Automated chemical synthesis

Edited by Ian R. Baxendale, Marcus Baumann and Richard Bourne

Imprint

Automated glycan assembly of a *S. pneumoniae* serotype 3 CPS antigen

Markus W. Weishaupt, Stefan Matthies, Mattan Hurevich, Claney L. Pereira, Heung Sik Hahm and Peter H. Seeberger[*]

Abstract

Vaccines against *S. pneumoniae*, one of the most prevalent bacterial infections causing severe disease, rely on isolated capsular polysaccharide (CPS) that are conjugated to proteins. Such isolates contain a heterogeneous oligosaccharide mixture of different chain lengths and frame shifts. Access to defined synthetic *S. pneumoniae* CPS structures is desirable. Known syntheses of *S. pneumoniae* serotype 3 CPS rely on a time-consuming and low-yielding late-stage oxidation step, or use disaccharide building blocks which limits variability. Herein, we report the first iterative automated glycan assembly (AGA) of a conjugation-ready *S. pneumoniae* serotype 3 CPS trisaccharide. This oligosaccharide was assembled using a novel glucuronic acid building block to circumvent the need for a late-stage oxidation. The introduction of a washing step with the activator prior to each glycosylation cycle greatly increased the yields by neutralizing any residual base from deprotection steps in the synthetic cycle. This process improvement is applicable to AGA of many other oligosaccharides.

Introduction

The Gram-positive encapsulated commensal bacterium *Streptococcus pneumoniae* [1-3] can cause serious medical conditions like pneumonia, meningitis, endocarditis and sepsis [4]. *S. pneumoniae* is the leading cause of vaccine-preventable deaths in children under five years worldwide [5]. Over 90 different serotypes of *S. pneumoniae* have been identified, each of which expresses a unique capsular polysaccharide (CPS) [6-9].

The *S. pneumoniae* serotype 3 CPS was first isolated in 1924 [10] and its exact chemical structure was finally elucidated in 1941 [11], as being composed of repeating units of β-(1,3)-linked cellobiuronic acid (Figure 1).

CPS plays a major role in *S. pneumoniae* virulence [12]. A commercial 17-valent polysaccharide vaccine was introduced in
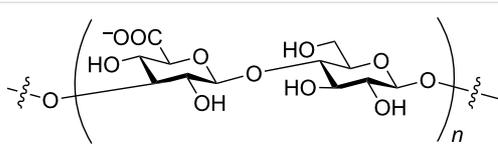
Figure 1: Disaccharide repeating unit of the *S. pneumoniae* serotype 3 CPS.

1977, followed by a 23-valent vaccine in 1983 [13-15]. Serotype 3 of *S. pneumoniae* is one of the most prevalent serotypes causing acute otitis media [16] and is one of the thirteen serotypes included in the blockbuster pneumococcal conjugate vaccine Prevnar 13® [17,18].

Vaccines against *S. pneumoniae* are usually manufactured using isolated CPS structures containing oligosaccharides of different lengths and frame shifts [19]. Synthetic oligosaccharide antigens enable structure–activity relationship (SAR) studies of bacterial antigens [20] to better understand antibody binding and help to improve existing vaccine formulations.

Two synthetic routes to prepare serotype 3 oligosaccharides have been developed and were applied to other uronic acid containing carbohydrate structures [21,22]. The first method uses only glucose building blocks to assemble oligosaccharides and introduces the C6 carboxylic acid moieties via a late-stage oxidation. Using this method, serotype 3 di-, tri- and tetrasaccharides were synthesized [23]. The other approach directly uses glucuronic acid building blocks as glycosylating agents. Due to the electron-withdrawing C6 carboxyl group, uronic acids exhibit a decreased reactivity both as glycosylating agents and as nucleophiles. Disaccharide building blocks containing glucuronic acid were used by de Jong et al. to prepare two different SP 3 trisaccharides [24]. In general, the late-stage-oxidation approach is often preferred since it circumvents the inherent reactivity issues associated with uronic acid building blocks [25-27].

Automated glycan assembly builds on monomeric building blocks that are incorporated during iterative glycosylations [28,29]. Here, a set of building blocks was identified that can be employed interchangeably in the automated syntheses of a wide variety of biologically relevant glycans. To minimize the post-automation chemical modifications and the loss of product, we assembled pneumococcal serotype 3 CPS structures utilizing glucose and glucuronic acid monosaccharide building blocks and thus avoided late-stage oxidations.

Results and Discussion

Mindful of this strategic framework, glucuronic acid building block **1** was designed (Figure 2). A levulinoyl (Lev) ester was chosen as temporary protecting group (TPG) since the Fmoc (fluorenylmethoxycarbonyl) group led to a loss of stereocontrol during glycosylations with this glucuronic acid (GlcA) building block (data not shown). Glucose building blocks **2** and **3** were equipped with two benzyl ethers to account for the low reactivity of glucuronic acids as glycosylating agents and carried either Fmoc or Lev groups. As solid support, we chose photolabile-linker-functionalized Merrifield resin **4** for its compatibility with the activation conditions for glycosyl phosphates, its mild cleavage conditions and the possibility to directly conjugate the product after global deprotection via the amine functional group [28]. The presence of glucuronic acids in the oligosaccharide sequence precludes the use of a base-labile linker due to the risk of elimination reactions [30].

The building blocks were synthesized in high yields using standard protecting group chemistry (see Supporting Information File 1). Solid support **4** was prepared according to an established procedure [28].

The automated glycosylation protocol employed three times three equivalents of building block to ensure complete glycosylation of the nucleophile (Scheme 1). The glycosyl phosphate building blocks **1** and **2** were activated by stoichiometric amounts of TMSOTf (trimethylsilyl trifluoromethanesulfonate) at −30 °C and reacted at this temperature for 30 min. Then the temperature was raised to −15 °C and maintained for 30 min. The temporary Fmoc protecting group was cleaved with triethylamine in DMF (*N,N*-dimethylformamide; 10% v/v). The Lev protecting group was removed using hydrazine monohydrate in pyridine/acetic acid (3:2 v/v).
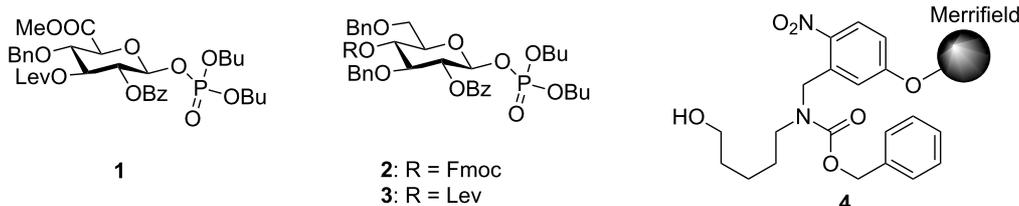
Figure 2: Building blocks and solid support for the automated solid-phase synthesis of *S. pneumoniae* serotype 3 CPS structures.
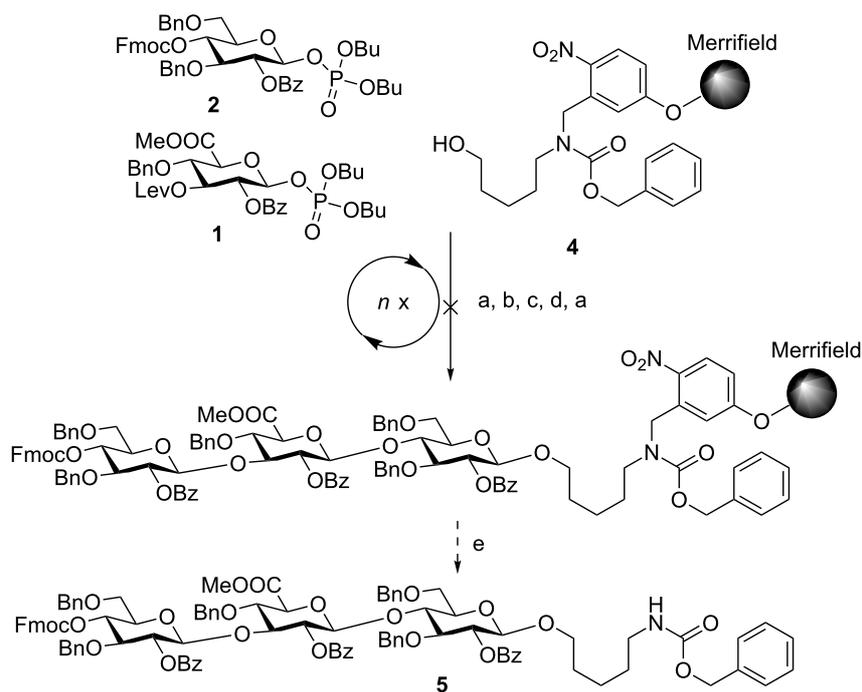
Scheme 1: Attempted assembly of SP3 trisaccharide **5** using glycosyl phosphate building blocks **1** and **2**. Reagents and conditions: a) **2** (3 equiv), TMSOTf, CH$_2$Cl$_2$, −30 °C (30 min) to −15 °C (30 min), n = 3; b) Et$_3$N in DMF (10% v/v), 25 °C (15 min), n = 3; c) **1** (3 equiv), TMSOTf, CH$_2$Cl$_2$, −30 °C (30 min) to −15 °C (30 min), n = 3; d) N$_2$H$_4$·H$_2$O, pyridine/AcOH (3:2 v/v), CH$_2$Cl$_2$, 30 min, n = 3; e) hv.

The crude oligosaccharide products were cleaved from the solid support by irradiation with UV light in a flow reactor [28] and analyzed by normal-phase HPLC (Figure 3).

Trisaccharide **6** lacking one C2-benzoate ester protecting group was identified as the main product. The unexpected side reaction was attributed to the basicity of the Fmoc deprotection

Figure 3: HPLC chromatogram of the crude products of the attempted AGA of SP3 trisaccharide **5**; conditions: YMC Diol 300, H/EtOAc, 0% EtOAc (5 min) to 55% EtOAc (70 min), ELSD.

solution. In addition, two deletion sequences (**7** and **8**) were also detected. Glycosylations mediated by the strongly acidic activator TMSOTf were found to be neutral when exiting the reaction vessel. An incomplete removal of the strongly basic deprotection solutions would result in quenching of the next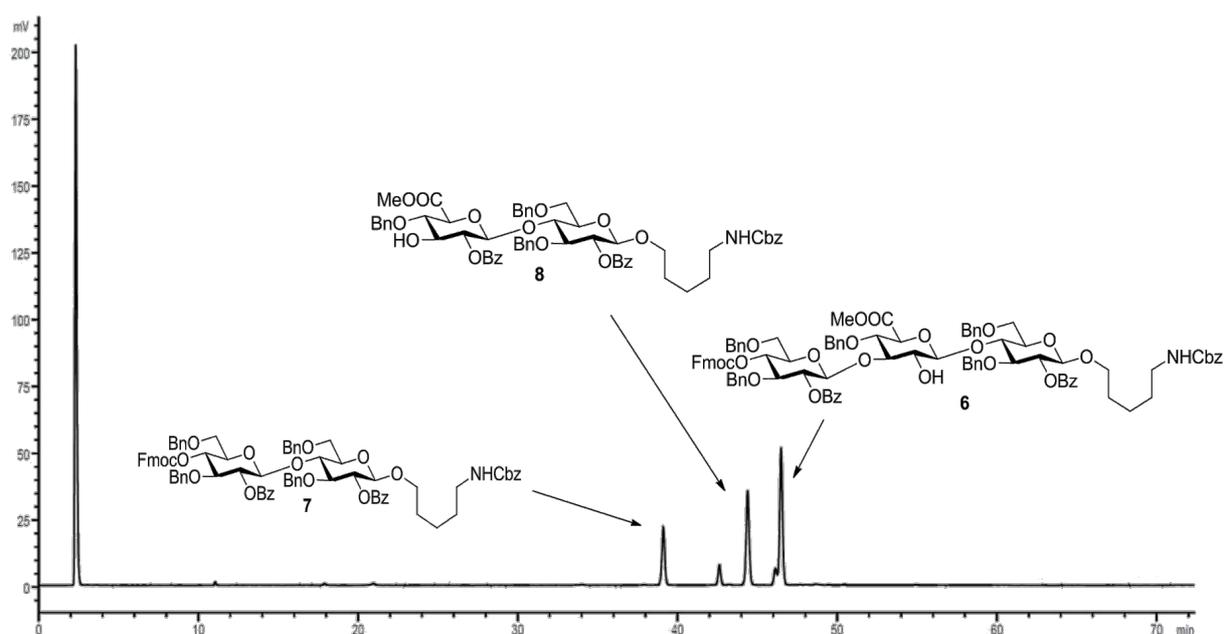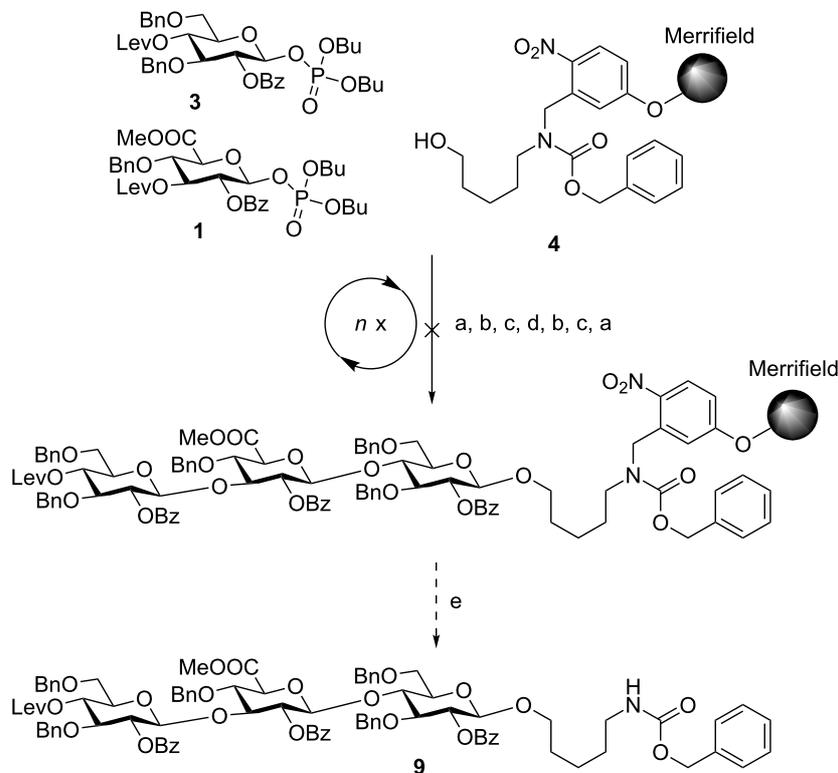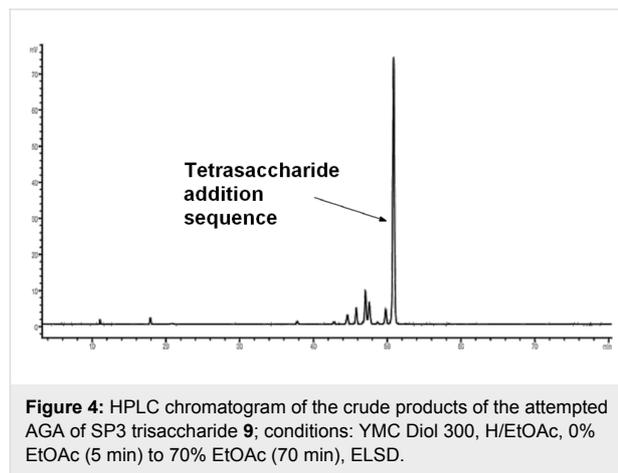 glycosylations. Indeed, test runs on the automated synthesis instrument illustrated regular washing steps following each deprotection failed to completely remove the deprotection solution. Therefore, an activator wash step was introduced between deprotection and glycosylation steps. In this step, the resin was washed with activator solution at −30 °C for one minute in order to neutralize any residual base. Remaining traces of water that would hydrolyze the glycosylating agent in the following glycosylation cycle are also effectively removed hereby. Furthermore, Fmoc-protected glucose building block **2** was replaced with Lev-protected **3**. The use of the buffered hydrazine solution for the cleavage of Lev TPGs was expected to prevent any undesired benzoyl ester cleavage. The trisaccharide synthesis was repeated using the same glycosylation conditions as in the previous synthesis (Scheme 2).

After each glycosylation step, the pH of the glycosylation solutions exiting the reaction chamber was tested and found to be strongly acidic. After cleavage from the solid support, HPLC analysis of the crude product showed one major product (Figure 4). However, MALDI–TOF MS analysis indicated that this fraction corresponded to a tetrasaccharide addition sequence, resulting from benzoyl ester cleavage and a double glycosylation in the last step (see Supporting Information File 1). This result was not expected as the buffered hydrazine deprotection protocol had never favored the formation of side

Figure 4: HPLC chromatogram of the crude products of the attempted AGA of SP3 trisaccharide **9**; conditions: YMC Diol 300, H/EtOAc, 0% EtOAc (5 min) to 70% EtOAc (70 min), ELSD.

Scheme 2: Attempted AGA of SP3 trisaccharide **9** using glycosyl phosphate building blocks **1** and **3**. Reagents and conditions: a) **3** (3 equiv), TMSOTf, CH$_2$Cl$_2$, −30 °C (30 min) to −15 °C (30 min), *n* = 3; b) N$_2$H$_4$·H$_2$O, pyridine/AcOH (3:2 v/v), CH$_2$Cl$_2$, 30 min, *n* = 3; c) TMSOTf, CH$_2$Cl$_2$, −30 °C (1 min), *n* = 1; d) **1** (3 equiv), TMSOTf, CH$_2$Cl$_2$, −30 °C (30 min) to −15 °C (30 min), *n* = 3; e) *hv*.

products in our hands. However, this finding also highlighted the efficiency of glycosylating agent **3** that can effectively glycosylate two free hydroxy groups in one step with nine equivalents of glycosylating agent **3**.

Different conditions for the cleavage of the Lev protecting group on solid support had been developed previously [24,31]. Performing the reaction at elevated temperature (40 °C), it is possible to use less hydrazine acetate (7.8 equivalents). Adapting these conditions to the automated synthesizer, each Lev deprotection was followed by an activator washing step. In order to test the modified deprotection conditions, glucuronic acid **1** was reacted with the linker, and the temporary Lev protecting group was removed using the adapted deprotection protocol (Scheme 3).

The HPLC analysis showed quantitative cleavage of the Lev protecting group without loss of the benzoyl ester to afford **10** (not shown).

With this encouraging result in hand, the synthesis of *S. pneumoniae* serotype 3 CPS trisaccharide **5** was attempted utilizing the new protocol for the removal of the Lev group (Scheme 4). In order to minimize the number of Lev deprotection steps, we

Scheme 3: Automated synthesis of linker-bound glucuronic acid **10** using glycosyl phosphate building block **1**. Reagents and conditions: a) **1** (3 equiv), TMSOTf, CH$_2$Cl$_2$, −30 °C (30 min) to −15 °C (30 min), *n* = 3; b) N$_2$H$_4$·OAc, pyridine/AcOH (4:1 v/v), 40 °C, 10 min, *n* = 2; c) *h*v.
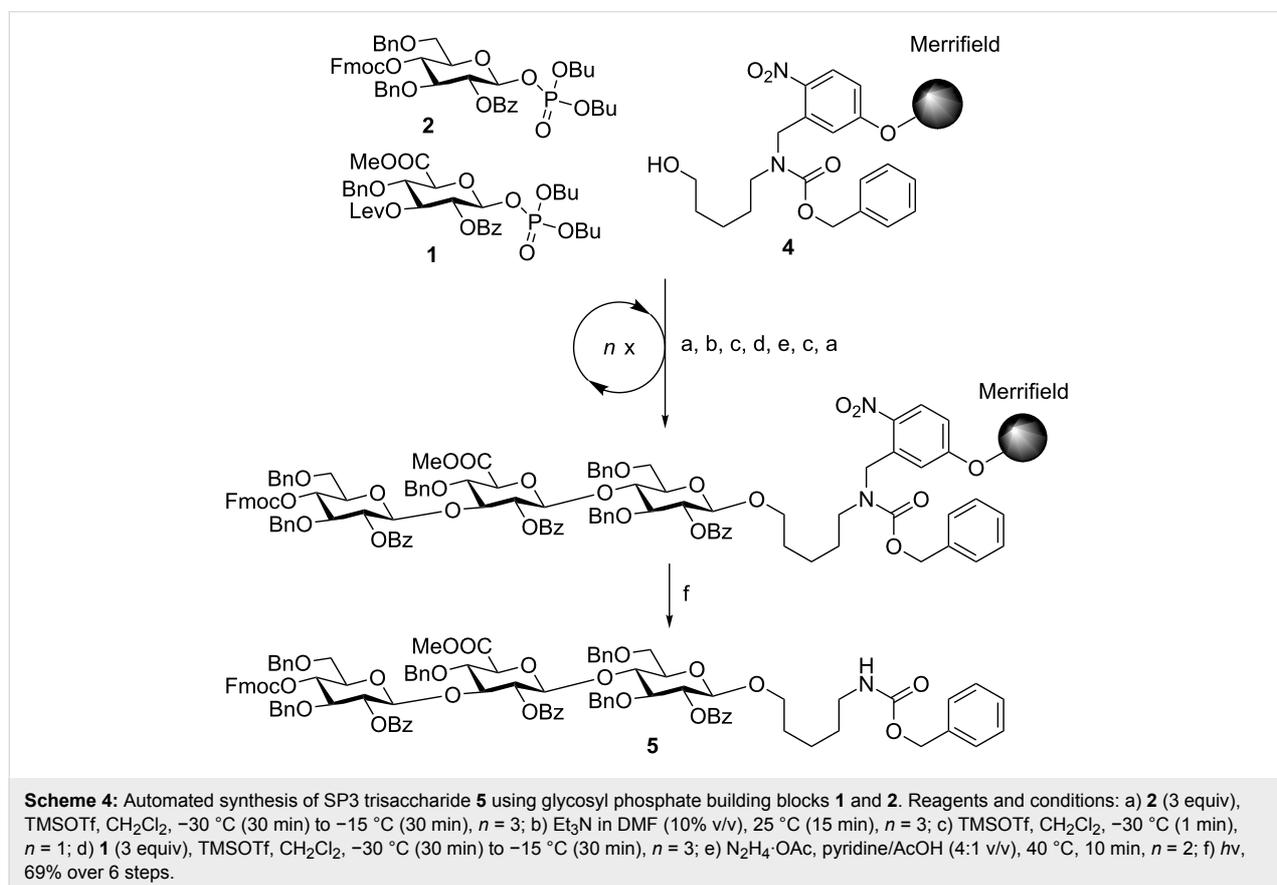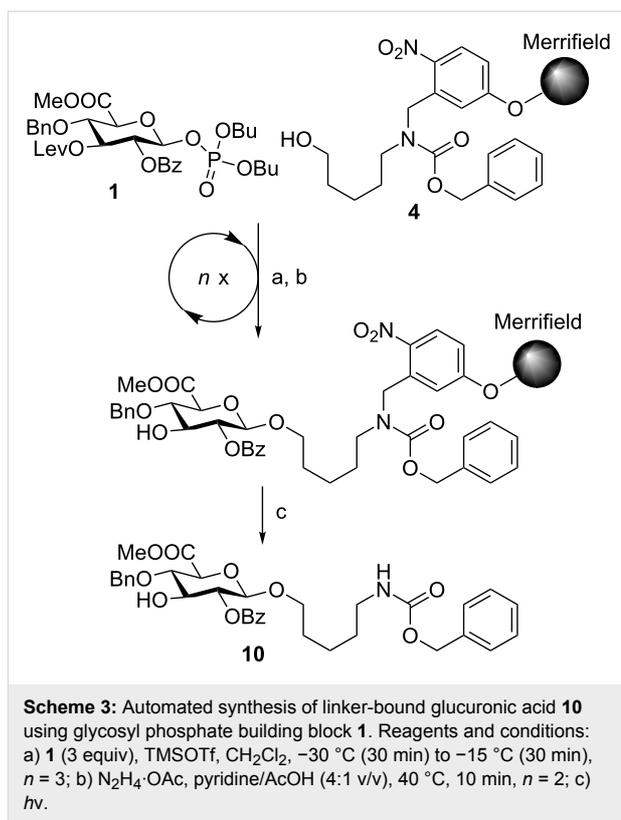

Scheme 4: Automated synthesis of SP3 trisaccharide **5** using glycosyl phosphate building blocks **1** and **2**. Reagents and conditions: a) **2** (3 equiv), TMSOTf, CH$_2$Cl$_2$, −30 °C (30 min) to −15 °C (30 min), *n* = 3; b) Et$_3$N in DMF (10% v/v), 25 °C (15 min), *n* = 3; c) TMSOTf, CH$_2$Cl$_2$, −30 °C (1 min), *n* = 1; d) **1** (3 equiv), TMSOTf, CH$_2$Cl$_2$, −30 °C (30 min) to −15 °C (30 min), *n* = 3; e) N$_2$H$_4$·OAc, pyridine/AcOH (4:1 v/v), 40 °C, 10 min, *n* = 2; f) *h*v, 69% over 6 steps.

returned to the initial strategy using Fmoc-protected glycosyl phosphate **2** as the glucose building block. This monomer did not suffer from a loss of stereocontrol as was observed in the case of the similarly protected GlcA building block.

The desired trisaccharide **5** was observed as the main product from the automated synthesis by HPLC analysis (Figure 5). The Lev protecting group had been removed quantitatively while no benzoyl ester cleavage was observed. None of the byproducts could be identified by either ESIMS or NMR.
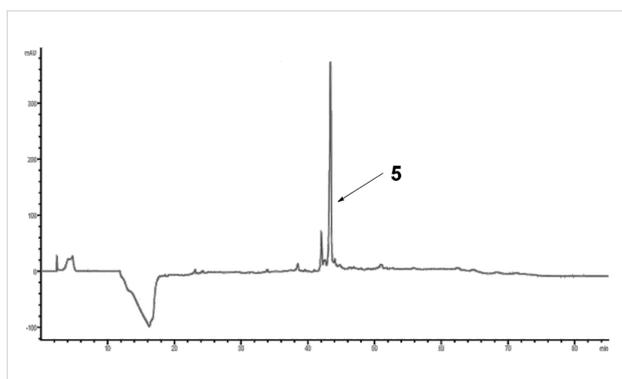

Figure 5: HPLC chromatogram of the crude products of the automated solid-phase SP3 trisaccharide **5** synthesis; conditions: YMC Diol 300, H/EtOAc, 0% EtOAc (5 min) to 60% EtOAc (60 min), 254 nm.

The *S. pneumoniae* serotype 3 trisaccharide **5** was isolated in 69% yield and deprotected in three steps. First, the methyl ester was removed under mild conditions using a mixture of lithium hydroxide and hydrogen peroxide to avoid elimination reactions which are common for uronic acid methyl esters under strongly basic conditions [30,32]. In the next step, the remaining esters were removed employing sodium hydroxide in methanol. Finally, catalytic hydrogenation using Pd(OH)$_2$/C in methanol/water/acetic acid (50:25:1 v/v/v) afforded the fully deprotected *S. pneumoniae* serotype 3 CPS antigen **11** in 71% yield over three steps (Scheme 5).

Conclusion

The first automated glycan assembly of a conjugation-ready *S. pneumoniae* serotype 3 trisaccharide **11** using glucuronic acid building blocks was achieved. The need for a late-stage oxidation was circumvented by using a novel glucuronic acid building block, thereby shortening the synthetic route by two steps. Selective C6-OH deprotection/oxidation steps on oligosaccharides are usually not very efficient (53% over two steps for a trisaccharide), and are characterized by decreasing yields with increasing chain length [23]. The GlcA building block proved to be an efficient glycosylating agent, that is expected to serve well in the synthesis of other oligosaccharide antigens. Liberation of the C3-OH group of glucuronic acid **1** for chain elongation proved delicate. Standard hydrazine cleavage conditions for the Lev protecting group also removed a benzoyl ester and lead to the formation of unwanted products. Using hydrazine acetate at slightly elevated temperatures (40 °C) [24,31] cleaved the levulinoyl groups on mono- and trisaccharides while retaining all benzoyl esters. The introduction of an activator washing step prior to each glycosylation greatly increased the reproducibility of the automated syntheses and is envisioned to increase efficacy of AGA for many other biologically relevant glycans in the future.

In conclusion, we have developed an efficient method for the synthesis of *S. pneumoniae* serotype 3 CPS structures. The products of these syntheses are currently used in the development of synthetic carbohydrate conjugate vaccines.

Supporting Information

Supporting Information File 1
Experimental details as well as full characterization of all new compounds.
[http://www.beilstein-journals.org/bjoc/content/supplementary/1860-5397-12-139-S1.pdf]
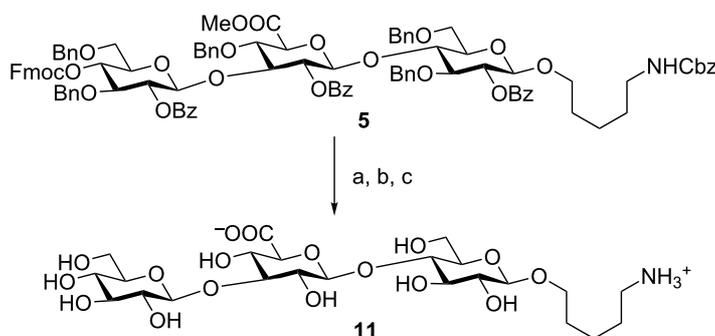
Scheme 5: Global deprotection of SP3 trisaccharide **5**. Reagents and conditions: a) LiOH, H$_2$O$_2$, THF, −5 °C to rt; b) NaOH, MeOH, 0 °C to rt; c) Pd(OH)$_2$/C, MeOH/H$_2$O/AcOH (50:25:1 v/v/v), 71% over 3 steps.

Acknowledgements

References

1. Friedländer, C. *Fortschr. Med.* **1883,** *1,* 715–733.
2. Pasteur, L. *Bull. Acad. Med. (Paris, Fr.)* **1881,** *10,* 94–103.
3. Sternberg, G. M. *Nat. Board Health Bull.* **1881,** *2,* 781–783.
4. Musher, D. M. *Clin. Infect. Dis.* **1992,** *14,* 801–809. doi:10.1093/clinids/14.4.801
5. O'Brien, K. L.; Wolfson, L. J.; Watt, J. P.; Henkle, E.; Deloria-Knoll, M.; McCall, N.; Lee, E.; Mulholland, K.; Levine, O. S.; Cherian, T. D. *Lancet* **2009,** *374,* 893–902. doi:10.1016/S0140-6736(09)61204-6
6. Henrichsen, J. *J. Clin. Microbiol.* **1995,** *33,* 2759–2762.
7. Lund, E.; Henrichsen, J. *Methods Microbiol.* **1978,** *12,* 241–262. doi:10.1016/S0580-9517(08)70365-9
8. Calix, J. J.; Nahm, M. H. *J. Infect. Dis.* **2010,** *202,* 29–38. doi:10.1086/653123
9. Park, I. H.; Pritchard, D. G.; Cartee, R.; Brandao, A.; Brandileone, M. C. C.; Nahm, M. H. *J. Clin. Microbiol.* **2007,** *45,* 1225–1233. doi:10.1128/JCM.02199-06
10. Heidelberger, M.; Avery, O. T. *J. Exp. Med.* **1924,** *40,* 301–317. doi:10.1084/jem.40.3.301
11. Reeves, R. E.; Goebel, W. E. *J. Biol. Chem.* **1941,** *139,* 511–519.
12. Moxon, E. R.; Kroll, J. S. *Clin. Diagn. Lab. Immunol.* **1990,** *150,* 65–85.
13. Austrian, R. *Rev. Infect. Dis.* **1981,** *3* (Suppl. 1), S1–S17. doi:10.1093/clinids/3.Supplement_1.S1
14. Austrian, R. *Rev. Infect. Dis.* **1989,** *11* (Suppl. 3), S598–S602. doi:10.1093/clinids/11.Supplement_3.S598
15. Robbins, J. B.; Austrian, R.; Lee, C.-J.; Rastogi, S. C.; Schiffman, G.; Henrichsen, J.; Makela, P. H.; Broome, C. V.; Facklam, R. R.; Tiesjema, R. H.; Parke, J. C., Jr. *J. Infect. Dis.* **1983,** *148,* 1136–1159. doi:10.1093/infdis/148.6.1136
16. Rodgers, G. L.; Arguedas, A.; Cohen, R.; Dagan, R. *Vaccine* **2009,** *27,* 3802–3810. doi:10.1016/j.vaccine.2009.04.021
17. Committee on Infectious Diseases. *Pediatrics* **2010,** *126,* 186–190.
18. Plosker, G. L. *Pediatr. Drugs* **2013,** *15,* 403–423. doi:10.1007/s40272-013-0047-z
19. Yu, X. H.; Sun, Y.; Frasch, C.; Concepcion, N.; Nahm, M. H. *Clin. Diagn. Lab. Immunol.* **1999,** *6,* 519–524.
20. Johnson, M. A.; Pinto, B. M. *J. Am. Chem. Soc.* **2002,** *124,* 15368–15374. doi:10.1021/ja020983v
21. Codée, J. D. C.; Christina, A. E.; Walvoort, M. T. C.; Overkleeft, H. S.; van der Marel, G. A. Uronic Acids in Oligosaccharide and Glycoconjugate Synthesis. In *Reactivity Tuning in Oligosaccharide Assembly;* Fraser-Reid, B.; Lopez, J. C., Eds.; Springer-Verlag: Berlin, 2011; Vol. 301, pp 253–289. doi:10.1007/128_2010_111
22. van den Bos, L. J.; Codée, J. D. C.; Litjens, R. E. J. N.; Dinkelaar, J.; Overkleeft, H. S.; van der Marel, G. A. *Eur. J. Org. Chem.* **2007,** 3963–3976. doi:10.1002/ejoc.200700101
23. Lefeber, D. J.; Kamerling, J. P.; Vliegenthart, J. F. G. *Chem. – Eur. J.* **2001,** *7,* 4411–4421. doi:10.1002/1521-3765(20011015)7:20<4411::AID-CHEM4411>3.0.CO;2-T
24. de Jong, A.-R.; Hagen, B.; van der Ark, V.; Overkleeft, H. S.; Codée, J. D. C.; van der Marel, G. A. *J. Org. Chem.* **2012,** *77,* 108–125. doi:10.1021/jo201586r
25. Slaghek, T.; Nakahara, Y.; Ogawa, T. *Tetrahedron Lett.* **1992,** *33,* 4971–4974. doi:10.1016/S0040-4039(00)61248-0
26. Wang, Z.; Xu, Y.; Yang, B.; Tiruchinapally, G.; Sun, B.; Liu, R.; Dulaney, S.; Liu, J.; Huang, X. *Chem. – Eur. J.* **2010,** *16,* 8365–8375. doi:10.1002/chem.201000987
27. Wu, X.; Cui, L.; Lipinski, T.; Bundle, D. R. *Chem. – Eur. J.* **2010,** *16,* 3476–3488. doi:10.1002/chem.200902460
28. Eller, S.; Collot, M.; Yin, J.; Hahm, H. S.; Seeberger, P. H. *Angew. Chem., Int. Ed.* **2013,** *52,* 5858–5861. doi:10.1002/anie.201210132
29. Weishaupt, M. W.; Matthies, S.; Seeberger, P. H. *Chem. – Eur. J.* **2013,** *19,* 12497–12503. doi:10.1002/chem.201204518
30. BeMiller, J. N.; Kumari, G. V. *Carbohydr. Res.* **1972,** *25,* 419–428. doi:10.1016/S0008-6215(00)81653-5
31. Walvoort, M. T. C.; Volbeda, A. G.; Reintjens, N. R. M.; van den Elst, H.; Plante, O. J.; Overkleeft, H. S.; van der Marel, G. A.; Codée, J. D. C. *Org. Lett.* **2012,** *14,* 3776–3779. doi:10.1021/ol301666n
32. Lucas, H.; Hasten, J. E. M.; van Dinther, T. G.; Meuleman, D. G.; van Aelst, S. F.; van Boeckel, C. A. A. *Tetrahedron* **1990,** *46,* 8207–8228. doi:10.1016/S0040-4020(01)81477-0

Flow carbonylation of sterically hindered *ortho*-substituted iodoarenes

Carl J. Mallia[1], Gary C. Walter[2] and Ian R. Baxendale[*1]

Abstract

The flow synthesis of *ortho*-substituted carboxylic acids, using carbon monoxide gas, has been studied for a number of substrates. The optimised conditions make use of a simple catalyst system compromising of triphenylphosphine as the ligand and palladium acetate as the pre-catalyst. Carbon monoxide was introduced via a reverse "tube-in-tube" flow reactor at elevated pressures to give yields of carboxylated products that are much higher than those obtained under normal batch conditions.

Introduction

Carbonylation reactions have received a great deal of attention both in batch as well as in flow (using plug/annular flow reactors [1-5] or "tube-in-tube" reactors [6-10]) and generally produce the desired products in good yields [11-14]. This is not the case though for the carbonylation of *ortho*-substituted substrates which are much more challenging as highlighted by the limited literature precedence [15-17]. However, these products are of considerable industrial importance, especially the amide and ester derivatives, which are commonly found in agrochemical active ingredients, for example tecloftalam, flutolanil, fluopyram and diflufenican. Likewise, in pharmaceutical compounds such as 2,4,5-trifluorobenzoic acid, which serve as a

starting material for several antibacterial drugs such as ciprofloxacin (Cipro™), norfloxacin (Noroxin™) and pefloxacin (Peflacine™).

The low catalyst turnover frequency (T.O.F.) and poor yields associated with *ortho*-substituted transformations are attributed to the carbon monoxide coordination to the intermediate aryl transition metal (i.e., Pd) complex which is inhibited by sterics [15]. Following oxidative addition of the aryl halide, an associative mechanism for the complexation of carbon monoxide on the d^8 square planar intermediate would occur prior to the key migratory insertion step. In the complex, the aryl group would

be oriented perpendicularly to the plane to minimise steric interactions thus placing the *ortho*-substituent directly over an axial site (Figure 1). The *ortho*-substituent therefore acts as a steric buttress hindering the approach of the incoming carbon monoxide thus slowing down the rate of the reaction. An X-ray structure of *trans*-bromo(*o*-tolyl)bis(triphenylphosphine)palladium(II) complex was reported by Cross et al. (Figure 2) [18]. The molecular structure of **1** comprises of a palladium atom with near perfect square planar geometry with a slight out of plane displacement of Br and C(1) where the Br–Pd–C(1) angle is 170.9°. As a whole, the molecule has approximate C_s symmetry with the PPh$_3$ ligands almost eclipsing each other if viewed along the P–Pd–P axis, with the tolyl group sandwiched between the two phenyl groups (Figure 2, structure B). Focusing on the tolyl group only, structure C (Figure 2) shows how the methyl of the tolyl group is placed straight over the axial position of the palladium. Structure D (Figure 2) is a top view of the crystal structure illustrating how the methyl group sits directly over the axial position of the palladium which would introduce steric effects inhibiting the CO coordination on the intermediate aryl complex.

As the carbonylation step becomes slower, the competing dehalogenation pathway becomes dominant resulting in overall

Figure 1: Steric interactions of the carbon monoxide coordination to the aryl complex intermediate.
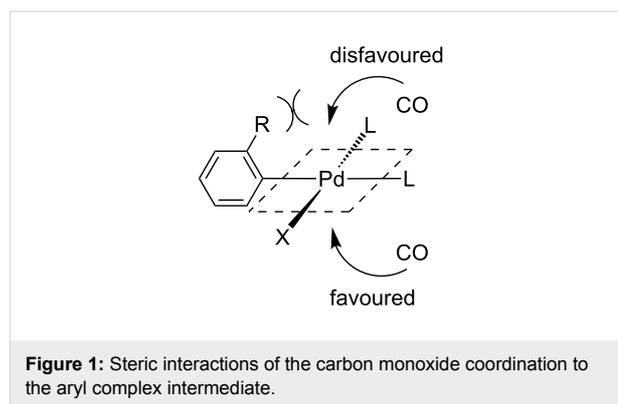
lower yields of the carbonylated product. In principle, increasing the carbon monoxide concentration (by increasing the carbon monoxide pressure) together with an increase in temperature, should promote the carbonylation. However, an increase in carbon monoxide concentration can also decrease the amount of active Pd^0 catalyst due to the π-acidic nature of carbon monoxide as a ligand, thus slowing down the reaction. Additionally, increasing the temperature will also increase the rate of side product formation. Consequently, optimisation of the carbon monoxide concentration and temperature is critical to obtaining a good yield of carbonylated *ortho*-substituted products.

Figure 2: A) molecular structure of complex **1**; B) ball and stick representation of X-ray structure; C) ball and stick representation of X-ray structure showing the tolyl group only; D) topside view of X-ray structure [18].
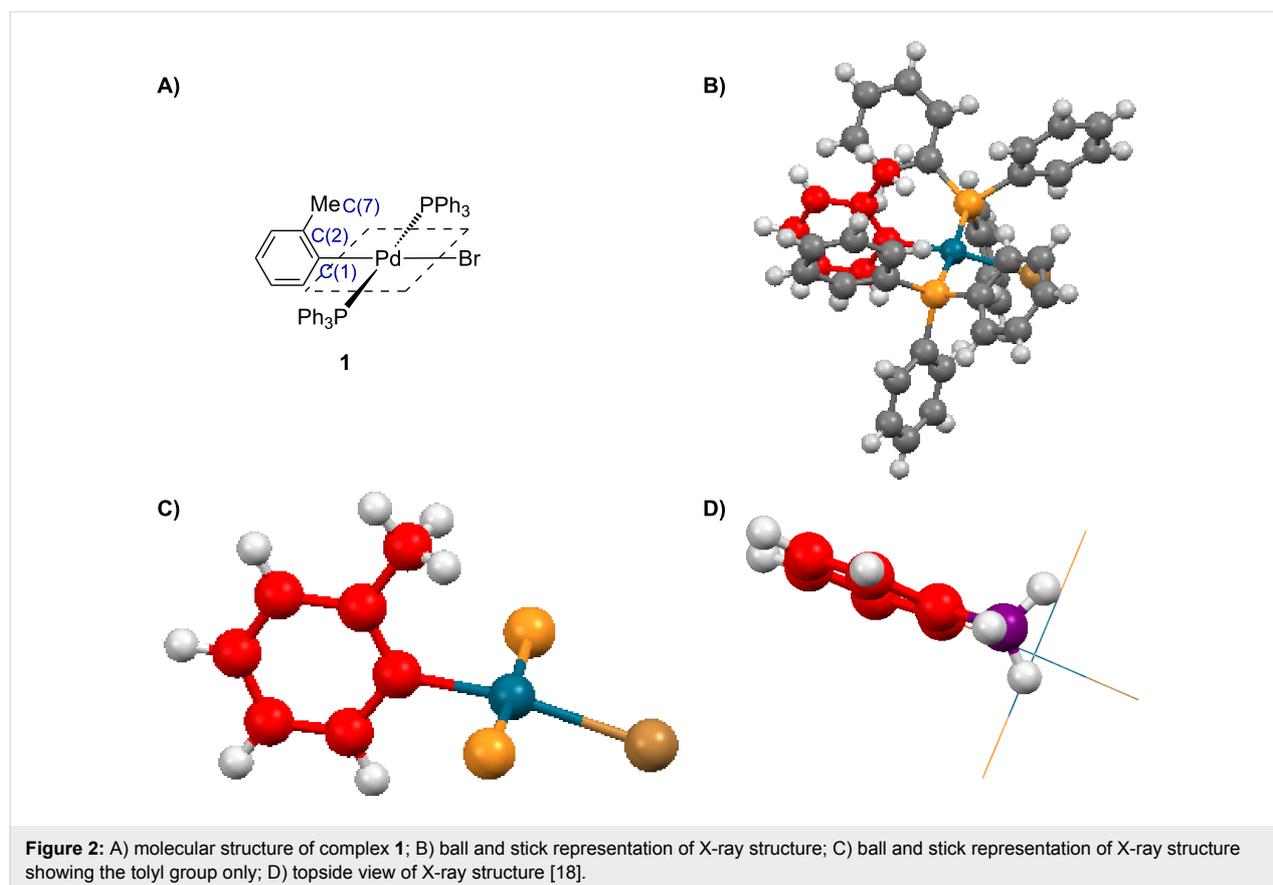
Results and Discussion

The application of flow chemistry [19,20] has been shown to be beneficial for many reactions that involve gases [21-29]. The efficient mixing along with high heat and mass transfer that are achieved through the use of small dimensioned channels such as those found in flow reactors, allow for the use of a wider range of reaction conditions which are otherwise difficult or impossible to achieve. The interfacial mixing area is also an important characteristic when gases are involved as this is an essential factor determining the solubility of a gas in the liquid phase. The interfacial area is generally very small when traditional batch chemistry equipment is used such as round bottom flasks. This also becomes proportionally smaller when larger volume flasks are used as in scale up procedures making the mass transfer even less efficient. In contrast, high interfacial areas can be achieved in flow reactors especially microchannel reactors (a = 3400–18000 m^2 m^{-3}) [30], which increases the mass transfer and thus helps solubilise the gases in the liquid phase.

In our work a reverse "tube-in-tube" reactor [31-33] was used to deliver the carbon monoxide to the reaction (Figure 3), as this was shown to be more efficient than an alternative plug flow system (Scheme 1) when evaluated on iodobenzene (**2**).

The "tube-in-tube" gas-liquid unit was attached to a commercial flow system; Vapourtec R2+ Series along with an R4 heating unit. Having established the reactor design, we next used 2-chloro-1-iodobenzene (**4**) as a model substrate for screening and identification of a set of general reaction conditions (Scheme 2). Initially, a fixed 5 mol % of Pd(OAc)$_2$ and 10 mol % of the phosphine ligand was investigated. It was
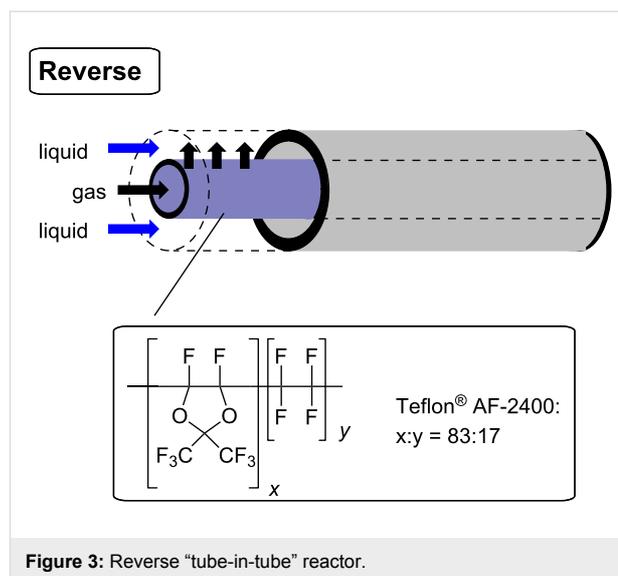
Figure 3: Reverse "tube-in-tube" reactor.

noted that the catalyst level could be reduced [34], but this amount allowed for an efficient catalytic process with short reaction times in the region of two hours, a good match for the flow system assembly [8]. Five different phosphine ligands were subsequently tested, three of which were monodentate with a variable cone angle (**6**–**8**; 145–256°) [35,36] and the other two bidentate phosphine ligands namely 1,4-bis(diphenylphosphino)butane (DPPB, **9**; βn = 98°) and Xantphos (**10**; 104 and 133°) with differing bite angles (Figure 4) [37-39].

Initially using 5 bar of carbon monoxide and a temperature of 110 °C, the five ligands gave similar yields, with DPPB (**9**) giving marginally the highest and X-Phos (**7**) the lowest isolat-
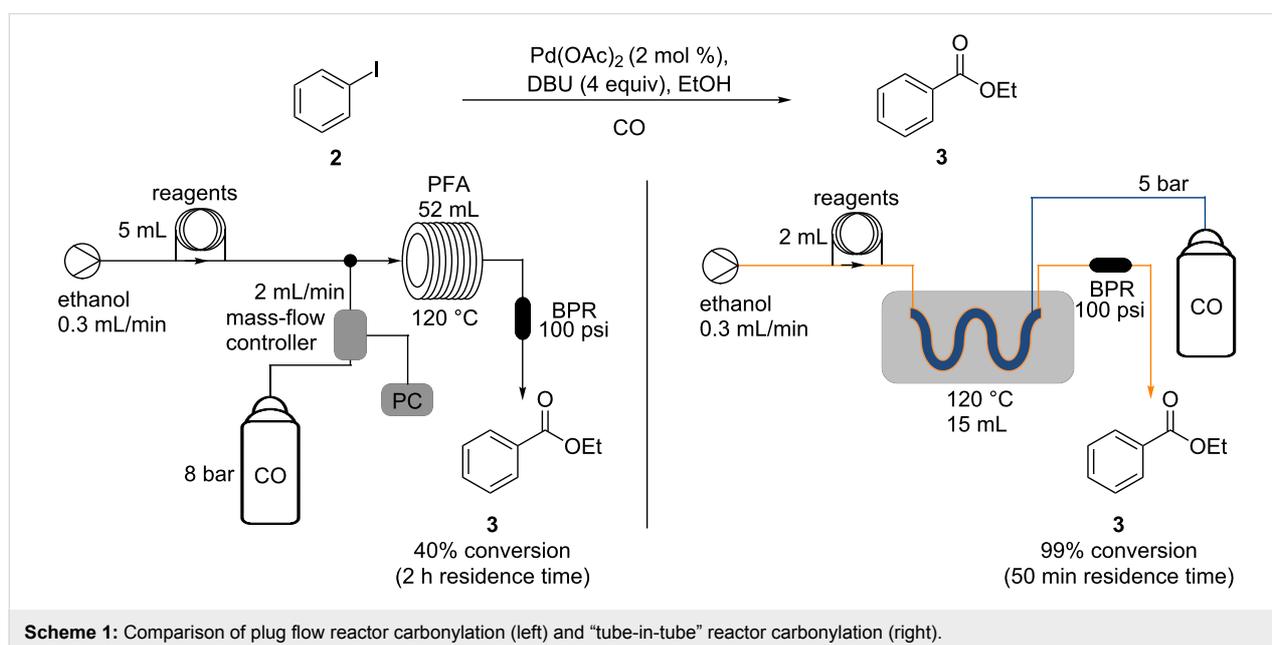
Scheme 1: Comparison of plug flow reactor carbonylation (left) and "tube-in-tube" reactor carbonylation (right).

Scheme 2: Schematic diagram of the flow process.

Figure 4: Phosphine ligands used for the *ortho*-carbonylation reaction.
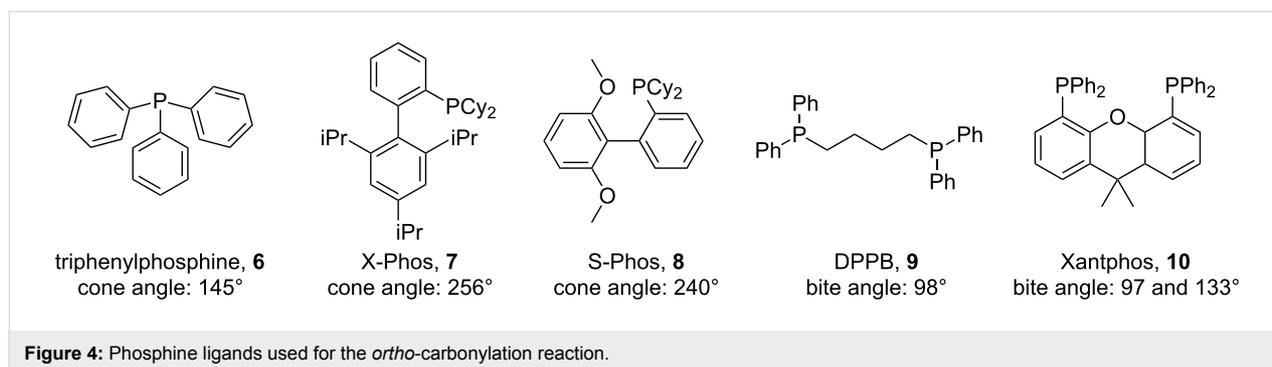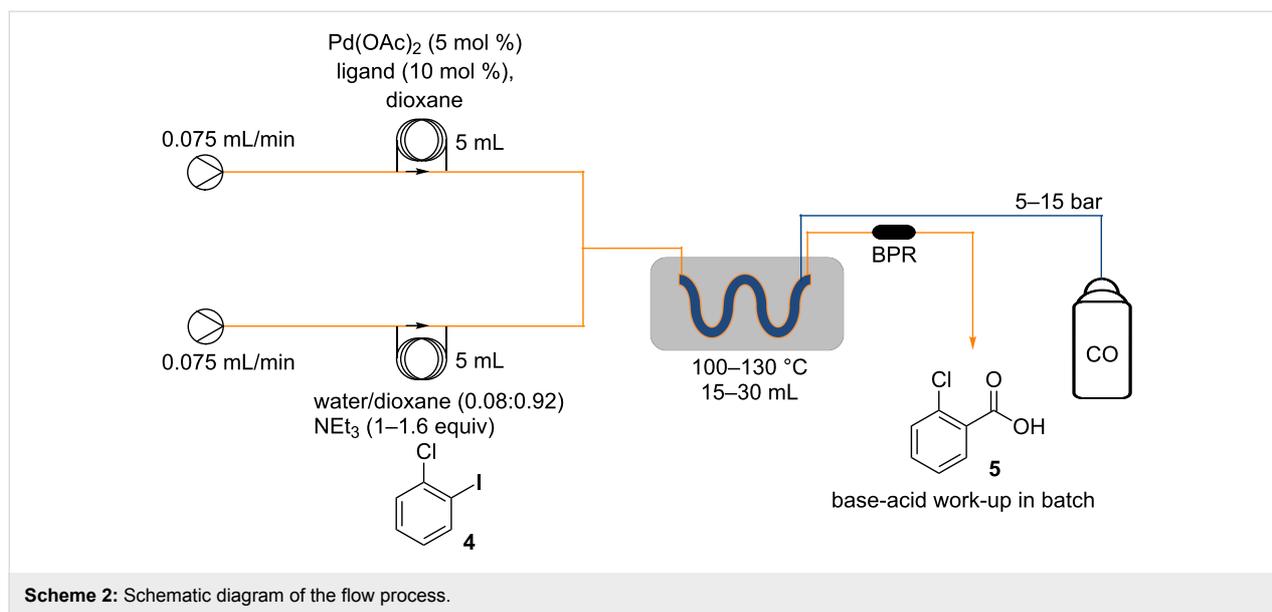
ed yield. However, the highest selectivities for the desired product were obtained with S-Phos (**8**) and triphenylphosphine (**6**) (Table 1, entries 2 and 5), with the difference between the conversion and the isolated yield mainly equating to the dehalogenated product namely, chlorobenzene.

Next changing the amount of triethylamine used from 1.1 equiv to 1.6 equiv and 2.0 equiv, respectively, did not significantly change the isolated yield of **5**. However, changing to the stronger base DBU (pK_a in water at 25 °C = 13.5) [40] dramatically reduced the isolated yield (Table 1, entry 8). A wider temperature range was also investigated (Table 1, entries 9–11). This resulted in only a small increase in the yield on going from 100 °C to 120 °C and a marginal decrease when the temperature was further increased to 130 °C. As there was no significant difference between 110 °C and 120 °C (Table 1, entries 5 and 10), the lower temperature was selected for the use in the next set of experiments. Interestingly the addition of up to 20 mol % of dimethylformamide (DMF) as an additive did not improve the yield which had been suggested by evaluation of

similar reactions in the literature [6,10]. However as anticipated, an increase in carbon monoxide pressure did pertain to a raise in product yield to 62% (Table 1, entries 12 and 13). In addition the effect of gas contact time was evaluated by employing two "tube-in-tube" reactors linked in series; albeit this resulted in only a modest improvement in yield (Table 1, entry 15). A further increase in product yield was observed when a larger excess of the triethylamine base (1.6 equiv) was used (Table 1, entry 16), but the isolated yield dropped with further equivalents of triethylamine (2.0 equiv; Table 1, entry 17). This indicated that the reaction was being inhibited by low pH which was generated at higher conversions when insufficient base was present to neutralise the carboxylic acid being formed. Interestingly, the requirement for a higher excess of base during initial screening (Table 1, entries 6 and 7) had been masked due to the initial low conversions achieved.

For comparison purposes, two batch carbonylation reactions were performed. The first of these batch reactions (conducted in a conventional laboratory set-up) used the palladium triphenyl-

Table 1: Optimisation for the carbonylation of *ortho*-substituted substrates in flow.
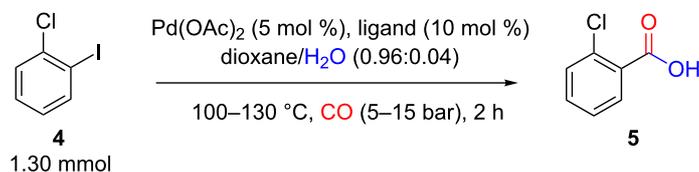
Entry	Ligand	Temperature (°C)	CO pressure (bar)	Conversion (%)	Isolated yield of **5** (%)
1	X-Phos	110	5	68	31
2	S-Phos	110	5	43	36
3	DPPB	110	5	90	38
4	Xantphos	110	5	57	36
5	PPh₃	110	5	44	36
6[a]	PPh₃	110	5	59	36
7[b]	PPh₃	110	5	80	33
8[c]	PPh₃	110	5	N/D	18
9	PPh₃	100	5	41	31
10	PPh₃	120	5	60	37
11	PPh₃	130	5	N/D	33
12[d]	PPh₃	110	10	67	46
13[d]	PPh₃	110	15	74	62
14[d,e]	PPh₃	110	15	N/D	31
15[f]	PPh₃	110	15	N/D	68
16[f,a]	PPh₃	110	15	99	90
17[f,b]	PPh₃	110	15	99	73

[a]1.6 equiv of base. [b]2.0 equiv of base. [c]1.1 equiv of DBU used instead of NEt₃. [d]10 mL reactor was not "tube-in-tube". [e]20 mol % DMF added. [f]2 × 15 mL "tube-in-tube" reactors used. N/D: not determined.

phosphine catalyst system under refluxing conditions with a double-walled balloon to deliver the carbon monoxide (Scheme 3). This would constitute a normal set-up used by many laboratory chemists when reactions involving gases are attempted if no specialised equipment is available. Two parallel reactions were preformed, one reaction was quenched after 2 hours and after purification yielded 5% of product **5**, while the second reaction was quenched after 24 h yielding 9% of purified **5**. The difference in the yields obtained in batch

when compared to the reactions conducted in flow, most probably arises from the fact that not enough carbon monoxide is being delivered to the reaction mixture. The dehalogenation pathway is then preferred yielding chlorobenzene as the main product.

The second batch reaction set-up, conducted in the departmental high pressure lab (HPL), was set up in a Parr autoclave using carbon monoxide at 15 bar and 110 °C for 2 hours. After
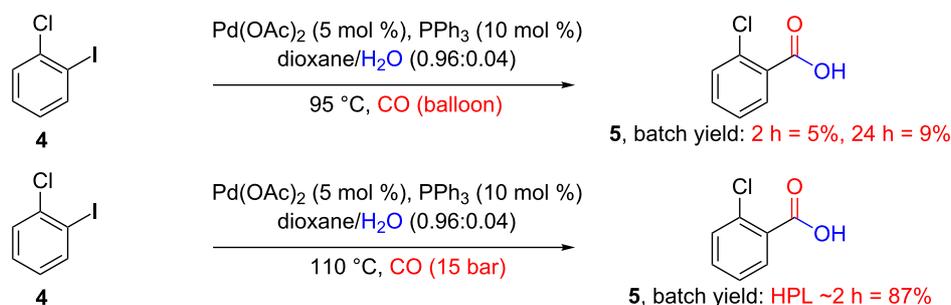
Scheme 3: The batch carbonylation of 2-chloro-1-iodobenzene in conventional lab (top) and using a Parr autoclave in high pressure lab (bottom).

purification, a yield of 87% for product **5** was obtained. This compares well with the flow protocol, however, the reaction "processing" time is in reality much longer due to the long cooling and heating times (4 h 15 min "processing" time, see experimental section in Supporting Information File 1 for more details). Also, the time required due to the extra precautionary measures needed when high pressure laboratory equipment is used means that the turnaround time is much longer. This makes the flow reactor more efficient in terms of processing time. Additionally, the added safety and potential benefits regarding scale up associated with the flow reactor makes this even more favourable.

Having identified a set of reaction conditions for successful carbonylation, a number of additional substrates were assessed to determine the generality of the flow process. No significant impact was seen on the overall yield by altering the *ortho*-sub-

stituent to a bromo, fluoro or trifluoromethyl group. However, a slight decrease associated with the larger sizes of bromo and trifluoromethyl groups may be inferred (Scheme 4, **11**, **13**). A more pronounced decrease in yield was obtained for substrates **14** and **15** (Scheme 4, 63% and 60%, respectively) probably due to the larger size of these groups and as well as electronic effects (the more electron withdrawing trifluoromethyl group substrate **13** gave a 71% yield). For comparisons of the sizes of the *ortho*-substituents used, A-values can be used as a guide (Cl: 0.43 kcal/mol, Br: 0.38 kcal/mol, F: 0.15 kcal/mol, OMe: 0.60 kcal/mol, CF_3: 2.10 kcal/mol and Me: 1.70 kcal/mol) [41]. This indicates interplay between electronic and steric factors.

Using a pyridine as a heteroaromatic substrate gave a lower but still acceptable yield of **16** compared to the phenyl equivalent (**5**). In general, substitution at the 4-position of the aryl gave moderate to good yields (Scheme 4, **17**–**21**) with weakly elec-

Scheme 4: Structures of *ortho*-substituted carboxylic acids prepared via a continuous flow hydroxy-carbonylation method.
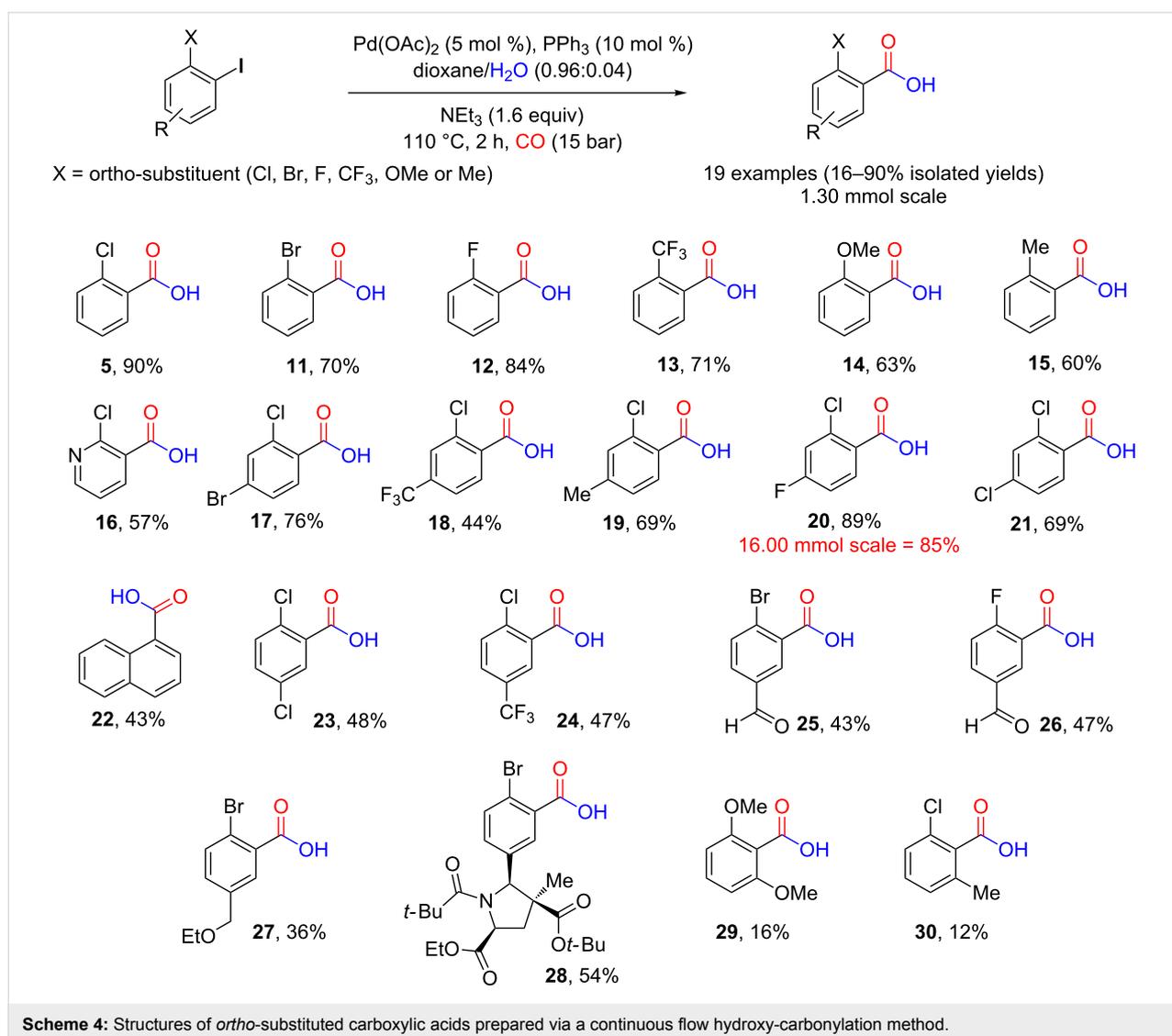
tron-withdrawing substituents or electron-donating groups giving better yields (Scheme 4, compounds **17**, **19–21**) than the more electron-withdrawing CF$_3$ group (Scheme 4, compound **18**). In the case of **22** the attached aromatic ring introduces both the ortho substituted sterics and the electronic effects from the additional aromatic ring attached. For comparison 2-iodonaphthalene (**31**) was carboxylated under the same conditions to give 2-naphthoic acid (**32**) showing that reducing the steric encumbrance at the ortho position improves the yield by 10% for this substrate (Scheme 5).

Moderate yields were obtained with 5-substited substrates (Scheme 4, compounds **23–30**). Both electron-withdrawing groups (Scheme 4, compounds **23–26**) and electron-donating groups gave similar yields (Scheme 4, compounds **27** and **28**) indicating that the inductive effects are not affecting the yields. Comparing the yields obtained for **27** and **28** also indicates that the sterics at the 5-position are not affecting the yield with a large group at the 5-position of substrate **30** [42] (see X-ray structure of substrate **33**, Figure 5) actually leading to a better yield than obtained for product **27** which contains the smaller ethoxy group at the 5-position.

The lowest yields of the array were obtained for compounds **29** and **30**, demonstrating the importance of sterics and electronics adjacent to the leaving group. In both cases, the carbon mon-oxide insertion is assumed to be slow as both axial positions of the aryl complex would be hindered, meaning the competing proton-dehalogenation pathway becomes preferred, giving 1,3-dimethoxybenzene as the main product, which was isolated in 31% yield in the case of **29** and 3-chlorotoluene in the case of **30** which was isolated in 52% yield (Scheme 4).

To demonstrate the potential scalability of the reaction conditions, the synthesis of compound **20** was repeated at 16 mmol scale, a factor of twelve times the original 1.3 mmol test scale (Scheme 6). The yield obtained for the larger scale was 85% which is consistent with the original 89% obtained at the 1.30 mmol scale, indicating that the processes is robust and reliably delivering 1.19 g h^{-1} of **20** in 85% isolated yield.

Conclusion
We have successfully demonstrated how flow chemistry can be used to enhance difficult transformations such as the palladium-catalysed hydroxy-carbonylation of *ortho*-substituted iodo-arenes. The optimised conditions were also demonstrated to work on a number of *ortho*-substituted substrates giving moderate to good yields. Comparison of **22** with **32** also showed that the steric encumbrance on the ortho position has an effect on the yield even when other electronic effects are in place such as those coming from the additional aromatic ring attached. A scale-up of the reaction conditions was performed providing comparable yields to those obtained from the initial smaller test scale. This method could thus be an efficient and scalable approach to synthesising important intermediates containing *ortho*-substituted carboxylic acids.

Scheme 5: Flow carbonylation of 2-iodonaphtalene.

Figure 5: X-ray structure of substrate **33**.

Scheme 6: Scale up synthesis of 2-chloro-4-fluorobenzoic acid (**20**).
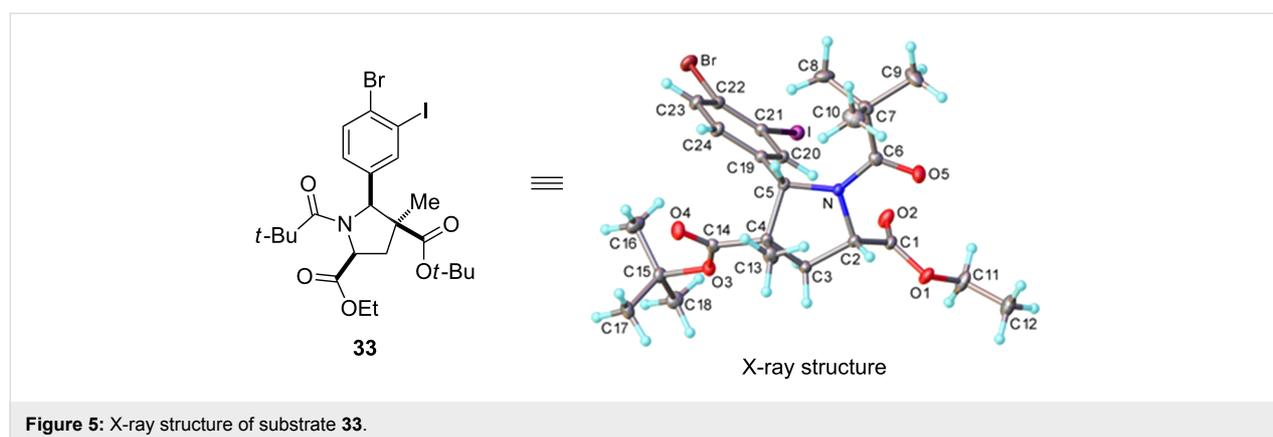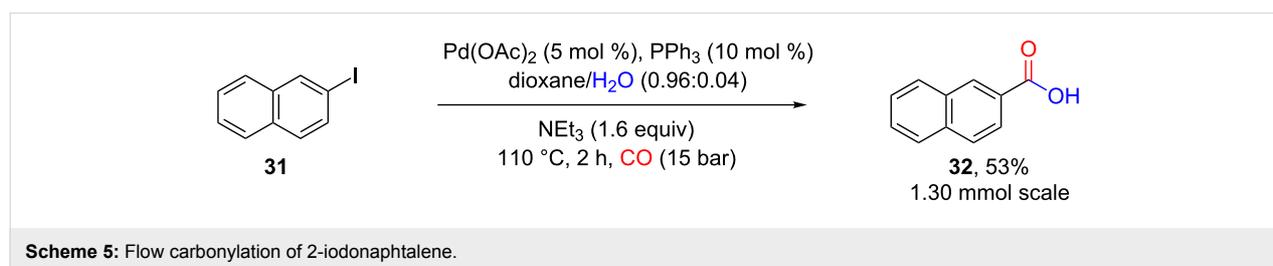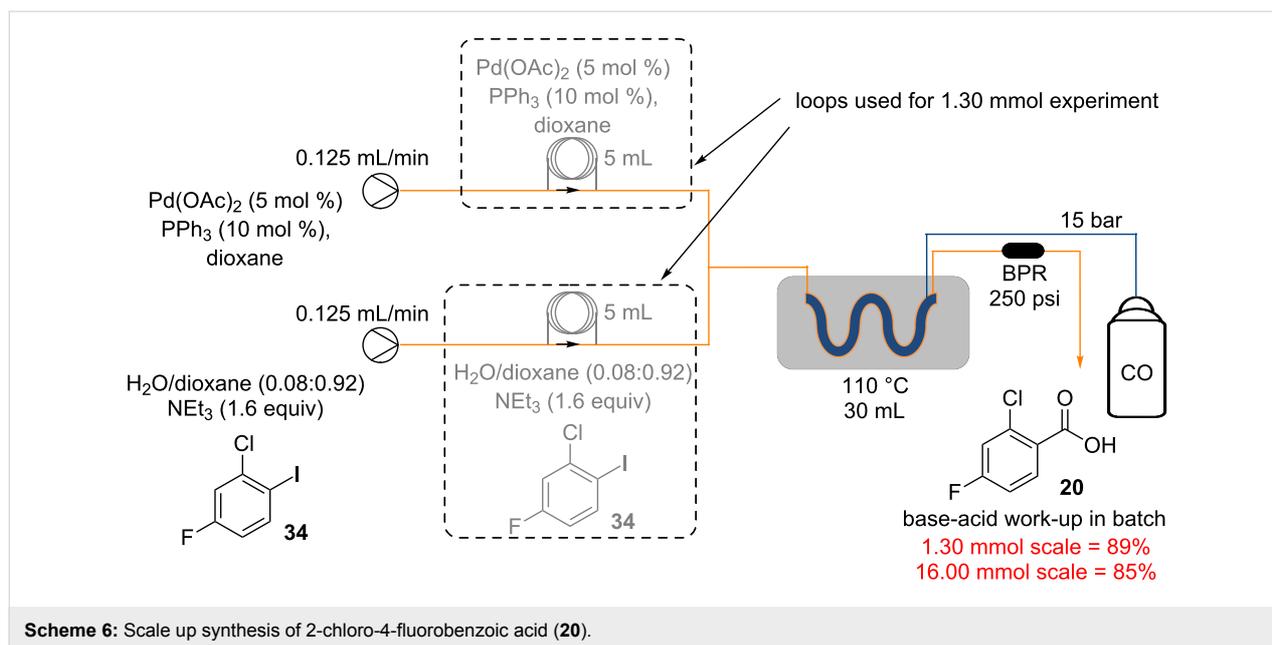
Experimental
See Supporting Information File 1 for full experimental data.

General notes
Warning
Carbon monoxide is highly toxic and extremely flammable gas. All reactions were carried out in well ventilated fume cupboards and carbon monoxide detectors were continuously used thought the process. High pressure lab facilities were used under the supervision of dedicated staff and all associated safety measures were taken. Parr autoclave was pressure tested at 80 bar before use.

Supporting Information

Supporting Information File 1
Experimental part.
[http://www.beilstein-journals.org/bjoc/content/supplementary/1860-5397-12-147-S1.pdf]

Supporting Information File 2
X-ray information data of compound **33**.
[http://www.beilstein-journals.org/bjoc/content/supplementary/1860-5397-12-147-S2.cif]

Acknowledgements

References
1. Miller, P. W.; Long, N. J.; de Mello, A. J.; Vilar, R.; Passchier, J.; Gee, A. *Chem. Commun.* **2006,** 546–548. doi:10.1039/B515710B
2. Rahman, M. T.; Fukuyama, T.; Kamata, N.; Sato, M.; Ryu, I. *Chem. Commun.* **2006,** 2236–2238. doi:10.1039/b600970k
3. Miller, P. W.; Long, N. J.; de Mello, A. J.; Vilar, R.; Audrain, H.; Bender, D.; Passchier, J.; Gee, A. *Angew. Chem., Int. Ed.* **2007,** *46,* 2875–2878. doi:10.1002/anie.200604541
4. Miller, P. W.; Jennings, L. E.; deMello, A. J.; Gee, A. D.; Long, N. J.; Vilar, R. *Adv. Synth. Catal.* **2009,** *351,* 3260–3268. doi:10.1002/adsc.200900563
5. Gong, X.; Miller, P. W.; Gee, A. D.; Long, N. J.; de Mello, A. J.; Vilar, R. *Chem. – Eur. J.* **2012,** *18,* 2768–2772. doi:10.1002/chem.201104059
6. Koos, P.; Gross, U.; Polyzos, A.; O'Brien, M.; Baxendale, I.; Ley, S. V. *Org. Biomol. Chem.* **2011,** *9,* 6903–6908. doi:10.1039/c1ob06017a
7. Mercadante, M. A.; Leadbeater, N. E. *Org. Biomol. Chem.* **2011,** *9,* 6575–6578. doi:10.1039/c1ob05808h
8. Brancour, C.; Fukuyama, T.; Mukai, Y.; Skrydstrup, T.; Ryu, I. *Org. Lett.* **2013,** *15,* 2794–2797. doi:10.1021/ol401092a
9. Fukuyama, T.; Mukai, Y.; Ryu, I. *Beilstein J. Org. Chem.* **2011,** *7,* 1288–1293. doi:10.3762/bjoc.7.149
10. Gross, U.; Koos, P.; O'Brien, M.; Polyzos, A.; Ley, S. V. *Eur. J. Org. Chem.* **2014,** 6418–6430. doi:10.1002/ejoc.201402804
11. Brennführer, A.; Neumann, H.; Beller, M. *Angew. Chem., Int. Ed.* **2009,** *48,* 4114–4133. doi:10.1002/anie.200900013
12. Wu, X.-F.; Neumann, H.; Beller, M. *Chem. Rev.* **2013,** *113,* 1–35. doi:10.1021/cr300100s
13. Brennführer, A.; Neumann, H.; Beller, M. *ChemCatChem* **2009,** *1,* 28–41. doi:10.1002/cctc.200900062
14. Grigg, R.; Mutton, S. P. *Tetrahedron* **2010,** *66,* 5515–5548. doi:10.1016/j.tet.2010.03.090

15. Barnard, C. F. J. *Org. Process Res. Dev.* **2008,** *12,* 566–574.
doi:10.1021/op800069w
16. Daniewski, A. R.; Liu, W.; Püntener, K.; Scalone, M.
Org. Process Res. Dev. **2002,** *6,* 220–224. doi:10.1021/op0102363
17. Ashfield, L.; Barnard, C. F. J. *Org. Process Res. Dev.* **2007,** *11,* 39–43.
doi:10.1021/op060193w
18. Cross, R. J.; Kennedy, A. R.; Muir, K. W.
Acta Crystallogr., Sect. C: Cryst. Struct. Commun. **1995,** *51,* 208–210.
doi:10.1107/S0108270194009042
19. Baumann, M.; Baxendale, I. R. *Beilstein J. Org. Chem.* **2015,** *11,*
1194–1219. doi:10.3762/bjoc.11.134
20. Pinho, V. D.; Gutmann, B.; Miranda, L. S. M.; de Souza, R. O. M. A.;
Kappe, C. O. *J. Org. Chem.* **2014,** *79,* 1555–1562.
doi:10.1021/jo402849z
21. Baxendale, I. R.; Brocken, L.; Mallia, C. J. *Green Process. Synth.*
2013, *2,* 211–230. doi:10.1515/gps-2013-0029
22. McQuade, D. T.; Seeberger, P. H. *J. Org. Chem.* **2013,** *78,* 6384–6389.
doi:10.1021/jo400583m
23. Baxendale, I. R. *J. Chem. Technol. Biotechnol.* **2013,** *88,* 519–552.
doi:10.1002/jctb.4012
24. Pastre, J. C.; Browne, D. L.; O'Brien, M.; Ley, S. V.
Org. Process. Res. Dev. **2013,** *17,* 1183–1191. doi:10.1021/op400152r
25. Wiles, C.; Watts, P. *Green Chem.* **2012,** *14,* 38–54.
doi:10.1039/C1GC16022B
26. Anderson, N. G. *Org. Process Res. Dev.* **2012,** *16,* 852–869.
doi:10.1021/op200347k
27. Wegner, J.; Ceylan, S.; Kirschning, A. *Adv. Synth. Catal.* **2012,** *354,*
17–57. doi:10.1002/adsc.201100584
28. Malet-Sanz, L.; Susanne, F. *J. Med. Chem.* **2012,** *55,* 4062–4098.
doi:10.1021/jm2006029
29. Wegner, J.; Ceylan, S.; Kirschning, A. *Chem. Commun.* **2011,** *47,*
4583–4592. doi:10.1039/c0cc05060a
30. Yue, J.; Chen, G.; Yuan, Q.; Luo, L.; Gonthier, Y. *Chem. Eng. Sci.*
2007, *62,* 2096–2108. doi:10.1016/j.ces.2006.12.057
31. Brzozowski, M.; O'Brien, M.; Ley, S. V.; Polyzos, A. *Acc. Chem. Res.*
2015, *48,* 349–362. doi:10.1021/ar500359m
32. O'Brien, M.; Baxendale, I. R.; Ley, S. V. *Org. Lett.* **2010,** *12,*
1596–1598. doi:10.1021/ol100322t
33. Yang, L.; Jensen, K. F. *Org. Process Res. Dev.* **2013,** *17,* 927–933.
doi:10.1021/op400085a
34. Fukuyama, T.; Totoki, T.; Ryu, I. *Green Chem.* **2014,** *16,* 2042–2050.
doi:10.1039/c3gc41789a
35. Immirzi, A.; Musco, A. *Inorg. Chim. Acta* **1977,** *25,* L41–L42.
doi:10.1016/S0020-1693(00)95635-4
36. Clavier, H.; Nolan, S. P. *Chem. Commun.* **2010,** *46,* 841–861.
doi:10.1039/b922984a
37. van Leeuwen, P. W. N. M.; Kamer, P. C. J.; Reek, J. N. H.; Dierkes, P.
Chem. Rev. **2000,** *100,* 2741–2769. doi:10.1021/cr9902704
38. Kamer, P. C. J.; van Leeuwen, P. W. N. M.; Reek, J. N. H.
Acc. Chem. Res. **2001,** *34,* 895–904. doi:10.1021/ar000060+
39. van der Veen, L. A.; Keeven, P. H.; Schoemaker, G. C.; Reek, J. N. H.;
Kamer, P. C. J.; van Leeuwen, P. W. N. M.; Lutz, M.; Spek, A. L.
Organometallics **2000,** *19,* 872–883. doi:10.1021/om990734o
40. Kaupmees, K.; Trummal, A.; Leito, I. *Croat. Chem. Acta* **2014,** *87,*
385–395. doi:10.5562/cca2472
41. Eliel, E. L.; Wilen, S. H.; Mander, L. N. *Stereochemistry of organic
compounds;* Wiley & Sons: New York, 1994.
42. Baumann, M.; Baxendale, I. R.; Kuratli, C.; Ley, S. V.; Martin, R. E.;
Schneider, J. *ACS Comb. Sci.* **2011,** *13,* 405–413.
doi:10.1021/co2000357

Catalytic Chan–Lam coupling using a 'tube-in-tube' reactor to deliver molecular oxygen as an oxidant

Carl J. Mallia[1], Paul M. Burton[2], Alexander M. R. Smith[2], Gary C. Walter[2] and Ian R. Baxendale[*1]

Abstract

A flow system to perform Chan–Lam coupling reactions of various amines and arylboronic acids has been realised employing molecular oxygen as an oxidant for the re-oxidation of the copper catalyst enabling a catalytic process. A tube-in-tube gas reactor has been used to simplify the delivery of the oxygen accelerating the optimisation phase and allowing easy access to elevated pressures. A small exemplification library of heteroaromatic products has been prepared and the process has been shown to be robust over extended reaction times.

Introduction

The functionalisation of aromatic and aliphatic amines has received considerable attention due to the number of biologically active compounds represented by these classes. For this reason different synthetic methods for C–N bond formation have been developed (Scheme 1) over the years with the general goal to overcome the shortcomings of the original Ullman [1] and Goldberg [2] methods relating to the harsh reaction conditions they employ. After a closer look at the work of Mitiga [3] on the Stille coupling reactions, Hartwig [4] and Buchwald [5] independently proposed a catalytic mechanism and later reported a tin free aryl–amine coupling reaction [6,7]. This major breakthrough made the C–N coupling reaction accessible to a wide range of substrates, including anilines, which did not react very well with the previous conditions. However, despite the improvements achieved with the Buchwald–Hartwig coupling, limitations such as sensitivity to air and moisture, functional group tolerance and the high cost of palladium, reignited the search for an improved method.

In 1998, the groups of Chan [8], Evans [9] and Lam [10] independently reported upon mild methods for C(aryl)–N and C(aryl)–O coupling reactions. Their methods made use of stoichiometric amounts of copper(II) acetate as the catalyst and boronic acids as the aryl donors. In the presence of a base, the

Scheme 1: Comparison of early C–N and C–O coupling reactions.
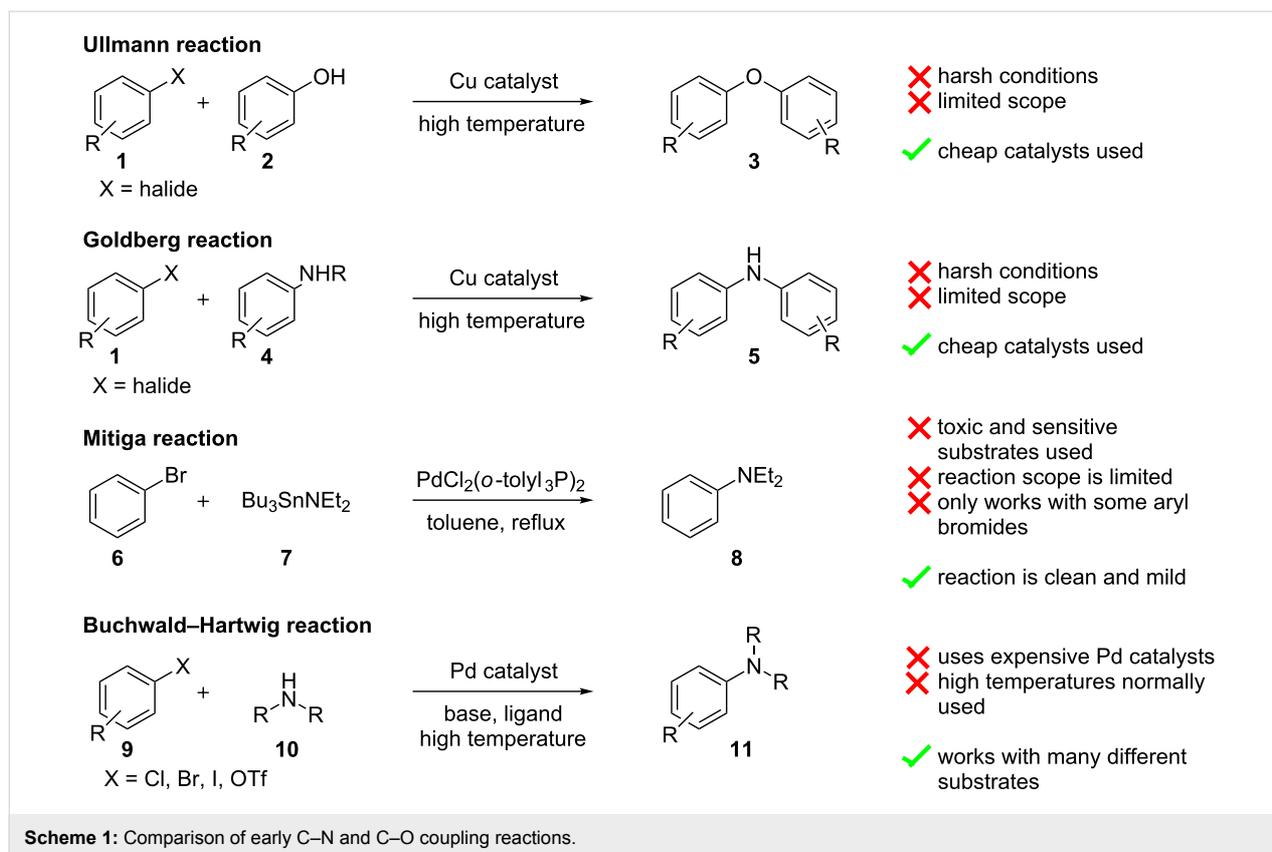
coupling could be performed at room temperature. These reactions were subsequently shown to work with a large number of nucleophiles and tolerated a variety of substrates, making the process one of the most efficient ways for C–N/O coupling [11]. Several modifications of the Chan–Lam reaction have been reported, expanding its scope and it has since been used to synthesise several biologically active compounds [11,12].

In 2009 the groups of Stevens and van der Eycken reported on the Chan–Lam reaction as a continuous flow protocol using copper(II) acetate (1.0 equiv), pyridine (2.0 equiv) and triethylamine (1.0 equiv) in dichloromethane [13]. Generally, when using anilines or phenols as the nucleophilic partner, moderate to good yields were obtained (56–71% yields, 9 examples). More recently the Tranmer group reported the use of a copperfilled column as a catalyst with TEMPO as the co-oxidant in acetonitrile (acetic acid additive) with moderate to good yields of the coupled products being obtained (25–79% yields, 16 examples) [14]. The use of a copper tubing which serves as both the reactor and the catalyst with *tert*-butyl peroxybenzoate as the oxidant in acetonitrile was also described but was outperformed by the copper filled column system. Although the use of elemental copper is potentially an improvement on the use of stiochiometric copper(II) acetate in continuous flow, the use of TEMPO or *tert*-butyl peroxybenzoate as a co-oxidant intro-

duces waste. Employing oxygen gas as an oxidant is preferred as it is cheap, renewable and environmentally benign. We therefore set out to develop a more atom economical way of catalysing the Chan–Lam reaction using a sub-stoichiometric amount of copper and oxygen gas as the oxidant.

The use of oxygen provides the necessary oxidant to reoxidise the Cu(I) that forms after the C–N reductive elimination back to Cu(II), allowing for sub-stoichiometric amounts of copper catalyst to be used [15,16]. Based upon our previous experience of using the reverse "tube-in-tube" reactor with other gases, it was decided that oxygen would be delivered via this reactor set-up (Figure 1).

Results and Discussion
In our initial screening, four different organic solvents with good oxygen absorption were investigated (toluene, dichloromethane, acetonitrile and ethyl acetate), however, Cu(OAc)$_2$ was only completely soluble in dichloromethane. Consequently dichloromethane was used as the reaction solvent. Unfortunately pumping dichloromethane through the HPLC pumps, used as part of the flow system, initially presented some issues. This was mainly due to cavitation which occurred just before the pump inlet, attributed to the shear forces present, causing outgassing (air). These bubbles, if allowed to enter the system
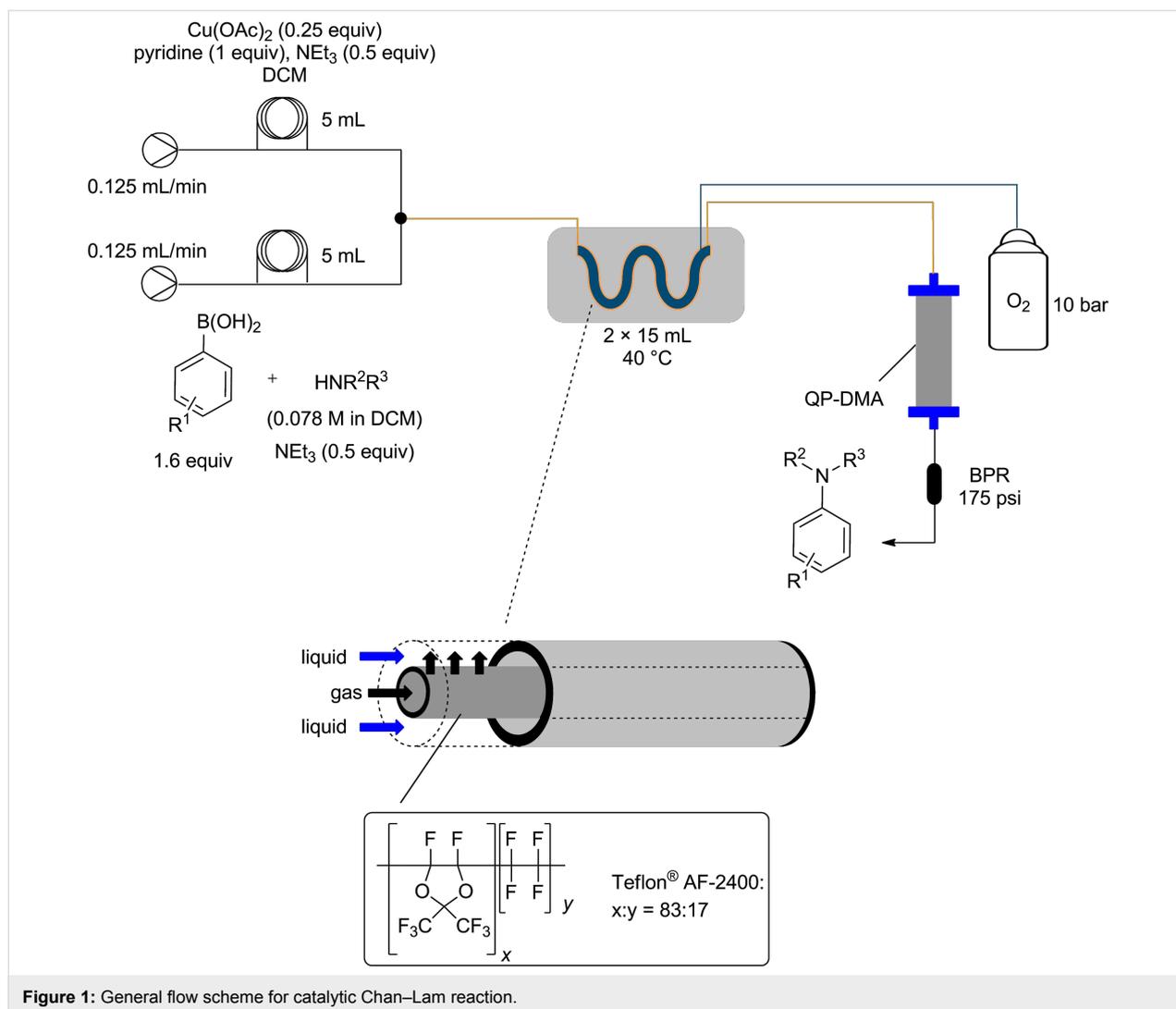
Figure 1: General flow scheme for catalytic Chan–Lam reaction.

disturbed the flow (or impaired the pump), resulting in unstable flow. The problem was solved when the dichloromethane used was sonicated (30 min of sonication per 500 mL of solvent) prior to use, it was then maintained under positive pressure at the inlet throughout the experiment (N_2 balloon was used for the positive pressure).

In an effort to identify the optimum conditions for the reaction process, the amount of copper catalyst and the oxygen pressure were studied (Table 1).

A set of control experiments with no oxygen was run and the amount of copper acetate catalyst was lowered from 1 to 0.25 equiv (entries 1–3, Table 1). As anticipated, with no oxidant to reoxidize the catalyst, the yield of **19** dropped in proportion to the amount of catalyst used. Next, whilst maintaining the amount of copper acetate (0.5 equiv), the effect of the oxygen pressure on conversion was investigated (entries

4–8, Table 1). A general increase in the yield of **19** was obtained on going from atmospheric to 10 bar after which a slight decrease in yield was encountered at higher pressures (Figure 2). This same decrease in yield was also observed when going from 10 bar to 12 bar of oxygen using 0.25 equiv of copper acetate (entries 9 and 10, Table 1).

When the amount of copper acetate was reduced to 0.1 equiv a drastic decrease in yield was observed indicating that the TOF of the catalyst prevented achievement of good yields within the time limits (residence time) of the flow reactor (entry 11, Table 1). A decrease in yield was also observed when the amount of boronic acid used was decreased to 1.4 equiv and 1.1 equiv, respectively (entries 12 and 13, Table 1). Changing the temperature from 20 °C to 50 °C did not greatly affect the yields obtained, with 40 °C giving the most promising result (entries 14–16, Table 1). However, it was observed that less particulate matter was formed in the reactor when higher tem-

Table 1: Optimisation of the Chan–Lam reaction in continuous flow.

Entry	Cu(OAc)$_2$ (equiv)	Boronic acid (equiv)	Temperature (°C)	O$_2$ pressure (bar)	NMR conversion (%)[a]
1	1.00	1.6	20	0	66
2	0.50	1.6	20	0	48
3	0.25	1.6	20	0	25
4	0.50	1.6	20	4	81
5	0.50	1.6	20	8	85
6	0.50	1.6	20	10	97
7	0.50	1.6	20	12	85
8	0.50	1.6	20	14	83
9	0.25	1.6	20	10	94
10	0.25	1.6	20	12	87
11	0.10	1.6	20	10	50
12	0.25	1.4	20	10	56
13	0.25	1.1	20	10	48
14	0.25	1.6	30	10	87
15	0.25	1.6	40	10	95
16	0.25	1.6	50	10	88
17[b]	0.25	1.6	40	10	93
18[c]	0.25	1.6	40	10	76

[a]Yields calculated using 1,3,5-trimethoxybenzene as an internal NMR standard and represents the average of two runs. [b]1.5 equiv of pyridine, [c]0.5 equiv of pyridine.

peratures were used (40 and 50 °C), which helps in avoiding possible reactor blockages. Finally, the amount of pyridine added was also studied. Decreasing the amount of pyridine (0.5 equiv, entry 18, Table 1) resulted in a lower yield (76%) while increasing the amount of pyridine (1.5 equiv, entry 18, Table 1) did not produce any noticeable change in the yield (93%). This indicates that the pyridine plays an important role in this coupling reaction which could be both due to its effect as a ligand and/or its solubility enhancement of the copper acetate.

The amount of triethylamine was not varied as its quantity was required to ensure the boronic acid remained soluble in the dichloromethane solvent.

To determine the time needed to reach steady state in the reactor, samples were periodically collected (every 2 min via an autosampler) and analysed by ^{1}H NMR spectroscopy using 1,3,5-trimethoxybenzene as an internal standard. As expected, the product started eluting after 120 min which corresponds
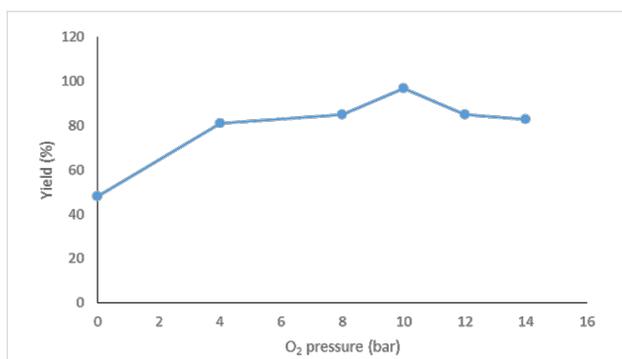
Figure 2: Observed trend for the effect of changing oxygen pressure on the NMR yield of **19**.

with the theoretical residence time. A lower yield was initially obtained for 120 min (85% yield) which then rapidly increased to 98% yield at 125 min. The yield then stabilised from 135 min at 96% indicating steady state was achieved.

As it had been determined that the amount of arylboronic acid excess could not be lowered (entries 12 and 13, Table 1), the use of a polymer supported scavenger was tested in an effort to sequester the excess boronic acid. A column of QP-DMA, a polymer-supported tertiary amine base, was placed in-line after the "tube-in-tube" reactor (Figure 1). It was found that this was sufficient to remove the majority of boronic acid without affecting the yield of the product (Figure 3). Ultimately as the
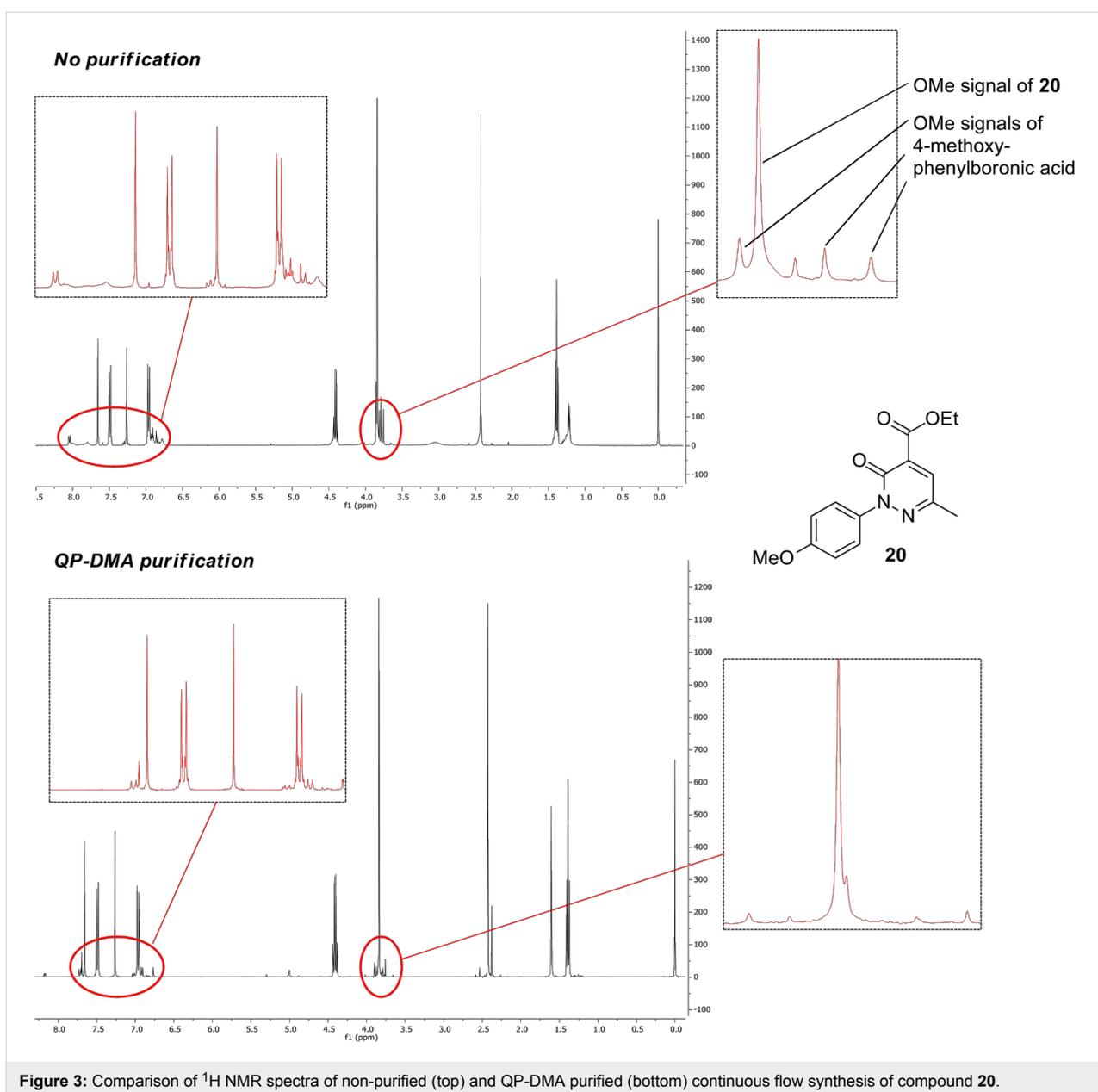
Figure 3: Comparison of ^{1}H NMR spectra of non-purified (top) and QP-DMA purified (bottom) continuous flow synthesis of compound **20**.

products were required for biological screening they were still purified by column chromatography, however, the reduction of the boronic acid excess made the chromatography far easier.

Reaction scoping and library preparation

Using the optimised conditions determined for the synthesis of compound **19**, a small library was prepared to demonstrate the scope of the reaction conditions. Excellent isolated yields were obtained when anilines were used as the nucleophilic partner with both 4-methoxyphenylboronic acid (90% yield of **21**) and phenylboronic acid (92% yield of **22**) as the aryl donors (Scheme 2). Phenylboronic acid also gave a moderate isolated yield when coupled with 3-amino-5-bromopyridine as the nucleophile (50% yield of **23**, Scheme 2) and a good isolated yield with the electron withdrawing 4-chloroaniline (71% yield of **24**, Scheme 2). Using *L*-tyrosine methyl ester as the nucleophile with phenylboronic acid, unfortunately, gave a poor isolat-

ed yield of 26% and also underwent some epimerisation (**25**, 53% ee determined by chiral HPLC, Scheme 2). Additionally, a small amount of the product (**25**) reacted further with phenylboronic acid through the phenol to give **26** in 3% isolated yield. In the case of *L*-leucine methyl ester an isolated yield of 60% was realised, but this substrate also underwent partial epimerisation (**27**, 71% ee determined by chiral HPLC, Scheme 2).

Using *N*-heterocyclic substrates as the nucleophilic partner with a range of different phenylboronic acids generally gave good isolated yields (**19**, **20**, **28–35**, Scheme 2). Using a pyradizine as a nucleophilic partner an 81% yield was obtained for the formation of **20**. However, using 3,4-dimethyl-1*H*-1,2,4-triazol-5(4*H*)-one (**39**), which was synthesised using a literature procedure [17,18] (Scheme 3), with 3,4-dimethoxyphenylboronic acid gave a lower yield of 26% (**28**, Scheme 2). It is not yet clear as to why such a low conversion and isolated yield was

Scheme 2: Scope of the catalytic Chan–Lam reaction in continuous flow.
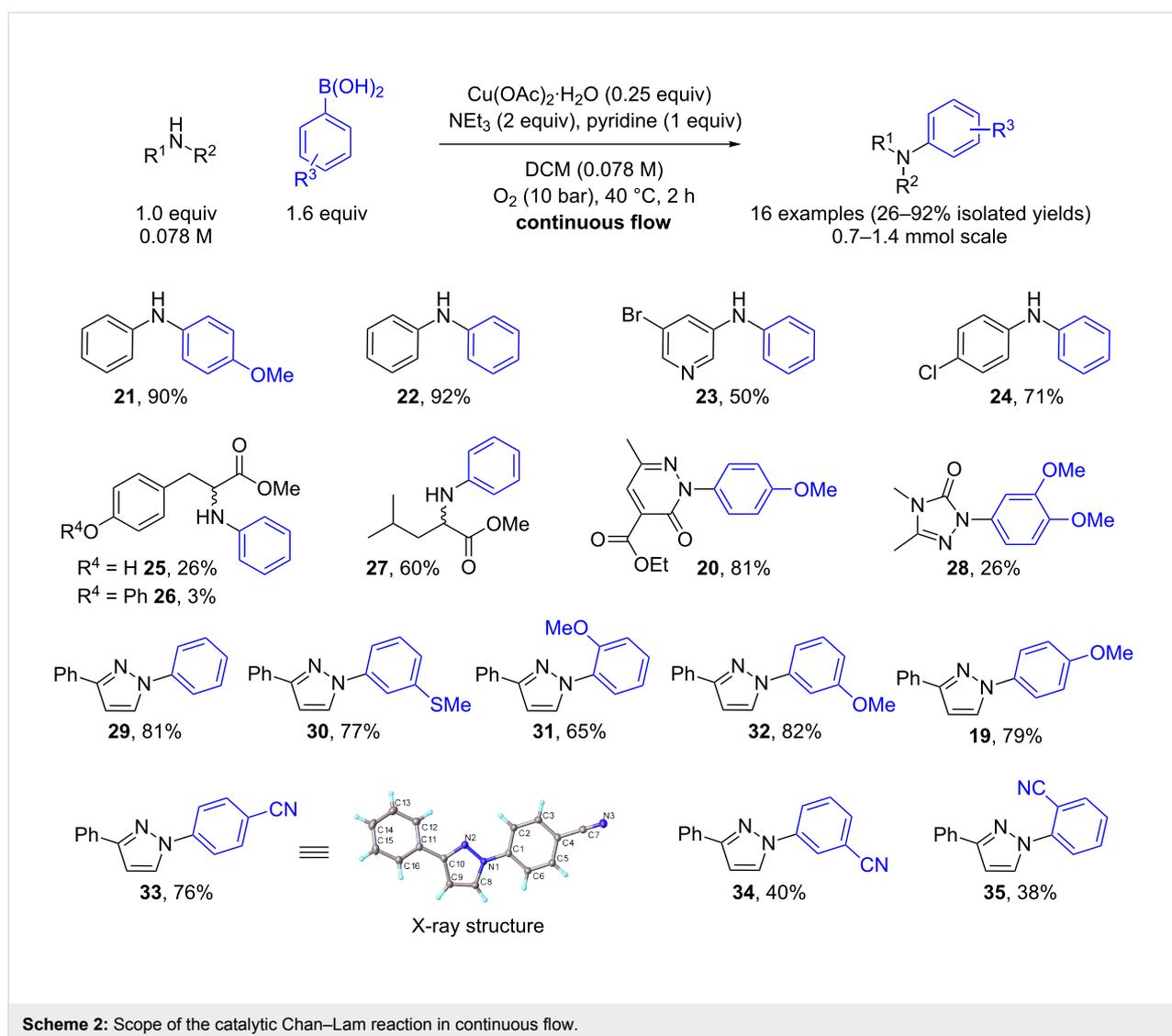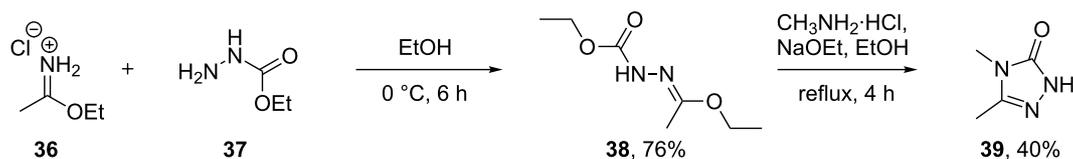
Scheme 3: Syntheses of substrate **39**.

obtained although the reduced nucleophilicity and higher potential for coordination of the triazole to the copper catalyst might inhibit catalyst turnover and account for this.

Alternatively, using 3-phenyl-1*H*-pyrazole (**18**) as the nucleophile with a number of different phenylboronic acids gave moderate to good yields (38–82% yields). In general electron-rich phenylboronic acids (**19**, **29–32**, Scheme 2) gave better yields than electron poor ones (**33–35**, Scheme 2). This is probably due to the more favourable thermodynamics with an increase in the electropositive nature of boron, which in turn increases the rate of the transmetallation step. Changing the group at the 4-position of the phenylboronic acid gave good yields for both electron-rich (**19**, 79% yield) and electron-poor (**33**, 76% yield) phenylboronic acids. On the other hand changing the group at the 3-position of the phenylboronic acid gave good yields for electron-rich (**30** and **32**, 77% and 82% yields, respectively) but only a moderate yield of 40% for electron-poor (**34**) phenyl-

boronic acids. Lower yields were also encountered for both electron-rich (65% yield) and electron-poor (38% yield) 2-substituted phenylboronic acids, most likely due to steric factors (**31** and **35**, Scheme 2).

It is noteworthy that for all of the 3-phenyl-1*H*-pyrazole couplings, only the 1,3-disubsituted pyrazole products were obtained with no 1,5-disubsituted isomers being detected. The regioselectivity of the 1,3-disubstituted pyrazoles was confirmed by NOESY NMR experiments (**30**, **33** and **35**, Figures 4–6) as well as comparison to known published data. In addition, an X-ray crystal structure for compound **33** was obtained and the connectivity confirmed. It was noted that several examples of literature reported cases where mixtures of regioisomers had been obtained were wrongly assigned.

The process described does have certain limitations. For certain nucleophilic substrates no products were obtained when C–N
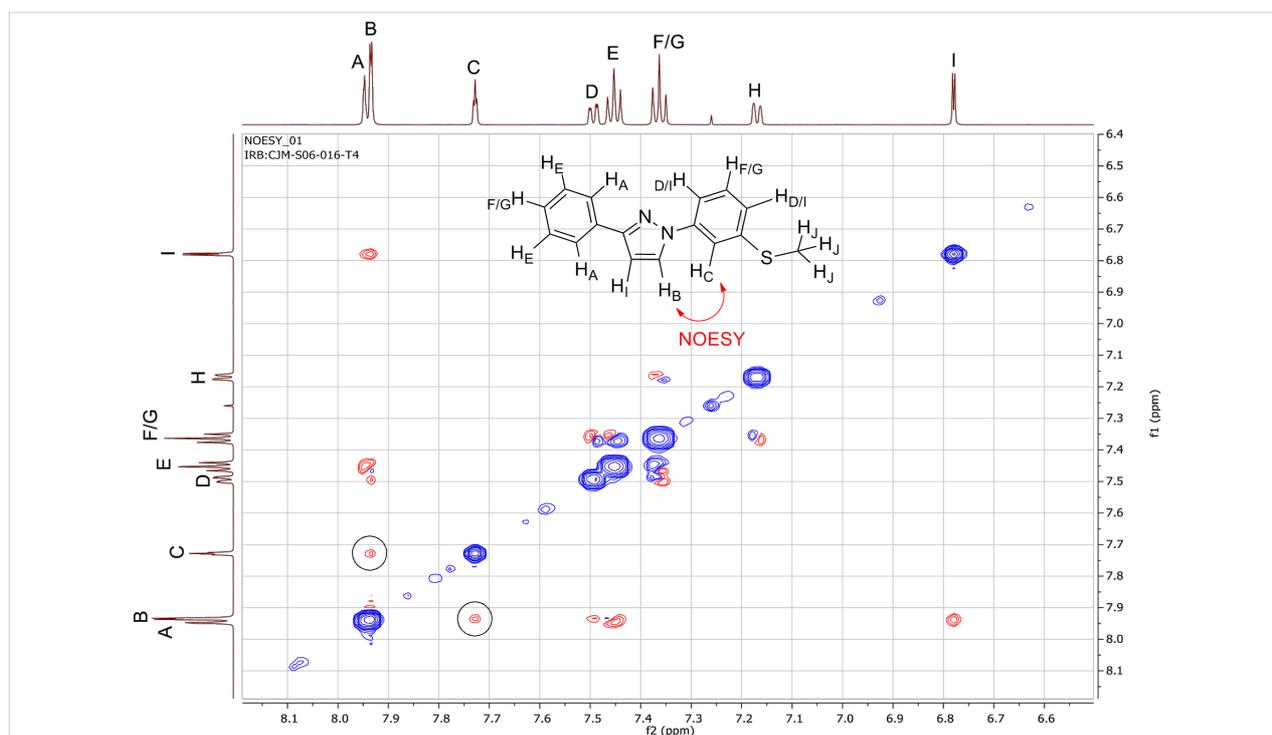
Figure 4: NOESY NMR spectrum for **30** with the characteristic NOESY signal encircled.
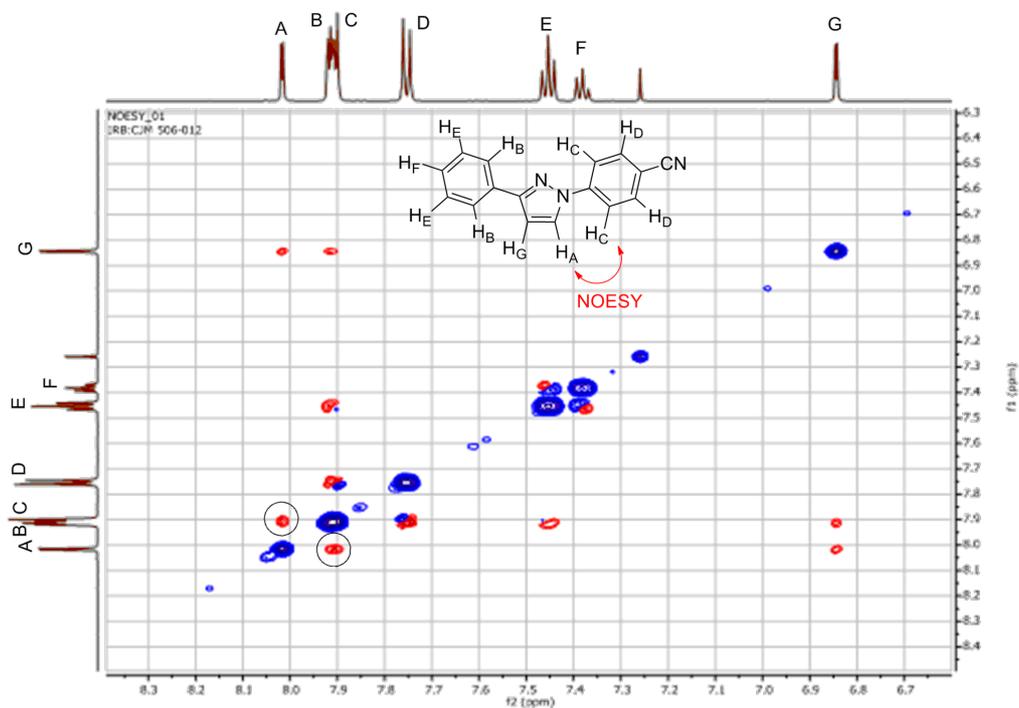
Figure 5: NOESY NMR spectrum for **33** with the characteristic NOESY signal encircled.
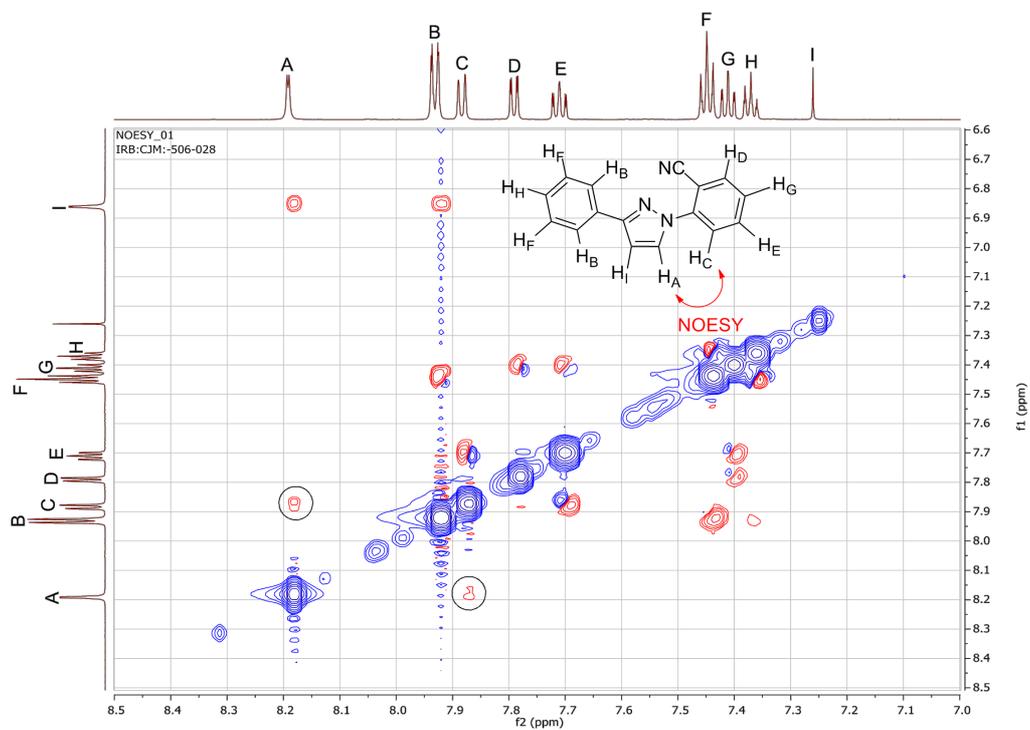
Figure 6: NOESY NMR spectrum for **35** with the characteristic NOESY signal encircled.

coupling with 4-methoxyphenylboronic acid (**17**) was attempted (Figure 7). In the case of substrate **40** precipitation occurred as soon as the two solutions came into contact at the T-piece mixer, which was probably due to strong coordination to the copper acetate by the imidazole ring. This made running this reaction problematic in flow due to the occurrence of reactor blocking. Other substrates proved unreactive. In the case of starting materials **41–43** the reduced nucleophilicity of these substrates might account for the lack of conversion. By comparison, all three substrates (**41–43**) also failed to react under batch conditions using 2 equiv of Cu(OAc)$_2$, 2 equiv of NEt$_3$ and 1 equiv of pyridine at 40 °C for 48 h confirming their low reactivity.

Reaction scaling

Finally, the robustness of the process and potential for scalability of the general reaction conditions was demonstrated by the synthesis of **19** at a 10 mmol scale, a factor of fourteen times the original 0.7 mmol test reaction (Scheme 4). A slightly improved isolated yield (81%) was obtained for the larger scale

experiment when compared to the 79% isolated yield obtained for the shorter run experiment. The consistency of the yields obtained indicates that the process is robust and without modification can reliably deliver 0.216 g h^{-1} of **19** at 81% isolated yield.

Conclusion

The use of flow chemistry for the C–N coupling through a catalytic Chan–Lam reaction has allowed for a safe and efficient introduction of oxygen through a reverse "tube-in-tube" reactor. Optimisation of the reaction conditions allowed for a scalable and efficient way for the continuous synthesis of a number of functionalised aromatic and aliphatic amines including a number of 1,3-disubstituted pyrazoles which were selectively obtained over the regioisomeric 1,5-disubstituted products. When compared to other published protocols it is clear that the use of sub-stoichiometric amounts of the copper catalysts presents an advantage over the stoichiometric amount used in the original flow studies [13]. Additionally, the use of oxygen as the oxidant offers improved atom economy over the use of systems such as TEMPO and *tert*-butyl peroxybenzoate [14]. We believe this
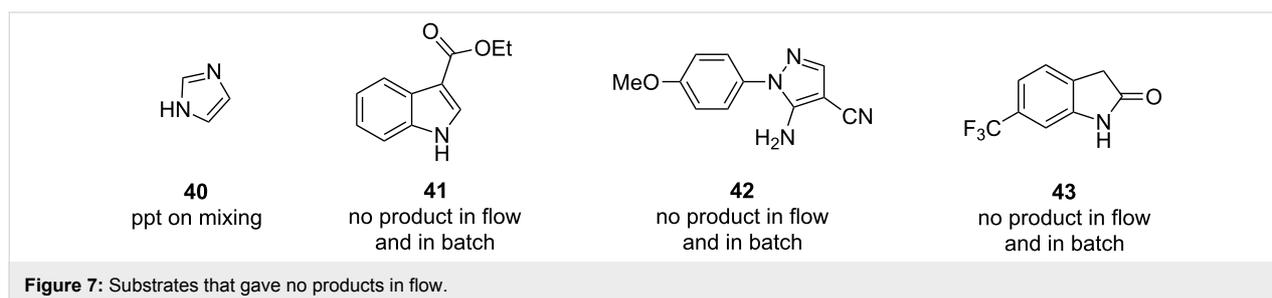
Figure 7: Substrates that gave no products in flow.
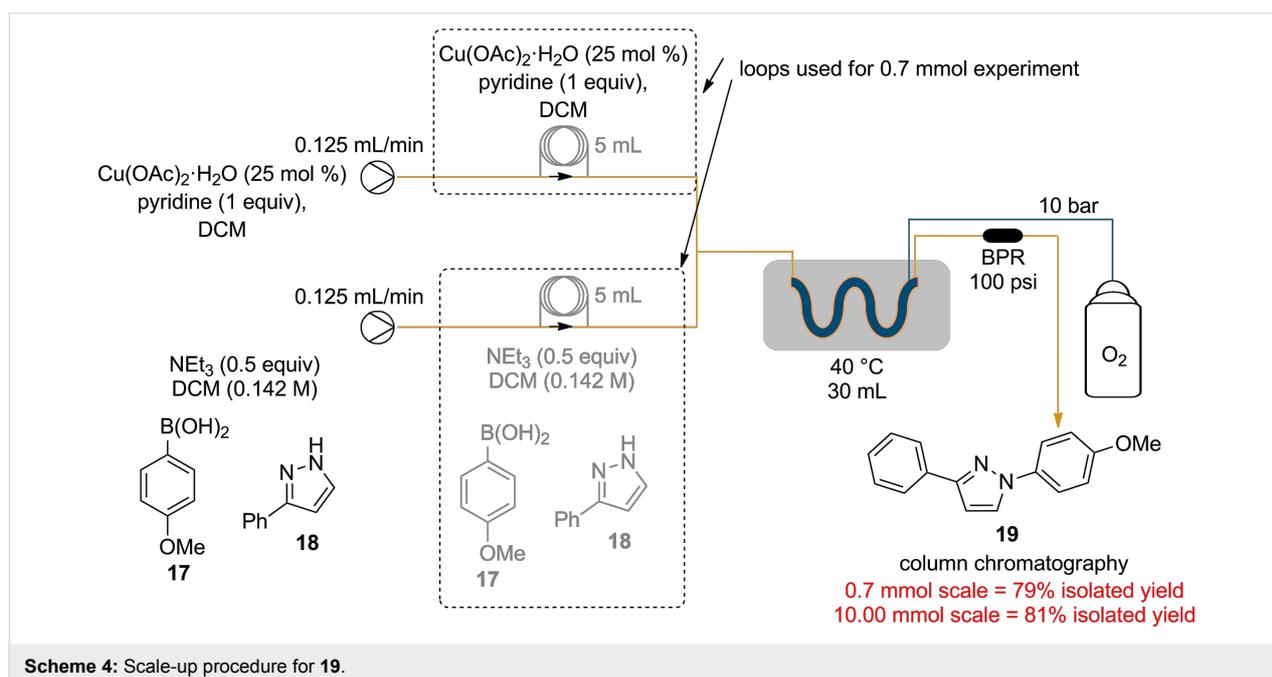
Scheme 4: Scale-up procedure for **19**.

approach therefore present several opportunities for laboratory chemists to utilise this valuable C/N coupling methodology.

Experimental
Warning: Oxygen is a highly flammable gas and all reactions were carried out in well ventilated fume cupboards

For the flow process, 0.781 mmol of the amine was dissolved in 5.5 mL of dichloromethane followed by 1.25 mmol of the boronic acid and NEt_3 (0.039 g, 54 µL, 0.391 mmol). Another solution containing $Cu(OAc)_2·H_2O$ (0.195 mmol, 0.25 equiv), NEt_3 (0.039 g, 54 µL, 0.391 mmol) and pyridine (0.062 g, 63 µL, 0.781 mmol) in 5.5 mL of dichloromethane was also prepared. The two solutions were separately introduced in a 5 mL loop as shown in Table 1. The pumps were each set at 0.125 mL/min to achieve a residence time of 2 h. Two reverse "tube-in-tube" reactors (supplied by Vapourtec) were used in series to achieve a combined reactor volume of 30 mL which were heated at 40 ºC. The reaction mixture was then passed through an Omnifit column (r = 0.33 cm, h = 10.00 cm) filled with QP-DMA followed by a back pressure regulator (175 psi). The crude reaction mixture was then passed through a plug of silica to remove most of the excess copper present and the organic solvent from eluent evaporated under reduced pressure. The resultant crude material was then purified using flash chromatography.

Supporting Information

Supporting Information File 1
Experimental procedures and characterization data for all new compounds.
[http://www.beilstein-journals.org/bjoc/content/supplementary/1860-5397-12-156-S1.pdf]

Acknowledgements

References

1. Ullmann, F.; Sponagel, P. *Ber. Dtsch. Chem. Ges.* **1905,** *38,* 2211–2212. doi:10.1002/cber.190503802176
2. Goldberg, I. *Ber. Dtsch. Chem. Ges.* **1906,** *39,* 1691–1692. doi:10.1002/cber.19060390298
3. Kosugi, M.; Kameyama, M.; Migita, T. *Chem. Lett.* **1983,** *12,* 927–928. doi:10.1246/cl.1983.927
4. Paul, F.; Patt, J.; Hartwig, J. F. *J. Am. Chem. Soc.* **1994,** *116,* 5969–5970. doi:10.1021/ja00092a058
5. Guram, A. S.; Buchwald, S. L. *J. Am. Chem. Soc.* **1994,** *116,* 7901–7902. doi:10.1021/ja00096a059
6. Guram, A. S.; Rennels, R. A.; Buchwald, S. L. *Angew. Chem., Int. Ed. Engl.* **1995,** *34,* 1348–1350. doi:10.1002/anie.199513481
7. Louie, J.; Hartwig, J. F. *Tetrahedron Lett.* **1995,** *36,* 3609–3612. doi:10.1016/0040-4039(95)00605-C
8. Chan, D. M. T.; Monaco, K. L.; Wang, R.-P.; Winters, M. P. *Tetrahedron Lett.* **1998,** *39,* 2933–2936. doi:10.1016/S0040-4039(98)00503-6
9. Evans, D. A.; Katz, J. L.; West, T. R. *Tetrahedron Lett.* **1998,** *39,* 2937–2940. doi:10.1016/S0040-4039(98)00502-4
10. Lam, P. Y. S.; Clark, C. G.; Saubern, S.; Adams, J.; Winters, M. P.; Chan, D. M. T.; Combs, A. *Tetrahedron Lett.* **1998,** *39,* 2941–2944. doi:10.1016/S0040-4039(98)00504-8
11. Rao, K. S.; Wu, T.-S. *Tetrahedron* **2012,** *68,* 7735–7754. doi:10.1016/j.tet.2012.06.015
12. Fischer, C.; Koenig, B. *Beilstein J. Org. Chem.* **2011,** *7,* 59–74. doi:10.3762/bjoc.7.10
13. Singh, B. K.; Stevens, C. V.; Acke, D. R. J.; Parmar, V. S.; Van der Eycken, E. V. *Tetrahedron Lett.* **2009,** *50,* 15–18. doi:10.1016/j.tetlet.2008.09.159
14. Bao, J.; Tranmer, G. K. *Tetrahedron Lett.* **2016,** *57,* 654–657. doi:10.1016/j.tetlet.2015.12.107
15. King, A. E.; Brunold, T. C.; Stahl, S. S. *J. Am. Chem. Soc.* **2009,** *131,* 5044–5045. doi:10.1021/ja9006657
16. King, A. E.; Huffman, L. M.; Casitas, A.; Costas, M.; Ribas, X.; Stahl, S. S. *J. Am. Chem. Soc.* **2010,** *132,* 12068–12073. doi:10.1021/ja1045378
17. Kahveci, B. *Molecules* **2005,** *10,* 376–382. doi:10.3390/10020376
18. Ün, R.; Îkizler, A. *Chim. Acta Turc.* **1975,** *3,* 113–132.

The in situ generation and reactive quench of diazonium compounds in the synthesis of azo compounds in microreactors

Faith M. Akwi and Paul Watts[*]

Abstract

In this paper, a micro-fluidic optimized process for the continuous flow synthesis of azo compounds is presented. The continuous flow synthesis of Sudan II azo dye was used as a model reaction for the study. At found optimal azo coupling reaction temperature and pH an investigation of the optimum flow rates of the reactants for the diazotization and azo coupling reactions in Little Things Factory-MS microreactors was performed. A conversion of 98% was achieved in approximately 2.4 minutes and a small library of azo compounds was thus generated under these reaction conditions from couplers with aminated or hydroxylated aromatic systems. The scaled up synthesis of these compounds in PTFE tubing (i.d. 1.5 mm) was also investigated, where good reaction conversions ranging between 66–91% were attained.

Introduction

Going green, a familiar catch phrase in the chemical industry, in addition to environment protection laws have influenced and also triggered the development of cleaner methods of production. The production of azo compounds is one controversial sector of the fine chemical industry; color is highly desired and used in almost everything, but the waste generated from the production of these compounds is detrimental to the environment and human health.

Following the principles of green chemistry [1,2] such as less hazardous chemical synthesis, efficient atom economy, reduction of waste produced, some alternative cleaner methods for

the synthesis of azo dyes have been developed. These methods are however only representative of particular coupling agents and diazotized amines. Nonetheless they highlight the green benefits that they offer.

For example Noroozi-Pesyan et al. synthesized azo dyes by grinding derivatives of aniline with solid sodium nitrite in the presence of *p*-toluenesulfonic acid [3]. It was found that the yield of isolated azo dyes obtained increased with an increase in electron donor strength of the coupling compound. This method eliminates the use of alkaline and acidic solutions (Scheme 1).

In another method developed by Rahimizadeh et al., ferric hydrogen sulfate was used as a catalyst to synthesize azo compounds from aromatic amines and 2-naphthol. The method boasts of shorter reaction times [4] with high yields (Scheme 2).

Mirjalili et al. also used silica supported boron trifluoride and was able to carry out diazotization at room temperature [5] after they discovered that the diazonium salts obtained were stable at

room temperature even in their dry state. In addition, the method also facilitated short reaction times and provided high yields (Scheme 3).

A number of other methods have been developed for the green synthesis of azo compounds [6-16]. Thus far, the above examples concentrate on modifying the procedure of diazotization and azo coupling (using compounds that impart green benefits to the process or make it environment friendly, i.e., short reaction times thus less energy is required for the process, high yield thus low amount of waste generated, etc). Equally, process equipment can also be changed or modified to achieve the above mentioned green benefits in addition to other advantages.

For example, isolated diazonium salts are known to be hazardous due to their explosive and unstable nature. However, microreactor technology makes it possible to safely perform reactions with unstable intermediates [17] such as these, as well as those that give rise to explosive [18] and hazardous products [19]. The small reagent volumes used in microreactors also
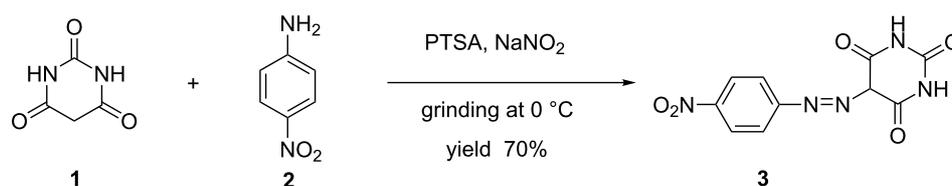
Scheme 1: PTSA-catalyzed diazotization and azo coupling reaction.
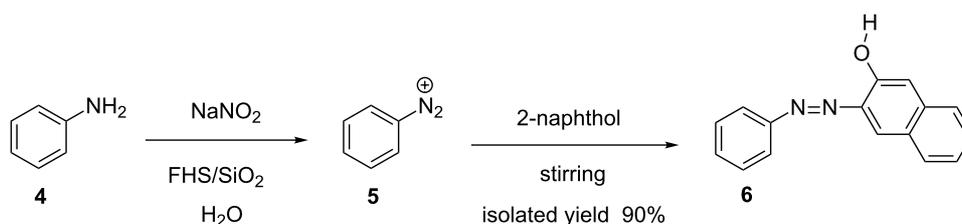
Scheme 2: Ferric hydrogen sulfate (FHS) catalyzed azo compound synthesis.
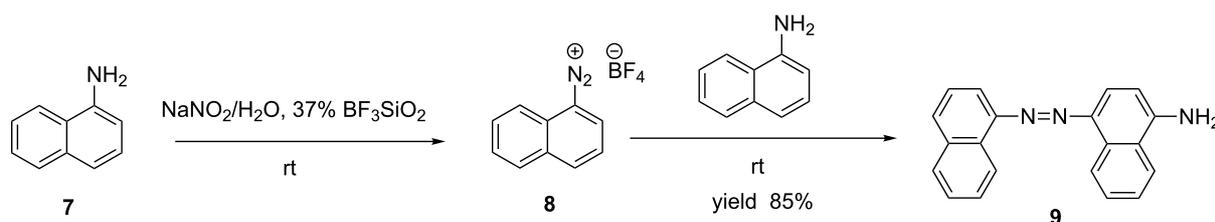
Scheme 3: Synthesis of azo compounds in the presence of silica supported boron trifluoride.

reduce the amount of acidic and alkaline waste associated with the synthesis of azo compounds during research and development.

In the conventional way of performing reactions, the amount of waste generated is dealt with at the end of the reaction. On the contrary, microreactor technology enables the reduction of waste generated by increasing the atom efficiency of reactions and in so doing, the quantity of starting materials is reduced in turn minimizing the amount of waste generated. This aspect of microreactor technology will definitely prove to be quite important in the synthesis of these compounds more so that their production, however important they are, has adverse effects on the environment, mammals [20,21] and aquatic life. Even with a number of dye degradation techniques [22] currently being employed in waste water treatment, a certain percentage of the dyestuffs is still found in water bodies. This therefore is motivation for developing better methods or techniques or processes that can be used independently or in conjunction with the existing techniques. Microreactor technology is one such technology that can be used in the manufacture of these dyes. If used in conjunction with existing azo dye degradation techniques the amount of waste generated can easily be managed.

Hisamoto et al., for example, used 'phase transfer synthesis' in micro-chips for a diazo-coupling reaction [23]. The authors did not however employ a phase transfer catalyst, but rather the principle to increase the reaction selectivity in the diazo coupling of 5-methylresorcinol (**10**) to *p*-nitrobenzene diazonium tetrafloroborate (**11**) in a biphasic laminar flow reaction system. The bi-phasic reaction media consisted of compound **10** dis-

solved in the organic phase, ethyl acetate ($C_4H_8O_2$) and **11** in the aqueous phase (Scheme 4). The large specific interfacial areas and reduced molecular diffusion distances were found to have played a role in avoiding the undesirable side reaction, thus increasing the atom economy in the reaction. This in turn reduces the amount of waste generated after the reaction. A reaction conversion of almost 100% was attained in 2.3 seconds. The same reaction performed at a macro scale and at a strong stirring rate providing a calculated specific interfacial area of 40 cm^2, gave a comparable conversion to that attained at a micro scale (calculated specific interfacial area of 80 cm^2).

In the synthesis of azo dyes and pigments, the cost of production and quality of the product cannot be over looked. Wille et al., in their investigative research involving the synthesis of two azo pigments (yellow and red pigments) in microreactors [24], demonstrated that scaling out in the microreactors provided better and more consistent quality of the pigments as compared to scale up in the batch vessels.

Similarly, yellow pigment 12 (**15**) was also synthesized by Pennemann et al. (Scheme 5) using a micro-mixer apparatus [25]; the group's comparison of the results with the batch synthesis of the said pigment **15** affirmed the notion that mixing is an essential unit operation in the synthesis of azo pigments.

The pigment synthesized in a micro-mixer (25 μm channel width) at a flow rate of 30 mL/min had smaller pigment size distribution compared to the batch synthesized pigment. The fast mixing in the micro-mixer was noted to be responsible for
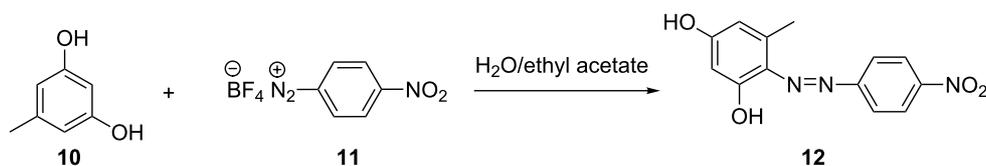
Scheme 4: Phase transfer catalyzed azo coupling of 5-methylresorcinol in microreactors.
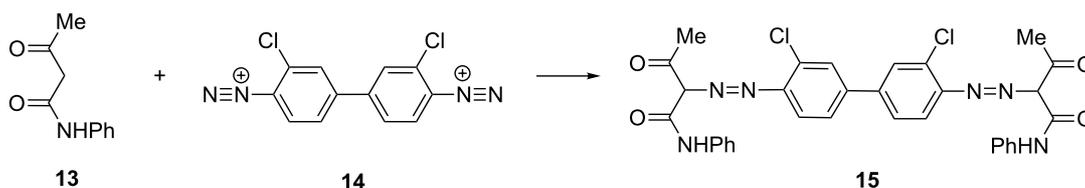
Scheme 5: Synthesis of yellow pigment 12 in a micro-mixer apparatus.

the improvement of glossiness (73%) and tinctorial strength (66%) of the yellow pigment thus yielding a good quality product.

With all the various applications of azo compounds previously mentioned, it is therefore important to develop an optimized process for their synthesis. This was achieved with the use of the microreactor technology. Since the benefits of microreactor technology are well documented in literature [26-30], the ease of reaction parameter optimization in the synthesis of azo compounds in microreactors is highlighted.

In this study, the continuous flow synthesis of Sudan II azo dye (**19**, Scheme 6) constituting of the diazotization of 2,4-dimethylaniline (**16**) and its in situ azo coupling to 2-naphthol (**18**) within LTF-MS microreactors was investigated.

Although various groups have investigated similar reactions in microreactors, to the best of our knowledge, there is no detailed study combining the effect of pH, temperature and flow rate on the azo coupling reaction. In addition, industry always questions why reactions are done in micro structured reactors rather than simple tubular reactors. As such, we extended this investigation to study the optimized conditions obtained within the LTF microreactors within PTFE tubing (i.d. 1.5 mm) in order to scale up the synthesis and to see if the size effect had any major implication on the reaction performance.

Results and Discussion
Azo coupling reaction in the synthesis of 1-((2,4-dimethylphenyl)azo)naphthalen-2-ol in LTF-MS microreactors
In an effort to exemplify the azo coupling of phenols as well as naphthol derivatives in alkaline reaction conditions, the synthesis of 1-((2,4-dimethylphenyl)azo)naphthalen-2-ol (**19**) also commonly known as Sudan II azo dye was used as a model reaction. The synthesis involved diazotization of 2,4-dimethyl-aniline (**16**) to form diazonium salt intermediate **17**, which is coupled with 2-naphthol (**18**) under alkaline conditions (Scheme 6). The experimental set up comprised of two

syringes, two syringe pumps and an LTF-MS microreactor placed into a temperature control bath (as shown in Figure 6 in the experimental section). Following the experimental procedures outlined, a range of reaction conditions were evaluated, where the pH value is that of the stock solution (Table 1).

Table 1: Data showing conversions attained at different reaction conditions.

Run	pH	Flow rate (mL/min)	Temperature (°C)	Conversion (%)
1	5.11	0.6	7	59
2	5.11	0.37	26	62
3	5.11	0.03	25	64
4	5.11	0.13	40	63
5	5.11	0.37	46	57
6	5.11	0.7	26	55
7	5.11	0.6	43	57
8	5.11	0.37	2	54
9	5.11	0.13	8	56
10	5.11	0.37	26	56
11	7.39	0.6	7	70
12	7.39	0.37	26	78
13	7.39	0.13	41	76
14	7.39	0.37	49	73
15	7.39	0.7	25	76
16	7.39	0.6	43	72
17	7.39	0.37	2	74
18	7.39	0.13	8	82
19	7.39	0.37	26	77
20	10.83	0.37	26	72
21	10.83	0.13	40	69
22	10.83	0.37	50	69
23	10.83	0.7	26	73
24	10.83	0.6	43	71
25	10.83	0.37	26	64

A quadratic model was fitted onto the resultant calculated conversions of 2-naphthol as obtained from reversed-phase HPLC analysis output. STATISCA 12 – Statsoft program was thereafter used to validate the model fitted. The findings of this investigation are presented here in the form of simple profile plots.
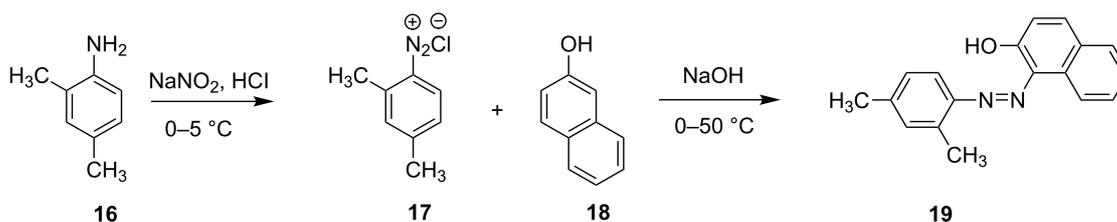
Scheme 6: Continuous flow synthesis of Sudan II azo dye in LTF-MS microreactors.

Effect of reaction temperature, flow rate and pH on the reaction conversion

The pH is of utmost importance in the azo coupling reaction, the second step in the synthesis of azo compounds. This reaction parameter is also dependent on the kind of coupling compound used [31]. For example, phenols are successfully coupled in alkaline conditions in which the phenolate ion is formed. These conditions provide the desired electron-releasing group thus facilitating the electrophilic substitution reaction to afford the azo compound. However, highly alkaline conditions are usually avoided as they lead to diazonium salt decomposition.

In the regression summary of the statistical data analysis (Table 2) of the observed data, it is seen from the *p*-values (0.067 and 0.084) associated with the estimated coefficients (b) of flow rate and temperature respectively, that these two reaction parameters seem not to have a significant effect on the reaction conversion in the experimental domain employed for this investigation. In contrast, pH is shown to be of importance in this reaction considering that the *p*-value associated with its estimated coefficient (b) is less than 0.005. Furthermore, evidence of a quadratic relationship between pH and reaction conversion was also seen (pH^2, $p < 0.005$). Similarly, there was also a slight indication of a quadratic relationship between temperature and the response (Temperature^2, $p = 0.076$). There were no interactions observed between the reaction parameters investigated.

In the plot (Figure 1), it is seen that at a flow rate of 0.03 mL/min, the pH has a non-linear relationship with the predicted conversion of the coupler. In addition, the predicted conversion increases with an increase in reaction pH in this experimental domain. The optimum pH that would provide the best conversion was predicted to be approximately 8.5 and the

Table 2: Statistical multiple regression analysis output.

			Regression summary for dependent variable: conversion %			
N = 25	b*	Std. Err. (of b*)	b	Std. Err. (of b)	t(19)	*p*-value
Intercept			−42.4512	10.97819	−3.86687	0.001038
pH	7.54901	0.772030	27.9443	2.85784	9.77812	0.000000
Flow rate	−0.15896	0.081676	-6.5854	3.38369	−1.94621	0.066572
Temperature	0.57407	0.315099	0.3187	0.17495	1.82187	0.084257
pH^2	−7.02309	0.774875	−1.6268	0.17949	−9.06351	0.000000
Temperature^2	−0.58488	0.311906	−0.0061	0.00325	−1.87518	0.076223

Figure 1: pH profile plot at constant flow rate of 0.03 mL/min.
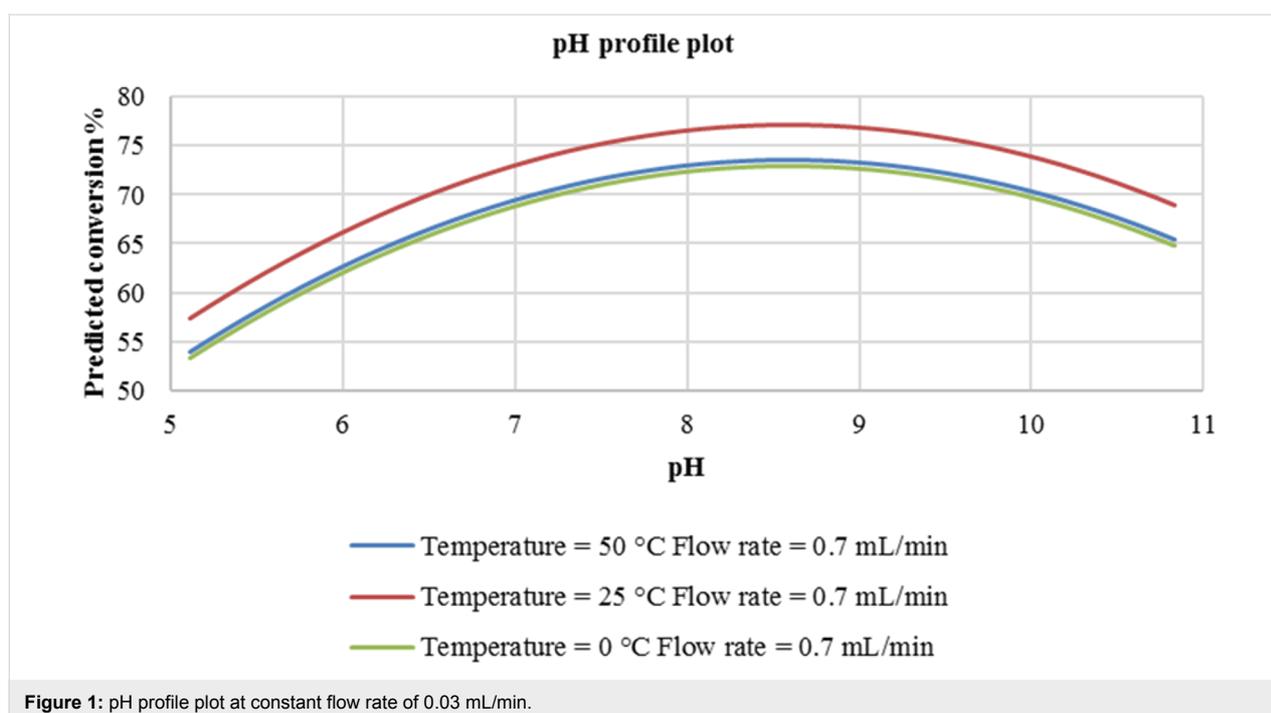
most suitable reaction temperature was found to be 25 °C. Therefore, at a pH of about 8.5 and a reaction temperature of 25 °C, a reaction conversion of approximately 80% should be attained. As expected, at highly alkaline conditions (pH 9–11), the reaction conversion is predicted to gradually decrease. It is also seen that at 0 °C and 50 °C, slightly lower conversion is predicted (approximately 74%–75%). This could be attributed to decomposition of the reaction intermediate at higher temperatures (50 °C) and lowered rate of reaction at lower temperatures (0 °C).

At a higher flow rate of 0.7 mL/min (Figure 2), a similar trend is observed with regard to the effect of pH on the reaction conversion. Similarly, a reaction temperature of 25 °C was predicted to provide optimum conversion (75%). At this reaction temperature (25 °C), the predicted reaction conversion at this flow rate, is slightly lower (75%) compared to that predicted at a flow rate of 0.03 mL/min (80%). It was then concluded that the flow rate of the reactants in this experimental domain had no significant effect on the reaction response. For information, this flow rate range covers a residence time of 0.37 to 0.86 minutes.

Azo coupling reaction in the synthesis of 4-(2-(4-nitrophenyl)diazenyl)-*N*-phenyl-benzenamine in LTF-MS microreactors

The synthesis of azo compounds involving couplers containing aminated aromatic systems is usually carried out in slightly acidic reaction conditions. The synthesis of 4-(2-(4-nitrophenyl)diazenyl)-*N*-phenylbenzenamine was an interesting choice for demonstrating the synthesis of azo compounds involving couplers containing aminated aromatic systems.

It involves the diazotization of *p*-nitroaniline **2** to form **20** which is subsequently coupled to **21**. Diphenylamine (**21**), the coupler used in this reaction is sparingly soluble in aqueous media thus rendering it quite difficult to use in this synthesis and as such, methanol was used as the azo coupling reaction media (Scheme 7). It is due to this that the pH of the diazonium compound solution was buffered to the preferred values for the reaction investigation as opposed to the conventional buffering of the coupler solution. Following the experimental procedures, a range of reaction conditions were evaluated (Table 3).

A Logit model was then fitted onto the resultant calculated conversions of diphenylamine as obtained from reversed phase HPLC analysis output. STATISCA 12 – Statsoft program was thereafter used to validate the model fitted (see Supporting Information File 1). The result of this investigation is also presented here in form of simple profile plots.

Effect of reaction pH, temperature and flow rate on the reaction conversion

Azo coupling reactions involving aromatic amines as coupling agents are carried out in mildly acidic conditions such that a water-soluble protonated version of the aromatic amine, which

Figure 2: pH profile plot at a constant flow rate of 0.7 mL/min.
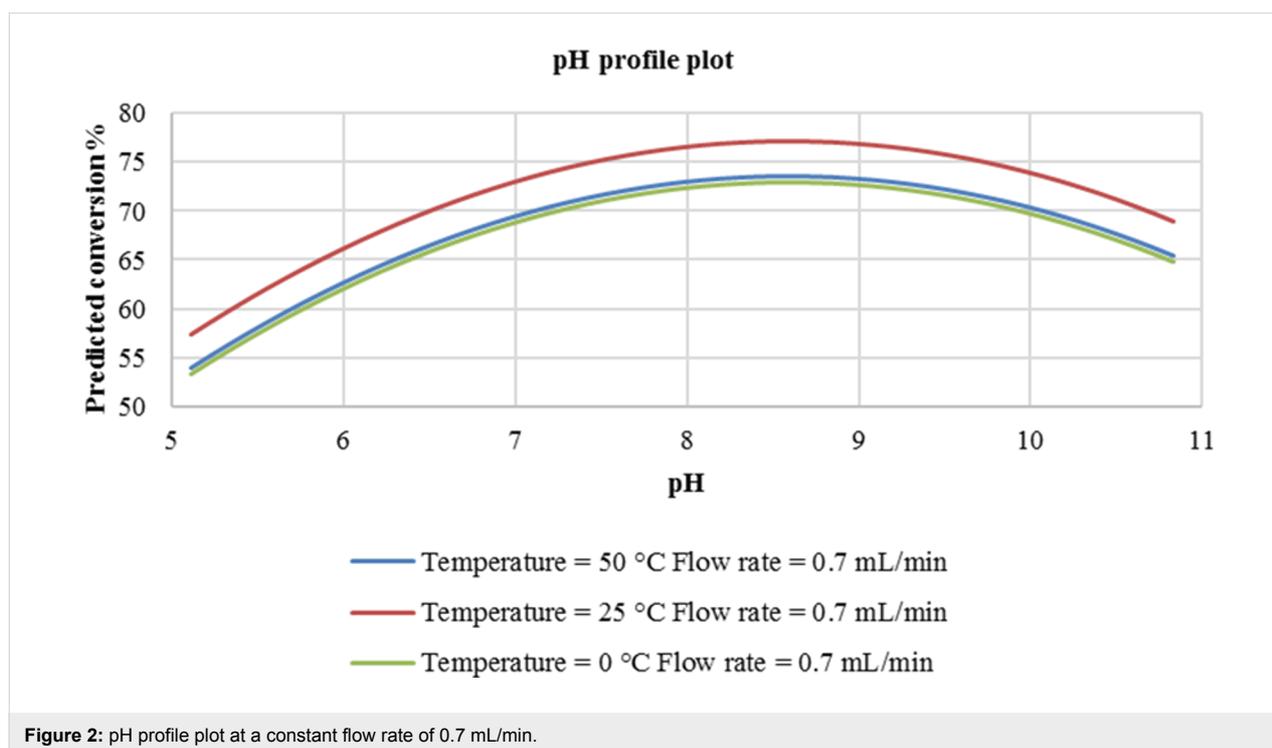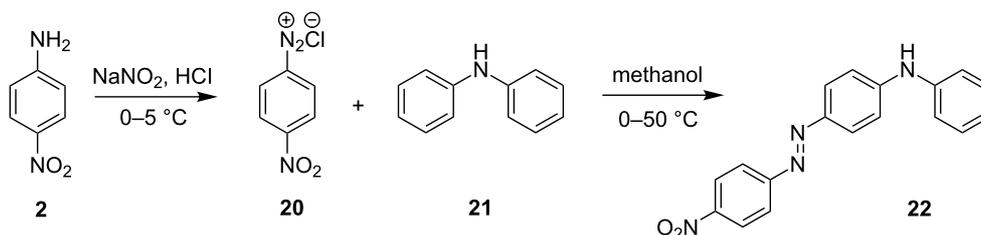
Scheme 7: Azo coupling reaction under acidic conditions.

Table 3: Data showing the conversion attained at various reaction conditions.

Run	pH	Flow rate (mL/min)	Temperature (°C)	Conversion (%)
1	3.5	0.6	6	84
2	3.5	0.37	26	89
3	3.5	0.13	41	85
4	3.5	0.37	47	83
5	3.5	0.7	26	78
6	3.5	0.6	41	83
7	3.5	0.37	3	84
8	3.5	0.13	7	83
9	3.5	0.37	26	83
10	5.66	0.6	8	92
11	5.66	0.37	26	93
12	5.66	0.13	43	91
13	5.66	0.37	50	90
14	5.66	0.7	25	96
15	5.66	0.6	42	86
16	5.66	0.37	2	97
17	5.66	0.13	7	96
18	5.66	0.37	26	99
19	6.94	0.6	7	81
20	6.94	0.37	25	74
21	6.94	0.13	8	86
22	6.94	0.7	43	70
23	6.94	0.13	2	86
24	6.94	0.37	26	56
25	6.94	0.37	7	58
26	6.94	0.6	50	64
27	6.94	0.37	43	86

is more reactive than its unprotonated version is availed; it is also obvious that the protonation also renders the aromatic ring less nucleophilic.

In this reaction, like the one previously discussed, pH plays an important role and significantly affects the reaction conversion ($p < 0.005$) moreover (Table 4), it also has a non-linear effect on this response (pH^2, $p < 0.005$). Conversely, within this experimental domain, there is evidence (Flow rate, $p = 0.116$) that shows that the flow rate of the reactants has a negligible effect on the reaction conversion. Looking at the *p*-value associated with the estimated coefficient (b) of the reaction temperature (temperature, $p = 0.012$), there is a slight indication of its significance on the reaction conversion.

It is also demonstrated in Figure 3 that the effect of pH on the azo coupling reaction is quite conspicuous. It is seen that the reaction flourishes at a mildly acidic pH that being between 5.5 and 6.0 while temperature is predicted not to have a tremendous effect on the reaction conversion (Figure 3). A variation in reaction temperature between 0 °C and 50 °C provides a very slight improvement in conversion (from 82% to 95%).

The flow rate of the reactants (diazotized primary amine and coupler) was also investigated as mentioned earlier on. As is shown in Figure 4, based on the predicted conversion, there is no difference in carrying out the reaction at either 0.03 mL/min or 0.7 mL/min.

Moving on to the reaction temperature, unlike pH, it has a more or less linear relationship with predicted reaction conversion. There is a slight drop in the predicted conversion as the reaction temperature is increased from 0 °C to 50 °C. This is clearly shown in Figure 5 below.

An increase in the flow rate from 0.03–0.7 mL/min at a constant pH of 5.66 causes a 2% drop in predicted conversion whereas an increase in the reaction temperature from 0–50 °C at flow rates of 0.03, 0.33 and 0.7 mL/min at constant pH 5.66 is shown to lead to a less than 5% drop in the predicted conversion. It was thereafter concluded that in this experimental domain, the reaction temperature had no significant effect on the reaction conversion. For both reactions investigated thus far, it was found that the flow rate of the reactants in the chosen experimental domain had little or no significant effect on the reaction conversion.

Table 4: Statistical multiple regression analysis output.

N = 24	b*	Std. Err. (of b*)	b	Std. Err. (of b)	t(19)	*p*-value
			Regression summary for dependent variable: logit			
Intercept			8.14853	1.409724	5.78023	0.000014
pH	−9.27407	1.208038	−4.48258	0.583899	−7.67697	0.000000
Temperature	0.29741	0.107162	0.01204	0.004340	2.77534	0.012053
Flow rate	0.17639	0.107167	0.61041	0.370851	1.64596	0.116214
pH^2	9.30475	1.208036	0.43744	0.056793	7.70238	0.000000
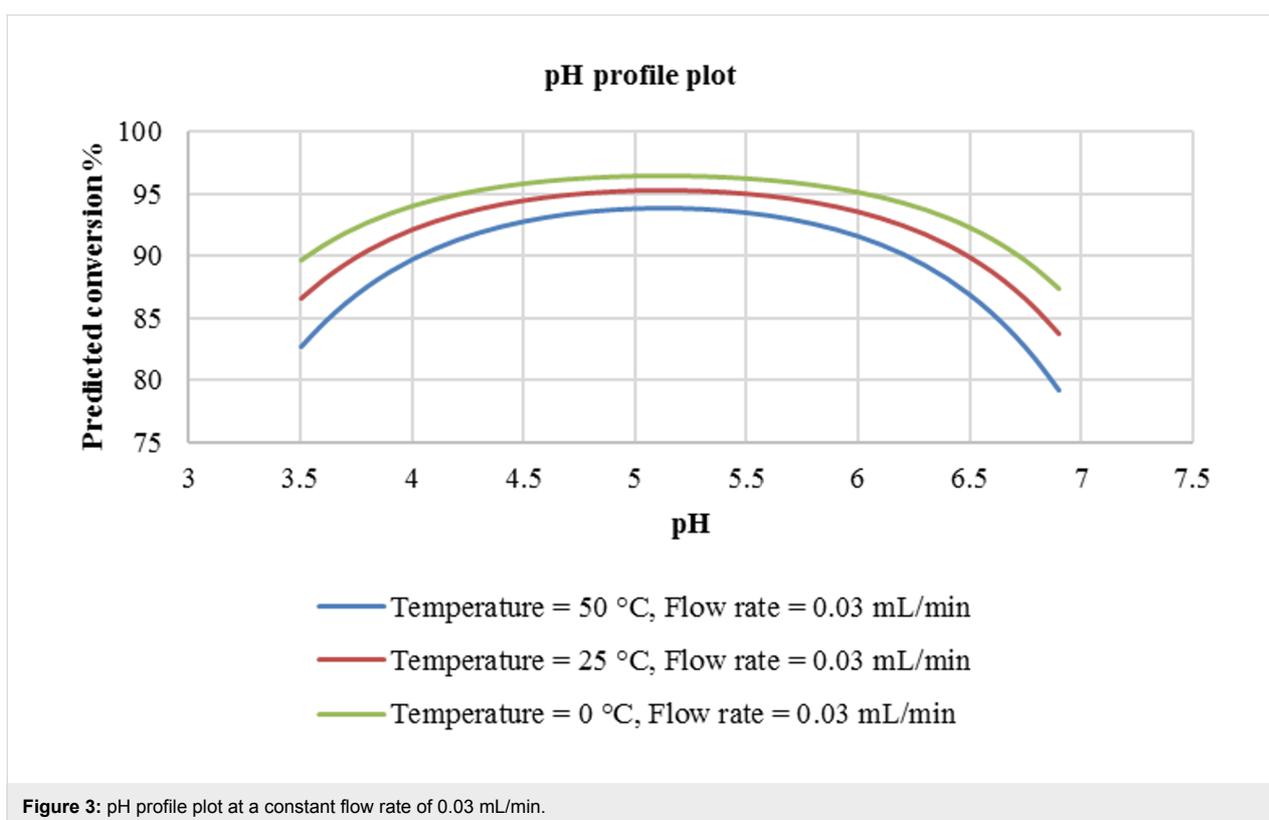
Figure 3: pH profile plot at a constant flow rate of 0.03 mL/min.

The effect of reaction parameters i.e. flow rate, temperature and pH on azo coupling reactions in the synthesis of azo compounds under acidic and alkaline reaction conditions in LTF-MS microreactors however, was successfully demonstrated. We therefore went ahead to fully make good use of the benefits that microreactor technology offers to organic syntheses such as this one by performing both reaction steps in continuous flow reactors.

Continuous flow synthesis of Sudan II azo dye in LTF-MS microreactors

Having determined the reaction parameters that affect the azo coupling reaction in the synthesis of Sudan II azo dye, an attempt to perform both reaction steps involved in this synthesis in continuous flow reactors was thus made. This was achieved in LTF-MS reactors with the aid of statistical modeling where the continuous flow synthesis of Sudan II azo dye was optimized and used a model reaction.

Based on the statistical experimental central composite design used for the optimization of this synthesis, no descriptive trends showing the effect of the flow rates of reactants on the conversion of 2-naphthol could be obtained. At all varied reaction parameters in the 20 experiments carried out, the response was relatively the same with no clear cut trends observed as is shown in Table 5. A quadratic regression model was then fitted

Figure 4: pH profile plot at constant flow rate of 0.7 mL/min.

Figure 5: Temperature profile plot at constant pH 5.66.
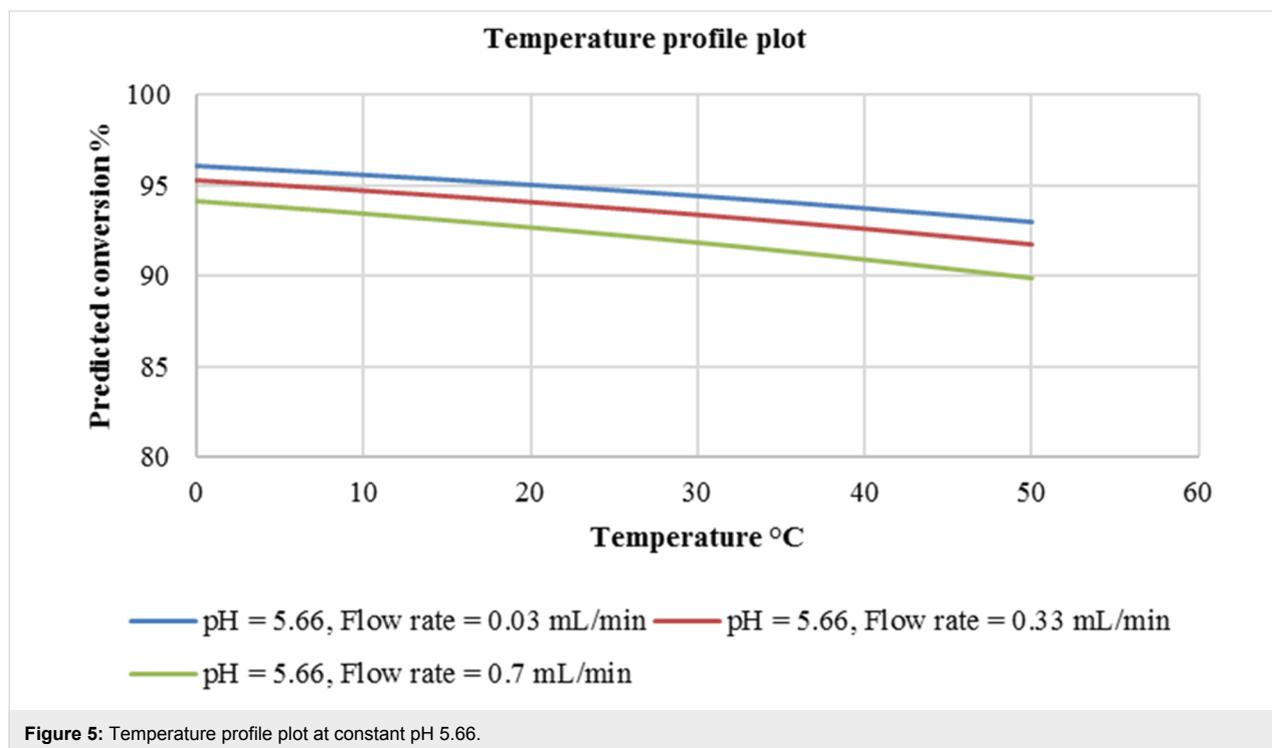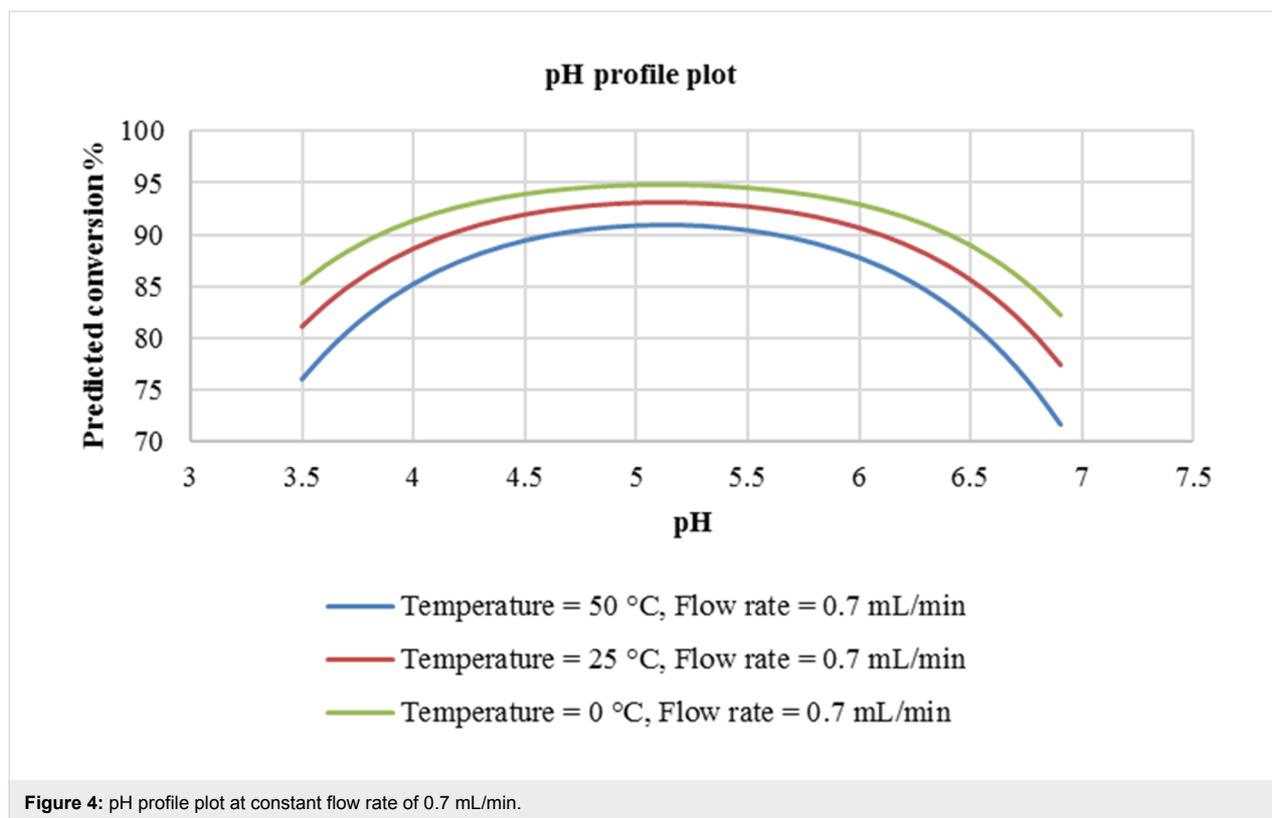
onto the observed data and no outliers were found during this model fitting procedure in addition, there were also no indications of either synergistic or antagonist interactions between the independent variables (see Supporting Information File 1). On further statistical analysis of this data, it was found that there is some evidence that supports the notion that the flow rate of the

Table 5: Data showing conversions attained at various reaction conditions.

Run	Amine + HCl (mL/min)[a]	Sodium nitrite (mL/min)[b]	Coupler (mL/min)[c]	Conversion (%)
1	0.20	0.01	0.07	98
2	0.09	0.03	0.07	97
3	0.30	0.03	0.07	97
4	0.26	0.02	0.03	99
5[d]	0.20	0.03	0.07	98
6	0.26	0.04	0.03	99
7	0.13	0.02	0.10	93
8	0.26	0.04	0.10	98
9[d]	0.20	0.03	0.07	98
10	0.13	0.04	0.10	96
11	0.20	0.05	0.07	96
12	0.20	0.03	0.12	95
13	0.20	0.03	0.01	96
14[d]	0.20	0.03	0.07	95
15	0.13	0.04	0.03	96
16[d]	0.20	0.03	0.07	95
17[d]	0.20	0.03	0.07	95
18	0.13	0.02	0.03	98
19[d]	0.20	0.03	0.07	98
20	0.26	0.02	0.10	97

[a]Amine-flow rate of HCl + amine (2,4-dimethylaniline) solution, [b]nitrite-flow rate of sodium nitrite solution, [c]coupler-flow rate of coupler (2-naphthol) solution. [d]center point.

(amine + HCl) solution in this particular experimental domain has the most effect on the conversion (Partial correlation: 0.406, $p = 0.094$). The R-square value corresponding to the three variables investigated was also found to be nil which indicated that there was no correlation between the variables investigated.

The reaction conditions at the center point (run with letter 'd' in the Table 5 above) of the central composite design used for the optimization were therefore used to generate a small library of compounds. Before embarking on this task, a confirmatory experiment to ascertain the reproducibility of the reaction output at these reaction conditions was performed and indeed a similar result was obtained (Table 6).

Table 6: Confirmatory experiment for the chosen reaction parameters for the synthesis.

Run	Amine + HCl (mL/min)[a]	Sodium nitrite (mL/min)[b]	Coupler (mL/min)[c]	Conversion (%)
1	0.2	0.03	0.07	98
2	0.2	0.03	0.07	98

[a]Amine-flow rate of HCl + amine (2,4-dimethylaniline) solution, [b]nitrite-flow rate of sodium nitrite solution, [c]coupler-flow rate of coupler (2-naphthol) solution.

The continuous flow synthesis of 2-naphtholic, phenolic and similar azo compounds in LTF-MS microreactors

At the reactant flow rates stated in the confirmatory experiment in Table 6, similar azo compounds were synthesized. To our delight, the reaction conditions were robust since comparable high conversions were also attained for the synthesis of similar azo compounds regardless of the substituent groups present on the coupler as well as diazotizable amine. This is shown in Table 7.

The continuous flow scaled-up synthesis of 2-naphtholic, phenolic and similar azo compounds in LTF-MS microreactors

In the synthesis of azo compounds, there is usually formation of a precipitate, which renders this reaction problematic in microreactors due to blockages. The geometrical specifications of the microchannel are very important, so much that these dictate the concentration of the reagents used for the reaction, amount of solvent added to facilitate quick dissolution of particulates as they are formed as well as the output of the reaction, i.e., conversion, yield and or even selectivity. The scaled-up synthesis of these compounds in PTFE tubing of 1.5 mm internal diameter is herein reported. The experimental set up of the scaled-up synthesis is shown in the experimental section (Figure 8). A comparison of the two microreactor systems, i.e., LTF-MS and the PTFE tubing microreactor systems is presented in Table 8. The reactions were conducted at appropriate flow rates so as to maintain the same residence time used in the LTF-MS microreactors.

It was found that the synthesis of these compounds in a simple set up comprising of PTFE tubing (i.d. 1.5 mm) provided comparable conversions to those attained in the LTF-MS microreactors despite the geometrical specifications of the two reactor systems being quite different. It should also be noted that the PTFE tubing is much cheaper than the glass LTF-MS and at the internal diameter of the PTFE tubing used there were no occurrences of blockages witnessed due to precipitate formation. This is particularly important since the amount of solvent used in the reactions can be kept at a bare minimum. Despite the fact that the geometrical specifications of the two reactor systems (LTF-MS microreactors and PTFE tubing) were quite different, the drop in conversion is not massive and can be circumvented by increasing the residence time in order to achieve even better conversions.

Conclusion

From our proof of concept investigation, the desired temperature and pH in the azo coupling of hydroxylated or aminated couplers in the synthesis of azo compounds was determined. It

Table 7: Azo compounds synthesized under alkaline and acidic azo coupling conditions.

Run	Diazotizable amine	Coupler	Product	Conversion
1				97%
2				88%
3				95%
4				80%
5				92%
6				80%
7				88%
8				84%
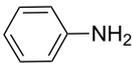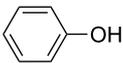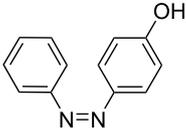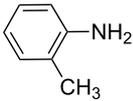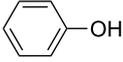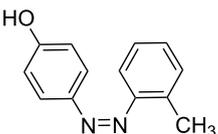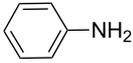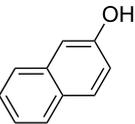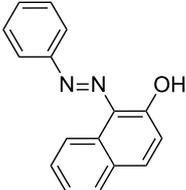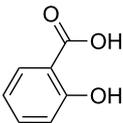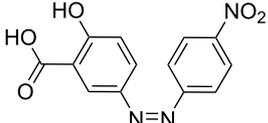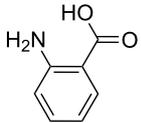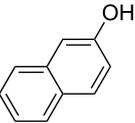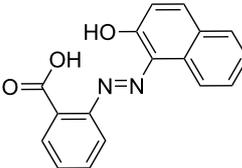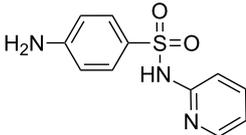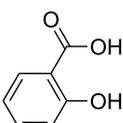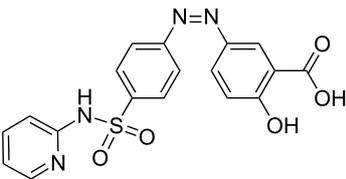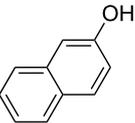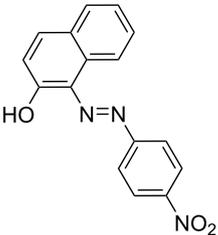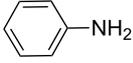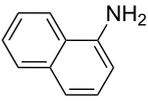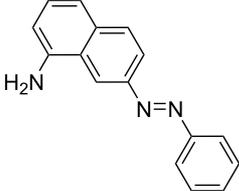
Table 7: Azo compounds synthesized under alkaline and acidic azo coupling conditions. (continued)
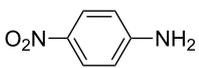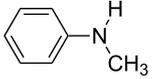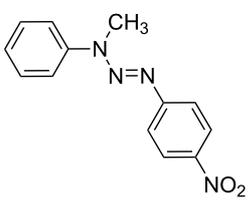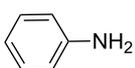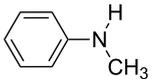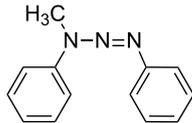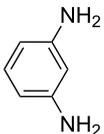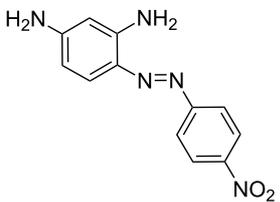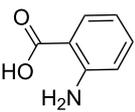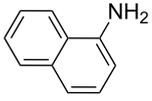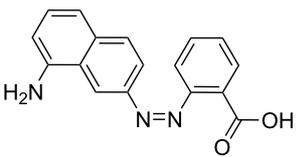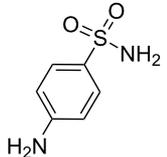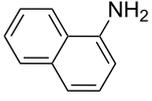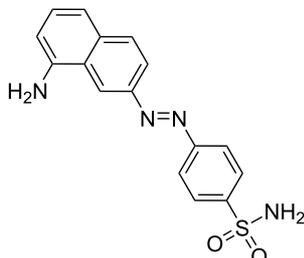
9	O_2N—⟨⟩—NH_2	⟨⟩—N(H)—CH_3	Ph—N(CH_3)—N=N—⟨⟩—NO_2	87%
10	⟨⟩—NH_2	⟨⟩—N(H)—CH_3	H_3C—N(Ph)—N=N—Ph	79%
11	O_2N—⟨⟩—NH_2	H_2N-⟨⟩-NH_2	H_2N,NH_2-⟨⟩—N=N—⟨⟩—NO_2	89%
12	HO(O)C—⟨⟩—H_2N	naphthyl-NH_2	H_2N-naphthyl—N=N—⟨⟩—C(O)OH	90%
13	H_2N—⟨⟩—S(O)(O)NH_2	naphthyl-NH_2	H_2N-naphthyl—N=N—⟨⟩—S(O)(O)NH_2	88%
14	⟨⟩(NH_2)(CH_3)	naphthyl-NH_2	H_3C-⟨⟩—N=N—naphthyl-NH_2	82%

was found that at slightly alkaline conditions (pH 8.55) and at a temperature of 25 °C, excellent conversions were attained in the azo coupling reaction of the diazonium salt solution of 2,4-dimethylaniline to 2-naphthol whereas the azo coupling reaction of the diazonium salt solution of *p*-nitroaniline to diphenylamine was found to thrive at a pH of 5.71 and at a temperature of 25 °C. It should be noted that the data generated was obtained in a very short time. On the down side, for a couple of experiments, samples could not be collected due to the limitations of the microreactor used. There were blockages observed due to precipitation of the product in the microreactor channels. This was particularly observed in the synthesis of 1-((2,4-dimethylphenyl)azo)naphthalen-2-ol at slow flow rates, temperatures close to 25 °C and pH greater than 7. Nonetheless, the effect of the reaction parameters on the azo coupling reaction in the synthesis of azo compounds was shown. To the best of our knowledge, this investigation is the first of its kind to expound the effect of pH, flow rate and temperature on the azo coupling reaction in the synthesis of azo compounds. A simple and fast continuous flow process was also thereafter developed for the

Table 8: Comparison of reaction conversion attained from two continuous flow reactor systems.

Run	Diazotizable amine	Coupler	Product	Conversion	
				LTF-MS (CD: 1.0 mm)	PTFE (i.d.: 1.5 mm)
1				97%	90%
2				88%	91%
3				95%	69%
4				80%	71%
5				92%	70%
6				80%	70%
7				88%	67%
8				89%	80%
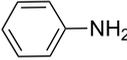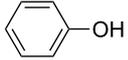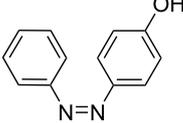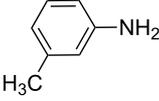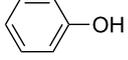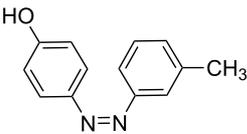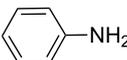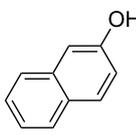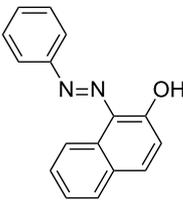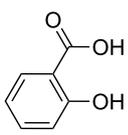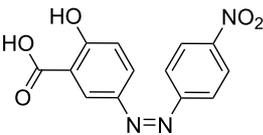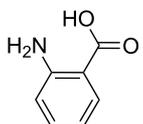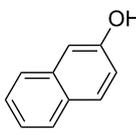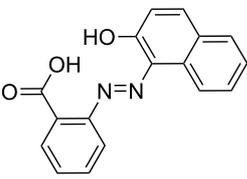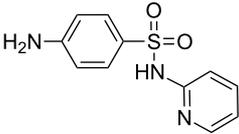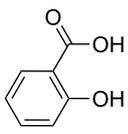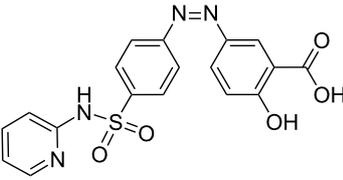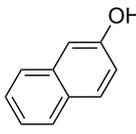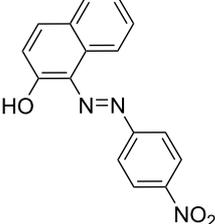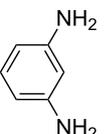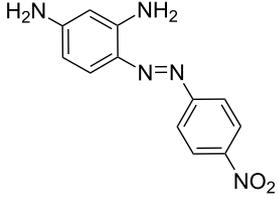
Table 8: Comparison of reaction conversion attained from two continuous flow reactor systems. (continued)
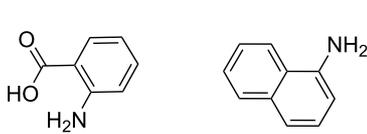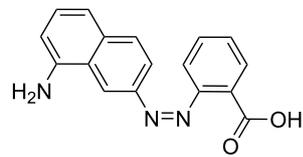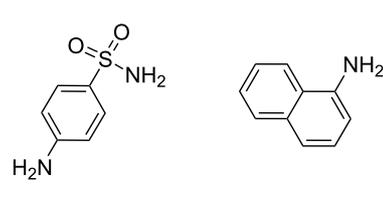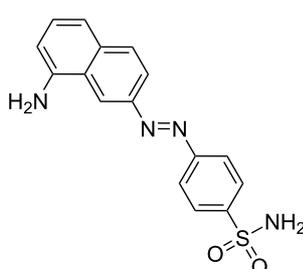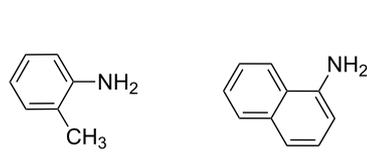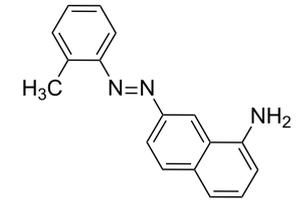
9				90%	72%
10				88%	78%
11				82%	66%

synthesis of naphtholic, phenolic and similar azo dyes. The robustness of the process was clearly demonstrated. In addition, an easy scale-up strategy was also established where it was found that the synthesis of these compounds in a simple continuous flow set up consisting of T-mixers and PTFE tubing (i.d.: 1.5 mm) provided relatively satisfactory reaction conversions moreover no occurrence of blockages was observed when this set up was in use. This finding is of importance especially when it comes to an increasing reaction throughput by the numbering up technique. Ideally, in evaluating the performance of two reactor systems in a chemical synthesis, it is important to keep most factors constant especially those pertaining to the geometry of the reactor channel as this can affect the reaction output. Albeit comparable reaction conversions were attained from the two reactor systems investigated, it is worth determining the role that the difference in geometrical structure had to play in the data observed in this study.

Experimental

All chemicals and solvents used were of analytical grade. ^{1}H and ^{13}C NMR spectra were recorded on a Bruker Avance-400 (400 MHz).

Microreactor set up; azo coupling reactions in the synthesis of azo compounds

Using two (1 mL) SGE glass syringes and PTFE tubing of 0.5 mm internal diameter, the reactants (diazonium salt and azo

coupling component solutions) were fed to an LTF-MS (Volume: 0.2 mL, channel size: 1 mm, geometry: 115 × 60 × 6 mm) microreactor plate (Figure 6). The microreactor plate was dipped into a temperature control bath and delivery of the reactants to the plates was enabled by two Chemyx fusion 100 classic syringe pumps.
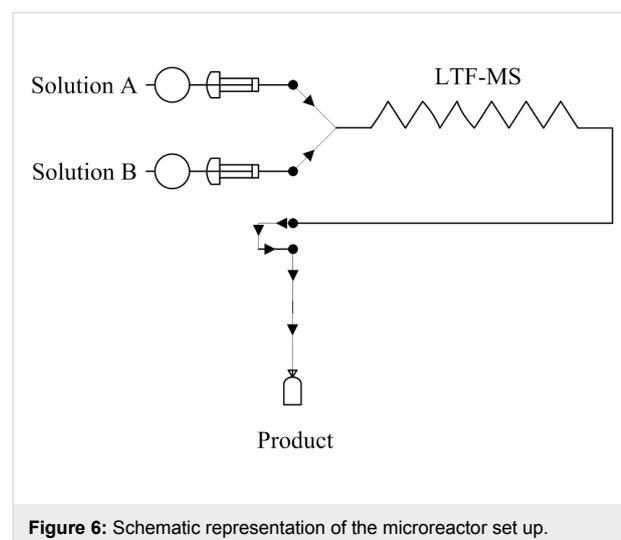
Figure 6: Schematic representation of the microreactor set up.

Preparation of reactant solutions

Solution A (diazotized primary aromatic amine): 2,4-dimethyl-aniline (0.2918 g) was dissolved in approximately 0.8 mL of

concentrated 32% HCl and cooled. To this cooled solution, 3 mL of cold sodium nitrite solution (0.29 g in 5 mL of distilled water) was added drop wise until the potassium starch iodide paper test was positive. DMF (20 mL) was added to this, after which the solution was made up to a volume (100 mL) with distilled water.

Solution B (coupler): 2-naphthol (0.35 g) was dissolved in 10% aqueous NaOH (10 mL) to which DMF (15 mL) was added. The pH of the solution was buffered to the appropriate pH intended for the investigation (pH 5.11, 7.39 and 10.83). The solution was then made up to a volume (50 mL) with distilled water.

Similarly, the reactant solutions A and B (diazotized primary aromatic amine and coupler) in the azo coupling of diazonium salt solution of *p*-nitroaniline to diphenylamine were prepared as follows:

Solution A (diazotized primary aromatic amine): *p*-nitroaniline (0.2918 g) was dissolved in hot concentrated 32% HCl (0.8 mL) and cooled. To this cooled solution, cold sodium nitrite solution (0.29 g in 5 mL of distilled water) was added drop wise until the potassium starch iodide paper test was positive. DMF (20 mL) was added to this after which the pH of the solution was buffered to afford the various working pH intended for the study (pH: 3.5, 5.66 and 6.94). The solution was then made up to a volume (100 mL) with distilled water.

Solution B (coupler): diphenylamine (0.35 g) was dissolved in methanol (50 mL).

Azo coupling reactions in microreactors

A central composite experimental design with a total of 12 experiments was used for each of the optimization studies at the various pH levels for the two reactions. The experiments were performed in a randomized manner. In addition, the flow rate of the solutions A and B was also varied as is shown in Table 9 below. The temperature of the batch diazotization reaction was kept constant at 0 °C while that of the azo coupling reaction.

Table 9: Experimental domain.

Reaction parameters	Minimum	Maximum
Flow rate (mL/min)	0.03	0.7
Temperature (°C)	0	50

Microreactor set up; continuous flow synthesis of azo compounds

Using three (5 mL) SGE glass syringes and PTFE tubing (i.d. 0.5 mm, length: 340.2 mm connecting from the first reactor plate to the second reactor plate and 380.7 mm connecting from the second reactor plate to the sample collection bottle) reactant solutions A (amine + HCl solution), B (sodium nitrite solution) and C (coupler) were fed into two LTF-MS microreactor plates (reactor volume: 0.2 mL, channel size: 1 mm, geometry: 115 × 60 × 6 mm) joined by PTFE tubing (i.d. 0.5 mm). The delivery of the reactants was enabled by three Chemyx Fusion 100 classic syringe pumps as shown in Figure 7. The reaction temperature for the diazotization (0 °C) and azo coupling (25 °C) reactions was maintained with the aid of an ice and water bath respectively.
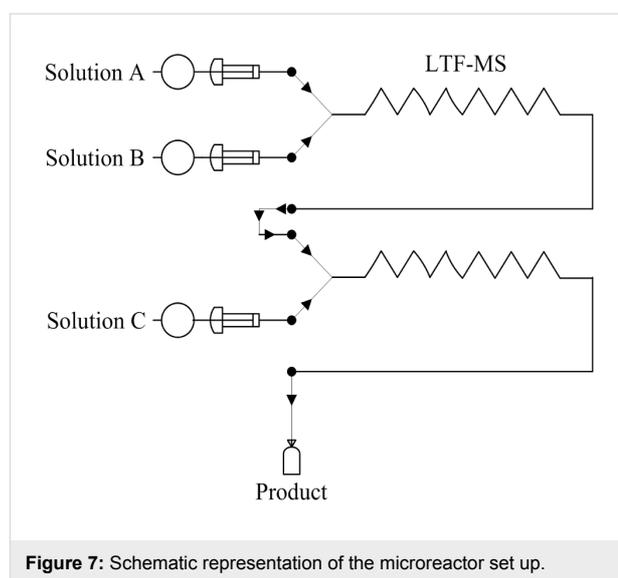
Figure 7: Schematic representation of the microreactor set up.

Preparation of reactant solutions

Solution A (amine + HCl solution): 2,4-dimethylaniline (0.2918 g) was dissolved in approximately 0.8 mL of concentrated 32% HCl. DMF (20 mL) was added to this, after which the solution was made up to a volume (100 mL) with distilled water.

Solution B (sodium nitrite solution): Sodium nitrite (0.2914 g) was dissolved in DMF (5 mL) and made up to a volume (50 mL) with distilled water.

Solution C (coupler): 2-naphthol (0.35 g) was dissolved in 10% aqueous NaOH (10 mL) to which DMF (15 mL) was added. The pH of the solution was adjusted to 8.55–9 with 10% glycine solution. The solution was then made up to a volume (50 mL) with distilled water.

For the azo coupling reactions performed in acidic reaction media, the reactant solution C was prepared as follows.

Solution C (coupler): 1-naphthylamine (0.3477 g) was dissolved in glacial acetic acid (10 mL of 10% glacial acetic acid solution) and buffered to a pH of approximately 5.77–6. The solution was then made up to volume (50 mL) with distilled water.

Microreactor diazotization and consequent azo coupling reactions

A central composite experimental design with a total of 20 experiments was used for this optimization study, where the diazotization of 2,4-dimethylaniline and its in situ azo coupling to 2-naphthol was used as a model reaction. The experiments were performed in a randomized manner. The temperature of the diazotization reaction was kept constant at 0 °C while that of the azo coupling reaction was kept at 25 °C (Table 10).

Scaled up microreactor diameter set up: PTFE tubing i.d. 1.5 mm

Keeping the residence time established in the optimization reactions constant, the scale up was carried out in PTFE tubing (i.d.

Table 10: Experimental domain.

Reaction parameters	Minimum	Maximum
HCl + amine (mL/min)	0.09	0.3
Sodium nitrite (mL/min)	0.01	0.05
Coupler (mL/min)	0.01	0.12

1.5 mm, length: 150.93 mm and 155.43 mm for the diazotization and azo coupling reactions, respectively). Using three SGE glass syringes and two 3-Way-Tee mixers (Omnifit labware, Pore size: 8.0 mm i.d., 0.5-4 mm OD), the delivery of reactant solutions A (amine + HCl solution), B (sodium nitrite solution) and C (coupler) into the PTFE tubing (i.d. 1.5 mm) was enabled by three Chemyx Fusion 100 classic syringe pumps (Figure 8). The reaction temperature for the diazotization reaction was kept at 0 °C with the aid of ice. The azo coupling reaction was performed at room temperature (25 °C).

Sample preparation

The microreactor set up was stabilized for 10 minutes between each experiment. In order to obtain substantial amount of sam-
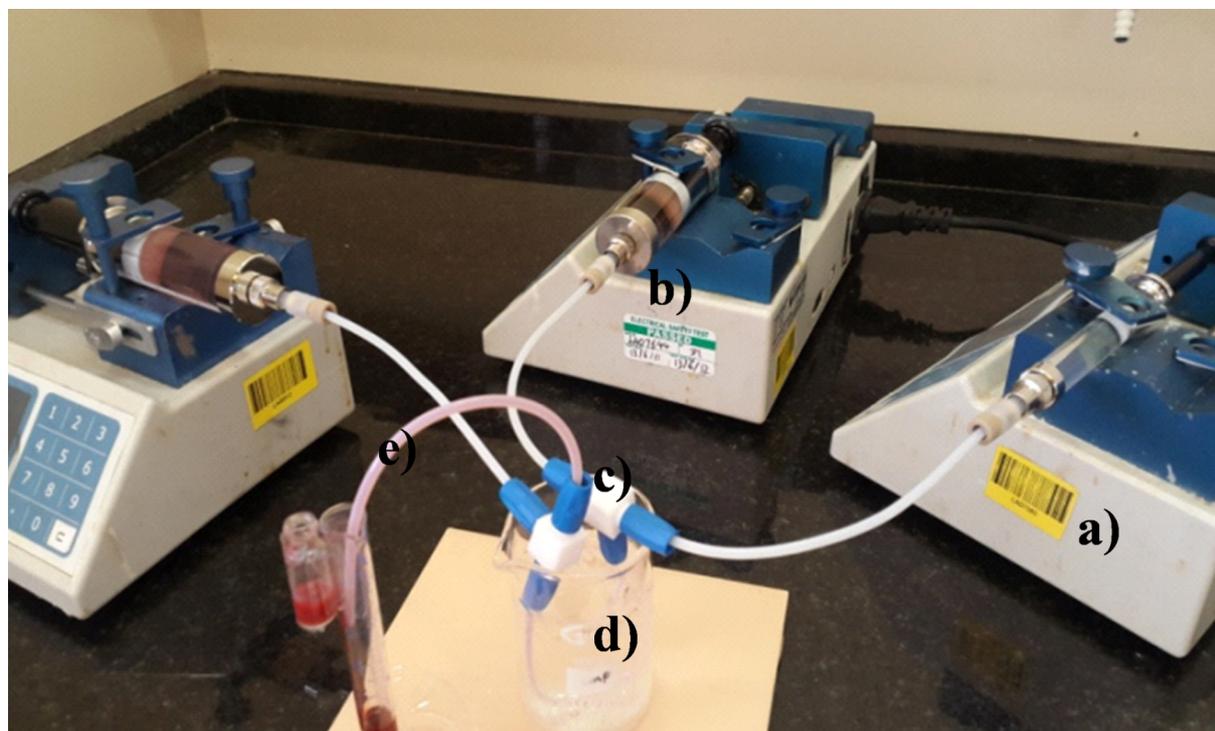
Figure 8: Scaled up microreactor set up: PTFE tubing i.d. 1.5 mm a) Chemyx Fusion 100 classic syringe pump, b) SGE glass syringe, c) T-mixer, d) Ice bath: Diazotization reaction and e) Room temperature: Azo coupling reaction.

ples for analysis, they were collected for a period of 1 minute each in a sample vial containing HCl (0.2 mL of 1 M). The mixture was then diluted with DMF (1 mL).

Sample analysis

Off-line reversed phase HPLC using a Phenomenex Luna 5 μ C18 100 A (250 × 4.60 mm × 5 microns) column under the following conditions; flow rate: 1.2 mL/min, mobile phase (acetonitrile 0.1% formic acid (75:25)) equipped with a variable wavelength detector was used for sample analysis. The external standard calibration HPLC method was used to quantify the amount of coupler utilized in the reaction. The wavelength used for quantification of the 2-naphthol was 349 nm.

Data analysis

The total volume of samples collected ($tvs_{collected}$) was calculated by multiplying the total flow rate of the reactant solutions (tfr_{ABC}) by the total sample collection time ($t_{collection}$). The reaction time was calculated by dividing the total reaction space volume i.e. the total volume of the two LTF-MS plates, the PTFE tubing used to join the two mixers and also that leading to the final outlet: the point of sample collection by the total flow rate of reactant solutions (tfr_{ABC}). For purposes of data analysis, all flow rates were converted to liters/minute.

Supporting Information

Supporting Information File 1

Additional diagrams and NMR spectra.
[http://www.beilstein-journals.org/bjoc/content/supplementary/1860-5397-12-186-S1.pdf]

Acknowledgements

References

1. James, C. H. In *Handbook of Green Chemistry and Technology;* Clark, J.; Macquarrie, D., Eds.; John Wiley & Sons, Ltd., 2002; pp 10–27.
2. Anastas, P.; Eghbali, N. *Chem. Soc. Rev.* **2009,** *39,* 301–312. doi:10.1039/b918763b
3. Noroozi-Pesyan, N.; Khalafy, J.; Malekpoor, Z. *Prog. Color, Color. Coat.* **2009,** *2,* 61–70.
4. Rahimizadeh, M.; Eshghi, H.; Shiri, A.; Ghadamyari, Z.; Matin, M. M.; Oroojalian, F.; Pordeli, P. *J. Korean Chem. Soc.* **2012,** *56,* 716–719. doi:10.5012/jkcs.2012.56.6.716
5. Mirjalili, F. B. B.; Bamoniri, A.; Akbari, A. *Curr. Chem. Lett.* **2012,** *1,* 109–114. doi:10.5267/j.ccl.2012.6.002
6. Bamoniri, A.; Pourali, A. R.; Nazifi, M. R. S. *Iran. J. Catal.* **2012,** *2,* 185–189.
7. Caldarelli, M.; Baxendale, I. R.; Ley, S. V. *Green Chem.* **2000,** *2,* 259–264. doi:10.1039/b000816h
8. Grirrane, A.; Corma, A.; García, H. *Science* **2008,** *322,* 1661–1664. doi:10.1126/science.1166401
9. Zhao, R.; Tan, C.; Xie, Y.; Gao, C.; Liu, H.; Jiang, Y. *Tetrahedron Lett.* **2011,** *52,* 3805–3809. doi:10.1016/j.tetlet.2011.05.054
10. Moglie, Y.; Vitale, C.; Radivoy, G. *Tetrahedron Lett.* **2008,** *49,* 1828–1831. doi:10.1016/j.tetlet.2008.01.053
11. Velasco, M. I.; Kinen, C. O.; de Rossi, R. H.; Rossi, L. I. *Dyes Pigm.* **2011,** *90,* 259–264. doi:10.1016/j.dyepig.2010.12.009
12. Damodaran, B.; Litka, J.; Lalithambika, M. *Synth. Commun.* **2003,** *33,* 863–869. doi:10.1081/SCC-120016343
13. Valizadeh, H.; Amiri, M.; Shomali, A.; Hosseinzadeh, F. *J. Iran. Chem. Soc.* **2011,** *8,* 495–501. doi:10.1007/bf03249083
14. Qiao, R.-Z.; Zhang, Y.; Hui, X.-P.; Xu, P.-F.; Zhang, Z.-Y.; Wang, X.-Y.; Wang, Y.-L. *Green Chem.* **2001,** *3,* 186–188. doi:10.1039/b103840k
15. Dabbagh, H. A.; Teimouri, A.; Chermahini, A. N. *Dyes Pigm.* **2007,** *73,* 239–244. doi:10.1016/j.dyepig.2005.12.002
16. Zarei, A.; Hajipour, A. R.; Khazdooz, L.; Mirjalili, B. F.; Chermahini, A. N. *Dyes Pigm.* **2009,** *81,* 240–244. doi:10.1016/j.dyepig.2008.10.011
17. Wootton, R. C. R.; Fortt, R.; de Mello, A. J. *Lab Chip* **2002,** *2,* 5–7. doi:10.1039/b111286d
18. Delville, M. M. E.; Nieuwland, P. J.; Janssen, P.; Koch, K.; Van Hest, J. C. M.; Rutjes, F. P. J. T. *Chem. Eng. J.* **2011,** *167,* 556–559. doi:10.1016/j.cej.2010.08.087
19. Struempel, M.; Ondruschka, B.; Daute, R.; Stark, A. *Green Chem.* **2008,** *10,* 41–43. doi:10.1039/b710554a
20. Chung, K.-T. *J. Environ. Sci. Health, Part C: Environ. Carcinog. Ecotoxicol. Rev.* **2000,** *18,* 51–74. doi:10.1080/10590500009373515
21. Wang, C.; Yediler, A.; Lienert, D.; Wang, Z.; Kettrup, A. *Chemosphere* **2002,** *46,* 339–344. doi:10.1016/s0045-6535(01)00086-8
22. Rai, H. S.; Bhattacharyya, M. S.; Singh, J.; Bansal, T. K.; Vats, P.; Banerjee, U. C. *Crit. Rev. Environ. Sci. Technol.* **2005,** *35,* 219–238. doi:10.1080/10643380590917932
23. Hisamoto, H.; Saito, T.; Tokeshi, M.; Hibara, A.; Kitamori, T. *Chem. Commun.* **2001,** 2662–2663. doi:10.1039/b106494k
24. Wille, C.; Gabski, H.-P.; Haller, T.; Kim, H.; Unverdorben, L.; Winter, R. *Chem. Eng. J.* **2004,** *101,* 179–185. doi:10.1016/j.cej.2003.11.007
25. Pennemann, H.; Forster, S.; Kinkel, J.; Hessel, V.; Löwe, H.; Wu, L. *Org. Process Res. Dev.* **2005,** *9,* 188–192. doi:10.1021/op049789e
26. Anderson, N. G. *Org. Process Res. Dev.* **2012,** *16,* 852–869. doi:10.1021/op200347k
27. De Zani, D.; Colombo, M. *J. Flow Chem.* **2012,** *2,* 5–7. doi:10.1556/jfchem.2012.00020
28. Webb, D.; Jamison, T. F. *Chem. Sci.* **2010,** *1,* 675–680. doi:10.1039/c0sc00381f
29. Newman, S. G.; Jensen, K. F. *Green Chem.* **2013,** *15,* 1456–1472. doi:10.1039/c3gc40374b
30. Martin, L. J.; Marzinzik, A. L.; Ley, S. V.; Baxendale, I. R. *Org. Lett.* **2011,** *13,* 320–323. doi:10.1021/ol1027927
31. Christie, R. M. *Colour Chemistry*. The Royal Society of Chemistry: Thomas Graham House., 2001; pp 51–55.

Development of a continuous process for α-thio-β-chloroacrylamide synthesis with enhanced control of a cascade transformation

Olga C. Dennehy[1], Valérie M. Y. Cacheux[1], Benjamin J. Deadman[1,§], Denis Lynch[1], Stuart G. Collins[*1], Humphrey A. Moynihan[*1] and Anita R. Maguire[*2]

Abstract

A continuous process strategy has been developed for the preparation of α-thio-β-chloroacrylamides, a class of highly versatile synthetic intermediates. Flow platforms to generate the α-chloroamide and α-thioamide precursors were successfully adopted, progressing from the previously employed batch chemistry, and in both instances afford a readily scalable methodology. The implementation of the key α-thio-β-chloroacrylamide casade as a continuous flow reaction on a multi-gram scale is described, while the tuneable nature of the cascade, facilitated by continuous processing, is highlighted by selective generation of established intermediates and byproducts.

Introduction

Since the efficient and highly stereoselective transformation of α-thioamides to the corresponding α-thio-β-chloroacrylamides derivatives was first reported [1,2], the considerable synthetic utility of these heavily functionalized acrylamide compounds has been well documented [3]. The predominant site of reactivity is at the electrophilic β-carbon, which results from the combined influence of the amide and chloro substituents, mitigating the electron-donating effect of the sulfide moiety. Nucleophilic substitution [4], Diels–Alder reactions [5] and 1,3-dipolar cycloadditions [6-9], and oxidation of the sulfide group [10-12] are among a wide array of transformations which have been successfully applied to these compounds (Scheme 1).
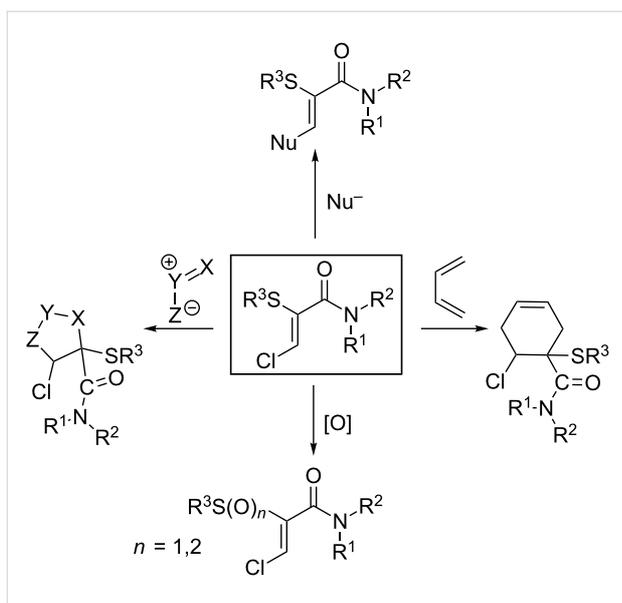
Scheme 1: Reaction pathways of α-thio-β-chloroacrylamides.

In order to fully exploit the synthetic potential of these β-chloroacrylamides, however, a means of ready access to appreciable quantities of material is required. Preparation of α-thio-β-chloroacrylamides typically results from a three-step synthetic route, culminating in a final cascade/domino reaction [13] where a toluene solution of α-thioamide and NCS is subjected to a 'hot plunge' by placing it into an oil bath at 90 °C (Scheme 2). While this route has consistently provided a robust means of generating the desired β-chloroacrylamides at scales of 1–10 g, it suffers from several disadvantages which impact on the ease of scale-up.

The preparation of the α-chloroamide **1** is exothermic and requires significant external cooling, an undesirable feature for scale-up. The synthesis of the α-thioamide **2** involves prior generation of fresh sodium ethoxide from sodium metal. Furthermore, this α-thioamide protocol, at high pH, ordinarily does not go to completion, leaving unreacted starting material and forming impurities which are subsequently removed by chro-

matographic purification. Finally, the optimized conditions for the final cascade transformation employ rapid heating via 'hot-plunge' in order to minimize the formation of process impurities during the initial heating phase [1]. This efficient rapid heating poses practical difficulties for scale-up and, furthermore, chromatographic separation is required to remove product impurities.

The nature of the aforementioned difficulties outlined are, however, largely specific to the scale-up of batch chemistry. A continuous processing approach frequently possesses advantages over the batch equivalent, as has been extensively documented [14-22]. When combined with automated operation, it allows for enhanced reproducibility and access to extreme conditions, which, along with improved heat and mass transfer, all facilitate significant ease of scale-up. The reaction control afforded by use of high surface-area-to-volume ratio tubular reactors, specifically with respect to dissipation of heat, offers a safety profile unique to flow chemistry. Continuous processing also provides the capacity to continuously generate hazardous reagents and intermediates in small quantities, in situ, and transferred directly into a reaction stage without operator handling [21-26]. As rapid heat transfer (steps 1 and 3) and greater reaction control (steps 2 and 3) were identified as the key challenges to be overcome, we envisaged that continuous processing could facilitate the preparation of large quantities of α-thio-β-chloroacrylamide with reduced purification requirements. The goal of this study was to develop an optimized process for the synthesis of α-thio-β-chloroacrylamides, employing a model system with *N*-4′-methylphenyl-(*Z*)-3-chloro-2-(phenylthio)propenamide (*Z*-**3**) as the target product. This optimized process would utilise flow chemistry as a key enabling technology to overcome the aforementioned challenges.

Results and Discussion
Preparation of α-chloroamide

The synthesis of α-chloroamide **1** is highly exothermic, due to the neutralisation of HCl – a byproduct – with triethylamine, and the need for effective heat removal imposes limitations on
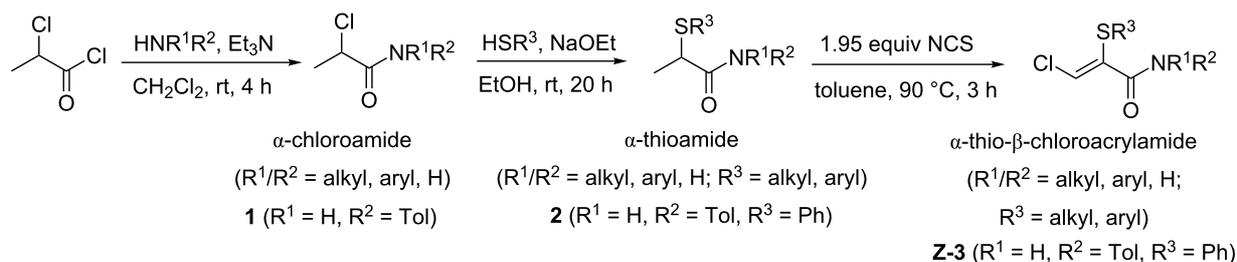
Scheme 2: Typical three-step batch preparation of α-thio-β-chloroacrylamide.

the batch scale-up of this step. It was envisaged that the efficient heat transfer properties of a high surface area tubular flow reactor would remove the need for external cooling of the reaction. To facilitate safe scale-up of this reaction we initially investigated a direct transfer of the batch process (Scheme 3) to continuous mode.

Scheme 3: Batch process for preparation of α-chloroamide **1**.
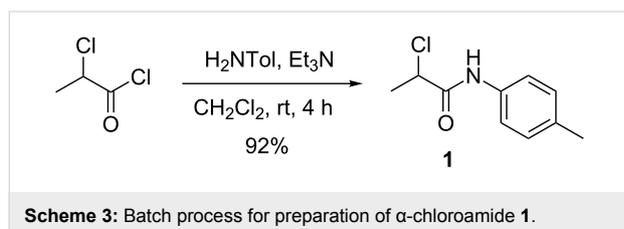
Although initial investigations involving small throughput had shown promise, the practicalities of employing dichloromethane at process scales caused us to consider alternative 'greener' solvent systems [27]. A screen of alternative solvents in batch test reactions revealed that, while the amide formation was tolerant to most solvents, rapid precipitation of triethylamine hydrochloride would be problematic in a continuous process. Indeed, trial runs of a continuous process in ethyl acetate resulted in immediate blockage of the flow reactor at the point of reagent mixing. To prevent blockages due to salt formation we investigated replacements for triethylamine that would produce a more soluble HCl salt. Diisopropylethylamine (DIPEA) was found to be a suitable base that allowed the continuous process to be carried out in ethyl acetate without any observed precipitation of the HCl salt. The 'greener' continuous amide formation (Scheme 4) was carried out on a large scale, producing 91 g (92% yield) of the α-chloroamide **1** over 5 hours of continuous operation, as a white crystalline solid after aqueous work-up and recrystallization.

Synthesis of α-thioamide

Driving the reaction to completion and avoiding the use of sodium metal were the key aims in transferring α-thioamide preparation from batch to flow. Although yields of 80–90% can be obtained under batch conditions, incomplete conversion to α-thioamide **2** necessitates a difficult, and often laborious, chromatographic separation, as starting material **1** and product **2** are poorly resolved. Indeed, high-purity batches of α-thioamide **2** are often not achieved by chromatography, with the resulting product typically ca. 94% pure by HPLC. It was also envisaged that the facility to superheat the solvent in a pressurised continuous platform could enable sodium ethoxide to be replaced by a weaker base, obviating the need for sodium metal.

At an early stage of process development, the possibility of telescoping the amide formation and thiolation steps was consid-

Scheme 4: Process for the conversion of 2-chloropropionyl chloride and *p*-toluidine to α-chloroamide **1** under optimized flow conditions.
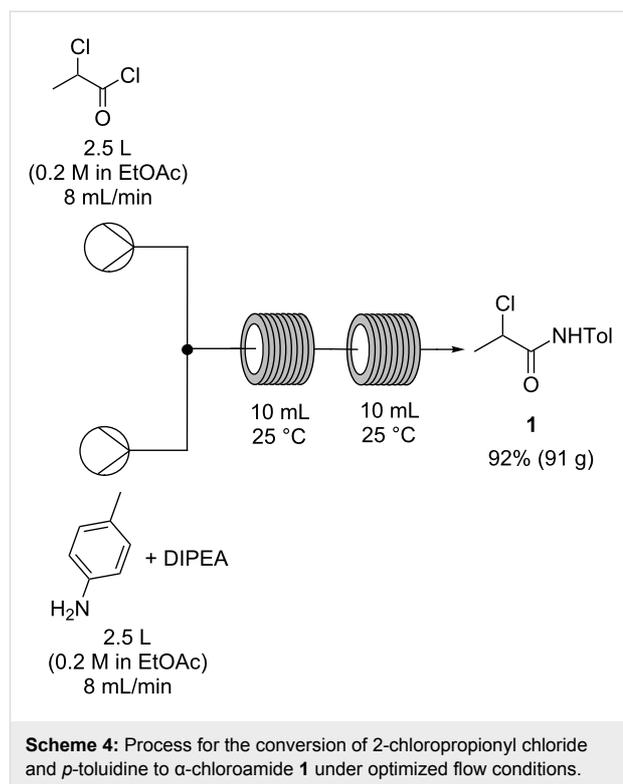
ered. Attempts were made to use triethylamine as the base in a continuous thiolation reaction, however, the reaction was found to progress slowly and a maximum conversion of 39% was observed by ^{1}H NMR spectroscopy. Elevating the temperature to 90 °C and employing DBU, as a more basic alternative to triethylamine, did not increase the reactivity. Hence, the focus was instead directed on converting the existing batch process (Scheme 2), with sodium ethoxide as base, into a stand-alone continuous process.

Initially, however, the sodium chloride byproduct was found to precipitate from ethanol causing blockages at the back-pressure regulator. As sodium chloride possesses a relatively low solubility in ethanol (ca. 0.055 g in 100 g of ethanol at 20 °C) compared to methanol (1.375 g in 100 g) [28], methanol was proposed as an alternative solvent. As ^{1}H NMR analysis indicated that the crude reaction product from batch tests (using methanol as solvent) consisted of 98% α-thioamide **2**, the process was subsequently transferred to a continuous flow system (Scheme 5).

A variety of temperatures (60–120 °C), bases (NaOMe, NaOH, Na_2CO_3) and concentrations (0.1–0.3 M) were investigated using methanol as solvent (see Supporting Information File 1), however, unreacted *α*-chloroamide **1** and diphenyl disulfide were detected as product components in all experiments. Direct sampling of the reaction mixture (system effluents) also showed

Scheme 5: Conversion of **1** to **2** in continuous mode using MeOH as solvent.
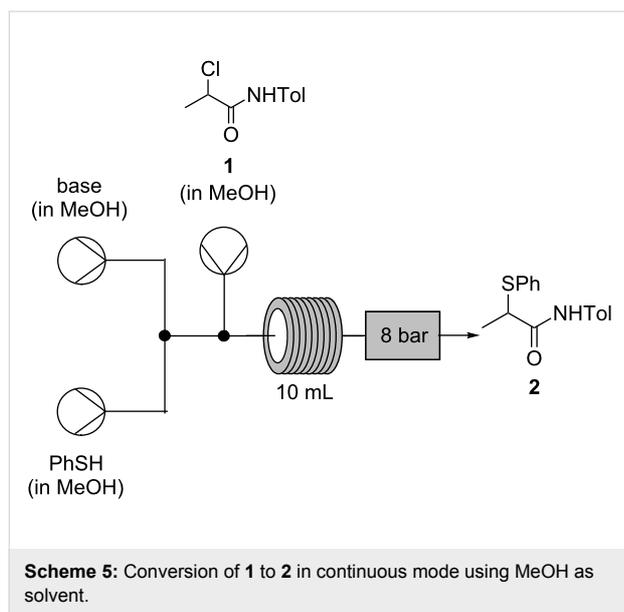
additional component peaks by HPLC analysis, which were not observed in material isolated after the reaction work-up. While temperatures above 100 °C or α-chloroamide **1** concentrations above 0.1 M were not found to be advantageous, sodium hydroxide demonstrated promising results when used as base.

With use of sodium hydroxide in mind, replacement of methanol with an ethanol/water mixture as solvent was subsequently examined. This solvent change was investigated in conjunction with further refinements to the stoichiometry of sodium hydroxide and thiophenol used, along with optimization of process temperature and residence time (Table 1).

Initially, when using 10 equivalents of sodium hydroxide, the best conversion to product **2** was obtained at a reaction temperature of 120 °C (entry 2, Table 1), with no unreacted α-chloroamide **1** detected by HPLC. Employing just 5 equivalents of hydroxide also provided an acceptable yield of α-thioamide **2** in all instances (entries 4–13, Table 1). The use of an excess of sodium hydroxide as base had removed the difficulty with unreacted starting material, presumably by hydrolysis of unreacted α-chloroamide **1** to more water soluble byproducts. In order to minimize the presence of diphenyl disulfide in the isolated product, the stoichiometry of thiophenol was also examined. Interestingly, a reduction in the excess of thiophenol to 1.05 equivalents was found to give a greater proportion of α-thioamide **2** and significantly reduced level of diphenyl disulfide (entries 7–13, Table 1).

After an improved stoichiometry of reagents had been established, lowering the residence time was investigated to facilitate efficient large scale synthesis by a continuous flow process.

Ultimately, a residence time of 5 min at 120 °C, using a 0.25 M concentration of α-chloroacrylamide, was found to give an acceptable quality of product **2**, with no detectable quantities of starting material **1** or diphenyl disulfide by HPLC analysis (entry 13, Table 1).

The optimized continuous process (Scheme 6) was then run on a 5 g scale with no observed loss of yield or purity. The α-thioamide **2**, which crystallized directly from the output of the flow process, was obtained in 71% yield and found to be >99% pure by HPLC analysis, compared to 94% purity for a typical batch preparation following chromatography.

Scheme 6: Optimized process for the conversion of α-chloroamide **1** to α-thioamide **2** under flow conditions.
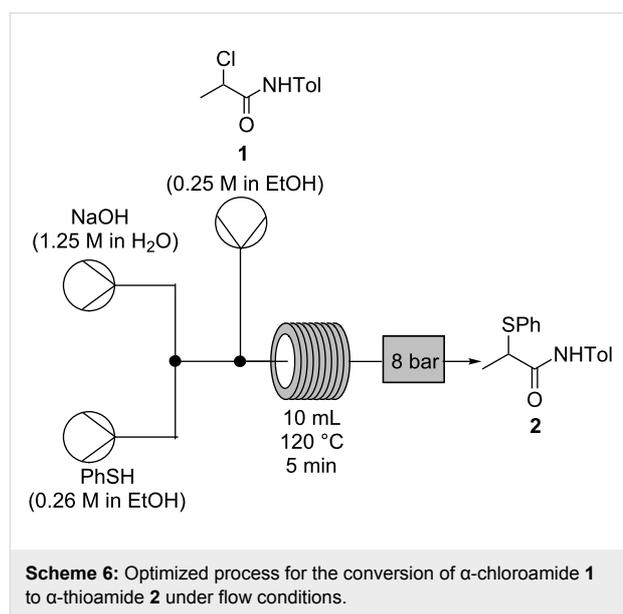
As transferring the α-thioamide preparation to a continuous platform had involved a number of important changes to the reaction conditions, it was decided to evaluate the optimized flow conditions (entry 13, Table 1) when applied to a batch process for comparison: 1.05 equivalents of thiophenol in ethanol mixed with an aqueous solution containing 5 equivalents of sodium hydroxide followed by heating to reflux for 1 hour. Initially on a 500 mg scale, a 97% yield of α-thioamide **2** was obtained, while operating at a higher concentration (increased from 0.25 M α-chloroamide **1** to 0.4 M α-chloroamide **1**) a yield of 94% was achieved on a 5 g scale, with the isolated product determined to be 99% pure by HPLC analysis. This process was ultimately carried out at a 20 g scale achieving 88% yield, again with 99% purity; the decrease in yield was offset by the increase in both productivity at this scale and product purity. The ability to operate effectively at higher concentrations in batch than in flow, in this case, made this batch process the optimum method of α-thioamide preparation, with a considerable reduction in reaction time from 10 hours to just 1 hour

Table 1: Optimization of temperature, thiophenol concentration, residence time and stoichiometry of base for conversion of **1** to **2** in continuous mode[a] using EtOH/H$_2$O as solvent.

Entry	Residence time (min)	Temp. (°C)	PhSH (equiv)	NaOH (equiv)	Product ratio			
					2 (%)[b]	**1** (%)[b]	PhSSPh (%)[b]	Other[c] (%)[b]
1	30	100	1.4	10	73.2	0	2.4	24.4
2	30	120	1.4	10	82.2	0	6.1	11.7
3	30	140	1.4	10	54.5	0	1.3	44.2
4	30	100	1.4	5	75.9	0	2.6	21.5
5	30	100	1.2	5	78.8	3.6	3.5	14.2
6	30	100	1.1	5	81.0	0.4	0.6	18.0
7	30	100	1.05	5	85.4	0	1.1	13.5
8	10	100	1.05	5	67.4	8.5	0.4	23.7
9	10	120	1.05	5	77.3	0	0.9	21.8
10	5	120	1.05	5	81.0	2.1	1.2	15.7
11	2	120	1.05	5	72.8	4.5	1.1	21.6
12	2	140	1.05	5	71.3	0	1.3	27.4
13[d]	5	120	1.05	5	74.1	0	0	25.9

[a]General conditions: 1 equiv α-chloroamide **1** (2 mL of a 0.1 M solution in EtOH) was reacted with PhSH (as a solution in EtOH) and NaOH (as a solution in H$_2$O). [b]Determined by HPLC analysis (peak area: see Supporting Information File 1) of samples taken directly from flow reactor as effluent solutions and diluted in MeCN prior to analysis. [c]Unisolated components, not present after work-up. [d]Reaction was run using 2 mL 0.25 M solution of α-chloroamide **1** in EtOH.

(for 20 g of **2**) and with a reduction of approximately one third in the required solvent volume, compared to the flow process. By comparison, the original batch process was typically run for 20 hours on scales up to 10 g.

As with the optimized flow process, direct crystallisation of the α-thioamide product **2** from this improved batch process was achieved by cooling and adding water as anti-solvent. This method of product isolation obviated the need for the arduous work-up – involving extraction into dichloromethane and several aqueous washes – associated with the original batch version, and gave material which was 99% purity or greater by HPLC analysis.

The stoichiometry of sodium hydroxide required for reaction completion was also considered as part of the batch comparison. Here, a reduction from 5 equivalents to 3 and subsequently to just 2 equivalents was found to be possible, with no discernible negative impact on the product formation. In the latter case, in batch the α-thioamide **2** was recovered in 92% yield and >99% purity by HPLC, when the reaction was performed on a 5 g scale. A subsequent batch run on a 20 g afforded an 89% yield, with the same level of product purity. It is, perhaps, worth noting that the high isolated yields obtained from the scaled-up reactions strongly suggest that the substantial quantities of 'other' components observed by HPLC analysis, but removed during work-up, are overestimated by detection at 250 nm

(Table 1). Such an overestimation is consistent with the presence of additional chromophores, when compared to the desired product, and would indicate that these observed components may contain an α,β-unsaturated carbonyl motif in their structures.

The value of exploring flow methodology, ultimately leading to an improved batch process, is keenly highlighted in this instance. The optimized batch process, developed through examining the use of continuous processing, can produce 20 g of pure material, with direct product precipitation/crystallization from the reaction solution (>99% pure by HPLC analysis), which has removed the requirements for isolation by extraction and subsequent chromatographic purification. HPLC analysis of

the current process – in either batch or flow – indicated complete consumption of the α-chloroamide **1**, without diphenyl disulfide formation, while an increase in yield from 80–90% to consistently over 90% has been achieved. Furthermore, the use of an inert atmosphere is no longer necessary as the decrease in reaction time has essentially eliminated the opportunity for aerobic oxidation of the thiophenolate anion to diphenyl disulfide, while sodium metal is no longer used as part of the process.

α-Thio-β-chloroacrylamide cascade in flow

Successful conversion of the β-chloroacrylamide cascade step from batch to flow posed a number of challenges. The reaction mechanism (Scheme 7) involves a complex cascade which also
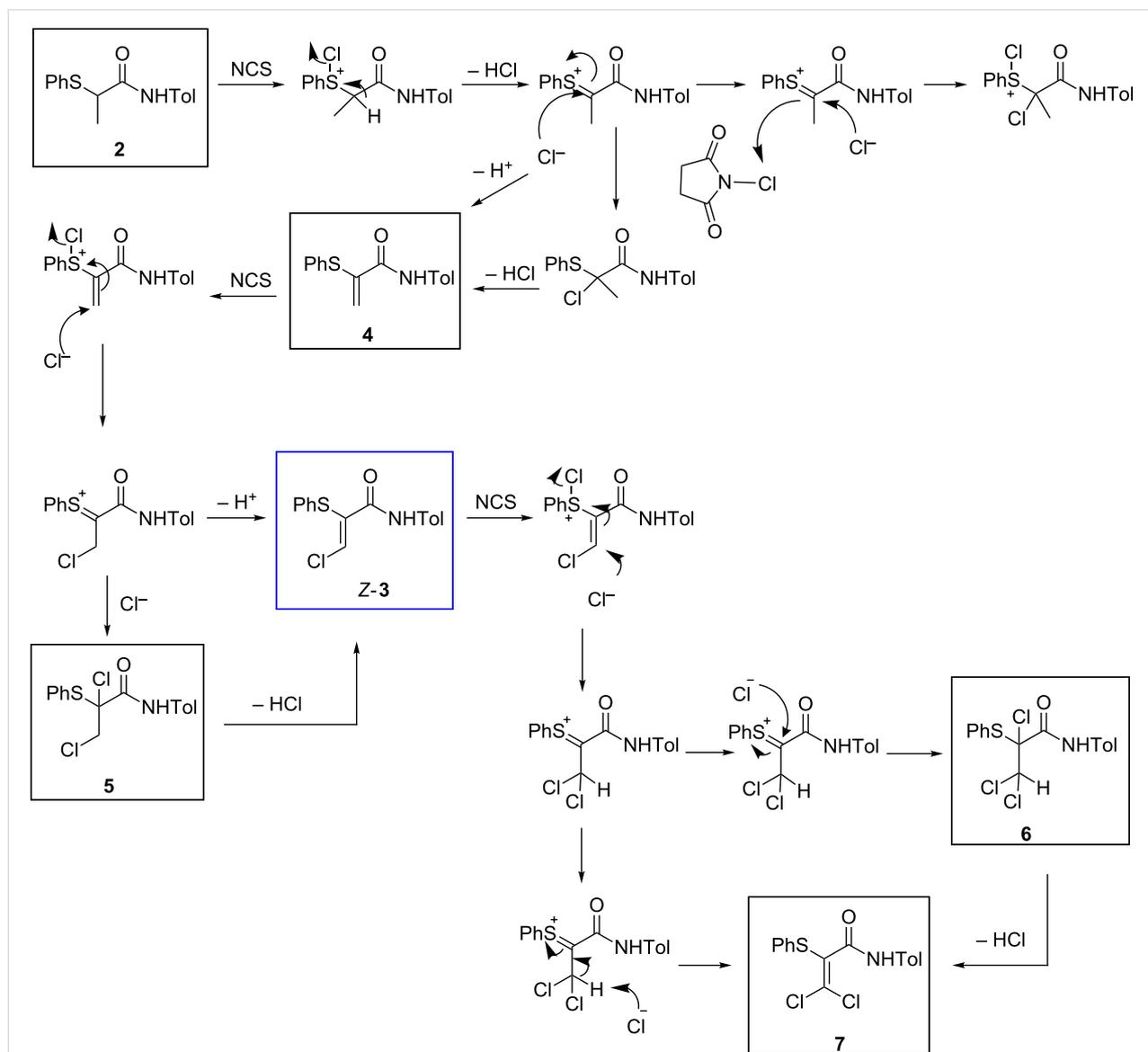
Scheme 7: Mechanism of the β-chloroacrylamide cascade process [29].

gives rise to several known impurities, including acrylamide **4**, dichloride **5**, trichloride **6** and dichloroacrylamide **7**.

In the optimized batch synthesis of α-thio-β-chloroacrylamide *Z*-**3** from the corresponding α-thioamide **2**, *N*-chlorosuccinimide (NCS) is added in one portion to a solution of **2** in toluene and the reaction mixture is immediately immersed in an oil bath at 90 °C (Scheme 2). Although this protocol performs well, giving 91% yield on a ca. 5 g scale [1], the practical challenges of achieving efficient rapid heating on a larger scale in batch made continuous processing an attractive alternative for scale-up due to its capacity for excellent temperature control. Efficient heat transfer due to the high surface, low volume geometry of tubular flow reactors makes it possible to achieve extremely rapid temperature transitions. It was envisaged that flowing the reaction through a heated section of tubing would be analogous to the batch 'hot plunge' method but with the capacity for faster heating of the reaction.

Given the superior performance of α-thioamide **2** synthesis in batch, the potential telescoping of the thiolation process with the β-chloroacrylamide cascade was not investigated. Furthermore, the potential vulnerability of α-thio-β-chloroacrylamides towards nucleophilic substitution by an aqueous ethanol compo-

nent of the reactant stream (from α-thioamide **2** preparation), particularly at elevated temperatures, strongly mitigated against integrating these steps.

For the batch process, the solubility of NCS in toluene has notable benefits: NCS is soluble in toluene at high temperatures, while the succinimide byproduct readily precipitates from toluene on cooling, allowing its convenient removal by filtration. In a continuous flow process, however, succinimide precipitation would cause blockage of the system.

Attempts at transferring the cascade reaction to a continuous platform began with direct adaptation of the existing batch process (Table 2). The solubility of NCS in toluene was found to be variable and often unsuitably low. Only batches of NCS which readily gave complete solutions were used and these batches were always either freshly recrystallized or commercial batches which were 'newly' opened prior to use. The reduced solubility of other batches was attributed to the partial hydrolysis of NCS upon intermittent exposure to ambient conditions over prolonged periods, also generating HCl.

Initial investigations using our prototype flow process employed 0.01 M solutions of NCS and starting material **2** in tolu-

Table 2: Initial flow process for conversion of **2** to *Z*-**3** using toluene as solvent.

Entry	Ratio 2:NCS[a]	Residence Time (min)	Product ratio			
			2 (%)[b]	4 (%)[b]	5 (%)[b]	Z-3 (%)[b]
1	1:2	20	19	15	18	47
2	1:2	50	21	19	0	60
3	1:2.3	20	22	8	20	46
4	1:3	20	25	1	12	62
5	1:1	20	21	77	<1	2

[a]Stoichiometric ratio of α-thioamide **2**:NCS controlled by manipulating the relative flow rates. [b]Molar ratio determined by HPLC analysis (peak area weighted for relative response factors of each component: see Supporting Information File 1) of samples taken directly from flow reactor as effluent solutions and diluted in MeCN prior to analysis.

ene. The equivalent of a 'hot-plunge' method was achieved by passing the reaction solution through a coiled tube reactor at 120 °C. The high surface area–volume ratio of tubular flow reactors is ideal for such rapid temperature transitions. It was noted that a relatively short residence time of only 20 min could be used, with a longer time of 50 min offering only a modest improvement on the reaction outcome (entries 1 and 2, Table 2). Indeed, the conversion of starting material **2** to acrylamide **4** was found to be closely comparable, indicating almost identical reaction progress, given the instability of dichloride **5**, which easily converts to the final product *Z*-**3**.

Increasing the amounts of NCS used was found to lead to a better conversion of acrylamide **4** to dichloride **5** or α-thio-β-chloroacrylamide *Z*-**3** (entries 3 and 4, Table 2), with only 1% of acrylamide **4** left unreacted with three equivalents of NCS used. When only an exact stoichiometric ratio (1:1) of NCS was used, the reaction stopped after the first chlorination step, leading to a reaction mixture which contained acrylamide **4** as the main product formed (entry 5, Table 2). This ability to halt the cascade at the acrylamide intermediate **4** or push through to the α-thio-β-chloroacrylamide *Z*-**3** highlights the enhanced control of reaction stoichiometry afforded by a continuous platform and offers the possibility to isolate selected intermediates

in the cascade reaction using a continuous process, more effectively than in batch and with greater flexibility.

Optimization of the cascade process using flow chemistry

In all the aforementioned cases (Table 2), around 20% of the starting material was consistently found to be unreacted. The key limitation to overcome was proposed to be the low solubility of NCS in toluene, and the consequent limitations to reactor throughput. To offset this difficulty, the use of alternative solvents was investigated. Acetonitrile was considered as a possible alternative solvent due to the high solubility of NCS it offers. Hence, preliminary experiments were carried out in order to compare its performance to toluene (Table 3), with the α-thioamide **2**:NCS ratio again adjusted by manipulating the concentration of the reagent solutions. In these experiments, the reaction conversions were determined using ^{1}H NMR analysis of the crude product material obtained, with characteristic proton signals of the β-carbon of the starting material **2**, intermediates **4** and **5**, and the desired product *Z*-**3** being easily identifiable.

Using toluene as a solvent for both reagents (α-thioamide **2** and NCS) leads to 10% unreacted acrylamide **4** (entry 1, Table 3).

Table 3: Solvent screen for conversion of **2** to *Z*-**3** in continuous mode.

Entry	[α-Thioamide **2**] (mM)	[NCS] (mM)	Solvent A/B	Product ratio				
				2 (%)[a]	**4** (%)[a]	**5** (%)[a]	*Z*-**3** (%)[a]	*E*-**3** (%)[a]
1	25	50	Tol/Tol	0	9.9	9.9	78.7	1.5
2	25	50	Tol/MeCN	0	4.3	0	81.4	14.3
3	25	50	MeCN/MeCN	0	0	0	86.9	13.1
4	200	400	Tol/MeCN	0	7.3	0	83.5	9.2
5	200	400	MeCN/MeCN	0	0	0	87.8	12.2

[a]Determined by ^{1}H NMR spectroscopy.

When a solution of **2** in toluene and a solution of NCS in acetonitrile were employed as the reactant streams, similar results were observed at either low or high concentration, in terms of residual acrylamide intermediate detected (entries 2 and 4, Table 3). However when acetonitrile was used as solvent for both reagents (α-thioamide **2** and NCS), full conversion to the final product *Z*-**3** was observed, at both high and low concentration of reagents (entries 3 and 5, Table 3). Use of high concentrations has the advantage of increasing process productivity. In this case (entry 5, Table 3), the production could be increased eight-fold for the same reaction time as entry 3 (25 min residence time). Furthermore, higher concentration of reagents enables greener synthesis by reducing solvent use.

Interestingly, during development studies on the conversion of α-thioamide **2** to α-thio-β-chloroacrylamide *Z*-**3** in acetonitrile, by flow or in batch, a new component of the cascade reaction was observed, which was identified as the (*E*)-α-thio-β-chloroacrylamide *E*-**3**.

An important feature of the experiments conducted on the β-chloroacrylamide cascade as a continuous process was the

complete absence of the over-chlorinated products **6** and **7**, which were not observed by HPLC analysis or ^{1}H NMR spectroscopy. In contrast, when similar conditions were employed in batch, significant formation of these byproducts was often in evidence [1]. The flow process for the conversion of α-thioamide **2** to α-thio-β-chloroacrylamide **3** which employed acetonitrile as solvent was therefore taken forward for optimization and scale-up (Table 4).

The residence time of the flow process was investigated to determine the completion time of the reaction, principally to minimize the extent of impurity formation due to over-reaction. The shortest possible effective residence time would be also preferable for larger scale operation in order to maximize the reactor throughput. The dichloride intermediate **5** was still present after a 2 min residence time (entry 5, Table 4), implying the reaction had not yet reached completion, while minor impurities remained at similar levels throughout all of the experiments. The succinimide byproduct was removed in the product work-up.

At lower reaction temperatures, large quantities of the dichloride **5** were observed (entries 6–8, Table 4), with correspond-

Table 4: Optimization of flow rates, residence time and temperature for conversion of **2** to *Z*-**3** in continuous mode[a].

Entry	Residence time (min)	Flow rate (mL/min)	Temp (°C)	Product ratio[b]			
				Z-**3** (%)[c]	*E*-**3** (%)[c]	**4** (%)[c]	**5** (%)[c]
1	25	0.2	120	88.2	11.8	0.0	0.0
2	15	0.3	120	87.6	12.4	0.0	0.0
3	10	0.5	120	86.9	13.1	0.0	0.0
4	5	1.0	120	85.5	14.5	0.0	0.0
5	2	2.5	120	72.8	13.7	0.0	13.5
6	2	2.5	80	4.9	2.3	0.0	92.7
7	2	2.5	90	9.5	3.1	0.0	87.4
8	2	2.5	100	17.3	4.4	0.0	78.3
9	2	2.5	130	84.0	16.0	0.0	0.0

[a]1 Equiv of α-thioamide **2** (4 mL of a 0.2 M solution in MeCN) was reacted with 2 equiv of NCS (4 mL of a 0.4 M solution in MeCN). [b]Unisolated components, not present after work-up were not included, but ranged from 5–10% by peak area. [c]Molar ratio determined by HPLC analysis (peak area weighted for relative response factors of each component: see Supporting Information File 1) of samples taken directly from flow reactor as effluent solutions and diluted in MeCN prior to analysis.

ingly low quantities of product *Z*-**3**. This finding is consistent with previous work showing that rapid heating resulted in a more efficient reaction cascade to the desired product *Z*-**3**, while slower heating leads to substantial quantities of reaction intermediates **4** and **5** as product impurities [3].

The stoichiometry of NCS used for the continuous process was also further optimized (Table 5). It was found that, at 130 °C, 2 equivalents of NCS resulted in the lowest levels of the impurities arising from reaction intermediates and over-chlorination byproducts while also achieving one of the highest conversions to the desired α-thio-β-chloroacrylamide *Z*-**3** (82.9%, entry 4, Table 5).

This process was then operated on a 30 g scale (Scheme 8) to produce 19.3 g (57% yield, >99% pure by HPLC analysis and ^{1}H NMR spectroscopy) of isolated α-thio-β-chloroacrylamide *Z*-**3** in less than 4 hours. The crude material was found to

consist only of a mixture of the *Z*- and *E*-isomers by ^{1}H NMR spectroscopy, with pure *Z*-**3** selectively recovered after recrystallization, albeit with a loss of isolated yield from this process. This is the first instance in which multi-gram quantities of the product *Z*-**3** have been isolated without the need for chromatography and on more than 3 times the scale which can be obtained in batch with the same reaction time [1]; the increase in quantity and the ease of purification compensates for the reduction in yield to 57%. The material obtained by concentration of the liquors recovered from recrystallization were found to consist mainly of *Z*-**3** and *E*-**3** by ^{1}H NMR spectroscopy. Purification of this material by chromatography gave an additional 11% yield of pure *Z*-**3** (3.7 g).

Conclusion

An efficient continuous flow methodology has been developed for the three-step synthesis of α-thio-β-chloroacrylamide *Z*-**3**, which has overcome the challenges to scale-up posed by the

Table 5: Optimization of NCS stoichiometry for conversion of α-thioamide **2** to α-thio-β-chloroacrylamide *Z*-**3** in continuous mode[a].

Entry	NCS equiv	Product ratio[b]				
		Z-**3** (%)[c]	*E*-**3** (%)[c]	**4** (%)[c]	**5** (%)[c]	**6** (%)[c]
1	1.7	68.8	13.1	18.1	0.0	0.0
2	1.9	73.8	14.1	12.1	0.0	0.0
3	1.95	76.5	14.8	8.6	0.0	0.0
4	2	82.9	15.8	1.3	0.0	0.0
5	2.05	81.6	15.9	1.4	0.0	1.1
6	2.1	81.3	15.3	1.7	0.0	1.7
7	2.2	69.4	11.9	0.0	0.0	18.7

[a]1 Equiv of α-thioamide **2** (4 mL of 0.2 M solution in MeCN) was reacted with NCS (4 mL of solution in MeCN) at 130 °C for 2 min, using a flow rate of 2.5 mL/min. [b]Molar ratio determined by HPLC analysis (peak area weighted for relative response factors of each component: see Supporting Information File 1) of samples taken directly from flow reactor as effluent solutions and diluted in MeCN prior to analysis. [c]Unisolated components, not present after work-up were not included, but ranged from 2–14% by peak area.

Scheme 8: Optimized flow process for conversion of α-thioamide **2** to α-thio-β-chloroacrylamide *Z*-**3**.
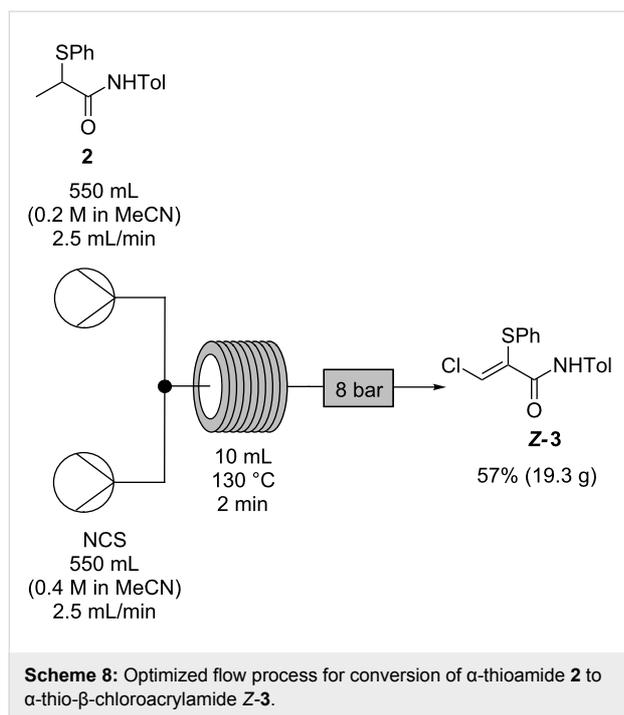
conventional batch preparation. This approach has yielded improvements in process safety, significantly reduced reaction times and increased product purity, obviating the need for chromatography. One process, preparation of α-thioamide **2** ultimately proved most efficient in batch, though the investigations performed in flow were critical to achieving the optimization. The easy access to synthetically useful amounts, afforded by a transfer to continuous processing, is expected to significantly increase the attractiveness of harnessing the enormous potential utility of α-thio-β-chloroacrylamides on a more widespread basis. Perhaps the most powerful outcome is the ability to control the β-chloroacrylamide cascade through continuous processing, leading to selective recovery of individual components of the reaction.

Supporting Information

Supporting Information File 1

General information, experimental procedures, analytical data and copies of NMR spectra of all compounds. [http://www.beilstein-journals.org/bjoc/content/supplementary/1860-5397-12-246-S1.pdf]

Acknowledgements

References

1. Murphy, M.; Lynch, D.; Schaeffer, M.; Kissane, M.; Chopra, J.; O'Brien, E.; Ford, A.; Ferguson, G.; Maguire, A. R. *Org. Biomol. Chem.* **2007,** *5,* 1228–1241. doi:10.1039/B618540A
2. Maguire, A. R.; Murphy, M. E.; Schaeffer, M.; Ferguson, G. *Tetrahedron Lett.* **1995,** *36,* 467–470. doi:10.1016/0040-4039(94)02288-M
3. Kissane, M.; Maguire, A. R. *Synlett* **2011,** 1212–1232. doi:10.1055/s-0030-1260559
4. Kissane, M.; Murphy, M.; O'Brien, E.; Chopra, J.; Murphy, L.; Collins, S. G.; Lawrence, S. E.; Maguire, A. R. *Org. Biomol. Chem.* **2011,** *9,* 2452–2472. doi:10.1039/c0ob00805b
5. Kissane, M.; Lynch, D.; Chopra, J.; Lawrence, S. E.; Maguire, A. R. *Org. Biomol. Chem.* **2010,** *8,* 5602–5613. doi:10.1039/c0ob00368a
6. Kissane, M.; Murphy, M.; Lynch, D.; Ford, A.; Maguire, A. R. *Tetrahedron* **2008,** *64,* 7639–7649. doi:10.1016/j.tet.2008.05.026
7. Kissane, M.; Lawrence, S. E.; Maguire, A. R. *Org. Biomol. Chem.* **2010,** *8,* 2735–2748. doi:10.1039/c002479a
8. Kissane, M.; Maguire, A. R. *Chem. Soc. Rev.* **2010,** *39,* 845–883. doi:10.1039/B909358N
9. Kissane, M.; Lawrence, S. E.; Maguire, A. R. *Tetrahedron* **2010,** *66,* 4564–4572. doi:10.1016/j.tet.2010.04.057
10. Kissane, M.; Lynch, D.; Chopra, J.; Lawrence, S. E.; Maguire, A. R. *Tetrahedron: Asymmetry* **2008,** *19,* 1256–1273. doi:10.1016/j.tetasy.2008.04.033
11. Kissane, M.; Lawrence, S. E.; Maguire, A. R. *Tetrahedron: Asymmetry* **2010,** *21,* 871–884. doi:10.1016/j.tetasy.2010.05.004
12. Kissane, M.; Murphy, M.; Lawrence, S. E.; Maguire, A. R. *Tetrahedron: Asymmetry* **2010,** *21,* 2550–2558. doi:10.1016/j.tetasy.2010.10.007
13. Tietze, L. F. *Chem. Rev.* **1996,** *96,* 115–136. doi:10.1021/cr950027e
14. Wegner, J.; Ceylan, S.; Kirschning, A. *Adv. Synth. Catal.* **2012,** *354,* 17–57. doi:10.1002/adsc.201100584
15. Wirth, T., Ed. *Microreactors in Organic Chemistry and Catalysis;* Wiley-VCH Verlag GmbH & Co. KGaA: Weinheim, Germany, 2013.
16. Baxendale, I. R.; Brocken, L.; Mallia, C. J. *Green Process. Synth.* **2013,** *2,* 211–230. doi:10.1515/gps-2013-0029
17. Pastre, J. C.; Browne, D. L.; Ley, S. V. *Chem. Soc. Rev.* **2013,** *42,* 8849–8869. doi:10.1039/c3cs60246j
18. Webb, D.; Jamison, T. F. *Chem. Sci.* **2010,** *1,* 675–680. doi:10.1039/c0sc00381f
19. McQuade, D. T.; Seeberger, P. H. *J. Org. Chem.* **2013,** *78,* 6384–6389. doi:10.1021/jo400583m
20. Hartman, R. L.; McMullen, J. P.; Jensen, K. F. *Angew. Chem., Int. Ed.* **2011,** *50,* 7502–7519. doi:10.1002/anie.201004637
21. Gutmann, B.; Cantillo, D.; Kappe, C. O. *Angew. Chem., Int. Ed.* **2015,** *54,* 6688–6728. doi:10.1002/anie.201409318
22. Movsisyan, M.; Delbeke, E. I. P.; Berton, J. K. E. T.; Battilocchio, C.; Ley, S. V.; Stevens, C. V. *Chem. Soc. Rev.* **2016,** *45,* 4892–4928. doi:10.1039/C5CS00902B
23. Deadman, B. J.; Collins, S. G.; Maguire, A. R. *Chem. – Eur. J.* **2015,** *21,* 2298–2308. doi:10.1002/chem.201404348
24. Müller, S. T. R.; Wirth, T. *ChemSusChem* **2015,** *8,* 245–250. doi:10.1002/cssc.201402874

25. Deadman, B. J.; O'Mahony, R. M.; Lynch, D.; Crowley, D. C.; Collins, S. G.; Maguire, A. R. *Org. Biomol. Chem.* **2016,** *14,* 3423–3431. doi:10.1039/C6OB00246C

26. Kopach, M. E.; Roberts, D. J.; Johnson, M. D.; McClary Groh, J.; Adler, J. J.; Schafer, J. P.; Kobierski, M. E.; Trankle, W. G. *Green Chem.* **2012,** *14,* 1524–1536. doi:10.1039/c2gc35050e

27. Prat, D.; Wells, A.; Hayler, J.; Sneddon, H.; McElroy, C. R.; Abou-Shehada, S.; Dunn, P. J. *Green Chem.* **2016,** *18,* 288–296. doi:10.1039/C5GC01008J

28. Pinho, S. P.; Macedo, E. A. *J. Chem. Eng. Data* **2005,** *50,* 29–32. doi:10.1021/je049922y

29. Foley, D. A.; Doecke, C. W.; Buser, J. Y.; Merritt, J. M.; Murphy, L.; Kissane, M.; Collins, S. G.; Maguire, A. R.; Kaerner, A. *J. Org. Chem.* **2011,** *76,* 9630–9640. doi:10.1021/jo201212p

The digital code driven autonomous synthesis of ibuprofen automated in a 3D-printer-based robot

Philip J. Kitson, Stefan Glatzel and Leroy Cronin[*]

Abstract

An automated synthesis robot was constructed by modifying an open source 3D printing platform. The resulting automated system was used to 3D print reaction vessels (reactionware) of differing internal volumes using polypropylene feedstock via a fused deposition modeling 3D printing approach and subsequently make use of these fabricated vessels to synthesize the nonsteroidal anti-inflammatory drug ibuprofen via a consecutive one-pot three-step approach. The synthesis of ibuprofen could be achieved on different scales simply by adjusting the parameters in the robot control software. The software for controlling the synthesis robot was written in the python programming language and hard-coded for the synthesis of ibuprofen by the method described, opening possibilities for the sharing of validated synthetic 'programs' which can run on similar low cost, user-constructed robotic platforms towards an 'open-source' regime in the area of chemical synthesis.

Introduction

The rapid expansion of 3D-printing technologies in recent decades has been one of the most promising developments in the fields of science and engineering [1]. This technology, along with the open-source ethos and large, committed user and developer base from which it benefits, has driven innovation in many areas of industrial and technological activity, from distributed manufacturing [2] to practical applications in the areas of medicine [3,4] and biology [5,6]. The use of 3D printers and

3D-printed objects has expanded rapidly, with this technology being applied to scientific disciplines as diverse as biomedical research [7-9], soft robotics [10,11] and materials science [12]. Our group has recently been investigating the use of 3D printing in the chemical sciences, in particular its potential to create 'reactionware' [13], that is, chemical reactors where the control which 3D printing offers over the topology, geometry and composition of a reactor [14] can have a significant influence on the

reaction outcomes. This utility has so far been demonstrated for a number of applications, from inorganic and organic synthetic [15,16] chemistry to hydrothermal synthesis [17], flow applications [18] and analytical chemistry [19]. One area of research where 3D printers themselves, rather than the products of 3D printing could have a large impact is in the field of laboratory automation.

The automation of laboratory processes has been continuing for as long as the technical abilities and engineering capacities have existed, with the first examples of such equipment appearing in the second half of the nineteenth century [20]. The development of such automation in industrial settings has been rapid, with the inherent flexibility of work in research laboratories leading to much slower adoption of routine automation. One of the barriers to large-scale adoption of laboratory automation technologies has been the traditionally high cost of such equipment which is often optimized for very specific routine tasks [21]. Indeed, one area in which these technologies have been slow to develop has been in the area of synthetic organic chemistry. In this field automation has largely been limited to flow chemistries for specific synthetic pathways [22]. Recently however more versatile equipment and synthetic strategies have been developed to cope with a broader range of target syntheses [23]. Whilst this equipment offers good value for high precision automation of these tasks the expansion of open-source technologies [24] such as 3D printing in the last decade dramatically expands the scope for versatile, low-cost robotics to become a practical reality across a range of modern scientific disciplines [25]. One of the most common types of user-built

3D printers is the RepRap, which has a large online, open-source support community for both hardware development of the printer as well as open-source software development, making it an ideal base for the production of automated laboratory equipment. RepRap 3D printers are often available in kit form and are inexpensive when compared to other laboratory equipment. A basic 3D printer capable of being modified to automate some laboratory functions can cost in the region of 600–700 €.

Herein we present the modification of a RepRap 3D printer to incorporate liquid handling components such that it can act as a unitary chemical synthesis robot which is capable of fabricating (3D printing) a reaction vessel and subsequently performing the complete synthesis of the common drug ibuprofen. Such low-cost, versatile robots could be adapted for use in a variety of settings, from developing laboratories and use in educational institutions to eventually expanding into a distributed manufacturing regime for chemical products.

Results and Discussion
RepRap 3D printer modification

The RepRap model modified for use was a prusa i3 model (see Figure 1). This is a fused deposition modelling (FDM)-type 3D printer, meaning it works on the principle of using a movable heated print head which extrudes molten or semi-molten material in pre-defined patterns onto a print bed by moving the heated extruder in the x and y directions. The print head is then incrementally raised in the z direction and the printing process repeated to produce the final object. Traditionally parts of this
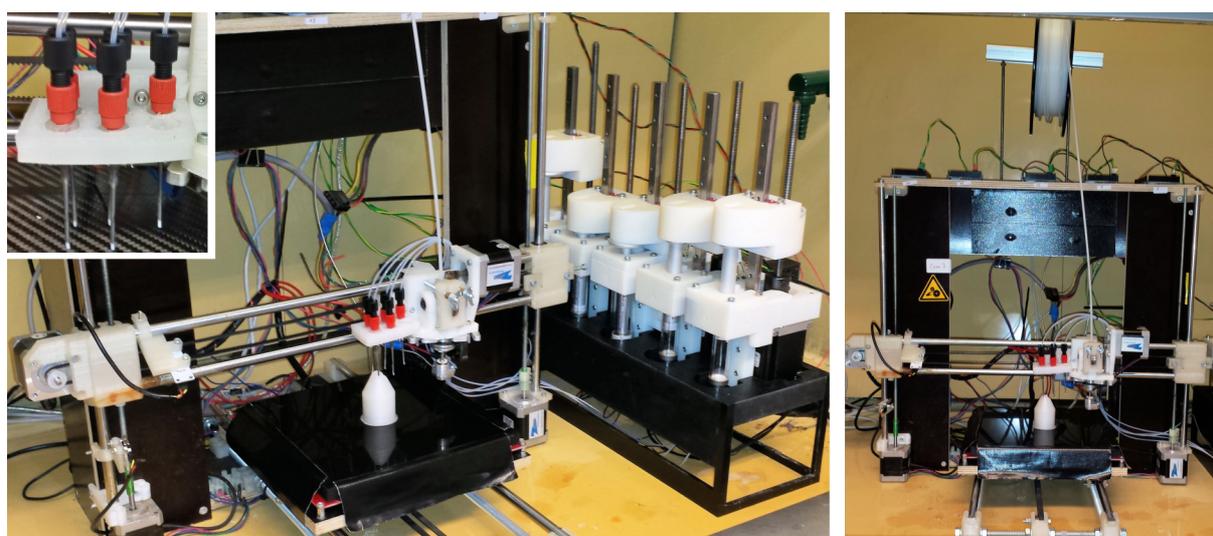
Figure 1: Prusa i3 RepRap printer modified for the automated synthesis of ibuprofen. Left: Full view of robotic platform set-up with a 3D-printed reaction vessel. Left inset: Dispensing needle carriage for 3D printing/liquid deposition. Right: Front view of the 3D-printing section of the robotic set-up with a 3D-printed reaction vessel showing the PP feedstock for reaction-vessel printing.

3D printer are constructed using components which are themselves 3D printed. These components would often be made from polylactic acid (PLA), a widely used 3D printing material. It was found, however, that it was better to construct certain components of the printer from 3D-printed polypropylene (PP) as PLA components degraded quickly if exposed to the chemical environment of a fume hood. The robot was required to have the capacity to both 3D print (for the reaction vessel) and dispense liquids, so the 3D-printing carriage was modified to incorporate both a heated extruder for 3D printing as well as a holder for the polytetrafluoroethylene (PTFE)-lined dispensing needles required for the liquid handling part (see Supporting Information File 1 for further details). These needles were connected by PTFE tubing (internal diameter 0.8 mm) to a number of automatable syringe pumps which have been developed by our group. These pumps were controlled individually by dedicated Arduino control boards and were coordinated via the process-control software developed for the robot. It was determined that the minimum number of pumps necessary to effect the synthesis of ibuprofen by our chosen route was five, to accommodate the starting materials and reagents required.

Synthetic strategy

The synthesis modified for use with our automated synthetic platform is a three-step synthesis of the popular nonsteroidal anti-inflammatory drug ibuprofen ((R,S)-2-(4-(2-methylpropyl)phenyl)propanoic acid) starting from isobutylbenzene and propanoic acid (see Scheme 1). These starting materials undergo a Friedel–Crafts acylation using trifluoromethanesulfonic (triflic) acid (CF_3SO_3H) as the Lewis acid catalyst to yield 4-isobutylpropiophenone (**2**). Once this is complete a solution of di(acetoxy)phenyl iodide ($PhI(OAc)_2$) and trimethyl orthoformate (TMOF) in methanol (MeOH) is added to the reaction mixture in order to induce a 1,2-aryl migration to produce the ibuprofen methyl ester (**3**). The latter is then hydrolysed in the final step by a potassium hydroxide solution to

produce the desired product **4** which can be retrieved after acidic work-up and column chromatography. This synthetic approach was developed by McQuade and co-workers [26] for the puposes of a continuous-flow synthesis of ibuprofen. The reaction was designed specifically such that the byproducts and excess reagents of each step were compatible with the subsequent transformations, eliminating the need for isolation and purification of intermediate products. This approach suited the development of our synthesis robot as the reaction could be performed in a one-pot manner, minimising the liquid handling necessary during the reaction sequence.

The synthetic route was modified to suit the capabilities of the automated robotic platform. For example it was not possible to completely seal the reaction vessel for the duration of the reaction, so it was not feasible to perform the reactions under inert gas atmosphere or to completely exclude atmospheric moisture from the reactions. The reaction vessels were designed to have a small aperture wide enough for only the insertion of the dispensing needle for each chemical to minimise as much as possible the interaction between the reaction and the outside atmosphere (see Figure 2). There were three reaction vessels used for the synthesis, with different capacities depending on the scale of the reaction performed. All vessels were printed using PP, a 3D-printable material which we have found to be compatible with a wide range of chemistries, including those used in this synthesis. The vessels were outwardly similar, but varied in internal volume with capacities with R1, R2 and R3 having total internal volumes of 5.96, 9.68 and 14.99 cm^3, respectively. In order to effectively print the PP reaction vessels it was necessary to replace the standard carbon fibre or glass-printing bed of the RepRap with a PP plate leading to better adhesion of the PP during printing. The print settings were adjusted such that the reaction vessels could be readily removed after the completion of the synthesis ready to repeat the process (see Supporting Information File 1 for more details).
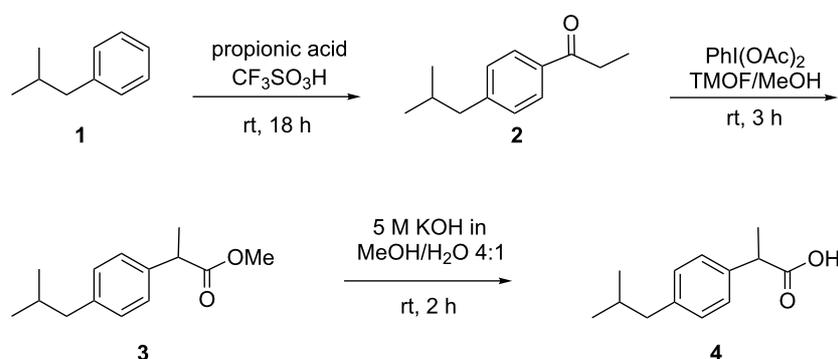
Scheme 1: Synthetic route chosen for automated synthesis robot.
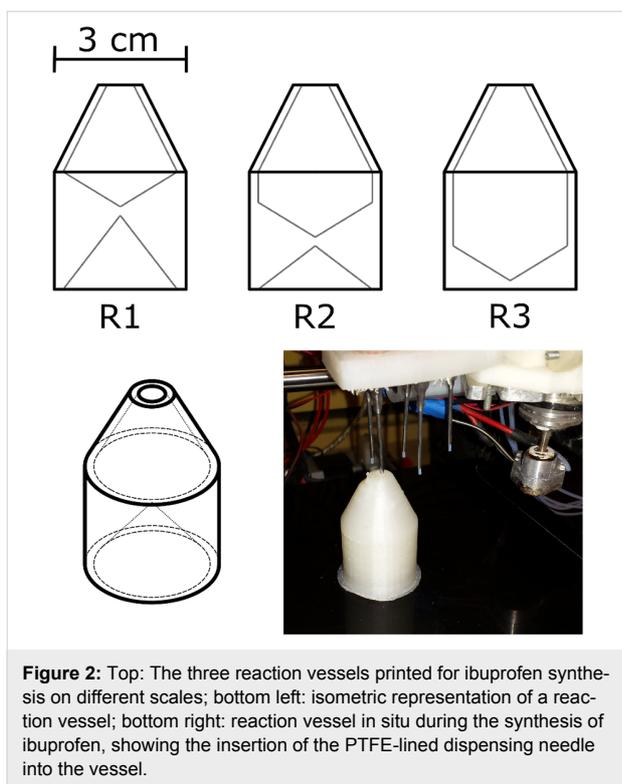
Figure 2: Top: The three reaction vessels printed for ibuprofen synthesis on different scales; bottom left: isometric representation of a reaction vessel; bottom right: reaction vessel in situ during the synthesis of ibuprofen, showing the insertion of the PTFE-lined dispensing needle into the vessel.

One of the drawbacks of using a PP-printing bed for the reactor fabrication was that, due to the poor thermal conductivity of PP, we were unable to use the RepRap's standard heated print bed to effectively heat the reaction mixture. This meant that the reactions of the sequence would have to be carried out at room temperature, leading to longer reaction times to achieve significant conversions for each of the reactions. Similarly, as it was desired that as much as possible of the equipment required for carrying out the reaction be contained entirely within the automated robotic platform it was decided not to include magnetic stirring of the reaction mixture. This would have involved the introduction of a magnetic stirring bar which could not be 3D printed and would have had to be supplied externally. In order to ensure an efficient mixing of the materials, therefore, the x–y carriage of the 3D-printing platform was programmed to oscillate rapidly in the y axis. The speed and amplitude of this oscillation could be adjusted as parameters in the control software, and were optimised at amplitude of oscillation of 30 mm at a speed of 50 mm s^{-1} for the automated reaction sequence. This proved to be sufficient for the effective mixing of the reaction media on the scales of the reaction vessels printed.

Taking all of these considerations into account the control software for the synthesis robot was designed to coordinate the movements of the 3D printer and liquid handling components in order to achieve the reaction vessel fabrication and chemical processing required for the synthesis of ibuprofen.

Process control software

The software control of the RepRap is also open source allowing the printer to be easily interfaced with user-developed modifications, allowing us to produce our own software for coordinating the 3D printing, liquid handling and reaction timing (see Scheme 2). The software to control our robotic platform was written in Python and the full source code is available from the authors. The control software was designed to be hardcoded for the specific actions required to synthesise Ibuprofen in the three-step synthesis described above, although it would be possible to build on the structure of the software to develop generic modules for liquid handling associated with the modified 3D-printer design, which could then be used to control the robot for a variety of synthetic applications. In this case the focus was on producing a single piece of software which could achieve the fabrication of a reaction vessel, and complete the synthesis of ibuprofen without human intervention other than to ensure the robot was supplied with the necessary reagents and materials (chemical starting materials and thermoplastic stock for the printing of the reaction vessel). This code could then act as a fully self-contained set of synthesis procedures which could be shared with other users as a pre-validated synthesis program to be used with similar robotic systems to achieve the same synthesis.

The control software was designed to first print the reaction vessel used for the ibuprofen synthesis. The software uses the API of an open source 3D-printer control software called Octo-Print (run from source code, available at http://octoprint.org/), which is used to send the gcode (i.e., the 3D-printing instructions) to the printer and perform the 3D printing of the reaction vessel. This process takes about two hours. After this the Octo-Print connection to the printer is terminated and the program connects directly to the firmware of the printer through a serial connection. This connection is used to send the movement commands the printer. The control software has a set definition of the position of each of the dispensing needles for the individual chemicals and the reaction vessel is designed in such a way that the opening for the vessel is positioned at the centre point of the print bed to ease the programming of the dispensing positions. Parameters such as the volume of each chemical to be dispensed into the robot, the amount by which the robot should overdraw each chemical (i.e., the dispensing volume plus an arbitrary amount to ensure that the full volume can be dispensed during the synthesis) are collected together in the source code as user definable variables which can be set depending on the scale of the synthesis required.

For debugging and optimisation purposes all of the programmed routines contain various debug levels where the program intercepts at predefined points (or in the highest level at every step)

Scheme 2: The digitisation of the synthesis of ibuprofen. This flow diagram shows the individual steps of the process control software written to control the chemical synthesis robot.
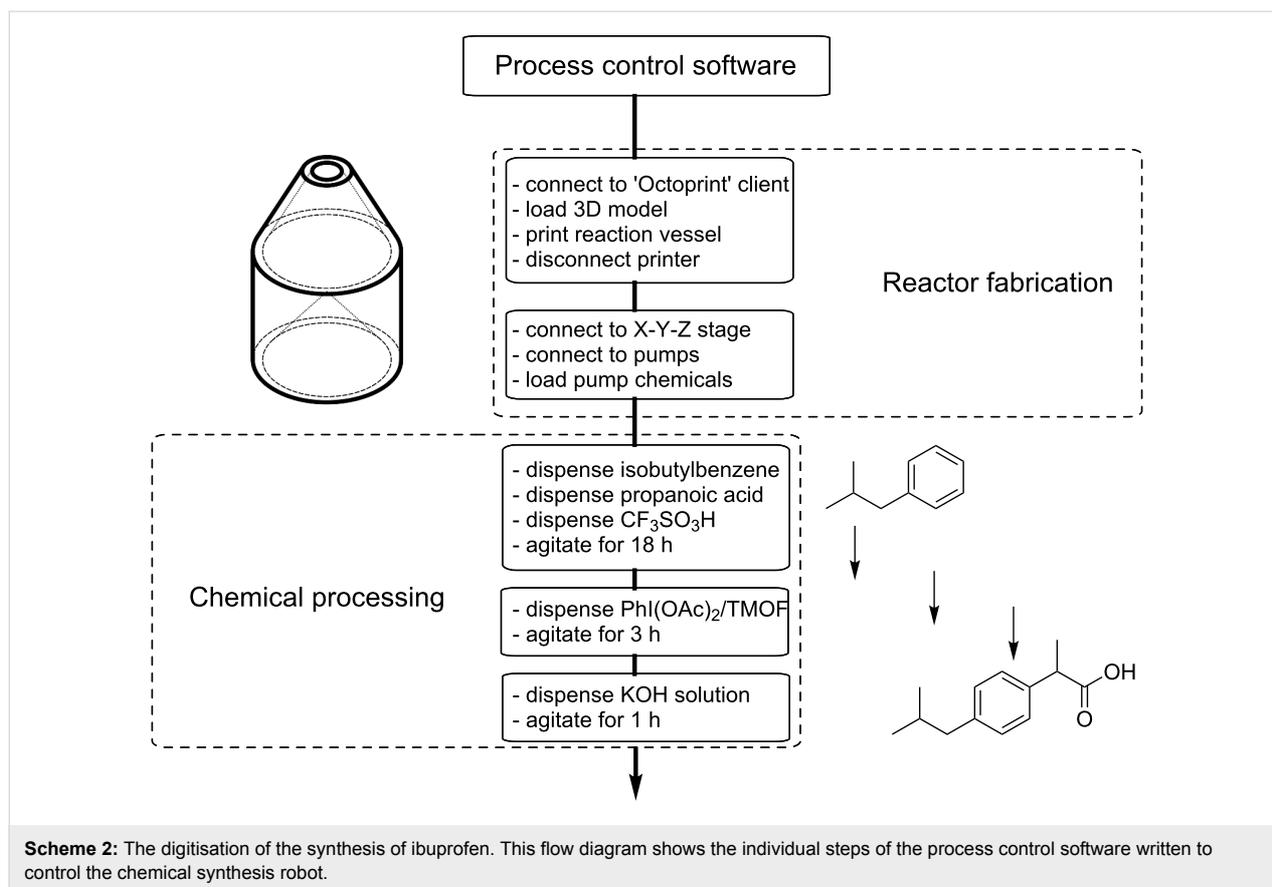
and waits for the user to acknowledge to go ahead or skip the current step. This is particularly useful when only a small part of the program needs to be tested in the bigger context of the rest of the source code. All working steps can simply be skipped without actually deactivating the responsible code.

Automated ibuprofen synthesis

The automated synthesis of ibuprofen is initiated with the running of the control software which then proceeds to print the specified reaction vessel. Once this was complete the appropriate pumps were charged with the starting materials solutions (see Table 1) and the control software continued with the automated reaction scheme until the final product solution was ready to be collected. The total time for the completed synthesis was approximately 24 hours, during which time the synthesis robot required little to no interaction from human operators.

For the first reaction, chloroform solutions of isobutylbenzene (1.0 M) and propanoic acid (1.0 M) were deposited into the reaction vessel, followed by the dropwise addition of triflic acid over the course of 10 min to minimise the exotherm produced. Once this process was completed the dispensing needle is raised from the aperture and the reaction is agitated. After 18 h of agitation the needle corresponding to the PhI(OAc)$_2$/TMOF

Table 1: Contents of the automated syringe pumps controlled by the automated synthesis robot.

Pump no.	Contents
1	isobutylbenzene[a]
2	propanoic acid[a]
3	triflic acid[b]
4	PhI(OAc)$_2$/MeOH/TMOF[c]
5	KOH[d]

[a]1.05 M in CHCl$_3$; [b]neat; [c]PhI(OAc)$_2$ was prepared as a 1.4 M solution in a mixture of MeOH/TMOF (1:0.8 v/v); [d]5 M in MeOH/H$_2$O 4:1.

solution is lowered into the aperture of the vessel and this solution is once again dispensed dropwise over the course of 10 min. This is followed by further agitation for 3 h, after which the final solution of KOH (5 M in MeOH/H$_2$O 4:1 v/v) is added, again dropwise over the course of 10 min, followed by agitation for 1 h. After this step the robot returns to its home position and the reaction mixture can be retrieved yielding, after acidic work-up and column chromatography, ibuprofen in yields of up to 34% over three steps (average of 6 automated runs). The PP reactors showed no evidence of degradation due to the reaction sequence performed, and could be effectively cleaned for reuse as a reaction vessel, all yields, however, were

calculated from fully automated runs of the control software including the reaction vessel printing stage. During the testing phase of the robot, the progress of each of the reactions was monitored by using the debug feature of the process control software. For this progression was paused after each stage and aliquots taken from the reaction mixture to be analysed by NMR to ensure the synthesis was proceeding as planned (giving approximate yields by ^{1}H NMR of 71% for the initial acylation step and 64% for the subsequent rearrangement, see Supporting Information File 1). Thus using the automation of the robot enables a 'debugging' of the chemical processes as well as the control software. However, once the synthetic procedure and parameters were defined the robot was capable of performing the reaction in an autonomous fashion (for a demonstration of the liquid handling steps of the automated reaction sequence, see Supporting Information File 3). Due to the automated nature of the process, the scale of the synthesis could be modified simply by adjusting the parameters in the process control program and ensuring that the reaction vessel design is appropriate for the reaction scale desired. To this end the synthesis of ibuprofen was completed on three different scales by fabricating different reaction vessels (R1–R3) and varying the software parameters controlling the volumes of each of the reaction solutions deposited. These could be easily tuned in the control software and the volumes required for each of these scales are summarised in Table 2. The yields from each of the scales of reaction described were similar (see Supporting Information File 1), however, it was found that further scale-up by increasing the reaction vessel volume (a fourth reaction vessel, R4, was also produced with an internal volume of 28.12 mL, see Supporting Information File 2 for dimensions) lead to reduced yields and longer reaction times. The maximum yield obtained using larger volume reactor vessels was approximately 12% isolated yield of ibuprofen. However the larger vessels also suffered from repeatability problems with less reliability in the yields obtained. These effects are presumably due to a less efficient mixing of the reaction media by agitation in the larger volume of the reaction vessel. This could be remedied by 'numbering up' the reaction vessels that the robotic platform prints in the initial stage and adjusting the control software such that several reactions could be run in parallel to increase the yield of ibuprofen.

Once the reaction sequence had been completed the final reaction mixture was removed from the reaction vessel by syringe and diluted with water. After acidic work-up the residue was purified by reversed-phase column chromatography on C18 (60% MeCN/H$_2$O) to give ibuprofen (**4**) as a white powder. The isolated and averaged yields obtained from six independent automated runs of the system at different scales are given in Table 3 below. There appears to be little depreciation of effi-

Table 2: Pump contents and reaction volumes.

Pump number	Withdrawn volume (mL)	Deposited volume (mL)	Reaction vessel
1	1.5	0.2	R1
		0.4	R2
		0.8	R3
2	1.5	0.2	R1
		0.4	R2
		0.8	R3
3	3.0	0.35	R1
		0.7	R2
		1.4	R3
4	10.0	1.5	R1
		3.0	R2
		6.0	R3
5	10.0	2.0	R1
		4.0	R2
		8.0	R3

Table 3: Isolated ibuprofen yields for automated synthesis.

Reaction vessel	Automated run	Ibuprofen yield, mg (%)	Average yield (%)
R1	1	15.9 (36)	32.1
	2	12.8 (29)	
	3	17.0 (39)	
	4	10.2 (24)	
	5	15.3 (35)	
	6	13.1 (30)	
R2	1	28.5 (33)	34.2
	2	26.7 (31)	
	3	33.2 (38)	
	4	31.0 (36)	
	5	27.5 (32)	
	6	29.9 (35)	
R3	1	60.1 (34)	33.7
	2	57.0 (33)	
	3	61.6 (36)	
	4	58.2 (34)	
	5	60.5 (35)	
	6	51.7 (30)	

ciency of the reaction sequence on the reaction scales with isolated yields varying from 24% to 38%.

Conclusion

By modifying a relatively inexpensive 3D-printing platform we were able to construct a unitary 'synthesis robot' which is capable of autonomously fabricating a reaction vessel and performing the liquid handling steps necessary to effect the synthesis of the common painkiller ibuprofen. This example demon-

strates the unique versatility of the current generation of open-source consumer robotic equipment to be modified for use in laboratory automation. Using this synthesis robot we were able to synthesise the popular drug ibuprofen on three different reaction scales using a piece of custom software to control the parameters of the synthesis. Future developments in this field could include the development of further open source solutions to allow robotic platforms to perform more of the routine functions of chemical synthesis such as work-up and purification routines. The widespread use of such low-cost automation of chemical synthesis could allow the development of an 'open source' approach to chemical synthesis itself where synthetic routines can be downloaded and tested by any laboratory with the necessary robotic platform, advances in the chemical automation equipment could then run in parallel with advances in the synthetic strategies used. Finally, this work shows how chemical synthesis can be fully digitized into a standalone code and autonomously run on a robotic system. Not only could this potentially overcoming reproducibility issues that can limit the exchange of synthetic chemistry, but allow users to share their code thereby allowing more complex molecules to be designed and made within autonomous chemical robots.

Supporting Information

Supporting information is available containing full experimental details, the source code of the process control software, along with information on the 3D printing settings for the reactor vessel fabrication. Also available are a video demonstrating the liquid handling for the automated reaction sequence and the .STL digital model files of the reactor vessels fabricated by the robotic platform.

Supporting Information File 1
Full experimental details, the source code of the process control software, along with information on the 3D printing settings for the reactor vessel fabrication.
[http://www.beilstein-journals.org/bjoc/content/supplementary/1860-5397-12-276-S1.pdf]

Supporting Information File 2
Digital 3D model files archive for the reaction vessels used.
[http://www.beilstein-journals.org/bjoc/content/supplementary/1860-5397-12-276-S2.zip]

Supporting Information File 3
Demonstration video of the liquid handling of the automated reaction sequence.
[http://www.beilstein-journals.org/bjoc/content/supplementary/1860-5397-12-276-S3.mp4]

References

1. Dimitrov, D.; Schreve, K.; de Beer, N. *Rapid Prototyping J.* **2006,** *12,* 136–147. doi:10.1108/13552540610670717
2. Bogers, M.; Hadar, R.; Bilberg, A. *Technol. Forecast. Social Change* **2016,** *102,* 225–239. doi:10.1016/j.techfore.2015.07.024
3. Rengier, F.; Mehndiratta, A.; von Tengg-Kobligk, H.; Zechmann, C. M.; Unterhinninghofen, R.; Kauczor, H.-U.; Giesel, F. L. *Int. J. Comput. Assisted Radiol. Surg.* **2010,** *5,* 335–341. doi:10.1007/s11548-010-0476-x
4. Skoog, S. A.; Goering, P. L.; Narayan, R. J. *J. Mater. Sci.: Mater. Med.* **2014,** *25,* 845–856. doi:10.1007/s10856-013-5107-y
5. Li, X.; Cui, R.; Sun, L.; Aifantis, K. E.; Fan, Y.; Feng, Q.; Cui, F.; Watari, F. *Int. J. Polym. Sci.* **2014,** No. 829145. doi:10.1155/2014/829145
6. Hollister, S. J. *Nat. Mater.* **2005,** *4,* 518–524. doi:10.1038/nmat1421
7. Boland, T.; Xu, T.; Damon, B.; Cui, X. *Biotechnol. J.* **2006,** *1,* 910–917. doi:10.1002/biot.200600081
8. Zhang, Y.; Tse, C.; Rouholamin, D.; Smith, P. J. *Cent. Eur. J. Eng.* **2012,** *2,* 325–335. doi:10.2478/s13531-012-0016-2
9. Kolesky, D. B.; Truby, R. L.; Gladman, A. S.; Busbee, T. A.; Homan, K. A.; Lewis, J. A. *Adv. Mater.* **2014,** *26,* 3124–3130. doi:10.1002/adma.201305506
10. Ilievski, F.; Mazzeo, A. D.; Shepherd, R. F.; Chen, X.; Whitesides, G. M. *Angew. Chem., Int. Ed.* **2011,** *50,* 1890–1895. doi:10.1002/anie.201006464
11. Wehner, M.; Truby, R. L.; Fitzgerald, D. J.; Mosadegh, B.; Whitesides, G. M.; Lewis, J. A.; Wood, R. J. *Nature* **2016,** *536,* 451–455. doi:10.1038/nature19100
12. Ivanova, O.; Williams, C.; Campbell, T. *Rapid Prototyping J.* **2013,** *19,* 353–364. doi:10.1108/RPJ-12-2011-0127
13. Symes, M. D.; Kitson, P. J.; Yan, J.; Richmond, C. J.; Cooper, G. J. T.; Bowman, R. W.; Vilbrandt, T.; Cronin, L. *Nat. Chem.* **2012,** *4,* 349–354. doi:10.1038/nchem.1313
14. Kitson, P. J.; Glatzel, S.; Chen, W.; Lin, C.-G.; Song, Y.-F.; Cronin, L. *Nat. Protoc.* **2016,** *11,* 920–936. doi:10.1038/nprot.2016.041
15. Dragone, V.; Sans, V.; Rosnes, M. H.; Kitson, P. J.; Cronin, L. *Beilstein J. Org. Chem.* **2013,** *9,* 951–959. doi:10.3762/bjoc.9.109
16. Kitson, P. J.; Symes, M. D.; Dragone, V.; Cronin, L. *Chem. Sci.* **2013,** *4,* 3099–3103. doi:10.1039/C3SC51253C
17. Kitson, P. J.; Marshall, R. J.; Long, D.; Forgan, R. S.; Cronin, L. *Angew. Chem., Int. Ed.* **2014,** *53,* 12723–12728. doi:10.1002/anie.201402654
18. Kitson, P. J.; Rosnes, M. H.; Sans, V.; Dragone, V.; Cronin, L. *Lab Chip* **2012,** *12,* 3267–3271. doi:10.1039/c2lc40761b
19. Mathieson, J. S.; Rosnes, M. H.; Sans, V.; Kitson, P. J.; Cronin, L. *Beilstein J. Nanotechnol.* **2013,** *4,* 285–291. doi:10.3762/bjnano.4.31
20. Olsen, K. *J. Lab. Autom.* **2012,** *17,* 469–480.

21. Boyd, J. *Science* **2002,** *295,* 517–518.
    doi:10.1126/science.295.5554.517
22. Ley, S. V.; Fitzpatrick, D. E.; Ingham, R. J.; Myers, R. M.
    Angew. Chem., Int. Ed. **2015,** *54,* 3449–3464.
    doi:10.1002/anie.201410744
23. Li, J.; Ballmer, S. G.; Gillis, E. P.; Fujii, S.; Schmidt, M. J.;
    Palazzolo, A. M. E.; Lehmann, J. W.; Morehouse, G. F.; Burke, M. D.
    Science **2015,** *347,* 1221–1226. doi:10.1126/science.aaa5414
24. Pearce, J. M. Introduction to Open-Source Hardware for Science.
    Open-Source Lab; Elsevier: Boston, 2014; pp 1–11.
    doi:10.1016/B978-0-12-410462-4.00001-9
25. Coakley, M.; Hurt, D. E. *J. Lab. Autom.* **2016,** *21,* 489–495.
26. Bogdan, A. R.; Poe, S. L.; Kubis, D. C.; Broadwater, S. J.;
    McQuade, D. T. *Angew. Chem., Int. Ed.* **2009,** *48,* 8547–8550.
    doi:10.1002/anie.200903055

Extrusion – back to the future: Using an established technique to reform automated chemical synthesis

Deborah E. Crawford

Review

Abstract

Herein, the benefits which extrusion can provide for the automated continuous synthesis of organic compounds are highlighted. Extrusion is a well-established technique that has a vital role in the manufacturing processes of polymers, pharmaceuticals and food products. Furthermore, this technique has recently been applied to the solvent-free continuous synthesis of co-crystals and coordination compounds including metal-organic frameworks (MOFs). To date, a vast amount of research has already been conducted into reactive extrusion (REX), particularly in the polymer industry, which in many cases has involved organic transformations, however, it has not received significant recognition for this. This review highlights these transformations and discusses how this previous research can be applied to the future of organic compound manufacture.

Review

Extrusion methodology

Extrusion is an umbrella term covering a family of processes that involves the movement of material through a confined space, most typically along a set of screws – screw extrusion. There are two main types of screw extrusion – single (SSE) and twin screw (TSE) (Figure 1) [1-3]. As the names suggest, SSE involves the movement of material by one screw, whereas TSE, which is more frequently employed, involves the movement of material by two, i.e., the material is conveyed from one screw to the other as it makes its way along the extruder barrel [4].

Both techniques process materials by mixing, heating and also by applying mechanical energy. The main forces present in an extrusion process are compression forces and shear. However, the methodology of each technique differs significantly, as well as the applications for which they are employed, for example SSE is typically used to carry out hot melt extrusion (HME), where the emphasis is on the melting of material for thorough mixing and processing [5]. The process can be adapted via modulation of the screw, as depicted in Figure 2, to make the
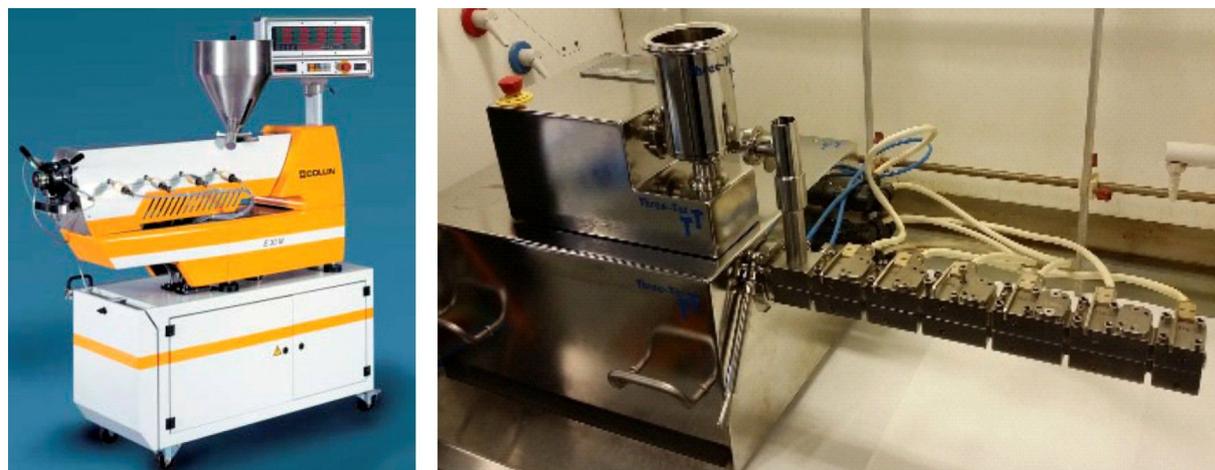
Figure 1: Typical pilot scale single screw extruder (left) and a laboratory scale twin screw extruder (right).

process more efficient. An industrial single screw extruder typically has a screw diameter ranging from anywhere between 1 inch and 24 inches. Principally, the root diameter (the diameter of the central part of the screw) of the screw increases along its length, this is to i) provide greater free volume at the beginning of the 'starve-fed' extruder for maximum feeding of material and ii) to increase the compressive forces at a later stage of the process, as a result of the volume being reduced, whilst a large amount of material is still present [3]. This also results in an increase of the shear applied to the material, as it experiences friction from moving between both the screw and the barrel walls. In addition, a kneading segment can be added at the end of the screw, to provide a region of intense mixing (with increased shear) before the material exists the extruder. It must be noted that the flow of material along a single screw extruder is essentially reliant on the feeding of material into the barrel, which provides a forward pressure so that the material can exit the barrel [5].

TSE however employs two intermeshing screws and it is mainly the movement of material from one screw to the other, and back again, that conveys the material along the barrel. The configuration of these screws is generally more intricate and typically comprised of a series of alternating conveying and kneading segments (Figure 3). The main advantage of employing modulated screws is that the screw configuration can be adjusted for each process. The conveying segments are generally of quite large channel depth, i.e., the radial distance between the flight tip and the screw root (ca. 2–3 mm for smaller extruders, and several centimetres or inches for extruders employed in industry), but again as with SSE, this channel depth decreases along the screw length, resulting in an increase of the compressive forces and shear. The equivalent to channel depth within continuous flow chemistry is typically very narrow of several millimetres. Furthermore, the kneading segments can be positioned at angles of 30º, 60º and 90º relative to each other, with the latter angle providing the greatest kneading (and shear). The kneading section can be quite hostile as it involves not just mixing, but also the grinding of the material, which resultantly leads to changes in the material properties, most commonly its rheology [3]. Furthermore, the mechanical energy applied to the system can be controlled by the screw profile, as well as the residence time which is not only dependent on screw speed, but on the configuration too, allowing it to be prolonged if required. Modification of the screw profile, by inserting additional segments or those of a different configuration, e.g., toothed seg-

Figure 2: PTFE screw employed in single screw extrusion, with increasing root diameter (RD) from 45 mm to 95 mm and a final kneading section.

Figure 3: Modulated stainless steel intermeshing co-rotating screws employed typically in twin screw extrusion, comprised of conveying and kneading segments.
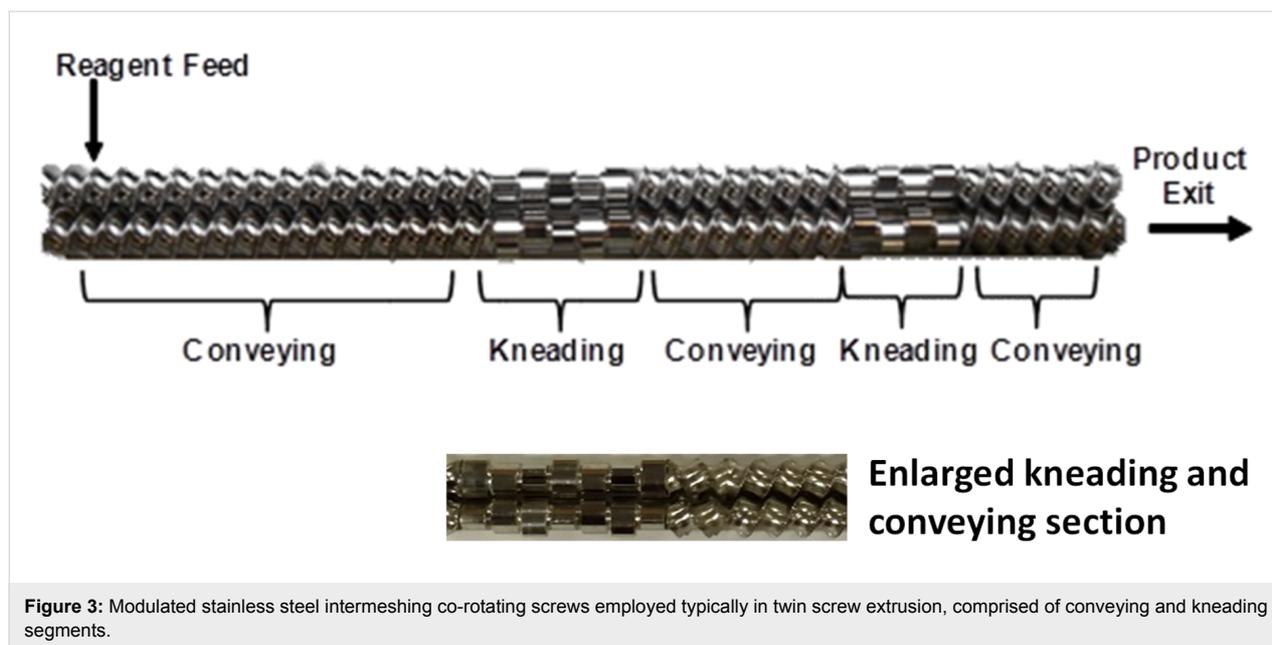
ments, can result in some control of the temperature as well, screw segments that apply greater mechanical energy may result in a greater amount of frictional heat being produced, particularly in comparison to those segments which provide less vigorous kneading.

Both single and twin screw extruders range from 10–443 mm in screw diameter [6] and extrusion processes are scalable to produce large quantities of materials in the range of tonnes per hour as a result of the extensive engineering research. Herein, a focused discussion of the reactive processes carried out by extrusion is provided. A substantial amount of the organic transformations carried out by extrusion has been in the polymer industry, however, most of these processes have been overlooked by synthetic chemists. In fact, the authors of these REX processes have focused mainly on optimising the process conditions and have not discussed the chemistry itself. It is hoped that this article will show readers that there is an extensive amount of research into continuous organic transformations by extrusion and encourage them to consider the potential that extrusion holds for continuous chemical synthesis, particularly under solvent-free conditions.

Reactive extrusion (REX)

Extrusion is employed most frequently in the polymer industry, generally for the dispersion of materials (e.g., graphene or quantum dots) into polymers [7]. However, REX is also employed as a technique to synthesise polymers or to carry out post synthetic polymer modification (e.g., functionalisation of polymer chains) via organic transformations, which in turn alters the properties of the materials [6].

Initially, the polymer industry employed only batch mixers to synthesise polymers and carry out post synthetic modification (PSM), however, this proved difficult and inefficient. This was due to a dramatic increase or change in the viscosity and rheology of the material, a common feature of REX, and therefore as reactions proceed, they can become very difficult to mix efficiently, leading to low conversions. A second problem associated with the change in viscosity is the resultant poor heat transfer, meaning that longer heating times are required, which often leads to polymer degradation. Employing extrusion overcame these issues. REX is now initially carried out in a batch mixer and the material is subsequently transferred to an extruder. This allows for fresh, thin reactive surfaces to be exposed, which encourages these reactions to go to completion [8]. Overall, the time required to carry out these processes was reduced, as well as the time during which the material is exposed to heat, therefore preventing polymer degradation [9,10].

There are five main types of reactive polymerisation for which extrusion has been employed, containing some clear examples of organic transformations. One of the most common forms is bulk polymerisation, involving the formation of a polymer (linear, branched and crosslinked) of high molecular weight starting from a series of monomers [11]. Bulk polymerisation will be discussed in detail, however, it is worthwhile noting the other various reaction types explored by extrusion:

- Grafting reactions – a grafted polymer is synthesised from the reaction of a polymer and a functionalised monomer [12].

- Functionalisation – this takes place on already prepared polymers, when the polymer is either functionalised by the modification or addition of a functional group [13].
- Controlled degradation – degradation and crosslinking of polymers to produce a product with controlled molecular weight distribution. This results in a higher number of active sites that can later be used for grafting [13].
- Reactive blending – this involves the extrusion of two or more compatible polymer blends, leading to the formation of a polymer–polymer complex [13].

Bulk polymerisation involves several common organic transformations, including living polymerisation, polyaddition, radical and polycondensation polymerisation. Living polymerisation, the most common transformation, involves the constant growth of a polymer chain where the ability to terminate the reaction is removed [14]. Again, there are several types of transformation including ionic polymerisation, ring opening metathesis, free radical and growth polycondensations [15]. All of which have been shown to be successful by extrusion.

Living polymerisation

There have been several publications on the use of living anionic polymerisations in the preparation of polystyrene. Höcker et al. have investigated the role of extrusion in i) the preparation of this polymer and ii) the sequential postsynthetic modification of polystyrene by isoprene [16]. The authors focus mainly on the engineering aspects of the project rather than the chemical reaction itself. The first part of the process involves the chemical reaction between styrene and *s*-BuLi, which is employed as an initiator (Scheme 1). The *s*-BuLi reacts with the double bond of styrene, initiating a homopolymerisation process. Once all the monomer is consumed, the polymer has a stable anionic

Scheme 1: Polymerisation of styrene using *s*-BuLi as an initiator.

polymer chain, which allows for further functionalisation by reaction with electrophilic functional groups.

The solution-based living polymerisation reactions are typically dependent on the solvent employed, temperature and concentration [17], however, when they are conducted by extrusion, they are carried out under solvent-free conditions, which is a major advantage. It must also be noted that to carry out a reaction solvent-free, when a pyrophoric reagent, such as *s*-BuLi, is involved is quite remarkable, and it is carried out as a continuous process and not on a small scale. This suggests that solvent-free extrusion can be on par with continuous flow technology, allowing a wider range of hazardous reagents to be used continuously and on large scale.

Furthermore, Höcker et al. report the post polymerisation of polystyrene with isoprene, which is actually carried out in the same processing line as the polymerisation of styrene, i.e., styrene is polymerised initially in the extruder barrel and isoprene is fed into the barrel at a later point to react with polystyrene in a second reaction (Scheme 2) [16]. This is an example of telescoping which is considered to be very advantageous in continuous flow technology for example. As a result of being able to carry out polymerisation and post polymerisation functionalisation by TSE, different polymer geometries can be achieved, for example a star or comb-shaped polymer [18,19].

Scheme 2: Telescoping process of the formation of polystyrene, followed by post polymerisation functionalisation with isoprene. The figure depicts the screw configuration employed and each reaction. Adapted from [16].

This indicates that large molecules of well-defined architecture, in addition to polymers, could be synthesised by TSE. It must also be noted that these processes were optimised in order to have throughput rates of ca. 3–10 kg h^{-1} (after both transformations have been carried out) [16]. Unfortunately, there is no example in the literature for this reaction carried out in batch, however, Meyer reports on the general scalability of batch polymerisation and comments that up to 200 kg d^{-1} quantities can be obtained. It must be noted, however, that the reaction reported by Höcker involves the use of *s*-BuLi, making the process more difficult, but still a greater throughput rate is obtained than that predicted by Meyer [20].

Free radical polymerisation involving deactivation polymerisation, iniferter polymerisation and reversible addition fragmentation chain transfer (RAFT) polymerisation, amongst others [21], has been studied extensively by extrusion to produce, for example, branched polypropylene, polyethylene and polylactide polymers. The process involves the production of a free radical at the end of an active polymer chain, and is further characterised as living free radical polymerisation due to the complete absence of a termination reaction [22]. Narayan et al. report the branching of polylactide by TSE, during which the molecular weight of polylactide was increased dramatically at 170–180 °C

[23]. This work highlights another advantage of extrusion in that the barrel can have separate heating zones (some also provide cooling), allowing the temperatures to be varied along the production line. In addition, due to the low free volume of the extruder barrel, but the high throughput rates achievable by extrusion, the material has a resultantly higher surface area exposed directly to heat. The material is exposed to heat usually only for a couple of minutes, which then avoids polymer degradation [3].

Narayan reports the addition of an initiator, Lupersol, a di-tertiary alkyl peroxide which produces free radicals in bulk, to the formation of polylactide. Another advantage is that Lupersol is a food additive and is approved by the Food and Drug Administration (FDA). Furthermore, the authors hypothesise a mechanism by which the branching of polylactide is occurring, suggesting that the initial polymer undergoes a hydrogen radical abstraction, followed by radical coupling and finally chain scission (Scheme 3) [23].

Polyaddition polymerisation

Another common form of polymerisation is polyaddition polymerisation, an example is the formation of polyurethane from a reaction between an isocyanate and a hydroxy functional group

Scheme 3: Proposed mechanism for the branching of polylactide. Adapted from [23].
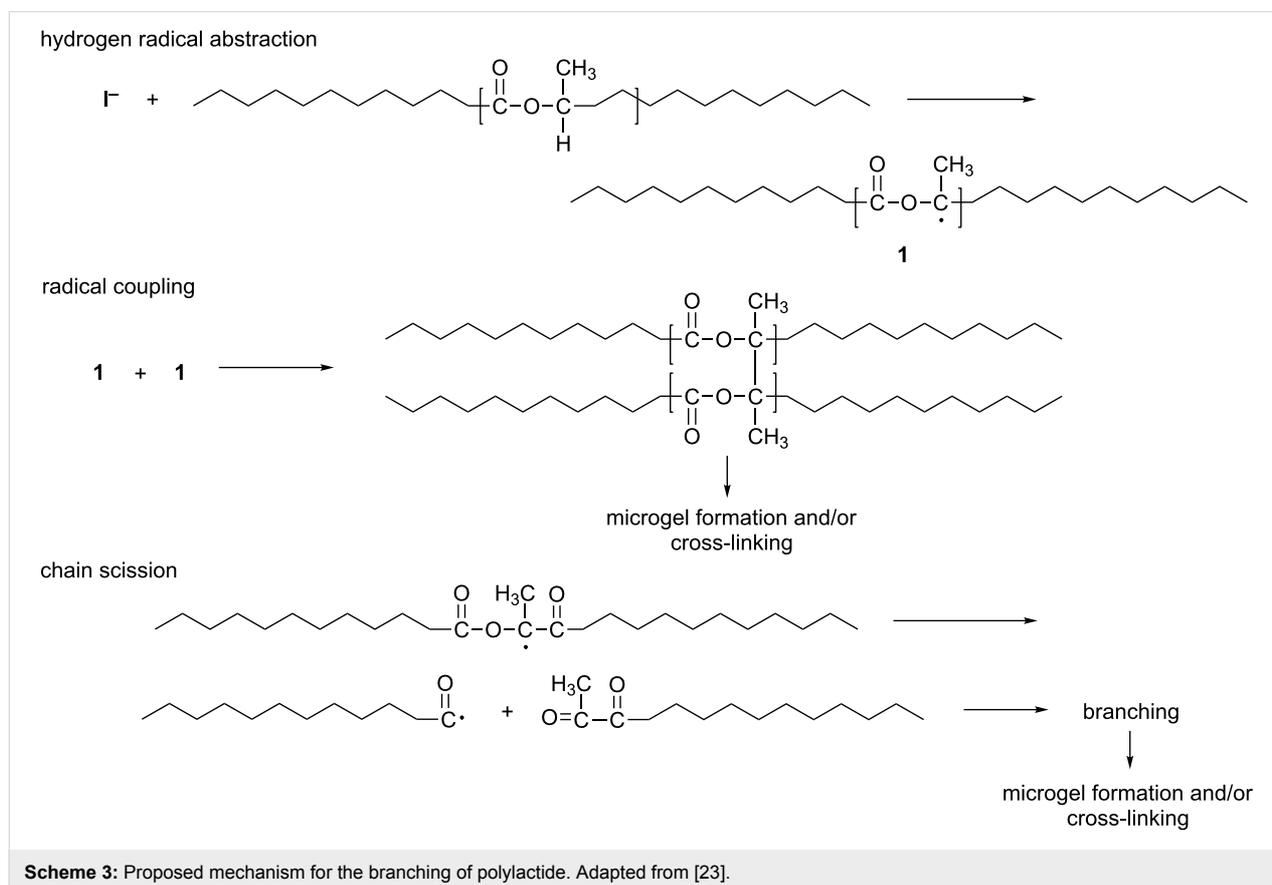
(Scheme 4). Polyaddition involves the addition of monomers onto an actively growing polymer chain; however, there is also 'step growth polymerisation' which is employed in the formation of polyurethane. Step growth polymerisation involves a gradual approach to the polymer by initially forming a dimer from multifunctional monomers, which then forms a trimer, then oligomer and finally a polymer (Figure 4) [24].
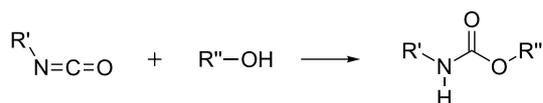
Scheme 4: Chemical reaction between isocyanate and an alcohol to form polyurethane.
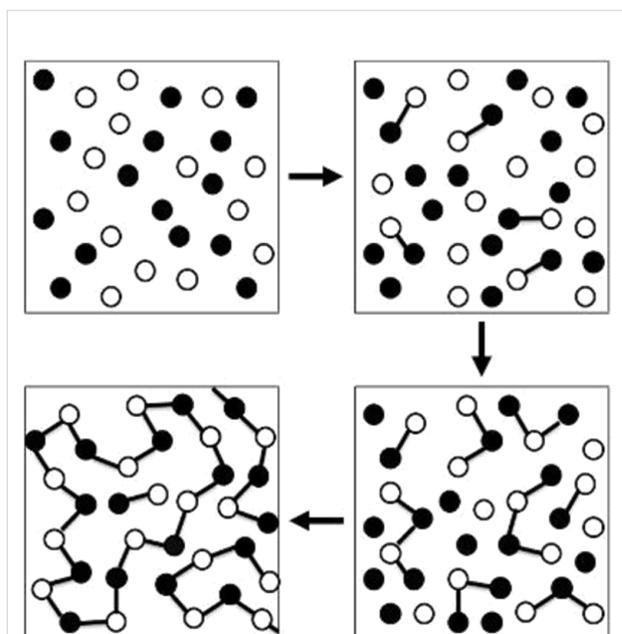
Figure 4: Representative diagram explaining the process involved in step growth polymerisation, which involves the formation of a dimer, then trimer followed by oligomer synthesis. Taken from [24].

Kim and Hyun report the synthesis of polyurethane, discussing the associated numerical simulation they conducted to determine the dependency of shear rate on viscosity, rheology and the kinetics of formation also. The authors report that a reaction between 4,4'-diphenylmethane diisocyanate, polycaprolactonediol and 1,4-butanediol takes place in a twin screw extruder, employing a screw speed of 15 rpm and a temperature of 60 °C [25]. This transformation was conducted in the presence of a catalyst – dibutyltin diaurate. The authors focus on the processing of this reaction rather than the chemistry taking place itself, however, this is one of the most traditional organic transformations carried out by TSE to date, carried out on a continuous scale whilst being metal catalysed by an organotin compound. It must be highlighted that the residence times for these reactions are relatively short at ca. 10 minutes, particularly upon comparison with the time required to carry out conventional organic synthesis, yet the process still forms the desired polymers of high molecular weight at moderate temperatures of 60 °C [25].

Polycondensation polymerisation

Finally, another important example of organic synthesis in the production of polymers is the polycondensation reaction to produce polymers such as polyamides. There are numerous patents on this application of polymer extrusion [26-28]. The reactions work very well by TSE as a result of being able to heat the extruder barrel to temperatures greater than that of boiling water. As a result, water (reaction byproduct) is removed during the extrusion process, driving the reactions to completion. Typically, reactions are carried out between diamines and an anhydride, dicarboxylic acid or a dicarbonyl compound (Scheme 5). Takekoshi et al. released a patent demonstrating the ability of extrusion to form a variety of different polyimides by extrusion in a completely solvent-free, continuous manner. Polycondensations were performed at temperatures between 210–350 °C, it can therefore be speculated that the high temperatures are required to accelerate the polymerisation reaction, rather than just drive off the water byproduct [29]. Batch synthesis of polyimide polymers typically involves mixing for 48 hours at temperatures ranging from room temperature to 250 °C [30].
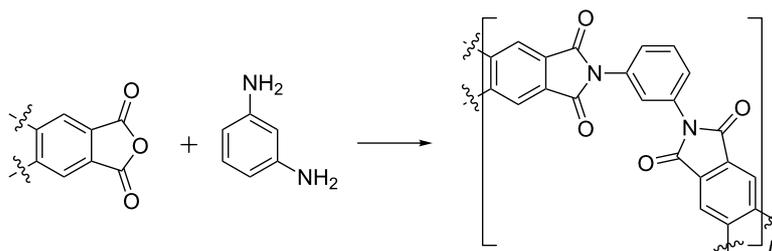
Scheme 5: Generic polycondensation reaction to produce polyamides.

Chemical synthesis by extrusion

Extrusion is heavily relied upon within the pharmaceutical industry with regards to the formulation of drugs and their incorporation into drug delivery systems. However, extrusion has not been employed to carry out any organic compound or active pharmaceutical ingredient (API) synthesis in this industry. There has been some research in the last decade demonstrating the preparation of cocrystals by hot melt extrusion (HME) and liquid assisted extrusion. This work has been essentially conducted by Amgen, preparing cocrystals consisting of a pharmaceutical component [31-33]. There is currently extensive research being carried out into the effectiveness of cocrystals as medicinal products due to the higher dissolution rates they provide. Therefore, in order to employ cocrystals as drugs available to patients, not only is research into their bioavailability being conducted, but also into manufacturing techniques that could be utilised for their production. Currently, research into non-solvent based synthetic methods is being pursued to eliminate the influence that the solvent has over the cocrystal formed.

Cocrystal formation

In 2009, Alvarez-Nunez et al. of Amgen used TSE to scale up the synthesis of a cocrystal which had already been reported to be synthesised successfully by ball milling (employing liquid-assisted grinding (LAG)). This was the first example demonstrating that mechanochemical synthesis could be scaled up to several hundred grams and carried out continuously by employing hot melt extrusion (HME) [31,34]. Initially two cocrystals were optimised – a cocrystal formed from caffeine and oxalic acid and another consisting of AMG517 (a selective TRPV1 antagonist) and sorbic acid [31].

Since the publication of this work, Moradiya et al. (of Amgen) have reported the synthesis of carbamazepine-saccharin cocrystals by both TSE and SSE techniques [35]. Moradiya et al. found some difficulties in regards to maintaining an exact stoichiometry of cocrystal components – any deviation from the correct stoichiometry could potentially lead to undesirable variations in the properties of the product. Kulkarni et al., however, demonstrated that this issue could be resolved by careful manipulation of the extruder temperature [36], demonstrating that in the extrusion of a 2:1 mixture of caffeine/malic acid, extrusion temperatures of below 104 °C favoured the formation of a 1:1 product. Increasing to above 104 °C however resulted in the subsequent melting of the 1:1 product, followed by formation of the desired 2:1 cocrystal.

There are now several examples of cocrystal formation by HME present in the literature (<30 publications, mainly from researchers at Amgen) and studies on the extrusion process

itself with regards to cocrystal manufacture is also gaining momentum. There are a few publications investigating the effect of screw speed and temperature on the process [37]. There is also an example in the literature demonstrating the utilisation of near-infrared spectroscopy for online monitoring to determine where in the extruder the cocrystal begins to form. Consequently this also provides feedback regarding screw configuration and deductions can be made as to whether sufficient mechanical energy is being applied in order to achieve 100% conversion to product for example [38].

Mechanistically, it was initially believed that the formation of a eutectic was vital to the formation of a cocrystal, but it has been reported that this is not always the case, in some cases it is the effect of high temperatures and screw configurations that has had the greatest influence. Furthermore, extrusion not only provides advantages to the formation of cocrystals by improving the manufacturing process, it has also been demonstrated to improve the properties of the materials. Alvarez-Nunez et al. report that in the formation of AMG517-sorbic acid cocrystal by extrusion, the N_2 Brunauer–Emmett–Teller (BET) surface area was greater than the conventionally prepared cocrystals, and there were also improvements to the bulk density and flow properties of the material [31]. As a result of these superior material properties, a final milling process step typically employed in the conventional synthesis to increase the surface area was removed.

Deep eutectic solvents

Deep eutectic solvents (DESs) – regarded as a new generation of ionic liquids – are two-component ionic solvents with melting points lower than either constituent of the mixture [39-42]. These materials are receiving a lot of attention due to their potential applications in metal deposition and as green media in chemical reactions [43]. James et al. have reported the preparation of DESs Reline 200 (choline chloride:urea, 1:2), choline chloride:zinc chloride (1:2) and choline chloride:D-fructose (1.6:1) by TSE [44]. Typically they are prepared by batch heating, but this is not always very effective on large scale, especially as processing of these mixtures results in a dramatic increase in viscosity, this then results in an uneven distribution of each component in the mixture [45]. Furthermore, it was reported that batch heating also resulted in the thermal degradation of choline chloride:D-fructose DES due to the caramelisation of D-fructose [45].

TSE overcame the problems identified by batch heating. The residence time for the continuous extrusion of the DES components was determined to be 4–8 minutes on average, producing quantities of ca. 0.4 kg h^{-1} (value of Reline 200 collected per hour) of DES [44]. The reaction times in the formation of DESs

was greatly decreased, and as a result, thermal degradation was avoided in those DESs containing D-fructose due to the short exposure times to heat (Figure 5). The authors made a direct comparison of the determined space time yields (STY) for the batch preparation versus continuous preparation, which were significantly different. The STY determined for the extrusion process was four orders of magnitude greater at 3250,000 kg m^{-3} d^{-1}, whereas batch synthesis was determined to be 500 kg m^{-3} d^{-1} [44]. Furthermore, these materials (particularly choline chloride/zinc chloride (1:2)) are known to be incredibly viscous and so very difficult to transport from the batch mixer into storage containers, but extrusion has avoided this issue as well, the material can be extruded directly into a storage container. This rules out the need for transfer and eliminates the loss of material upon that transfer. Therefore, it can be concluded that the use of TSE has improved the preparation of DESs and the quality of material obtained, which may in turn make them a more accessible media for metal processing or an alternative green solvent for synthesis [44].

Figure 5: Comparison of choline chloride/D-fructose DES prepared via twin screw extrusion (left) and conventional heating (right). Taken from [44].
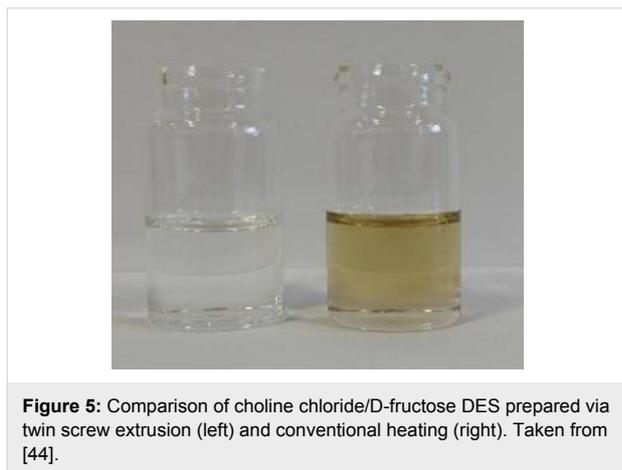
Metal-organic frameworks (MOFs)

The above examples of cocrystal and DES formation describe systems which involve the formation of eutectic and intermolecular interactions upon mixing, but these did not involve the formation of a covalent bond. However, James et al. report on the formation of covalent bonds in metal-organic frameworks (MOFs) and discrete metal complexes by TSE, under solvent-free conditions or in the presence of stoichiometric amounts of MeOH [2]. There is a lot of commercial interest into the use of MOFs for gas capture and chemical separations [46]. Recently, the first commercial use of MOFs has been reported and this involves the adsorption of ethylene gas from the ripening of fruit and vegetables postharvest [47]. As the commercial interest and usage of MOFs increases, the manufacture of these materials, which typically require solvothermal techniques, has become a key research area.

Mechanochemical synthesis of several MOFs has been reported typically by ball milling [48], and James et al. have scaled up the synthesis of HKUST-1, ZIF-8 and Al(fumarate)OH by TSE. Each synthesis involves the reaction between an organic ligand and metal salt. In the synthesis of ZIF-8 and Al(fumarate)OH, high temperatures were required in the absence of solvent, whereas the synthesis of HKUST-1 required stoichiometric amounts of EtOH at room temperature. STYs of 144,000 kg m^{-3} d^{-1} were reported for ZIF-8 and HKUST-1, and for the latter, the STY was three orders of magnitude greater than that reported for the conventional batch synthesis in the literature (Scheme 6) [2].

As with most examples discussed herein, the reaction times to form these MOFs were dramatically reduced from days (via solvothermal methods), to minutes (by TSE) [49]. Furthermore, the TSE products were of very high quality, comparable to the products obtained by batch, solvothermal methods. The N$_2$ BET surface areas of extruded MOFs were similar to, or greater than, that of MOFs prepared in batch. PXRD analysis also indicated that highly crystalline materials were produced from the extrusion process, prior to any post process purification [2].

Two discrete metal complexes have been synthesised by extrusion, involving the reaction between salenH$_2$ and nickel acetate dihydrate as well as the reaction between triphenylphosphine and nickel thiocyanate, both in the presence of stoichiometric amounts of MeOH (Figure 6) [2]. High-quality products were obtained, as determined by ^{1}H NMR spectroscopy, PXRD analysis (which gave sharp diffraction patterns, indicating high crystallinity) and elemental analysis. James et al. report that both of these complexes were isolated and characterised with the only post process workup involved was heating in an oven for two hours [2], which is highly advantageous. Typically, workup of these complexes would involve isolating a precipitate through filtration, followed by drying to remove the copious amounts of MeOH employed as the reaction media.

Conclusion

Organic synthesis is typically quite labour intensive and therefore industrialists are actively seeking ways to minimise the amount of labour required to manufacture organic compounds, particularly in an automated continuous fashion. In addition, they are also looking for techniques that still allow for compounds requiring many synthetic steps to be manufactured and preferably at a lower cost.

As discussed, extrusion has many roles within the food, polymer and pharmaceutical industries. Here we discussed how organic transformations have already been carried out by extrusion, hopefully allowing readers to understand that this tech-

Scheme 6: Synthesis of HKUST-1, ZIF-8 and Al(fumarate)OH by twin screw extrusion. Adapted from [2].

Figure 6: Synthesis of Ni(NCS)$_2$(PPh$_3$)$_2$ and [Ni(salen)] by twin screw extrusion. Adapted from [2].
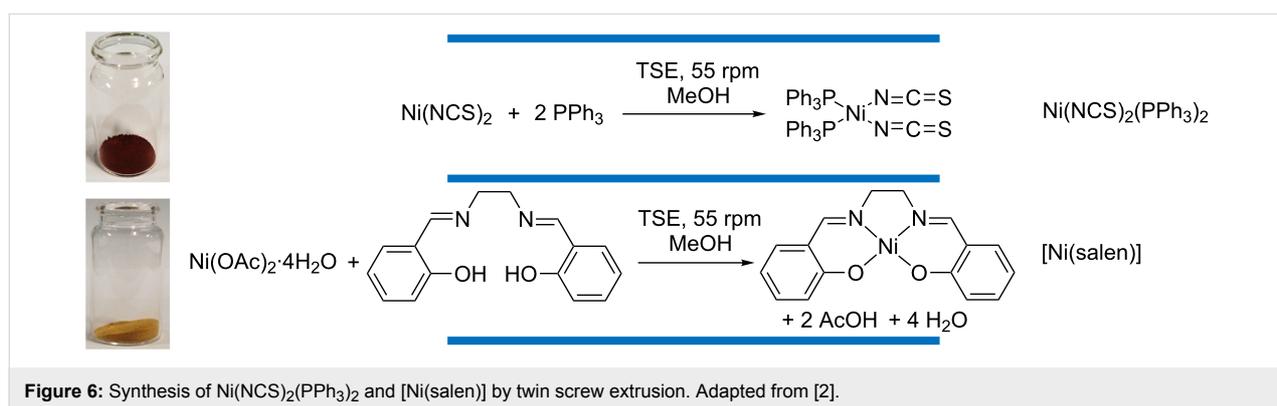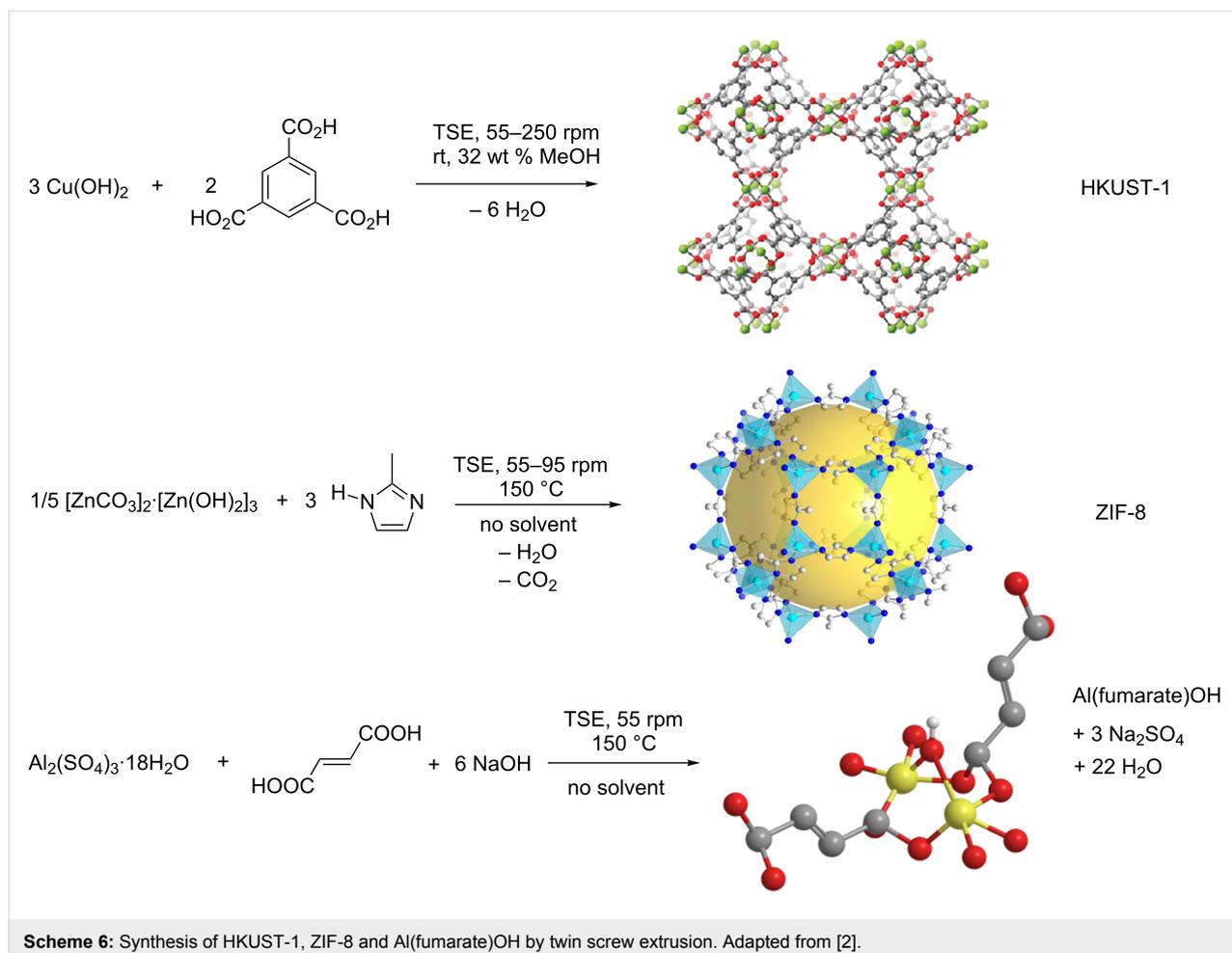
nique could have a future in organic synthesis. To validate this, we have reviewed briefly how the technique has been used for inorganic synthesis and the preparation of cocrystals. This is the first time that the work reviewed here has been highlighted as a form of organic synthesis. In fact, the authors of the work included put a great emphasis on the processing and applications of the polymers and thus do not discuss any of the chemistry that is involved. This may be the reason why these trans-

formations have been overlooked as organic synthesis, and it is hoped that we have highlighted this here.

Employing extrusion for chemical processes brings with it many advantages as discussed. However, there still remains some limitations that inhibits the potential of this technique in chemical synthesis, for example, reactions between two or more liquids have not been studied by extrusion and may be more

difficult to carry out. In fact, there are still very few examples of this reported in ball mill reactions. Secondly, although it has been described that pyrophoric materials can be used in the extruder, through the use of *s*-Buli by Höcker et al., reagents that are potentially explosive or can be ignited when dry or exposed to friction are too hazardous to be used in an extrusion process, therefore chemistry involving azides or hydrazines for example, would need to be avoided.

In summary, extrusion is a technique that has great potential for use in organic synthesis. It has already been demonstrated as a method to scale up synthesis carried out by ball milling, therefore there is very little preventing its use for the organic reactions that have been reported to be successful by ball milling also. Condensation reactions (e.g., Knoevenagel condensations, Michael additions and Aldol reactions) in particular are the most obvious reaction to be successful by extrusion due to its general success in the ball mill, and as their reactions can be accelerated by the simple removal of water (by heating for example).

Extrusion provides a way to achieve intimate mixing of the reagents, it also allows for the extent of mixing to be fine-tuned (via modification of the screw configuration), the extruder itself can be heated to several hundred degrees and if required, small amounts of solvent can be added to accelerate reactions (liquid-assisted grinding). Therefore, it can be concluded that the extruder provides most, if not all of the parameters that conventional solvent-based synthesis can provide. In fact, in regards to the current drive towards a more sustainable environment, the extruder is advantageous as the amount of solvent required is either reduced or eliminated. Furthermore, typically the reaction times are greatly reduced and telescoping can be achieved in the extrusion process as discussed.

Acknowledgements

References
1. Shah, S.; Maddineni, S.; Lu, J.; Repka, M. A. *Int. J. Pharm.* **2013,** *453,* 233. doi:10.1016/j.ijpharm.2012.11.001
2. Crawford, D.; Casaban, J.; Haydon, R.; Giri, N.; McNally, T.; James, S. L. *Chem. Sci.* **2015,** *6,* 1645. doi:10.1039/C4SC03217A
3. Wagner, J. R., Jr.; Mount, E. M., III; Giles, H. F., Jr. *Extrusion The Definitive Processing Guide and Handbook,* 2nd ed.; Elsevier: Oxford, UK, 2014.
4. Crawford, D. E.; Casaban, J. *Adv. Mater.* **2016,** *28,* 5747. doi:10.1002/adma.201505352
5. Janssen, L. P. B. M. *Twin Screw Extrusion;* Elsevier: New York, USA, 1978; Vol. 7.
6. Tzoganakis, C. *Adv. Polym. Technol.* **1989,** *9,* 321. doi:10.1002/adv.1989.060090406
7. Rauwendaal, C. *Polymer Extrusion,* 4th ed.; Hanser: Munich, 2001.
8. Tzoganakis, C. Ph.D. Thesis, McMaster University, Hamilton, Ontario, Canada, 1988.
9. Rauwendaal, C. *J. Polym. Eng. Sci.* **1981,** *21,* 1092. doi:10.1002/pen.760211608
10. Janssen, L. P. B. M. In *Proceedings of the 3rd International Conference on Reactive Processing of polymers,* Strasbourg, France; 1984; pp 151 ff.
11. Narayan, R.; Krishnan, M.; Snook, J. B.; Gupta, A.; DuBois, P. *Bulk Reactive Extrusion Polymerisation Process Producing Aliphatic Ester Polymer Compositions*. U.S. Patent US 5801224A, Sept 1, 1998.
12. Eisenbach, C. D.; Heinemann, T. *Macromolecules* **1995,** *28,* 4815. doi:10.1021/ma00118a006
13. Brown, S. B.; Orlando, C. M. *Encyclopedia of Polymer Science and Engineering,* 2nd ed.; Wiley-Interscience: New York, 1988; Vol. 14.
14. Jenkins, A. D.; Kratochvil, P.; Stepto, R. F. T.; Suter, U. W. *Pure Appl. Chem.* **1996,** *68,* 2287. doi:10.1351/pac199668122287
15. Szwarc, M. *Nature* **1956,** *178,* 1168. doi:10.1038/1781168a0
16. Michaeli, W.; Höcker, H.; Berghaus, U.; Frlngs, W. *J. Appl. Polym. Sci.* **1993,** *48,* 871. doi:10.1002/app.1993.070480512
17. Hadjichristidis, N.; Iatrou, H.; Pitsikalis, P.; Mays, J. *Prog. Polym. Sci.* **2006,** *31,* 1068. doi:10.1016/j.progpolymsci.2006.07.002
18. Efstratiadis, V.; Tselikas, Y.; Hadjichristidis, N.; Li, J.; Yunan, W.; Mays, J. W. *Polym. Int.* **1994,** *33,* 171. doi:10.1002/pi.1994.210330208
19. Rempp, P.; Franta, E.; Herz, J.-E. *Adv. Polym. Sci.* **1988,** *86,* 145. doi:10.1007/BFb0025276
20. Meyer, T. *Org. Process Res. Dev.* **2003,** *7,* 297. doi:10.1021/op025605p
21. Hu, G.-H.; Flat, J.-J.; Lambla, M. *Makromol. Chem., Macromol. Symp.* **1993,** *75,* 137. doi:10.1002/masy.19930750113
22. Jenkins, A. D.; Jones, R. G.; Moad, G. *Pure Appl. Chem.* **2009,** *82,* 483. doi:10.1351/PAC-REP-08-04-03
23. Carlson, D.; Dubois, P.; Nie, L.; Narayan, R. *Polym. Eng. Sci.* **1998,** *38,* 311. doi:10.1002/pen.10192
24. Website. http://www.polymerdatabase.com/polymer%20chemistry/Stepgrowth%20Polymerization.html (accessed Aug 23, 2016).
25. Hyun, M. E.; Kim, S. C. *Polym. Eng. Sci.* **1988,** *28,* 743. doi:10.1002/pen.760281107
26. Gallagher, P. E.; Greenberg, R. A. *Process for Preparing* Polyimides. U.S. Patent US 4835249 A, May 30, 1989.
27. Banucci, E. G.; Mellinger, G. A. *Melt polymerization method for making polyetherimides*. U.S. Patent US 4073773 A, Feb 14, 1978.
28. Schmidt, L. R.; Lovgren, E. M. *Liquid monomer feed pipe for continuous extrusion polymerization*. U.S. Patent US 4511535 A, April 16, 1985.
29. Takekoshi, T.; Kochanowski, J. E. *Methods for Making Polyetherimides*. U.S. Patent US 4011198, March 8, 1991.
30. Mittal, K. L. *Polyimides and Other High Temperature Polymers: Synthesis, Characterization and Applications;* CRC Press: New York, 2007; Vol. 4.
31. Medina, C.; Daurio, D.; Nagapudi, K.; Alvarez-Nunez, F. *J. Pharm. Sci.* **2010,** *99,* 1693. doi:10.1002/jps.21942
32. Ross, S. A.; Lamprou, D. A.; Douroumis, D. *Chem. Commun.* **2016,** *52,* 8772. doi:10.1039/C6CC01289B
33. Daurio, D.; Medina, C.; Saw, R.; Nagapudi, K.; Alvarez-Núñez, F. *Pharmaceutics* **2011,** *3,* 582. doi:10.3390/pharmaceutics3030582

34. Daurio, D.; Nagapudi, K.; Li, L.; Quan, P.; Alvarez-Nunez, F.
Faraday Discuss. **2014,** *170,* 235. doi:10.1039/C3FD00153A

35. Islam, M. T.; Scoutaris, N.; Maniruzzaman, M.; Moradiya, H. G.;
Halsey, S. A.; Bradley, M. S. A.; Chowdhry, B. Z.; Snowden, M. J.;
Douroumis, D. *Eur. J. Pharm. Biopharm.* **2015,** *96,* 106.
doi:10.1016/j.ejpb.2015.06.021

36. Kulkarni, C.; Wood, C.; Kelly, A. T.; Gough, T.; Blagden, N.;
Paradkar, A. *Cryst. Growth Des.* **2015,** *15,* 5648.
doi:10.1021/acs.cgd.5b00806

37. Liu, X.; Lu, M.; Guo, Z.; Huang, L.; Feng, X.; Wu, C. *Pharm. Res.* **2012,**
29, 806. doi:10.1007/s11095-011-0605-4

38. Moradiya, H.; Islam, M. T.; Woollam, G. R.; Slipper, I. J.; Hasley, S.;
Snowden, M. J.; Douroumis, D. *Cryst. Growth Des.* **2014,** *14,* 189.
doi:10.1021/cg401375a

39. Smith, E. L.; Abbott, A. P.; Ryder, K. S. *Chem. Rev.* **2014,** *114,* 11060.
doi:10.1021/cr300162p

40. Abbott, A. P.; Boothby, D.; Capper, G.; Davies, D. L.; Rasheed, R. K.
J. Am. Chem. Soc. **2004,** *126,* 9142. doi:10.1021/ja048266j

41. Zhang, Q.; De Oliveira Vigier, K.; Royer, S.; Jérôme, F.
Chem. Soc. Rev. **2012,** *41,* 7108. doi:10.1039/c2cs35178a

42. Dai, Y.; van Spronsen, J.; Witkamp, G.-J.; Verporte, R.; Choi, Y. H.
Anal. Chim. Acta **2013,** *766,* 61. doi:10.1016/j.aca.2012.12.019

43. Troter, D. Z.; Todorović, Z. B.; Dokić-Stojanović, D. R.;
Stamenković, O. S.; Veljković, V. B.
Renewable Sustainable Energy Rev. **2016,** *61,* 473.
doi:10.1016/j.rser.2016.04.011

44. Crawford, D. E.; Wright, L. A.; James, S. L.; Abbott, A. P.
Chem. Commun. **2016,** *52,* 4215. doi:10.1039/C5CC09685E

45. Hayyan, A.; Mjalli, F. S.; Al-Nashef, I. M.; Al-Wahaibi, T.;
Al-Wahaibi, Y. M.; Hashim, M. A. *Thermochim. Acta* **2012,** *541,* 70.
doi:10.1016/j.tca.2012.04.030

46. Furukawa, H.; Cordova, K. E.; O'Keeffe, M.; Yaghi, O. M. *Science*
2013, *341,* 6149. doi:10.1126/science.1230444

47. Website.
http://www.moftechnologies.com/2016/09/13/mof-announces-worlds-fir
st-commercial-application-decco-worldwide-mof-2016 (accessed Oct 1,
2016).

48. Zhan, G.; Zeng, H. C. *Chem. Commun.* **2017,** *53,* 72.
doi:10.1039/c6cc07094a

49. Czaju, A. U.; Trukhan, N.; Müller, U. *Chem. Soc. Rev.* **2009,** *38,* 1284.
doi:10.1039/b804680h

License and Terms

Solution-phase automated synthesis of an α-amino aldehyde as a versatile intermediate

Hisashi Masui[1], Sae Yosugi[1], Shinichiro Fuse[2] and Takashi Takahashi[*1]

Abstract

A solution-phase automated synthesis of the versatile synthetic intermediate, Garner's aldehyde, was demonstrated. *tert*-Butoxycarbonyl (Boc) protection, acetal formation, and reduction of the ester to the corresponding aldehyde were performed utilizing our originally developed automated synthesizer, ChemKonzert. The developed procedure was also useful for the synthesis of Garner's aldehyde analogues possessing fluorenylmethyloxycarbonyl (Fmoc) or benzyloxycarbonyl (Cbz) protection.

Introduction

Automated synthesis has attracted a great deal of attention in recent years because the automation of synthetic operations improves both the reproducibility and reliability of syntheses [1-4]. Synthetic chemists frequently perform repetitive processes such as the optimization of reaction conditions, construction of compound libraries, and preparation of synthetic intermediates. These operations are very time-consuming, and do not require expert knowledge and skills. Development of automated synthetic procedures and storage of relevant digital data allow anyone to reproduce the same results anytime and anywhere using the same apparatus and reagents. As a result, synthetic chemists can spend more time on advanced and chal-

lenging problems. We previously reported automated syntheses of various bioactive compounds [5-8], including taxol, using our originally developed solution-phase automated synthesizer, ChemKonzert [9].

Protected α-amino aldehydes are versatile intermediates for the synthesis of vicinal amino alcohols and important building blocks for various bioactive natural products [10-12]. In particular, Garner's aldehyde (**4a**) is very useful as a chiral building block [13-18]. It is sufficiently stable and its configurational rigidity allows stereoselective addition of nucleophiles to the aldehyde [19].

The most conventional synthesis of **4a** involves the protection of the amine, the carboxylic acid, and the alcohol moiety of serine, and the subsequent reduction of carboxylic acid derivatives such as ester [20-27], thioester [28], or Weinreb amide [29,30] to the aldehyde. In addition, Burke and co-workers reported an asymmetric hydroformylation of 2,2-dimethyl-2,3-dihydrooxazole for the synthesis of **4a** [31]. Although various syntheses of **4a** have been established, an automated synthesis has never been demonstrated. The automated synthesis of a versatile intermediate such as **4a** will improve the overall research efficiency of synthetic chemists. Herein, we report the first solution-phase automated synthesis of Garner's aldehyde (**4a**) and its analogues.

Results and Discussion

Our synthetic route is shown in Scheme 1. We planned to synthesize **4a** with various protecting groups from a commercially available amino ester through a three-step procedure utilizing the automated synthesizer, ChemKonzert (Figure 1).

Scheme 1: Automated synthesis of **4a**.
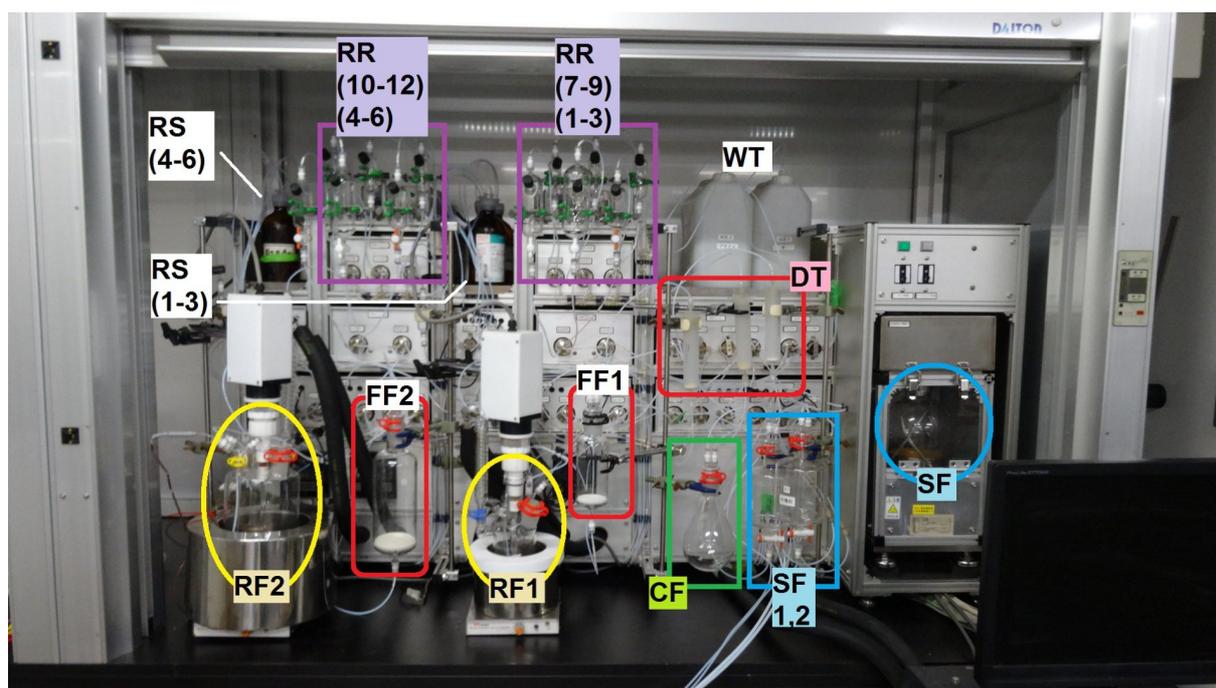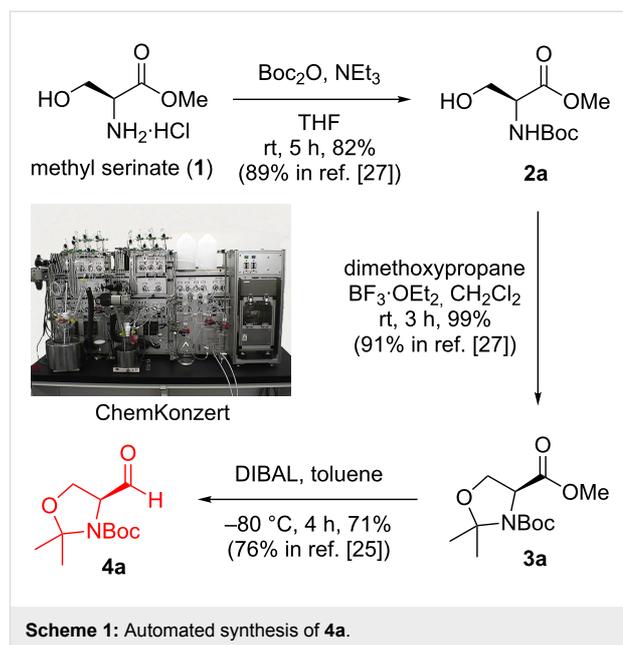
Figure 1: Full picture of ChemKonzert, showing two reaction vessels (RF1 and RF2), a centrifugal separator (SF, 700 mL), two receivers (SF1 and SF2, 500 mL), two glass filters (FF1 and FF2, 500 and 100 mL), 12 substrate and reagent reservoirs (RR1–RR12, 100–200 mL), six solvent and wash-solution bottles (RS1–RS6, 500 mL), three drying pads (DT1–DT3), a round-bottom flask (CF), two solvent tanks (WT1 and WT2), and a computer controller. Transfer of compounds from a server flask to a receiver flask through a Teflon tube is performed as shown below. The receiver flask is vacuumed by a diaphragm pump and N$_2$ flow pushes the compound into the server flask. The flow of liquid in the tube is monitored by a photosensor that detects the difference in reflective index between gas and liquid. All the gas/liquid flows are controlled by solenoid valves and/or rotary valves. This transfer system avoids direct contacts of pumps with compounds that frequently cause mechanical troubles of pumps. Formation of emulsions during phase separation is one of the common problems for liquid-phase automated synthesizers that can perform aqueous work-up. ChemKonzert uses a centrifuge instrument to solve this problem: the emulsified mixture is transferred to the separating flask and the phases are separated by centrifugation. The separated mixture is then transferred to a receiver flask from the lower layer by passing through a flow-type electroconductivity sensor, which detects the difference in conductivity between the organic phase and aqueous phase. When the sensor detects the boundary of the phases, the solenoid valve is changed to send the upper layer to a different receiver.

Figure 1 shows the automated synthesizer ChemKonzert and its various components. An automated synthesis of **4a** was examined utilizing ChemKonzert (Scheme 1). It is important to examine and check the reaction conditions manually before performing the automated synthesis. Therefore, we optimized the reaction time and the work-up method was modified. We started with the Boc protection of methyl L-serinate hydrochloride (**1**). The computer controlling the automated synthesizer was programmed with a specific procedure. The substrate, reagents, solvents, and wash solutions were added to the reaction vessel (RF1), reagent reservoir (RR1), solvent bottles (RS1–3), and wash solution bottles (RS4–6), respectively. A solution of methyl L-serinate hydrochloride in THF was stirred at 25 °C in RF1, to which a solution of triethylamine in THF and Boc$_2$O in THF was added. Originally, the respective solutions were loaded in the reagent reservoirs (RR1 and RR3). After stirring at 25 °C for 5 h, the reaction mixture was diluted with ethyl acetate from RS1 and was quenched by adding 1 M HCl from RR2. The reaction mixture was then transferred to the centrifugal separator (SF). After centrifugation, the two resulting phases were separated; their electroconductivities measured with a sensor and transferred to two receivers (SF1 and SF2). The aqueous phase in SF1 was returned to RF1. Ethyl acetate, from RS1, was added, and the mixture was stirred for 3 min and then transferred to SF. After performing the extraction, the combined organic mixture in the receiver (SF2) was washed with 10% aqueous NaCl solution from RS3. The organic layer was separated in SF, transferred to SF2, subsequently passed through a plug of anhydrous Na$_2$SO$_4$ (DT1) and collected in a round-bottom flask (CF1). The collected solution was manually concentrated in vacuo. The obtained residue was purified manually using silica gel column chromatography. Carbamate **2a** was obtained in 82% yield.

Acetal formation was also demonstrated using ChemKonzert. A solution of substrate **2a** in dichloromethane was stirred at 25 °C in the reaction vessel (RF1), to which a solution of 2,2-dimethoxypropane in dichloromethane and a solution of boron trifluoride·ethyl ether complex in dichloromethane were added. Originally, the respective solutions were loaded into the reagent reservoirs (RR1 and RR3). After stirring at 25 °C for 3 h, the reaction was quenched by adding 50% aqueous NaOH solution. When the NaOH solution was added to RF1, the yield of the target compound decreased because of the undesired hydrolysis of the acetonide. Therefore, the reaction mixture was transferred to the centrifugal separator (SF), NaOH solution was added to RF1 and the reaction mixture in SF was added to the NaOH solution in RF1. This reverse addition improved the yield. The subsequent automated aqueous work-up, manual concentration, and silica gel column chromatography afforded acetonide **3a** in 99% yield.

DIBAL reduction was also achieved using ChemKonzert. The amount of Rochelle salt required to diminish the aluminum salt generated from DIBAL was optimized in manual operation preliminarily. A solution of the substrate in toluene was stirred at −80 °C in the reaction vessel (RF1). A solution of DIBAL in toluene, originally loaded into the reagent reservoir (RR1), was added to RF1. After further stirring at −80 °C for 4 h, the reaction was quenched by adding saturated aqueous Rochelle salt solution at 25 °C from the solvent bottle RS2. The subsequent automated aqueous work-up, manual concentration, and silica gel column chromatography afforded **4a** in 71% yield. The observed yields of the automated syntheses were similar to those obtained from the corresponding reported manual syntheses (see Scheme 1).

Garner's aldehyde analogues containing a Fmoc [32] or Cbz [33-35] group were synthesized using the established procedure. Protection of the amino group in methyl serinate using Fmoc–OSu or CbzCl afforded the corresponding carbamates in good yields (Table 1, experimental details, see Supporting Information File 1). Acetal formation and reduction were performed by the developed procedure in ChemKonzert (Table 1).

Table 1: Automated synthesis of **4b** and **4c**.

PG	Protection	Acetal formation	Reduction
Fmoc	Fmoc–OSu, NaHCO$_3$, dioxane, H$_2$O, rt, 5 h, 97%	87%	22%
Cbz	CbzCl, NaHCO$_3$, dioxane, H$_2$O, rt, 5 h, 92%	80%	31%

The Garner's aldehydes containing an Fmoc or Cbz protecting group (PG) could be synthesized from the corresponding methyl ester; however, lower yields were obtained for the DIBAL reduction, probably due to the DIBAL-mediated removal of the carbamates [32].

Conclusion

In conclusion, the first solution-phase automated synthesis of **4a** (Boc protection) was demonstrated utilizing our originally developed automated synthesizer, ChemKonzert. The observed yields were comparable to those of the corresponding reported manual syntheses. In addition, **4b** and **4c** (Fmoc and Cbz protection) were also synthesized automatically according to the established procedure. Garner's aldehyde (**4a**) and its analogues are very important versatile intermediates. The automated synthesis of **4a** can be applied to the synthesis of various useful compounds containing a vicinal amino alcohol moiety.

Supporting Information

Supporting Information File 1

Synthetic procedures and ^{1}H NMR spectral data of compounds **2a–c**, **3a–c**, and **4a–c**.
[http://www.beilstein-journals.org/bjoc/content/
supplementary/1860-5397-13-13-S1.pdf]

Acknowledgements

References

1. Cork, D. G.; Sugawara, T., Eds. *Laboratory Automation in the Chemical Industries;* Marcel Dekker Inc.: New York, 2002. doi:10.1201/9780203908945
2. Li, J.; Ballmer, S. G.; Gillis, E. P.; Fujii, S.; Schmidt, M. J.; Palazzolo, A. M. E.; Lehmann, J. W.; Morehouse, G. F.; Burke, M. D. *Science* **2015,** *347,* 1221–1226. doi:10.1126/science.aaa5414
3. Adamo, A.; Beingessner, R. L.; Behnam, M.; Chen, J.; Jamison, T. F.; Jensen, K. F.; Monbaliu, J.-C. M.; Myerson, A. S.; Revalor, E. M.; Snead, D. R.; Stelzer, T.; Weeranoppanant, N.; Wong, S. Y.; Zhang, P. *Science* **2016,** *352,* 61–67. doi:10.1126/science.aaf1337
4. Seeberger, P. H.; Werz, D. B. *Nat. Rev. Drug Discovery* **2005,** *4,* 751–763. doi:10.1038/nrd1823
5. Doi, T.; Fuse, S.; Miyamoto, S.; Nakai, K.; Sasuga, D.; Takahashi, T. *Chem. – Asian J.* **2006,** *1,* 370–383. doi:10.1002/asia.200600156
6. Fuse, S.; Ikebe, A.; Oosumi, K.; Karasawa, T.; Matsumura, K.; Izumikawa, M.; Johmoto, K.; Uekusa, H.; Shin-ya, K.; Doi, T.; Takahashi, T. *Chem. – Eur. J.* **2015,** *21,* 9454–9460. doi:10.1002/chem.201500703
7. Fuse, S.; Okada, K.; Iijima, Y.; Munakata, A.; Machida, K.; Takahashi, T.; Takagi, M.; Shin-ya, K.; Doi, T. *Org. Biomol. Chem.* **2011,** *9,* 3825–3833. doi:10.1039/c0ob01169j
8. Tanaka, Y.; Fuse, S.; Tanaka, H.; Doi, T.; Takahashi, T. *Org. Process Res. Dev.* **2009,** *13,* 1111–1121. doi:10.1021/op9002455
9. Machida, K.; Hirose, Y.; Fuse, S.; Sugawara, T.; Takahashi, T. *Chem. Pharm. Bull.* **2010,** *58,* 87–93. doi:10.1248/cpb.58.87
10. Kher, S. S.; Penzo, M.; Fulle, S.; Finn, P. W.; Blackman, M. J.; Jirgensons, A. *Bioorg. Med. Chem. Lett.* **2014,** *24,* 4486–4489. doi:10.1016/j.bmcl.2014.07.086
11. Segade, Y.; Montaos, M. A.; Rodríguez, J.; Jiménez, C. *Org. Lett.* **2014,** *16,* 5820–5823. doi:10.1021/ol502958u
12. Vasudevan, N.; Kashinath, K.; Reddy, D. S. *Org. Lett.* **2014,** *16,* 6148–6151. doi:10.1021/ol503011g
13. Singh, P.; Manna, S. K.; Panda, G. *Tetrahedron* **2014,** *70,* 1363–1374. doi:10.1016/j.tet.2013.11.074
14. Takahata, H.; Banba, Y.; Ouchi, H.; Nemoto, H. *Org. Lett.* **2003,** *5,* 2527–2529. doi:10.1021/ol034886y
15. Sa-ei, K.; Montgomery, J. *Tetrahedron* **2009,** *65,* 6707–6711. doi:10.1016/j.tet.2009.05.029
16. Bhabak, K. P.; Proksch, D.; Redmer, S.; Arenz, C. *Bioorg. Med. Chem.* **2012,** *20,* 6154–6161. doi:10.1016/j.bmc.2012.08.035
17. Sudhakar, N.; Kumar, A. R.; Prabhakar, A.; Jagadeesh, B.; Rao, B. V. *Tetrahedron Lett.* **2005,** *46,* 325–327. doi:10.1016/j.tetlet.2004.11.035
18. Chen, J.; Chen, X.; Bois-Choussy, M.; Zhu, J. *J. Am. Chem. Soc.* **2006,** *128,* 87–89. doi:10.1021/ja0571794
19. Passiniemi, M.; Koskinen, A. M. P. *Beilstein J. Org. Chem.* **2013,** *9,* 2641–2659. doi:10.3762/bjoc.9.300
20. Karjalainen, O. K.; Koskinen, A. M. P. *Tetrahedron* **2014,** *70,* 2444–2448. doi:10.1016/j.tet.2014.02.020
21. Upadhyay, P. K.; Kumar, P. *Synthesis* **2010,** 3063–3066. doi:10.1055/s-0030-1258185
22. Garner, P.; Park, J. M. *Org. Synth.* **1992,** *70,* 18–28. doi:10.15227/orgsyn.070.0018
23. Foss, F. W., Jr.; Snyder, A. H.; Davis, M. D.; Rouse, M.; Okusa, M. D.; Lynch, K. R.; Macdonald, T. L. *Bioorg. Med. Chem.* **2007,** *15,* 663–677. doi:10.1016/j.bmc.2006.10.060
24. Ocejo, M.; Vicario, J. L.; Badía, D.; Carrillo, L.; Reyes, E. *Synlett* **2005,** 2110–2112. doi:10.1055/s-2005-871947
25. Dondoni, A.; Perroni, D. *Org. Synth.* **2000,** *77,* 64–77. doi:10.15227/orgsyn.077.0064
26. Jurczak, J.; Gryko, D.; Kobrzycka, E.; Gruza, H.; Prokopowicz, P. *Tetrahedron* **1998,** *54,* 6051–6064. doi:10.1016/S0040-4020(98)00299-3
27. Roush, W. R.; Hunt, J. A. *J. Org. Chem.* **1995,** *60,* 798–806. doi:10.1021/jo00109a008
28. Trajkovic, M.; Ferjancic, Z.; Saicic, R. N. *Tetrahedron: Asymmetry* **2012,** *23,* 602–604. doi:10.1016/j.tetasy.2012.03.019
29. Hoffman, T. J.; Kolleth, A.; Rigby, J. H.; Arseniyadis, S.; Cossy, J. *Org. Lett.* **2010,** *12,* 3348–3351. doi:10.1021/ol101145t
30. Cortes-Clerget, M.; Gager, O.; Monteil, M.; Pirat, J.-L.; Migianu-Griffoni, E.; Deschamp, J.; Lecouvey, M. *Adv. Synth. Catal.* **2016,** *358,* 34–40. doi:10.1002/adsc.201500794
31. Clemens, A. J. L.; Burke, S. D. *J. Org. Chem.* **2012,** *77,* 2983–2985. doi:10.1021/jo300025t
32. Rush, J.; Bertozzi, C. R. *Org. Lett.* **2006,** *8,* 131–134. doi:10.1021/ol052623t
33. Jiang, S.; Li, P.; Lai, C. C.; Kelley, J. A.; Roller, P. P. *J. Org. Chem.* **2006,** *71,* 7307–7314. doi:10.1021/jo061037q
34. Martin, N. I.; Woodward, J. J.; Winter, M. B.; Marletta, M. A. *Bioorg. Med. Chem. Lett.* **2009,** *19,* 1758–1762. doi:10.1016/j.bmcl.2009.01.076

35. Lingamurthy, M.; Jagadeesh, Y.; Ramakrishna, K.; Rao, B. V.
J. Org. Chem. **2016,** *81,* 1367–1377. doi:10.1021/acs.joc.5b02275

3D printed fluidics with embedded analytic functionality for automated reaction optimisation

Andrew J. Capel[1], Andrew Wright[1], Matthew J. Harding[1], George W. Weaver[1], Yuqi Li[1], Russell A. Harris[2], Steve Edmondson[3], Ruth D. Goodridge[4] and Steven D. R. Christie[*1]

Abstract

Additive manufacturing or '3D printing' is being developed as a novel manufacturing process for the production of bespoke micro- and milliscale fluidic devices. When coupled with online monitoring and optimisation software, this offers an advanced, customised method for performing automated chemical synthesis. This paper reports the use of two additive manufacturing processes, stereolithography and selective laser melting, to create multifunctional fluidic devices with embedded reaction monitoring capability. The selectively laser melted parts are the first published examples of multifunctional 3D printed metal fluidic devices. These devices allow high temperature and pressure chemistry to be performed in solvent systems destructive to the majority of devices manufactured via stereolithography, polymer jetting and fused deposition modelling processes previously utilised for this application. These devices were integrated with commercially available flow chemistry, chromatographic and spectroscopic analysis equipment, allowing automated online and inline optimisation of the reaction medium. This set-up allowed the optimisation of two reactions, a ketone functional group interconversion and a fused polycyclic heterocycle formation, via spectroscopic and chromatographic analysis.

Introduction

Additive manufacturing (AM), or as it is widely known '3D printing', is the internationally recognised term used to describe a wide range of manufacturing processes that can generate complex three-dimensional parts, often with geometries which would be extremely complex, or in some cases impossible to manufacture using more conventional subtractive manufacturing processes [1]. In AM, parts are built layer-by-layer, using processes such as material extrusion [2], material jetting [3], vat

photopolymerisation [4], sheet lamination [5], powder bed fusion [6], binder jetting and direct energy deposition [7,8]. AM has gained widespread academic and industrial use for a diverse set of applications ranging from biological to aeronautical [9,10]. However, more recent research has demonstrated the benefits of using 3D printing to produce microfluidic devices using AM techniques such as stereolithography (SL) [11], polymer jetting and fused deposition modelling (FDM) [12,13]. There is therefore considerable interest in the optimisation of chemical systems using this type of multifunctional continuous flow reactor. Notable recent work in this area has been carried out by Cronin [14], Ley [15] and Jensen [16]. This research highlights the array of benefits that manufacturing fluidic devices via AM processes can bring, including the ability to produce multimaterial parts with complex microscale features and embedded functionality, allowing inline and online optimisation of a reaction medium.

This paper presents a range of printed chemical reactors produced via the selective laser melting (SLM) and SL manufacturing processes. SLM is a powder-based additive manufacturing technique which uses a high-power energy source, typically a laser, to selectively melt a powder bed into a single solid body [17]. SLM can manufacture parts in a range of chemically inert and thermally stable metals such as stainless steel [18], aluminium and titanium [19,20], and is therefore an attractive technique for a number of industrial applications. SLM is capable of producing parts at a layer thickness as low as 20 μm, and with part geometries of +/− 0.1 mm being achieved over smaller parts, however, even highly optimised SLM processes can still experience problems with balling, thermal cracking, unwanted surface roughness and difficulty with removing un-melted powder from smaller cavities [6]. SL utilises layer-by-layer photopolymerisation of a liquid resin bath to generate fully dense polymer parts [21]. Typically these resins are complex formulations based around a small selection of UV-curable acrylates, epoxies and urethanes [4], whose poor mechanical and chemical properties can limit the application of SL manufactured parts. However, well maintained machines are capable of reproducibly producing parts at a layer thickness as low as 25 μm, making SL one of the most accurate and reproducible AM processes [4]. Both SLM and SL are therefore attractive manufacturing techniques for the production of milliscale chemical reactors.

This research investigates how these two innovative processes can be used to produce milliscale chemical reactors with increased analytical functionality, by embedding spectroscopic viewing windows across the reaction path length allowing inline UV–vis spectroscopic analysis of the reaction medium. The research also highlights the design freedom associated with

using AM processes, by designing custom reactor geometries which allow these devices to be integrated with existing laboratory flow and analysis equipment [22].

Results and Discussion

Previous work within this research group has demonstrated the flexibility of AM for the production of milliscale chemical reactors, with complex internal geometries as well as parts with embedded spectroscopic capability [11,23]. In order to fully utilise this flexibility, parts were designed which could be integrated with existing flow and analytical instrumentation. An ideal choice for this application is high-performance liquid chromatography (HPLC). HPLC instrumentation is widely available in most modern chemistry laboratories, and is ideally suited for use in flow applications. Modern HPLC systems are typically equipped with a binary or quaternary pumping system (flow rates ≈0.01–10 mL/min), thermostatted heated compartments (temperatures ≈20–100 °C), multiport sampling valves, as well as separation, purification and UV–vis spectroscopic analysis capability. The HPLC system, parts were also integrated with a commercially available Uniqsis FlowSyn module providing pumping and heating apparatus, allowing inline spectroscopic reaction analysis via a portable UV–vis light source and detector. This type of spectroscopy is often used for inline reaction analysis due to its rapid data generation, however, it can often be difficult to interpret for complex multifunctional systems. On the other hand, chromatographic analysis methods produce much more concise spectra allowing quantitative data to be extrapolated, however, they often suffer from lengthy method times significantly decreasing the reaction throughput [24,25].

The HPLC equipment set-up, which varied between experiments, was based around a four module Agilent 1100 series, with two binary pumping modules, a thermostatted column compartment module, a variable wavelength diode array detector (DAD) compartment with a standard flow cell, as well as an external six-port sampling valve. Using this set-up allowed the flow medium to be pumped through a temperature controlled reactor, which using a sampling valve would allow the reaction medium to either be collected, injected onto the HPLC column for separation or passed directly through a diode array detector. The column would be flushed with the mobile phase by the secondary pump, whilst being independently heated by the same thermostatted compartment. By integrating this system with 3D printed fluidic devices, it would be possible to perform automated inline and online analysis of the reaction media, affording substantial control over reaction residence time, temperature, and reagent composition. However, in order to achieve this level of control it was necessary to design custom software: a series of intuitive 'macro' programs, which

would allow the automated control of each module within the system. This required control over the Chemstation software that is the graphical user interface (GUI) for the Agilent HPLC system. This was achieved using MacroPad [26]. MacroPad is a software specifically designed for developing macros to control the Chemstation software. Through MacroPad, it is possible to access the Chemstation 'registers', which store all the input and output variables produced during the HPLC analysis. These registers allow control over variables such as reaction flow rates, temperature and pressure, as well as quantitative outputs such as spectroscopic and chromatographic data from any HPLC analysis undertaken. Using this software, it was possible to define the specific reaction and analysis conditions for each optimisation that was undertaken. More detailed descriptions of the function of the Chemstation macros and the SIMPLEX optimisation software are available in Supporting Information File 1. Both pieces of software allow user input, specifically defining the target variable to be optimized, e.g., absorption intensity or product peak area.

The large number of variables within the optimisation system and reactor design necessitated the generation of an idealised set of reaction conditions, allowing effective comparison of data sets. This reaction was the conversion of (*R*)-(−)-carvone (**1**) to its corresponding semicarbazone **2**, using semicarbazide and sodium acetate (Scheme 1). This reaction was selected because it would run smoothly at room temperature, and a mild solvent mixture such as methanol and water (MeOH/water) could be
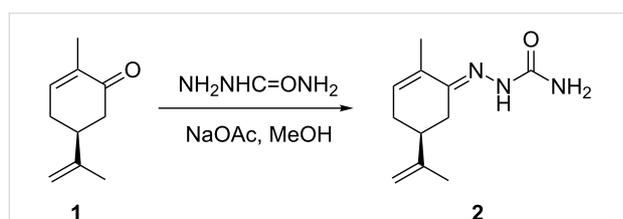
used with the less solvent-compatible parts. Differences between the UV–vis spectra of the starting material and the product can be used to follow the reaction optimization.

Reactor design 1 (RD1)

By mimicking the internal dimensions of the DAD compartment within an Agilent HPLC system, an inline spectroscopic flow cell could be realised (Figure 1). RD1 was therefore fabricated using a 3D Systems Viper si2 SL system from Accura 60 photoresin, with external geometries of $123 \times 67 \times 42$ mm (volume ≈ 68 cm^3), and a continuous cylindrical channel running throughout the part (channel diameter = 1.5 mm, channel length = 1600 mm, reaction volume = 2.8 mL). The external dimensions of the flow cell would match the internal dimensions of the DAD compartment, allowing the part to be held within by a commercially available sprung clip. The flow cell itself had a path length of 6 mm. One of the unique features of using AM to manufacture this type of part is that manufacturing costs are directly proportional to the volume of material used and not the complexity of the design. Despite the fact that the Accura 60 material has a high cost compared to conventional (non-SL) polymer materials, the material cost of RD1 is only around £17, making the SL process reasonably priced in comparison to other manufacturing processes.

The functionality of RD1 was determined via the use of an Ocean optics DH2000 light source (400 micron diameter illumination fibre, 600 micron collection fibre) and an Ocean Optics S2000 variable wavelength detector [27]. It was possible to determine the amount of stray light (predominantly from fluorescent strip lighting within the laboratory) being picked up by the detector when the light source was inactive (Figure 2). This demonstrated that due to the transparency of the Accura 60 resin to visible light, even though the part would be housed inside a dark chamber, ideally the detection wavelengths for this material should be kept below 400 nm. To confirm that the part functions correctly, a benzaldehyde solution (2 mmol in methanol), was flowed through RD1 with the resulting spectrum

Scheme 1: The reaction of (*R*)-(−)-carvone (**1**) with semicarbazide to form the corresponding semicarbazone **2**.

Figure 1: CAD model of SL reactor design RD1 (left), RD1 with attached sprung clip (centre), commercially available Agilent flow cell (right). External dimensions of RD1 are 123 (length) × 67 (width) × 42 mm (depth).

Figure 2: Energy versus wavelength spectra comparing the amount of stray light being picked up by the detector using both RD1 and a commercial flow cell (left), normalised absorption spectra of a benzaldehdye solution passing through both RD1 and a commercial flow cell (right).

being compared to that achieved through the Ocean Optics flow cell. Having normalised the data it was clear that the two spectra were very similar above wavelengths of around 260 nm.

RD1 was therefore tested using the carvone functional group interconversion previously outlined (Scheme 1) and would be fully automated, using the spectroscopic data generated from the inline flow cell as the controlling output that would run the Chemstation control macros and optimisation software. The software was set to optimise for maximum UV–vis absorbance due to the semicarbazone by automatically varying both temperature and flow rate. For this optimisation an Agilent 1100 series binary pumping module was used to pump the two reagent flows, which passed through a 5 mL stainless steel coil reactor. This reactor was attached to a heating mandrel, and heated using the temperature controlled heating module of a Uniqsis FlowSyn. The flow would then pass into a six-port valve, allowing it to be redirected into either a collection vial, or pass through RD1 for spectroscopic data collection (Figure 3 and Table 1).

The analysis macro used during this specific optimisation would monitor the intensity of absorption at a single predetermined

Figure 3: Reactor set-up for carvone optimisation using RD1 as an inline spectroscopic flow cell. Reagents were pumped using an Agilent 1100 series HPLC pumping module. A Uniqsis FlowSyn was used to heat and cool the 5 mL stainless steel coil reactor. The flow passed onto a stand-alone six-port valve, whereby samples were either passed into a collection vial or passed through RD1 which sat within the DAD compartment of the same Agilent 1100 series HPLC.

Table 1: Conditions and limits for the optimisation used in tandem with RD1. Ketone **1** concentration 0.40 mmol/L, semicarbazide concentration 1.20 mmol/L.

Optimisation variable	Value
flow rate range	0.2–1 mL/min
temperature range	25–80 °C
SIMPLEX temperature variation	5 °C
SIMPLEX flow rate variation	0.1 mL/min
maximum data points	30

wavelength (275 nm). At this wavelength the carvone starting material has very low absorbance, whereas the semicarbazone product has significant absorbance. The increase in intensity of absorbance at this value could therefore be attributed to the presence of an increased concentration of the reaction product. Prior to each new set of experimental conditions, the flow cell would be flushed with a MeOH/water mix (1:1 ratio), allowing the detector to establish a new baseline. Figure 4 shows the reactor held in place in the HPLC compartment.

Figure 4: RD1 held in place within the DAD compartment of an Agilent 1100 HPLC.

The optimisation was run over the period of approximately 8 h, generating 30 data points within the allowable temperature and flow rate range (Figure 5). Successive points were automatically selected by the SIMPLEX algorithm using previous results, in order to find the optimum conditions. This produced the optimal data point as being 69 °C and 0.27 mL/min (Figure 5). This initial optimisation methodology was able to quickly identify the trend towards higher yield with higher temperatures and lower flow rates. This type of analysis is ideal for fast data generation. Indeed, with this type of analysis the biggest delay within the system was the wait for the heating and cooling of the reactor between analysis points. However, this analysis method did have a number of features which could be improved upon with future design alterations. The use of both a FlowSyn and HPLC system made it complex to co-ordinate both pieces of instrumentation. Also the reaction could not be carried out at uniform temperature throughout due to poor thermal conductivity and stability of the Accura material that RD1 was manufactured with. It was hypothesised however, that both of these features could be overcome by manufacturing reactors via the SLM process, allowing the parts to be manufactured from thermally conductive and thermally stable metals that could be designed to retrofit to any off-the-shelf heating device (see RD2 below).

Figure 5: Optimisation plot for the SIMPLEX optimisation of semicarbazone **2**. Optimum reaction conditions within the specified system were found to a flow rate of 0.27 mL/min and a temperature of 69 °C.

Reactor design 2 (RD2)

Agilent HPLC systems are equipped with two programmable temperature controlled column compartments, which allow temperatures to be independently heated up to 100 °C and simultaneously selected by the user. This will allow a bespoke chemical reactor to be placed into one of these compartments, whilst allowing the inline separation and analysis of reaction products downstream of the device. This set-up allows the temperature controlled reaction, purification, analysis and optimisation of a reaction medium all within a single piece of common laboratory equipment. RD2 was therefore designed to match the internal dimensions of the heated column compartment of an Agilent 1100 series HPLC system (Figure 6). The part was fabricated using a Renishaw AM 250 system from Ti-6Al-4V alloy, with external geometries of $100 \times 20 \times 20$ mm (volume = 31.6 cm^3) and a continuous cylindrical channel running throughout (channel diameter = 2 mm, channel length = 3200 mm, theoreti-
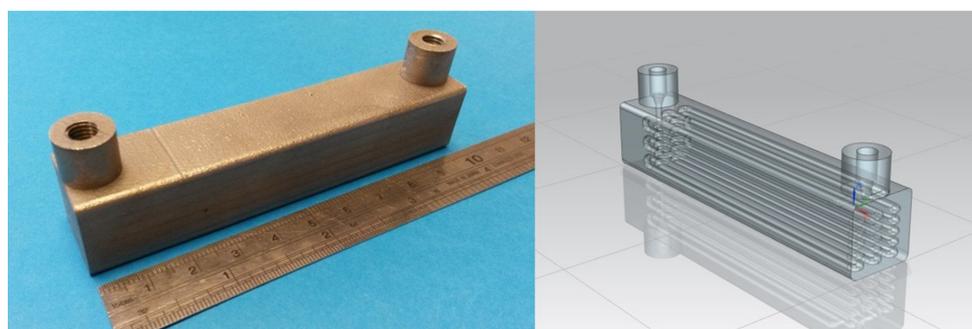
Figure 6: SLM reactor RD2 (left), CAD model of RD2 (right). External dimensions of RD2 are 100 (length) × 20 (width) × 20 mm (depth).

cal reaction volume = 10 mL). The titanium alloy used to manufacture the part is thermally stable across a substantial temperature range, and chemically compatible with a wide range of organic solvents and reagents, making it ideally suited to continuous flow chemistry.

The part was again tested using the semicarbazide preparation previously outlined (Scheme 1), and automated through the Chemstation software. For this optimisation an 1100 series binary pump module was used to pump the two reagent flows directly through RD2. The part was placed into the HPLC column compartment (Figure 7), and heated using the temperature control settings within the Chemstation software. The flow would then pass into a six port sampling valve, allowing the material to pass into either a collection vial, or be injected directly onto the HPLC column for purification and further analysis. To verify the actual temperature versus the set temperature, we flowed a methanol/water mix through the set-up and measured the temperature at the reactor exit. We did see an offset of around 5 °C for every set increase of 20 °C. Whilst there is predictability in this, this confirms that accurate reaction temperature measurement would be desirable in future design. For further details regarding the experimental set-up see Supporting Information File 1.

Figure 7: RD2 held in place within the thermostatted Agilent 1100 series column department.

The specific macro used during this optimisation was set up to calculate the peak area for both the carvone starting material, as well as the semicarbazone product. The percentage conversion of the starting material was then outputted as a single value. The

optimisation was run over the period of around 24 hours, generating 40 data points within the allowable temperature and flow rate range (Figure 8). This produced the optimal reaction conditions as being 79.6 °C and 0.24 mL/min, which had a conversion of 56%. Again the system was able to identify the general trend towards higher yields at lower flow rates and higher temperatures. However, switching from spectroscopic to chromatographic analysis caused a significant increase in the amount of time required to complete the optimisation, with each data point taking around 35 minutes to generate. However, the system did produce much more easily-quantifiable spectra resulting in a significant improvement in the reliability and accuracy of the data generated.
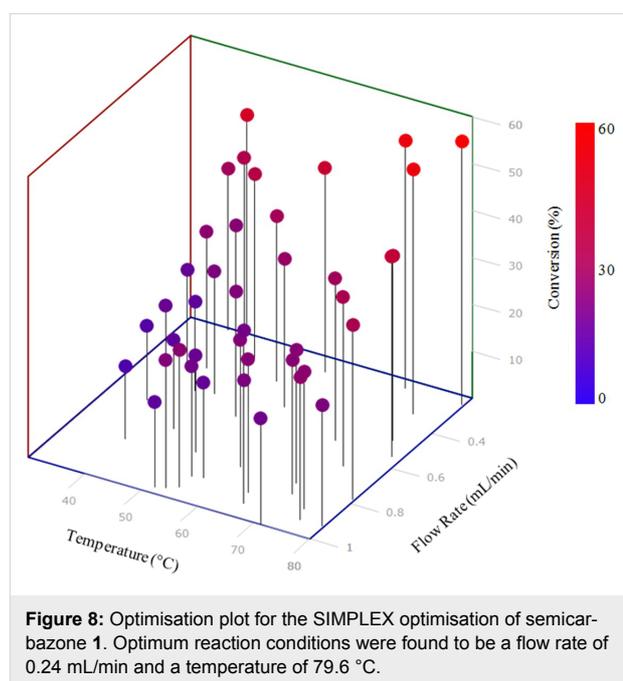
Figure 8: Optimisation plot for the SIMPLEX optimisation of semicarbazone **1**. Optimum reaction conditions were found to be a flow rate of 0.24 mL/min and a temperature of 79.6 °C.

The thermal and chemical stability of the Ti-6Al-4V alloy used to manufacture RD2 opened up a much wider range of potential chemical syntheses possible using this device. It was hypothesised that integrating RD2 with a commercially available FlowSyn module would allow a much larger chemical space to be analysed (<200 °C). The formation of a fused polycyclic heterocycle **5** (Scheme 2), from pentafluoropyridine (**3**) and 2-(methylamino)phenol (**4**), was chosen as this would
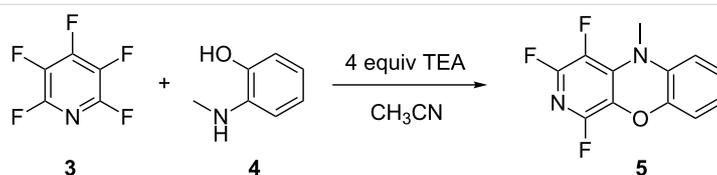
Scheme 2: The reaction of pentafluoropyridine (**3**) with 2-(methylamino)phenol (**4**) to form the corresponding fused polycyclic heterocycle **5**.

generate a more complex optimisation set with two starting materials, the reaction product as well as any potential reaction intermediates and unwanted side products. The reaction would also require elevated temperatures as well as a solvent system which would have proved destructive to the Accura resin used to manufacture RD1. These types of fused polycyclic heterocycles are of significant interest, as they have been shown to have significant antitrypanosomal activities against *Trypanosoma brucei rhodesiense,* with low or no toxicity towards mammalian cells [28], thus testing the system against a real research problem.

The reaction set-up for this optimisation consisted of RD2 being held into place on the chip heater of a FlowSyn system by a metal clip. The system was allowed to reach temperature with solvent pumping throughout the system, before switching to a reagent flow. The product from each optimisation point was collected and analysed via UV–vis spectroscopy at a wavelength of 330 nm. For further details regarding the experimental set-up see Supporting Information File 1.

The optimisation generated two optimal data points at 0.24 mL/min and 156 °C, and 0.24 mL/min and 170 °C, respectively (Figure 9). Despite a 12-fold increase in reaction conversion over the course of the optimisation, the optimum data point generated correlated to only around 23.4% conversion. This output does perhaps suggest that at a lower flow rate, or higher residence time, a more optimal set of reaction conditions could be realised. Limitations of the current pumping system used above made it impractical to drop to a lower flow rate, however, the inherent benefit of AM processes is that a new reactor design with a larger internal reaction volume can be realised within a short time period. In this manner AM affords the opportunity to design and develop reactor geometries, specifically tailored to the individual needs of the reaction in use, be that in terms of reactor dimensions or specific analysis sites located throughout the port, in a highly cost and time efficient manner. If coupled with HPLC purification of target compounds, it

offers a rapid method for generation of quantitites of compounds for further testing.

Figure 9: Optimisation plot for the SIMPLEX optimisation of the fused polycyclic heterocycle **5**. Two optimal data points at 0.24 mL/min and 156 °C, and 0.24 mL/min and 170 °C were found.
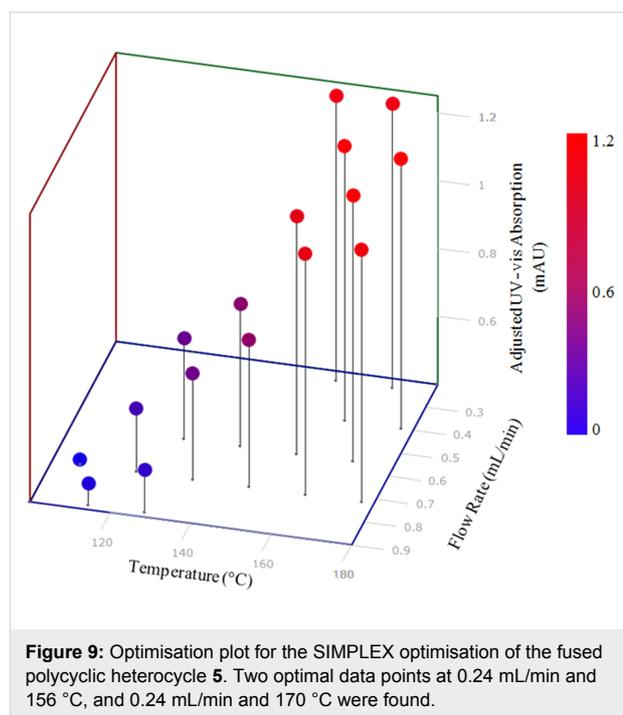
Reactor design 3 (RD3)

Having previously demonstrated that it was possible to manufacture a flow cell with in-build windows from polymer via the SL process (RD1), it was logical to produce a similar part from metal. This would allow high and low-temperature reactions to be undertaken, in a much larger range of chemical reagent and solvents. RD3 was again produced using a Renishaw AM 250 system from Ti-6Al-4V alloy, with external geometries of $89 \times 27 \times 38$ mm (volume = 24.6 cm^3) and a continuous cylindrical channel running throughout (channel diameter = 2 mm, channel length = 190 mm, reaction volume = 0.6 mL) (Figure 10). Like RD1, the external dimensions of the flow cell would match the internal dimensions of the DAD compartment,
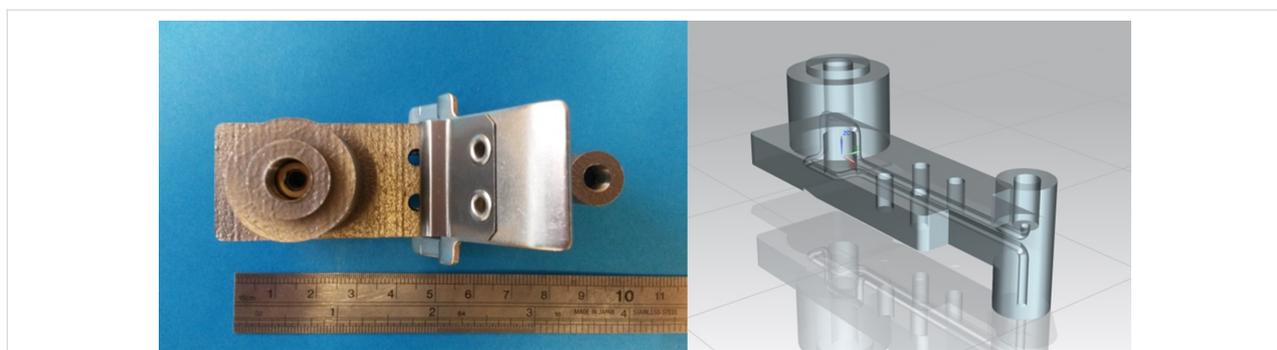
Figure 10: SLM reactor design RD3 (left), CAD model of RD3 (right). External dimensions of RD3 are 89 (length) × 27 (width) × 38 mm (depth).

whereby a flow cell of path length 2 mm would sit approximately half way along the flow path . For further details regarding the experimental set-up see Supporting Information File 1.

Again the part was tested using the model semicarbazone reaction and the same optimisation set-up used during the testing of RD1. However, the 5 mL stainless steel reaction coil previously used was replaced by RD3, which sat in the temperature controlled column compartment of the HPLC. This increased the total internal reaction volume to around 10.3 mL. This set-up meant that the entire reaction, analysis and optimisation would be performed within a single HPLC system, using only AM parts. The optimisation was run over the period of about 6 hours, generating 20 data points within the allowable temperature and flow rate range. This produced the optimal data point as being 75 °C and 0.2 mL/min (Figure 11). Both RD2 and RD3 have demonstrated the immense potential of AM processes to not only manufacture bespoke and customisable geometries which can be integrated with existing laboratory equipment, but also to manufacture functional chemical and thermally compatible reactors with embedded functionality.

the AM process allowed the generation of a selection of custom built metal and polymer parts. These parts were designed so that they could be integrated with existing pieces of flow and analysis instrumentation, as well as housing analytical functionality in the form of spectroscopic windows. By integrating this type of custom-made device with a piece of intuitive software, it was possible to develop a fully automated flow system capable of generating a significant amount of data at discrete locations within the flow system. There is therefore significant future research scope in this area where additive manufacturing offers the ability to embed analytical technology in reactors in innovative ways.

Supporting Information

Supporting Information File 1
General considerations, macros and experimental data.
[http://www.beilstein-journals.org/bjoc/content/supplementary/1860-5397-13-14-S1.pdf]

Acknowledgements

References

1. Wong, K. V.; Hernandez, A. *ISRN Mech. Eng.* **2012,** No. 208760. doi:10.5402/2012/208760
2. Masood, S. H. *Rapid Prototyp. J.* **1996,** *2,* 24–33. doi:10.1108/13552549610109054
3. Shallan, A. I.; Smejkal, P.; Corban, M.; Guijt, R. M.; Breadmore, M. C. *Anal. Chem.* **2014,** *86,* 3124–3130. doi:10.1021/ac4041857
4. Melchels, F. P. W.; Feijen, J.; Grijpma, D. W. *Biomaterials* **2010,** *31,* 6121–6130. doi:10.1016/j.biomaterials.2010.04.050
5. Friel, R. J.; Harris, R. A. *Procedia CIRP* **2013,** *6,* 35–40. doi:10.1016/j.procir.2013.03.004
6. Kruth, J. P.; Froyen, L.; Van Vaerenbergh, J.; Mercelis, P.; Rombouts, M.; Lauwers, B. *J. Mater. Process. Technol.* **2004,** *149,* 616–622. doi:10.1016/j.jmatprotec.2003.11.051
7. Bai, Y.; Williams, C. B. *Rapid Prototyp. J.* **2015,** *21,* 177–185. doi:10.1108/RPJ-12-2014-0180
8. Carroll, B. E.; Palmer, T. A.; Beese, A. M. *Acta Mater.* **2015,** *87,* 309–320. doi:10.1016/j.actamat.2014.12.054
9. Zein, I.; Hutmacher, D. W.; Tan, K. C.; Teoh, S. H. *Biomaterials* **2002,** *23,* 1169–1185. doi:10.1016/S0142-9612(01)00232-0
10. Brandl, E.; Baufeld, B.; Leyens, C.; Gault, R. *Phys. Procedia* **2010,** *5,* 595–606. doi:10.1016/j.phpro.2010.08.087
11. Monaghan, T.; Harding, M. J.; Harris, R. A.; Friel, R. J.; Christie, S. D. R. *Lab Chip* **2016,** *16,* 3362–3373. doi:10.1039/C6LC00562D

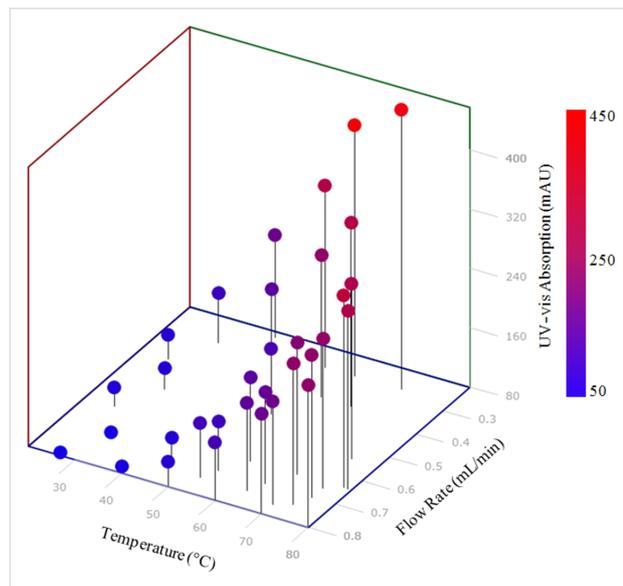**Figure 11:** Optimisation plot for the SIMPLEX optimisation of semicarbazone **2**. Optimum reaction conditions were found to be a flow rate of 0.2 mL/min and a temperature of 75 °C.

Conclusion

AM has been shown to be a highly versatile manufacturing process for the production of multifunctional bespoke flow reactors. This allows conceptual parts to be realised within a short time period, and consequently a rapid optimisation of the designed geometry can be achieved. The customisable nature of

12. Anderson, K. B.; Lockwood, S. Y.; Martin, R. S.; Spence, D. M. *Anal. Chem.* **2013,** *85,* 5622–5626. doi:10.1021/ac4009594

13. Capel, A. J.; Edmondson, S.; Christie, S. D. R.; Goodridge, R. D.; Bibb, R. J.; Thurstans, M. *Lab Chip* **2013,** *13,* 4583–4590. doi:10.1039/c3lc50844g

14. Tsuda, S.; Jaffery, H.; Doran, D.; Hezwani, M.; Robbins, P. J.; Yoshida, M.; Cronin, L. *PLoS One* **2015,** *10,* e0141640. doi:10.1371/journal.pone.0141640

15. Fitzpatrick, D. E.; Battilocchio, C.; Ley, S. V. *Org. Process Res. Dev.* **2016,** *20,* 386–394. doi:10.1021/acs.oprd.5b00313

16. Moore, J. S.; Smith, C. D.; Jensen, K. F. *React. Chem. Eng.* **2016,** *1,* 272–279. doi:10.1039/C6RE00007J

17. Yadroitsev, I.; Smurov, I. *Phys. Procedia* **2011,** *12,* 264–270. doi:10.1016/j.phpro.2011.03.034

18. Rombouts, M.; Kruth, J. P.; Froyen, L.; Mercelis, P. *CIRP Ann.* **2006,** *55,* 187–192. doi:10.1016/S0007-8506(07)60395-3

19. Louvis, E.; Fox, P.; Sutcliffe, C. J. *J. Mater. Process. Technol.* **2011,** *211,* 275–284. doi:10.1016/j.jmatprotec.2010.09.019

20. Thijs, L.; Verhaeghe, F.; Craeghs, T.; Van Humbeeck, J.; Kruth, J.-P. *Acta Mater.* **2010,** *58,* 3303–3312. doi:10.1016/j.actamat.2010.02.004

21. Sager, B.; Rosen, D. W.; Shilling, M.; Kurfess, T. R. Experimental Studies in Stereolithography Resolution. In *Proceedings of the Annual International Solid Freeform Fabrication Symposium,* The Fourteenth Solid Freeform Fabrication (SFF) Symposium, Austin, TX, Aug 4–6, 2003; University of Texas at Austin: Austin, TX, 2003; pp 70–81.

22. Kitson, P. J.; Glatzel, S.; Chen, W.; Lin, C.-G.; Song, Y.-F.; Cronin, L. *Nat. Protoc.* **2016,** *11,* 920–936. doi:10.1038/nprot.2016.041

23. Monaghan, T.; Capel, A. J.; Christie, S. D.; Harris, R. A.; Friel, R. J. *Composites, Part A* **2015,** *76,* 181–193. doi:10.1016/j.compositesa.2015.05.032

24. Holmes, N.; Akien, G. R.; Savage, R. J. D.; Stanetty, C.; Baxendale, I. R.; Blacker, A. J.; Taylor, B. A.; Woodward, R. L.; Meadows, R. E.; Bourne, R. A. *React. Chem. Eng.* **2016,** *1,* 96–100. doi:10.1039/C5RE00083A

25. Sans, V.; Cronin, L. *Chem. Soc. Rev.* **2016,** *45,* 2032–2043. doi:10.1039/C5CS00793C

26. MacroPad. http://waleson.eu/products/macropad/ (accessed Jan 15, 2015).

27. OceanOptics. http://www.oceanoptics.com/ (accessed Jan 15, 2015).

28. Brown-Barber, C. J. Ph.D. Thesis, Georgia State University, Atlanta, GA, USA, 2010.

Diels–Alder reactions of myrcene using intensified continuous-flow reactors

Christian H. Hornung[*], Miguel Á. Álvarez-Diéguez, Thomas M. Kohl and John Tsanaktsidis

Full Research Paper	Open Access

Address:
CSIRO Manufacturing, Bag 10, Clayton South, Victoria 3169, Australia

Email:
Christian H. Hornung[*] - christian.hornung@csiro.au

* Corresponding author

Abstract

This work describes the Diels–Alder reaction of the naturally occurring substituted butadiene, myrcene, with a range of different naturally occurring and synthetic dienophiles. The synthesis of the Diels–Alder adduct from myrcene and acrylic acid, containing surfactant properties, was scaled-up in a plate-type continuous-flow reactor with a volume of 105 mL to a throughput of 2.79 kg of the final product per day. This continuous-flow approach provides a facile alternative scale-up route to conventional batch processing, and it helps to intensify the synthesis protocol by applying higher reaction temperatures and shorter reaction times.

Introduction

Over the past years, great attention has been devoted to finding alternative, renewable feedstocks to fossil oil for the production of fuel and industrial chemicals. Especially, high value added products from fine chemicals, specialty chemicals or the pharmaceuticals sector allow for a 'drop-in' replacement of existing, fossil resources based synthesis routes with economic alternatives based on renewable sources. Besides chemical platforms based on sugar, lignin or fatty acid containing feedstocks, terpenes present another plant derived feedstock which is of great interest for a variety of industrial applications, first and foremost in the fragrance and flavor industries, but also in the pharmaceutical and chemical industries [1-3]. Myrcene is a naturally occurring, acyclic monoterpene which is used industrially for the manufacture of flavoring substances and fragrances; in research it is used as a model compound for a series of different reactions and in the synthesis of complex natural products, including several pheromones [3]. Myrcene is a colorless oil and exists as two isomers, the synthetic α-myrcene, containing an isopropenyl group, and the naturally occurring β-myrcene (which will be referred to in the following only as "myrcene"

(**1**), see Scheme 1, vide infra). It can be found in significant quantities (up to 39%) in the essential oils of several plants, such as wild thyme [4], ylang-ylang [5], bay leaf [6], juniper berries [7], lemongrass [8], or parsley [9], and in smaller percentages (<5%) in hops [3], celery [3], dill [9], rosemary [3], tarragon [10] and nutmeg [3] to name but a few. A review by Behr and Johnen [3] describes the manufacture of myrcene from other terpenes, as well as several synthetic routes based on this versatile and reactive starting material to form alcohols, esters, amines, chlorides, dimers, polymers and even complex natural products, amongst others. At present myrcene (**1**) is manufactured industrially from turpentine; the distillate of pine resin [3]. One of the main components of turpentine is β-pinene, from which myrcene can be synthesized upon thermal isomerization at temperatures between 400 and 600 °C. This was first described by Goldblatt and Palkin in 1947 [11]. Myrcene is a very versatile molecule that can act as the starting material for several valuable compounds. The industrial production of a series of top-selling flavors and fragrances are based on myrcene, such as geraniol, nerol, linalool, menthol, citral, citronellol or citronellal [3]. The terminal diene moiety present in myrcene allows for a reaction with a suitable dienophile following the Diels–Alder reaction mechanism. Dahill et al. describe the synthesis of the Diels–Alder adduct of myrcene and acrylonitrile for the use as an odorant in the perfume industry [12]. A series of Diels–Alder reactions of myrcene (**1**) and another sesquiterpene, farnesene, with various dienophiles have been reported by Tabor et al. [13] for the use as solvents and surfactants.

The emergence of compact continuous-flow reactors has begun to transform the way chemical synthesis is conducted in research laboratories and small manufacturing over the past few years [14-21]. In several applications, where reaction times are short and heat management is important, intensified continuous processes inside tubular or plate-type flow reactors can successfully replace batch methodologies classically carried out in stirred glass vessels. We have demonstrated the benefits of this superior heat management in previous work looking at exothermic radical polymerizations in continuous flow [22,23]. Over the past years, Diels–Alder reactions of isoprene using laboratory-scale flow reactors were studied by different research groups [24,25]. A continuous-flow reactor can offer a range of benefits over batch processing, with the enhanced heat and mass transfer arguable being one of the most important. In many cases increased control over the process and improvements in product quality are the result. Herein, we describe the synthesis of several Diels–Alder adducts made from myrcene (**1**) and a series of dienophiles, which contain carboxylic acids, esters or acid anhydrides. In particular, the reaction of myrcene (**1**) with acrylic acid (**2b**) was investigated in detail, through batch and continuous-flow methods. The intensified flow process presents a more compact and efficient alternative to classic batch manufacture for the production of Diels–Alder adduct surfactants from myrcene.

Results and Discussion

The solution-phase Diels–Alder reactions presented herein follow the general reaction pathway shown in Scheme 1. The

Scheme 1: Diels–Alder reaction of myrcene (**1**), with various dienophiles **2**.
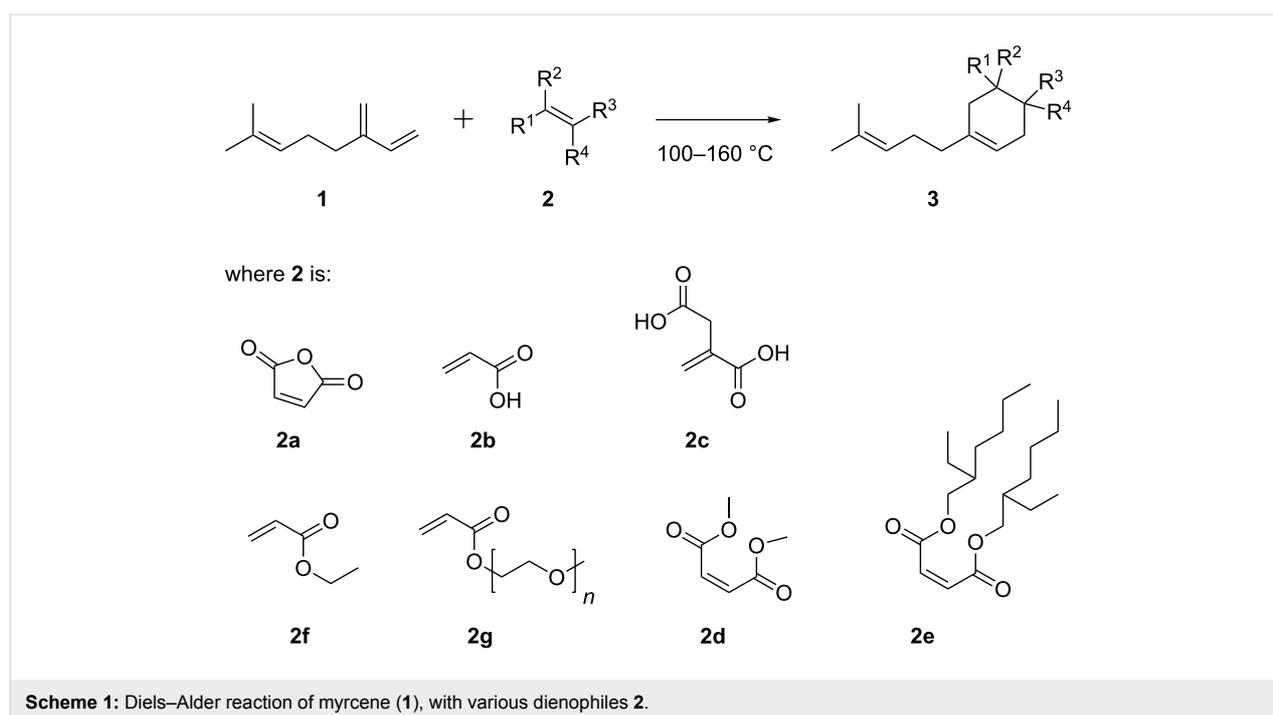
conjugated diene myrcene (**1**) was reacted with a series of dienophiles **2** to form the Diels–Alder adducts **3**.

Before investigating this reaction for continuous-flow processing, we first undertook a series of batch experiments to explore the reactivity of the different dienophiles shown in Scheme 1. These experiments were carried out on a batch microwave-reactor system (see experimental section) at temperatures between 100 and 140 °C, and the results are presented in Table 1.

Table 1: Reagents, reaction conditions and results for small scale batch reaction of myrcene with various dienophiles.

entry	dienophile	solvent[a]	T [°C]	reaction time	conversion [%][b]
1.1	**2a**	THF	100	5 min	90
1.2	**2b**	toluene	140	1 h	98
1.3	**2c**	iPrOH	140	10 h	70
1.4	**2d**	neat	140	10 h	97
1.5	**2e**	neat	140	10 h	93
1.6	**2f**	neat	120	5 h	96
1.7	**2g**	neat	140	10 h	48

[a]Entries 1.1 to 1.3 were reacted with an initial myrcene concentration, $c_{MYR,0}$, of 2.8 mol/L; all entries were reacted with a myrcene to dienophile ratio, R, of 0.9; [b]conversions were calculated based on NMR.

Maleic anhydride (**2a**) proved to be the most reactive of the dienophiles used in this study with reaction completion occurring after a few minutes at 100 °C. Other activated dienophiles such as acrylic acid (**2b**) and ethyl acrylate (**2f**) reached high conversions in excess of 90% after 1 to 5 h and the maleates **2d** and **2e** required up to 10 h reaction time at 140 °C to reach near-completion. The slowest reactions were observed using itaconic acid (**2c**) and the PEG containing acrylate **2g**. Acrylic acid (**2b**) was selected for further study given our interest in products with surfactant properties, and the preferable reaction kinetics

of the acrylic acid–myrcene system. Table 2 presents a set of experiments using this system, at different process conditions and in different solvents; samples were analyzed over time in order to establish kinetic profiles of these reactions. Figure 1 shows the kinetic profiles of the reactions presented in Table 2.

All reactions followed an expected trend, asymptotically approaching full conversion with increasing reaction time. While both EtOAc and toluene produced similarly fast kinetic data with conversions around 95% after 40 to 60 min toluene was preferred due to its higher boiling point. Figure 1b shows the influence of temperature and the ratio of starting materials. These experiments also showed trends as were expected. Values for the reaction rate constant, *k*, calculated from these experiments, are presented in Table 2 and are within expected limits when compared to literature values. More details on the derivation of the *k* values and the literature references can be found in Supporting Information File 1. After the Diels–Alder reaction was optimized in batch on a small scale (typically 2 mL reaction volume) the process was scaled-up first on a Vapourtec R2/R4 tubular flow reactor to a reaction volume of typically 20 mL and then on a Chemtrix Plantrix® MR260 plate flow reactor to a reaction volume of typically 200 mL (see also experimental section). The results from these continuous-flow experiments are shown in Table 3.

The 10-times scale-up in the tubular flow reactor and the 100 times scale-up in the plate flow reactor resulted in similar, if not slightly higher conversions than the batch experiments (see Figure 2). The two continuous reactors produced high-quality material at steady state conditions. The reaction profile in the plate flow reactor was quantified by taking samples at the outlet of the reactor over the entire duration of one experiment. These profiles are very uniform with steep fronts and tails and a flat steady state region, suggesting that the residence time distribution inside the reactor is narrow and close to plug flow. One

Table 2: Solvents, reaction conditions, conversions and reaction rate constants, *k*, for small scale batch reactions of myrcene (**1**) with acrylic acid (**2b**); for further details on derivation of *k* values see Supporting Information File 1.

entry	solvent	$c_{MYR,0}$ [mol L^{-1}][a]	R [–][b]	T [°C]	reaction time [h]	conversion [%][c]	$k \times 10^3$ [L mol^{-1} s^{-1}][d]
2.1	EtOAc	2.8	0.9	120	2	92	0.53
2.2	EtOAc	2.8	0.9	140	2	99	3.44
2.3	toluene	2.8	0.9	100	2	84	0.27
2.4	toluene	2.8	0.9	120	2	95	1.14
2.5	toluene	2.8	0.9	140	2	99	4.75
2.6	toluene	2.9	1.1	160	1	~100	27.05
2.7	toluene	2.9	1.2	160	1	~100	–

[a]Initial myrcene concentration; [b]ratio of myrcene to acrylic acid; [c]conversions were calculated based on NMR; [d]k was derived from kinetic studies plotted in Figure 1 for entries 2.1 to 2.6, as in these experiments R was close to 1 (between 0.9 and 1.1).
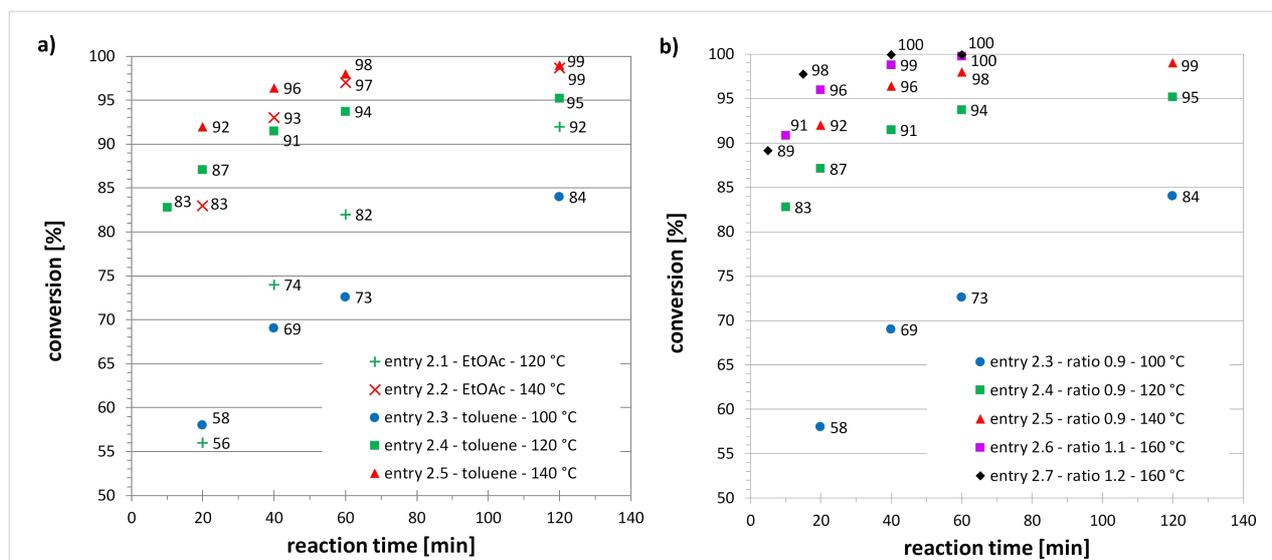
Figure 1: Kinetic studies of the Diels–Alder reaction between myrcene (**1**) and acrylic acid (**2b**); a) for different solvents and temperatures, ratio of myrcene to acrylic acid: 0.9; b) for different starting material ratios and temperatures, solvent: toluene.

Table 3: Solvents, reaction conditions and results for the continuous-flow reaction of myrcene (**1**) with acrylic acid (**2b**) in a tubular flow reactor (reactor volume: 20 mL) and a plate flow reactor (reactor volume: 105 mL); all entries were reacted with a myrcene to dienophile ratio, *R*, of 0.9, and $c_{MYR,0}$ of 2.8 mol/L.

entry	reactor	solvent	*R* [–]	*T* [°C]	residence time [min]	conversion [%][a]
3.1	tubular	EtOAc	0.9	140	20	75
3.2	tubular	EtOAc	0.9	140	30	95
3.3	tubular	EtOAc	0.9	140	40	99
3.4	tubular	toluene	0.9	120	40	93
3.5	tubular	toluene	0.9	140	40	99
3.6	plate	toluene	0.9	112	40	85
3.7	plate	toluene	0.9	130	40	93
3.8	plate	toluene	1.1	140	40	~100
3.9	plate	toluene	1.1	160	30	99

[a]Conversions were calculated based on NMR.

of these profiles is shown in Figure S4 (Supporting Information File 1). The fastest conditions investigated herein were 30 min in the plate reactor at 160 °C giving 99% conversion of **2b** and a yield of 94% of a semi-crystalline product (Table 3, entry 3.9). As part of the scale-up investigations, we also performed the Diels–Alder reaction of myrcene (**1**) and **2b** in a 6 mm i.d. stainless steel tubular flow reactor with a reaction volume of 108 mL. A few minutes after start of the reaction, however, we observed a pressure increase in the reactor which was caused by fouling occurring in the reactor entrance section and ultimately led to complete blockage of the tube at this point. This is believed to be caused by a side reaction of **2b** and myrcene (**1**) forming polymeric material, which built up on the metal walls of the reactor, ultimately leading to the complete blockage. The mechanism and circumstances of this side-reaction are unknown; it only occurred in the stainless steel reactor and not in the PFA tubing of the Vapourtec R-series flow reactor or the silicon carbide module of the plate flow reactor. Hence, it was postulated that a metal catalyzed polymerisation on the stainless steel reactor tubes might have occurred, however, this could not be confirmed. Further details on these observations can be found in Supporting Information File 1.

Using ^{13}C NMR an approximate ratio of the two isomers, **3**-3 and **3**-4 (see Figure 2), was calculated for the continuous-flow reactions performed between 140 and 160 °C (see Table 3). The amount of Diels–Alder adduct with the carboxylic acid located in the 3-substituted position, **3**-3, was always larger than the 4-substituted adduct, **3**-4, with an average **3**-3/**3**-4 ratio of 7:3 (3-substituted adduct was between 68 and 71%).

Figure 2: Comparison of conversions in three different reactors for the Diels–Alder reaction of myrcene (**1**) with acrylic acid (**2b**) in toluene; the reaction forms two isomers, **3**-3 and **3**-4; reaction temperature for these experiments: 120, 130 or 140 °C, reaction time: 40 min; photographic images of a tubular reactor coil of the Vapourtec R2/R4 flow reactor [26] and of the plate reactor module of the Chemtrix Plantrix® MR260 [27].

For Table 3, entry 3.9, the yield of the semi-crystalline product after solvent removal was 94%. The production capacity (PC) and the space time yield (S.T.Y.) can be calculated based on the amount of isolated product, m_P, using Equations 1 and 2.

$$PC = \frac{m_P \dot{V}}{V_{SS}} \qquad (1)$$

$$S.T.Y. = \frac{PC}{V_R} \qquad (2)$$

Here, $\dot{V}$ is the total volumetric flow rate through the reactor, V_{SS} the combined volume of both stock solutions and V_R the volume of the flow reactor. Running the plate reactor at 160 °C (Table 3, entry 3.9), we managed to achieve a production capacity of 116.3 g/h, which equates to an S.T.Y. of 1.11 kg L^{-1} h^{-1}. Parallel to the scale-up in the plate flow reactor, we also scaled up the process in batch to a 6 L scale using a jacketed stirred tank reactor. Here, the reaction was run for ~10 h at 100 °C in order to reach completion, compared to only 30 min at 160 °C in continuous flow.

Preliminary experiments were carried out looking at the surfactant properties of the Diels–Alder adduct of myrcene (**1**) and **2b**. The results were promising and showed that the product was able to stabilize emulsions for several hours compared to several seconds or minutes in the control experiments without the Diels–Alder adduct. Further details on these surfactant tests are presented in Supporting Information File 1.

Conclusion

We have investigated the Diels–Alder reaction of myrcene (**1**) with a range of different dienophiles at temperatures between 100 and 160 °C. The Diels–Alder reaction of myrcene (**1**) with acrylic acid (**2b**), yielding a carboxylic acid containing surfactant, was scaled-up in a plate-type continuous-flow reactor and a batch stirred tank. The use of continuous-flow processing allows for an efficient synthesis of large quantities of the Diels–Alder adduct and we managed to scale-up the reaction of myrcene (**1**) with acrylic acid (**2b**) inside the 105 mL flow reactor to a throughput of 2.79 kg of the final product per day. The small dimensions of the fluidic channels inside the tubular and the plate-type flow reactors ensured that heat and mass transfer were efficient and fast, and that the reaction could be operated under 'quasi isothermal' conditions (i.e., with negligible deviations from the set temperature in the entire bulk reaction volume of the reactor). This resulted in a much more uniform reaction profile than in batch stirred tanks, allowing for a much shorter reaction time than classically applied in batch operations.

Experimental

Materials and analysis

The reactants myrcene (**1**, 90% purity), maleic anhydride (**2a**), acrylic acid (**2b**), itaconic acid (**2c**), dimethyl maleate (**2d**), ethyl acrylate (**2f**) and poly(ethylene glycol) methyl ether acrylate (PEGA, **2g**) were obtained from Sigma-Aldrich; bis(2-ethylhexyl) maleate was provided by TriTech Lubricants. The solvents tetrahydrofuran (THF), ethyl acetate (EtOAc), toluene, dichloromethane (DCM) and isopropanol (iPrOH) were obtained from Merck KGaA. All reagents and solvents were used without further purification.

Reaction conversions were calculated from ^{1}H NMR spectra, which were recorded on a Bruker AC-400 spectrometer in deuterated chloroform (from Cambridge Isotope Laboratories Inc.). Conversion calculations were based on clearly identifiable and non-convoluted peaks of remaining starting material and generated product. The residual solvent peak at δ = 7.26 ppm was used as an internal reference. Product compositions were analyzed by GC–FID and GC–MS; details for both can be found in Supporting Information File 1. The GC–FID results were also used to confirm NMR conversions and to calculate GC-based yields.

Batch Diels–Alder reaction

The following procedure is typical for the preparation of the Diels–Alder adduct of myrcene (**1**) and a series of different dienophiles. A reactant solution of myrcene (**1**, 811 mg of myrcene stock solution with a 90% purity, 5.36 mmol of myrcene), **2b** (429 mg, 5.95 mmol), in EtOAc (0.49 mL), was premixed and filled into a sealed microwave vial. The reaction was conducted in a laboratory microwave reactor (Biotage Initiator) at 140 °C with a reaction time of 2 h. A transparent, faintly yellow solution was obtained after reaction, from which the conversion was determined by ^{1}H NMR. The solvent was evaporated under reduced pressure to yield a yellow semi-crystalline paste. Detailed reaction conditions and reagent compositions for each batch experiment can be found in Table 1 and Table 2. For kinetic studies, small samples of the reaction mixture for ^{1}H NMR were withdrawn through the septum of the microwave reactor glass vial using a syringe. For this the microwave reaction was stopped at various points in time over the course of the reaction, namely at 20, 40, 60 and 120 min.

Continuous-flow Diels–Alder reaction using a Vapourtec R2/R4 flow reactor

The following procedure is typical for the preparation of the Diels–Alder adduct of myrcene (**1**) and acrylic acid (**2b**) in a tubular flow reactor. Two reactant solutions were prepared, one containing myrcene (16.22 g of myrcene stock solution with a 90% purity, 107.16 mmol of myrcene) in EtOAc (1.98 mL), and

the other containing **2b** (8.58 g, 119.06 mmol), in EtOAc (7.75 mL). The two solutions were continuously mixed in a T-piece and then fed into a Vapourtec R2/R4 flow reactor set-up [26], consisting of two 1.0 mm i.d. perfluoroalkoxy alkane (PFA) reactor coil modules in series (10 mL each – total reactor volume: 20 mL). The pump flow rate of the myrcene solution was set to 0.3 mL·min^{-1}, the pump flow rate of the acrylic acid solution was set to 0.2 mL·min^{-1}. This resulted in a total flow rate of 0.5 mL·min^{-1} and a mean hydraulic residence time of 40 min inside the two PFA reactor coils (the mean hydraulic residence time is defined as 'flow rate/reactor volume'). The reaction was conducted at 140 °C. The product, a transparent, faintly yellow solution, was collected at the reactor outlet, after passing through a 75 psi back-pressure regulator. From this solution, the reaction conversion was determined by ^{1}H NMR. Afterwards, the solvent was evaporated under reduced pressure to yield a yellow semi-crystalline paste. Detailed reaction conditions and reagent compositions for each experiment in the tubular flow reactor can be found in Table 3.

Continuous-flow Diels–Alder reaction using a Chemtrix MR260 flow reactor

The following procedure is typical for the preparation of the Diels–Alder adduct of myrcene (**1**) and acrylic acid (**2b**) in a silicon carbide plate-type flow reactor. Two reactant solutions were prepared, one containing myrcene (208.2 g of myrcene stock solution with a 90% purity, 1.375 mol of myrcene) in toluene (21.2 mL), and the other containing **2b** (90.1 g, 1.250 mol), in toluene (80.1 mL). The two feed solutions were pumped using two Teledyne Isco D-series dual syringe pumps (100 DX, with Hastelloy™ syringes) and were continuously mixed in a T-piece. After mixing, the combined starting material solution was fed into a Chemtrix Plantrix® MR260 [27] plate-type flow reactor. This plate flow reactor configuration consisted of a series of 3M™ silicon carbide microstructured plates (see also Figures S2 and S3 in Supporting Information File 1), which was thermally regulated by a Lauda Integral XT 150 heater/chiller unit. The total reactor volume was 105 mL. An SSI Prep 100 dual piston pump with PEEK pump heads was used to flush the reactor before and after the reaction with toluene. The pump flow rate of the myrcene solution was set to 2.21 mL·min^{-1}, the pump flow rate of the acrylic acid solution was set to 1.30 mL·min^{-1}. This resulted in a total flow rate of 3.51 mL·min^{-1} and a reaction time of 30 min inside the plate flow reactor. The reaction was conducted at 160 °C. The product, a transparent, faintly yellow solution, was collected at the reactor outlet, after passing through a stainless steel Swagelok® R3A series adjustable high pressure valve. This valve was used as a back pressure regulator, in order to set the pressure inside the reactor to between 8 and 10 bar (116 to 145 psi) during operation. From the resulting product solution, the reaction

conversion was determined by ^{1}H NMR. Afterwards, the solvent was evaporated under reduced pressure to yield a yellow semi-crystalline paste. Detailed reaction conditions and reagent compositions for each experiment in the plate-type flow reactor can be found in Table 3.

Supporting Information

Supporting Information File 1

Analysis procedures, calculation of *k*-values, reactor performance profiles, reactor fouling, emulsion stabilizing properties, copies of ^{1}H and ^{13}C NMR and of GC-FID spectra.

[http://www.beilstein-journals.org/bjoc/content/supplementary/1860-5397-13-15-S1.pdf]

Acknowledgements

The authors thank Charlotte Wiles from Chemtrix BV for helpful discussions and Matthew Waterford and Stuart Littler for assistance with the operation of the Chemtrix Plantrix® MR260 reactor.

References

1. Romeo, L. M.; Catalina, D.; Lisbona, P.; Lara, Y.; Martínez, A. *Greenhouse Gases: Sci. Technol.* **2011,** *1,* 72. doi:10.1002/ghg3.5
2. Gallezot, P. *Catal. Today* **2007,** *121,* 76. doi:10.1016/j.cattod.2006.11.019
3. Behr, A.; Johnen, L. *ChemSusChem* **2009,** *2,* 1072. doi:10.1002/cssc.200900186
4. Wilden, K.-G.; Alanko, P.; Uotila, M. *Ann. Bot. Fenn.* **1977,** *14,* 29.
5. Fekam Boyom, F.; Amvam Zollo, P. H.; Menut, C.; Lamaty, G.; Bessière, J. M. *Flavour Fragrance J.* **1996,** *11,* 333. doi:10.1002/(SICI)1099-1026(199611)11:6<333::AID-FFJ582>3.0.CO; 2-O
6. Abaul, J.; Bourgeois, P.; Bessiere, J. M. *Flavour Fragrance J.* **1995,** *10,* 319. doi:10.1002/ffj.2730100506
7. Bonaga, G.; Galletti, G. C. *Anal. Chim. Acta* **1985,** *75,* 131.
8. Shu, C.-K.; Lawrence, B. M. Reasons for the Variation in Composition of Some Commercial Essential Oils. In *Spices, Flavour Chemistry and Antioxidant Properties;* Risch, S. J.; Ho, C.-T., Eds.; American Chemical Society Symposium Series, Vol. 660; American. Chemical Society: Washington, 1997; pp 138–159. doi:10.1021/bk-1997-0660.ch012
9. Orav, A.; Kailas, T.; Jegorova, A. *Proc. Est. Acad. Sci., Chem.* **2003,** *52,* 147–154.
10. Verma, M. K.; Anand, R.; Chisti, A. M.; Kitchlu, S.; Chandra, S.; Shawl, A. S.; Khajuria, R. K. *J. Essent. Oil-Bear. Plants* **2010,** *13,* 331.
11. Goldblatt, L. A.; Palkin, S. *Process for converting nopinene to myrcene.* U.S. Patent US2420131, May 6, 1947.
12. Dahill, R. J., Jr. *Myrcene-methacrylonitrile adducts.* U.S. Patent US3714220, Jan 30, 1973.
13. Tabor, R.; Bernhardt, R. J.; Luxem, F. J.; Yao, C.; Wallace, G. J. *Surfactants and Solvents Containing Diels-Alder Adducts.* WO Patent WO2013148842, Oct 3, 2013.
14. Blacker, A. J.; Breen, J. R.; Bourne, R. A.; Hone, C. A. The Growing Impact of Continuous Flow Methods on the Twelve Principles of Green Chemistry. *Green and Sustainable Medicinal Chemistry;* The Royal Society of Chemistry, 2016; pp 140–155.
15. Ley, S. V.; Fitzpatrick, D. E.; Ingham, R. J.; Myers, R. M. *Angew. Chem.* **2015,** *127,* 3514. doi:10.1002/ange.201410744
16. Myers, R. M.; Fitzpatrick, D. E.; Turner, R. M.; Ley, S. V. *Chem. – Eur. J.* **2014,** *20,* 12348. doi:10.1002/chem.201402801
17. Elvira, K. S.; Casadevall i Solvas, X.; Wootton, R. C. R.; deMello, A. J. *Nat. Chem.* **2013,** *5,* 905. doi:10.1038/nchem.1753
18. Wiles, C.; Watts, P. *Green Chem.* **2012,** *14,* 38. doi:10.1039/C1GC16022B
19. Watts, P.; Wiles, C. *J. Chem. Res.* **2012,** *36,* 181. doi:10.3184/174751912X13311365798808
20. Ehrfeld, W.; Hessel, V.; Löwe, H. *Microreactors: New Technology for Modern Chemistry;* Wiley-VCH Verlag GmbH: Weinheim, 2000. doi:10.1002/3527601953
21. Baxendale, I. R.; Hornung, C.; Ley, S. V.; de Mata Muñoz Molina, J.; Wikström, A. *Aust. J. Chem.* **2013,** *66,* 131. doi:10.1071/CH12365
22. Micic, N.; Young, A.; Rosselgong, J.; Hornung, C. H. *Processes* **2014,** *2,* 58. doi:10.3390/pr2010058
23. Hornung, C. H.; Guerrero-Sanchez, C.; Brasholz, M.; Saubern, S.; Chiefari, J.; Moad, G.; Rizzardo, E.; Thang, S. H. *Org. Process Res. Dev.* **2011,** *15,* 593. doi:10.1021/op1003314
24. Hornung, C. H.; Mackley, M. R.; Baxendale, I. R.; Ley, S. V. *Org. Process Res. Dev.* **2007,** *11,* 399. doi:10.1021/op700015f
25. McMullen, J. P.; Jensen, K. F. *Org. Process Res. Dev.* **2011,** *15,* 398. doi:10.1021/op100300p
26. Vapourtec Ltd.. http://www.vapourtec.co.uk/home.
27. Chemtrix BV. http://www.chemtrix.com/.

Self-optimisation and model-based design of experiments for developing a C–H activation flow process

Alexander Echtermeyer[1,2], Yehia Amar[2], Jacek Zakrzewski[2] and Alexei Lapkin[*2,§]

Full Research Paper

Address:
[1]Aachener Verfahrenstechnik – Process Systems Engineering, RWTH Aachen University, Aachen, Germany and [2]Department of Chemical Engineering and Biotechnology, University of Cambridge, Cambridge, United Kingdom

Email:
Alexei Lapkin[*] - aal35@cam.ac.uk

* Corresponding author
§ + 44 1223 334796

Abstract

A recently described $C(sp^3)$–H activation reaction to synthesise aziridines was used as a model reaction to demonstrate the methodology of developing a process model using model-based design of experiments (MBDoE) and self-optimisation approaches in flow. The two approaches are compared in terms of experimental efficiency. The self-optimisation approach required the least number of experiments to reach the specified objectives of cost and product yield, whereas the MBDoE approach enabled a rapid generation of a process model.

Introduction

The development of manufacturing processes to produce functional molecules, such as pharmaceuticals or fine chemicals, often relies on experience and trial-and-error, rather than on mechanistic process models [1]. The only reason for this is the complexity of chemistry and the duration of time required for the development of good mechanistic models. A game changer in this area is the recently emerged field of automated continuous-flow experiments driven by algorithms for sequential design of experiments (DoE), which significantly reduce the effort in running routine reactions and generating data for optimisation of reaction conditions [2-7]. An illustration of the concept is shown in Figure 1.

Mainly, self-optimisation experimental platforms are used to rapidly obtain optimal reaction conditions using either flow [8-10] or batch experiments [11]. In these cases, the optimisation is driven by the global or target optimisation towards the selected performance criteria. This is rather different from the objectives of model development. In the case of model development, the key criterions are the ability of a model to describe

Figure 1: A framework of closed-loop or self-optimisation combining smart DoE algorithms, process analytics, chemoinformatics and automated reactor systems.
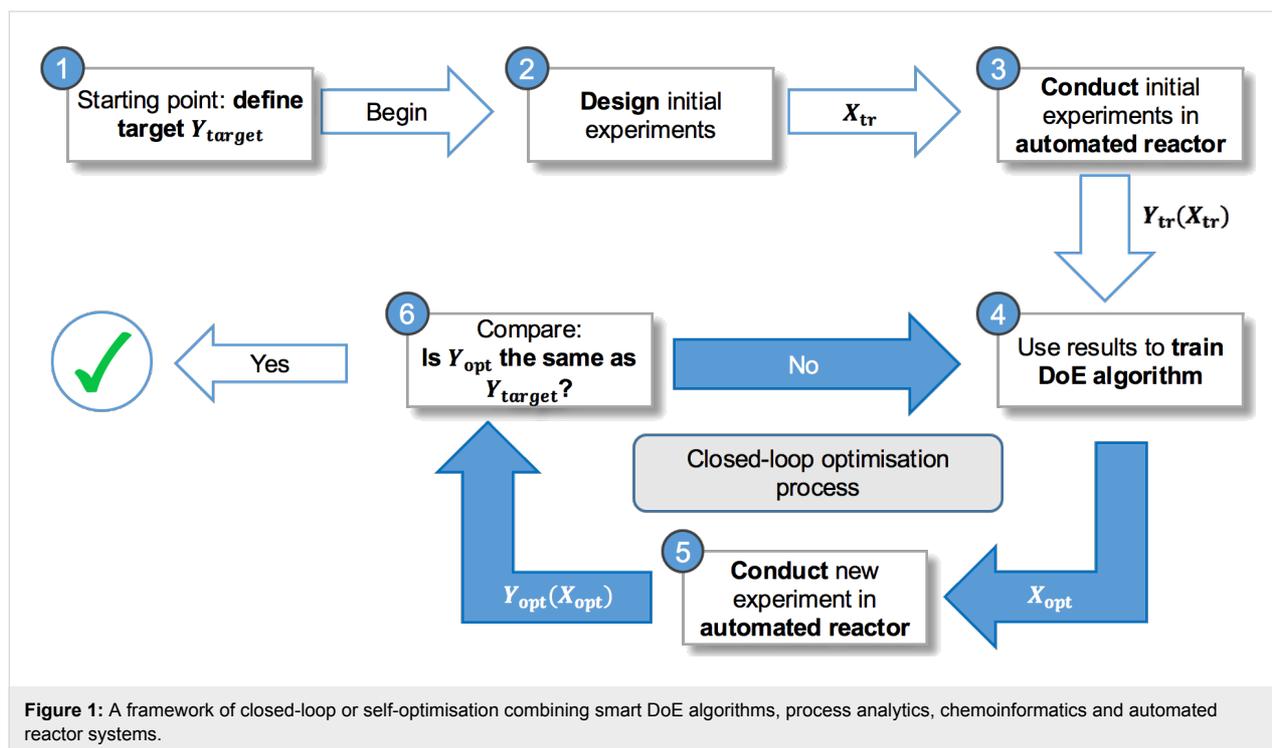
the observed experimental data and to predict process performance under unseen conditions. Thus, experiments required for model development are frequently what would be considered as 'bad' experiments in the case of optimisation.

A model-development framework has been demonstrated on the basis of an automated microreactor experimental system for several complex reactions [8,12,13]. The framework uses factorial design of experiments to obtain an initial data set for parameter estimation, followed by an iterative search with online model discrimination and parameter estimation, guided by D-optimal design. In a different approach, transient data from continuous-flow experiments were used to identify parameters of a known mechanistic scheme to discriminate between several alternative model structures and to identify model parameters, but no specific design of experiments method was used [14].

The framework proposed in the present publication is using a model-based design of experiments method (MBDoE) [15-17], which incorporates the model with its parameters, as well as details of the experimental setup, such as measurement accuracy and experimental limitations, to design the most informative experiments. This approach requires some model structures to be known a priori which may restrict the methodology to reactions with known mechanism, or to empirical parametric models. A discussion of how a priori knowledge of chemistry, i.e., reaction mechanisms, is included in self-optimisation and model-development frameworks is not well documented in the

literature. Very recently we have shown that a priori knowledge in the form of density functional theory level (DFT) mechanistic calculations can be used to propose process models and to perform in silico design of novel flow processes [18]. In this publication, we present an extension of this methodology, in which an initial process model is developed through a MBDoE methodology coupled with an automated self-optimisation flow system.

This approach was tested on the Pd-catalysed C–H activation reaction of **1** resulting in the formation of an aziridine **2** (Scheme 1) [19]. The reaction was recently discovered [20] and its mechanism studied [21] and later proven [18]. A simplified mechanism is shown in Scheme 2. In the reaction of interest, the starting material **1**, an aliphatic secondary amine, is converted into an intermediate species **B** in a catalytic first step and

Scheme 1: Catalytic reaction scheme showing C–H activation of an aliphatic secondary amine **1** to form the aziridine product **2** [19,20]. Orange rings show C–H and C–N bonds in the substrate and the product, respectively, indicating the location of the C–H activation.

Scheme 2: A simplified reaction mechanism based on literature [21], showing intermediate **B** and the side reaction compounds **1**·HOAc and **A**. The key step includes the C–H activation. **1**: starting material, **1**·HOAc: coordinated starting material, Pd(OAc)$_2$: catalyst, **2**: product, PhI(OAc)$_2$: oxidant.

consecutively transformed to product **2** in the second step, which comprises the C–H activation. In addition to the main reaction pathway, **B** can form the relatively unreactive resting state complex **A**, and compound **1** can also form a coordinated species **1**·HOAc upon protonation with a molecule of acetic acid. This limits the formation of **A** due to reduced concentration of **1**.

Table 1 gives an overview of the a priori knowledge used in this study. Fast reaction steps were lumped into a single one, containing the critical C–H activation, and described by reaction rate constant k_3 in Scheme 2. Empirical information provided constraints of process conditions, such as temperature and concentration ranges, whereas initial values of kinetic parameters were estimated based on a DFT model. Further details can be found in Supporting Information File 1.

Here we demonstrate an MBDoE approach on the basis of the model structure and the initial model parameters from DFT calculations and using automated flow experiments. We then use the obtained process model to develop a surrogate model for optimisation, and compare the different methodologies: classical kinetic modeling approach, MBDoE with automated flow experiments and black-box optimisation in achieving the different objectives of the methods.

Results and Discussion
Experimental system for model development and optimisation in flow
Although a number of experimental systems for self-optimisation were reported in the literature, this number is fairly small and very few examples of using flow experiments for model development are reported [8,9]. In this study a commercial

Table 1: Details of information considered as a priori knowledge in this study and source of this knowledge.

A priori knowledge	Source
reaction mechanism, concentration constraints of species due to degradation of starting material and product.	[21]
Gibbs free energies of reaction, obtained from DFT study.	[18]
target values based on best results from previous experimental study.	[18]
physical constraints (maximum oxidant concentration to prevent crystallisation, maximum temperature to prevent excessive catalyst decomposition).	empirical
technical details of experimental set-up (e.g., variance of gas chromatography (GC) used in variance model for MBDoE, minimum and maximum flow rates).	empirical

Vapourtec R2+/R4 system was used with a standard 10 mL coiled reactor. To save on expensive reagents, reagents and catalyst were injected using 2 mL sample loops, with the solvent being continuously pumped between the reaction slugs. The two employed sample loops were filled with the same reaction mixture (further information on sample preparation is given in Supporting Information File 1) to avoid potential experimental errors due to inaccuracies of generating mixtures with specific concentrations by pumps. Laminar flow through long pipes will necessarily cause dispersion, which dictates the minimum reaction slug length that can be used. This was determined experimentally, which also allowed to develop the method of detection of the reaction slugs (by a flow UV cell) and the protocol for GC sampling. A schematic depiction of the experimental system is shown in Figure 2.

Physical model generation and refinement

The initial model structure and parameters were taken from the earlier published DFT study of the reaction [18]. Performing MBDoE in the process modelling software gPROMS [22] resulted in a design indicating the experimental conditions, the reaction times and the number of samples required in each experiment for the estimation of a particular parameter or the combination of parameters. Table 2 shows the different experiments conducted for estimation of the given parameters. Each experiment refers to a particular composition of the reaction mixture, but with various reaction times for each sample within the experiment. Neither in the MBDoE step for $k_{j,ref}$ nor in the step for $E_{a,j}$ could an experiment be designed for the estimation of all parameters simultaneously. This is likely due to correlations between the parameters, which is common for reaction

networks and consecutive reactions. To overcome this problem, sophisticated decoupling techniques and special design criteria considering direct measures of correlation could be used [23,24]. However, as shown by Franceschini and Macchietto, a simple design-by-grouping method can also yield reasonable results [25]. Following this approach experiments were designed for either a single or groups of parameters. Parameters, which showed a maximum in their normalised local sensitivity curves in the same time interval were grouped together. This is reasonable, as a sample taken in this time interval likely yields sensible data for the estimation of the respective parameters. As can be seen from Figure S9 (Supporting Information File 1), all parameters of the same type showed maximum sensitivity in approximately the same time interval. Hence, all possible combinations of single and grouped parameters were tested in the two MBDoE steps and those with the lowest correlation, maximum number of included parameters and a t-value larger than a reference t-value were selected. It is worth noting, that this method overcomes problems with parameter correlations during the experimental design for parameter subgroups and the subsequent estimation. The effects of the neglected parameter correlation may reoccur during the overall parameter estimation, but can be reduced due to the refinement of the parameters in the subgroups.

The best possible design with minimum analytical effort was selected. It can be seen from Table 2 that the t-test is successful for the experiments 1–3. This is not surprising as possible correlations between the parameters are neglected by splitting them into subgroups or even singles. For the experiments 4, 5 and 6 (Table 2) not all parameters pass the t-test. The best possible ex-
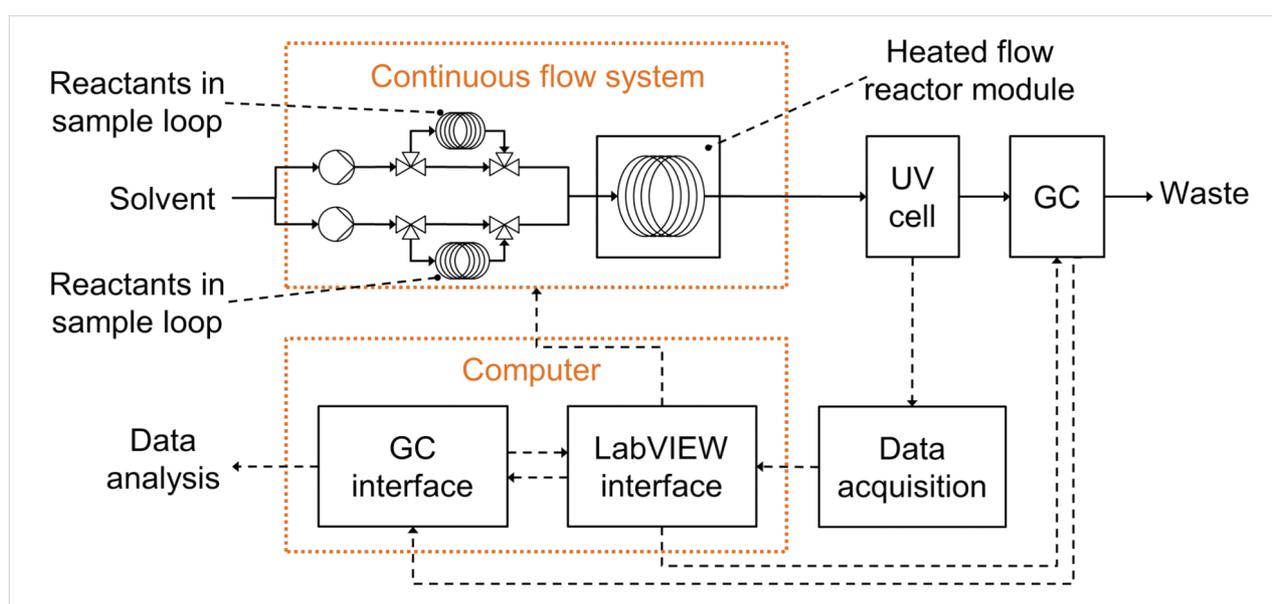
Figure 2: Schematics of the automated continuous-flow system used for model development and 'black-box' sequential optimisation.

Table 2: Results of the MBDoE for kinetic parameters, showing the number of samples needed in the experiment and the statistical t-test results.

Experiments	Parameter(s)	Number of samples	t-value	t_{ref}
1	$k_{0,ref}$	7	76.19	2.92
2	$k_{2,ref}$	6	23.36	2.92
3	$k_{3,ref}$	5	23.36	2.92
4	$k_{0,ref}, k_{2,ref}, k_{3,ref}$	11	5.34, 0.03, 6.42	1.94
5	$E_{a,0}, E_{a,2}, E_{a,3}$	11	0.05, 0.04, 2.88	1.94
6	$E_{a,0}, E_{a,2}, E_{a,3}$	11	0.63, 0.25, 2.33	1.94
7	$E_{a,0}, E_{a,2}$	10	2.79, 17.1	2.02
8	$E_{a,0}, E_{a,3}$	10	3.99, 46.8	1.94

perimental design was selected. Due to failed estimability analysis, no experiment design included parameters for the reaction $j = 1$. Experimental conditions associated with each experiment sequence are given in Supporting Information File 1, Table S4 and Table S5.

Parameter estimation and comparison of effort

For the investigated reaction in Scheme 2, Zakrzewski et al. generated and validated a kinetic model using a classical kinetic approach [18]. For this they used 38 batch experiments, each comprising approximately 10 sample points at different reaction times, which in total resulted in more than 400 sample points used for the estimation of kinetic model parameters. In contrast to that, we used MBDoE and flow experiments. As Table 2 shows, the MBDoE resulted in 8 experiments with a total of 71 samples required to determine the model parameters. These numbers highlight the benefit of MBDoE for parameter estimation, reducing the consumption of materials, cost and time associated with sample generation. Due to some failed experiments only 64 experimental sample points were used for the model development.

The parameter estimation was employed to obtain estimates of the kinetic parameters $k_{j,ref}$ and $E_{a,j}$, where $j \in \{0, 1, 2, 3\}$ in a two-step procedure using standard solver settings in gPROMS. By applying the initial guesses for the parameters, each experiment was first used to estimate only the parameter for which it was designed, while keeping the others fixed at their current values. Afterwards, all experiments were included in an overall estimation with the parameter values obtained from the previous estimations as new initial guesses to account for possible parameter correlations, which were neglected by grouping the parameters. Even though no experiment design comprised the parameters for reaction $j = 1$ specifically, they were still included in the overall estimation to refine their initial values as much as

possible. To avoid stopping the estimation at undesired local optima, several such estimation runs were performed. The final results of the obtained parameter values are shown in Table 3. The final values of parameters $k_{1,ref}$ and $E_{a,1}$ do not differ much from the initial guesses, which is not surprising as the estimability analysis had already predicted a weak influence of $k_{1,ref}$ and $E_{a,1}$ on the model output, i.e., this cannot be estimated with precision. However, this was not necessary, as the parameters do not change the model prediction. Therefore, also the very large 95% confidence interval can be explained. For all other parameters, the difference between initial guess and final value is significant, which might be caused be the simplifications employed for computing the guesses and the uncertainty of the DFT calculation in the exponentially amplified van't Hoff equation. The 95% confidence intervals for the parameters of reaction $j = 0$ are both one magnitude smaller than the final parameter values indicating sufficiently low uncertainty and good significance. The confidence intervals for the parameters of reaction $j \in \{2, 3\}$ are larger than the final parameter value. However, as the values for $k_{j,ref}$ and $E_{a,j}$ can only be positive, this indicates still some level of uncertainty in the parameters estimates. This uncertainty is further revealed by a comparison of the t-values and the reference t-values. For the overall estimation of $k_{j,ref}$ it was impossible to attain t-values exceeding the reference t-value, even though $k_{0,ref}$ comes close. Furthermore, the predicted t-values from the MBDoE, shown in Table 2, could not be reached. In the overall estimation of $E_{a,j}$ three out of four parameters could not be estimated with high statistical significance. Only for $E_{a,0}$ the t-test was satisfied with a t-value close to the predicted one in Table 2. The problem of diminished statistical significance of the estimates is likely due to practical identifiability issues as the measurement data employed for the estimation was affected by experimental errors. Additionally, parameter correlation effects reappeared during the overall estimation making it more difficult to obtain useful results.

Table 3: Results of the parameter estimation showing the final values, initial guesses, 95% confidence intervals (CI) and t-values for each of the 8 parameters.

Parameter	Initial guess	Final value	Units	95% CI	t-values
$k_{0,ref}$	3.019	3.035	L mol^{-1} s^{-1}	±0.396	1.403[a]
$k_{1,ref}$	2,551,604	2,728,600	L mol^{-1} s^{-1}	±4.817·10^{11}	2.49·10^{-6} [a]
$k_{2,ref}$	8,591	16,997	L mol^{-1} s^{-1}	±6.282·10^{5}	0.012[a]
$k_{3,ref}$	0.001756	0.140378	s^{-1}	±8.175	0.012[a]
$E_{a,0}$	84,132	128,517	J mol^{-1}	±5.152·10^{4}	2.495[b]
$E_{a,1}$	45,019	44,941	J mol^{-1}	±1.709·10^{10}	2.63·10^{-6} [b]
$E_{a,2}$	59,508	20,995	J mol^{-1}	±3.525·10^{6}	0.006[b]
$E_{a,3}$	98,831	144,942	J mol^{-1}	±3.517·10^{6}	0.041[b]

[a]Refers to t_{ref} = 1.725 and [b]refers to t_{ref} =1.688.

Figure 3 shows a comparison of the simulated model response incorporating the final parameter values vs the experimentally observed product concentrations for the experiments 4 and 8 of the MBDoE in Table 2. These show a reasonably good model fit. Only experiments suggested by MBDoE were conducted to generate data for parameter estimation. Thus, as the method did not suggest samples to be taken at reaction times longer than 50 minutes in experiment 4, Figure 3a, or between zero and 24 minutes in experiment 8, Figure 3b, there was no data collected. In total, 8 such experiments were conducted, four for each of the two parameter types (shown in Supporting Information File 1).

Despite the remaining uncertainty in some of the parameters, indicated by the large 95% confidence intervals, the quality of model prediction was considered to be good-enough for the purpose of in silico training of the smart DoE algorithm for

target optimisation. Thus, the final parameter values in Table 3 were accepted and used in the model employed for the subsequent in silico target optimisation steps.

Improvement of process conditions using an a priori model and in silico optimisation

Access to automated experimental systems allows to perform black-box sequential optimisation using sequential DoE algorithms. However, if a process model is available, there exist two more options for optimisation: optimisation using the available process model directly, or optimisation using a surrogate model. The latter is frequently used in expensive computer experiments, and in the case of large-scale process simulations, when evaluations of process models is computationally too expensive. In the case of our test reaction the MBDoE approach enabled us to develop a reasonably good process model in a small number of flow experiments. We can use this process model to perform
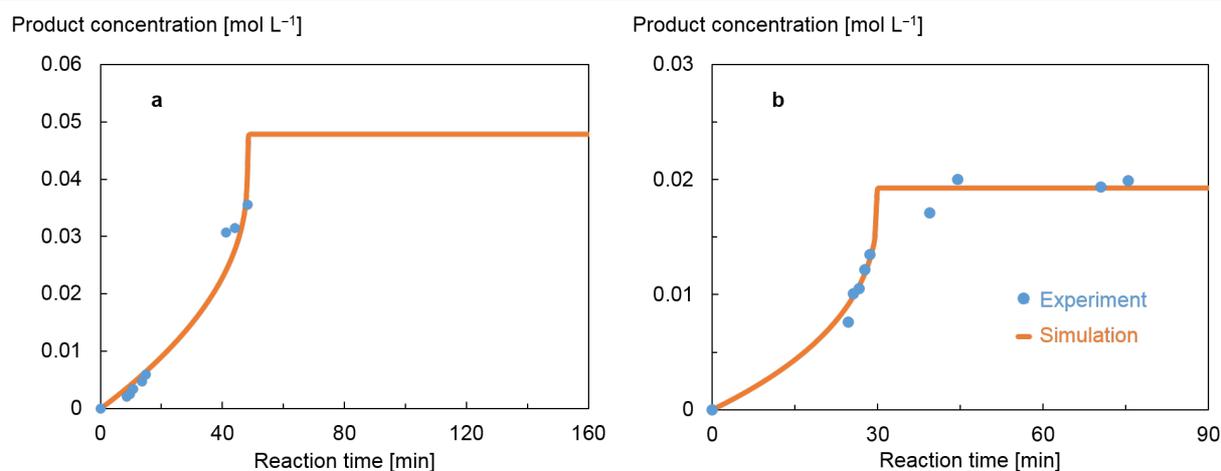
Figure 3: Results of experiments from the MBDoE in Table 2, conducted for parameter estimation, and their corresponding simulated model responses based on the estimated parameters. The only experiments conducted were those calculated by the MBDoE, defined by the sampling times and recipes suggested. (a) Experiment 4 conducted at a reference temperature of 70 °C to estimate rate constants. (b) Experiment 8 used for determining activation energies, at 75 °C.

optimisation. Although this model is not expensive to evaluate we resorted to building a surrogate model, which allowed us to use an efficient target optimisation algorithm we have demonstrated earlier [11,26]. Target optimisation is significantly easier compared to global optimisation as the optimiser is allowed to stop after finding only few conditions that satisfy a target, compared to the problem of finding a global optimal.

The target functions and their corresponding values in the optimisation presented below were the yield, *y*, of **2** defined in Equation 2, with a desired value of 100%, and a specific cost function given in Equation 3 with a target value of 2,108 £ h kg^{-1}. This cost function was selected to account for the material and energy consumption, and the reaction time with respect to the amount of product **2**. Thus, $cost_{el}$ and $cost_i$ represent the electricity and material costs, whereas W_{el} and $m_{i,0}$ denote the consumed electricity and materials, respectively. The product output $\dot{m}_2$ with

$$\dot{m}_2 = \frac{m_2}{t_{reaction}} \qquad (1)$$

combines the amount of product **2** with the necessary reaction time. The cost target value was derived based on a reaction with the shortest reaction time and highest yield, identified from a series of prior experiments (see Table S2 and Figure S5 in Supporting Information File 1 for further details) [18].

$$y = \frac{m_2 - m_{2,0}}{m_{1,0}} \cdot 100\% = 100\% \qquad (2)$$

$$cost = \frac{cost_{el}W_{el} + \sum cost_i m_{i,0}}{\dot{m}_2} = 2,108 \text{ £ h kg}^{-1} \qquad (3)$$

The surrogate model was trained on the 64 experimental points obtained for model parameter identification. In case of an unknown mechanism, the experiments for mechanism discovery could also be included in the training set, which leads to a data-efficient approach. However, they might not be the most informative for training the surrogate. The output of the surrogate model is the suggested next experiment to perform, which was used as an input to the process model. Upon reaching the targets in silico after a number of optimisation iterations, the successful input conditions were verified experimentally, to confirm the predictions.

The in silico results for the optimisation target cost and yields are shown in Figure 4 and Table 4. It can be seen that out of 174 iterations, several points were very close to the targets and two optimal sets of conditions satisfy both targets (these iterations are marked with stars). The simulation results of the two identified successful sets of conditions both predict a yield of 98.72%. The experimentally obtained yields in the validation of the two sets of conditions were determined to be >99%, which is caused by the uncertainty of the applied GC method including sample preparation, which lead to ±1% variance in the yield value. The algorithm is not expected to exhibit fast convergence, since it is exploring the reaction space to develop a better statistical model. The physical experiments performed thereafter confirmed prediction of the successfully attained target

Figure 4: Results of in silico iterations of the multi-objective active learner (MOAL) algorithm [26]. Each iteration produces two resulting values, one for yield and one for the cost function. Targets were 100% for yield and 2,108 k£ h kg^{-1} for the cost function. Green stars signify experiments that satisfy the selected targets.
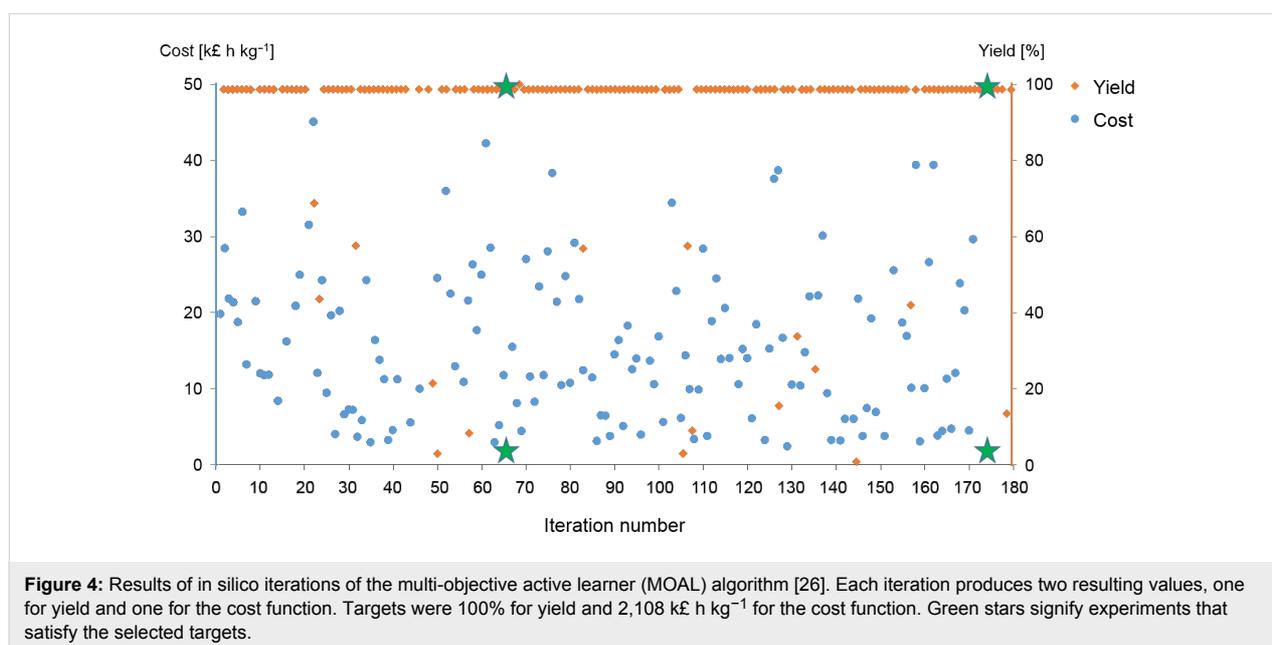
Table 4: Experimental conditions and results of the experimental validation of the two successful predictions that met the target specifications.[a]

Iteration	T [°C]	$t_{reaction}$ [min]	R_{acid-1}	R_{cat-1}	Yield [%]	Cost [k£ h kg^{-1}]
66	107	9	46.1	0.077	>99 (98.72)	1.79 (1.92)
174	101	10	41.4	0.077	>99 (98.72)	1.79 (1.93)

[a]R_{acid-1}: ratio of the concentrations of acetic acid and compound **1**, R_{cat-1}: ratio of the concentrations of catalyst and compound **1**. Values in brackets are the predicted values by the physical model. Further information regarding the experimental conditions is given in Supporting Information File 1, Table S6.

values. Hence, only the successful predicted experimental conditions X_{opt} were tested in real experiments, which saved time, cost and material, otherwise associated with testing false predicted reactions.

The cost target was more difficult to reach than the yield target, which was already fulfilled after the first iteration and later for most of the proposed experiments. This can be seen by the large fluctuation in the cost values for the proposed experiments over the 174 iterations. One possible reason might be the structure of the cost function with many input variables and strong sensitivity with regards to product amount and reaction time. The reaction conditions shown in Table 4 indicate relatively similar conditions with respect to temperature, reaction time as well as acid and catalyst loading, and do not at this stage demonstrate a case of multimodality.

We have also applied the same target optimisation algorithm for direct improvement of this chemical system as a 'black-box' sequential optimisation. For this approach five experiments were used as a training set, using Latin Hypercube space filling algorithm; the results are shown in Supporting Information File 1, Table S7 (Expt. 1–5). Figure 5 shows results of the initial set of experiments on the left side of the plot. It is noted that two of the five training experiments did incidentally meet the target value for yield at the conditions set. All outputs, regardless whether they reached the desired target values, were included into the training set and the algorithm was re-trained on the updated set once more. This iterative process was conducted six times. After a single iteration, the results of the first suggested set of conditions were already more promising than any of the training points. The target for yield has been met, as perhaps expected as it was optimal for two of the training exam-
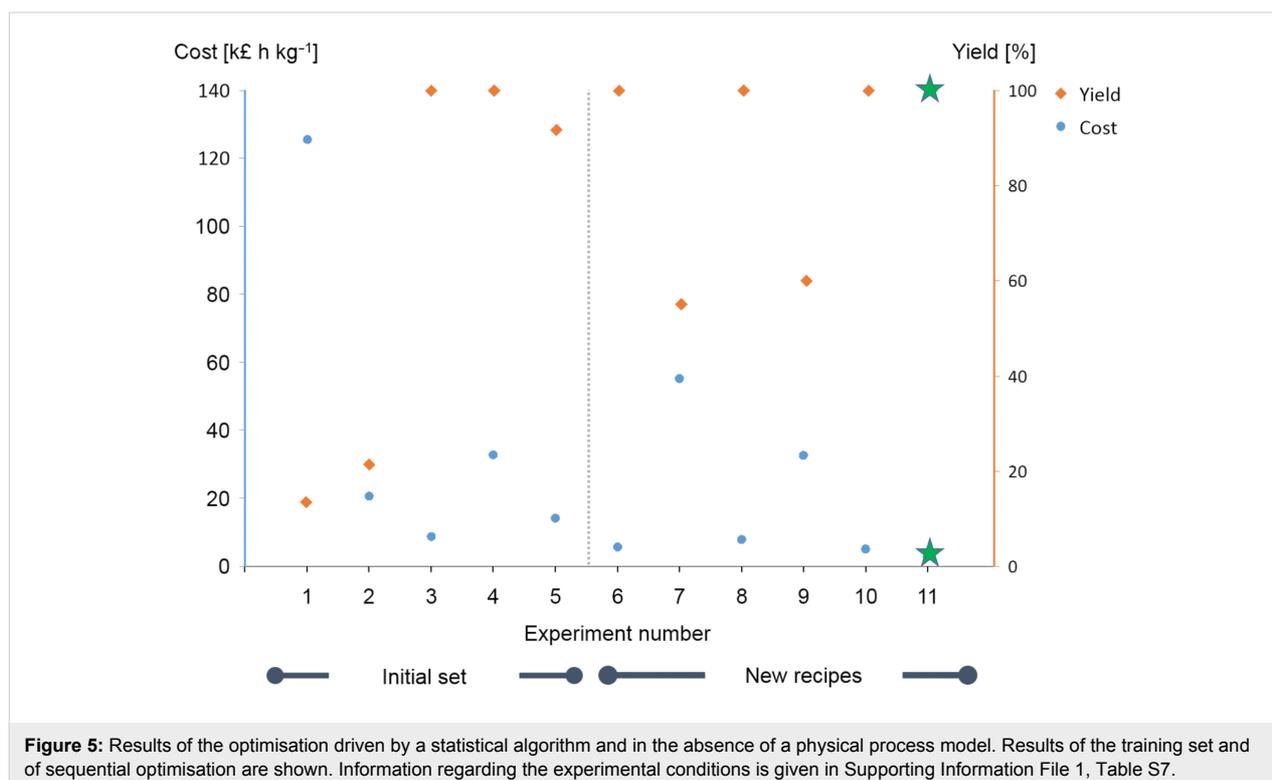
Figure 5: Results of the optimisation driven by a statistical algorithm and in the absence of a physical process model. Results of the training set and of sequential optimisation are shown. Information regarding the experimental conditions is given in Supporting Information File 1, Table S7.

ples as well, and the value for cost has been significantly reduced, getting closer to the pre-defined target. Whilst it is observed that experiments 7 and 9 have a large margin of error with regards to the targets, this is due to the exploration function of the algorithm.

Four of the new suggested experimental conditions achieved high yields with the accepted accuracy and had lower cost scores than even the lowest that was found in the initial set. The recipe at the 6th and final iteration following the training set corresponds to a temperature of 102 ºC, reaction time of 15 minutes, acid–substrate ratio of 27.85 and catalyst–substrate ratio of 0.084. With these final conditions, the algorithm converged as both targets were met simultaneously for the first time.

Comparison of the two optimisation approaches

In this work we used the automated flow set-up combined with MBDoE approach to rapidly develop a good-enough process model, which was then used to train a surrogate model and perform a target optimisation. This resulted in two new sets of reaction conditions which both provided better results than the ones obtained previously. In our second approach we used the experimental flow system as a 'black-box' and employed the same statistical target optimisation algorithm to experimentally find the conditions that satisfy the set targets. In this specific case the 'black-box' target optimisation is extremely efficient and found suitable reaction conditions within a very small number of experiments. However, no knowledge about the system was generated. The approach of using automated flow experiments in combination with MBDoE allows to minimise experimental effort compared to classical kinetic studies, but results in a process model that can be directly used in optimisation. This approach is clearly preferred for the cases when a model structure could be identified. There would be many practical cases when due to complexity of chemistry it would be unrealistic to develop a physical model within a reasonable timescale. Then the 'black-box' approach is a viable option.

Conclusion

In conclusion, we present an approach of using model-based design of experiments, based on the first principles model structure, in automated flow experiments, and coupling of the process models with a statistical machine learning based target optimisation. We demonstrate that MBDoE offers a significant potential for efficient and rapid generation of process models in flow experiments. The developed process model enables in silico training of the optimisation surrogate model and cost effective determination of process conditions that satisfy the set performance targets. While this is certainly faster than physical

experiments, we also show that the self-optimisation works well when trained on a space-filling method to avoid many necessary experiments for model generation. This results in a set of experiments that reach the pre-defined targets in six iterations, although it does not provide any process knowledge. Hence, a combined approach, leading to generation of a surrogate model and a physical model has unique advantages of rapid optimisation and simultaneous generation of process knowledge.

Experimental
Reaction system and analysis
All reactions were performed in continuous segmented flow using the R2$^+$/R4 system by Vapourtec, see Figure 2. The reaction mixture segments and the solvent were pumped through a 10 mL polytetrafluoroethylene (PTFE) tubular reactor and quenched in an ice bath at the reactor outlet. A minimum segment volume of 2 mL was found to be necessary to avoid dispersion effects in the centre of the segment. The segments were detected using the in-line UV cell, which allowed automatic triggering of the GC (Agilent 6850) to sample the segment at its centre. The flow GC vial was designed by Daniel Geier and Ralf Thelen from the Institut für Technische und Makromolekulare Chemie (ITMC) at RWTH Aachen University and manufactured in-house in Cambridge. GC analysis was performed for product **2** with an accuracy of ±0.0005 mol L^{-1}. Due to the decomposition of **1·HOAc**, **B** and **A** to **1** during sampling following a reaction, the reaction mixture was analysed for species **1** prior to beginning a reaction, with an accuracy of ±0.0003 mol L^{-1}. All communication between instruments was custom-coded in LabVIEW and communication with Vapourtec was via its proprietary Excel interface. Further details of the set-up and the on-line auto-sampling strategy, as well as a protocol for sample preparation and experiment execution are provided in Supporting Information File 1.

Materials
Toluene (Sigma-Aldrich, anhydrous, 99.8%), acetic acid (Sigma-Aldrich, ReagentPlus, ≥99.0%), acetic anhydride (Sigma-Aldrich, ReagentPlus, ≥99.0%), 1,1,2,2-tetrachloroethane (Sigma-Aldrich, reagent grade, ≥98.0%), palladium(II) acetate (Sigma-Aldrich, reagent grade, 98.0%, no further purification steps were applied, the same batch was used for all experiments, stored according to manufacturer's suggestions), (diacetoxyiodo)benzene (Sigma-Aldrich, ≥98.0%) were all used as received. 3,3,5,5-Tetramethylmorpholin-2-one was synthesised as described elsewhere [18].

Model development and analysis
A process model was developed on the basis of the previously discussed reaction mechanism and DFT estimates of the rate constants (see Table S1, Supporting Information File 1) [18].

The kinetic model was developed as a well-stirred tank reactor. The model includes kinetic equations, energy and material balances as well as constitutive equations. A lumped model was created as each reaction segment was assumed to be ideally mixed; thus no excess volume was considered for mixing. As the reaction takes place in a homogeneous liquid phase, and as the tube dimensions are small, there was no need to account for mass transfer effects. For simplicity, the slightly endothermic nature and hence the heat of reaction for the C–H activation was neglected.

The temperature effect in the reaction steps shown in Scheme 2 were expressed using the Arrhenius equation in its re-parametrised form, shown in Equation 4 and Equation 5 [27,28]. This facilitates subsequent parameter estimation by decoupling the kinetic parameters of each reaction. Assuming equilibrium for the three reversible reaction steps in Scheme 2, the 8 kinetic parameters of interest in this reaction sequence were the reference reaction rate constants ($k_{j,ref}$) and activation energies ($E_{a,j}$), where $j \in \{0, 1, 2, 3,\}$ given by Equation 4 and Equation 5).

$$k_j = k_{j,ref} \cdot e^{\frac{E_{a,j}}{R}\left(\frac{1}{T} - \frac{1}{T_{ref}}\right)} \tag{4}$$

$$k_{j,ref} = A \cdot e^{\frac{E_{a,j}}{R T_{ref}}} \tag{5}$$

The temperature-dependent volumetric reaction rates $R_{i,j}^V$ of compound i in the reaction j were modelled by Equation 6, in which $v_{i,j}$ are the stoichiometric coefficients of a compound i in the reaction j, c_i denotes the molar concentration of the compound i, k_j represents the reaction rate constant of the reaction j and $n_{i,j}$ gives the order of the reaction. All reaction steps in Scheme 2 were found to be first order with respect of the participating compounds, except for the oxidant PhI(OAc)$_2$ which is of zero-order dependency [21].

$$R_{i,j}^V = v_{i,j} k_j \prod c_{i,j}^{n_{i,j}} \tag{6}$$

In addition, the overall and the component mole balances, Equation 7 and Equation 8, were written for the process model, where V denotes the reaction volume.

$$\frac{dn}{dt} = V \sum_{i=1}^{n_{comp}} \sum_{j=1}^{n_{reac}} R_{i,j}^V \tag{7}$$

$$\frac{dn_i}{dt} = V \sum_{j=1}^{n_{reac}} R_{i,j}^V \tag{8}$$

The balances were constructed for a single reaction mixture segment, which was assumed to behave as a batch reactor, as samples were taken in the dispersion-free centre of the segment.

For the purpose of calculating the cost associated with heating the system, a steady state energy balance, Equation 9, was established.

$$W_{el} = \frac{Q_{heat}}{\eta_{heat}} = \frac{n_0 \overline{c_{p,0}}\left(T - T_0\right)}{\eta_{heat}} \tag{9}$$

were η_{heat} denotes an overall efficiency of conversion of electrical into thermal energy of the reaction mixture segment. This efficiency was determined experimentally for the employed reactor system by measuring the electrical power input to the Vapourtec heating system needed to increase the temperature of a reaction mixture stream with a set flowrate and of known composition, thus with known molar flow and heat capacity, from ambient temperature of approx. 20 °C to a reaction temperature of 70 °C. By inserting these values into Equation 10, the value for the energy-conversion efficiency was calculated and kept constant.

$$\eta_{heat} = \frac{\dot{n}_0 \overline{c_{p,0}}\left(T - T_0\right)}{P_{el,Vapourtec}} \tag{10}$$

To complete the process model, simple constitutive equations were applied and initial parameter values were computed. The latter were identified based on Gibbs free energies of reaction for the chemical system, which were obtained from a priori DFT calculations with an accuracy of ±7 kJ mol⁻¹ [18]. These values were related to kinetic parameters through the exponential van't Hoff equation.

Subsequently, the model was investigated and tested for identifiability to ensure its structural soundness, i.e., that it can be used to uniquely determine its parameters. This was done using an established method, detailed elsewhere [29,30]. It is worth noting that structural identifiability is tested under the assumption of noise-free measurement data and no uncertainty of the model. Thus, it does not necessarily imply practical identifiability as the measurement data for the parameter estimation is usually superimposed by noise and errors [31]. Thereafter, an estimability analysis, based on visual inspection of the local dynamic sensitivity curves [32], confirmed that all parameters

except those for reaction with $j = 1$ can be determined with sufficient accuracy. For this reaction step, low sensitivity of the measurable quantity, concentration of compound **2**, was found (see Supporting Information File 1, Figure S9 for further details). The local dynamic sensitivity curves of the remaining parameters were used to identify the time intervals with the maximum sensitivity of the parameters (see Supporting Information File 1, Figure S9), indicating reasonable sample points to obtain sensible measurement data for parameter estimation.

The physical model was implemented in gPROMS. The D-optimality criterion was selected to refine the model using the model-based design of experiments (MBDoE) and parameter estimation suite of gPROMS by employing standard solver settings. Further details on this procedure are given in Supporting Information File 1 together with constraints employed for the experiment control variables in the MBDoE optimisation problem (Equations S8–S21, Supporting Information File 1).

The experimental design and parameter estimation strategy included two steps. In the first step, experiments were designed at a reference temperature $T_{ref} = 70\ °C$ to eliminate $E_{a,j}$ as a parameter in each reaction j, see Equation 4 and Equation 5). A t-test was used as a statistical method for judging the increase in precision of the predicted parameter and, hence, the statistical significance of the estimates which is attained if the predicted t-value exceeds a reference value t_{ref}. The performed experiments would therefore generate data to enable estimation of the reference reaction rate constants $k_{j,ref}$ independent of $E_{a,j}$. After these parameters have been determined to sufficient accuracy, they were kept constant and experiments were designed at temperatures different from T_{ref} in the second step to obtain data for the subsequent estimation of $E_{a,j}$. The combination of MBDoE and subsequent parameter estimation was repeated twice in both steps to increase parameter precision, whilst keeping the experimental effort low. This was necessary to ensure good parameter improvement in the case of poor initial parameter guesses.

Algorithm for statistical optimisation

One key element of the proposed framework for self-optimisation of reaction conditions is the statistical multi-target optimisation method. For this purpose, the multi-objective active learner (MOAL) algorithm coded in the numerical computing environment MATLAB (v.2015b) was adopted, which combines Gaussian processes as a surrogate model with the concept of mutual information and a genetic algorithm [26]. To apply it to the chemistry under investigation, the algorithm was provided with specified targets Y_{target} for the optimisation and defined experiment design variables $X = [T, t_{reaction}, c_{1,0}, c_{AcOH,0}, c_{cat,0}]$ as the degrees of freedom. The latter were bounded by the corresponding constraints (see Supporting

Information File 1 for details). A set of 2,000 randomly generated candidate solutions, uniformly distributed within the allowed design space was employed, because the algorithm works with discrete evaluation techniques for the optimisation. The initial training set $[X_{tr}, Y_{tr}(X_{tr})]$ contained the input variables X_{tr} and measurements of the corresponding target values $Y_{tr}(X_{tr})$, which were adopted from the MBDoE approach. It was updated continuously, so that at each iteration of the algorithm, a new training point was added. Binary Gaussian process classification was included into the algorithm to account for feasible and infeasible solutions in X, hence learning the promising regions of the design space and evolving some internal process knowledge stepwise with each new iteration. An infeasible solution could occur if an experiment fails in the laboratory. Thus, each point in the training was equipped with one more value, providing information on its feasibility (1) or infeasibility (−1). The current limitation of this approach is that it does not automatically distinguish if the experiment failure identifies the region of design space where the specific reaction is not working, or the failure was due to a random fluke and the same experiment, if repeated, would be successful. There is a way of dealing with this problem, which we will implement, when the algorithm will be published.

After classification of the candidate solutions and training samples, the Gaussian process was trained by fitting the so called hyperparameters of its covariance and likelihood functions by maximising the marginal likelihood with a conjugate gradient optimiser. In this way, a statistical surrogate model was created to provide an approximated response surface for the underlying problem of investigation. This response surface was used to evaluate the feasible candidate solutions and subsequently identify a best solution $\widetilde{Y}_{opt}(\widetilde{X}_{opt})$ with corresponding experimental conditions $\widetilde{X}_{opt}$. As only discrete candidate solutions were evaluated by this method, the Non-dominated Sorting Genetic Algorithm-II (NSGA-II) was employed for perturbation of $\widetilde{Y}_{opt}(\widetilde{X}_{opt})$ to explore the neighbourhood for further refinement of the generated solution. The resulting combination of input and output conditions were subsequently assessed against the targets. If the targets were attained within acceptable tolerance, the results were accepted and the statistical algorithm converged. Otherwise, the results were fed back into the training set and a new iteration was started.

In silico optimisation

The in silico optimisation process was initiated by first training the MOAL algorithm (with the data generated for the purpose of parameter estimation of the physical model described above). This enables the algorithm to construct a statistical surrogate model and suggest a set of experimental conditions which might give results that are closer to the targets. This set is then fed into

the physical model to predict what outputs are expected as though the experiment had been conducted. This process is repeated until the required tolerance is reached. A margin of tolerance was included, such that results within 10 and 1.5% of the target values for cost and yield, respectively, were taken as successful, due to the expected difficulty in achieving those targets. Subsequently, the successful reaction conditions found in silico were tested experimentally. In the case of failure, the experimental results were fed back into the algorithm and the target optimisation loop starts again. Otherwise, the algorithm converged and suitable experimental conditions were identified.

In principle, standard optimisation approaches employing the physical model directly to identify optimum operating conditions could be used, but would give poor results in case of uncertainty and restricted validity of the physical model. However, by applying the MOAL algorithm, technical difficulties regarding multi-objective global optimisation can be overcome. Furthermore, the proposed optimisation procedure can deal with potential uncertainties and restricted validity in the physical model. This is achieved by the machine learning functionalities of the MOAL algorithm, which retrain the algorithm not just on the physical model but also on unsuccessful experiments, erroneously predicted as suitable by the physical model. Thus, it obtains information beyond the capabilities of the physical

model. An additional point is, that the MOAL algorithm proved to be especially suited for the detection of multiple possible solutions to indicate multimodality, which is challenging for standard optimisation methods, but can yield valuable information in the current case.

Statistical closed-loop optimisation

Statistical target optimisation was performed using the MOAL algorithm. Latin hypercube sampling (LHS) was used to discretise the experimental space initially. An overview of this sampling strategy is laid out for one variable in Figure S10 in Supporting Information File 1. A uniform distribution was taken for the input variables and hence the cumulative distribution function was linear. In this case k is five and N was the number of initial experiments to be conducted, which was decided to be five. This number of initial training experiments was selected as in the previous application of the MOAL algorithm for laboratory optimisation [11], the same number of training samples was applied for an optimisation of two targets, but with a 14 dimensional design space, instead of five dimensions in the current case. Still, the algorithm converged within 17 iterations (including the five training experiments). Hence, we assumed, that for the current work with less design space dimensions, the algorithm would learn the response surface as fast as it was the case for its previous application.

Table 5: Nomenclature.

Symbol	Definition	Units
η_{heat}	heat efficiency	–
$v_{i,j}$	stoichiometric coefficient of component i in reaction j	–
A	pre-exponential factor in Arrhenius equation	case dependent
cost	investigated target value	£ h kg^{-1}
cost$_{el}$, *cost*$_i$	cost of electricity, cost of material component i	case dependent
$c_{i,0}$	initial component concentration	mol L^{-1}
$\overline{c_{p,0}}$	average molar heat capacity	J mol^{-1} K^{-1}
$E_{a,j}$	activation energy of reaction j	J mol^{-1}
$k_{j,ref}$	reference rate of reaction in reaction j	case dependent
m_i, $m_{i,0}$	mass of component i, initial mass of component i	kg s^{-1}
n_i, n_0	number of moles of component i, total number of moles initially	mol
$P_{el,Vapoutec}$	electrical power uptake of Vapourtec flow system	W
Q_{heat}	heat	J
R	universal gas constant	J mol^{-1} K^{-1}
$R_{i,j}^{V}$	reaction rate of component i in reaction j	mol L^{-1} s^{-1}
t, $t_{reaction}$	time, reaction time	s, min
T, T_{ref}, T_0	temperature, reference temperature, initial temperature	°C
V	volume of system	L
W_{el}	electrical work	J
X	experiment design variables	–

Table 5: Nomenclature. (continued)

$\widetilde{X}_{opt}$	proposed suboptimal inputs	–
X_{opt_1}	proposed optimal inputs	–
X_{tr}	input training matrix	–
y	yield	%
Y_{target}	target outputs matrix	–
$\widetilde{Y}_{opt}(\widetilde{X}_{opt})$	proposed suboptimal outputs	–
Y_{opt_i}	proposed optimal outputs	–
Y_{tr}	output training matrix	–

Supporting Information

Supporting Information File 1
Details of experimental set-up and protocols, table of a priori data taken from our previous study, details of model development, MBDoE results, and LHS results.
[http://www.beilstein-journals.org/bjoc/content/supplementary/1860-5397-13-18-S1.pdf]

Acknowledgements

References

1. Dolas, R. T.; Siddheshwar, S. S.; Somwanshi, S. B.; Merekar, A. N.; Godge, R. K.; Pattan, S. R. *Int. J. Curr. Trend. Pharm. Res.* **2013,** *5,* 137–143.
2. Sans, V.; Cronin, L. *Chem. Soc. Rev.* **2016,** *45,* 2032–2043. doi:10.1039/C5CS00793C
3. Ley, S. V.; Fitzpatrick, D. E.; Myers, R. M.; Battilocchio, C.; Ingham, R. J. *Angew. Chem., Int. Ed.* **2015,** *54,* 2–17. doi:10.1002/anie.201410932
4. Houben, C.; Lapkin, A. A. *Curr. Opin. Chem. Eng.* **2015,** *9,* 1–7. doi:10.1016/j.coche.2015.07.001
5. McMullen, J. P.; Jensen, K. F. *Org. Process Res. Dev.* **2010,** *14,* 1169–1176. doi:10.1021/op100123e
6. McMullen, J. P.; Stone, M. T.; Buchwald, S. L.; Jensen, K. F. *Angew. Chem., Int. Ed.* **2010,** *49,* 7076–7080. doi:10.1002/anie.201002590
7. McMullen, J. P.; Jensen, K. F. *Annu. Rev. Anal. Chem.* **2010,** *3,* 19–42. doi:10.1146/annurev.anchem.111808.073718
8. Reizman, B. J.; Jensen, K. F. *Acc. Chem. Res.* **2016,** *49,* 1786–1796. doi:10.1021/acs.accounts.6b00261
9. McMullen, J. P.; Jensen, K. F. *Org. Process Res. Dev.* **2011,** *15,* 398–407. doi:10.1021/op100300p
10. Parrott, A. J.; Bourne, R. A.; Akien, G. R.; Irvine, D. J.; Poliakoff, M. *Angew. Chem., Int. Ed.* **2011,** *50,* 3788–3792. doi:10.1002/anie.201100412
11. Houben, C.; Peremezhney, N.; Zubov, A.; Kosek, J.; Lapkin, A. A. *Org. Process Res. Dev.* **2015,** *19,* 1049–1053. doi:10.1021/acs.oprd.5b00210
12. Reizman, B. J.; Jensen, K. F. *Org. Process Res. Dev.* **2012,** *16,* 1770–1782. doi:10.1021/op3001838
13. Moore, J. S.; Jensen, K. F. *Org. Process Res. Dev.* **2012,** *16,* 1409–1415. doi:10.1021/op300099x
14. Hone, C. A.; Holmes, N.; Akien, G. R.; Bourne, R. A.; Muller, F. L. *React. Chem. Eng.* **2017.** doi:10.1039/C6RE00109B
15. Walter, E.; Pronzato, L. *Automatica* **1990,** *26,* 195–213. doi:10.1016/0005-1098(90)90116-Y
16. Espie, D.; Macchietto, S. *AIChE J.* **1989,** *35,* 223–229. doi:10.1002/aic.690350206
17. Franceschini, G.; Macchietto, S. *Chem. Eng. Sci.* **2008,** *63,* 4846–4872. doi:10.1016/j.ces.2007.11.034
18. Zakrzewski, J.; Smalley, A. P.; Kabeshov, M. A.; Gaunt, M. J.; Lapkin, A. A. *Angew. Chem., Int. Ed.* **2016,** *55,* 8878–8883. doi:10.1002/anie.201602483
19. Hu, X. E. *Tetrahedron* **2004,** *60,* 2701–2743. doi:10.1016/j.tet.2004.01.042
20. McNally, A.; Haffemayer, B.; Collins, B. S. L.; Gaunt, M. J. *Nature* **2014,** *510,* 129–133. doi:10.1038/nature13389
21. Smalley, A. P.; Gaunt, M. J. *J. Am. Chem. Soc.* **2015,** *137,* 10632–10641. doi:10.1021/jacs.5b05529
22. Process Systems Enterprise. gPROMS. https://www.psenterprise.com/products/gproms. 1997-2005.
23. Franceschini, G.; Macchietto, S. *AIChE J.* **2008,** *54,* 1009–1024. doi:10.1002/aic.11429
24. Franceschini, G.; Macchietto, S. *Ind. Eng. Chem. Res.* **2008,** *47,* 2331–2348. doi:10.1021/ie071053t
25. Franceschini, G.; Macchietto, S. *Ind. Eng. Chem. Res.* **2007,** *46,* 220–232. doi:10.1021/ie060758c
26. Peremezhney, N.; Hines, E.; Lapkin, A.; Connaughton, C. *Eng. Optim.* **2014,** *46,* 1593–1607. doi:10.1080/0305215X.2014.881997
27. Asprey, S. P.; Naka, Y. *J. Chem. Eng. Jpn.* **1999,** *32,* 328–337. doi:10.1252/jcej.32.328
28. Agarwal, A. K.; Brisk, M. L. *Ind. Eng. Chem. Process Des. Dev.* **1985,** *24,* 203–207. doi:10.1021/i200028a034

29. Asprey, S. P.; Macchietto, S. *Comput. Chem. Eng.* **2000,** *24,* 1261–1267. doi:10.1016/S0098-1354(00)00328-8

30. Grewal, M.; Glover, K. *IEEE Trans. Autom. Control* **1976,** *21,* 833–837. doi:10.1109/TAC.1976.1101375

31. Galvanin, F.; Ballan, C. C.; Barolo, M.; Bezzo, F. *J. Pharmacokinet. Pharmacodyn.* **2013,** *40,* 451–467. doi:10.1007/s10928-013-9321-5

32. McLean, K. A. P.; McAuley, K. B. *Can. J. Chem. Eng.* **2012,** *90,* 351–366. doi:10.1002/cjce.20660

Continuous-flow synthesis of highly functionalized imidazo-oxadiazoles facilitated by microfluidic extraction

Ananda Herath and Nicholas D. P. Cosford[*]

Abstract

A versatile continuous-flow synthesis of highly functionalized 1,2,4-oxadiazoles starting from carboxylic acids is reported. This process was applied to the multistep synthesis of imidazo[1,2-*a*]pyridin-2-yl-1,2,4-oxadiazoles, using a three reactor, multistep continuous-flow system without isolation of intermediates. This continuous-flow method was successfully combined with a single-step liquid–liquid microextraction unit to remove high boiling point polar solvents and impurities and provides the target compounds in high purity with excellent overall yields.

Introduction

The design and execution of scalable and economically viable processes for the preparation of biologically active small molecules is a major hurdle in modern organic synthesis. The development of batch processes that combine multiple reactions into "one-pot" have been used successfully in some cases [1-6]. However, this approach has a number of drawbacks, primarily because of mutual interference between various reactive components. Recently, continuous-flow chemistry has emerged as a powerful technique in organic synthesis. This is in part due to the potential for integrating individual reaction steps and subsequent separations into a single streamlined process [7-14].

On the other hand, a significant challenge in flow chemistry is the formation of insoluble intermediates in the reactor. This can often be prevented by using polar organic solvents such as dimethylformamide (DMF) [7-9,15]. However, the challenges of removing large amounts of high boiling solvents during the purification and isolation process can limit scalability and efficiency. Furthermore, many useful synthetic reactions are incompatible with the use of DMF as a solvent. Recently several unit operations have successfully been implemented in continuous-flow syntheses to allow separations and purifications in a continuous fashion, such as liquid–liquid microextrac-

tion [12,16-20] or microfluidic distillation [21,22]. Herein we describe the utilization of liquid–liquid microextraction to facilitate a complex, multistep flow synthesis process.

Our research in the field of flow synthesis has focused on developing continuous-flow chemistry methods to access complex, drug-like molecules from readily available precursors without isolation of intermediates. We have shown that the "telescoping" of multiple synthetic steps into a single continuous process provides an efficient method for the production of heterocyclic compound libraries in sufficient quantities for biological screening in high-throughput assay formats as well as follow-up confirmatory studies. We previously reported a method for the preparation of 1,2,4-oxadiazoles in an uninterrupted continuous-flow sequence using arylnitriles and acyl chloride precursors [9]. We also reported the flow synthesis of highly functionalized imidazo[1,2-*a*]heteroaryl derivatives from readily available starting materials in a single continuous process [7]. We now report an efficient continuous-flow procedure for the synthesis of 1,2,4-oxadiazoles directly from arylnitriles and carboxylic acid derivatives. We further demonstrate the incorporation of this procedure into a continuous, three-microreactor method for the highly efficient preparation of a diverse library of imidazo-oxadiazole derivatives. Moreover, this continuous-flow method was successfully combined with a single-step liquid–liquid microextraction unit to remove high boiling point polar solvents and impurities.

Results and Discussion

Historically the 1,2,4-oxadiazole scaffold has been used by medicinal chemists as a ubiquitous bioisosteric replacement of amide and ester functionalities in a wide variety of biologically active compounds [23,24]. This motif is found in several drugs

and drug leads including sphingosine-1-phosphate 1 (S1P$_1$) receptor agonists [25-27] and metabotropic glutamate subtype 5 (mGlu$_5$) receptor negative allosteric modulators (NAMs) [25,28-30]. Most synthetic efforts toward the preparation of these heterocyclic systems utilize a multistep, in-flask approach as illustrated by the synthesis of S1P$_1$ agonists (Scheme 1). Thus, a typical batch synthesis entails the formation of an amidoxime by reacting an arylnitrile with hydroxylamine in the presence of a base [29-31]. The amidoxime is then combined with a carboxylic acid derivative in the presence of a coupling reagent. The target oxadiazole is then formed via an intramolecular cyclodehydration (Scheme 1) [27,32-34].

For our initial studies on the development of a flow synthesis of 1,2,4-oxadiazoles we focused on the reaction of *N*-hydroxynicotinimidamide with 3-bromobenzoic acid (Table 1). Screening a variety of reaction conditions using a single microreactor we found that the combination of EDC/HOBt/DIPEA (1:1:1) for 10 min at 150 °C provided the best conditions for complete conversion of 3-bromobenzoic acid to the corresponding 1,2,4-oxadiazole derivative (Table 1, entry 5). The use of *N,N*-dimethylformamide (DMF) as a solvent resulted in competitive amide formation from the decomposition product of DMF at high temperature. In order to prevent this we switched to *N,N*-dimethylacetamide (DMA) as the solvent.

We next focused our efforts on combining this optimized oxadiazole ring-closure procedure with our previously reported flow synthesis of amidoximes by the reaction of hydroxylamine with precursor aryl- and heteroarylnitriles (Table 2). These two reactions were successfully perfomed in flow with slight modifications to the reaction conditions to generate a variety of 1,2,4-oxadiazoles (Table 2). Reactions of arylnitriles having electron-
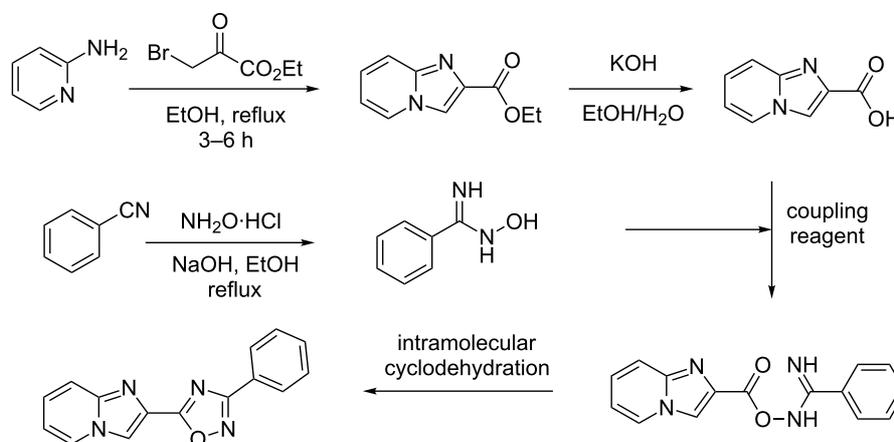
Scheme 1: In-flask (batch) preparation of imidazo[1,2-*a*]pyridin-2-yl-1,2,4-oxadiazoles (S1P$_1$ agonists) [27].

Table 1: Optimization of the flow synthesis of 1,2,4-oxadiazoles.
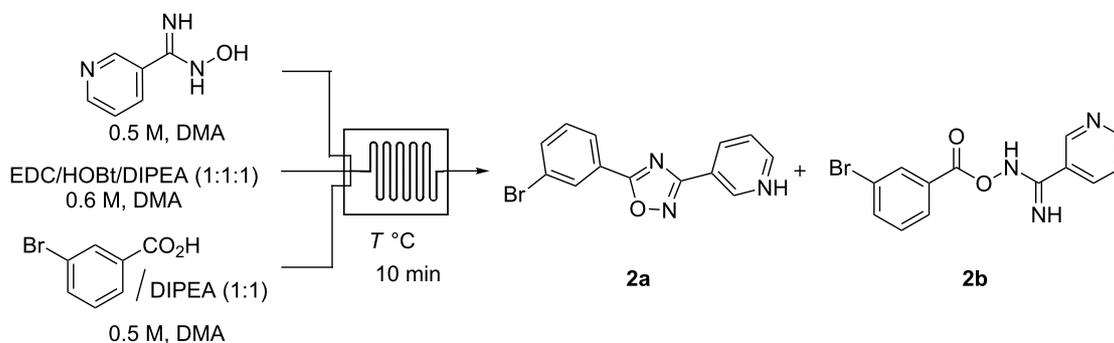
Entry	T [°C]	Product Ratio **2a:2b**[a]
1	50	0:100[b]
2	75	3:97
3	100	18:82
4	125	80:20
5	150	99:1

[a]Compound ratios were determined using LC–MS (see Figure S1 in Supporting Information File 1). [b]Compound **2a** was not observed.

donating (Table 2, entry 7) or electron-withdrawing groups (Table 2, entries 1, 2, 4 and 8) proceeded efficiently in good to excellent overall yields. Additionally, a range of aliphatic and aromatic acids were tolerated under these reaction conditions to produce the corresponding oxadiazoles in high yields. Several advantages of this methodology compared to our previously reported flow synthesis should be noted. First, this method is more facile because no cooling step is necessary before flowing into the second microreactor. Secondly, many more carboxylic acid derivatives are readily available (purchased or easily synthesized) than acyl chlorides allowing access to greater diversity. Finally, this method is easily adaptable to the synthesis of compounds with increasing complexity, as shown by our next set of experiments.

To demonstrate the utility of the newly developed methodology, our next goal was to incorporate a carboxylic acid synthesis step into the flow process. As noted above, we previously reported the continuous-flow synthesis of imidazo[1,2-*a*]pyridine-2-carboxylic acids in a single, uninterrupted process directly from readily available starting materials. We hypothesized that incorporating this step into our new oxadiazole synthesis would provide access to diverse imidazo[1,2-*a*]pyridin-2-yl-1,2,4-oxadiazoles of biological importance [27]. The flow platform we were using, the Syrris AFRICA® flow system, is limited to two heated reactors. To overcome this issue a third reactor was placed in a heated silicone oil bath and a flow system was

assembled as shown in Table 3. The first reaction, the formation of imidazo[1,2-*a*]pyridine-2-carboxylic acid, was performed in a 1000 µL reactor (glass chip) at 100 °C. The acid exiting the first reactor was combined with EDC/HOBt/DIPEA (1:1:1) in a T-mixer. The synthesis of amidoxime was achieved by placing a second reactor (250 µL glass chip) in a heated silicone oil bath at 100 °C. The product stream was next introduced into a third reactor (1000 µL) and mixed with the stream exiting from the T-mixer at 150 °C. Initial studies suggested that premixing of acid and coupling reagent was efficient and provided better yields. The substrate scope of this continuous flow method is shown in Table 3. Thus, this flow method delivers a diverse array of drug-like heterocycles in good overall yields.

Although this multistep continuous-flow method allowed the construction of complex molecules rapidly without the need for purification and isolation of intermediates, lower flow rates and small reactors limited the scalability of the method. As noted previously, the use of high boiling point solvents, such as DMA, are less attractive during scale-up due to the difficulty of removal of these solvents during purification. Consequently the current method is limited to small scale library synthesis. Therefore, our next goal was to convert this microfluidic procedure to a sequence that would deliver compounds on a larger scale. To this end, we first focused our attention on increasing the throughput of the reaction by using the larger tubing and tube

Table 2: Synthesis of 1,2,4-oxadiazoles via a continuous microreactor sequence from arylnitriles and carboxylic acids.

250 µL

NH$_2$OH·HCl/ArCN/DIPEA (1:1.05:3) 0.4 M, DMA

100 °C

1000 µL

EDC/HOBt/DIPEA (1:1:1) 0.6 M, DMA

R^{1}CO$_2$H/DIPEA (1:1) 0.5 M, DMA

150 °C
15 min
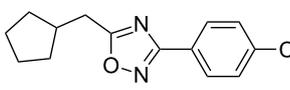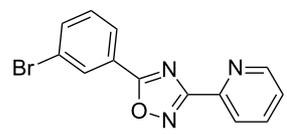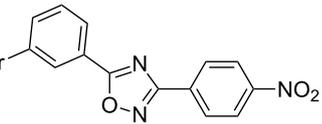
Entry	Compound	Yield (%)[a]	Entry	Compound	Yield (%)[a]
1	(structure)	81	5	(structure)	69
2	(structure)	53	6	(structure)	80
3	(structure)	75	7	(structure)	78
4	(structure)	88	8	(structure)	69

[a]Isolated yield after chromatographic purification of the crude reaction mixture.

reactors available in the Vapourtec R series flow system. We also increased the flow rate to maintain a residence time of 12 min in the third reactor (Scheme 2). Next, a microfluidic liquid–liquid extraction module (the AFRICA® FLLEX) was incorporated at the end of the flow sequence to remove the high boiling point solvent (DMA). Initial studies using a single microreactor and dichloromethane as the organic extraction phase demonstrated proof-of-concept that the microfluidic extraction could be used in the oxadiazole flow synthesis procedure (see Supporting Information File 1). However, the optimized method employs the introduction of toluene and water into the microfluidic extraction module to efficiently remove the DMA and avoid the use of a halogenated solvent, as shown in Scheme 2 and Scheme 3. The reaction mixture exiting from the third reactor is mixed with water and toluene using an external pump before entering the phase separation device. On a preparative scale using this flow reaction setup, the desired oxadiazole derivatives were obtained in good yield with a throughput of ~0.5 g/h. To demonstrate the utility of this new method we synthesized the mGlu$_5$ NAM (Table 2, entry 3) on a gram scale in high yield (3.5 g, 70%). With the same optimized flow method we also synthesized 5-(6-bromoimidazo[1,2-*a*]pyridin-2-yl)-3-(4-chlorophenyl)-1,2,4-oxadiazole on a gram scale (2 g, 42%) rapidly and efficiently (Scheme 3).

Several advantages of this methodology compared to the standard batch synthesis should be noted. First, a fully automated flow method permits the rapid construction of libraries of highly functionalized oxadiazole derivatives. Second, imidazo[1,2-*a*]pyridin-2-yl-1,2,4-oxadiazoles, a scaffold with activity as S1P$_1$ agonists, are prepared directly from commercially available building blocks in a single continuous process without isolating intermediates. As noted previously, the standard in-flask (batch) synthesis of these compounds involves multiple reaction steps requiring work-up and purification of several intermediates. Furthermore, liquid–liquid microextrac-

Table 3: Continuous-flow process for the synthesis of imidazo[1,2-*a*]pyridin-2-yl-1,2,4-oxadiazoles.

Entry	Compound	Yield (%)[a]	Entry	Compound	Yield (%)[a]
1		46	7		59
2		32	8		35
3		44	9		35
4		42	10		29
5		55	11		20
6		59	12		25

[a]Isolated yield after chromatographic purification of the crude reaction mixture.

tion removes high boiling point solvent and impurities from the product. Finally, this new process with liquid–liquid extraction allows easy scale-up and eliminates the tedious high boiling point solvent removal step.

Conclusion

In summary, we have developed a telescoped continuous-flow method for the synthesis of diversely substituted imidazo[1,2-*a*]pyridine-2-yl-1,2,4-oxadiazole derivatives directly from com-

Scheme 2: Gram-scale synthesis of mGlu$_5$ NAM by continuous flow in combination with microfluidic extraction.

Scheme 3: Gram-scale synthesis of imidazo[1,2-*a*]pyridin-2-yl-1,2,4-oxadiazole S1P$_1$ agonist scaffold by continuous flow combined with microfluidic extraction.
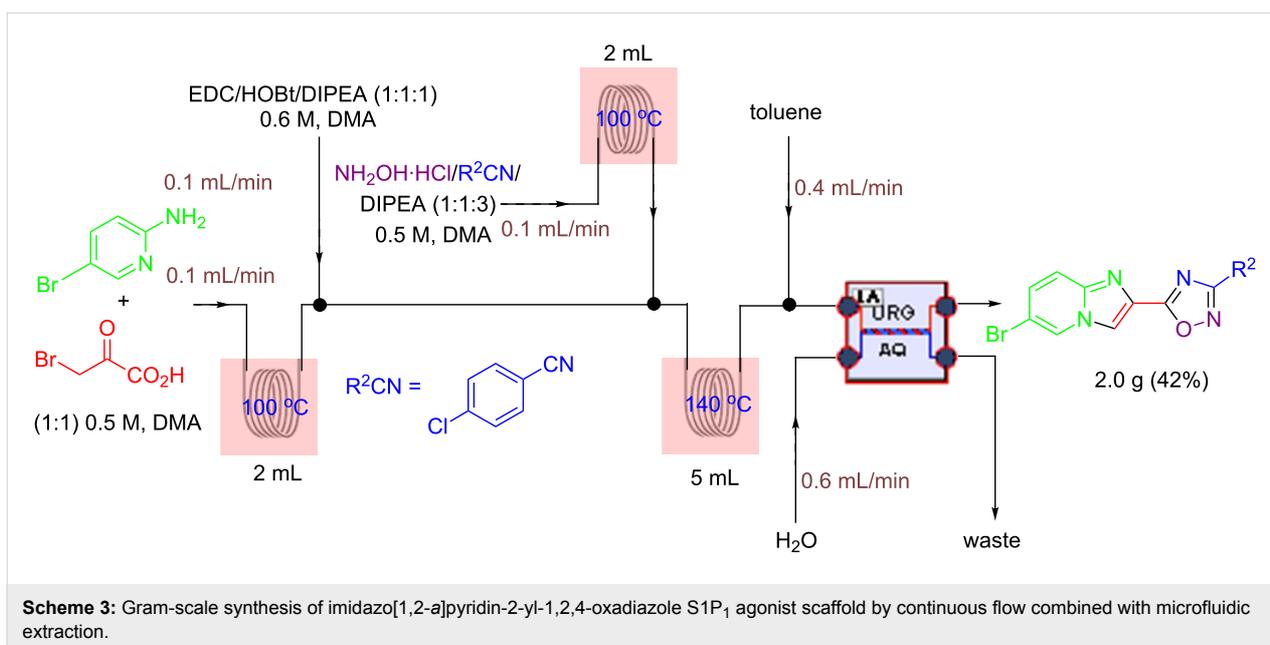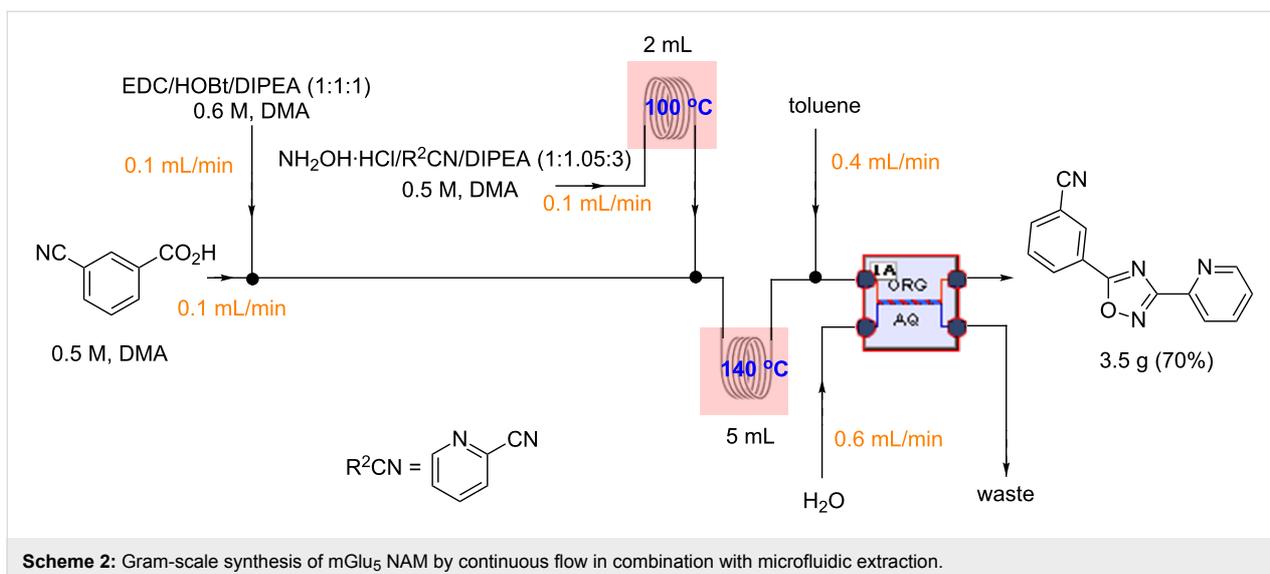
mercial nitriles, aminopyridine carboxylic acids and hydroxyl-amine. Moreover, we demonstrated that a liquid–liquid microextraction unit can be utilized to remove high polar water soluble solvents and impurities from products. This scalable method provides the desired oxadiazole derivatives at a rate of ≈0.5 g/h and represents a significant advantage over batch synthesis. We anticipate that these advances will facilitate the rapid synthesis of these biologically important compounds.

Experimental

All reagents were used as received unless otherwise noted. ^{1}H and ^{13}C spectra were obtained in CDCl$_3$ at room temperature, unless otherwise noted, on a JEOL (JNM-CS400) 400 MHz

instrument. Chemical shifts of ^{1}H NMR spectra were recorded in parts per million (ppm) on the δ scale from an internal standard of residual CDCl$_3$ (7.24 ppm). Chemical shifts of ^{13}C NMR spectra were recorded in ppm from the central peak of CDCl$_3$ (77.0 ppm) on the δ scale. High-resolution ESI–TOF mass spectra were acquired from the Mass Spectrometry Core at the Sanford Burnham Prebys Medical Discovery Institute (Orlando, Florida). LC–MS analyses were carried out on a Shimadzu LC–MS 2010 Series LC System with a Kromasil 100 5 micron C18 column (50 × 2.1 mm i.d.). Continuous-flow (microreactor) experiments were carried out using a Syrris AFRICA apparatus or a Vapourtec R Series Flow Chemistry System.

General procedure for the optimization of the flow synthesis of 1,2,4-oxadiazoles (Table 1)

The reaction was conducted in a glass reactor consisting of a 1.0 mL retention unit and three inlets. Streams of EDC/HOBt/DIPEA (1:1:1, 25 μL/min, 0.6 M, DMA), acid/DIPEA (1:1, 25 μL/min, 0.5 M, DMA) and a solution of amidoximes (25 μL/min, 0.5 M, DMA) were combined in the glass reactor at different temperatures for 10 min of residence time. Reactions were monitored by LC–MS analysis and showed that the conversion of the 3-bromobenzoic acid to the corresponding 1,2,4-oxadiazole was optimal at 150 °C (Table 1, entry 5).

General procedure for the synthesis of 1,2,4-oxadiazoles via a continuous microreactor sequence from arylnitriles and acids (Table 2)

A solution of ArCN/NH$_2$OH·HCl/DIPEA (1.05:1:3, 0.4 M, DMA) was introduced to a glass microreactor (250 μL) heated at 100 °C. The stream exiting from the first reactor was combined with streams of the acid/DIPEA (1:1, 25.0 μL/min, 0.5 M, DMA) and EDC/HOBt/DIPEA (1:1:1, 25 μL/min, 0.6 M, DMA) in a second glass reactor (1.0 mL) at 150 °C for 15 min of residence time. This reaction was carried out with a back pressure of 4.0 bar. The reaction mixture was mixed with excess water and extracted three times with dichloromethane. The combined organic layers were washed with brine, dried over magnesium sulfate, filtered, and concentrated and the residue was purified via automated flash chromatography (SiO$_2$) to afford the desired product (CombiFlash® Rf, 12 g flash column). The solvent gradient was 90% hexane to 50% ethyl acetate over 15 min at a flow rate of 15 mL/min.

General procedure for the continuous flow synthesis of imidazo[1,2-*a*]pyridin-2-yl-1,2,4-oxadiazoles (Table 3)

The first reaction, the formation of imidazo[1,2-*a*]pyridine-2-carboxylic acid, was carried out in a 1000 μL reactor (glass chip) at 100 °C. The acid exiting the first reactor was combined with EDC/HOBt/DIPEA (1:1:1, 0.5 M, DMA) in a T-mixer. The synthesis of amidoxime (ArCN/NH$_2$OH·HCl/DIPEA (1.1:1:3), 0.4 M, DMA) was achieved by placing a second reactor (250 μL glass chip) in a heated silicone oil bath at 100 °C. This stream was next introduced into a third reactor and mixed with the stream exiting from the T-mixer at 150 °C. The stream exiting the third chip was collected after passing through the back pressure regulator. This reaction was carried out with a back pressure of 4.0 bar. The reaction mixture was mixed with excess water and extracted three times with dichloromethane. The combined organic layers were washed with brine, dried over magnesium sulfate, filtered, and concentrated and the

residue was purified via automated flash chromatography (SiO$_2$) to afford the desired product (CombiFlash® Rf, 12g flash column). The solvent gradient was 90% hexane to 50% ethyl acetate over 15 min at a flow rate of 15 mL/min.

Supporting Information

LC traces for optimization of oxadiazole synthesis (Table 1), details of liquid–liquid microextraction with FLLEX module including LC traces, general and detailed synthetic procedures with full characterization data for compounds, and ^{1}H NMR and ^{13}C NMR spectral traces of all compounds.

Supporting Information File 1
Experimental data.
[http://www.beilstein-journals.org/bjoc/content/supplementary/1860-5397-13-26-S1.pdf]

Acknowledgements

References

1. Hansen, K. B.; Hsiao, Y.; Xu, F.; Rivera, N.; Clausen, A.; Kubryk, M.; Krska, S.; Rosner, T.; Simmons, B.; Balsells, J.; Ikemoto, N.; Sun, Y.; Spindler, F.; Malan, C.; Grabowski, E. J. J.; Armstrong, J. D., III. *J. Am. Chem. Soc.* **2009,** *131,* 8798–8804. doi:10.1021/ja902462q
2. Broadwater, S. J.; Roth, S. L.; Price, K. E.; Kobašlija, M.; McQuade, D. T. *Org. Biomol. Chem.* **2005,** *3,* 2899–2906. doi:10.1039/b506621m
3. Hyde, A. M.; Buchwald, S. L. *Angew. Chem., Int. Ed.* **2008,** *47,* 177–180. doi:10.1002/anie.200704529
4. Tietze, L. F.; Brasche, G.; Gericke, K. M. *Domino Reactions in Organic Synthesis;* Wiley: Weinheim, 2006. doi:10.1002/9783527609925
5. Tietze, L. F. *Chem. Rev.* **1996,** *96,* 115–136. doi:10.1021/cr950027e
6. Enders, D.; Grondal, C.; Hüttl, M. R. M. *Angew. Chem., Int. Ed.* **2007,** *46,* 1570–1581. doi:10.1002/anie.200603129
7. Herath, A.; Dahl, R.; Cosford, N. D. P. *Org. Lett.* **2010,** *12,* 412–415. doi:10.1021/ol902433a
8. Herath, A.; Cosford, N. D. P. *Org. Lett.* **2010,** *12,* 5182–5185. doi:10.1021/ol102216x
9. Grant, D.; Dahl, R.; Cosford, N. D. P. *J. Org. Chem.* **2008,** *73,* 7219–7223. doi:10.1021/jo801152c
10. Baxendale, I. R.; Ley, S. V.; Mansfield, A. C.; Smith, C. D. *Angew. Chem., Int. Ed.* **2009,** *48,* 4017–4021. doi:10.1002/anie.200900970
11. Usutani, H.; Tomida, Y.; Nagaki, A.; Okamoto, H.; Nokami, T.; Yoshida, J.-i. *J. Am. Chem. Soc.* **2007,** *129,* 3046–3047. doi:10.1021/ja068330s
12. Sahoo, H. R.; Kralj, J. G.; Jensen, K. F. *Angew. Chem., Int. Ed.* **2007,** *46,* 5704–5708. doi:10.1002/anie.200701434

13. Bogdan, A. R.; Mason, B. P.; Sylvester, K. T.; McQuade, D. T. *Angew. Chem., Int. Ed.* **2007,** *46,* 1698–1701. doi:10.1002/anie.200603854
14. Webb, D.; Jamison, T. F. *Chem. Sci.* **2010,** *1,* 675–680. doi:10.1039/c0sc00381f
15. Pagano, N.; Herath, A.; Cosford, N. D. P. *J. Flow Chem.* **2011,** *1,* 28–31. doi:10.1556/jfchem.2011.00001
16. Aota, A.; Nonaka, M.; Hibara, A.; Kitamori, T. *Angew. Chem., Int. Ed.* **2007,** *46,* 878–880. doi:10.1002/anie.200600122
17. Kralj, J. G.; Sahoo, H. R.; Jensen, K. F. *Lab Chip* **2007,** *7,* 256–263. doi:10.1039/B610888A
18. Dessimoz, A.-L.; Cavin, L.; Renken, A.; Kiwi-Minsker, L. *Chem. Eng. Sci.* **2008,** *63,* 4035–4044. doi:10.1016/j.ces.2008.05.005
19. Maruyama, T.; Matsushita, H.; Uchida, J.-i.; Kubota, F.; Kamiya, N.; Goto, M. *Anal. Chem.* **2004,** *76,* 4495–4500. doi:10.1021/ac049844h
20. Noël, T.; Kuhn, S.; Musacchio, A. J.; Jensen, K. F.; Buchwald, S. L. *Angew. Chem., Int. Ed.* **2011,** *50,* 5943–5946. doi:10.1002/anie.201101480
21. Hartman, R. L.; Sahoo, H. R.; Yen, B. C.; Jensen, K. F. *Lab Chip* **2009,** *9,* 1843–1849. doi:10.1039/b901790a
22. Hartman, R. L.; Naber, J. R.; Buchwald, S. L.; Jensen, K. F. *Angew. Chem., Int. Ed.* **2010,** *49,* 899–903. doi:10.1002/anie.200904634
23. Diana, G. D.; Volkots, D. L.; Nitz, T. J.; Bailey, T. R.; Long, M. A.; Vescio, N.; Aldous, S.; Pevear, D. C.; Dutko, F. J. *J. Med. Chem.* **1994,** *37,* 2421–2436. doi:10.1021/jm00041a022
24. Borg, S.; Vollinga, R. C.; Labarre, M.; Payza, K.; Terenius, L.; Luthman, K. *J. Med. Chem.* **1999,** *42,* 4331–4342. doi:10.1021/jm990197+
25. Li, Z.; Chen, W.; Hale, J. J.; Lynch, C. L.; Mills, S. G.; Hajdu, R.; Keohane, C. A.; Rosenbach, M. J.; Milligan, J. A.; Shei, G.-J.; Chrebet, G.; Parent, S. A.; Bergstrom, J.; Card, D.; Forrest, M.; Quackenbush, E. J.; Wickham, L. A.; Vargas, H.; Evans, R. M.; Rosen, H.; Mandala, S. *J. Med. Chem.* **2005,** *48,* 6169–6173. doi:10.1021/jm0503244
26. Buzard, D.; Han, S.; Thoresen, L.; Moody, J.; Lopez, L.; Kawasaki, A.; Schrader, T.; Sage, C.; Gao, Y.; Edwards, J.; Barden, J.; Thatte, J.; Fu, L.; Solomon, M.; Liu, L.; Al-Shamma, H.; Gatlin, J.; Le, M.; Xing, C.; Espinola, S.; Jones, R. M. *Bioorg. Med. Chem. Lett.* **2011,** *21,* 6013–6018. doi:10.1016/j.bmcl.2011.05.110
27. Canne Bannen, L.; Chan, D. S.-M.; Gu, X.-H.; Mac, M. B.; Ng, S.; Wang, T.-L.; Wang, Y.; Xu, W. Imidazo[1,2-*a*]pyridine Derivatives, Their Use as S1P1 Agonists and Methods for Their Production. WO Patent WO2010065760 A1, June 10, 2010.
28. Zhang, H.-Z.; Kasibhatla, S.; Kuemmerle, J.; Kemnitzer, W.; Ollis-Mason, K.; Qiu, L.; Crogan-Grundy, C.; Tseng, B.; Drewe, J.; Cai, S. X. *J. Med. Chem.* **2005,** *48,* 5215–5223. doi:10.1021/jm050292k
29. Roppe, J.; Smith, N. D.; Huang, D.; Tehrani, L.; Wang, B.; Anderson, J.; Brodkin, J.; Chung, J.; Jiang, X.; King, C.; Munoz, B.; Varney, M. A.; Prasit, P.; Cosford, N. D. P. *J. Med. Chem.* **2004,** *47,* 4645–4648. doi:10.1021/jm049828c
30. Van Wagenen Bradford, C.; Stormann, T. M.; Moe, S. T.; Sheehan, S. M.; Mcleod, D. A.; Smith, D. L.; Isaac, M. B.; Slassi, A. Heteropolycyclic Compounds and Their Use as Metabotropic Glutamate Receptor Antagonists. WO Patent WO2001012627, Feb 22, 2001.
31. Eloy, F.; Lenaers, R. *Chem. Rev.* **1962,** *62,* 155–183. doi:10.1021/cr60216a003
32. Wang, Y.; Miller, R. L.; Sauer, D. R.; Djuric, S. W. *Org. Lett.* **2005,** *7,* 925–928. doi:10.1021/ol050007r
33. Adib, M.; Jahromi, A. H.; Tavoosi, N.; Mahdavi, M.; Bijanzadeh, H. R. *Tetrahedron Lett.* **2006,** *47,* 2965–2967. doi:10.1016/j.tetlet.2006.02.102
34. Evans, M. D.; Ring, J.; Schoen, A.; Bell, A.; Edwards, P.; Berthelot, D.; Nicewonger, R.; Baldino, C. M. *Tetrahedron Lett.* **2003,** *44,* 9337–9341. doi:10.1016/j.tetlet.2003.10.055

NMR reaction monitoring in flow synthesis

M. Victoria Gomez and Antonio de la Hoz[*]

Review

Address:
Área Química Orgánica, Facultad de Químicas, Universidad de
Castilla-La Mancha, Avda. Camilo José Cela nº 10, E-13071 Ciudad
Real, Spain and Instituto Regional de Investigación Científica
Aplicada (IRICA), Avda. Camilo José Cela s/n, E-13071 Ciudad Real,
Spain

Email:
Antonio de la Hoz[*] - Antonio.Hoz@uclm.es

* Corresponding author

Keywords:
expert systems; flow chemistry; microcoil; NMR probes

Abstract

Recent advances in the use of flow chemistry with in-line and on-line analysis by NMR are presented. The use of macro- and
microreactors, coupled with standard and custom made NMR probes involving microcoils, incorporated into high resolution and
benchtop NMR instruments is reviewed. Some recent selected applications have been collected, including synthetic applications,
the determination of the kinetic and thermodynamic parameters and reaction optimization, even in single experiments and on the μL
scale. Finally, software that allows automatic reaction monitoring and optimization is discussed.

Introduction

New enabling technologies have facilitated the transition from
traditional chemistry to a more automated approach that will be
the chemistry of the 21st century [1,2]. The objective is that the
reaction, analysis and work-up can be performed in an auto-
matic and continuous manner, but optimization and scale-up
represent a new step forward towards the full automation of the
chemical process [3]. The final objective is to save time for
chemists to focus on the more technical work and to spend
their time planning, interpreting results and developing new
projects.

In this regard, flow chemistry is the central motif of this auto-
mated approach. In contrast to batch mode, in flow chemistry
the starting materials are continuously introduced into the flow

reactor (e.g., a microreactor or a column) and the product is
continuously eluted from the end of the flow reactor. This ap-
proach can be used from microscale to laboratory scale and
even to production scale [4,5].

Some important advantages of flow chemistry are:

- Diffusion is clearly improved with regard to chemistry in
  batch (reagents and products), thus leading to improved
  heat and mass transfer.
- The surface to volume ratio increases with regard to
  reactions in batch. This enables good control of the reac-
  tion temperature and resolves the problems of highly
  exothermic reactions.

- Dangerous or air- and moisture-sensitive compounds can be used safely due to the small amounts of reagents and the use of a closed system with efficient control of pressure.
- The use of solvents can be minimized since concentrations can be increased up to the limit of solubility.
- Coupling with other enabling technologies is very simple and more efficient than in batch (photochemistry, electrochemistry, microwave, ultrasound, etc.) [6-9].

In this regard, in a recent paper a compact reconfigurable flow system was described for the continuous flow production of pharmaceuticals. The system comprised different types of preparation, reaction and elaboration modules that could be coupled in different configurations and the authors used them to prepare from hundreds to thousands of doses of pharmaceuticals that fulfilled the quality standards of the pharmacopeia [10].

In research laboratories that focus on rapid, reproducible and efficient analysis and optimization, and on the production scale for quality control, the coupling of flow and microreactor technology with a good analytical method is a prerequisite. Several analytical methods have been used and these include fluorescence, ultraviolet–visible (UV–vis), RAMAN, infrared (IR) and nuclear magnetic resonance (NMR) spectroscopy and mass spectrometry (MS). The use of a particular technique depends on the application, on the characteristics of the analyte and the ease of coupling with the flow system [11,12].

In this paper we focus on the coupling of nuclear magnetic resonance spectroscopy with flow and microreactor systems for the rapid analysis and optimization of reaction parameters and conditions. The use of this technique in mechanistic studies is also discussed.

Review
Commercial flow probes
NMR spectroscopy is based on the absorption of radiofrequency radiation to produce absorption on the nuclear spin level when nuclei are submitted to a strong magnetic field [13]. NMR spectroscopy is one of the most powerful and versatile methods for structural determination, enabling qualitative and quantitative analysis of samples. It can be applied to almost all elements in the periodic table, the only requirement being the presence of an isotope, not necessarily the most abundant, that shows magnetic properties.

The main drawback of NMR spectroscopy is that the sensitivity is very low when compared with other spectroscopic techniques such as UV, since the difference in population between the ground and the excited state is very low and is strongly de-

pendent on the permanent magnetic field (B_0) applied. This limitation is compensated by using stronger magnetic fields, which results in more complex, large and expensive NMR instruments and/or the development of specialized probes. Although the low sensitivity of NMR spectroscopy is a disadvantage for an analytical method, the power of this technique in structural determination compensates for its limitations.

The application of NMR spectroscopy to analytical chemistry in flow, preparative flow chemistry and microreactor technology requires the use of specially designed equipment, especially flow probes, flow cells or specialized microfluidic coils. In most cases, high-resolution NMR instruments are used but the high cost of these systems and the large space required limit their application on the laboratory scale and lab-on-a-chip. Recently, benchtop low field NMR instruments have been introduced in flow chemistry to overcome these limitations, with the advantage of lower cost and better integration with the continuous flow platform since the whole system can be set up in a fume hood. The main drawback of these systems is the lower resolution and sensitivity as compared to high resolution NMR instruments, which limits the application of benchtop NMR instruments to relatively simple structures.

Two classes of flow probes have been designed depending on the position of the sample tube, which can be vertical (denoted below as type 1) or horizontal (denoted below as type 2) (Figure 1), and the shape of the RF coil for transmitting and receiving, namely saddle-shaped when the sample tube is placed vertically and solenoidal when the sample tube is placed horizontally [14]. Manufacturers have designed commercial NMR flow probes of type 1 that can be integrated into their high and low-resolution NMR instruments. Type 2 probes have been designed by different research groups and integrated into standard NMR instruments.

Flow probes can further be classified as 'room temperature probes' if the RF coils and the sample are at similar temperatures or as 'cryogenic probes' if the RF coils are insulated from the sample chamber and kept cold.

The development of commercial NMR flow probes requires a different design when compared to the standard tube-based probes. For the design of a NMR flow probe, similarly to the design of a new probe head, careful choice of the components should be made in order to have an optimal resolution, sensitivity and RF homogeneity, but in addition, other factors should be taken into account because of working on-flow. Hence, the design should allow a high filling factor, the flash out of air bubbles and the displacement of the existing fluid in the detection volume by the incoming fluid instead of just mix with it,
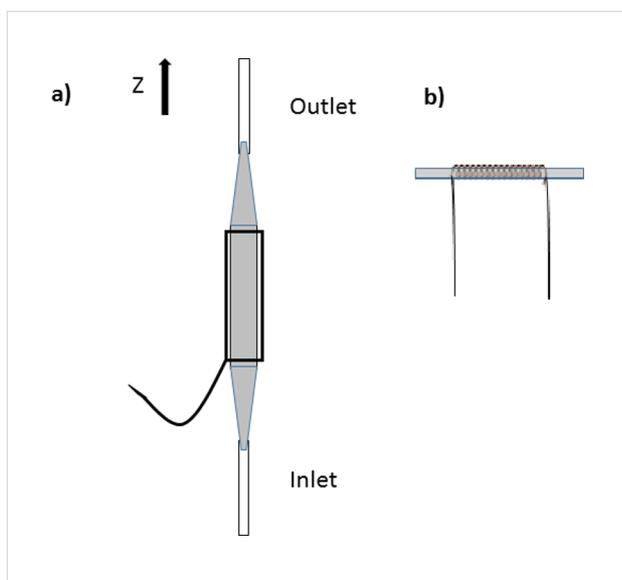
Figure 1: Graphical representation of (a) conventional flow cell with a saddle-shaped RF coil and (b) flow capillary with a solenoid coil.

among other issues [14]. Hence, the flow cell is a sample tube (made of glass or quartz) with openings at the top (outlet) and at the bottom (inlet) to enable connection to the flow system. NMR flow cells generally have a larger inner diameter at the centre than at the ends (Figure 1). The larger central portion of the flow cell is the sample chamber, i.e., the detection zone. The smaller segments at the ends correspond to the inlet and the outlet stems. When designing a flow cell, the total volume of the sample chamber is considered to be the minimum volume and this must be twice the active volume. This ratio is similar to that found for 5 mm NMR tubes in standard probes.

Flow cells are usually made of quartz, although Pyrex®, sapphire and alumina can also be considered. Quartz is the material of choice because of its uniformity, purity and mechanical strength. Moreover, quartz is a machinable material and shows excellent electrical properties. Tubing connections are made of PEEK (poly-ether-ketone) due to the strength of this material. However, PEEK has three main drawbacks, it absorbs DMSO and CH_3OH, it is not compatible with acids and it does not have a good turn radius.

Finally, most standard flow probes include pulsed-field gradient hardware, which enables interesting uses for the probe such as gradient shimming, solvent suppression pulse sequences (i.e., WET, which is especially suitable for applications in flow), and the use of pulse sequences that incorporate gradients, nowadays commonly found within most NMR experiments.

Considering the points outlined above, several advantages of flow NMR over traditional NMR can be envisaged. Firstly, ad-

ditional time is not required to lock or shim each sample when the solvent is kept constant during the experiment. Secondly, deuterated solvents are not required because of WET solvent suppression and also because locking is not required. Thirdly, more samples can be analyzed automatically from microtiter plates, thus avoiding the use and possible breakage of glass sample tubes.

Microcoil probes
An interesting way to increase the sensitivity of NMR is the use of microcoil probes [15,16]. Based on the reciprocity principle [15], it has been shown that for a constant length-to-diameter ratio, the NMR detector (i.e., coil) sensitivity is inversely proportional to its diameter. For a volume-limited sample, the signal is maximized when the coil is scale-down to enclose this volume sample. Although these probes show several advantages, as for instance are the coupling into continuous flow systems and its integration in compact magnets due to their lower requirements for the spatial B_0 field homogeneity, the construction of the probe for the highest sensitivity and resolution is a challenging task. The latter falls outside the scope of this review and instead, we will describe the types and features of microcoil probes in this section and its integration with flow systems in the following sections.

An important requirement in NMR spectroscopy is that a sufficiently strong B_1 is generated perpendicular to the static B_0 field. The geometry of the coil is very important in order to generate a homogeneous B_1 field over the entire sample volume. Hence, the geometry of the coil should be optimized in order to obtain the highest possible sensitivity and resolution. The most widely used geometries for NMR coils are represented in Figure 2. The most typical geometry used in commercial solution NMR probes is the saddle type. Although this geometry generates a very homogeneous magnetic field orthogonal to the permanent field B_0, it is not suitable for miniaturization. As a consequence, the saddle coil it is not used in small-volume NMR applications.

The main geometries reported for microcoils are, solenoidal, flat helical (also called planar microcoils), microslot and stripline (Figure 2). Below, the planar and solenoid coils are discussed more in detail as they are the most reported in literature.

Microsolenoid coils
A coil of helical geometry is wrapped around a capillary adopting the size and shape of the sample and therefore, a good filling factor is achieved. Solenoid coils have been investigated in detail. A representative example was reported by Sweedler et al. [17] who designed a microsolenoid coil with a detection cell
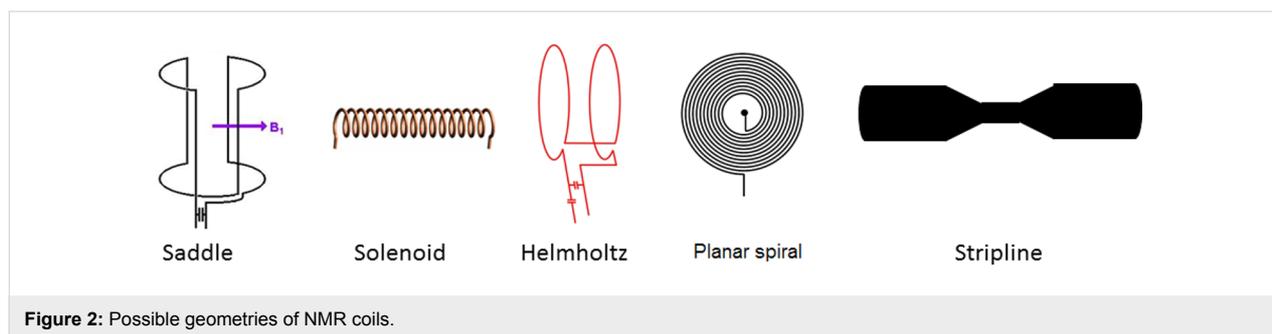
Figure 2: Possible geometries of NMR coils.

volume of ca. 5 nL, and line widths of only 0.6 Hz for a neat ethylbenzene sample. Recently, a new manufacturing procedure, by using a sacrificial layer and a combination of solvents, has been reported by Gruschke et al. [18] yielding a maximized and optimum filling factor compared to former procedures as hollow microcoils are encased in external support structures. A new methodology for the easy fabrication of solenoid coils has been reported by Saggiomo and Velders [19] using 3D-printing technology. The authors described an easy two-step ABS (acrylonitrile butadiene styrene) scaffold removal method to obtain a 3D printed device inserted in a block of PDMS (polydimethylsiloxane). The authors tested this methodology for the creation of microfluidic devices but they also fabricated a simple, cheap and sensitive NMR microsolenoid [19] with a detection volume of only 2 μL. Integration with a 9.4 T superconducting magnet allowed them to obtain high-resolution NMR spectra.

The main advantages of microsolenoid coils are: Excellent B_1-field uniformity and B_1/i field efficiency resulting in a high signal-to-noise ratio (SNR). In comparison to planar coils, the solenoid have lower resistance, better nutation curves (reaching the ideal sinusoidal behaviour) representing a much more uniform B_1 field than planar coils, however solenoid coils show lower resolution than planar coils in a comparative study reported by Popovic et al. [20] when both types of coils were fabricated following the same process.

And the main disadvantages of microsolenoid coils: Tedious manufacturing procedure especially for very small volumes as well as encountering the optimum position of the sample in the coil. Solenoid coils are usually wound by hand, resulting in a low reproducible and very time-consuming process.

Planar coils

Spiral planar coils were introduced in NMR spectroscopy derived from the semi-conductor industry by means of microfabrication techniques. Planar coils were studied in detail by Popovic et al. [21] as an alternative to solenoid coils. Planar coils show the following advantages:

They can be batch-fabricated with submicrometer resolution and with a high degree of geometric precision and reproducibility by standard photolithographic techniques. In addition, they can be integrated with chip-based microfluidic systems. To end with the advantages, planar coil facilitate an increased throughput since an array of planar coils and microfluidic channels can be manufactured by microfabrication techniques [15,16,21].

The disadvantages of planar coils are: Planar coils suffer of a high series resistance resulting in a low SNR as the latter is dominated by the thermal noise of the coil. The SNR depends on the geometrical features of the coil. For instance, the number of turns is crucial since a large number of turns can increase the unitary field produced by the coil but will also lead to higher resistance [21]. It is believed that the nearby windings of the coil induce static field distortions resulting in lower resolution and sensitivity in the NMR spectrum [22]. The optimum dimensions for a planar microcoil were presented by van den Berg et al. [23] and obtained from finite-element simulations [24]. High SNR were obtained at a low-field magnet. Another disadvantage of planar coils is the weak and inhomogenous B_1-field produced by the coil resulting in a non-sinusoidal nutation curve and in low SNR of the free induction decay [20].

Despite these disadvantages, interesting applications of planar microcoils can be found in literature. Hence, Velders et al. [25] studied supramolecular interactions by ^{19}F NMR spectroscopy at the picomole level. This application takes advantage of the high sensitivity and large chemical-shift dispersion of this nucleus. The authors determined the association constant of the complex of $NaPF_6$ with α-cyclodextrin at the picomole level with a detection volume of 50 nL and using non-deuterated solvents [25].

To conclude with the different coil geometries, microslot NMR microprobes and stripline coils show also interesting applications in small-volume NMR spectroscopy. A microslot consists of a dual-layer metallic microstrip that can have submicrometer dimensions. These coils produce field lines that are more homo-

geneous than those obtained with planar coils or just a metallic wire and find applications even for NMR metabolomics [26]. Stripline coils represent a simple and effective coil design with interesting applications even as detectors in DNP methods [22,27]. Stripline coils produce high and homogeneous B_1 field, can be integrated on a microfluidic chip and show scalability as reported by Kentgens et al. [22].

Applications of flow NMR in reaction monitoring

Keifer defined flow-NMR [28] as any NMR technique in which the sample flows through a tube into the NMR probe at some time during the measurement process.

The first reported use of a flow-NMR technique was in 1951 [29], when the ^{1}H spectrum of water (doped with FeCl$_3$) was recorded as it flowed through the NMR probe. In the seventies, a group of related techniques that were variously called 'stopped-flow NMR' [30], 'rapid-injection NMR' [31], 'continuous-flow' NMR [32], or just 'flow NMR' [33] were introduced and their use has continued to the present day. All of these techniques involve the use of standard NMR probes and do not require specialized equipment.

The introduction of LC–NMR was a natural development, although LC–NMR requires the use of an NMR probe that is dedicated solely to the observation of a sample flowing through tubing from another source. This requirement led to the investigation, design and development of the NMR flow probe. Several techniques were developed for the integration of the two systems, such as on-flow and stopped-flow LC–NMR. In the on-flow technique the solvent stream flows continuously during the analysis. However, one important problem that must be addressed is to achieve a good NMR signal-to-noise ratio. This limitation is more important than the chromatographic resolution. The NMR signal-to-noise ratio can be improved by signal averaging, but this approach usually requires the flow to be stopped for substantial periods of time.

The terms in-line and on-line analysis have been commonly used. 'In-line' and 'on-line' refer to methods of analysis that do not require the manual transfer of samples [34]. When the NMR probe and the reaction system are connected in-series, all of the reaction mixture passes through the NMR instrument and is continuously analyzed. This method is called in-line analysis. This configuration minimises the time-lag between reaction and analysis. For on-line analysis the NMR system is not directly connected to the reaction system and the sample is transferred from the reaction to the analysis system with representative aliquots collected periodically during the reaction. This method is simpler and can be used when direct connection is difficult to

be analyzed by NMR. A similar definition is provided by the FDA: "on-line: Measurement where the sample is diverted from the manufacturing process, and may be returned to the process stream. In-line: Measurement where the sample is not removed from the process stream and can be invasive or non-invasive" [35].

If the solvent contains protons, solvent suppression pulse sequences have to be used to obtain a good quality NMR spectrum. The first sequences used were presaturation and binomial sequences. The introduction of the WET sequence for solvent suppression was an important advance. WET has several advantages in that solvent suppression is fast, so it works well with flowing samples, it can supress multiple solvent lines and it is more frequency selective than other techniques. In contrast, pre-saturation do not work well in flowing samples and it is slower in its recycle rate. WET has also been incorporated into all of the standard 2D NMR sequences [28]. As an example Figure 3 shows a NOESY pulse sequence in which the WET sequence is incorporated into the end of the mix delay.
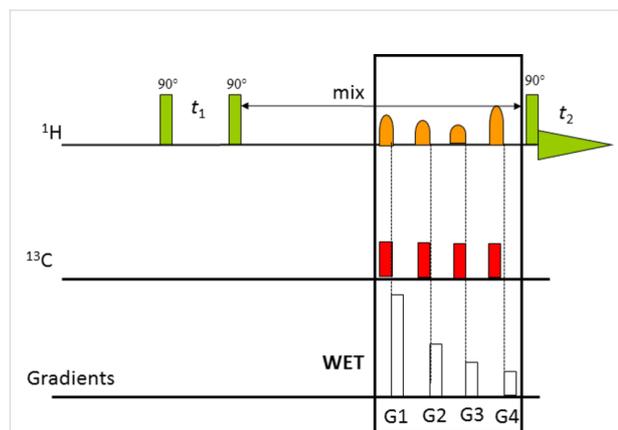
Figure 3: The NMR pulse sequence used for NOESY with WET solvent suppression [28].

NMR spectroscopy can be coupled to most separation techniques, including gas chromatography (GC), supercritical fluid chromatography (SFC), gel-permeation chromatography (GPC), high-performance liquid chromatography (HPLC), capillary electrophoresis (CE), capillary LC–NMR (CapLC–NMR), capillary electrochromatography-NMR (CEC–NMR), capillary isotachophoresis (cITP) and size-exclusion chromatography-NMR (SEC–NMR) [28].

Hyphenation is another important field in which separation and analytical techniques are combined. Hyphenation involves adding on other analytical techniques, almost as if they were

'building blocks', for instance, LC–NMR–MS, which was first described in 1995.

Flow Injection Analysis-NMR (FIA–NMR) and Direct Injection-NMR (DI–NMR) were the first non-chromatographic flow-NMR methodologies to be introduced. By simply removing the chromatography column LC–NMR produces FIA–NMR, a technique that has the capability of performing multiple analyses rapidly.

In contrast to FIA–NMR, DI–NMR lacks a mobile phase, just the solvent to dissolve the sample and some additional to rinse the flow cell. Also, the pump is simplified and the sample is injected directly into the flow probe to give a simple flow-NMR system. Applications of DI–NMR include combinatorial chemistry for the analysis of libraries [36], analysis of biofluids for clinical diagnosis [37] and metabolomics [38].

Applications in organic synthesis

In this section we will discuss some recent selected examples of the application of NMR reaction monitoring in flow chemistry. These examples include the design of flow systems, the use of standard NMR instruments and flow probes, the use of micro-coils and finally the use of flow-NMR for kinetic and mechanistic studies and for the optimization of synthetic processes.

Marquez et al. [39] developed a new NMR flow tube for the use in a standard 5 mm NMR probe (Figure 4). This system allows experiments to be carried out on flowing samples. The authors tested this flow tube to monitor the standard reaction of *p*-phenylenediamine and isobutyraldehyde to form the diimine product and good results and reproducibility were obtained.

The authors consider that this technology can be used to determine the mechanistic and kinetic aspects of reactions without a specialized flow probe and using different kinds of spectrometers with varying magnetic field strengths.

Danielli et al. [40] described the application of Benchtop NMR spectroscopy in flow reactions (SpinSolve from Magritek at 60 MHz). They considered that the field homogeneity and sensitivity that compact NMR spectrometers provide is sufficient to analyze small molecules at concentrations of 1 mmol L^{-1} in single-scan experiments. As a proof-of-concept,
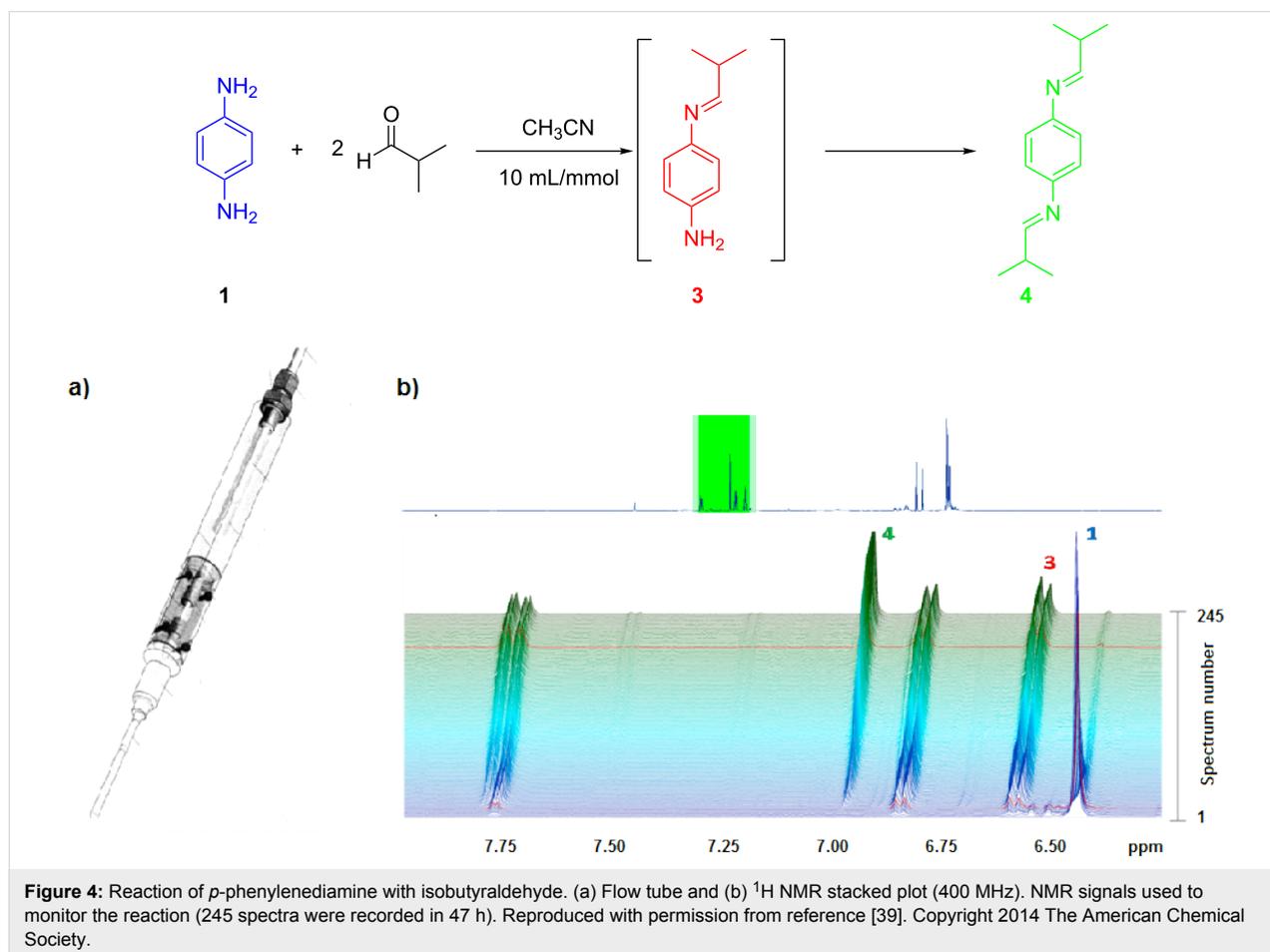
Figure 4: Reaction of *p*-phenylenediamine with isobutyraldehyde. (a) Flow tube and (b) ^{1}H NMR stacked plot (400 MHz). NMR signals used to monitor the reaction (245 spectra were recorded in 47 h). Reproduced with permission from reference [39]. Copyright 2014 The American Chemical Society.

they studied the transfer hydrogenation process of aceto-phenone with isopropanol catalysed by iridium complexes. The reaction was performed in batch and the sample was introduced into the magnet with a pump and Teflon tubing to form a closed circuit, at a flow rate of 1 mL min^{-1}. The kinetic rate could be studied as a function of the catalyst concentration and good agreement was found with the results obtained by gas chromatography. As expected for a first-order reaction, a linear dependence of the kinetic constant on the catalyst concentration was found.

An interesting point to consider is the comparison of in-line and off-line analysis. For example, Duchateau et al. [41] described the preparation of Grignard reagents from aryl halides and magnesium using a fluidized bed reactor under continuous-flow conditions. In a second flow reactor the Grignard was reacted with CO_2 to obtain carboxylic acids (Figure 5). The whole process was monitored by on-line ^{1}H NMR spectroscopy using a low field NMR instrument (Spinsolve-60 from Magritek).

The reaction was analysed by in-line NMR and off-line with a standard NMR tube. In the first case, the amount of oxidized Grignard reagent was significantly lower, showing the advan-

tages of in-line measurements. In the in-line experiment the reaction mixture was introduced into the flow NMR cell at 1 mL min^{-1} showing a conversion of about 80% in 70 min.

In this regard, Foley et al. [42] reported a comparison of three different methods for the analysis of flow reactions: online NMR, static NMR tubes, and periodic inversion of NMR tubes, using a high-resolution NMR instrument (400 MHz). Both studied reactions, heterogeneous reactions with long reaction times and homogeneous reactions with short reaction times showed that mixing has an important effect on the final result.

A careful evaluation of the three analytical methods and reaction conditions showed that the NMR technique has a significant influence on the results of the analysis. Considering the application of interest, the choice of one or other method could be crucial. In this regard, flow NMR gives more accurate results for kinetic studies, while static NMR is suitable to obtain structural information and determination of the mechanism.

The NMR instrument should also be evaluated considering that high-resolution NMR instruments are expensive, in terms of

Figure 5: Scheme and experimental setup of the flow system.
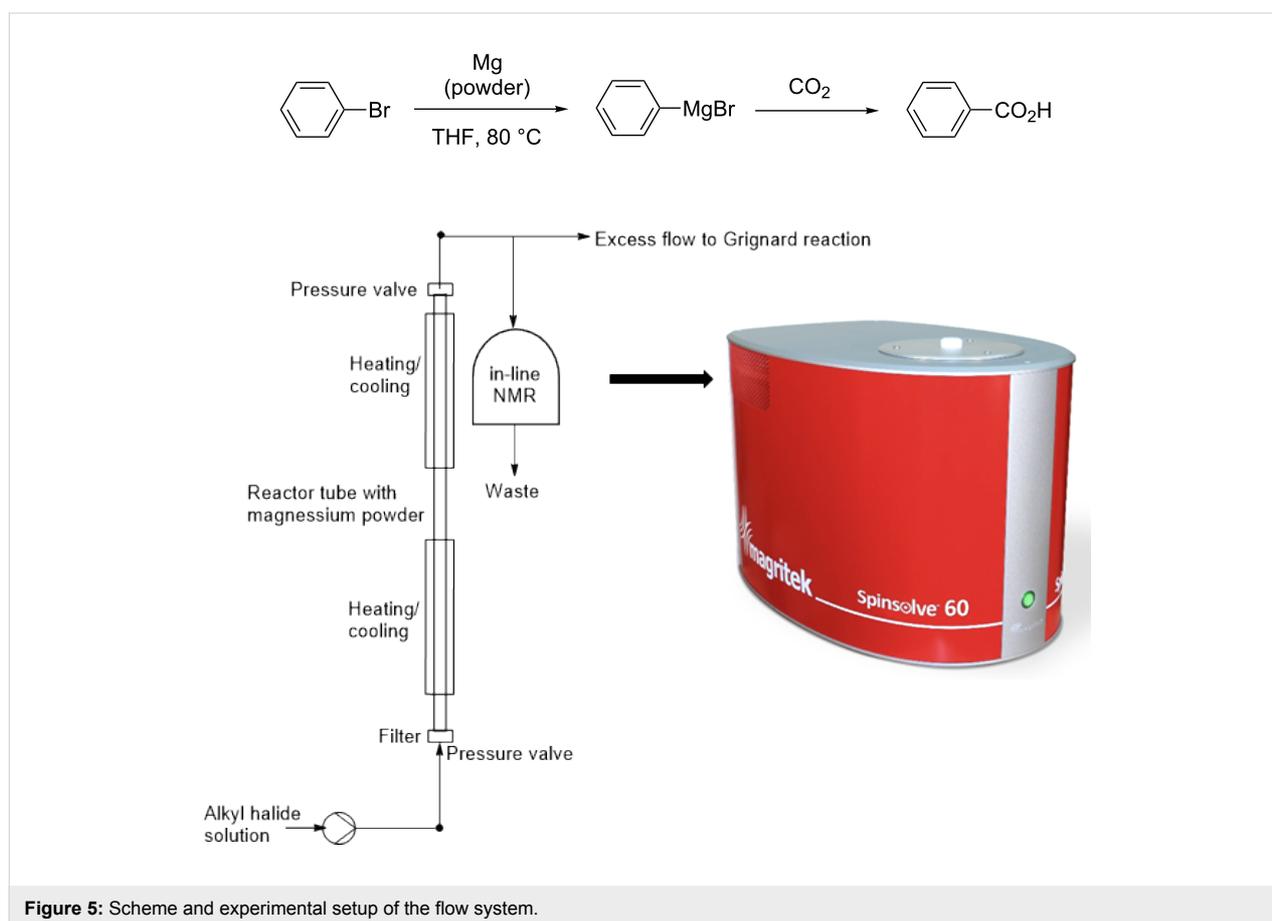
both acquisition and maintenance, and they require special laboratory installation. Benchtop NMR instruments have low cost and low maintenance; they can be easily placed in a conventional laboratory fume hood and transported to the required place.

Elipe and Milburn [43] studied the pros and cons of a benchtop NMR instrument at 45 MHz (Pico Spin-45). For this purpose, they studied reactions like the Fisher esterification, Suzuki reactions, and oxime formation and they analyzed the samples by simple injection of aliquots in the inlet port through an HPLC filter using non-deuterated solvents.

The major advantages of low field NMR arise from its simplicity, especially the fact that they do not require cryogenic liquids for the magnet, and they have reduced maintenance costs and also simpler handling and operation. Although there is a clear reduction in the sensitivity with regard to high field instruments, it is possible to obtain a ratio of up to 10:1 and this is sufficient for many applications. The major problems arise in reactions involving complex structures with small chemical shift dispersion and second-order coupling, which produce complex spectra with several overlapping signals. Finally, many low field instruments are supplied without variable temperature units and this limits the application to reactions at room temperature or close to the temperature of the magnet (25–50 °C, 42 °C in this case).

Another issue that must be considered when using benchtop NMR instruments is the use of magnetic stirrers, which can generate fluctuating magnetic fields that interfere with the NMR measurement if they are close to the magnet in the fume hood

[40]. Consequently, it is advisable to use mechanical stirrers for such reactions.

As pointed out above, the use of microcoils increases the sensitivity in NMR analysis. Moreover, it is possible to use these in conjunction with microreactors and consequently to design integrated systems that can be classified in the lab-on-a-chip methodology.

An interesting example was developed by Kentgens et al. [44], who designed a stripline microcoil for NMR studies coupled to a microreactor (Figure 6). The system was coupled to a custom-made NMR probe and inserted into a high-resolution NMR instrument (600 MHz). As pointed out above, the authors demonstrated that stripline microcoils show higher sensitivity than solenoid and planar microcoils with a line of <1 Hz in ethanol. As a proof-of-concept, the integrated flow system (microreactor-stripline NMR chip) was tested in the acylation of benzyl alcohol with acetyl chloride (Figure 7) using DIPEA as the base. The kinetics were studied by in situ monitoring and it was found that 70% conversion was achieved after 3 minutes. Broadening observed in the DIPEA signals is a consequence of protonation.

This example clearly shows that it is possible to integrate in one compact system the microreactor and the NMR chip to analyze raw samples and to apply this system to monitor reactions in a lab-on-a-chip approach.

Kinetic and mechanistic studies

The rapid analysis produced in flow NMR can be used for the detection of reactive intermediates and consequently for
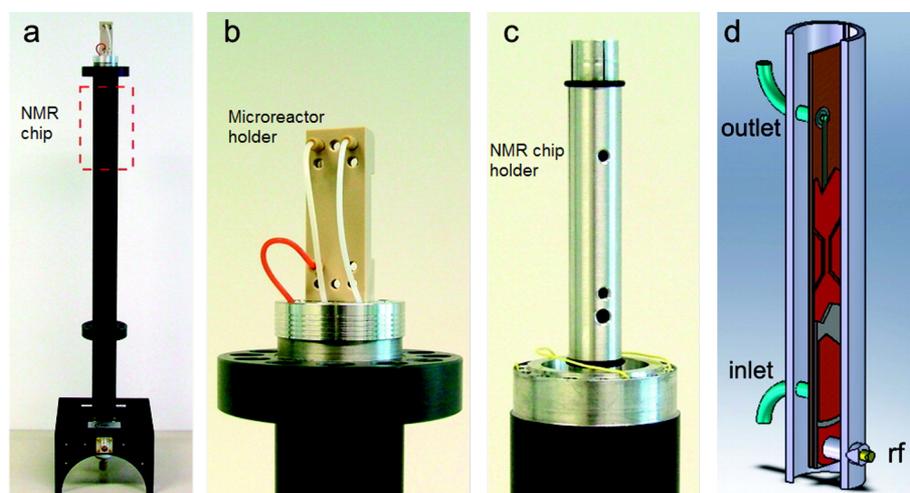
Figure 6: (a) Microfluidic probe. (b) Microreactor holder. (c) Stripline NMR chip holder. (d) Arrangement of the microfluidic chip in the holder. Reproduced with permission from reference [44]. Copyright 2009 The American Chemical Society.

Figure 7: Acetylation of benzyl alcohol. Spectra at (a) 9 s and (b) 3 min. Stoichiometry: benzyl alcohol/DIPEA/acetyl chloride 1:1:1.2. Reproduced with permission from reference [44]. Copyright 2009 The American Chemical Society.
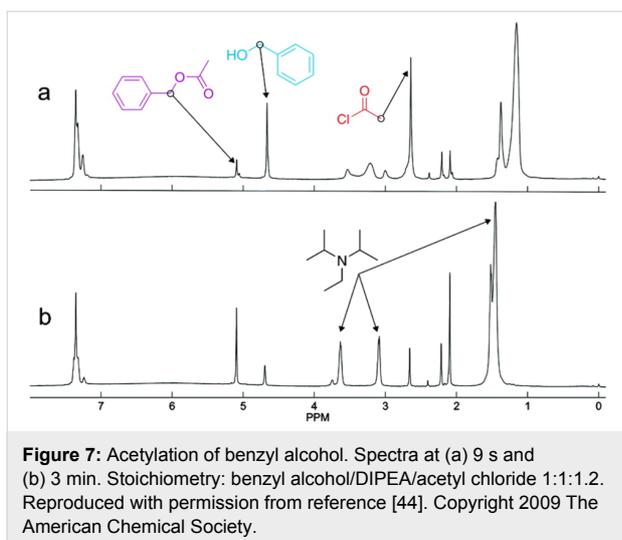
studying reaction mechanisms and the rapid optimization of a chemical process.

The first example was described by Nakakoshi et al. [45], who developed a micro-channelled cell for synthesis and monitoring (MICCS) (Figure 8) and this was integrated into a 500 MHz NMR instrument.

The system was used to elucidate the mechanism of the radical addition to an oxime ether with triethylborane (Scheme 1). The use of the NMR micro flow cell permitted the detection of intermediate A, which is unstable but is crucial for the elucidation of the reaction mechanism.

The authors consider that this system has several advantages over other methods: (i) detection of short-lived intermediates is possible, (ii) two-step chemical reactions can be observed, (iii) reaction conditions can be examined very easily by real-time monitoring and (iv) integration of small amounts of products and intermediates would be possible [45].

Harbou et al. [46] performed a kinetic study on the multicomponent reaction of acetaldehyde and water to produce poly(oxymethylmethylene)glycols. They used a new microreactor probe head that combined online flow ^{1}H NMR spectroscopy (400 MHz) using microreactor technology (Figure 9).

The microreactor NMR probe head was operated in stopped-flow. Under these conditions, the NMR flow cell is quickly filled with the reacting mixture of the desired overall composition because of the high flow rates used. The flow is then stopped and the NMR flow cell is used as a batch reactor in

Figure 8: a) Design of MICCS and b) schematic diagram of MICCS–NMR [45]. CH_2Cl_2 solutions of oxime ether and triethylborane were introduced into MICCS by two inlet ports and mixed at the first Y-shape channel (Flow rate 5 µL min^{-1}). A CH_2Cl_2 solution of methanol was introduced and mixed with reaction mixture at the second Y-shape channel to quench the reaction. Reproduced with permission from reference [45]. Copyright 2007 John Wiley and Sons.

Scheme 1: Proposed reaction mechanism.
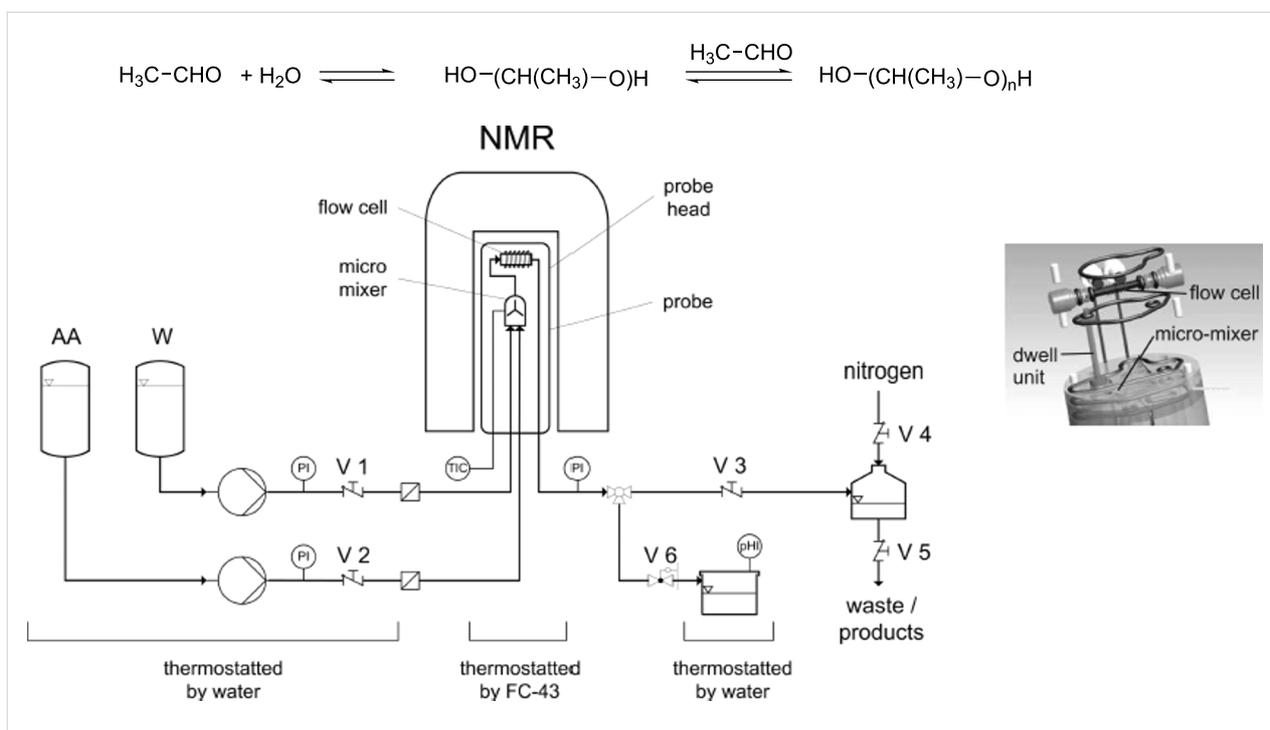
Figure 9: Flowsheet of the experimental setup used to study the reaction kinetics of the oligomer formation in mixtures of acetaldehyde (AA) and water (A) (Flow rates V_{AA} 254 µL min^{-1} and V_W 748 µL min^{-1}). Reproduced with permission from reference [46]. Copyright 2014 The American Chemical Society.

which the reaction is monitored online. The outlet line of the NMR probe head is connected to a vessel, which is pressurized with nitrogen to apply a back-pressure and thus adjusts the system pressure. In this way a new kinetic model could be developed for this reaction taking into consideration a wide range of temperatures and pH values. The results obtained extend the knowledge of the reaction kinetics for this industrially important system.

Similarly, Steinhof et al. [47] studied the equilibria and kinetics of the reaction of 1,3-dimethylurea with formaldehyde, which is

a model for the industrially relevant urea–formaldehyde system. The reaction was performed in a batch reactor and the analysis was carried out using a commercial NMR flow probe (Figure 10).

The design represented in Figure 10 allows the regulation of the molar ratio of reagents for the kinetic experiments (urea/formaldehyde from 1:1 to 4:1) as well as the temperature and pH, which were constantly measured. The reaction mixture flowed to the NMR instrument (400 MHz) by way of a pump and, before entering the NMR flow probe, the sample was filtered
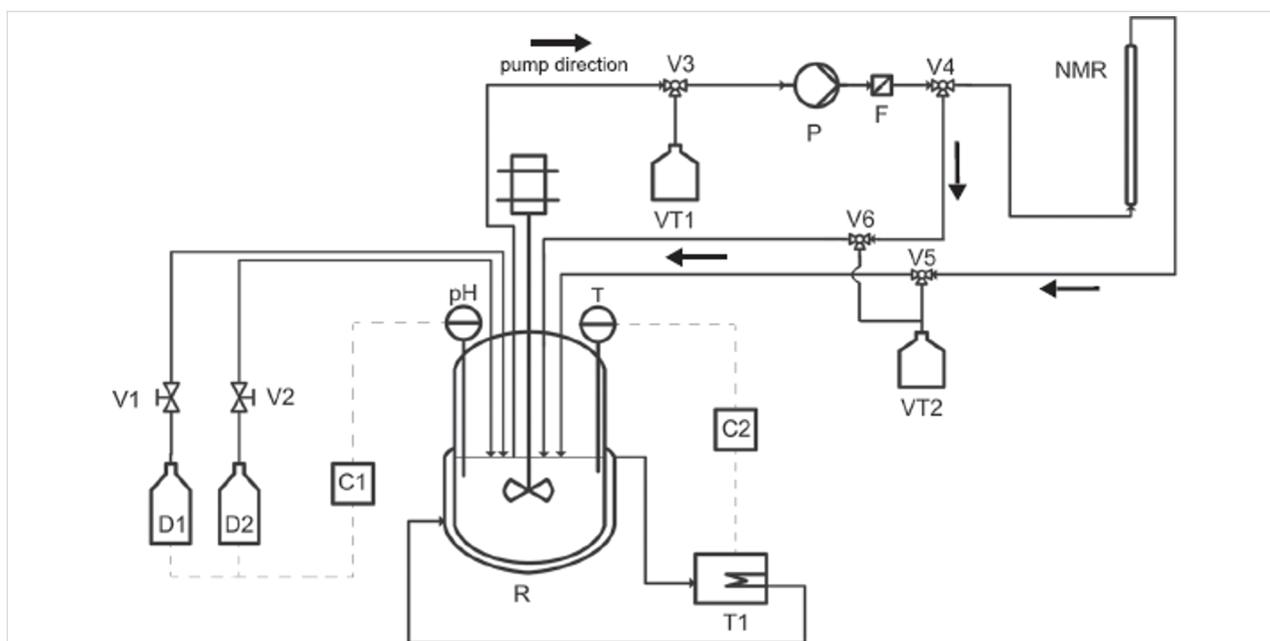
Figure 10: Design of the experimental setup used to combine on-line NMR spectroscopy and a batch reactor. Reproduced with permission from reference [47]. Copyright 2015 John Wiley and Sons.

and the volume selected with a split valve. In order to estimate the equilibrium time the authors performed dilutions using a micromixer prior to the NMR probe. In this way, it was possible to elucidate the reaction kinetics of the reaction system, including the main reaction pathways and also the side reactions, and to detect several intermediates including the formation of an ether bridge (Figure 11).

Gomez et al. [48] reported the first contribution that combines microstructured NMR probes with microliter continuous-flow microwave-assisted organic reactions. A microfluidic NMR chip with a planar microcoil and a detection volume of 6 nL was used for detection (Figure 12a). The specially designed microwave reactor has a small cavity in which a Weflon^{TM} (15% carbon filled PTFE) bar is introduced to ensure almost in-
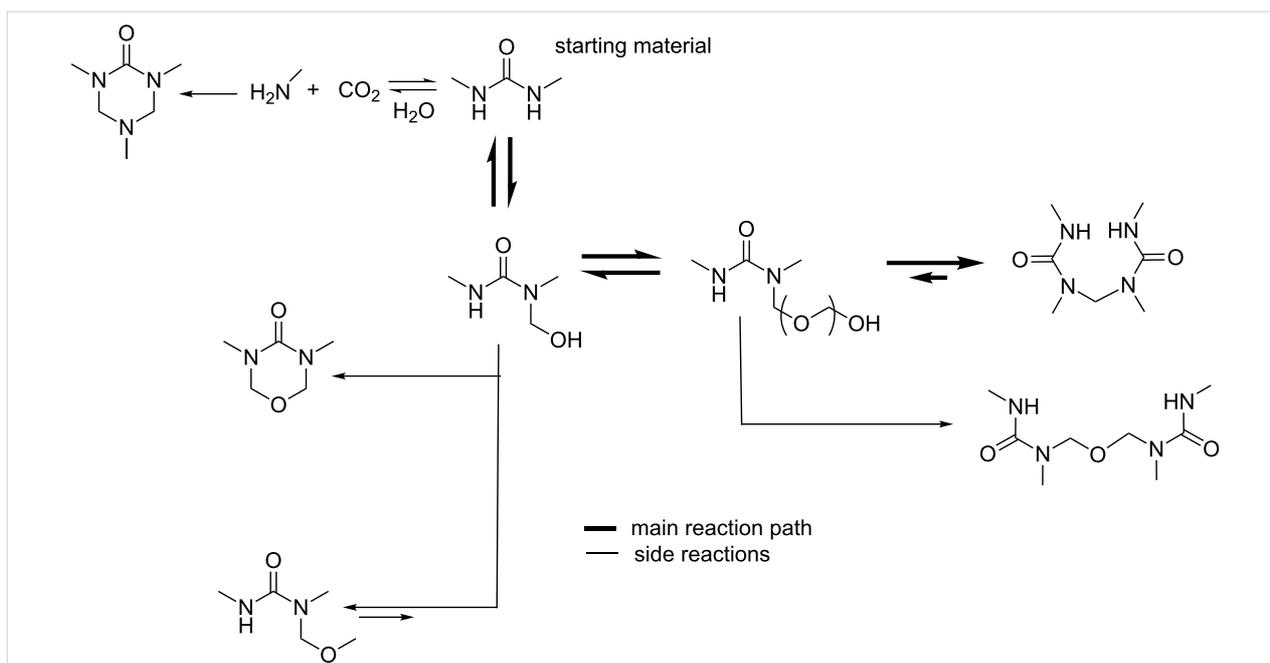
Figure 11: Reaction system 1,3-dimethylurea/formaldehyde. Main reaction pathway and side reactions [47].

Figure 12: (a) Experimental setup for the reaction. (b) Reaction samples analyzed independently by NMR. (c) Plot of conversion vs time at different temperatures determined by NMR. All of the data points for a certain temperature were collected from a single flow experiment. Reproduced with permission from reference [48]. Copyright 2010 The Royal Society of Chemistry.
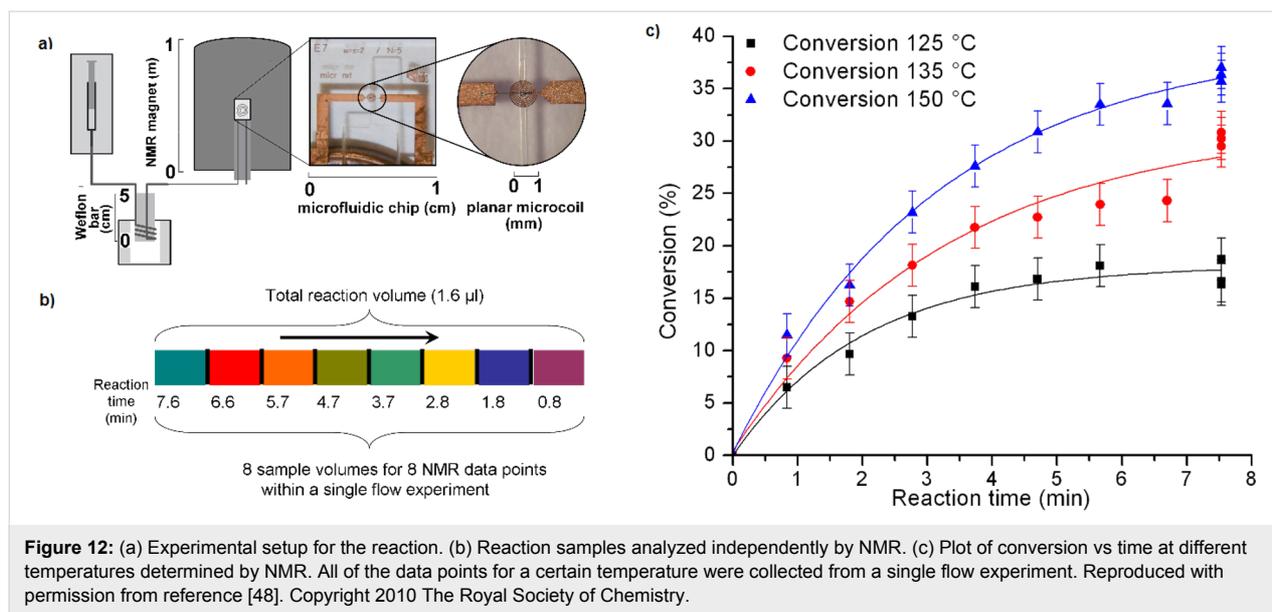
stantaneous heating. A fused silica capillary is wrapped around the Weflon™ bar to ensure efficient heat transfer and the total reaction volume was 2 μL. The minimal capillary thickness also permits rapid cooling of the reaction prior to NMR analysis in a 300 MHz NMR instrument.

Considering that the detection volume is smaller than the reaction volume (Figure 12b), different fractions of the initial reaction volume can be analyzed independently. In this way, it is possible to analyze reaction volumes submitted to different irradiation times in the same on-flow experiment.

As a model reaction, the cycloaddition of 2,5-dimethylfuran with dimethyl acetylenedicarboxylate in toluene was studied. With this system the authors could optimize the reaction conditions in a rapid manner with the consumption of very small amounts of solvent and reagents (Figure 12c). It is interesting to note that this set-up worked with standard, non-deuterated solvents.

This result showed how the synergistic interaction of microwave irradiation as the energy source and the rapid reaction characterization available with NMR and flow techniques can be used for rapid optimization in a single experiment in short time and with very small solvent volumes.

Determination of the kinetic parameters for a reaction usually requires the measurement of the initial reaction rate for different initial substrate concentrations and temperatures, and fitting of the data to the corresponding reaction rate law. Overall this is a very time-consuming process. However, the use of flow-NMR techniques leads to a marked reduction in the time required for

kinetic analysis. In this respect, Gomez et al. [49] reported an efficient flow system to determine kinetic information in a single experiment by taking advantage of the ability of the NMR chip, again a planar microcoil, to analyze very small volumes.

Bearing in mind once again that the detection volume is much smaller than the reaction volume, it is possible to extract information at the onset and during the steady state of the reaction, and to analyze the data to determine the kinetic parameters in a single non-isothermal on-flow experiment of 10 minutes and with a total volume of less than 50 μL.

The first cohort consists of sample volumes ranging from monitoring time zero to t_R and the second cohort spans from t_R to $2t_R$. For the first cohort, the time spent in the microreactor is equal to the monitoring time t. The second cohort of sample fractions always spends time t_R in the microreactor (Figure 13a).

In zone a, every data point corresponds to a different temperature (Figure 13b). Zone b' shows a constant temperature value (different to zone a). Zone c includes the first data points for samples that entered the microreactor before temperature stabilization, each with a different temperature value. Finally, zone d includes the data points that experienced the constant temperature of 393 K for 4 minutes (but with a difference in 'starting' concentration from that of zone b').

Fitting these data, i.e., temperature, temperature gradients, starting concentration and residence times, against a reaction conversion model enables the reaction order, rate constant,

Figure 13: (a) Schematics of two microreactor cohorts of sample fractions. (b) Reaction product concentration (M) versus monitoring time (s) for the synthesis of 5-methyl-3-phenylisoxazole in methanol at an overall flow rate of 5 µL/min (initial concentration, 0.35 M). Every data point corresponds to a 2.5 µL fraction. (c) Table with differences between the zones (a + b, b', c, d) in residence time, temperature, and concentration. Flow-NMR analysis were performed in a 400 MHz instrument. Reproduced with permission from reference [49]. Copyright 2015 The American Chemical Society.

Arrhenius parameters, pre-exponential factor, and activation energy values to be determined in a rapid manner from one single flow experiment.

The two latter examples reported by Gomez et al. [48,49] illustrate the advantages of combining microprobes with flow techniques. The capabilities of the microcoil of analysing very small sample volumes enable the division of the reactor volume in different portions of different experimental conditions, allowing a fast collection of experimental data and therefore, a fast optimization of reaction conditions and determination of kinetic parameters. On the other hand, some limitations and problems are encountered when combining microcoils with flow techniques. The usual limitations of working on flow NMR (i.e., clogging, bubbles, precipitation and dirty flow cells among others) are present at this small scale [28].

Finally, Cronin et al. [50] described a synthetic platform that incorporates a flow reactor, an in-line benchtop NMR instrument (Spinsolve from Magritek) to monitor the organic reactions, and a control system to analyze NMR (via Labview software) data and optimize the reaction conditions. They performed a range of reactions including imine formation (Figure 14), electrophilic fluorinations and Diels–Alder reactions. This system was employed to perform kinetic studies, in-line structural characterization including DEPT spectra, 2D-NMR spectroscopy, ^{19}F NMR spectroscopy and monitoring of the stereoselectivity in Diels–Alder reactions and self-optimization of flow conditions

using a modified version of the Nelder–Mead algorithm. For the NMR integral data for each experiment, the algorithm (Figure 15) selects the composition and residence time for each experiment.

Figure 14: NMR analysis of the reaction of benzaldehyde (2 M in CH$_3$CN) and benzylamine (2 M in CH$_3$CN) (1:1), residence time, 30 min. Reproduced with permission from reference [50]. Copyright 2015 The Royal Society of Chemistry.
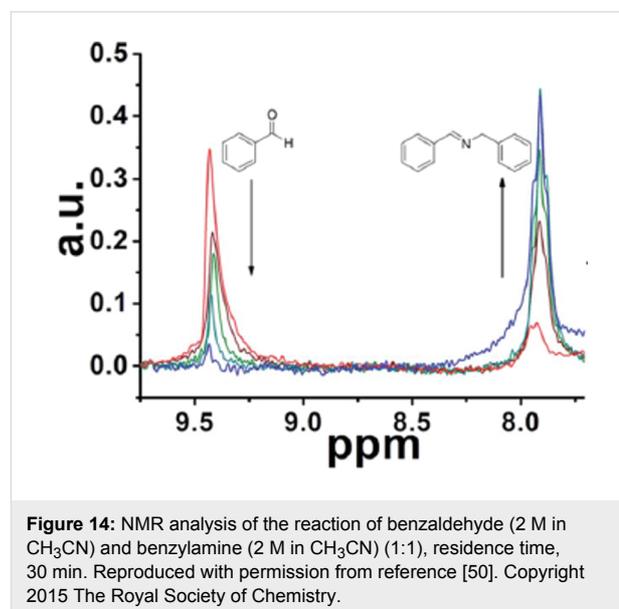
This study showed the potential of the combined use of flow-chemistry, real-time on-line analysis, especially by flow-NMR, and design of experiments (DOE) for the characterization and self-optimization of chemical reactions.

Figure 15: Flow diagram showing the self-optimizing reactor system. Reproduced with permission from reference [50]. Copyright 2015 The Royal Society of Chemistry.
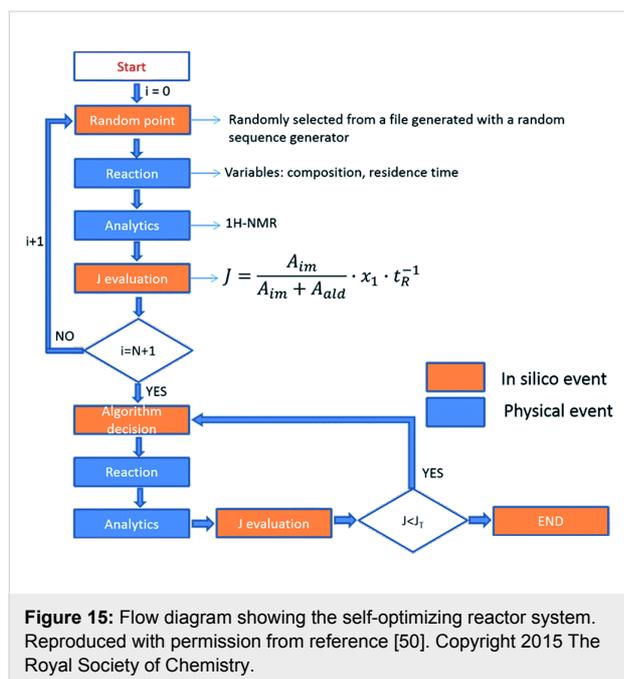
Conclusion

Real-time analysis of a reaction is one of the key principles of green chemistry [51] for pollution prevention. However, on-line and in-line analysis together with the use of flow chemistry and the appropriate software for analysis, determination of the kinetic and thermodynamic parameters and for process optimization, are a key for a new type of chemistry in the 21st century.

In this regard, the use of NMR spectroscopy is probably the most interesting technique of choice. Although NMR spectroscopy lacks the high sensitivity of other analytical techniques such as MS, IR, and UV–vis, it is possibly the most powerful method for structural determination and it provides an excellent platform for analysis and characterization of the reaction product.

Besides the low sensitivity of flow NMR spectroscopy some other limitations can be found. They are specific of each technique or to its combination. These limitations include:

- Clogging of the capillary tubing by precipitation of the sample, that produces a mechanical blockage and is increasingly important as the diameter of the capillary is reduced.
- Formation of bubbles it is always a problem but especially if they get into the flow NMR cell since they can distort the NMR lineshape.
- Pressure produced when using gases may produce bubbles and a reduction of the sensitivity of the NMR instrument.

- In flow reaction, a laminar flow should be assured ($Re < 2000$) avoiding a turbulent flow ($Re > 3000$). The NMR coil require a uniform magnetic susceptibility in the whole sample that cannot be assured with a turbulent flow. This problem may occur also if mixing of the components is not perfect or even when using mixtures of deuterated and non-deuterated solvents, since they have different magnetic susceptibilities.

All these limitations may affect the reproducibility and the accuracy of the quantitative analysis of the reaction, especially if mixing is not perfect, the analyzed sample may be not representative of the whole reaction.

Finally, this is an interdisciplinary field with implications in chemistry, physics, engineering and mathematics and with many possibilities of development and innovation. Further developments in microchip technology, microcoils (higher sensitivity, broadband and 2D NMR applications [52]) and improved sensitivity for benchtop NMR instruments, together with the development of new and improved software for product analysis and reaction optimization, will extend and popularize the application of these methodologies.

Acknowledgements

References

1. Fitzpatrick, D. E.; Battilocchio, C.; Ley, S. V. *ACS Cent. Sci.* **2016,** *2,* 131–138. doi:10.1021/acscentsci.6b00015
2. Ley, S. V.; Fitzpatrick, D. E.; Myers, R. M.; Battilocchio, C.; Ingham, R. J. *Angew. Chem., Int. Ed.* **2015,** *54,* 10122–10136. doi:10.1002/anie.201501618
3. Kobayashi, S. *Chem. – Asian J.* **2016,** *11,* 425–436. doi:10.1002/asia.201500916
4. Wirth, T., Ed. *Microreactors in Organic Synthesis and Catalysis;* Wiley: Weinheim, Germany, 2008.
5. Mark, D.; Haeberle, S.; Roth, G.; von Stetten, F.; Zengerlez, R. *Chem. Soc. Rev.* **2010,** *39,* 1153–1182. doi:10.1039/b820557b
6. Albini, A.; Germani, L. *Photochemical Methods.* In *Handbook of Synthetic Photochemistry;* Albini, A.; Fagnoni, M., Eds.; Wiley-VCH: Weinheim, Germany, 2010.
7. Yoshida, J.-i.; Kataoka, K.; Horcajada, R.; Nagaki, A. *Chem. Rev.* **2008,** *108,* 2265–2299. doi:10.1021/cr0680843
8. Kise, N.; Mimura, R. *Tetrahedron: Asymmetry* **2007,** *18,* 988–993. doi:10.1016/j.tetasy.2007.04.014
9. Glasnov, T. N.; Kappe, C. O. *Chem. – Eur. J.* **2011,** *17,* 11956–11968. doi:10.1002/chem.201102065

10. Adamo, A.; Beingessner, R. L.; Behnam, M.; Chen, J.; Jamison, T. F.; Jensen, K. F.; Monbaliu, J.-C. M.; Myerson, A. S.; Revalor, E. M.; Snead, D. R.; Stelzer, T.; Weeranoppanant, N.; Wong, S. Y.; Zhang, P. *Science* **2016,** *352,* 61–67. doi:10.1126/science.aaf1337

11. Yue, J.; Schouten, J. C.; Nijhuis, T. A. *Ind. Eng. Chem. Res.* **2012,** *51,* 14583–14609. doi:10.1021/ie301258j

12. Sans, V.; Cronin, L. *Chem. Soc. Rev.* **2016,** *45,* 2032–2043. doi:10.1039/C5CS00793C

13. Günther, H. *NMR Spectroscopy. Basic Principles, Concepts, and Applications in Chemistry;* Wiley-VCH: Weinheim, Germany, 2013.

14. Haner, R. L.; Keifer, P. A. *Flow Probes for NMR Spectroscopy. Encyclopedia of Magnetic Resonance;* John Wiley & Sons, 2009; pp 1–11. And references therein.

15. Fratila, R. M.; Velders, A. H. *Annu. Rev. Anal. Chem.* **2011,** *4,* 227–249. doi:10.1146/annurev-anchem-061010-114024

16. Zalesskiy, S. S.; Danieli, E.; Blümich, B.; Ananikov, V. P. *Chem. Rev.* **2014,** *114,* 5641–5694. doi:10.1021/cr400063g

17. Olson, D. L.; Peck, T. L.; Webb, A. G.; Magin, R. L.; Sweedler, J. V. *Science* **1995,** *270,* 1967–1970. doi:10.1126/science.270.5244.1967

18. Kamberger, R.; Moazenzadeh, A.; Korvink, J. G.; Gruschke, O. G. *J. Micromech. Microeng.* **2016,** *26,* 065002. doi:10.1088/0960-1317/26/6/065002

19. Saggiomo, V.; Velders, A. H. *Adv. Sci.* **2015,** *2,* 1500125. doi:10.1002/advs.201500125

20. Ehrmann, K.; Saillen, N.; Vincent, F.; Stettler, M.; Jordan, M.; Wurm, F. M.; Besse, P.-A.; Popovic, R. *Lab Chip* **2007,** *7,* 373–380. doi:10.1039/b614044k

21. Massin, C.; Vincent, F.; Homsy, A.; Ehrmann, K.; Boero, G.; Besse, P.-A.; Daridon, A.; Verpoorte, E.; de Rooij, N. F.; Popovic, R. S. *J. Magn. Reson.* **2003,** *164,* 242–255. doi:10.1016/S1090-7807(03)00151-4

22. van Bentum, P. J. M.; Janssen, J. W. G.; Kentgens, A. P. M.; Bart, J.; Gardeniers, J. G. E. *J. Magn. Reson.* **2007,** *189,* 104–113. doi:10.1016/j.jmr.2007.08.019

23. Wensink, H.; Hermes, D. C.; van den Berg, A. In *High signal to noise ratio in low field NMR on chip: simulations and experimental results,* Int. Workshop Micro Electromech. Syst., 7th, Maastricht, Netherland; 2004.

24. Meeker, D. Finite Element Method Magnetics. http://www.femm.info/wiki/HomePage (accessed Jan 11, 2017).

25. Gómez, M. V.; Reinhoudt, D. N.; Velders, A. H. *Small* **2008,** *4,* 1293–1295. doi:10.1002/smll.200701306

26. Krojanski, H. G.; Lambert, J.; Gerikalan, Y.; Suter, D.; Hergenröder, R. *Anal. Chem.* **2008,** *80,* 8668–8672. doi:10.1021/ac801636a

27. Sharma, M.; Janssen, G.; Leggett, J.; Kentgens, A. P. M.; van Bentum, P. J. M. *J. Magn. Reson.* **2015,** *258,* 40–48. doi:10.1016/j.jmr.2015.06.007

28. Keifer, P. A. *Flow techniques in NMR spectroscopy. Annual reports on NMR spectroscopy;* Elsevier, 2007; Vol. 62, pp 1–47. And references therein.

29. Suryan, G. *Proc. - Indian Acad. Sci., Sect. A* **1951,** *33,* 107–111.

30. Sudmeier, J. L.; Pesek, J. J. *Inorg. Chem.* **1971,** *10,* 860–863. doi:10.1021/ic50098a040

31. McGarrity, J. F.; Prodolliet, J.; Smyth, T. *Org. Magn. Reson.* **1981,** *17,* 59–65. doi:10.1002/mrc.1270170114

32. Bayer, E.; Albert, K. *J. Chromatogr. A* **1984,** *312,* 91–97. doi:10.1016/S0021-9673(01)92766-9

33. McGarrity, J. F.; Ogle, C. A.; Brich, Z.; Loosli, H. R. *J. Am. Chem. Soc.* **1985,** *107,* 1810–1815. doi:10.1021/ja00293a002

34. Browne, D. L.; Wright, S.; Deadman, B. J.; Dunnage, S.; Baxendale, I. R.; Turner, R. M.; Ley, S. V. *Rapid Commun. Mass Spectrom.* **2012,** *26,* 1999–2010. doi:10.1002/rcm.6312

35. http://www.fda.gov/downloads/Drugs/GuidanceComplianceRegulatoryInformation/Guidances/UCM070305 (accessed Jan 11, 2017).

36. Leo, G. C.; Krikava, A.; Caldwell, G. W. *Anal. Chem.* **2003,** *75,* 1954–1957. doi:10.1021/ac026389l

37. Potts, B. C. M.; Deese, A. J.; Stevens, G. J.; Reily, M. D.; Robertson, D. G.; Theiss, J. *J. Pharm. Biomed. Anal.* **2001,** *26,* 463–476. doi:10.1016/S0731-7085(01)00430-7

38. Teng, Q.; Ekman, D. R.; Huang, W.; Collette, T. W. *Analyst* **2012,** *137,* 2226–2232. doi:10.1039/c2an16251b

39. Foley, D. A.; Bez, E.; Codina, A.; Colson, K. L.; Fey, M.; Krull, R.; Piroli, D.; Zell, M. T.; Marquez, B. L. *Anal. Chem.* **2014,** *86,* 12008–12013. doi:10.1021/ac502300q

40. Danieli, E.; Perlo, J.; Duchateau, A. L. L.; Verzijl, G. K. M.; Litvinov, V. M.; Blümich, B.; Casanova, F. *ChemPhysChem* **2014,** *15,* 3060–3066. doi:10.1002/cphc.201402049

41. Goldbach, M.; Danieli, E.; Perlo, J.; Kaptein, B.; Litvinov, V. M.; Blümich, B.; Casanova, F.; Duchateau, A. L. L. *Tetrahedron Lett.* **2016,** *57,* 122–125. doi:10.1016/j.tetlet.2015.11.077

42. Foley, D. A.; Dunn, A. L.; Zell, M. T. *Magn. Reson. Chem.* **2016,** *54,* 451–456. doi:10.1002/mrc.4259

43. Elipe, M. V. S.; Milburn, R. R. *Magn. Reson. Chem.* **2016,** *54,* 437–443. doi:10.1002/mrc.4189

44. Bart, J.; Kolkman, A. J.; Oosthoek-de Vries, A. J.; Koch, K.; Nieuwland, P. J.; Janssen, H. J. W. G.; van Bentum, J. P. J. M.; Ampt, K. A. M.; Rutjes, F. P. J. T.; Wijmenga, S. S.; Gardeniers, H. J. G. E.; Kentgens, A. P. M. *J. Am. Chem. Soc.* **2009,** *131,* 5014–5015. doi:10.1021/ja900389x

45. Nakakoshi, M.; Ueda, M.; Sakurai, S.; Asakura, K.; Utsumi, H.; Miyata, O.; Naito, T.; Takahashi, Y. *Magn. Reson. Chem.* **2007,** *45,* 989–992. doi:10.1002/mrc.2087

46. Scheithauer, A.; Brächer, A.; Grützner, T.; Zollinger, D.; Thiel, W. R.; von Harbou, E.; Hasse, H. *Ind. Eng. Chem. Res.* **2014,** *53,* 17589–17596. doi:10.1021/ie5033556

47. Steinhof, O.; Scherr, G.; Hasse, H. *Magn. Reson. Chem.* **2016,** *54,* 457–476. doi:10.1002/mrc.4274

48. Gomez, M. V.; Verputten, H. H. J.; Díaz-Ortız, A.; Moreno, A.; de la Hoz, A.; Velders, A. H. *Chem. Commun.* **2010,** *46,* 4514–4516. doi:10.1039/b924936b

49. Gomez, M. V.; Rodríguez, A. M.; de la Hoz, A.; Jimenez-Marquez, F.; Fratila, R. M.; Barneveld, P. A.; Velders, A. H. *Anal. Chem.* **2015,** *87,* 10547–10555. doi:10.1021/acs.analchem.5b02811

50. Sans, V.; Porwol, L.; Dragone, V.; Cronin, L. *Chem. Sci.* **2015,** *6,* 1258–1264. doi:10.1039/C4SC03075C

51. Anastas, P. T.; Warner, J. C. *Green Chemistry: Theory and Practice;* Oxford University Press: New York, 1998.

52. Fratila, R. M.; Gomez, M. V.; Sýkora, S.; Velders, A. H. *Nat. Commun.* **2014,** *5,* No. 3025. doi:10.1038/ncomms4025

A chemoselective and continuous synthesis of *m*-sulfamoylbenzamide analogues

Arno Verlee[1], Thomas Heugebaert[1], Tom van der Meer[2,3], Pavel I. Kerchev[2,3], Frank Van Breusegem[2,3] and Christian V. Stevens[*1]

Abstract

For the synthesis of *m*-sulfamoylbenzamide analogues, small molecules which are known for their bioactivity, a chemoselective procedure has been developed starting from *m*-(chlorosulfonyl)benzoyl chloride. Although a chemoselective process in batch was already reported, a continuous-flow process reveals an increased selectivity at higher temperatures and without catalysts. In total, 15 analogues were synthesized, using similar conditions, with yields ranging between 65 and 99%. This is the first automated and chemoselective synthesis of *m*-sulfamoylbenzamide analogues.

Introduction

Small molecules are commonly used for their ability to regulate or assist in different biological processes. Typically, drug development starts with the screening of large libraries of relatively similar compounds, where only milligrams of material are needed for primary testing. Upon identification of a primary hit, the synthetic protocol must then be quickly expanded to tens of grams for early in vivo toxicity studies and hundreds of grams for further toxicology studies and clinical trials [1]. These swiftly changing requirements appear throughout the clinical development of active pharmaceutical ingredients (APIs) and

place specific and conflicting burdens on synthetic protocols. An early synthesis must be extremely fast and flexible, as current high-throughput compound screening takes less than one week for a set of 10,000 compounds [2], which is far beyond the current synthetic capabilities. Once a suitable hit is identified on the other hand, the synthetic prerequisites change completely, and a robust and scalable protocol is needed. Over the past few years, flow chemistry has emerged as a potential solution to these conflicting prerequisites [3-11]. Flow processing is suitable for automation, thus allowing the fast synthesis of com-

pound libraries, but as opposed to, e.g., combinatorial chemistry, the developed protocols are directly useful for scale-up. A class of small molecules where these principles can apply for are *m*-sulfamoylbenzamides. These compounds proved to be effective against Huntington's and Parkinson's disease [12-14]. They inhibit the Sirtuin 2 (SIRT2) deacetlyse protein (Figure 1, **AK-1**, **AK-7**) resulting in improved motor skills [12,13,15]. Furthermore, *m*-sulfamoylbenzamide analogues (Figure 1, **C2-8**) are able to suppress polyglutamine (polyQ) aggregation [14], which is a major cause of neurodegeneration in Huntington's disease. Although there are numerous reports available on the study of these analogues, an automated, chemoselective alternative to the synthesis is not yet available.

Figure 1: *m*-Sulfamoylbenzamides as Sirtuin 2 inhibitors (SIRT2) or suppressor of polyglutamine aggregation (polyQ).
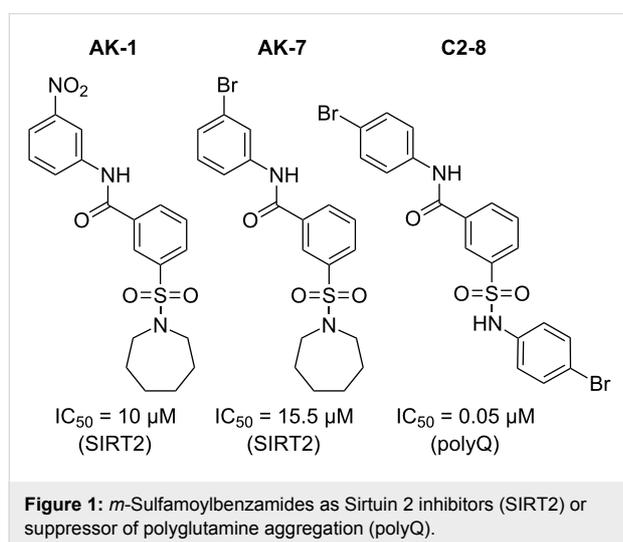
The most common synthetic approach starts from *m*-(chlorosulfonyl)benzoic acid [15-17]. This synthetic approach is a two-step procedure and therefore needs two subsequent work-up steps, limiting the yield and resulting in a more time-consuming synthetic approach. Yang et al. [18] reported a one-pot synthetic strategy for *m*-sulfamoylbenzamide analogues starting from *m*-(chlorosulfonyl)benzoyl chloride. In this study the difference in reactivity between the sulfonyl and aroyl chloride is exploited resulting in a chemoselective synthesis for these analogues. The yields varied between 46% and quantitative yield, relatively short reaction times were required and dichloromethane was used as solvent.

The coupling of carboxylic acids with amines in flow through a benzotriazole activation [19], or with immobilized reagents as for the synthesis of grossamide [20] is already known. However, we wanted to use *m*-(chlorosulfonyl)benzoyl chloride since this can be synthesized in one single step. Furthermore, acid chlorides show a high reactivity [21] making *m*-(chlorosulfonyl)benzoyl chloride an ideal starting material as was

shown by Yang et al. [18]. By transferring this reaction to a multistep flow set-up, we envisioned an improved chemoselectivity. This phenomenon is not unusual for flow chemistry. Typical batch reactions are mixed by stirring; however, perfect homogeneity is not immediately obtained. Ideal mixing conditions can only be achieved with microreactors or micromixers [22]. The small diameters of these microreactors lead to almost ideal mixing conditions [23-26], resulting in an improved chemoselectivity. Furthermore, the use of an automated process leads to the possibility to produce libraries of compounds in a fast manner. In addition, an alternate biocompatible and water miscible solvent would result in a flexible and automated chemoselective synthesis, delivering stock solutions suitable for initial testing at the outlet of the reactor.

Results and Discussion
Development of a continuous-flow process
Although a continuous-flow process shows many advantages compared to batch reactions, there are some difficulties which should be overcome or be avoided. A general concern is the clogging of the channels. There are numerous reports about handling solids in flow. For example, the use of ultrasound [27-32] can reduce the particle size of the precipitates, and preventing the clogging of the small channels. A second example is the Coflore agitating cell reactor [32]. This type of reactor uses transverse mixing motions which keeps the solids in suspension, and prevents clogging. The Coflore reactor was successfully used for the synthesis of *N*-iodomorpholinium hydroiodide salt [33]. However, it takes specialized machinery and time to develop a system which can pump slurries. Therefore, a reduction in the formation of solids is preferable. Furthermore, we wanted to avoid the use of dichloromethane as solvent and use a biocompatible and water miscible alternative.

A series of initial batch reactions were performed to evaluate the potential of a chemoselective synthesis as a continuous process. As bench mark, aniline and azepane were used as first and second reagent, respectively. After addition of the first reactant and completion of the reaction (followed by TLC) the second reactant was added. The chemoselectivity was determined by LC–MS analysis.

In the initial screening, tetrahydrofuran (THF) was chosen as solvent (c_{final} = 100 mM), however, precipitation of the ammonium salts was unavoidable. The results of this screening did show that the use of catalysts, such as pyridine or dimethylaminopyridine (DMAP), is unnecessary in batch or continuous flow. This is not surprising since a similar result is reported for the reaction of amines with sulfonyl chlorides [34]. Triethylamine was added as base for the capture of hydrogen chloride which is produced during the reaction. Nonetheless, the precipi-

tation of anilinium salts and/or triethylamonium salts could not be avoided in THF, even at lower concentrations (c_{final} = 10 mM). Due to the reactivity of the aroyl and sulfonyl chloride, water, DMF or DMSO cannot be used to dissolve the salts. Therefore, acetonitrile (CH_3CN) was used instead. CH_3CN is a more polar solvent compared to THF, however, the salts which were formed during the reaction still precipitated (c_{final} = 100 mM and 40 mM). At lower concentrations (c_{final} = 10 mM), the precipitation of the formed salts was not observed. Furthermore, the chemoselectivity was increased, being 80% for 10 mM and 73% for 100 mM.

Screening for the optimal chemoselectivity

Since the formation of precipitants can be avoided using CH_3CN at a final compound concentration of 10 mM, the synthesis can be further optimized in continuous flow. To get the optimal selectivity and reaction conditions, different parameters were screened (residence time/flow rate and reactor temperature). The advantage of the serial use of two microreactors is

that two different temperatures can be used. Three solutions were made: F_1 and F_2 having a concentration of 40 mM, and F_3 having a concentration of 20 mM. After addition of the three reaction streams, with the flow rate of F_3 being twice as high as for F_1 and F_2, the final concentration is 10 mM. This corresponds to the end concentration of the selected batch reaction. The results of screening of residence time/flow rate and reactor temperature are presented in Table 1. The optimal conditions and selectivity are obtained for a flow rate of 125 µL/min for starting materials **1** and **2a** and 250 µL/min for reactant **2b**. The temperature for the first microreactor was kept at 20 °C to avoid coupling with the sulfonyl chloride. The second reactor was kept at 40 °C. This increase in temperature enables the coupling with the less reactive sulfonyl chloride, and prevents the use of catalysts.

With this process, an automated and chemoselective continuous synthesis was obtained for *m*-sulfamoylbenzamide analogues. Furthermore, the chemoselectivity was increased signif-

Table 1: Screening results of the different conditions for the best chemoselectivity with aniline and azepane as (F_2) and (F_3), respectively.

Run	Flow rate 1 (µL/min)	Flow rate 2 (µL/min)	T_1 (°C)	Chemoselectivity (%)
1	50	100	0	91
2	75	150	0	80
3	25	50	10	89
4	50	100	10	91
5	75	150	10	93
6	100	200	10	92
7	125	250	10	89
8	75	150	20	92
9	100	200	20	93
10	125	250	20	94
batch	–	–	0	80[a]
batch	–	–	20	75[a]

[a]Reaction performed in batch with a final concentration of 10 mM.

icantly compared to the batch reaction due to the quasi-ideal mixing conditions, and therefore avoiding coupling with the sulfonyl chloride which is less reactive compared to the aroyl chloride [35]. For the reactions in batch, an average chemoselectivity of 80% was obtained while for the synthesis in continuous flow with CH_3CN the average chemoselectivity is 94%. This indicates that these optimized mixing conditions are crucial for an improved chemoselective synthesis. Interestingly, the temperatures used for the first coupling ($T_1 = 20$ °C) are substantially higher compared to the batch reactions (0 °C), while the chemoselectivity is still maintained. This effect is also linked to the optimized mixing conditions enabling higher temperatures without losing chemoselectivity, while increasing the reaction rate. This adds also significantly to an increased sustainability of the process since no cooling capacity is required.

This process can be used for a range of *m*-sulfamoylbenzamide analogues (vide infra). However, if the first reagent (F_2) is a secondary amine, the chemoselectivity decreases substantially when the current process is used. Secondary amines are more nucleophilic as compared to primary amines, resulting in a higher percentage of sulfonylation. To improve the chemoselec-

tivity when using secondary amines, an additional screening was performed with azepane and aniline as first and second reagent, respectively. Initially, we tried to increase the selectivity by decreasing the temperature. Unfortunately, the reaction mixtures obtained showed the presence of several side products, and the decrease in temperature did not appear to result in a substantial increase in chemoselectivity. Therefore, it was decided to first optimize the chemoselectivity for compound **4** (Table 2). This simplified the reaction mixture substantially. The temperature was kept at −15 °C and the final concentration of compound **4** was varied between 20 mM and 5 mM. By decreasing the concentration, the chemoselectivity increased substantially from 45% for 40 mM to 89% for 5 mM.

Using the lower substrate concentration, an optimization of the second reaction step was performed, using azepane as the first and aniline as the second reactant. The concentrations used were 5 mM for F_1 and F_2 and 2.5 mM for F_3. This leads to a final concentration of 1.25 mM. However, due to the increased flow rate, the second coupling step with aniline could not reach full conversion. Even by increasing the temperature for this step up to 75 °C, full conversion was not obtained. Therefore, DMAP was used as a base instead of triethylamine in F_3.

Table 2: Screening results of the different conditions for the best chemoselectivity with azepane as (F_2).
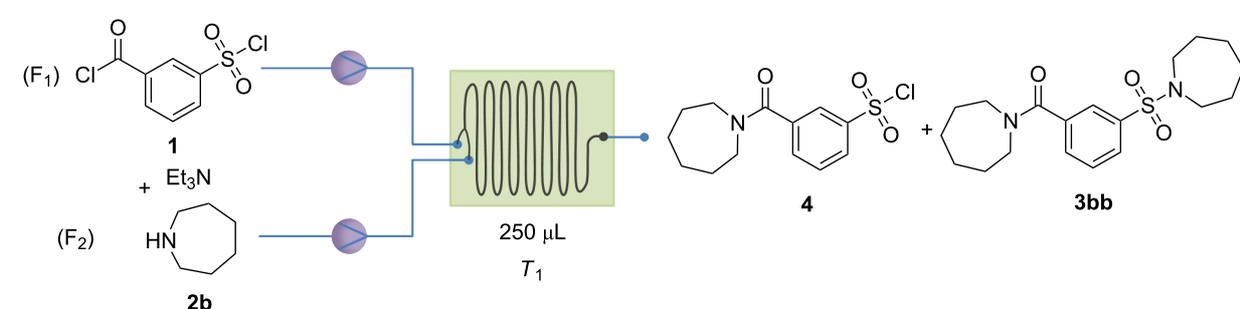
Run	Flow rate (µL/min)	Concentration F_1 and F_2 (mM)	Final concentration (mM)	**4** (%)	**3bb** (%)
1	50	40	20	29	36
2	100	40	20	29	36
3	200	40	20	28	36
4	50	20	10	37	32
5	100	20	10	60	20
6	150	20	10	47	27
7	100	10	5	63	19
8	150	10	5	71	15
9	200	10	5	64	18
10	200	5	2.5	67	17
11	400	5	2.5	74	13
12	600	5	2.5	82	9

DMAP serves both as a base and catalyst for the reaction with the sulfonyl chloride group. The temperature in the second reation chip was kept at 75 °C and by using DMAP as a base, full conversion was obtained. The effect of the temperature and the flow rate were evaluated and the results are shown in Table 3. The highest chemoselectivity (82%) was obtained for a flow rate of 500 µL/min for F_1 and F_2 and 1000 µL/min for F_3 at a temperature of 0 °C and 75 °C in chip 1 and chip 2, respectively. It should be noted that not the reaction temperature, but rather the substrate concentration is the main variable determining chemoselectivity (compare Table 3, entries 2 and 5). The chemoselectivity in flow was again higher compared to the batch conditions due to quasi-ideal mixing conditions.

Medium-throughput synthesis

To evaluate the flexibility of both processes, a range of molecules were synthesized on small scale. In total, 49 molecules could be readily used for a medium-throughput screening for pharmaceutical applications. The chemoselectivity was measured by LC–MS and is presented in Table 4. The chemose-

lectivity varied between 50 and 99%. Apart from the reactions involving 3-fluoroaniline, the chemoselectivity was above 70% for primary amines and above 60% for secondary amines. The side products which are being formed are the double substituted analogues **3aa**, **3bb**, **3cc**, **3dd**, **3ee, 3ff** or **3ee** depending on the amines which were used. As such, we synthesized these compounds (chemoselectivity >99%) so that they can function as a negative control in the direct screening, to exclude false positives. Synergistic effects were not taken into account but, the screening of these analogues should already give a good indication which compounds are of interest.

Medium throughput synthesis if F_2 are primary amines

Between each sample a washing step with CH_3CN was included to eliminate any side reaction of undesired amines in the system. For the washing step, a flow rate of 1000 µL/min was applied for a duration of 4 minutes. This implements a total washing volume of 12 mL, which is 8 times the total volume of the flow system. The equilibration time was 11.5 minutes and

Table 3: Screening results of the different conditions for the best chemoselectivity with azepane and aniline as (F_2) and (F_3), respectively.
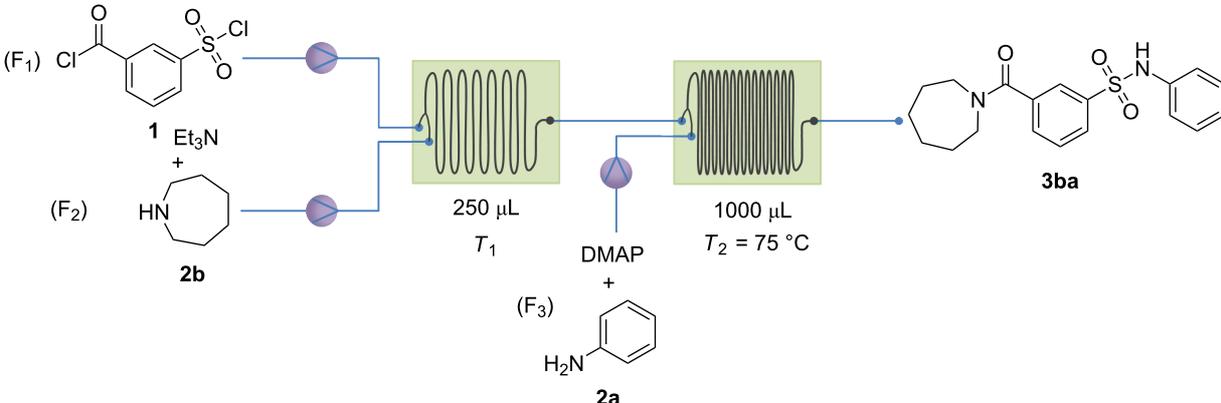
Run	Flow rate 1 (µL/min)	Flow rate 2 (µL/min)	T_1 (°C)	Chemoselectivity (%)
1	300	600	−15	39
2	400	800	−15	79
3	500	1000	−15	57
4	300	600	0	53
5	400	800	0	80
6	500	1000	0	82
7	600	1200	0	52
8	200	400	10	41
9	300	600	10	50
10	400	800	10	40
batch	–	–	0	59[a]

[a]Reaction performed in batch with a final concentration of 1.25 M.

the collecting time 1.5 minutes resulting in a reaction time of 13 minutes. The volume collected for each sample was 750 µL, and a total reaction time, including the washing step, of 17 minutes is required. On a 24 h basis, a total of 84 compounds can be synthesized in continuous flow, and used for a medium-throughput screening with primary amines as first reactant. The final concentration of each sample was 10 mM and can be diluted with a factor 100 resulting in a concentration of 100 µM. In each sample, only 1% (v/v) of CH_3CN would be present.

Medium throughput synthesis if F_2 are secondary amines

If the first reagent is a secondary amine, the washing step remains the same and the volume collected was 1000 µL. The equilibration time was 5 minutes and the collecting time together with the equilibration time was 5 minutes and 20 seconds. The total reaction time, including the washing step,

was approximately 10 minutes. This leads to 144 compounds on a daily basis. The final concentration of each sample was 1.25 mM and can be diluted with a factor 12.5 resulting in a concentration of 100 µM. In each sample 8% (v/v) of CH_3CN would be present. The next step is to produce these compounds on a larger scale. From Table 4, 15 analogues were chosen and produced on a larger scale (vide infra).

Synthesis of a small library in continuous flow

The use of flow chemistry facilitated greatly the synthesis of an extended library of compounds. Different *m*-sulfamoylbenz-amide analogues were synthesized in continuous flow. From Table 4, 15 analogues were produced on a larger scale to exemplify the direct scalability of the developed protocol. For these reactions the required amount of product was aimed at 100–200 mg which took about 3 hours of production. Compound **3cb**, which corresponds with **AK-7**, was also produced on gram scale which took approximately 24 hours. Table 5

Table 4: Chemoselectivity (%) of the medium-throughput synthesis in continuous flow.

(F3) → (F2)	2a	2b	2c	2d	2e	2f	2g
2a	99 **3aa**	94 **3ab**	95 **3ac**	64 **3ad**	95 **3ae**	83 **3af**	94 **3ag**
2b	82 **3ba**	99 **3bb**	83 **3bc**	77 **3bd**	76 **3be**	70 **3bf**	74 **3bg**
2c	83 **3ca**	94 **3cb**	99 **3cc**	64 **3cd**	94 **3ce**	84 **3cf**	97 **3cg**
2d	64 **3da**	59 **3db**	53 **3dc**	99 **3dd**	58 **3de**	68 **3df**	85 **3dg**
2e	93 **3ea**	94 **3eb**	94 **3ec**	63 **3ed**	99 **3ee**	86 **3ef**	94 **3eg**
2f	77 **3fa**	73 **3fb**	71 **3fc**	50 **3df**	77 **3fe**	99 **3ff**	72 **3fg**
2g	68 **3ga**	69 **3gb**	83 **3gc**	63 **3gd**	60 **3ge**	61 **3gf**	99 **3gg**
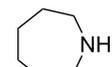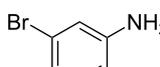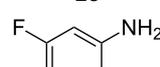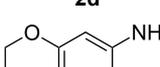
Table 5: Library of 15 *m*-sulfamoylbenzamide analogues synthesized in continuous flow.
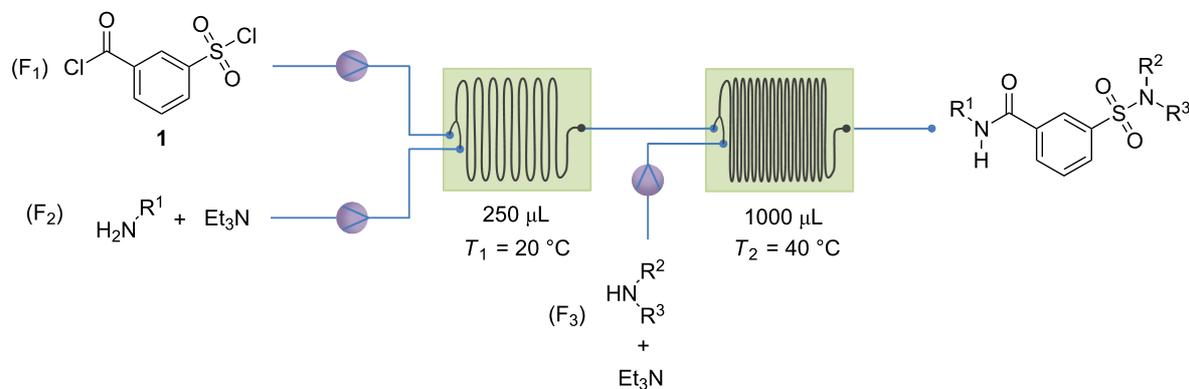
Compound	(F₂)	(F₃)	Chemoselectivity (%)	Yield (%)	Quantity (mg)
3aa			–	95	140
3ab			94	75	197
3ac			95	78	94
3ae			95	76	92
3ag			94	74	88
3ca			83	70	83
3cb			94 / 87[a]	78 / 80	93 / 2447
3cc			–	99	97
3ce			94	81	77
3cg			97	77	96
3ea			93	80	96
3eb			94	78	94

Table 5: Library of 15 *m*-sulfamoylbenzamide analogues synthesized in continuous flow. (continued)
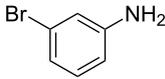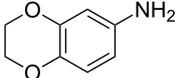
3ec	Br—⟨phenyl⟩—NH₂	94	72	87
3ee	⟨benzodioxane⟩—NH₂	–	98	117
3eg	⟨piperidine⟩NH	94	77	93

ᵃReduced chemoselectivity due to leakage during the reaction.

shows 15 analogues synthesized in continuous flow. The chemoselectivity varied between 83 and 97%, the remaining 17–3% were symmetrical *m*-sulfamoylbenzamides. After work-up and purification the yield was between 70 and 99%. These results indicate that both processes are applicable to a large variety of *m*-sulfamoylbenzamides.

Conclusion

A chemoselective, automated process is developed for the synthesis of *m*-sulfamoylbenzamide analogues. The used solvent is acetonitrile and the reactions in continuous flow showed an increased chemoselectivity compared to the batch reactions due to the ideal mixing conditions. Using secondary amines, a decrease in substrate concentration was essential to selectively obtain amides over sulfonamides. It was shown that the procedure can easily be used for the synthesis of a compound library suitable for initial screening; and that the optimized synthetic conditions are directly transferrable should the resulting hits be needed in gram-scale for further evaluation.

Experimental
General

All chemicals were purchased by either Sigma-Aldrich or TCI chemicals. Commercially available products were used without additional purification. NMR spectra were recorded at 400 MHz (^{1}H) and 100 MHz (^{13}C) in CDCl$_3$ with tetramethylsilane as internal standard or DMSO-d_6 on a Bruker Avance III Nanobay 400 MHz spectrometer at room temperature. The automated continuous synthesis was conducted using a commercially available continuous-flow system (syrris AFRICA, Figure 2).

Representative procedure for *m*-sulfamoyl-benzamide analogues

a) Continuous process with primary amines as F$_1$: Triethyl-amine and a primary amine (F$_1$) were dissolved in acetonitrile (c = 40 mM), *m*-chlorosulfonylbenzoyl chloride (F$_2$) was dissolved in the same solvent in a separate volumetric flask (c = 40 mM). A third solution was prepared with triethylamine and the second reactant (F$_3$) (c = 20 mM). The flow process is

Figure 2: Syrris AFRICA system.

presented in Table 1; reactants **1** and **2x** were mixed together in reactor 1 at 20 °C at a flow rate of 125 μL/min. The reaction mixture was then pumped to reactor 2, which was kept at 40 °C. The third reactant (**2y**) was then added at a flow rate of 250 μL/min. The residence times were 1 min and 2 min, respectively. Once the mixture passed both reactors, the final compound concentration was 10 mM and could be used as a stock solution for initial screening. For the larger scale experiments, the work-up procedure was similar to a batch reaction. The solvent was removed in vacuo and the remaining oil was dissolved in diethyl ether. It was subsequently washed with a hydrogen chloride solution of 1 M and with a saturated sodium bicarbonate solution. The organic phase was dried with $MgSO_4$, the solvent was evaporated in vacuo, and the residue was purified by either preparative thin-layer chromatography or by recrystallization.

b) Continuous process with secondary amines as F_1: Triethylamine and a secundary amine (F_1) were dissolved in acetonitrile (c = 5 mM), *m*-chlorosulfonylbenzoyl chloride (F_2) was dissolved in acetonitrile in a second volumetric flask (c = 5 mM). A third solution was prepared with dimethylaminopyridine (DMAP) and the second reactant (F_3) (c = 2.5 mM). The flow process is presented in Table 3; reactants **1** and **2x** were mixed together in reactor 1 at 0 °C at a flow rate of 500 μL/min. The reaction mixture was then pumped to reactor 2, which was kept at 75 °C. The third reactant (**2y**) was then added at a flow rate of 1000 μL/min. The residence times were 0.25 min and 0.5 min, respectively. Once the mixture passed both reactors, the final compound concentration was 1.25 mM and could be used as a stock solution for screening.

Supporting Information

Supporting Information File 1
Experimental part.
[http://www.beilstein-journals.org/bjoc/content/
supplementary/1860-5397-13-33-S1.pdf]

References

1. Gutmann, B.; Cantillo, D.; Kappe, C. O. *Angew. Chem., Int. Ed.* **2015,** *54,* 6688–6728. doi:10.1002/anie.201409318
2. Macarron, R.; Banks, M. N.; Bojanic, D.; Burns, D. J.; Cirovic, D. A.; Garyantes, T.; Green, D. V. S.; Hertzberg, R. P.; Janzen, W. P.; Paslay, J. W.; Schopfer, U.; Sittampalam, G. S. *Nat. Rev. Drug Discovery* **2011,** *10,* 188–195. doi:10.1038/nrd3368
3. Jiménez-González, C.; Poechlauer, P.; Broxterman, Q. B.; Yang, B.-S.; am Ende, D.; Baird, J.; Bertsch, C.; Hannah, R. E.; Dell'Orco, P.; Noorman, H.; Yee, S.; Reintjens, R.; Wells, A.; Massonneau, V.; Manley, J. *Org. Process Res. Dev.* **2011,** *15,* 900–911. doi:10.1021/op100327d
4. Thayer, A. M. *Chem. Eng. News* **2014,** *92,* 13–21.
5. Poechlauer, P.; Manley, J.; Broxterman, R.; Gregertsen, B.; Ridemark, M. *Org. Process Res. Dev.* **2012,** *16,* 1586–1590. doi:10.1021/op300159y
6. Baxendale, I. R.; Braatz, R. D.; Hodnett, B. K.; Jensen, K. F.; Johnson, M. D.; Sharratt, P.; Sherlock, J.-P.; Florence, A. J. *J. Pharm. Sci.* **2015,** *104,* 781–791. doi:10.1002/jps.24252
7. Rodrigues, T.; Schneider, P.; Schneider, G. *Angew. Chem.* **2014,** *126,* 5858–5866. doi:10.1002/ange.201400988
8. Malet-Sanz, L.; Susanne, F. *J. Med. Chem.* **2012,** *55,* 4062–4098. doi:10.1021/jm2006029
9. Poechlauer, P.; Colberg, J.; Fisher, E.; Jansen, M.; Johnson, M. D.; Koenig, S. G.; Lawler, M.; Laporte, T.; Manley, J.; Martin, B.; O'Kearney-McMullan, A. *Org. Process Res. Dev.* **2013,** *17,* 1472–1478. doi:10.1021/op400245s
10. Baumann, M.; Baxendale, I. R. *Beilstein J. Org. Chem.* **2015,** *11,* 1194–1219. doi:10.3762/bjoc.11.134
11. Porta, R.; Benaglia, M.; Puglisi, A. *Org. Process Res. Dev.* **2016,** *20,* 2–25. doi:10.1021/acs.oprd.5b00325
12. Taylor, D. M.; Balabadra, U.; Xiang, Z.; Woodman, B.; Meade, S.; Amore, A.; Maxwell, M. M.; Reeves, S.; Bates, G. P.; Luthi-Carter, R.; Lowden, P. A. S.; Kazantsev, A. G. *ACS Chem. Biol.* **2011,** *6,* 540–546. doi:10.1021/cb100376q
13. Chopra, V.; Quinti, L.; Kim, J.; Vollor, L.; Narayanan, K. L.; Edgerly, C.; Cipicchio, P. M.; Lauver, M. A.; Choi, S. H.; Silverman, R. B.; Ferrante, R. J.; Hersch, S.; Kazantsev, A. G. *Cell Rep.* **2012,** *2,* 1492–1497. doi:10.1016/j.celrep.2012.11.001
14. Zhang, X.; Smith, D. L.; Meriin, A. B.; Engemann, S.; Russel, D. E.; Roark, M.; Washington, S. L.; Maxwell, M. M.; Marsh, J. L.; Thompson, L. M.; Wanker, E. E.; Young, A. B.; Housman, D. E.; Bates, G. P.; Sherman, M. Y.; Kazantsev, A. G. *Proc. Natl. Acad. Sci. U. S. A.* **2005,** *102,* 892–897. doi:10.1073/pnas.0408936102
15. Khanfar, M. A.; Quinti, L.; Wang, H.; Choi, S. H.; Kazantsev, A. G.; Silverman, R. B. *Eur. J. Med. Chem.* **2014,** *76,* 414–426. doi:10.1016/j.ejmech.2014.02.003
16. Dolle, R.; Worm, K.; Zhou, Q. Sulfamoyl benzamide derivatives and methods of their use. U.S. Patent US20060079557 A1, April 13, 2006.
17. Choi, S. H.; Quinti, L.; Kazantsev, A. G.; Silverman, R. B. *Bioorg. Med. Chem. Lett.* **2012,** *22,* 2789–2793. doi:10.1016/j.bmcl.2012.02.089
18. Yang, Y.-L.; Rajagopal, B.; Liang, C.-F.; Chen, C.-C.; Lai, H.-P.; Chou, C.-H.; Lee, Y.-P.; Yang, Y.-L.; Zeng, J.-W.; Ou, C.-L.; Lin, P.-C. *Tetrahedron* **2013,** *69,* 2640–2646. doi:10.1016/j.tet.2013.01.028
19. Seghers, S.; Van Waes, F. E. A.; Cukalovic, A.; Monbaliu, J.-C. M.; De Visscher, J.; Thybaut, J. W.; Heugebaert, T. S. A.; Stevens, C. V. *J. Flow Chem.* **2015,** *5,* 220–227. doi:10.1556/1846.2015.00029
20. Baxendale, I. R.; Griffiths-Jones, C. M.; Ley, S. V.; Tranmer, G. K. *Synlett* **2006,** 427–430. doi:10.1055/s-2006-926244
21. Movsisyan, M.; Heugebaert, T. S. A.; Dams, R.; Stevens, C. V. *ChemSusChem* **2016,** *9,* 1945–1952. doi:10.1002/cssc.201600348
22. Yoshida, J.-i.; Takahashi, Y.; Nagaki, A. *Chem. Commun.* **2013,** *49,* 9896–9904. doi:10.1039/C3CC44709J
23. Darvas, F.; Hessel, V.; Dorman, G. *Flow chemistry;* De Gruyter: Berlin, 2014.
24. Reschetilowski, W., Ed. *Microreactors in Preparative Chemistry;* Wiley-VCH: Weinheim, 2013. doi:10.1002/9783527652891
25. Wirth, T., Ed. *Microreactors in Organic Synthesis and Catalysis,* 2nd ed.; Wiley-VCH: Weinheim, 2013. doi:10.1002/9783527659722

26. Hessel, V.; Schouten, J. C.; Renken, A.; Wang, Y.; Yoshida, J.-i. *Handbook of Micro Reactors;* Wiley-VCH: Weinheim, 2009.

27. Sedelmeier, J.; Ley, S. V.; Baxendale, I. R.; Baumann, M. *Org. Lett.* **2010,** *12,* 3618–3621. doi:10.1021/ol101345z

28. Cantillo, D.; Damm, M.; Dallinger, D.; Bauser, M.; Berger, M.; Kappe, C. O. *Org. Process Res. Dev.* **2014,** *18,* 1360–1366. doi:10.1021/op5001435

29. DeAngelis, A.; Wang, D.-H.; Buchwald, S. L. *Angew. Chem., Int. Ed.* **2013,** *52,* 3434–3437. doi:10.1002/anie.201208544

30. Hartman, R. L.; Naber, J. R.; Zaborenko, N.; Buchwald, S. L.; Jensen, K. F. *Org. Process Res. Dev.* **2010,** *14,* 1347–1357. doi:10.1021/op100154d

31. Noël, T.; Naber, J. R.; Hartman, R. L.; McMullen, J. P.; Jensen, K. F.; Buchwald, S. L. *Chem. Sci.* **2011,** *2,* 287–290. doi:10.1039/C0SC00524J

32. Hartman, R. L. *Org. Process Res. Dev.* **2012,** *16,* 870–887. doi:10.1021/op200348t

33. Browne, D. L.; Deadman, B. J.; Ashe, R.; Baxendale, I. R.; Ley, S. V. *Org. Process Res. Dev.* **2011,** *15,* 693–697. doi:10.1021/op2000223

34. Niu, B.; Xie, P.; Zhao, W.; Zhou, Y.; Bian, Z.; Pittman, C. U., Jr.; Zhou, A. *RSC Adv.* **2014,** *4,* 43525–43528. doi:10.1039/C4RA06810F

35. Barr, C. R.; Salminen, I. F.; Weissberger, A. *J. Am. Chem. Soc.* **1951,** *73,* 4131–4133. doi:10.1021/ja01153a023

Continuous *N*-alkylation reactions of amino alcohols using γ-Al$_2$O$_3$ and supercritical CO$_2$: unexpected formation of cyclic ureas and urethanes by reaction with CO$_2$

Emilia S. Streng[1], Darren S. Lee[1], Michael W. George[*1,2] and Martyn Poliakoff[*1]

Address:
[1]School of Chemistry, University of Nottingham, University Park, Nottingham, NG7 2RD, UK and [2]Department of Chemical and Environmental Engineering, University of Nottingham Ningbo China, 199 Taikang East Road, Ningbo 315100, China

Email:
Michael W. George[*] - mike.george@nottingham.ac.uk;
Martyn Poliakoff[*] - martyn.poliakoff@nottingham.ac.uk

* Corresponding author

Keywords:
continuous flow; heterocycle; *N*-alkylation; self-optimisation; supercritical CO$_2$

Abstract

The use of γ-Al$_2$O$_3$ as a heterogeneous catalyst in scCO$_2$ has been successfully applied to the amination of alcohols for the synthesis of *N*-alkylated heterocycles. The optimal reaction conditions (temperature and substrate flow rate) were determined using an automated self-optimising reactor, resulting in moderate to high yields of the target products. Carrying out the reaction in scCO$_2$ was shown to be beneficial, as higher yields were obtained in the presence of CO$_2$ than in its absence. A surprising discovery is that, in addition to cyclic amines, cyclic ureas and urethanes could be synthesised by incorporation of CO$_2$ from the supercritical solvent into the product.

Introduction

N-alkylated amines are an important motif present in a range of pharmaceutically and industrially useful chemicals; the alkylation of amines is a commonly used reaction in process R&D toward the synthesis of drug candidates [1-3]. Traditional methods to produce such compounds frequently employ toxic alkylating agents or harsh reagents that can generate stoichiometric quantities of waste, e.g., boron salts from reductive amination [4]. Hydrogenation offers a greener approach but is often only applicable to simple substrates due to chemoselectiv-

ity issues. An approach that has received much attention recently is the concept of hydrogen borrowing catalysis [5-19]. The coupling of alcohols and amines is made possible by the catalysts ability to take two H atoms from the alcohol, oxidising it to an aldehyde. The aldehyde then reacts with the amine affording an imine, which is subsequently reduced by transferring two H atoms back from the catalyst. In this case the only byproduct is water. Another approach to *N*-alkylation in which water is the only byproduct is the direct substitution of alcohols

with amines. It is an attractive method; however, it requires significant activation of the alcohol or amine to proceed efficiently, and often a heterogeneous catalyst at elevated temperature and/or pressure is employed [20-28]. As these reactions are mostly carried out in high pressure systems, they are particularly suitable for the use of supercritical solvents. Supercritical solvents are highly compressed and/or heated gases that are beyond the critical point (e.g., the critical point for CO_2 is 31.1 °C and 73.9 bar); in this phase the gas exhibits unique properties and behaves both like a liquid and gas. Using inert supercritical gases as reaction solvents is a greener alternative to using conventional flammable or toxic solvents; furthermore post-reaction separation is simplified as the gas/liquid phases separate upon cooling. The use of supercritical methanol (scMeOH) for *N*-alkylation reactions has been reported before [29,30].

Our own investigations with heterogeneous catalysis in supercritical carbon dioxide (scCO$_2$) have mainly been focused on continuous flow systems and the etherification of alcohols, where alcohols are activated by heterogeneous catalysts [31-38]. We have usually employed γ-alumina as the catalyst, as this is a simple, readily available and environmentally benign catalyst that is often overlooked and it is used merely as a support for other catalysts [39-43]. The use of γ-alumina for the methylation of aniline with dimethyl carbonate has been reported [44]. In this paper, we chose to study the intramolecular and intermolecular alkylation of amino alcohols using γ-Al_2O_3 with scCO$_2$ as the solvent and employed self-optimisation [45,46] to explore the defined parameter space to effectively identify the highest yielding and optimal conditions in a relatively short timeframe.

Results and Discussion

To investigate our hypothesis that γ-Al_2O_3 with scCO$_2$ could be successfully applied to the amination of alcohols, we chose to employ a self-optimising reactor (Figure 1, see Supporting Information File 1 for details) to streamline the optimisation process using 5-amino-1-pentanol (**1**) as the model substrate and methanol as the alkylating agent (Scheme 1). For this reaction, self-optimisation is important as multiple products were identified that could form in parallel; from **1** the possible prod-

ucts we expected to see were a mixture of piperidine (**2a**), *N*-methylpiperidine (**2b**), *N*- and *O*-methylated **1**, as well as oligomers. We chose to target **2b** only for self-optimisation.
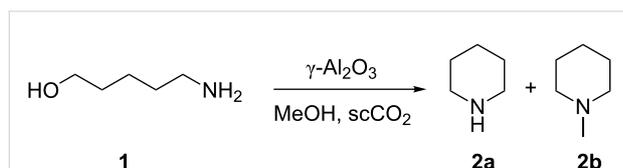
We targeted *N*-methylpiperidine (**2b**) using the self-optimisation approach with SNOBFIT as the optimising algorithm [47] and GC analysis as the analytical tool providing the responses for the self-optimisation. This methodology allows high yielding conditions to be found, minimising the formation of byproducts. The temperature and the flow rate of the reaction were optimised in both the presence and absence of scCO$_2$ (Figure 1).

Figure 1: Simplified schematic demonstrating a self-optimising reactor [34,35,37,44]. The reagents are pumped into the system where they are mixed and then flowed through a reactor filled with catalyst. The output of the reactor is analysed by an on-line GC. The response (e.g., yield) of this analysis is then sent to an optimising search algorithm (e.g., SNOBFIT), which then changes the conditions (e.g., flow rates and temperature) in order to maximise the response of the analysis.

The results of the optimisations are shown in Figure 2, and the conditions with the highest yields of **2b** are shown in Table 1. During these experiments the parameter space was extensively studied and high yields were achieved at several different conditions. This provides confidence that our optimal yield was the global optimum within the studied limits of the reaction. It can be seen from Figure 2 that, when the reaction was carried out in scCO$_2$, high yields (up to 96%) for **2b** were achieved (Figure 2a, Table 1, entries 1–3). In the absence of scCO$_2$ the percentage yield was good but the highest yields were ca. 8–11% less (Figure 2b, Table 1, entries 4–6) compared to when scCO$_2$ was present. Clearly scCO$_2$ is beneficial as a solvent in the formation of **2b**.

The optimal region for synthesising **2b** turned out to be quite broad, as high yields were obtained at a variety of conditions. At lower flow rates (0.1 mL min^{-1}) and hence longer residence times, yields of 94% were observed at 310 °C (Table 1, entry 2). Increasing the temperature by 30 °C led to an increase in the

Scheme 1: Target reaction – intramolecular cyclisation of **1** followed by *N*-methylation with methanol to yield **2b**.

Figure 2: Result of the SNOBFIT optimisation for *N*-methylpiperidine (**2b**) with and without CO_2 showing yields ≥70%. Figure a (left) shows the yields for the experiment carried out in scCO_2 at different temperatures and flow rates; Figure b (right) shows the results without CO_2. Conditions: Temperature 250–350 °C, substrate flow (0.5 M solution in MeOH) 0.1–0.5 mL min^{-1}, 100 bar, when applicable 0.5 mL min^{-1} CO_2.

Table 1: The highest yields of **2b** found by the optimisations carried out with CO_2 (entries 1–3) and without CO_2 (entries 4–6).[a]

Entry	T (°C)	Flow rate (mL min^{-1})	Yield **2b** (%)[b]
1[c]	340	0.3	94
2[c]	310	0.1	94
3[c]	330	0.15	96
4[d]	350	0.4	86
5[d]	350	0.3	85
6[d]	350	0.5	83

[a]0.5 M solution of **1** in MeOH, 100 bar system pressure. [b]Yields based on GC analysis. [c]With 0.5 mL min^{-1} CO_2. [d]No CO_2 used.

rate of cyclisation and methylation which then allowed for faster flow rates to be used under this operating temperature whilst still maintaining the same yield of **2b** (Table 1, entry 1). Hence, three times the amount of material could be processed in the same time using this elevated temperature, i.e., higher productivity.

After optimisation with the model substrate **1** in methanol, the application of these reaction conditions to a small range of different alcohols was studied. Initially we repeated the model reaction to demonstrate that the approach is repeatable and that the conditions found during the optimisation were indeed the optimum (N.B. We chose the conditions that afforded the highest yield). Pleasingly, full conversion of **1** was obtained and an identical yield of **2b** was observed (Table 2, entry 1). After showing that the conditions were repeatable, we applied them to

several different alcohols by flowing a starting mixture of **1** with the alcohol as the solvent (Table 2, entries 2–4). As might be expected, the cyclisation to *N*-alkylated piperidines was observed for the primary alcohols. The yield of the corresponding *N*-alkylated piperidine falls as the longer chain alcohols are reacted. When the secondary alcohol isopropanol was used as the solvent, no *N*-alkylation was observed and piperidine **2a** was found as the major product. As this catalyst system has been used previously for the etherification of alcohols [31-38], it is possible that ethers of the alcohols could be formed. In the case of **2d,** dibutyl ether was the major byproduct, but in most other cases only small amounts of the corresponding ethers were observed. When the reaction with isopropanol was

Table 2: Cyclisation and *N*-alkylation of **1** with different alcohols.[a]

Entry	R =	Yield (%)[b,c]
1	Me **2b**	94%
2	Et **2c**	82%
3	*n*-Bu **2d**	73%
4	iPr **2e**	0% (**2a** 80%)

[a]Conditions: **1** (0.5 M in ROH), 340 °C, substrate flow: 0.3 mL min^{-1}, CO_2 flow: 0.5 mL min^{-1}, 100 bar.; [b]Determined by GC analysis of the reaction mixture. [c]The remaining materials are unidentified side products.

repeated without scCO$_2$ the same selectivity was observed. However, when primary alcohols were run in the absence of scCO$_2$ the yields of the corresponding *N*-alkylated products were lower and more piperidine **2a** was observed. These results suggest that the rate of intermolecular alkylation is faster in scCO$_2$, while the rate of intramolecular cyclisation is not significantly affected by the presence of scCO$_2$ and thus proceeds faster than the intermolecular reaction.

We also explored the cyclisation and *N*-alkylation of different amino alcohol substrates. Initially we investigated the effect of simply changing the alkane chain length. Starting with 4-amino-1-butanol (**3**) under the model conditions afforded the desired *N*-methylpyrrolidine (**4**) in 95% yield. Extending the alkyl chain using 6-amino-1-hexanol (**5**), however, favoured methylation over intramolecular cyclisation as only 20% of the cyclised product **6** was observed. The major product was 6-(dimethylamino)-1-methoxyhexane (**7**, Scheme 2), which was formed by both *O*- and *N*-methylation of the starting material. Self-optimisation of the reaction of this substrate was performed in order to try and locate the optimal conditions for the highest yield of **6**. Within the parameters explored, it was found that higher reac-

tion temperatures increased the selectivity and yield of **6** up to 55%. This relatively modest yield could not be optimised further.

Ethanolamine **8** was used to explore the potential competition between the intra- and intermolecular etherification and amination. In this case we observed no azridine or *N*-methylaziridine, which would be expected from the intramolecular closure of **8**, consistent with the results observed with bromoalkylamines [48], and suggesting the rate of closure for three-membered rings is slower than that of five- and six-membered rings. We cannot rule out the formation of aziridine as an intermediate in the formation of the dimeric products that were observed. The reaction with ethanolamine yielded three products (Table 3), *N*-methylmorpholine (**9**), 1,4-dimethylpiperazine (**10**) and the fully *N*- and *O*-methylated ethanolamine **11**. Under the standard conditions, **11** was the major product, and as the temperature was increased, the amount of **10** increased. When the parameter space was explored using the self-optimisation approach the selectivity to **10** was increased to 63%. The etherification/deamination pathway forming **9** could not be optimised above 11% as the dehydration or methylated products were
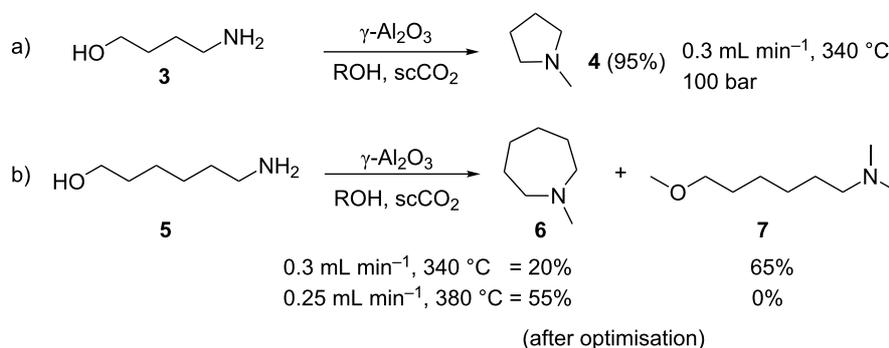
Scheme 2: Cyclisation and *N*-alkylation of 1,4- and 1,6-amino alcohols.

Table 3: Reactions of ethanolamine.[a]
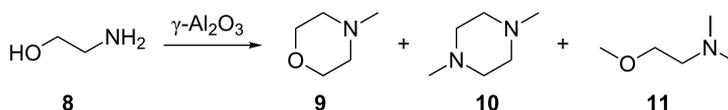
Entry	Flow rate (mL min^{-1})	Temperature (°C)	Conversion (%)	Selectivity (%)[b]		
				9	**10**	**11**
1[a]	0.3	340	100	<1	13	72
2[c]	0.1	370	100	11	48	0
3[c,d]	0.1	360	100	5	63	3

[a]Conditions: **8** 0.5 M (or 1.0 M) solution in MeOH, 0.5 mL min^{-1} CO$_2$, 100 bar; [b]Based on GC analysis of the reaction mixture, remaining material is a mixture of unidentified side products; [c]Substrate 1.0 M solution in MeOH; [d]After self-optimisation had been run targeting high yield of **10**.

present as the major products in all cases. These results prompted us to explore the use of more functionalised amino alcohols in an attempt to access these heterocycles more cleanly and to allow us to further examine the deamination reactivity that produces **9**.

Diethanolamine **12** is expected to produce a cleaner cyclisation pathway to *N*-methylmorpholine (**9**) via intramolecular etherification. When diethanolamine **12** in methanol was reacted using the standard conditions (Table 1, entry 1), *N*-methylmorpholine (**9**) was obtained but only in 24% yield; however, when the conditions were changed in an attempt to optimise the yield, it became apparent that the reactivity of **12** was more complicated. Running the reaction at 380 °C and 0.3 mL min^{-1} resulted in 46% of **9** being obtained but, at lower temperatures, different products were obtained. For example, when the reaction was run at 250 °C (Table 4, entry 1), oxazolidinone **13** was observed as the major product (52%) together with **14**, a dimer of the starting material **12** as the main byproduct (42%).

Formation of **13** involves incorporation of the CO_2 solvent into the product. Despite the very large number of reactions studied in $scCO_2$, there are relatively few examples of incorporation of CO_2 into the product. In this case, incorporation presumably occurs via the formation of a carbamate intermediate. This surprising formation of **13** suggests the incorporation of CO_2 into **12** with the dimer formation as a competing reaction. In fact, when further conditions were studied, it became apparent that the dimer **14** could be formed from oxazolidinone **13** as increasing the residence time led to an increase in selectivity of **14**

over **13** (Table 4, entry 2). Indeed, when **13** was used as the starting material, the major product that was isolated was **14**; and this reactivity of **13** has been reported previously in batch reactions [49]. Increasing the residence time further (Table 4, entry 3) resulted in the oxazolidinone **13** not being detected and **14** was the major product together with a small quantity of mono *O*-ethylated **14**. Reducing the temperature gave a better selectivity to the oxazolidinone **13** (Table 4, entry 4) and lowering the concentration, increased the conversion but gave a poor selectivity (Table 4, entry 5). Increasing the pressure to 150 bar had a positive effect on the selectivity toward **13** (Table 4, entry 6) and increasing the concentration of **12** to 1 M gave the highest selectivity for **13** (Table 4, entry 7). Further increasing the temperature to 275 °C only served to increase the selectivity towards **14** (Table 4, entry 8). From these conditions, it appears that the incorporation of CO_2 is fast but the rate of conversion to **14** is dependent on the pressure of the system, the temperature of the reactor, the residence time and to some extent the concentration of the amino alcohol in the alcohol. A higher pressure of CO_2 appears to slow the rate of conversion of **13** to **14**, whilst elevated temperatures appear to accelerate the rate. Increasing the residence time allows more time for **13** to be converted into **14** and hence the higher selectivity for it and the appearance of trace amounts of mono- and bis-ethylated **14**.

We have studied the incorporation of CO_2 further by investigating the reaction of *N*-(2-aminoethyl)ethanolamine **15**. The use of **15** as a starting material might be expected to produce high selectivity for the corresponding imidazolidinone **16** via the incorporation of CO_2. The competing oxazolidinone formation

Table 4: Showing the effect of conditions on the reaction of diethanolamine **12** to form carbamate **13** and piperazine **14**.[a]
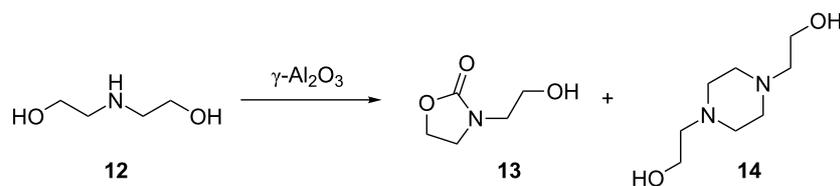
Entry	Conc. (M)	T (°C)	P (bar)	Flow rate (mL min^{-1})	Conv. (%)[b]	Selectivity (%)[b]	
						13	**14**
1	0.5	250	100	0.3	53	52	42
2	0.5	250	100	0.2	98	20	65
3	0.5	250	100	0.1	100	0	61[c]
4	0.5	240	100	0.3	48	69	26
5	0.2	250	100	0.3	80	42	38
6	0.2	250	150	0.3	73	65	19
7	1.0	250	150	0.2	56	73	22
8	1.0	275	100	0.2	100	8	63[d]

[a]**12** in ethanol, 0.5 mL min^{-1} CO_2. [b]Based on GC analysis of the reaction mixture. [c]12% of mono-*O*-ethylated **14**. [d]Trace of mono- and bis-ethylated **14**.

should be limited as the nucleophilicity of nitrogen is more than that of the oxygen. Furthermore, the formation of dimers were expected to be supressed as **16** does not contain a "CO_2 unit" that can serve as a leaving group. This was indeed the case as, at 250 °C, 85% selectivity, 70% yield for **16** was observed when the reaction was run in $scCO_2$ (Scheme 3a). In the absence of CO_2 as a solvent the formation of imidazolidinone **16** was not observed. When the starting solution was pre-saturated with CO_2 and run in the absence of CO_2 as a solvent, **16** was formed in 62% selectivity, 15% yield from 24% conversion of the starting material. This poor conversion suggests that CO_2 is needed in an excess for the reaction to be successful, and the use of CO_2 as the solvent as well as a reagent in this case provides the highest possible concentration of CO_2. To establish whether any dimers are formed when **16** is exposed to the catalyst bed for an extended time or to higher reaction temperatures, a solution of **16** in iPrOH (0.5 M) was flowed at 250 and 275 °C, but no dimers were detected and unreacted **16** was the main product observed. The reaction of **15** with CO_2 could be supressed using higher temperatures, for example at 380 °C in methanol the intramolecular cyclisation is favoured and *N,N'*-dimethylpiperazine (**10**) is obtained as the major product in 68% yield (Scheme 3b, 380 °C at 1 mL min^{-1}), and no imidazolidinone **16** was detected.

Scheme 3: a) Reactions highlighting the incorporation of CO_2 in to **16**. b) High temperature reaction of **15** yielding *N,N'*-dimethylpiperazine (**10**).
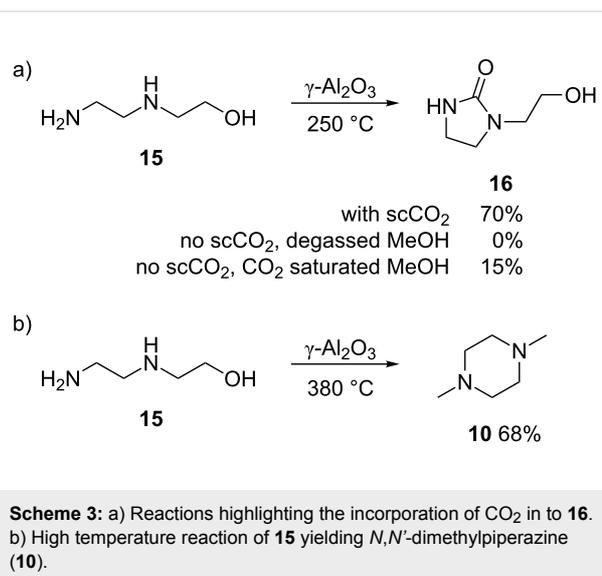
Conclusion

Using a self-optimising reactor and a simple heterogeneous catalyst, γ-Al_2O_3, moderate to high yields of several alkylated cyclic amines, formed in a two-step intramolecular cyclisation/ *N*-alkyation reaction, using amino alcohols and simple alcohols has been achieved (Scheme 4).

Scheme 4: Summary of products obtained from the reactions of amino alcohols over γ-Al_2O_3 in $scCO_2$.
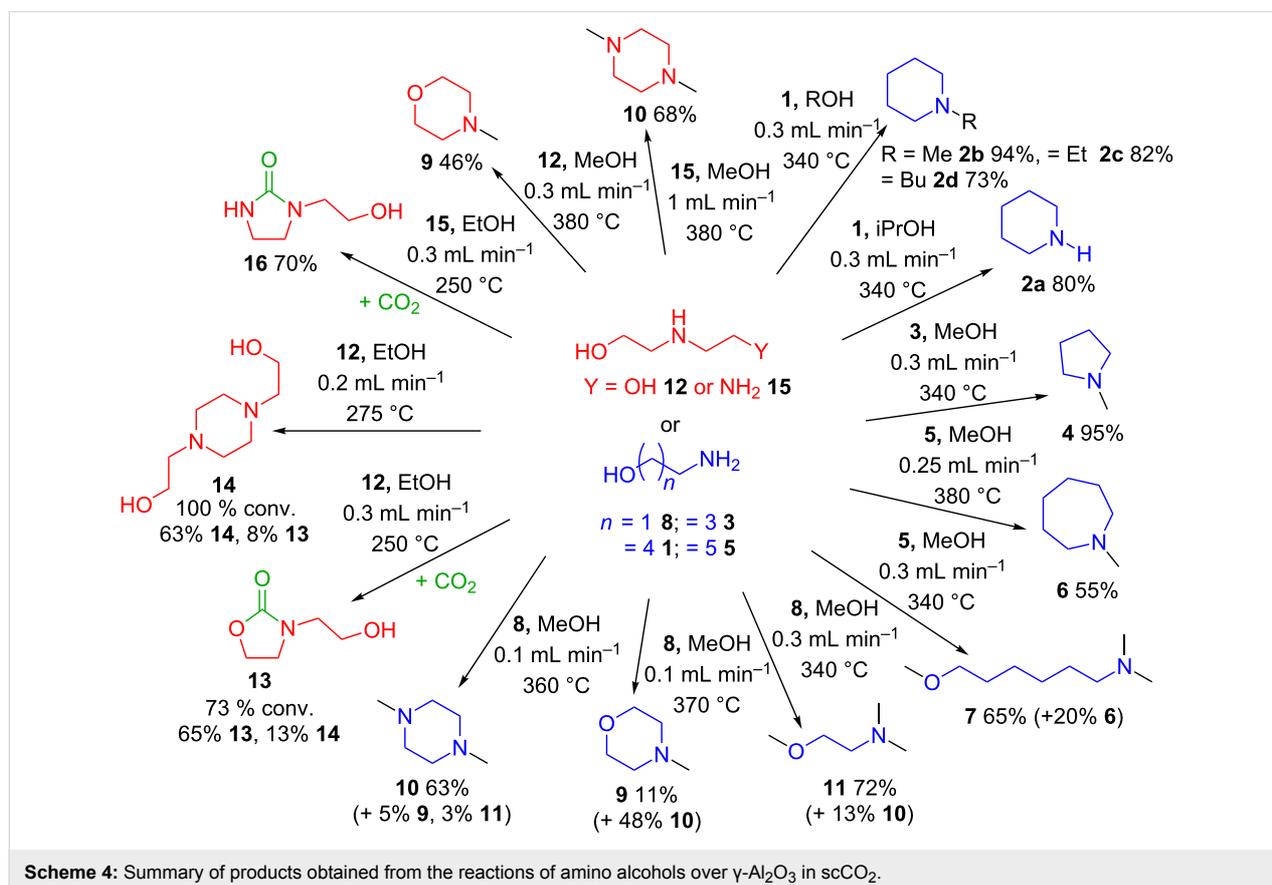
Using scCO$_2$ as the solvent proved to be beneficial to the yield of cyclic *N*-alkylated amines, in particular for the *N*-alkylation step which was arrested in the absence of scCO$_2$. The intramolecular cyclisation of the amino alcohols was favoured at higher temperatures in both the presence and absence of scCO$_2$. Increasing the primary alcohol length led to slightly lower yields of the target products whereas secondary alcohols did not react with the amines at all. Varying the chain length of the amino alcohol produced the corresponding *N*-alkylated five- (**4**) and seven-membered ring (**6**), three-membered aziridine rings were not detected. Competing *N*- and *O*-alkylation was observed at higher temperatures with ethanolamine (**8**) and 6-amino-1-hexanol (**5**), suggesting ring closure is slower in these cases. Ethanolamine (**8**) produced dimers as the major products, mainly via the amination pathway; however, some esterification/deamination was observed as *N*-methylmorpholine (**9**) was also detected. CO$_2$ incorporation in **12** and **15** was perhaps the most surprising result as this occurred at lower temperatures compared to the cyclisation, however at higher temperatures intramolecular reactions were favoured. The formation of oxazolidinones was shown to be reversible releasing CO$_2$ as dimers are formed. Imidazolidinones were shown to be stable to further reaction and no release of CO$_2$ was observed under the conditions studied. Further optimisation and investigations into the incorporation of CO$_2$ are in progress.

Experimental

CAUTION! The described reactions involve high pressures and require equipment (Figure 3) with appropriate pressure ratings.

All reagents and solvents were purchased from commercial sources and used as received. CO$_2$ was supplied by BOC Gases (99.8%). The γ-alumina (PURALOX NWa155) was supplied by SASOL. It was sieved before use, to obtain the desired particle
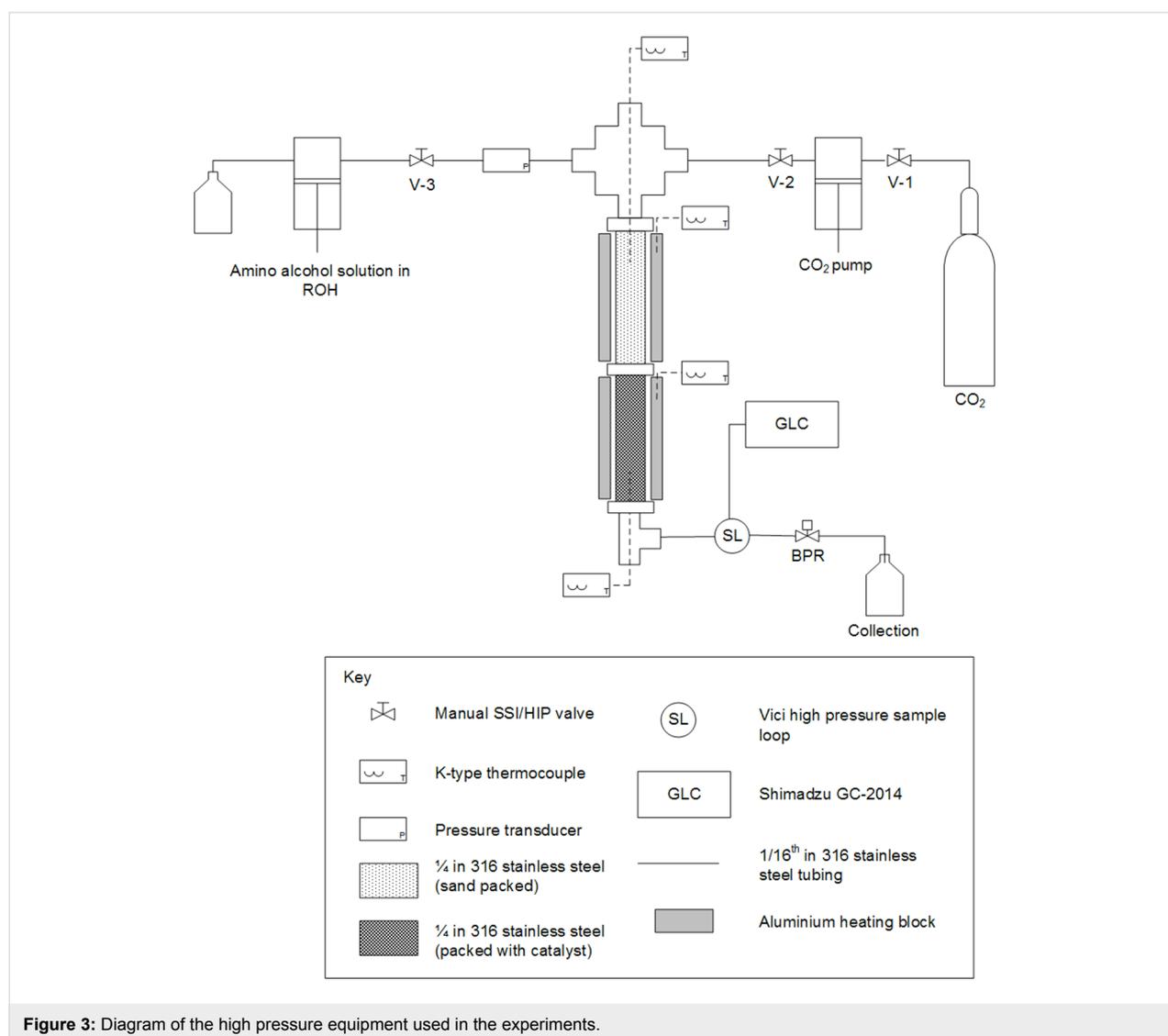
Figure 3: Diagram of the high pressure equipment used in the experiments.

size (125–170 μm), which was used as the catalyst. Reaction mixtures were analysed using GC, GC–MS, ^{1}H and ^{13}C NMR. Compounds **1a–c**, **4**, **9**, **10**, **13**, **14**, **16** were obtained from Aldrich and used as standards. **1d,e** [50], **6** [51], **7** [52], and **11** [53] were identified as previously described in the literature.

GC analysis was carried out using the following instrument and conditions: Online Shimadzu GC-2014 with a high pressure sample loop and an OPTIMA delta-3 column (30 m, 0.25 mm ID, 0.25 μm FT): hold 50 °C 4 min, ramp to 100 °C at 25 °C/min, ramp to 250 °C at 10 °C/min, hold for 2 min, pressure 132.1 kPa, purge 3.0 mL/min split ratio 40.

The high pressure continuous set-up (Figure 3) employed in the described reactions consisted of a HPLC pump through which a solution of the desired amino alcohol in an alcoholic solvent was delivered. A stainless steel reactor (1/4'' tube, 1.83 mL volume) was packed with γ-alumina (approx. 2 g) and attached below a pre-heater column (1/4'' tube, 1.83 mL volume) that was packed with sand to increase mixing. A crosspiece was used to mix the CO_2 and reagent flows before the reactors and the resulting product mixture was collected downstream of the back pressure regulator. The sampling to the on-line GC was done with a high pressure sample loop (Vici, 0.5 μL), which allowed a sample to be taken from the reaction flow. During optimisations a sample was taken once the conditions had been changed and stable state had been reached (10 min).

Some experiments were carried out by using a self-optimising reactor which has been described in detail previously [34,35,37]. All SNOBFIT [47] optimisations were performed within the following limits: Temperature 250–380 °C and flow rate 0.1–1.0 mL min^{-1}. The number of points produced by each call to SNOBFIT (n_{req}) was 6, and 10% of all the points were requested as global points (p = 0.1). The results at each condition were determined by GC analysis (programme time 20–23 min) and the pressure of the system was controlled by a back-pressure regulator at the outlet and was adjusted manually.

Supporting Information

Supporting Information File 1
Experimental data.
[http://www.beilstein-journals.org/bjoc/content/supplementary/1860-5397-13-36-S1.pdf]

Acknowledgements

References

1. Constable, D. J. C.; Dunn, P. J.; Hayler, J. D.; Humphrey, G. R.; Leazer, J. L., Jr.; Linderman, R. J.; Lorenz, K.; Manley, J.; Pearlman, B. A.; Wells, A.; Zaks, A.; Zhang, T. Y. *Green Chem.* **2007,** *9,* 411–420. doi:10.1039/B703488C
2. Lawrence, S. A. *Amines: Synthesis, Properties and Applications;* Cambridge University Press: Cambridge, 2004.
3. Carey, J. S.; Laffan, D.; Thomson, C.; Williams, M. T. *Org. Biomol. Chem.* **2006,** *4,* 2337–2347. doi:10.1039/b602413k
4. Salvatore, R. N.; Yoon, C. H.; Jung, K. W. *Tetrahedron* **2001,** *57,* 7785–7811. doi:10.1016/S0040-4020(01)00722-0
5. Marichev, K. O.; Takacs, J. M. *ACS Catal.* **2016,** *6,* 2205–2210. doi:10.1021/acscatal.6b00175
6. Bhawal, B. N.; Morandi, B. *ACS Catal.* **2016,** *6,* 7528–7535. doi:10.1021/acscatal.6b02333
7. Shimizu, K. *Catal. Sci. Technol.* **2015,** *5,* 1412–1427. doi:10.1039/C4CY01170H
8. Li, Q.-Q.; Xiao, Z.-F.; Yao, C.-Z.; Zheng, H.-X.; Kang, Y.-B. *Org. Lett.* **2015,** *17,* 5328–5331. doi:10.1021/acs.orglett.5b02685
9. Leonard, J.; Blacker, A. J.; Marsden, S. P.; Jones, M. F.; Mulholland, K. R.; Newton, R. *Org. Process Res. Dev.* **2015,** *19,* 1400–1410. doi:10.1021/acs.oprd.5b00199
10. Yan, T.; Feringa, B. L.; Barta, K. *Nat. Commun.* **2014,** *5,* No. 5602. doi:10.1038/ncomms6602
11. Obora, Y. *ACS Catal.* **2014,** *4,* 3972–3981. doi:10.1021/cs501269d
12. Watson, A. J. A.; Williams, J. M. J. *Science* **2010,** *329,* 635–636. doi:10.1126/science.1191843
13. Lamb, G. W.; Al Badran, F. A.; Williams, J. M. J.; Kolaczkowski, S. T. *Chem. Eng. Res. Des.* **2010,** *88,* 1533–1540. doi:10.1016/j.cherd.2010.04.005
14. Hamid, M. H. S. A.; Allen, C. L.; Lamb, G. W.; Maxwell, A. C.; Maytum, H. C.; Watson, A. J. A.; Williams, J. M. J. *J. Am. Chem. Soc.* **2009,** *131,* 1766–1774. doi:10.1021/ja807323a
15. Del Zotto, A.; Baratta, W.; Sandri, M.; Verardo, G.; Rigo, P. *Eur. J. Inorg. Chem.* **2004,** 524–529. doi:10.1002/ejic.200300518
16. Fujita, K.; Li, Z.; Ozeki, N.; Yamaguchi, R. *Tetrahedron Lett.* **2003,** *44,* 2687–2690. doi:10.1016/S0040-4039(03)00371-X
17. Watanabe, Y.; Tsuji, Y.; Ohsugi, Y. *Tetrahedron Lett.* **1981,** *22,* 2667–2670. doi:10.1016/S0040-4039(01)92965-X
18. Grigg, R.; Mitchell, T. R. B.; Sutthivaiyakit, S.; Tongpenyai, N. *J. Chem. Soc., Chem. Commun.* **1981,** 611–612. doi:10.1039/c39810000611
19. Bui-The-Khai; Concilio, C.; Porzi, G. *J. Org. Chem.* **1981,** *46,* 1759–1760. doi:10.1021/jo00321a056
20. Su, J.; Li, X.; Chen, Y.; Cui, Y.; Xu, J.; Qian, C.; Chen, X. *RSC Adv.* **2016,** *6,* 55643–55649. doi:10.1039/C6RA07998A
21. Li, Y.-Q.; Chen, Y.-B.; Huang, Z.-Z. *Chin. Chem. Lett.* **2014,** *25,* 1540–1544. doi:10.1016/j.cclet.2014.07.006
22. Yang, J.-M.; Jiang, R.; Wu, L.; Xu, X.-P.; Wang, S.-Y.; Ji, S.-J. *Tetrahedron* **2013,** *69,* 7988–7994. doi:10.1016/j.tet.2013.07.010
23. Pathare, S. P.; Akamanchi, K. G. *Appl. Catal., A* **2013,** *452,* 29–33. doi:10.1016/j.apcata.2012.11.017
24. Zhao, Y.; Foo, S. W.; Saito, S. *Angew. Chem., Int. Ed.* **2011,** *50,* 3006–3009. doi:10.1002/anie.201006660

25. Motokura, K.; Nakagiri, N.; Mizugaki, T.; Ebitani, K.; Kaneda, K.
J. Org. Chem. **2007,** *72,* 6006–6015. doi:10.1021/jo070416w

26. Ko, A.-N.; Yang, C.-L.; Zhu, W.-d.; Lin, H.-e. *Appl. Catal., A* **1996,** *134,*
53–66. doi:10.1016/0926-860X(95)00209-X

27. Brown, A. B.; Reid, E. E. *J. Am. Chem. Soc.* **1924,** *46,* 1836–1839.
doi:10.1021/ja01673a011

28. Frankland, P. F.; Challenger, F.; Nicholls, N. A. *J. Chem. Soc., Trans.*
1919, *115,* 198–205. doi:10.1039/CT9191500198

29. Oku, T.; Ikariya, T. *Angew. Chem., Int. Ed.* **2002,** *41,* 3476–3479.
doi:10.1002/1521-3773(20020916)41:18<3476::AID-ANIE3476>3.0.CO
;2-5

30. Oku, T.; Arita, Y.; Tsuneki, H.; Ikariya, T. *J. Am. Chem. Soc.* **2004,** *126,*
7368–7377. doi:10.1021/ja048557s

31. Gray, W. K.; Smail, F. R.; Hitzler, M. G.; Ross, S. K.; Poliakoff, M.
J. Am. Chem. Soc. **1999,** *121,* 10711–10718. doi:10.1021/ja991562p

32. Walsh, B.; Hyde, J. R.; Licence, P.; Poliakoff, M. *Green Chem.* **2005,** *7,*
456–463. doi:10.1039/b413890b

33. Gooden, P. N.; Bourne, R. A.; Parrott, A. J.; Bevinakatti, H. S.;
Irvine, D. J.; Poliakoff, M. *Org. Process Res. Dev.* **2010,** *14,* 411–416.
doi:10.1021/op900307w

34. Parrott, A. J.; Bourne, R. A.; Akien, G. R.; Irvine, D. J.; Poliakoff, M.
Angew. Chem., Int. Ed. **2011,** *50,* 3788–3792.
doi:10.1002/anie.201100412

35. Bourne, R. A.; Skilton, R. A.; Parrott, A. J.; Irvine, D. J.; Poliakoff, M.
Org. Process Res. Dev. **2011,** *15,* 932–938. doi:10.1021/op200109t

36. Jumbam, D. N.; Skilton, R. A.; Parrott, A. J.; Bourne, R. A.;
Poliakoff, M. *J. Flow Chem.* **2012,** *2,* 24–27.
doi:10.1556/jfchem.2012.00019

37. Skilton, R. A.; Parrott, A. J.; George, M. W.; Poliakoff, M.; Bourne, R. A.
Appl. Spectrosc. **2013,** *67,* 1127–1131. doi:10.1366/13-06999

38. Skilton, R. A.; Bourne, R. A.; Amara, Z.; Horvath, R.; Jin, J.;
Scully, M. J.; Streng, E.; Tang, S. L. Y.; Summers, P. A.; Wang, J.;
Pérez, E.; Asfaw, N.; Aydos, G. L. P.; Dupont, J.; Comak, G.;
George, M. W.; Poliakoff, M. *Nat. Chem.* **2015,** *7,* 1–5.
doi:10.1038/nchem.2143

39. Hammerschmidt, W.; Baiker, A.; Wokaun, A.; Fluhr, W. *Appl. Catal.*
1986, *20,* 305–312. doi:10.1016/0166-9834(86)80022-7

40. Bai, G. Y.; Li, Y.; Yan, X.; He, F.; Chen, L. *React. Kinet. Catal. Lett.*
2004, *82,* 33–39. doi:10.1023/B:REAC.0000028802.66602.0f

41. Nagaiah, K.; Rao, A. S.; Kulkarni, S. J.; Subrahmanyam, M.;
Rao, A. V. R. *J. Catal.* **1994,** *147,* 349–351. doi:10.1006/jcat.1994.1147

42. Wu, Z.; Wang, H.; Sun, M.; Du, X.; Chen, L.; Li, Y.
Res. Chem. Intermed. **2012,** *38,* 1149–1157.
doi:10.1007/s11164-011-0450-4

43. Wu, Z.; Yang, F.; Wang, H.; Ma, J.; Chen, L.; Li, Y.
React. Kinet., Mech. Catal. **2012,** *106,* 485–493.
doi:10.1007/s11144-012-0447-z

44. Amara, Z.; Streng, E. S.; Skilton, R. A.; Jin, J.; George, M. W.;
Poliakoff, M. *Eur. J. Org. Chem.* **2015,** 6141–6145.
doi:10.1002/ejoc.201500980

45. Reizman, B. J.; Jensen, K. F. *Acc. Chem. Res.* **2016,** *49,* 1786–1796.
doi:10.1021/acs.accounts.6b00261

46. Fabry, D. C.; Sugiono, E.; Rueping, M. *Isr. J. Chem.* **2014,** *54,*
341–350. doi:10.1002/ijch.201300080

47. Huyer, W.; Neumaier, A. *ACM Trans. Math. Software* **2008,** *35,* No. 9.
doi:10.1145/1377612.1377613

48. Freundlich, H.; Salomon, G. *Ber. Dtsch. Chem. Ges. A* **1933,** *66,*
355–357. doi:10.1002/cber.19330660308

49. Arrowood, T.; MacDonald, J. Preparation of Dihydroxyethyl Piperazine.
U.S. Pat. Appl. US20150274682 A1, Oct 1, 2015.

50. Katritzky, A. R.; Fan, W.-Q. *J. Org. Chem.* **1990,** *55,* 3205–3209.
doi:10.1021/jo00297a041

51. Reeves, J. T.; Tan, Z.; Marsini, M. A.; Han, Z. S.; Xu, Y.;
Reeves, D. C.; Lee, H.; Lu, B. Z.; Senanayake, C. H. *Adv. Synth. Catal.*
2013, *355,* 47–52. doi:10.1002/adsc.201200835

52. Barbry, D.; Hasiak, B. *Collect. Czech. Chem. Commun.* **1983,** *48,*
1734–1744. doi:10.1135/cccc19831734

53. Remenar, J. F.; Lucht, B. L.; Collum, D. B. *J. Am. Chem. Soc.* **1997,**
119, 5567–5572. doi:10.1021/ja970029b

Continuous-flow processes for the catalytic partial hydrogenation reaction of alkynes

Carmen Moreno-Marrodan, Francesca Liguori and Pierluigi Barbaro[*]

Abstract

The catalytic partial hydrogenation of substituted alkynes to alkenes is a process of high importance in the manufacture of several market chemicals. The present paper shortly reviews the heterogeneous catalytic systems engineered for this reaction under continuous flow and in the liquid phase. The main contributions appeared in the literature from 1997 up to August 2016 are discussed in terms of reactor design. A comparison with batch and industrial processes is provided whenever possible.

Introduction

The catalytic partial hydrogenation of alkynes to alkenes in the liquid phase is a reaction of high relevance to the manufacture of a multitude of fine chemicals [1] including pharmaceutical building blocks, agrochemicals, food additives, flavours and fragrances [2,3]. It is also crucial in the bulk polymer industry to achieve the complete elimination of alkynes and alkadienes from alkene feedstocks [4,5]. The chemistry of these processes is dominated by heterogeneous palladium catalysts, particularly based on solid-supported Pd nanoparticles (PdNP) [6,7]. On the industrial scale, alkynes partial hydrogenations are usually carried out under batch conditions using Lindlar-type catalysts,

consisting in relatively high amounts of Pd (5 wt %) and Pb (2–3%) deposited onto $CaCO_3$ [8,9], whose active sites nature is not fully characterized yet [10,11]. Besides the use of toxic lead, satisfactory catalyst performances often require a careful control of the hydrogen uptake and use of an excess of amine (quinoline) modifier [12,13], with serious drawbacks in terms of process economy, environmental impact and product separation management. The development of cost-effective, well-defined, efficient and environmentally friendly catalytic systems for the partial hydrogenation reaction of alkynes is thus of utmost importance [14,15].

Compared to batch setups, considerable process intensification [16,17] to this regard can be provided by continuous-flow operations either in terms of safety, purification, waste emission, durability, reproducibility, automation, energy and space consumption [18,19]. Particularly, continuous-flow catalysis may enhance the performance of a given catalyst while reducing the number of processing steps [20,21], which may result in a significant contribution to the reduction of the high E-factor (kg waste generated/kg product) usually observed in the fine-chemicals sector [22,23], as a consequence of the additives and manipulations required to achieve satisfactory selectivity. Indeed, the implementation of continuous-flow practices in the pharmaceutical industry is considered one of the most strategic fields of innovation toward greener manufacturing methods [24,25]. Nonetheless, in order to be competitive on the large-scale, continuous-flow systems for the catalytic hydrogenation of alkynes should not only provide their intrinsic benefits over conventional batch processes, but also be advantageous, or at least equal, either in terms of productivity per unit active metal, volume or time, absence of additives or catalyst lifetime [26,27].

In the present paper we shortly review the heterogeneous catalytic systems engineered for the partial hydrogenation reaction of substituted and unsubstituted alkynes under continuous flow and in the liquid phase, covering the main contributions appeared in the literature from 1997 up to August 2016. Some aspects of the topic have been surveyed in the past [28,29]. Details of alkyne hydrogenation reactions in general, including mechanism [30,31], kinetics [32,33], adsorption phenomena [34,35], thermodynamics [36,37], structure–activity relationships [38,39] have been extensively described elsewhere, therefore they are out of the scope of this review. Herein the focus is on the various catalytic reactor systems and technological solutions reported in the literature for this process, aimed at illustrating the state of the art in the field and the benefits of the approach. Generalities on theory and methods for flow chemistry can be found in excellent textbooks and reviews [40,41] and will not be treated in detail.

The present review could have been structured according to different variables, i.e., the metal catalyst involved, the type of support material, the reactor design or the hydrogen source. We decided to break down the manuscript on the basis of the substrates examined in order to allow an easier comparison among different reactors performance and highlight the potential benefits of one catalytic system over the others.

Review
The issue of selectivity

A major challenge in alkynes partial hydrogenation is to achieve 100% selectivity to the desired product at the highest conversion level [42,43]. The conventional heterogeneous catalysts often show selectivity issues owing to many potential side reactions, particularly in relation to chemoselectivity, i.e., over-hydrogenation of alkenes to alkanes [44,45], resistance of other functional groups (ketones [46,47], amines [48,49], azides [50]), regioselectivity [51,52], isomerization [53,54] and oligomerization [55,56] competitive reactions. In addition, whenever an internal alkyne is to be hydrogenated, stereoselectivity must also be considered [57] (Scheme 1). The main byproduct usually obtained is the over-hydrogenation one, which results in conversion and selectivity to be inversely proportional. Selectivity in partial hydrogenation is ruled by the relative rates of the first and second hydrogenation steps, as well as by the adsorption strengths of alkyne and alkene over the metal catalyst surface. Other side-products may include those due to dimerization and isomerization reactions, depending on the substrate.

Several approaches were developed to enhance the selectivity of the batch hydrogenation processes, including tuning of the reaction conditions, use of less conventional metals [58,59], alloys [60,61] or oxide active phases [62] and engineering of single-site heterogeneous catalysts [63,64]. A more usual strategy is the so-called "selective poisoning", i.e., the improvement of the catalyst's selectivity by the addition of variable, often large, amount of contaminants, either organic ligands (quinolone [65,66], phosphine [67]), carbon monoxide [68], sulfides [69], sulfoxides [70,71] defined as "reaction modifiers", or metal ions (Cu, Pb) [72], polymers/surfactants [73] defined "catalyst modifiers", whose common purpose is to decrease the hyperactivity of the (Pd) metal. It is clear that, besides the use and consumption of toxic/expensive substances, drawbacks in terms of cata-
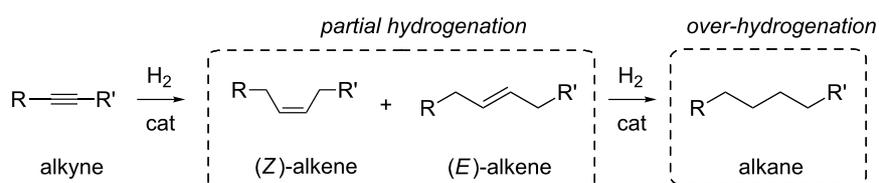
Scheme 1: Common reaction pathways for alkyne hydrogenation reactions.

lyst reuse and deactivation pose severe limitations in the utilization of this approach.

As it will be illustrated in the following sections, hydrogenation under continuous-flow conditions may represent a favourable alternative. Catalytic flow systems have shown to be extremely beneficial for carrying out chemical processes that are difficult to perform under batch conditions, e.g., involving reactive intermediates or competitive reactions [74,75]. Compared to batch setups, performing reactions under continuous flow allows a fine tuning of the contact time between intermediates and catalytic active phase, which may result in improved selectivity, with no need of additives [76].

Reactor and catalyst design

In contrast to unselective processes in the gas phase (e.g., for bulk chemicals production), whose fast interaction with the catalyst may ensure satisfactory conversions under the reaction conditions, selective liquid phase flow processes for the fine-chemicals synthesis, including partial hydrogenations, usually requires a more intimate contact with the heterogeneous catalyst to be efficient. One example is the so-called "confinement effect" found in mesoporous catalytic materials [77,78].

Catalytic hydrogenations are conveniently achieved under flow using fixed bed devices, wherein the size of the inner diameter of reactor channels distinguishes between micro (10–500 μm) or mesofluidic (500 μm up to several mm) reactors [79,80]. This size range may allow for the production of mg to tens of tons of target compound per year [81]. Despite the several possible reactor arrangements and catalyst morphologies falling within the above classification [82,83], herein we decided to break down the systems according to the main types reported in the literature for the catalytic partial hydrogenation reaction of alkynes, i.e., capillary, packed-bed, honeycomb and monolithic reactors. A schematic representation of these reactors is shown in Figure 1. Other reactor types (e.g., fluidized bed reactor, wherein the solid catalyst is suspended in a fluid) have not been reported for liquid-phase alkyne hydrogenations and will not be discussed.

Capillary reactors (10–1000 μm internal diameter, 0.1–30 m length) are routinely used in the lab-scale synthesis due to the ease of operations, negligible heat effects and fast reactants mixing [84,85]. Issues may arise from miniaturization of the catalysts, where the most common approach is to immobilize the catalyst onto the inner wall of the capillary support (catalytic wall reactors) [86,87] or to pack the powdered catalyst into the microchannels [88], the latter strategy being prone to significant pressure drops due to either the swelling or the size of the catalyst. It is important mentioning that different flow regimes

Figure 1: Schematic representation of most common reactor types for batch and continuous-flow partial hydrogenation of alkynes. Particles, layer or body of the catalyst in grey.
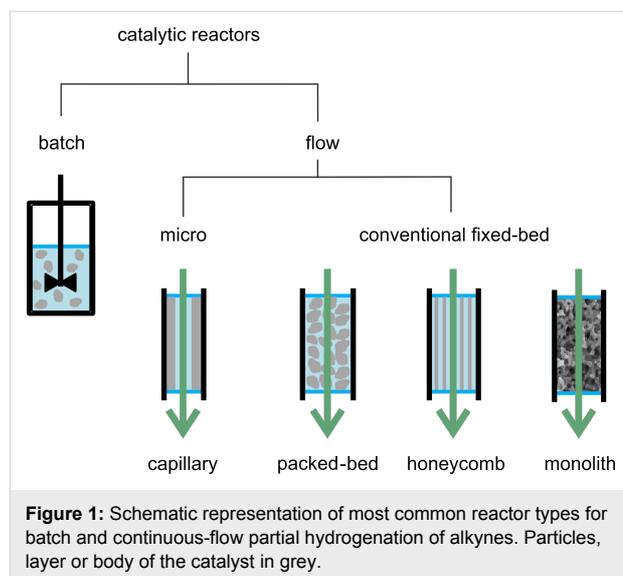
can be attained in miniaturized channels, depending on the gas and liquid rates, as these may affect both conversion and selectivity of the process (Figure 2).

Figure 2: Schematic representation of flow regimes in microchannels; (a) bubbly flow, (b) slug/Taylor or segmented flow, (c) churn flow, (d) slug/annular flow, (e) annular flow.
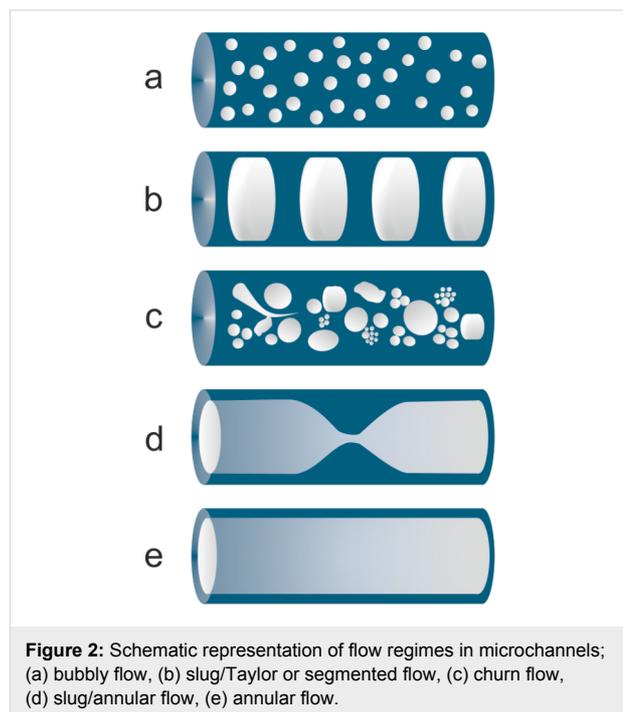
Packed-bed reactors are among the most used systems since they are relatively simple to handle, easy to operate and can accommodate beds with a broad range of physical dimensions and shapes. Commonly used packed catalysts consist of metal nanoparticles (MNP) immobilized onto a variety of porous solid supports, either pellets or powders of various grain size (in the range μm to mm). The preferred choice are mesoporous

supports (2–50 nm cavity size), due to the enhanced contact with the reagents because of the high surface area [89,90] and the effective "steric" stabilization of the embedded metal nanoparticle catalysts [91,92]. However, mesoporous catalysts may suffer from pore clogging, active sites accessibility, mass transfer limitations, and lack of reproducibility. Additional stabilization of MNP can be also achieved either by: the "electrostatic" effect of charged functional groups grafted to the support, a common strategy in gel-type resins (e.g., sulfonic resins) [93]; the strong metal–support interactions, particularly for inorganic oxide materials, e.g., TiO_2 [94,95]. Besides contributing to catalyst resistance by hampering the loss and the size increase of active sites, MNP stabilization is a key factor to limit the amount of metal leached in solution, an issue of utmost importance for the reduction of metal residues in the food and pharmaceuticals manufacture industry [96]. The choice of appropriate support materials is therefore critical to this purpose. Alternative strategies to reduce metal contamination include the use of metal scavengers, usually in the form of a downstream located cartridge [97].

Honeycomb (or foam) catalysts consist of inert carrier materials with millimetre size parallel channels (or cavities) obtained by extrusion, onto which a catalytically active layer is deposited, usually a porous inorganic oxide bonded to the support surface and containing precious metal sites (washcoat) [98,99]. They are largely reported in the chemical engineering literature for gas-phase, unselective thermal processes [100,101].

A monolith is "a shaped, fabricated intractable article with a homogeneous microstructure that does not exhibit any structural components distinguishable by optical microscopy" [102]. According to this definition, honeycombs do not fall within this category. In the recent years, porous monoliths have attracted considerable interest in several flow-through applications for the fine chemistry, including chromatography and catalysis [103,104]. Monolithic reactors may surpass most drawbacks typical of packed-bed systems, including high pressure drops, low contacting efficiency, large distribution of residence times, formation of hot-spots or stagnation zones, which results in poorly controlled fluid dynamics, hence in low catalyst productivity and selectivity [105,106]. Particularly, monoliths featuring a 3D isotropic, hierarchically porous network of narrowly size distributed, interconnected macropores (1–30 μm) and mesopores within the struts (6–50 nm) have shown a unique hydrodynamic behavior in the liquid phase [107,108], which addresses the need of both efficient processing (within small pores) and effective mass transport (by macropores) [109,110]. This kind of monolith obtained by spinodal decomposition joins the advantages of high surface area typical of mesoporous mate-

rial, spanning from 200 to 1200 $m^2 g^{-1}$ [111] with a high permeability typical of macropores, which results in a very efficient mass transfer [112]. According to Darcy's law, describing the flow of a fluid through a porous medium, hierarchically porous monoliths show a very low pressure drop Δp per unit reactor length L ($\Delta p/L = (\mu v)/k$, μ viscosity; v linear velocity), thanks to the high permeability coefficient $k > 0.25$ μm^2, which is proportional to the macroporous size D^2 [113]. The catalytic performance of these monoliths has been compared in continuous flow as a single piece or packed-bed (ground monolith 60–120 μm) and in batch arrangements. The better productivity was clearly demonstrated for the entire monolith under flow in the hydrogenation reaction of cyclohexene, resulting in turnover frequencies of 1673, 1131 and 932 h^{-1} and space-time-yields of 4.02, 0.95 and 0.01 $kg_{product} L_{reactor}^{-1} h^{-1}$, respectively [109]. An analogous permeability was observed under flow for 1D nanostructured support materials (vide infra).

A typical equipment for liquid-phase continuous-flow hydrogenations is sketched in Figure 3. Usually, concurrent, controlled flows of substrate solution and H_2 gas are allowed to flow through the catalytic reactor. Reaction products are collected at the reactor outlet. Typical residence times for alkynes partial hydrogenations, which defines the amount of time that the reaction mixture spends inside the reactor (the volume of the reactor divided by the volumetric flow rate) [114], are in the range 10–1000 s, corresponding to 5 μL/min (for capillary reactors) up to 3 mL/min of substrate solution flow. Hydrogen flow rates (and pressures) are adjusted to have typical H_2: substrate molar ratios inside the reactor in the range of 1–30.
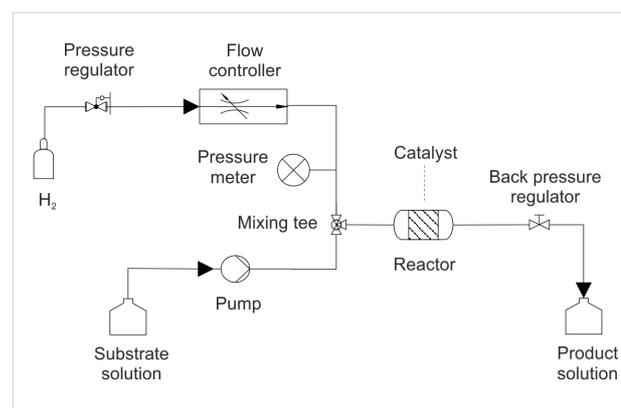
Figure 3: Sketch of typical continuous flow apparatus for liquid-phase catalytic alkynes hydrogenation reactions.

Hydrogenation of terminal alkynes

Various terminal alkynes have been hydrogenated under continuous-flow conditions using supported catalysts. The substrates and the commonly observed products with the labelling adopted in the present review are shown in Scheme 2. Representative
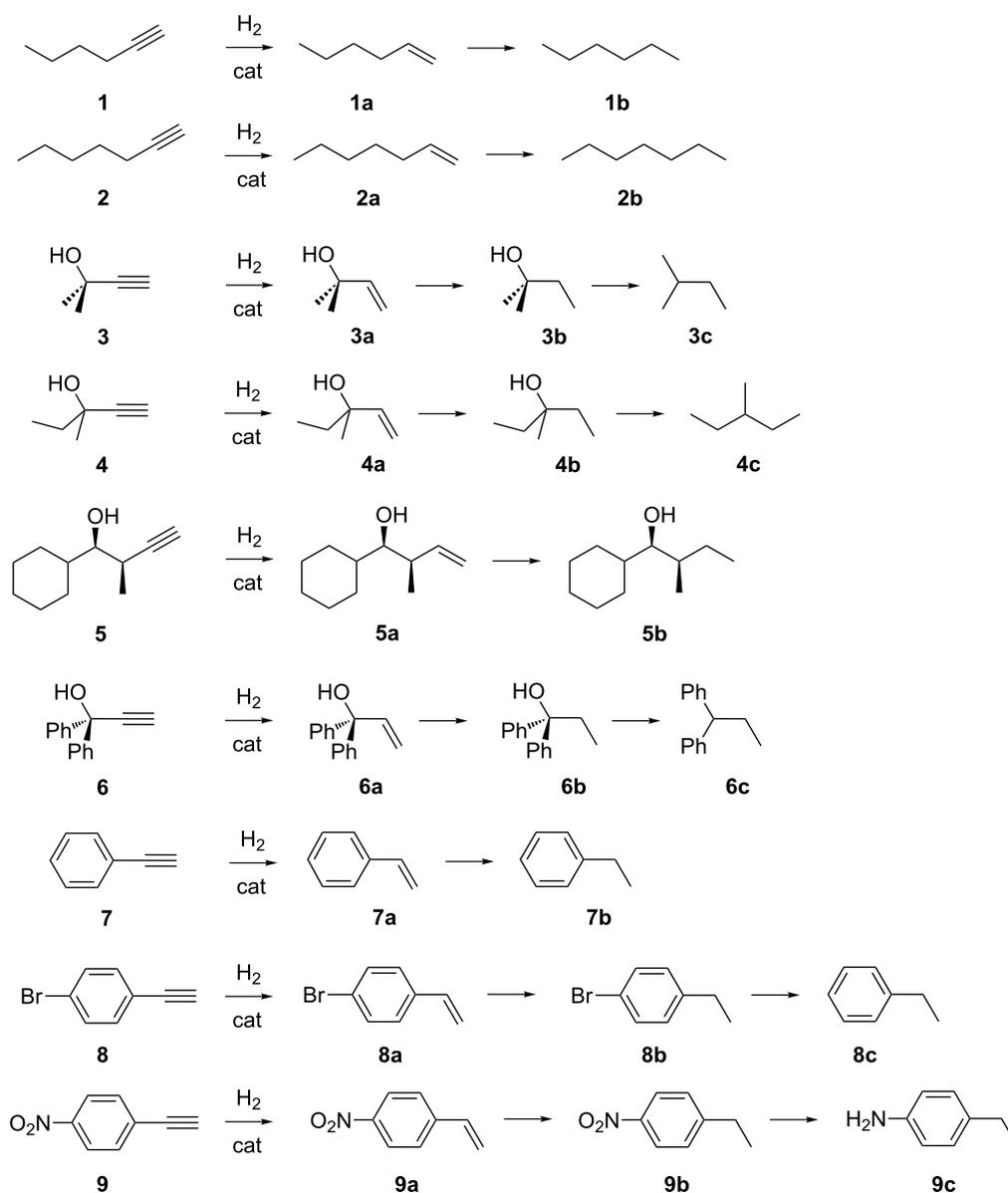
Scheme 2: Hydrogenation reactions of terminal alkynes with potential products and labelling scheme.

data are summarized in Table 1, in which conversions are indicated and catalysts' efficiencies are expressed in terms of selectivity, yield of indicated product, mass productivity ($mol_{product}\ g_{metal}^{-1}\ h^{-1}$) and space-time-yield (STY) [115]. Whenever available, the best compromise results between conversion and selectivity are reported.

1-Hexyne and 1-heptyne

The partial hydrogenation of 1-hexyne (**1**) produces 1-hexene (**1a**), one of the most commercially important linear α-olefins used in copolymerization processes [116,117]. High density polyethylene (HDPE) and linear low density polyethylene (LLDPE) contain approximately 2–4% and 8–10% of **1a**, re-

spectively [118]. 1-Hexene can be produced in ca. 91% yield under batch conditions using bimetallic Pd (4 wt %)–Cu (2 wt %) catalysts immobilized onto silica (298 K, 1 bar H_2) [65].

1-Hexyne was used as benchmark substrate to compare the efficiency of various packed-bed hydrogenation catalysts under continuous flow. Outstanding **1a** yields were obtained either using the Lindlar catalyst (84.6%) under smooth reaction conditions (298 K, 1 bar H_2, Table 1, entry 1) or 16.2 wt % $CeO_2@TiO_2$ (97%), the latter resulting in a very high STY for **1a** (18.86 kg $L^{-1}\ h^{-1}$) under solvent-free conditions (Table 1, entry 2) [119]. Use of cerium oxide is certainly advantageous in

Table 1: Representative continuous flow catalytic processes for liquid-phase partial hydrogenation of terminal alkynes.

entry	alkyne	reactor[a]	catalyst	T (K)	conv.[b] (%)	selectivity[c] (%)	yield[d] (%)	prod.[d,e] (mol g_M^{-1} h^{-1})	STY[d] (kg L^{-1} h^{-1})	ref.
1	**1**	PB	5% Pd(Pb)@CaCO$_3$	293	90[f]	94	84.6	2.9	1.65	[119]
2	**1**	PB	16.2% CeO$_2$@TiO$_2$	413	97[g,h]	100	97.0	1.1	18.86	[119]
3	**1**	PB	0.6% Pd(HHDMA)@C	293	30[f]	97	29.1	0.8	0.13	[121]
4	**1**	PB	0.5% Pd(HHDMA)@TiS	293	30[f]	96	28.8	0.9	0.13	[121]
5	**1**	PB	1.0% Pd@Al$_2$O$_3$	293	30[f]	67	20.1	0.3	0.09	[121]
6	**1**	PB	0.5% Pd@mpg-C3N4	343	–[i,j]	90	–[i]	13.3	–[i]	[122]
7	**1**	PB	1.3% Ag@SiO$_2$	373	30[k]	95	28.5	0.1	0.13	[123]
8	**1**	PB	1% Au@TiO$_2$	373	40[k]	95	38.0	0.1	0.17	[123]
9	**1**	PB	1% Ag@TCM-mpg-C3N4	303	–[i,k]	100	–[i]	0.9	0.56	[124]
10	**3**	C	1% Pd$_{25}$Zn$_{75}$@TiO$_2$	333	>99[l]	90	89.4	5.3	<0.01	[131]
11	**3**	M	0.67% Pd@MonoBor	294	92[l]	94	86.4	16.2	1.52	[136]
12	**3**	PB	0.5% Pd@TiNT	294	75[l]	83	62.2	82.3	7.36	[137]
13	**3**	PB	0.6% Pd(HHDMA)@C	293	30[f]	100	30.0	0.9	0.17	[121]
14	**3**	PB	0.5% Pd(HHDMA)@TiS	293	30[f]	96	28.8	1.0	0.16	[121]
15	**3**	PB	5% Pd(Pb)@CaCO$_3$	293	30[f]	83	24.9	0.1	0.14	[123]
16	**3**	PB	1.3% Ag@SiO$_2$	373	30[k]	100	30.0	0.1	0.17	[123]
17	**3**	PB	1% Au@TiO$_2$	373	30[k]	100	30.0	0.1	0.17	[123]
18	**3**	PB	0.5% Pd@mpg-C3N4	343	–[i,j]	90	–[i]	13.2	–[i]	[122]
19	**3**	PB	0.1% Pd@NKZPDB-5	294	>99[l]	60	59.4	5.8	0.17	[141]
20	**4**	C	0.02 wt % Pd@Al$_2$O$_3$	293	94[f]	83	78.0	–[i]	–[i]	[142]
21	**5**	PB	5% Pd(Pb)@CaCO$_3$	298	95[k]	100	95	–[i]	–[i]	[143]
22	**6**	M	0.67% Pd@MonoBor	294	85[l]	84	71.3	0.9	0.20	[136]
23	**6**	PB	0.5% Pd@TiNT	294	78[l]	89	69.4	20.0	4.37	[137]
24	**6**	PB	5% Pd(Pb)@CaCO$_3$	293	30[f]	100	30.0	0.1	0.39	[123]
25	**6**	PB	16% CeO$_2$@TiO$_2$	413	51[g]	100	51.0	<0.1	0.29	[119]
26	**6**	PB	1.3% Ag@SiO$_2$	373	30[k]	96	28.8	0.1	0.38	[123]
27	**6**	PB	1% Au@TiO$_2$	373	30[k]	100	30.0	0.1	0.39	[123]
28	**7**	PB	16% CeO$_2$@TiO$_2$	413	100[g]	100	100.0	<0.1	0.25	[119]
29	**7**	M	0.67% Pd@MonoBor	294	98[l]	96	93.7	2.9	0.33	[136]
30	**7**	PB	0.5% Pd@TiNT	294	83[l]	82	68.1	6.5	0.71	[137]
31	**7**	PB	5% Pd(Pb)@CaCO$_3$	293	30[f]	98	29.4	0.1	0.17	[123]
32	**7**	PB	1.3% Ag@SiO$_2$	373	30[k]	100	30.0	0.1	0.18	[123]
33	**7**	PB	1% Au@TiO$_2$	373	30[k]	96	28.8	0.1	0.17	[123]
34	**7**	PB	0.3% Au@TiO$_2$	333	99[m]	100	99	1.9	0.67	[151]

[a]Reactor type: C, capillary; PB, packed-bed; M, monolithic. [b]Substrate conversion. [c]Selectivity to the alkene product, e.g., **1a** / (**1a** + **1b**). [d]Calculated on the basis of the alkene product. [e]Calculated on bulk supported metal loading. [f]1 bar H$_2$. [g]90 bar H$_2$. [h]Solvent-free. [i]Not available. [j]5 bar H$_2$. [k]10 bar H$_2$. [l]1 – 2.7 bar H$_2$. [m]No H$_2$ pressure specified.

terms of catalyst cost, however, it requires much stronger reaction conditions to afford conversions analogous to that of Pd (413 K, 90 bar H$_2$). Comparable selectivities, although at lower conversion level, were reported using ligand-modified Pd catalysts, namely hexadecyl-2-hydroxyethyl-dimethylammonium dihydrogen phosphate (HHDMA), commercially available under the name NanoSelect^{TM} [120]. Low-content, colloidal

HHDMA-palladium catalysts onto on activated carbon (Table 1, entry 3) or titanium silicate (Table 1, entry 4) provided selectivities for **1a** of 97% and 96% respectively. As expected, "bare" 1% Pd@Al$_2$O$_3$ (Table 1, entry 5) showed to be poorly selective (67%), resulting in considerable amounts of oligomers and over-hydrogenated product **1b** [121]. The performance of the above systems was compared with that of a single-site catalyst

based on Pd atoms confined into the "six-fold cavities" of a mesoporous polymeric graphitic carbon nitride (mpg-C3N4, Figure 4a) [122]. The catalyst showed the highest productivity in the series (13.3 mol_{1a} g_{Pd}^{-1} h^{-1}), under fairly mild conditions (343 K, 5 bar H_2) (Table 1, entry 6), which was attributed to the facile hydrogen activation and alkyne adsorption on the atomically dispersed Pd sites. Electrostatic stabilization of Pd atoms was ascribed to a strong interaction with the nitrogen-coordinating species on the basis of DFT calculations. Effective stabilization also prevented site aggregation, resulting in pretty constant catalytic activity over a 20 h time-on-stream.

As an alternative to poisoned PdNP, use of other noble metals was also explored, although with lower catalysts efficiency. For instance, Ag@SiO2 (Table 1, entry 7) and Au@TiO2 (Table 1, entry 8) provided **1a** with modest yields and productivities under more severe reaction conditions compared to Pd (373 K, 10 bar H_2) [123]. Interestingly, the productivity of these systems could be significantly improved by adopting the same atomic level dispersion approach above described for palladium. Thus, Ag onto tricyanomethanide doped mpg-C3N4 provided comparatively much higher reaction rate for **1a** (0.9 mol g_{Pd}^{-1} h^{-1}) (Table 1, entry 9) [124], that confirms the effectiveness of the strategy.

The continuous flow partial hydrogenation of 1-heptyne (**2**) to 1-heptene (**2a**), an additive for lubricants and a surfactant [125], was also reported using packed 2% Pd@Al2O3 catalyst, showing 49% selectivity at 81% conversion under room temperature and 1 bar H_2 (STY for **2a**: 0.12 kg L^{-1} h^{-1}), with no detectable signs of deactivation over 6 h reaction time [126].

2-Methyl-3-butyn-2-ol and 3-methyl-1-pentyn-3-ol

The catalytic partial hydrogenation reaction of 2-methyl-3-butyn-2-ol (**3**) is an in-depth studied process, mainly because the alkene product (**3a**) is an important intermediate for the industrial synthesis of vitamins (A, E), as well as a variety perfumes [127,128]. The current manufacturing process is

based on the Lindlar or other Pd-based heterogeneous catalysts under batch conditions. Yields of the desired product are in the range of 95–97%, however, with fast catalyst deactivation due to degradation of the support or sintering of metal particles [129,130].

Reports exist on the partial hydrogenation of **3** under continuous flow. Best results in terms of alkene yield (89%) were reported for a capillary microreactor (10 m length, 250 μm i.d., 110 nm film thickness) operating under annular two-phase flow regime, and whose inner walls were coated with a bimetallic Pd25Zn75 catalyst onto mesoporous TiO2 (Table 1, entry 10). Selectivity could be further improved (97%) by addition of harmful pyridine [131]. The rather systematic kinetic study showed the significant selectivity increase (ca. 10%) by addition of Zn to the monometallic Pd catalysts, even at high substrate concentrations (up to 0.45 M). Selectivity enhancement could be attributed to a Pd site-isolation effect, similar to that found in Lindlar catalysts, which reduces the number of multiple interactions of the adsorbed intermediate alkene with active hydrogen species. It must be noted, however, the low STY value provided by this reactor type (less than 0.01 kg L^{-1} h^{-1}) due to the low substrate fed allowed (max. 14 μL min^{-1}). A lower selectivity was observed for the corresponding batch setup that was justified in terms of a slightly different concentration of active sites in the catalysts, as a result of the different preparation procedures. Similar findings were observed for an analogous Pd@TiO2 capillary reactor (annular flow), which showed ca. 15% higher selectivity compared to the corresponding batch system, although under slightly different reaction conditions [132]. The result was attributed to the shorter contact time between reagent and catalyst in that case.

In a different approach, PdNP were immobilized onto an open-cell macroporous (10 μm pore size), polymeric borate monolith, that was grown in situ within the walls of a commercial, tubular glass reactor (MonoBor, reactor volume 176 μL, Figure 5) [133]. The monolithic support was specifically designed to

Figure 4: Structure of Pd@mpg-C3N4 (a), Pd(HHDMA)@C (b), Pd(Pb)@CaCO3 (c) and Pd@Al2O3 (d) catalysts. The structures depict the increasing size of the active ensemble, from a single Pd atom (a) to a bare PdNP of approximately 800 atoms (d). The inset in (a) shows a characteristic six-fold cavity (orange) in the carbon nitride structure. C light grey, N dark blue, O red, Pb grey, Pd light blue. Adapted with permission from [122] , © 2015 John Wiley and Sons.

allow for the immobilization of Pd particles at non-coordinating borate sites within a rigid, highly-cross linked solid matrix (Figure 6) [134,135]. Under mild conditions (294 K, 1.4 bar H_2), alkene **3a** was obtained with good yield (93.9% sel. at 92% conv.) and productivity (1.52 kg L^{-1} h^{-1}) (Table 1, entry 11) [136]. The latter value was attributed to the macroporosity and to the poor swelling volume of the support material, which allow for high flow rates to be attained with low back-pressure evolution (methanol solution 0.1 M, 0.6 mL min^{-1}, H_2 pressure drop 0.4 bar).

Figure 5: Sketch of composition (left) and optical image of Pd@MonoBor monolithic reactor (right). Adapted with permission from [136], © 2013 Elsevier.

Figure 6: X-ray tomography 3D-reconstruction image of MonoBor [133]. Unpublished image from the authors.
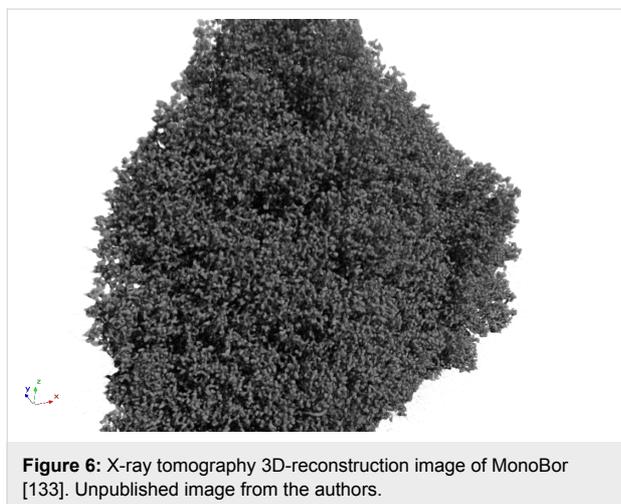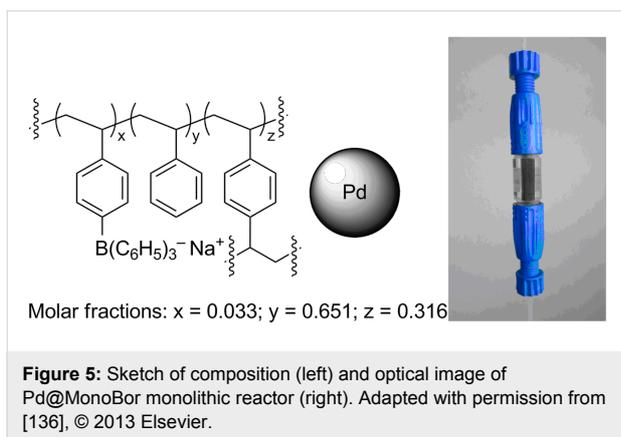
The highest productivity in the continuous partial hydrogenation of **3** (82.3 mol g_{Pd}^{-1} h^{-1}, Table 1, entry 12), was obtained using a packed-bed catalyst based on PdNP onto the outer surface of titanate nanotubes (Figure 7), that was justified in terms of both accessibility of Pd sites and high permeability of the packed 1D tubular material (weight hourly space velocity, $g_{substrate}$ $g_{catalyst}^{-1}$ h^{-1} ca. 11088 h^{-1}) [137,138]. In fact, much lower efficiency was observed under analogous flow conditions using Pd immobilized into the pores of conventional mesoporous powder titania.

Figure 7: Representative TEM image of titanate nanotubes with immobilized PdNP (arrows). Adapted with permission from [137], © 2016 John Wiley and Sons.
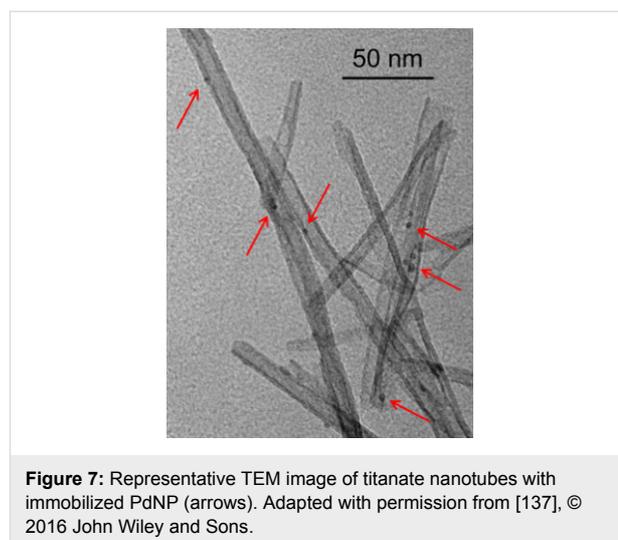
Analogous benefits in liquid phase flow operations were obtained by using nanostructured fibrous materials, that was attributed to the enhanced mass transfer of the one-dimensional packed support [139]. It is worth noticing that this result was obtained as a consequence of the so-called "Rational Catalyst Design" approach [140], applied to the hydrogenation of 2-methyl-3-butyn-2-ol as a case study [29]. In this approach, an optimized catalyst was designed by the integration of the catalyst performances at increasing length scales, from the nanoscale (active metal nanoparticles), to the mesoscale (support) and macroscale (reactor). Thus, after identification of the optimal shape and size of PdNP for the hydrogenation of **3**, the ex-situ particles were deposited onto a ZnO/Sintered Metal Fibers support, having selected this material for its excellent mass transfer properties. The catalyst was then integrated into a bubble column flow reactor with staged catalytic layers, showing two order magnitude higher productivity compared to Lindlar catalyst [141].

Low to moderate yields and productivities for **3a** were reported by using conventional packed-bed catalysts, either HHDMA-modified (Table 1, entries 13, 14) [121], Lindlar (Table 1, entry 15) or non-palladium based (Table 1, entries 16, 17) [123]. As above discussed for **1**, single-atom catalysts resulted in high productivity, however, direct comparison of product yield with other systems is not possible due to insufficient experimental data (Table 1, entry 18) [122]. PdNP onto hybrid zirconia/polyvinyl alcohol matrix (NKZPD) were also described, providing **3a** in moderate selectivity (60%) at full conversion and mild conditions (Table 1, entry 19) [142].

The partial hydrogenation reaction of the parent alkyne 3-methyl-1-pentyn-3-ol (**4**) was also reported under continuous flow. Similarly to what described above for **1** and **3**, the hydro-

genation of **4** to **4a** was investigated in detail by comparing the selectivity of diverse Pd packed-bed catalysts at the same substrate conversion level (30%). The study confirmed the efficiency of the catalysts to decrease in the order Pd(HHDMA)@C > Pd(HHDMA)@TiS > Lindlar > Pd@Al$_2$O$_3$ (from 100 to 67%) [121]. This selectivity trend was explained in terms of both adsorption mode on and relative accessibility to Pd active sites, depending on surface potentials and hindrance of modifiers, on the basis of density functional theory and molecular dynamics calculations. The rationale was summarized in the so-called thermodynamic selectivity concept, that is "a selective catalyst involves strong adsorption of the alkyne and a low stability to the adsorbed alkene" [121]. In bare Pd catalysts, such as Pd@Al$_2$O$_3$, or in alloyed Pd catalysts, such as Lindlar, the intermediate alkene is strongly adsorbed on Pd surface (exothermic process), thereby favouring further reaction with H$_2$ and reducing selectivity. In bulky ligand-modified catalysts, such as Pd(HHDMA)@C, the adsorption process is slightly endothermic and selectivity is enhanced.

A high yield of **4a** (78%) was also obtained by means of a capillary microreactor consisting in a mesoporous Al$_2$O$_3$-coated commercial fused-silica column with embedded PdNP (530 μm i.d., 25 cm length, 6 μm thick layer) (Table 1, entry 20) [143]. Experiments were performed in a segmented flow regime (H$_2$ gas/ethanol solution), so that the flow pattern enhanced the contact with the catalyst on the wall and minimize diffusion limits (Figure 2). Without bubbles, the yield of **4a** would have been ca. 57% at the same residence time. The catalyst was used for weeks without significant deactivation.

1-Cyclohexyl-2-methyl-3-butyn-1-ol

In the course of their studies on diastereoselective chain-elongation reactions, Ley and Baxendale reported the hydrogenation of (1*R*,2*R*)-1-cyclohexyl-2-methyl-3-butyn-1-ol (**5**), where the partial reduction of the triple bond is achieved in the presence of stereogenic centres [144]. The alkene **5a** was obtained in 95% yield, without compromising the starting diastereomeric ratio (4.3:1), using the Lindlar catalyst packed into a commercial H-Cube® apparatus under mild hydrogenation conditions (298 K, 10 bar H$_2$, Table 1, entry 21).

1,1-Diphenyl-2-propyn-1-ol

High yields of alkene **6a** were obtained by partial hydrogenation of 1,1-diphenyl-2-propyn-1-ol (**6**) using the monolithic Pd@MonoBor catalyst under smooth flow conditions (294 K, 84% selectivity at 85% conversion, Table 1, entry 22) [136]. Neither significant catalyst efficiency decay over 8 h reaction period was detected (Figure 8), nor an evidence for Pd leaching in solution was provided by ICP-OES throughout the reaction. This finding was justified by the effective electrostatic stabiliza-

tion of PdNP by the charged -B(C$_6$H$_4$)$^-$ groups onto the polymeric solid matrix. A small activity loss was attributed to poisoning by dimers and other byproducts adsorbed on the catalyst surface, as described for other batch Pd catalysts [145]. Under analogous conditions, Pd@TiNT gave **6a** in comparable yield (69.4%), although with remarkably higher productivity (for **6a**: 20.0 mol g$_{Pd}^{-1}$ h^{-1}) (Table 1, entry 23) [137], as previously outlined in the case of alkyne **3**.

Figure 8: Conversion and selectivity vs. time-on-stream for the continuous-flow hydrogenation of **6** over Pd@MonoBor catalyst (methanol solution 0.16 mL min^{-1}, H$_2$ 1.00 mL min^{-1} @ 1.29 bar, rt). Reprinted with permission from [136], © 2013 Elsevier.
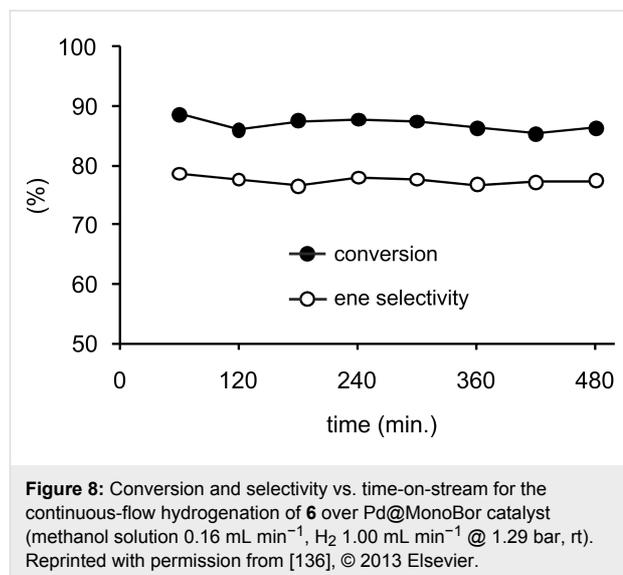
These latter results outperform those obtained at higher reaction temperatures using packed catalysts onto conventional supports, including Lindlar, CeO$_2$@TiO$_2$, Ag@SiO$_2$ and Au@TiO$_2$ (Table 1, entries 24–27), although the data are not properly comparable because they refer to significantly lower conversion levels (30–50%) [119,123]. The partial hydrogenation of **6** to **6a** under batch conditions was also described in 82–90% yield using phosphinated polymer incarcerated palladium catalysts [146].

The hydrogenation reaction of the bulky alkyne 1,1-diphenyl-2-propyn-1-ol (**6**) provides an interesting discussion example on how the relationship between catalyst architecture and substrate hindrance affects catalyst activity, even if not directly related to continuous flow operation conditions. It was proposed that ligand-modified surfaces, such as Pd(HHDMA)@C, are three-dimensional catalytic ensembles whose organic capping layer cannot be penetrated with ease by larger alkynes (Figure 4b) [121]. This justifies for the inactivity of Pd(HHDMA)-type catalysts toward the hydrogenation of **6**, while they are quite active in short-chain alkynes hydrogenation, e.g., **3** (Table 1, entries 13, 14) [123]. On the other hand, "naked" and Pb-poisoned palladium surfaces are 2D catalytic architectures (Figure 4c,d), which are amenable of alkynes adsorption irre-

spective of the chain length, thus resulting in high hydrogenation activity anyway. The selectivity is ruled by, e.g., site-isolation effects (Pd–Pd) in that case.

Phenylacetylene

The liquid-phase partial hydrogenation of phenylacetylene **7** was successfully achieved in the past using batch Pd catalysts (0.15–5% wt), with typical **7a** yields in the range of 60–70% [147,148]. More recently, a number of catalytic flow reactors were also described for this process. Best yields (94–100%) were achieved using either 16% CeO$_2$@TiO$_2$ (100%) [119] or Pd@MonoBor catalyst [136], under 90 bar H$_2$ and 413 K or 1.3 bar H$_2$ and 294 K, respectively (Table 1, entries 28, 29). As above reported for other substrates, best results in terms of productivity were provided by the monolithic and the titanate nanotubes-supported Pd catalysts (2.9–6.5 mol g$_{Pd}^{-1}$ h^{-1}, Table 1, entries 29, 30) [137]. Lower performances were observed using packed-bed catalysts and conventional support materials [123], an amorphous Pd$_{81}$Si$_{19}$ alloy catalyst in supercritical CO$_2$ (76% sel. at 91% conversion, 358 K) [149] or a capillary reactor (i.d. 250 μm) internally coated with Pd-doped mesoporous titania film (95% sel. at 30% conversion, 323 K) [150] (Table 1, entries 31–33).

The reduction of **7** to **7a** was also reported by transfer hydrogenation using formic acid / triethylamine as hydrogen source and packed Au@TiO$_2$ (rutile) catalyst [151]. An outstanding 99.7% yield was achieved at 333 K, corresponding to a productivity for **7a** of 1.9 mol g$_{Pd}^{-1}$ h^{-1} (Table 1, entry 34). This value was considerably higher (ca. 40%) than that obtained for the batch-type reaction under identical conditions. The selectivity toward **7a** was retained during the continuous operations, while a progressive decrease of conversion from 99% to 85% was observed after 3 h time on stream, that was partially recovered by treatment with acetone.

1-Bromo-4-ethynylbenzene and 1-ethynyl-4-nitrobenzene

The hydrogenations of **7**, 1-bromo-4-ethynylbenzene (**8**) and 1-ethynyl-4-nitrobenzene (**9**) were also reported with modest yields to **7a** (56%), (**8a**) (21%) and (**9a**) (21%), eventually with the addition of triethylamine, using a packed-bed multichannel catalytic reactor. The catalyst was based on PdNP onto trimodal (micro, meso), hierarchical porous synthetic carbon [152]. No catalyst deactivation was detected over 5 hours continuous runs (333 K, 1 bar H$_2$).

A perusal of Table 1 shows that identification of the most versatile partial hydrogenation flow system for terminal alkynes, either catalyst or reactor, is prevented by significant substrate specificity, lack of experimental data or choice of parameter to be compared either selectivity, productivity or STY. As representative example for selected catalysts and substrates **3**, **6** and **7**, one can infer that CeO$_2$@TiO$_2$ usually provides better selectivity compared to other systems with strong substrate dependence (such as Pd(HHDMA)@C, see above discussion) (Figure 9). However, data are not available at the same conversion level, yet not directly comparable. Comparison in terms of, e.g., productivity is limited due to the same reason.
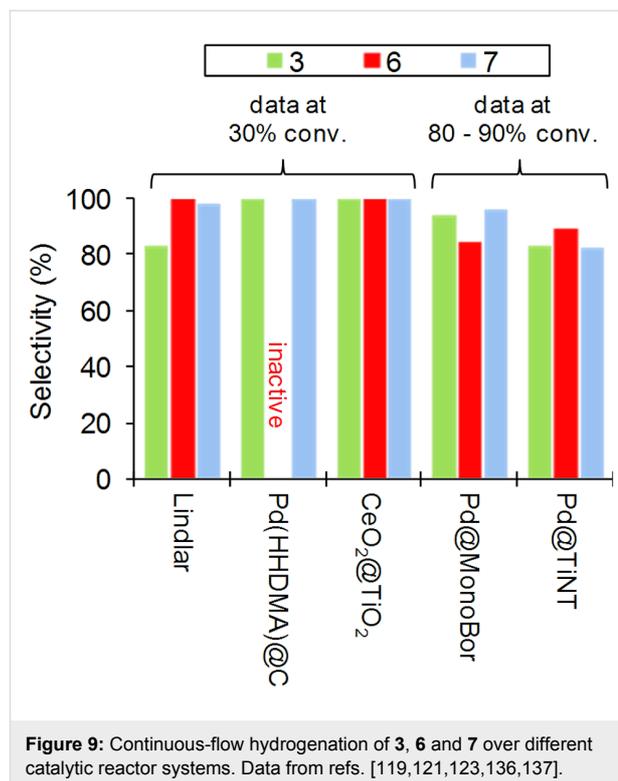
Figure 9: Continuous-flow hydrogenation of **3**, **6** and **7** over different catalytic reactor systems. Data from refs. [119,121,123,136,137].

Hydrogenation of internal alkynes

Compared to terminal alkynes, the partial hydrogenation reaction of internal alkynes is more challenging and intriguing owing to the stereoselectivity involved (usually *cis*) and to the large use of the products thereof in the fine-chemical industry. Most significant substrates examined in the literature under the continuous-flow catalysis conditions are reported in Scheme 3.

3-Hexyne

Analogously to the earlier discussed hydrogenation of 1-hexyne (see above), the continuous flow, partial hydrogenation of 3-hexyne (**10**) to *cis*-3-hexene (**10a**) has been extensively examined by comparing the efficiency of various packed-bed supported catalysts [119,121,123]. In all cases, irrespective of the metal or the support, the catalysts yielded the *cis*-alkene product with selectivity ≥89%, with the exception Pd/Al$_2$O$_3$ (Table 2, entry 1), in line with the previous observation on the selectivity to 1-hexene. The trend regarding catalysts efficiency
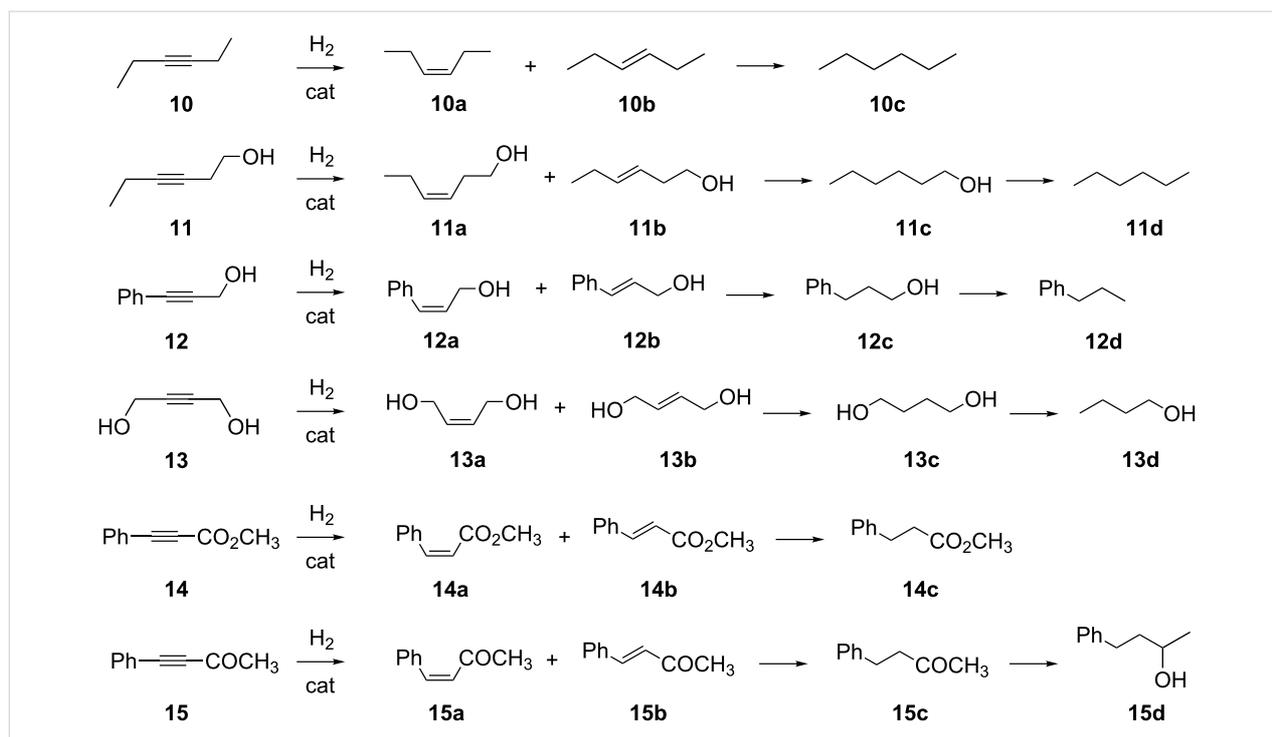
Scheme 3: Hydrogenation reactions of internal alkynes with potential products and labelling scheme.

was also very similar. High yields of **10a** (>87%) were observed for the Lindlar and the TiO$_2$-supported ceria catalysts, with a better productivity for the former (Table 2, entries 2, 3). All the other catalysts, including the HHDMA ligand modified-Pd one (Table 2, entries 4, 5) and the Ag and Au-based catalysts (Table 2, entries 7, 8) showed comparable selectivity, although at a lower conversion level. No data regarding the long-term catalysts stability were provided. Exceptionally high productivity was once again obtained for **10a** by the isolated Pd atoms catalyst Pd@mpg-C3N4 (11.3 mol g$_{Pd}^{-1}$ h^{-1}, Table 2, entry 6) [123].

3-Hexyn-1-ol and 3-phenyl-2-propyn-1-ol

The *cis*-partial hydrogenation product of 3-hexyn-1-ol (**11**), the so-called leaf alcohol **11a**, is an important product widely used as fragrance or perfumes component [153,154]. It is industrially obtained with a production volume of 400 t/y in ca. 96% selectivity at 99% conversion by means of a conventional Lindlar-based batch process [155,156]. Several systems have been reported on the lab scale for the catalytic hydrogenation of **11** under continuous-flow conditions.

An accurate study was carried out using the Pd@MonoBor monolithic catalyst [136], showing how the subtle effect of fine adjustments of concurrent flows of methanol substrate solution and H$_2$ gas may tune the conversion and selectivity of the process. As anticipated for similar hydrogenation systems,

under the same solution flow rate (i.e., keeping constant the residence time τ), an increase in the H$_2$ flow rate (i.e., the H$_2$/substrate molar ratio) resulted in a higher conversion and in a lower ene- and *Z/E* selectivity (Figure 10a). An increase in the solution flow rate (i.e., a decrease in τ) under a constant the H$_2$/substrate molar ratio resulted in a conversion decrease, but in a selectivity enhancement (Figure 10b). A reproducible selectivity/conversion diagram could be drawn on this basis, as reported in Figure 10c. Best compromise results between selectivity and conversion resulted in 87% **11a** yield (95% ene selectivity, of which 93% *cis*, at 99% conversion) under mild conditions (294 K, residence time 42 s, ratio H$_2$/**11** = 2.7, Table 2, entry 9). Pd@MonoBor is the first catalyst reported for the production of **11a** under continuous flow showing selectivity comparable to that of the industrial process, with additional benefits of lower noble metal content, no presence of toxic Pb or other additives [157]. The performance of Pd@MonoBor also compared favourably with that of other conventional batch systems [158,159]. Selectivity enhancement in the batch alkynes semi-hydrogenation was reported using egg-shell type catalyst. This was attributed to the short contact time of the intermediate alkene with the metal located on the catalyst surface, so that the alkene is quickly removed from the active phase with no possibility of further reduction [160]. A similar effect was invoked for Pd@MonoBor, whose site accessibility is hampered by the low swelling of the support in methanol solvent. Better swelling would allow the solvent to diffuse thor-

Table 2: Representative continuous flow catalytic processes for liquid-phase partial hydrogenation of internal alkynes.

entry	alkyne	reactor[a]	catalyst	T (K)	conv.[b] (%)	selectivity		yield[e] (%)	prod.[f,g] (mol g_M^{-1} h^{-1})	STY[f] (kg L^{-1} h^{-1})	ref.
						ene[c] (%)	Z/E[d] (%)				
1	**10**	PB	1.0% Pd@Al$_2$O$_3$	293	30[h]	–[i]	53	15.9	0.3	0.07	[121]
2	**10**	PB	5% Pd(Pb)@CaCO$_3$	293	93[h]	–[i]	94[j]	87.4	3.1	1.73	[119]
3	**10**	PB	16% CeO$_2$@TiO$_2$	413	93[k]	–[i]	100	93.0	< 0.1	0.18	[119]
4	**10**	PB	0.6% Pd(HHDMA)@C	293	30[h]	–[i]	97	29.1	0.8	0.13	[121]
5	**10**	PB	0.5% Pd(HHDMA)@TiS	293	30[h]	–[i]	100	30.0	0.9	0.14	[121]
6	**10**	PB	0.5% Pd@mpg-C3N4	343	–[i,l]	–[i]	90	–[i]	11.3	1.64	[122]
7	**10**	PB	1.3% Ag@SiO$_2$	373	30[m]	–[i]	89	26.7	0.1	0.12	[123]
8	**10**	PB	1% Au@TiO$_2$	373	30[m]	–[i]	94	28.2	0.1	0.13	[123]
9	**11**	M	0.67% Pd@MonoBor	294	> 99[n]	95	93	87.5	6.8	0.75	[136]
10	**11**	PB	0.5% Pd@TiNT	294	88[n]	94	93	76.9	40.6	4.24	[137]
11	**11**	PB	0.73% Pd@TiO$_2$	294	84[n]	80	85	57.1	19.2	0.20	[137]
12	**11**	PB	1.2% Pd@SiO$_2$	294	40[n]	87	93	32.4	7.1	1.43	[137]
13	**11**	PB	5% Pd(Pb)@CaCO$_3$	294	99[n]	64	62	39.4	0.2	0.10	[136]
14	**11**	PB	1.25% Pd/Dowex-Li	294	75[n]	80	89	53.4	2.3	0.73	[161]
15	**11**	PB	5% Pd@C	294	94[n]	22	81	16.8	0.9	0.16	[140]
16	**11**	PB	0.1% Pd@NKZPDB-5	294	99[n]	83	83	68.2	11.4	0.43	[141]
17	**11**	M	1.3% Pd@SiO$_2$ monolith	298	85[n]	80	80	54.4	0.5	0.17	[162]
18	**11**	M	0.2% Pd@TiO$_2$ monolith	294	61[n]	63	87	33.7	1.8	0.51	[163]
19	**12**	M	0.67% Pd@MonoBor	294	96[n]	79	95	71.9	0.8	0.12	[136]
20	**13**	M	0.67% Pd@MonoBor	294	93[n]	75	100	70.2	3.3	0.32	[136]
21	**13**	HC	0.5% Pd@Al$_2$O$_3$	328	90[o]	99	100	89.8	0.7	–[i]	[170]
22	**13**	PB	0.5% Pd@Al$_2$O$_3$	328	90[o]	94	93	78.7	1.0	–[i]	[170]
23	**13**	PB	5% Pd@C	323	92[p]	100	97	89.6	–[i]	–[i]	[172]
24	**14**	M	0.67% Pd@MonoBor	294	90[n]	91	96	79.2	6.1	1.09	[136]
25	**15**	M	0.67% Pd@MonoBor	294	92[n]	93	50	42.8	1.1	0.17	[136]

[a]Reactor type: C, capillary; PB, packed-bed; HC, honeycomb; M, monolithic. [b]Substrate conversion. [c]Selectivity to the alkene product, e.g., (**11a** + **11b**)/(**11a** + **11b** + **11c** + **11d**). [d]Selectivity to the Z-alkene product, e.g., **11a**/(**11a** + **11b**). [e]Yield of Z-alkene. [f]Calculated on the Z-alkene product. [g]Calculated on bulk supported metal loading. [h]1 bar H$_2$. [i]Not available. [j]Selectivity calculated as **10a**/(**10a** + **10b** + **10c**). [k]90 bar H$_2$. [l]5 bar H$_2$. [m]10 bar H$_2$. [n]1–2.7 bar H$_2$ K. [o]2 bar H$_2$. [p]10 bar H$_2$.

oughly the support, thereby producing a larger number of substrate–catalyst interactions, which results in lower alkene selectivity. The reaction using Pd@MonoBor was monitored for 14 h time-on-stream, showing no appreciable decay of conversion or selectivity (Figure 11). The catalyst could be reused several times with neither significant activity drop nor palladium leaching in solution detected.

Under comparable **11a** yield (76.9%), better productivity was shown by the packed Pd@titanate nanotubes catalyst (for **11a**: 40.6 mol g_{Pd}^{-1} h^{-1}, Table 2, entry 10) [137], analogously to what above described for the partial hydrogenation of **3**. As for

Pd@MonoBor, the high selectivity observed in this case was attributed to the short contact time of the intermediate alkene with the Pd sites located onto the outer surface of the catalyst. Indeed, an excellent product yield was obtained for short residence times (13 s), that suggests a high contribution to catalytic activity by easy accessible PdNP. No catalyst efficiency decay was observed over 6 h time-on-stream.

Worse performances were shown by other Pd packed-bed catalysts using conventional support materials, including mesoporous titania powder, mesoporous Davisil silica, Lindlar, gel-type Dowex resin, carbon (Table 2, entries 11–15), with the

Figure 10: Continuous-flow hydrogenation of **11** over Pd@MonoBor catalyst. a) Conversion and selectivity as a function of H$_2$ flow rate and H$_2$:**11** molar ratio under fixed residence time τ 42 s (solution flow rate 0.25 mL min^{-1}). b) Conversion and selectivity as a function of solution flow rate and residence time under fixed H$_2$:**11** molar ratio 2.7. c) selectivity/conversion diagram at: ○ fixed H$_2$:**11** ratio = 2.7 and residence time 33–59 s, • fixed residence time 42 s and H$_2$:**11** ratio range 2.0–2.7. Data from ref. [136].

Figure 11: Conversion and selectivity vs time-on-stream for the continuous-flow hydrogenation of **11** over Pd@MonoBor catalyst (methanol solution 0.25 mL min^{-1}, H$_2$ 1.35 mL min^{-1} @ 2.2 bar, rt). Reprinted with permission from [136], © 2013 Elsevier.

Figure 12: Continuous-flow hydrogenation reaction of **11** over packed-bed catalysts. Adapted with permission from [137], © 2016 John Wiley and Sons.

latter showing the highest rate of over-hydrogenation to 1-hexanol (**11c**, yield >70%, Figure 12) [136,137,161]. Good yield (68.2%) and productivity (11.4 mol g$_{Pd}^{-1}$ h^{-1}) of **11a** were obtained by packing pellets of a hybrid zirconia/polyvinyl-alcohol matrix with embedded PdNP (Table 2, entry 16) [142].

Catalysts based on PdNP immobilized into the mesopores of hierarchically ordered meso- and macroporous inorganic silica [162] and titania monoliths [163] (Figure 13), were also reported showing moderate yields and remarkable catalyst stability over a period of 24 h (Table 2, entries 17, 18).

The heterogeneous hydrogenation of the parent alkyne substrate 3-phenyl-2-propyn-1-ol (**12**) is of interest because the corresponding alkene, the cinnamyl alcohol (**12a** + **12b**), is used in the formulation of perfumes and other personal care products [164]. The highest selectivity so far reported in batch conditions was observed using dendron-stabilized PdNP catalysts with quinoline additives (97% ene, 98% Z) [165]. The only ex-
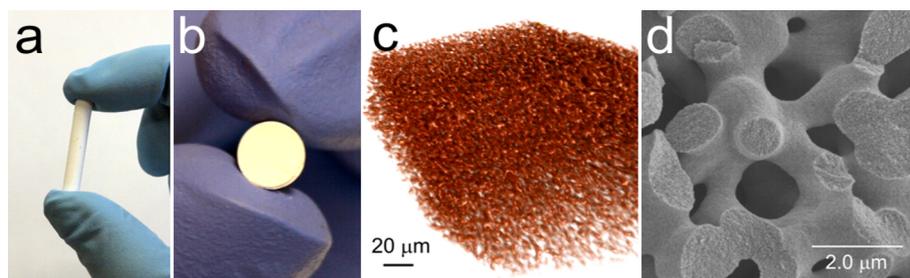
Figure 13: Images of the bimodal TiO$_2$ monolith with well-defined macroporosity: (a, b) optical; (c) X-ray tomography; (d) scanning electron microscopy. Reprinted with permission from [163], © 2012 American Chemical Society.

ample described under continuous flow used the Pd@monobor catalysts to achieve a 96% conversion and 79% selectivity to alkene and 95% to the *Z* isomer (Table 2, entry 19) [136].

2-Butyne-1,4-diol

From an industrial point of view, there is a great interest in the selective semi-hydrogenation reaction of 2-butyne-1,4-diol (**13**) under flow conditions, since *cis*-2-butene-1,4-diol (**13a**) is an important intermediate in the synthesis of antibiotics, vitamins A and B$_6$, several insecticides and antitumoral chemicals [166]. Currently, **13a** is manufactured from **13** in ca. 5000 t/y by a batch process under elevated pressures and/or temperatures, using 0.5% Pd@Al$_2$O$_3$ catalysts doped with Cd, Zn, Bi or Te [167]. On the laboratory scale, it is obtained with high selectivity (70–99% at 80–90% conversion) by the same route, using various supports and additives (including Zn, NH$_3$, pyridine, KOH) [168,169].

Under the conditions of continuous-flow catalysis, Pd@MonoBor provided **13a** in moderate yields (70.2%) and high productivity (3.3 mol g$_{Pd}^{-1}$ h^{-1}) at 294 K, with the formation of butyraldehyde byproducts in addition to the saturated alcohols **13c** and **13d**, as commonly reported in the literature for this substrate (Table 2, entry 20) [136].

Better product purity, but lower productivity, was observed using conventional flow reactors at higher reaction temperatures. Thus, Pd@Al$_2$O$_3$ catalysts, either as wash-coated honeycomb or as egg-shell particles packed-bed setups, resulted in a high ene- and *cis* selectivity (>93%) at 90% conversion at 328 K (Table 2, entries 21, 22) [170]. In that study, a comparison between honeycomb and packed-bed systems was carried out introducing the additional variables of cocurrent downflow contactor (CDC) and a trickle bed reactor (TBR) setups, that hinders a proper rationale of efficiency differences. However, the superior performance of honeycombs was highlighted both in terms of selectivity and productivity to **13a**. Supported Pd@Al$_2$O$_3$ was also reported by the group of A. N. Tsoligkas

where a circular capillary reactor was used in co-current downflow mode under Taylor flow regime (also known as slug and segmented flow) [171]. Selectivity to the *cis* isomer could be tuned by varying the liquid and the gas bubble slug length in that case. The optimized conditions showed slightly lower ene selectivity (91.4%) for this type of reactor. Similarly, commercial 5% Pd@charcoal operating in a slurry-type mode resulted in high selectivity in the presence of KOH and 323 K (Table 2, entry 23) [172].

As an alternative to palladium, a 1 wt % platinum catalyst supported onto calcium carbonate was also reported, however, with no practical advantages over Pd in terms of partial hydrogenation (27% ene selectivity at 78% conversion and 373 K) [173].

Methyl phenylpropiolate and 4-phenyl-3-butyn-2-one

The continuous hydrogenation of internal alkynes in presence of other functional groups other than alcohols was examined, for instance using the carbonyl derivatives methyl phenylpropiolate (**14**) and 4-phenyl-3-butyn-2-one (**15**). Both compounds were hydrogenated using the Pd@Monobor monolithic catalyst under mild conditions with >91% ene selectivity, and *cis* selectivity of 96% and 50%, respectively, at conversions higher than 90% (Table 2, entries 24, 25) [136]. Comparable selectivity results were obtained in batch using the Lindlar catalysts [174,175], Pd onto pumice [176] or onto nitrogen-doped carbon nanofibers [177], in the presence of 2.5–30% amine additives.

A variety of other single alkyne substrates have been hydrogenated under continuous-flow conditions using packed catalysts consisting of immobilized metal complexes. We refer the readers to the specific literature for these systems [178,179].

Substrate scope

An explanation for efficiency differences observed in catalytic flow reactors in relation to the molecular structure and/or sub-

stituent groups of alkynes substrates is not apparent due to a number of reasons.

For example, although a higher selectivity in partial hydrogenation was reported for 1-hexyne (67%, **1**) compared to 1-heptyne (ca. 90%, **2**) under analogous conditions (30% conversion, room temperature, 1 bar H_2, hydrocarbon solvent), hydrogenation experiments were carried out using different catalysts, namely 1% Pd@Al$_2$O$_3$ for **1** [121] and 2% Pd@Al$_2$O$_3$ for **2** [126], and reactor setups. Therefore, any effect of the alkyl chain length is to be considered with care in this case. Studies were reported for the continuous hydrogenation of 1-hexyne and 1-decyne by 16% CeO$_2$@TiO$_2$ catalyst under the same experimental conditions, showing a positive effect of chain length on selectivity (ca. 4% increase at full conversion) [119]. No justification for this evidence was proposed, however, a lower stability of the active site-adsorbed alkene intermediate with increasing steric hindrance may be hypothesized, which results in fewer interactions with hydrogen species, thus in enhanced the selectivity of the process [180].

On the other hand, a slightly negative effect of the alkyl substituent length on the selectivity of 2-methyl-3-butyn-2-ol (**3**) and 3-methyl-1-pentyn-3-ol (**4**) alcohols hydrogenation was demonstrated, for different Pd packed catalysts under the same conditions and substrate conversion [121]. Selectivity for **3** was equal or higher to that of bulkier **4**, irrespective whether Pd(HHDMA)@C, Pd(HHDMA)@TiS, Lindlar or Pd@Al$_2$O$_3$ catalyst was used (Figure 14).

Similarly, the hydrogenation of 2-methyl-3-butyn-2-ol (**3**) and 1,1-diphenyl-2-propyn-1-ol (**6**), bearing methyl and phenyl substituents, respectively, has been explored with a variety of catalytic flow reactors. While direct comparison in terms of substrate conversion is prevented by non-uniformity of reaction conditions, the dearth of a common trend emerges in terms of selectivity at the same level of conversion. An overall picture of experimental findings is summarized in Table 3. Selectivity for **6** is higher than that of **3** for Pd@TiNT and Lindlar packed catalysts, whereas the reverse is observed for monolithic Pd@MonoBor and packed Ag@SiO$_2$. Given the large differences in the reactor systems, no rationale for these data can be hypothesized in the absence of theoretical or mechanistic studies.

Phenylacetylene (**7**), 1-bromo-4-ethynyl benzene (**8**) and 1-ethynyl-4-nitrobenzene (**9**) were hydrogenated using a Pd@C catalyst with trimodal pore-size distribution [152]. The chemoselectivity to the corresponding alkene product showed to follow the order **7** >> **8** > **9**, under the same reaction conditions and comparable conversion. This result may be attributed to the
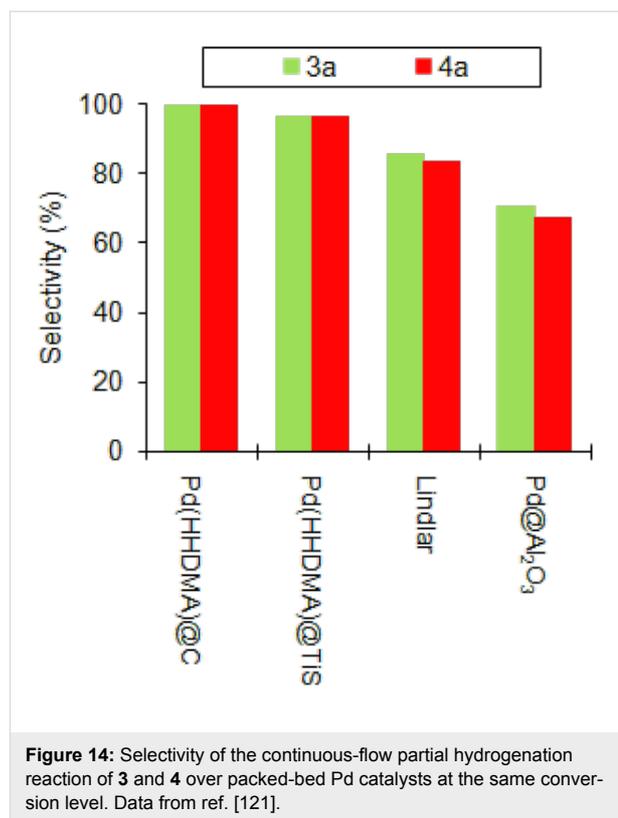
Figure 14: Selectivity of the continuous-flow partial hydrogenation reaction of **3** and **4** over packed-bed Pd catalysts at the same conversion level. Data from ref. [121].

Table 3: Relative selectivity in the continuous-flow partial hydrogenation reaction of **3** and **6** at comparable conversion level.

catalyst	alkyne		ref.
	3	**6**	
0.67% Pd@MonoBor[a]	higher		[136]
0.5% Pd@TiNT[b]		higher	[137]
5% Pd(Pb)@CaCO$_3$[c]		higher	[123]
16% CeO$_2$@TiO$_2$[d]	equal		[123]
1.3% Ag@SiO$_2$[e]	higher		[123]
1% Au@TiO$_2$[e]	equal		[123]

[a]ca. 90% conversion, 293 K, ca. 1.5 bar H_2. [b]ca. 75% conversion, 293 K, ca. 2.7 bar H_2. [c]30% conversion, 293 K, 1 bar H_2. [d]30% conversion, 413 K, 40 bar H_2. [e]30% conversion, 373 K, 10 bar H_2.

increasing stabilization of the intermediate alkene due to the electron-withdrawing properties of the alkyne substituents (nitro > bromo >> unsubstituted).

Data were reported for the partial hydrogenation of 3-hexyne (**10**) and the parent alcohol 3-hexyn-1-ol (**11**) by mean of Lindlar catalysts (Table 2, entries 2 and 13) [119,136]. At comparable substrate conversion, the selectivity was significantly lower for the latter. Based on DFT calculations, a similar effect was justified for the hydrogenation of alkynols in terms

of strong adsorption of alcohols on the Pd surface, that increases the contact time with catalyst, thereby resulting in lower selectivity [121].

The continuous hydrogenation of 3-phenyl-2-propyn-1-ol (**12**), methyl phenylpropiolate (**14**) and 4-phenyl-3-butyn-2-one (**15**), bearing -CH$_2$OH, -CO$_2$CH$_3$ and -COCH$_3$ substituents at the 1-position of phenylacetylene moiety, respectively, was investigated using the Pd@MonoBor catalyst [136]. Although a conversion and productivity trend cannot be highlighted due to the lack of experimental data under the same reaction conditions (concentration, H$_2$:substrate molar ratio), the ene selectivity showed to decrease in the order **15** > **14** > **12** at comparable conversions (90–96%), that can be related to the stabilization of the alkene product by the deactivating keto groups, despite a contribution of adsorption energy of alcohol group cannot be ruled out.

Conclusion

The selective, partial hydrogenation reaction of C≡C bonds is a process of high relevance in the current manufacturing technology of a variety of intermediates for the fine-chemical industry. The conventional batch processes employing Pd catalysts are often problematic because of selectivity issues, need of toxic additives, high metal loadings and limited catalyst resistance. Ever increasing environmental and economic constraints have boosted the development of innovative catalytic materials and processes with improved performance and lower environmental impact.

Great advancements have been achieved in the recent years in the design of continuous-flow systems for alkynes partial hydrogenation, showing efficiency that often surpass that of the industrial protocols. Two main elements of comparison can be highlighted.

Batch versus flow setup. While experimental comparison can be easily carried out, continuous-flow reactors are practically advantageous with respect to the corresponding batch systems in the instance that the same catalyst produces at least the same amount of desired product per mole of metal and unit time, under similar reaction conditions. Most examples illustrated above show that this is indeed the case. Selectivities comparable to that of batch systems have been achieved using flow reactors, with the unquestionable advantage that no additives are usually required. Higher activity of continuous-flow versus stirred-tank batch reactors was attributed to faster molecular flow to and from the active sites, as a consequence of both the larger surface area of the catalyst in contact with the reagents (convective mass transfer), and a more efficient permeation of fluids through the material (diffusive mass transfer), which

facilitates a reaction transition from a diffusion-controlled to kinetic-limited regime [163,181]. The non-accumulation of co-products adsorbed on the catalyst surface may also significantly contribute to the minimization of active site inhibition under the conditions of continuous flow [27].

Flow reactor design. Performance differences among different continuous-flow reactor designs are difficult to rationalize due to the number of additional variables related to the catalyst involved, which include:

- the role played by the supported metal, e.g., type, loading, MNP size, shape and location [182,183]),

- the role played by the support material, e.g., acid/base properties [184,185], morphology, grain size [186], porosity [187], strong metal–support interactions, swelling propensity [188]). In propyne hydrogenation, for instance, catalyst resistance was shown to decrease with increasing acidity of the support [189].

In order to establish a proper comparison, the experimental conditions should also be reproduced with care. In alkynes partial hydrogenation, the higher the conversion, the lower is the selectivity. Therefore, selectivity of different systems shall be compared at the same conversion level, or better, selectivity/conversion diagrams shall be obtained by investigation of appropriate operating windows in relation to reagents flow rates, residence time, hydrogen/substrate ratio. Comparison between different systems requires a systematic study enucleating the contribution of each of the above factors, which is usually hampered by the lack or inhomogeneity of experimental data. In practice, to the best of our knowledge, no such analysis was carried out comparing the same catalyst under analogous flow reaction conditions in different reactor setups for liquid phase alkynes hydrogenation. Comparison between monolithic and packed (crushed material) arrangements was reported for Pd@TiO$_2$ monolith catalyst and cyclohexene hydrogenation [163].

Despite no general conclusion can be drawn, structured monolithic reactors have usually shown superior performance with respect of packed-bed systems [162,163]. Due to their high permeability, monolithic materials allow for high substrate flow rates, weight hourly space velocities and low H$_2$ back-pressures. As a consequence, the residence time of the intermediate alkene formed by hydrogenation is very short and it is continuously removed from the active sites with limited chance of further reduction. This results in an enhanced selectivity and productivity of semi-hydrogenation compound. When conventional (packed) mesoporous heterogeneous catalysts are used, the substrate undergoes a significant interaction with the metal sites

inside the pores. The intermediate alkene is not swept away fast enough and it can react again before leaving the catalyst, thus resulting in a preferential formation of over-hydrogenation product at the same conversion level [190].

The activity of Pd-based catalysts is acknowledged to increase with decreasing particle size [191,192]. However, controversial statements can be found in the literature regarding the catalyst selectivity [193,194]. In the case of 2-methyl-3-butyn-2-ol (**3**) hydrogenation, the optimal catalyst in terms of desired partial hydrogenation productivity was established to be based on cubic PdNP of 3–5 nm length [195]. The combination of small metal particle size (high activity) and high flow rates (short contact time), as, e.g., in 1D materials or macroporous monoliths, seems, therefore, beneficial for continuous-flow partial hydrogenation of alkynes. In conclusion, the identification of the most effective and versatile catalytic system is difficult, since the choice is ruled by a variety factors to be evaluated, including selected performance indicators (product purity, productivity) and technical/economic parameters (cost and lifetime of the catalyst, reproducibility, reaction conditions, e.g., temperature, hydrogen pressure).

References

1. Pollak, P. *Fine Chemicals: The Industry and the Business;* Wiley-Interscience: Hoboken, 2007.
2. Chen, B.; Dingerdissen, U.; Krauter, J. G. E.; Lansink Rotgerink, H. G. J.; Möbus, K.; Ostgard, D. J.; Panster, P.; Riermeier, T. H.; Seebald, S.; Tacke, T.; Trauthwein, H. *Appl. Catal., A* **2005,** *280,* 17–46. doi:10.1016/j.apcata.2004.08.025
3. Nishimura, S. *Handbook of Heterogeneous Catalytic Hydrogenation for Organic Synthesis;* Wiley: New York, 2001; p 148.
4. Molnár, A.; Sárkány, A.; Varga, M. *J. Mol. Catal. A* **2001,** *173,* 185–221. doi:10.1016/S1381-1169(01)00150-9
5. Borodzínski, A.; Bond, G. C. *Catal. Rev.: Sci. Eng.* **2006,** *48,* 91–144. doi:10.1080/01614940500364909
6. King, A. O.; Larsen, R. D.; Negishi, E.-i. Palladium-Catalyzed Heterogeneous Hydrogenation. In *Handbook of Organopalladium Chemistry for Organic Synthesis;* Negishi, E., Ed.; Wiley: New York, 2002; pp 2719 ff. doi:10.1002/0471212466.ch124
7. Vilé, G.; Albani, D.; Almora-Barrios, N.; López, N.; Pérez-Ramírez, J. *ChemCatChem* **2016,** *8,* 21–33. doi:10.1002/cctc.201501269
8. Lindlar, H. *Helv. Chim. Acta* **1952,** *35,* 446–450. doi:10.1002/hlca.19520350205
9. Lindlar, H.; Dubuis, R. *Org. Synth.* **1966,** *46,* 89. doi:10.15227/orgsyn.046.0089
10. García-Mota, M.; Gómez-Díaz, J.; Novell-Leruth, G.; Vargas-Fuentes, C.; Bellarosa, L.; Bridier, B.; Pérez-Ramírez, J.; López, N. *Theor. Chem. Acc.* **2011,** *128,* 663–673. doi:10.1007/s00214-010-0800-0
11. McEwen, A. B.; Guttieri, M. J.; Maier, W. F.; Laine, R. M.; Shvo, Y. *J. Org. Chem.* **1983,** *48,* 4436–4438. doi:10.1021/jo00171a069
12. Jung, A.; Jess, A.; Schubert, T.; Schütz, W. *Appl. Catal., A* **2009,** *362,* 95–105. doi:10.1016/j.apcata.2009.04.026
13. Campos, K. R.; Cai, D.; Journet, M.; Kowal, J. J.; Larsen, R. D.; Reider, P. J. *J. Org. Chem.* **2001,** *66,* 3634–3635. doi:10.1021/jo015514a
14. Studt, F.; Abild-Pedersen, F.; Bligaard, T.; Sørensen, R. Z.; Christensen, C. H.; Nørskov, J. K. *Science* **2008,** *320,* 1320–1322. doi:10.1126/science.1156660
15. Armbrüster, M.; Kovnir, K.; Friedrich, M.; Teschner, D.; Wowsnick, G.; Hahne, M.; Gille, P.; Szentmiklósi, L.; Feuerbacher, M.; Heggen, M.; Girgsdies, F.; Rosenthal, D.; Schlögl, R.; Grin, Y. *Nat. Mater.* **2012,** *11,* 690–693. doi:10.1038/nmat3347
16. Stankiewicz, A. I.; Moulijn, J. A. *Chem. Eng. Prog.;* 2000; Vol. January, pp 22–34.
17. Wiles, C.; Watts, P. *Green Chem.* **2014,** *16,* 55–62. doi:10.1039/C3GC41797B
18. Ricciardi, R.; Huskens, J.; Verboom, W. *ChemSusChem* **2015,** *8,* 2586–2605. doi:10.1002/cssc.201500514
19. Myers, R. M.; Fitzpatrick, D. E.; Turner, R. M.; Ley, S. V. *Chem. – Eur. J.* **2014,** *20,* 12348–12366. doi:10.1002/chem.201402801
20. Lucarelli, C.; Vaccari, A. *Green Chem.* **2011,** *13,* 1941–1949. doi:10.1039/c0gc00760a
21. Andrews, I.; Dunn, P.; Hayler, J.; Hinkley, B.; Hughes, D.; Kaptein, B.; Lorenz, K.; Mathew, S.; Rammeloo, T.; Wang, L.; Wells, A.; White, T. D. *Org. Process Res. Dev.* **2011,** *15,* 22–30. doi:10.1021/op1003105
22. Sheldon, R. A.; Arends, I. W. C. E.; Hanefeld, U. *Green Chemistry and Catalysis;* Wiley-VCH: Weinheim, 2007. doi:10.1002/9783527611003
23. Baxendale, I. R. *J. Chem. Technol. Biotechnol.* **2013,** *88,* 519–552. doi:10.1002/jctb.4012
24. Newman, S. G.; Jensen, K. F. *Green Chem.* **2013,** *15,* 1456–1472. doi:10.1039/c3gc40374b
25. Baumann, M.; Baxendale, I. R. *Beilstein J. Org. Chem.* **2015,** *11,* 1194–1219. doi:10.3762/bjoc.11.134
26. Jiménez-González, C.; Poechlauer, P.; Broxterman, Q. B.; Yang, B.-S.; am Ende, D.; Baird, J.; Bertsch, C.; Hannah, R. E.; Dell'Orco, P.; Noorman, H.; Yee, S.; Reintjens, R.; Wells, A.; Massonneau, V.; Manley, J. *Org. Process Res. Dev.* **2011,** *15,* 900–911. doi:10.1021/op100327d
27. Anderson, N. G. *Org. Process Res. Dev.* **2012,** *16,* 852–869. doi:10.1021/op200347k
28. Cossar, P. J.; Hizartzidis, L.; Simone, M. I.; McCluskey, A.; Gordon, C. P. *Org. Biomol. Chem.* **2015,** *13,* 7119–7130. doi:10.1039/C5OB01067E
29. Crespo-Quesada, M.; Cárdenas-Lizana, F.; Dessimoz, A.-L.; Kiwi-Minsker, L. *ACS Catal.* **2012,** *2,* 1773–1786. doi:10.1021/cs300284r
30. Bond, G. C. *Metal-catalysed Reactions of Hydrocarbons;* Springer: New York, 2005; p 292.
31. Nikolaev, S. A.; Zanaveskin, L. N.; Smirnov, V. V.; Averyanov, V. A.; Zanaveskin, K. L. *Russ. Chem. Rev.* **2009,** *78,* 231–247. doi:10.1070/RC2009v078n03ABEH003893
32. Bos, A. N. R.; Westerterp, K. R. *Chem. Eng. Process.* **1993,** *32,* 1–7. doi:10.1016/0255-2701(93)87001-B
33. Natividad, R.; Cruz-Olivares, J.; Fishwick, R. P.; Wood, J.; Winterbottom, J. M. *Fuel* **2007,** *86,* 1304–1312. doi:10.1016/j.fuel.2006.12.005
34. Guo, X. C.; Madix, R. J. *J. Catal.* **1995,** *155,* 336–344. doi:10.1006/jcat.1995.1215

35. Studt, F.; Abild-Pedersen, F.; Bligaard, T.; Sørensen, R. Z.; Christensen, C. H.; Nørskov, J. K. *Angew. Chem., Int. Ed.* **2008,** *47,* 9299–9302. doi:10.1002/anie.200802844

36. Tysoe, W. T.; Nyberg, G. L.; Lambert, R. M. *J. Chem. Soc., Chem. Commun.* **1983,** 623–625. doi:10.1039/c39830000623

37. López, N.; Vargas-Fuentes, C. *Chem. Commun.* **2012,** *48,* 1379–1391. doi:10.1039/C1CC14922A

38. Bridier, B.; López, N.; Pérez-Ramírez, J. *Dalton Trans.* **2010,** *39,* 8412–8419. doi:10.1039/c0dt00010h

39. García-Mota, M.; Bridier, B.; Pérez-Ramírez, J.; López, N. *J. Catal.* **2010,** *273,* 92–102. doi:10.1016/j.jcat.2010.04.018

40. Jakobsen, H. A. *Chemical Reactor Modeling;* Springer: Berlin, 2008.

41. Darvas,, F.; Hessel, V.; Dorman, G., Eds. *Flow Chemistry;* De Gruyter: Berlin, 2014; Vol. 1, Fundamentals.

42. Oger, C.; Balas, L.; Durand, T.; Galano, J.-M. *Chem. Rev.* **2013,** *113,* 1313–1350. doi:10.1021/cr3001753

43. Joannet, E.; Horny, C.; Kiwi-Minsker, L.; Renken, A. *Chem. Eng. Sci.* **2002,** *57,* 3453–3460. doi:10.1016/S0009-2509(02)00215-4

44. Lindlar, H.; Dubuis, R. *Org. Synth. Coll.;* 1973; Vol. 5, p 880.

45. Kiwi-Minsker, L.; Crespo-Quesada, M. *Chimia* **2011,** *65,* 699–703. doi:10.2533/chimia.2011.699

46. Guo, C.; Lu, X. *Tetrahedron Lett.* **1991,** *32,* 7549–7552. doi:10.1016/0040-4039(91)80531-A

47. Nicolaou, K. C.; Xu, J.-Y.; Kim, S.; Ohshima, T.; Hosokawa, S.; Pfefferkorn, J. *J. Am. Chem. Soc.* **1997,** *119,* 11353–11354. doi:10.1021/ja973000g

48. Hamprecht, D.; Josten, J.; Steglich, W. *Tetrahedron* **1996,** *52,* 10883–10902. doi:10.1016/0040-4020(96)00629-1

49. Knight, D. W.; Little, P. B. *Tetrahedron Lett.* **1998,** *39,* 5105–5108. doi:10.1016/S0040-4039(98)00937-X

50. Nowak, W.; Gerlach, H. *Liebigs Ann. Chem.* **1993,** 153–159. doi:10.1002/jlac.199319930128

51. Organ, M. G.; Ghasemi, H. *J. Org. Chem.* **2004,** *69,* 695–700. doi:10.1021/jo035376k

52. Gueugnot, S.; Alami, M.; Linstrumelle, G.; Mambu, L.; Petit, Y.; Larchevêque, M. *Tetrahedron* **1996,** *52,* 6635–6646. doi:10.1016/0040-4020(96)00316-X

53. Dobson, N. A.; Eglinton, G.; Krishnamurthi, M.; Raphael, R. A.; Willis, R. G. *Tetrahedron* **1961,** *16,* 16–24. doi:10.1016/0040-4020(61)80050-1

54. Winterbottom, J. M.; Marwan, H.; Stitt, E. H.; Natividad, R. *Catal. Today* **2003,** *79–80,* 391–399. doi:10.1016/S0920-5861(03)00069-5

55. Middleton, R. L.; Lambert, R. M. *Catal. Lett.* **1999,** *59,* 15–20. doi:10.1023/A:1019027311804

56. Protasova, L. N.; Rebrov, E. V.; Choy, K. L.; Pung, S. Y.; Engels, V.; Cabaj, M.; Wheatley, A. E. H.; Schouten, J. C. *Catal. Sci. Technol.* **2011,** *1,* 768–777. doi:10.1039/c1cy00074h

57. Hamilton, C. A.; Jackson, S. D.; Kelly, G. J.; Spence, R.; de Bruin, D. *Appl. Catal., A* **2002,** *237,* 201–209. doi:10.1016/S0926-860X(02)00332-0

58. Vilé, G.; Baudouin, D.; Remediakis, I. N.; Copéret, C.; López, N.; Pérez-Ramírez, J. *ChemCatChem* **2013,** *5,* 3750–3759. doi:10.1002/cctc.201300569

59. Nikolaev, S. A.; Smirnov, V. V. *Catal. Today* **2009,** *147,* S336–S341. doi:10.1016/j.cattod.2009.07.032

60. Tew, M. W.; Emerich, H.; van Bokhoven, J. A. *J. Phys. Chem. C* **2011,** *115,* 8457–8465. doi:10.1021/jp1103164

61. Baber, A. E.; Tierney, H. L.; Lawton, T. J.; Sykes, E. C. H. *ChemCatChem* **2011,** *3,* 607–614. doi:10.1002/cctc.201000309

62. Vilé, G.; Bridier, B.; Wichert, J.; Pérez-Ramírez, J. *Angew. Chem., Int. Ed.* **2012,** *51,* 8620–8623. doi:10.1002/anie.201203675

63. Kyriakou, G.; Boucher, M. B.; Jewell, A. D.; Lewis, E. A.; Lawton, T. J.; Baber, A. E.; Tierney, H. L.; Flytzani-Stephanopolous, M.; Sykes, E. C. H. *Science* **2012,** *335,* 1209–1212. doi:10.1126/science.1215864

64. Liguori, F.; Moreno-Marrodan, C.; Barbaro, P. *Chin. J. Catal.* **2015,** *36,* 1157–1169. doi:10.1016/S1872-2067(15)60865-8

65. Spee, M. P. R.; Boersma, J.; Meijer, M. D.; Slagt, M. Q.; van Koten, G.; Geus, J. W. *J. Org. Chem.* **2001,** *66,* 1647–1656. doi:10.1021/jo001246p

66. Nijhuis, T. A.; van Koten, G.; Kapteijn, F.; Moulijn, J. A. *Catal. Today* **2003,** *79–80,* 315–321. doi:10.1016/S0920-5861(03)00055-5

67. Shen, R.; Chen, T.; Zhao, Y.; Qiu, R.; Zhou, Y.; Yin, S.; Wang, X.; Goto, M.; Han, L.-B. *J. Am. Chem. Soc.* **2011,** *133,* 17037–17044. doi:10.1021/ja2069246

68. Derrien, M. L. *Stud. Surf. Sci. Catal.* **1986,** *27,* 613–666. doi:10.1016/S0167-2991(08)65364-1

69. Mori, A.; Miyakawa, Y.; Ohashi, E.; Haga, T.; Maegawa, T.; Sajiki, H. *Org. Lett.* **2006,** *8,* 3279–3281. doi:10.1021/ol061147j

70. Mitsudome, T.; Takahashi, Y.; Ichikawa, S.; Mizugaki, T.; Jitsukawa, K.; Kaneda, K. *Angew. Chem., Int. Ed.* **2013,** *52,* 1481–1485. doi:10.1002/anie.201207845

71. Takahashi, Y.; Hashimoto, N.; Hara, T.; Shimazu, S.; Mitsudome, T.; Mizugaki, T.; Jitsukawa, K.; Kaneda, K. *Chem. Lett.* **2011,** *40,* 405–407. doi:10.1246/cl.2011.405

72. McQuillin, F. J.; Ord, W. O.; Simpson, P. L. *J. Chem. Soc.* **1963,** 5996–6003. doi:10.1039/jr9630005996

73. Semagina, N.; Kiwi-Minsker, L. *Catal. Rev.: Sci. Eng.* **2009,** *51,* 147–217. doi:10.1080/01614940802480379

74. Wegner, J.; Ceylan, S.; Kirschning, A. *Adv. Synth. Catal.* **2012,** *354,* 17–57. doi:10.1002/adsc.201100584

75. Webb, D.; Jamison, T. F. *Chem. Sci.* **2010,** *1,* 675–680. doi:10.1039/c0sc00381f

76. Levenspiel, O. *Chemical Reaction Engineering,* 3rd ed.; John Wiley & Sons: New York, 1999.

77. Goettmann, F.; Sanchez, C. *J. Mater. Chem.* **2007,** *17,* 24–30. doi:10.1039/B608748P

78. Pan, X.; Bao, X. *Acc. Chem. Res.* **2011,** *44,* 553–562. doi:10.1021/ar100160t

79. Wegner, J.; Ceylan, S.; Kirschning, A. *Chem. Commun.* **2011,** *47,* 4583–4592. doi:10.1039/c0cc05060a

80. Irfan, M.; Glasnov, T. N.; Kappe, C. O. *ChemSusChem* **2011,** *4,* 300–316. doi:10.1002/cssc.201000354

81. Kockmann, N.; Gottsponer, M.; Zimmermann, B.; Roberge, D. M. *Chem. – Eur. J.* **2008,** *14,* 7470–7477. doi:10.1002/chem.200800707

82. Kashid, M. N.; Kiwi-Minsker, L. *Ind. Eng. Chem. Res.* **2009,** *48,* 6465–6485. doi:10.1021/ie8017912

83. Harriot,, P. *Chemical Reactors Design;* Marcel Dekker: New York, 2002. doi:10.1201/9780203910238

84. Munirathinam, R.; Huskens, J.; Verboom, W. *Adv. Synth. Catal.* **2015,** *357,* 1093–1123. doi:10.1002/adsc.201401081

85. Jähnisch, K.; Hessel, V.; Löwe, H.; Baerns, M. *Angew. Chem., Int. Ed.* **2004,** *43,* 406–446. doi:10.1002/anie.200300577

86. Kobayashi, J.; Mori, Y.; Okamoto, K.; Akiyama, R.; Ueno, M.; Kitamori, T.; Kobayashi, S. *Science* **2004,** *304,* 1305–1308. doi:10.1126/science.1096956

87. Hornung, C. H.; Hallmark, B.; Mackley, M. R.; Baxendale, I. R.; Ley, S. V. *Adv. Synth. Catal.* **2010,** *352,* 1736–1745. doi:10.1002/adsc.201000139

88. Bogdan, A. R.; Mason, B. P.; Sylvester, K. T.; McQuade, D. T. *Angew. Chem.* **2007,** *119,* 1728–1731. doi:10.1002/ange.200603854

89. Kolev, N. *Packed bed columns: for absorption, desorption, rectification and direct heat transfer;* Elsevier: Amsterdam, 2006.

90. Fogler, H. S. *Essentials of Chemical Reaction Engineering;* Prentice Hall: Upper Saddle River, 2011.

91. Corain, B.; Jerabek, K.; Centomo, P.; Canton, P. *Angew. Chem., Int. Ed.* **2004,** *43,* 959–962. doi:10.1002/anie.200352640

92. Bönnemann, H.; Richards, R. M. *Eur. J. Inorg. Chem.* **2001,** 2455–2480. doi:10.1002/1099-0682(200109)2001:10<2455::AID-EJIC2455>3.0.CO;2-Z

93. Roucoux, A.; Schulz, J.; Patin, H. *Chem. Rev.* **2002,** *102,* 3757–3778. doi:10.1021/cr010350j

94. Lewera, A.; Timperman, L.; Roguska, A.; Alonso-Vante, N. *J. Phys. Chem. C* **2011,** *115,* 20153–20159. doi:10.1021/jp2068446

95. Kim, W.-J.; Moon, S. H. *Catal. Today* **2012,** *185,* 2–16. doi:10.1016/j.cattod.2011.09.037

96. European Agency for the Evaluation of Medicinal Products, *Note for guidance on specification limits for residues of metal catalysts,* EMEA/CHMP/SWP/4446/2000, February 2008.

97. Baumann, M.; Baxendale, I. R.; Ley, S. V. *Mol. Diversity* **2011,** *15,* 613–630. doi:10.1007/s11030-010-9282-1

98. Cybulski, A.; Moulijn, J. A. *Structured Catalysts and Reactors;* Marcel Dekker Ltd.: New York, 2005; p 19. doi:10.1201/9781420028003

99. Heck, R. M.; Gulati, S.; Farrauto, R. J. *Chem. Eng. J.* **2001,** *82,* 149–156. doi:10.1016/S1385-8947(00)00365-X

100. Tomašić, V.; Jović, F. *Appl. Catal., A* **2006,** *311,* 112–121. doi:10.1016/j.apcata.2006.06.013

101. Nativibad, R.; Kulkarni, R.; Nuithitikul, K.; Raymahasay, S.; Wood, J.; Winterbottom, J. M. *Chem. Eng. Sci.* **2004,** *59,* 5431–5438. doi:10.1016/j.ces.2004.09.011

102. Alemán, J.; Chadwick, A. V.; He, J.; Hess, M.; Horie, K.; Jones, R. G.; Kratochvíl, P.; Meisel, I.; Mita, I.; Moad, G.; Penczek, S.; Stepto, R. F. T. *Pure Appl. Chem.* **2007,** *79,* 1801–1829. doi:10.1351/pac200779101801

103. Nakanishi, K.; Tanaka, N. *Acc. Chem. Res.* **2007,** *40,* 863–873. doi:10.1021/ar600034p

104. Sachse, A.; Galarneau, A.; Coq, B.; Fajula, F. *New J. Chem.* **2011,** *35,* 259–264. doi:10.1039/c0nj00965b

105. Stankiewicz, A. *Chem. Eng. Sci.* **2001,** *56,* 359–364. doi:10.1016/S0009-2509(00)00236-0

106. Sachse, A.; Galarneau, A.; Fajula, F.; Di Renzo, F.; Creux, P.; Coq, B. *Microporous Mesoporous Mater.* **2011,** *140,* 58–68. doi:10.1016/j.micromeso.2010.10.044

107. Nakanishi, K. In *Hierarchically Structured Porous Materials;* Su, B.; Sanchez, C.; Yang, X., Eds.; Chapter 8; Wiley-VCH: Weinheim, 2012.

108. Feinle, A.; Elsaesser, M. S.; Hüsing, N. *Chem. Soc. Rev.* **2016,** *45,* 3377–3399. doi:10.1039/C5CS00710K

109. Galarneau, A.; Sachse, A.; Said, B.; Pelisson, C.-H.; Boscaro, P.; Brun, N.; Courtheoux, L.; Olivi-Tran, N.; Coasne, B.; Fajula, F. *C. R. Chim.* **2016,** *19,* 231–247. doi:10.1016/j.crci.2015.05.017

110. Grano, A. J.; Sayler, F. M.; Smått, J. H.; Bakker, M. G. *J. Porous Mater.* **2014,** *21,* 1113–1122. doi:10.1007/s10934-014-9861-0

111. Nakanishi, K. *J. Porous Mater.* **1997,** *4,* 67–112. doi:10.1023/A:1009627216939

112. Galarneau, A.; Abid, Z.; Said, B.; Didi, Y.; Szymanska, K.; Jarzębski, A.; Tancret, F.; Hamaizi,, H.; Bengueddach, A.; Di Renzo, F.; Fajula, F. *Inorganics* **2016,** *4,* 9–34. doi:10.3390/inorganics4020009

113. Whitaker, S. *Ind. Eng. Chem.* **1969,** *61,* 14–28. doi:10.1021/ie50720a004

114. Nauman, E. In *Handbook of Industrial Mixing: Science and Practice;* Paul, E. L.; Atiemo-Obeng, V. A.; Kresta, S. M., Eds.; Chapter 1; Wiley: New York, 2003.

115. Pletcher, D.; Walsh, F. *Industrial Electrochemistry;* Springer: London, 1990; p 83.

116. Redshaw, C.; Tang, Y. *Chem. Soc. Rev.* **2012,** *41,* 4484–4510. doi:10.1039/c2cs35028a

117. Krentsel, B. A.; Kissin, Y. V.; Kleiner, V. J.; Stotskaya, L. L. *Polymers and Copolymers of Higher Alpha-Olefins;* Carl Hanser Verlag: Munich, 1997.

118. Van Puyvelde, P.; Velankar, S.; Moldenaers, P. *Curr. Opin. Colloid Interface Sci.* **2001,** *6,* 457–463. doi:10.1016/S1359-0294(01)00113-3

119. Vilé, G.; Wrabetz, S.; Floryan, L.; Schuster, M. E.; Girgsdies, F.; Teschner, D.; Pérez-Ramírez, J. *ChemCatChem* **2014,** *6,* 1928–1934. doi:10.1002/cctc.201402124

120. Kirby, F.; Moreno-Marrodan, C.; Baán, Z.; Bleeker, B. F.; Barbaro, P.; Berben, P. H.; Witte, P. T. *ChemCatChem* **2014,** *6,* 2904–2909. doi:10.1002/cctc.201402310

121. Vilé, G.; Almora-Barrios, N.; Mitchell, S.; López, N.; Pérez-Ramírez, J. *Chem. – Eur. J.* **2014,** *20,* 5926–5937. doi:10.1002/chem.201304795

122. Vilé, G.; Albani, D.; Nachtegaal, M.; Chen, Z.; Donsova, D.; Antonietti, M.; López, N.; Pérez-Ramírez, J. *Angew. Chem., Int. Ed.* **2015,** *54,* 11265–11269. doi:10.1002/anie.201505073

123. Vilé, G.; Pérez-Ramírez, J. *Nanoscale* **2014,** *6,* 13476–13482. doi:10.1039/C4NR02777A

124. Chen, Z.; Pronkin, S.; Fellinger, T.-P.; Kailasam, K.; Vilé, G.; Albani, D.; Krumeich, F.; Leary, R.; Barnard, J.; Thomas, J. M.; Perez-Ramírez, J.; Antonietti, M.; Dontsova, D. *ACS Nano* **2016,** *10,* 3166–3175. doi:10.1021/acsnano.5b04210

125. Bridger, R. F. Alpha-olefin polymers as lubricant viscosity properties improvers (Mobil Oil Corporation). U.S. Patent US4613712 (A) , Sept 23, 1986.

126. Al-Herz, M.; Simmons, M. J. H.; Wood, J. *Ind. Eng. Chem. Res.* **2012,** *51,* 8815–8825. doi:10.1021/ie201955m

127. 3-Buten-2-ol, 2-methyl, CAS No.: 115-18-4, UNEP Publications, International Programme on Chemical Safety (IPCS).

128. Baglai, A. K.; Gurarii, L. L.; Kuleshov, G. G. *J. Chem. Eng. Data* **1988,** *33,* 512–518. doi:10.1021/je00054a035

129. Semagina, N.; Renken, A.; Laub, D.; Kiwi-Minsker, L. *J. Catal.* **2007,** *246,* 308–314. doi:10.1016/j.jcat.2006.12.011

130. Crespo-Quesada, M.; Grasemann, M.; Semagina, N.; Renken, A.; Kiwi-Minsker, L. *Catal. Today* **2009,** *147,* 247–254. doi:10.1016/j.cattod.2008.09.035

131. Rebrov, E. V.; Klinger, E. A.; Berenguer-Murcia, A.; Sulman, E. M.; Schouten, J. C. *Org. Process Res. Dev.* **2009,** *13,* 991–998. doi:10.1021/op900085b

132. Okhlopkova, L. B.; Kerzhentsev, M. A.; Ismagilov, Z. R. *Kinet. Catal.* **2016,** *57,* 497–503. doi:10.1134/S0023158416040091

133. Liguori, F.; Coiai, S.; Passaglia, E.; Barbaro, P. *Macromolecules* **2013,** *46,* 5423–5433. doi:10.1021/ma401120v

134. Illner, P.; Puchta, R.; Heinemann, F. W.; van Eldik, R. *Dalton Trans.* **2009,** 2795–2801. doi:10.1039/b820940e

135. Nieto, S.; Pérez, J.; Riera, L.; Riera, V.; Miguel, D. *Chem. Commun.* **2009,** 3279–3281. doi:10.1039/b823460d

136. Liguori, F.; Barbaro, P. *J. Catal.* **2014,** *311,* 212–220. doi:10.1016/j.jcat.2013.11.027

137. Linares, N.; Moreno-Marrodan, C.; Barbaro, P. *ChemCatChem* **2016,** *8,* 1001–1011. doi:10.1002/cctc.201501126

138. Burwell, R. L., Jr. *Pure Appl. Chem.* **1976,** *46,* 71–90. doi:10.1351/pac197646010071
IUPAC, *Manual of Symbols and Terminology for Physicochemical Quantities and Units* - Appendix II.

139. Semagina, N.; Grasemann, M.; Xanthopoulos, N.; Renken, A.; Kiwi-Minsker, L. *J. Catal.* **2007,** *251,* 213–222. doi:10.1016/j.jcat.2007.06.028

140. Centi, G.; Perathoner, S. *CATTECH* **2003,** *7,* 78–89. doi:10.1023/A:1023849024050

141. Grasemann, M.; Renken, A.; Kashid, M.; Kiwi-Minsker, L. *Chem. Eng. Sci.* **2010,** *65,* 364–371. doi:10.1016/j.ces.2009.06.063

142. Liguori, F.; Barbaro, P.; Sawa, H. *Appl. Catal., A* **2014,** *488,* 58–65. doi:10.1016/j.apcata.2014.09.029

143. Bakker, J. J. W.; Zieverink, M. M. P.; Reintjens, R. W. E. G.; Kapteijn, F.; Moulijn, J. A.; Kreutzer, M. T. *ChemCatChem* **2011,** *3,* 1155–1157. doi:10.1002/cctc.201100044

144. Carter, C. F.; Lange, H.; Sakai, D.; Baxendale, I. R.; Ley, S. V. *Chem. – Eur. J.* **2011,** *17,* 3398–3405. doi:10.1002/chem.201003148

145. Besson, M.; Gallezot, P. *Catal. Today* **2003,** *81,* 547–559. doi:10.1016/S0920-5861(03)00153-6

146. Nishio, R.; Sugiura, M.; Kobayashi, S. *Org. Biomol. Chem.* **2006,** *4,* 992–995. doi:10.1039/b517181d

147. Mastalir, A.; Király, Z.; Berger, F. *Appl. Catal., A* **2004,** *269,* 161–168. doi:10.1016/j.apcata.2004.04.012

148. Starodubtseva, E. V.; Vinogradov, M. G.; Turova, O. V.; Bumagin, N. A.; Rakov, E. G.; Sokolov, V. I. *Catal. Commun.* **2009,** *10,* 1441–1442. doi:10.1016/j.catcom.2009.03.012

149. Tschan, R.; Wandeler, R.; Schneider, M. S.; Schubert, M. M.; Baiker, A. *J. Catal.* **2001,** *204,* 219–229. doi:10.1006/jcat.2001.3364

150. Rebrov, E.V.; Berenguer-Murcia, A.; Skelton, H. E.; Johnson, B. F. G.; Schouten, J.C. *10th International Conference on Microreaction Technology*, New Orleans, Louisiana, April 2008.

151. Li, S.-S.; Tao, L.; Wang, F.-Z.-R.; Liu, Y.-M.; Cao, Y. *Adv. Synth. Catal.* **2016,** *358,* 1410–1416. doi:10.1002/adsc.201501183

152. Fan, X.; Sans, V.; Sharma, S. K.; Plucinski, P. K.; Zaikovskii, V. A.; Wilson, K.; Tennison, S. R.; Kozynchenko, A.; Lapkin, A. A. *Catal. Sci. Technol.* **2016,** *6,* 2387–2395. doi:10.1039/C5CY01401H

153. Warr, J.; Fraser, S.; Gouault, O. Sensitive skin perfumes (Takasago Perfumery Co., Ltd.). Eur. Pat. Appl. EP 1964542, Sept 3, 2008.

154. Choi, J. Y.; Jeon, B. B.; Seo, H. J. Perfum composition for expressing the fragrance of green tea flower (Amorepacific Corp.). WO patent WO 2007055493, May 18, 2007.

155. Bönnemann, H.; Brijoux, W.; Siepen, K.; Hormes, J.; Franke, R.; Pollmann, J.; Rothe, J. *Appl. Organomet. Chem.* **1997,** *11,* 783–796. doi:10.1002/(SICI)1099-0739(199710/11)11:10/11<783::AID-AOC630 >3.0.CO;2-#

156. Bönnemann, H.; Brijoux, W.; Schulze Tilling, A.; Siepen, K. *Top. Catal.* **1997,** *4,* 217–227. doi:10.1023/A:1019152625358

157. European Agency for the Evaluation of Medicinal Products, *Note for Guidance on Specification Limits for Residues of Metal Catalysts*, CPMP/SWP/QWP/ 4446/00, June 2002.

158. Roelofs, J. C. A. A.; Berben, P. H. *Chem. Commun.* **2004,** 970–971. doi:10.1039/b400737a

159. Witte, P. T. Process for the preparation of an aqueous colloidal precious metal suspension (BASF Catalysts LLC). WO patent WO 2009096783, Aug 6, 2009.

160. Witte, P. T.; Boland, S.; Kirby, F.; van Maanen, R.; Bleeker, B. F.; de Winter, D. A. M.; Post, J. A.; Geus, J. W.; Berben, P. H. *ChemCatChem* **2013,** *5,* 582–587. doi:10.1002/cctc.201200460

161. Moreno-Marrodan, C.; Barbaro, P.; Catalano, M.; Taurino, A. *Dalton Trans.* **2012,** *41,* 12666–12669. doi:10.1039/c2dt31626a

162. Sachse, A.; Linares, N.; Barbaro, P.; Fajula, F.; Galarneau, A. *Dalton Trans.* **2013,** *42,* 1378–1384. doi:10.1039/C2DT31690K

163. Linares, N.; Hartmann, S.; Galarneau, A.; Barbaro, P. *ACS Catal.* **2012,** *2,* 2194–2198. doi:10.1021/cs3005902

164. Thomas, J.; Kuruvilla, K. M. In *Handbook of Herbs and Spices,* 2nd ed.; Peter, K. V., Ed.; Woodhead Publ.: Cambridge, 2012; Vol. 1, pp 182–196. doi:10.1533/9780857095671.182

165. Mizugaki, T.; Murata, M.; Fukubayashi, S.; Mitsudome, T.; Jitsukawa, K.; Kaneda, K. *Chem. Commun.* **2008,** 241–243. doi:10.1039/B710860E

166. Rode, C. V. *J. Jpn. Pet. Inst.* **2008,** *51,* 119–133. doi:10.1627/jpi.51.119

167. Hoffmann, H.; Boettger, G.; Bör, K.; Wache, H.; Kräfje, H.; Cörning, W. Catalyst for partial hydrogenation (BASF AG). U.S. Patent US 4001344 (A), Jan 4, 1977.

168. Isaeva, V. I.; Tkachenko, O. P.; Afonina, E. V.; Kozlova, L. M.; Kapustin, G. I.; Grünert, W.; Solov'eva, S. E.; Antipin, I. S.; Kustov, L. M. *Microporous Mesoporous Mater.* **2013,** *166,* 167–175. doi:10.1016/j.micromeso.2012.04.030

169. Semagina, N.; Joannet, E.; Parra, S.; Sulman, E.; Renken, A.; Kiwi-Minsker, L. *Appl. Catal., A* **2005,** *280,* 141–147. doi:10.1016/j.apcata.2004.10.049

170. Fishwick, R. P.; Natividad, R.; Kulkarni, R.; McGuire, P. A.; Wood, J.; Winterbottom, J. M.; Stitt, E. H. *Catal. Today* **2007,** *128,* 108–114. doi:10.1016/j.cattod.2007.06.030

171. Tsoligkas, A. N.; Simmons, M. J. H.; Wood, J.; Frost, C. G. *Catal. Today* **2007,** *128,* 36–46. doi:10.1016/j.cattod.2007.07.001

172. Winterbottom, J. M.; Marwan, H.; Viladevall, J.; Sharma, S.; Raymahasay, S. *Stud. Surf. Sci. Catal.* **1997,** *108,* 59–66. doi:10.1016/S0167-2991(97)80888-9

173. Rode, C. V.; Tayade, P. R.; Nadgeri, J. M.; Jaganathan, R.; Chaudhari, R. V. *Org. Process Res. Dev.* **2006,** *10,* 278–284. doi:10.1021/op050216r

174. Belger, C.; Neisius, N. M.; Plietker, B. *Chem. – Eur. J.* **2010,** *16,* 12214–12220. doi:10.1002/chem.201001143

175. Boldrini, G. P.; Bortolotti, M.; Mancini, F.; Tagliavini, E.; Trombini, C.; Umani-Ronchi, A. *J. Org. Chem.* **1991,** *56,* 5820–5826. doi:10.1021/jo00020a025

176. Gruttadauria, M.; Liotta, L. F.; Noto, R.; Deganello, G. *Tetrahedron Lett.* **2001,** *42,* 2015–2017. doi:10.1016/S0040-4039(01)00065-X

177. Lee, Y.; Motoyama, Y.; Tsuji, K.; Yoon, S.-H.; Mochida, I.; Nagashima, H. *ChemCatChem* **2012,** *4,* 778–781. doi:10.1002/cctc.201200058

178. Horváth, H. H.; Papp, G.; Csajági, C.; Joó, F. *Catal. Commun.* **2007,** *8,* 442–446. doi:10.1016/j.catcom.2006.07.016

179. Neumann, K. T.; Klimczyk, S.; Burhardt, M. N.; Bang-Andersen, B.; Skrydstrup, T.; Lindhardt, A. T. *ACS Catal.* **2016,** *6,* 4710–4714. doi:10.1021/acscatal.6b01045

180. Teschner, D.; Borsodi, J.; Wootsch, A.; Révay, Z.; Hävecker, M.; Knop-Gericke, A.; Jackson, S. D.; Schlögl, R. *Science* **2008,** *320,* 86–89. doi:10.1126/science.1155200

181. El Kadib, A.; Chimenton, R.; Sachse, A.; Fajula, F.; Galarneau, A.; Coq, B. *Angew. Chem., Int. Ed.* **2009,** *48,* 4969–4972. doi:10.1002/anie.200805580

182. Semagina, N.; Kiwi-Minsker, L. *Catal. Lett.* **2009,** *127,* 334–338. doi:10.1007/s10562-008-9684-1

183. Telkar, M. M.; Rode, C. V.; Chaudhari, R. V.; Joshi, S. S.; Nalawade, A. M. *Appl. Catal., A* **2004,** *273,* 11–19. doi:10.1016/j.apcata.2004.05.056

184. Berguerand, C.; Yuranov, I.; Cárdenas-Lizana, F.; Yuranova, T.; Kiwi-Minsker, L. *J. Phys. Chem. C* **2014,** *118,* 12250–12259. doi:10.1021/jp501326c

185. Seki, T.; Grundwaldt, J.-D.; van Vegten, N.; Baiker, A. *Adv. Synth. Catal.* **2008,** *350,* 691–705. doi:10.1002/adsc.200700532

186. Perego, C.; Peratello, S. *Catal. Today* **1999,** *52,* 133–145. doi:10.1016/S0920-5861(99)00071-1

187. Taguchi, A.; Schüth,, F. *Microporous Mesoporous Mater.* **2005,** *77,* 1–45. doi:10.1016/j.micromeso.2004.06.030

188. Knapik, A.; Drelinkiewicz, A.; Waksmundzka-Góra, A.; Bukowska, A.; Bukowski, W.; Noworól, J. *Catal. Lett.* **2008,** *122,* 155–166. doi:10.1007/s10562-007-9362-8

189. Wehrli, J. T.; Thomas, D. J.; Wainwright, M. S.; Trimm, D. L.; Cant, N. W. *Appl. Catal.* **1991,** *70,* 253–262. doi:10.1016/S0166-9834(00)84168-8

190. Louis, B.; Laugel, G.; Pale, P.; Maciel Pereira, M. *ChemCatChem* **2011,** *3,* 1263–1272. doi:10.1002/cctc.201100110

191. Ruta, M.; Semagina, N.; Kiwi-Minsker, L. *J. Phys. Chem. C* **2008,** *112,* 13635–13641. doi:10.1021/jp803800w

192. Gross, E.; Liu, J. H.-C.; Toste, F. D.; Somorjai, G. A. *Nat. Chem.* **2012,** *4,* 947–952. doi:10.1038/nchem.1465

193. Borodziński, A.; Bond, G. C. *Catal. Rev.: Sci. Eng.* **2008,** *50,* 379–469. doi:10.1080/01614940802142102

194. Tew, M. W.; Miller, J. T.; van Bokhoven, J. A. *J. Phys. Chem. C* **2009,** *113,* 15140–15147. doi:10.1021/jp902542f

195. Crespo-Quesada, M.; Yarulin, A.; Jin, M.; Xia, Y.; Kiwi-Minsker, L. *J. Am. Chem. Soc.* **2011,** *133,* 12787–12794. doi:10.1021/ja204557m

Automating multistep flow synthesis: approach and challenges in integrating chemistry, machines and logic

Chinmay A. Shukla[1,2] and Amol A. Kulkarni[*,1,2,§]

Review

Address:
[1]Academy of Scientific and Innovative Research (AcSIR),
CSIR-National Chemical Laboratory (NCL) Campus, Pune 411008,
India and [2]Chem. Eng. & Proc. Dev. Div., CSIR-National Chemical
Laboratory, Dr. Homi Bhaba Road, Pashan, Pune 411008, India

Email:
Amol A. Kulkarni[*] - aa.kulkarni@ncl.res.in

* Corresponding author
§ Tel: +91 20 25902153

Abstract

The implementation of automation in the multistep flow synthesis is essential for transforming laboratory-scale chemistry into a reliable industrial process. In this review, we briefly introduce the role of automation based on its application in synthesis viz. auto sampling and inline monitoring, optimization and process control. Subsequently, we have critically reviewed a few multistep flow synthesis and suggested a possible control strategy to be implemented so that it helps to reliably transfer the laboratory-scale synthesis strategy to a pilot scale at its optimum conditions. Due to the vast literature in multistep synthesis, we have classified the literature and have identified the case studies based on few criteria viz. type of reaction, heating methods, processes involving in-line separation units, telescopic synthesis, processes involving in-line quenching and process with the smallest time scale of operation. This classification will cover the broader range in the multistep synthesis literature.

Introduction
Multistep flow synthesis

In the recent time the concept of flow chemistry has become an important milestone in organic and materials synthesis. It has also been proven to be successful for a large number of reactions and the natural evolution of flow synthesis was to extend for its applicability to complex chemistries and large molecules [1-4]. In general, the complexity of synthesis depends upon the method and/or a number of steps and/or specific functional activity, etc. Most of the useful synthetic organic compounds involve a series of chemical transformations of very different nature, which can be termed simply as 'multistep synthesis'. The final products can have applications in fine chemicals, agrochemicals, and pharmaceuticals. Multistep syntheses enable the synthesis of complex molecules, which otherwise would be practically impossible if performed in a single step. In multistep flow synthesis, the general approach is to mix the reagents in a suitable micromixer followed by a flow reactor (usually

depicted in the form of a helical coil or a packed column), which is maintained at a desired temperature or a given temperature profile. The outlet stream of the reactor is subsequently mixed with the new reagent and allowed to react for further transformation and so on [5,6]. The multistep synthesis may or may not involve inline separation units and also in-line analytical tools to monitor the process. The multistep synthesis where the intermediate separation or work-up is not required is conventionally termed as 'one pot' synthesis, which is also called 'telescopic' synthesis when carried out in a continuous mode. A separation or purification step is required if (i) there is a need to isolate the necessary phase or isomer or (ii) to switch to a new solvent due to chemical compatibility or (iii) due to an unviable boiling point or (iv) for the cases where the side-product/byproduct can significantly affect the yield of the subsequent reaction step.

Reactions involved in a multistep synthesis can be classified in many ways. The general approach for classification of reactions is based on the activation methods like radical reaction, electrophilic reaction, electrochemical reaction, photochemical reaction, microwave, etc. On the other hand, it is also possible and in many times necessary to classify the reactions on the basis of the number of phases (gas G, liquid L, and solid S) involved in the reaction (viz. single-phase or homogeneous reaction and multiphase reactions). In single-phase homogeneous reactions, the reactants and products are soluble in the solvent or the reaction medium. Multiphase reactions involve two or more immiscible phases like G-L [7], L-L [8], G-L-L, L-S [9] and G-L-S [4] reactions. Sometimes for such reactions, phase-transfer catalysts are involved in enhancing the mass transfer rates or even one of the products needs to be isolated continuously to shift the equilibrium.

Recently excellent literature has been published on the synthesis of high-value compounds using a multistep synthesis approach [3,4,7,9-24]. Several integrated protocols have been developed for generating a library of compounds [12,25-27]. In-line separators like scavenging columns [22,25-28], liquid–liquid extractors (based on gravity or membrane) [3,23,29], distillation [30], etc. also facilitate continuous separation and significantly reduce the time for process development. Recent reviews on multistep synthesis clearly highlight the potential application of multistep syntheses in fine and pharmaceutical industries [5,31,32]. However, while continuous-flow synthesis helps to reduce the reaction time scales significantly, complex work-up and offline analysis are some of the bottlenecks of easy implementation of multistep flow synthesis. It also brings the need for automation. Automation in chemical synthesis is not new for the chemical industry. However, for the multistep flow synthesis of high-value molecules where each

reaction step demands a very different set of optimal parameters to maximize the yield for that step, automating the synthesis approach will help in integrating the decision making, design of experiments and actual synthesis [33]. This will also help to identify the limitations of combining (and not integrating) reactions with separations/work-up. Usually, automation is not as straightforward as it gets depicted from the existing literature on flow synthesis. Automation involves the development of protocols for analysis of a situation (based on the input information in terms of the desired conversion, selectivity, impurity profiling), real-time integration with the process analytical tools and decision-making protocols for identifying the next set of conditions needed to move in the direction that leads to optimal performance (objective function). While these protocols can be implemented using a suitable software, necessarily embedded hardware with excellent accuracy that corroborates with the chemistry is also needed. It is evident that automation and machine based logical decision making will be the next logical evolution of flow synthesis, which would help in speeding up the optimization, process development and actual translation of chemistry to products.

This implies that integration of various core and peripheral domains from the relevant sciences and engineering is absolutely essential and unavoidable to automate on-demand and end-to-end synthesis of important molecules [34]. Interdisciplinary research with long-term sustainability objectives and scientific interactions with industries can only help to find useful solutions. This implies that the compartmental approach followed by the synthesis community (which is necessary only while conceiving a new creative chemistry) needs to be changed at a certain stage by looking at their creative invention as a process rather than remaining limited to lab-scale methods to be the first-to-demonstrate. First-to-demonstrate a complex synthesis should immediately or even right from the beginning should allow the approach to be looked through a process angle, which will help the creativity of synthesis to blossom into a process. This review paper uses multistep flow synthesis and automation as two different yet largely interdependent domains to show how an automated platform can be built to deliver more from synthesis, viz. in terms of data, consistency, and reproducibility.

Review
Automation in flow synthesis
Automation in target specific as well as routine chemical synthesis will be among the most likely happening things in the time to come [35,36]. The role of automation in the flow synthesis can be categorized into three levels. Each level or component of automation has a very different objective, complexity, and relevance to synthesis.

I) Auto-sampling and analysis: In such cases, there is no control structure or Design of Experiment (DoE). Here automation is responsible for in-line monitoring of reactants, intermediates or products at the outlet of the reactors or separators. It may also involve in-line measurement of other process parameters (often not shown in the literature) like temperature, pressure, pH, level, etc. [33]. Such automation is useful for screening a large library of potential drug candidates. For example, Guetzoyan et al. have demonstrated the use of automation for synthesizing imidazo[1,2-*a*]pyridines, potential GABA$_A$ agonists [12].

II) Optimization: For a set synthesis protocol usually an optimization of conditions to maximize the yield of the desired product brings the need of repetitive work, which can be transformed to an automated synthesis platform (viz. vapourtec, H-cube, etc.). It is always possible to develop customized automation platforms that suit for specific synthesis and building such avenues using well-established programming tools like Lab View is always beneficial. In such cases, the DoE or optimization algorithm is coupled with automation protocols to find the optimal conditions. In-line analytical techniques can be coupled with a computer which manipulates the process conditions like temperature, flow rate, pressure, pH, etc., to achieve the desired objective (in most cases yield of the desired reaction) [37-40]. The control structure is not present in such cases as it does not have a real-time feedback system. An excellent review by Fabry et al. [41] on self-optimizing reactor systems is a useful resource to visualize the evolution of flow synthesis. However, as of now the self-optimizing reactor systems are limited to single-step syntheses and will need complex algorithms to evolve them to multistep syntheses. Although it is claimed that self-optimizing systems will lead to time and cost savings, selection of appropriate optimization algorithm and the algorithm development remains critical. Moore and Jensen have studied the optimization of a Paal–Knorr synthesis using various optimization algorithms [42]. Figure 1 shows the number of experiments for various optimization algorithms at an optimal temperature of 130 °C. The authors have clearly demonstrated that selecting the appropriate optimization algorithm is essential for minimizing the number of experiments thus saving time and resources. This analysis is extremely important when the reactants and reagents are extremely expensive or have a very small active life. However, if the number of experiments is going beyond 20–25, it would be advisable to generate kinetic data instead and use the appropriate chemical reaction engineering model to optimize the process [43]. Chemical reaction engineering models give more insight by allowing estimating the concentration and temperature profiles inside the reactor. Whenever it is not possible to insert temperature sensors along the flow reactor/microreactor due to its compact

dimensions (although miniaturized sensors are available almost everywhere), the temperature should be monitored at the inlet (preferably at mixing points) and outlet of the reactor [44]. In such cases, reaction engineering models are useful for the prediction of the temperature profile inside the reactor and to investigate if any hot spot is occurring inside the reactor. Reizman and Jensen demonstrated the use of the automated platform for estimating kinetics parameters of a series-parallel substitution reaction [38]. Reizman et al. have studied Suzuki–Miyaura cross-coupling optimization using a DoE-based algorithm and feedback system [45]. The authors studied both continuous and discrete variables for optimization. Recently Fitzpatrick and Ley have demonstrated the use of automation for integrating batch and flow reactors on a single platform [46]. Their process also involved extraction and distillation operations.

Figure 1: A number of experiments for various optimization algorithms [46].
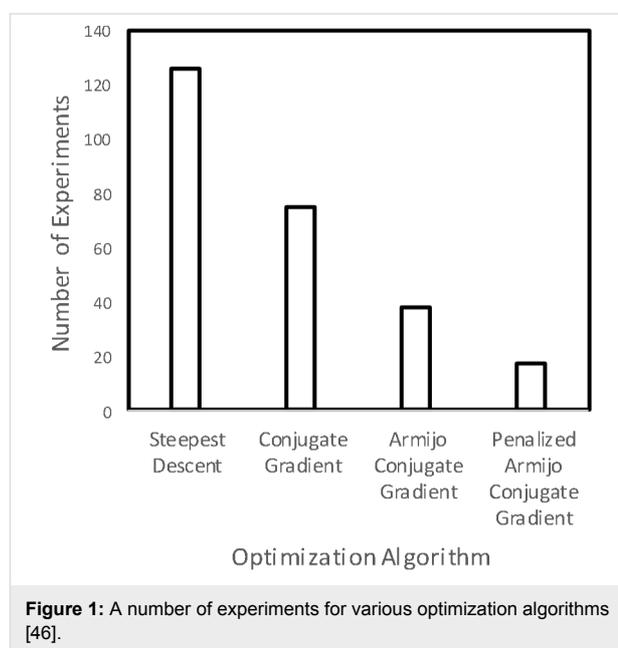
III) Automation for control: The third and the most important purpose of automation is to control the process variables like temperature, pressure, and flow rate at the given set point so that it helps indirectly to control the reaction rates and pH of the reaction mixture. The objective of controlling certain parameters within a range usually needs accuracy in measurements as well as in terms of response time. In such cases, there is no DoE but the objective is to maintain a steady state process at optimal conditions through an appropriate control strategy. In general, automated control strategies are commonly implemented for bench scale, pilot scale, and commercial scale manufacturing of chemicals, and not at laboratory scale. However, this feature becomes important for multistep synthesis as for taking into account any feedback effect in the entire synthesis protocol, minor variation in the operating conditions at any stage can

trigger a forward or backward effect leading to change in the reactor performance. Recently a few such works on the use of control systems for multistep synthesis of APIs and drugs are reported in the literature [3,8,19,24].

With this objective of implementing automation in synthesis, in the next section, we touch upon the automation at different scales and then focus on the possible ways in which multistep flow synthesis needs to be carried out to enhance the productivity and reliability of a synthesis protocol.

Automation in lab-scale environment: Automation can significantly improve the productivity of lab scale experiments and also aid speeding up the synthesis of a library of compounds and drug discovery process [47]. The chemical library has to go through high-throughput screening (about 100,000 compounds/day approximately) using robots [48]. In multistep synthesis off-line analysis actually becomes a bottleneck as it does not allow the real-time changes to be imposed at the inlet conditions for minor variations in the product quality. Automated in-line analysis has (to some extent) addressed this issue provided the response time from the systems is shorter than the time scales that control the reaction. Reliability and reproducibility of an experiment also improve significantly under automated environment [49]. With a significant portion of literature, falling under the non-reproducibility crisis, automation will make chemistry and methods as reliable as it was over several decades ago [50]. By using automation for measuring and reporting the scientific data, one can increase the value of the published work, patents, etc., by many folds. Automation is a powerful tool if used correctly, but can also be expensive if not utilized correctly [13].

Automation in chemical plants: The role of automation in chemical industries is to enhance the product quality, reduce the dependence on the availability of human being, improve process safety, efficiently utilize the plant resources and minimize the emissions [51]. Process automation is in great demand in various industrial sectors like chemical industry, power generation industry and petroleum industry. In the recent years, the pharmaceutical industries have been experiencing growing demands for process automation services like hardware and standard software. Stephanopoulos has reviewed the process control approach in chemical plants in detail [52]. The process control system should be designed to achieve the control objectives which are generally defined by the process or chemical engineers. The control objectives include both normal and special purpose operations. Normal operation during synthesis is controlling the process/reaction at optimum conditions. Special purpose operations may include start-up (viz. starting a continuous stirred tank reactor, adding a highly reactive reagent

to the reactor, etc.), shut-down (viz. stopping the reaction, giving rapid cooling to the reaction mixture, etc.), change-over (viz. switching from reactant to solvent, changing or recovering the catalyst activity, etc.), override and emergency situations (viz. forcefully quenching the reaction). There should also be a sequence of operation procedures which can take the process from one state of operating conditions to another state of operation. Dynamic simulations can be a useful tool to study the special purpose operations (viz. start-up, shut-down, etc.) and also the forward and backward effects due to operating condition variations in the multistep synthesis. Understanding the forward and backward effects in multistep synthesis is essential for successful translation of chemistry into an industrial process.

Accurate measurements of process variables are the most critical part of the process control. The process variables that are often measured are temperature, pressure, flow, liquid level, density, composition, pH and viscosity. Details of different sensors or transmitters for measuring these variables can be found in standard process control and instrumentation textbooks [53-56]. Before automating any process it is necessary to understand that the simplest control system that will do the desired job is the best one and one must understand the process thoroughly before controlling it [57].

The fundamental step for designing a control system is to identify the controlled variable. A controlled variable can be the outlet temperature of a heat exchanger or a reactor, the outlet composition of the reactor, the system pressure, the liquid level of a tank or a crystallizer, the pH, etc. Selection of controlled variables is done by engineering judgment based on process understanding. The next step is to identify manipulating variables and formulate a control loop [52]. Generally, there are many options available in manipulation variables which make developing control loops challenging. As a thumb rule, flow rates are generally avoided as a manipulating variable when the flow rate is high or temperature is very high or the process stream is in slurry form (suspension of solids in liquids) or contains dosing of solids or has corrosive materials. Pressure is also generally avoided as a manipulating variable when the liquid is volatile or the process stream is a two-phase mixture. Recently, Movsisyan et al. have reviewed the application of flow reactors for hazardous reactions [1]. Although the flow reactors allow such reactions to be carried in a safer manner controlling such reactors at production scale could be challenging.

Recently, automation is also used for Hazard and Operability (HAZOP) analysis in chemical industries [58,59]. In HAZOP analysis, the aim is to systematically identify all the possible

abnormal process deviations, its causes and its adverse effects in the chemical plant. HAZOP analysis is generally time-consuming and labour-intensive.

The recent advances in multistep synthesis have shown promising outcomes at lab scale especially for the synthesis of high-value drugs [4,7,11,17,21,23,60]. However, converting these chemistries into industrial processes is still challenging. While several industries provide solutions for scale-up of lab processes [61-67] usually their hands-on experience to decide the control strategy while automating a flow chemistry always offers better solutions than what one expects theoretically. Before analysing these complex syntheses, it is worth appreciating that a few successful demonstrations of an end-to-end manufacturing process for high-value drug compounds are already reported in the literature [3,8,19,24]. In this review, we have critically analysed a few multistep syntheses of high-value drugs using an approach that involves various unit operations like filtration, evaporation, membrane separation, liquid–liquid extraction, etc. We have also suggested some guidelines for these multistep syntheses for transforming these lab scale chemistries to automated pilot scale processes. At pilot or production scale, automation is largely employed for controlling and maintaining the process at a steady state. Here we have suggested some simple control strategies which can be adapted even for scale-up. With each process having different chemistries, unit operations and operating conditions, the operating protocol and control strategy may change every time making it a challenging task.

Approach and selection criteria

The case studies discussed in the later section includes control strategies for various types of reactions, viz. homogeneous reactions, gas–liquid reactions, gas–liquid–solid reactions and also for various unit operations including heat exchangers, evaporators, membrane extractors, etc. However, similar control strategies can also be employed for other chemistries/processes which are not included in the present case studies. Each case study is transformed in the form of a Piping and Instrument Diagram (P&ID) that makes a process engineer understand the flow of processes and associated measurement instruments. The P&ID includes engineering details of equipment, instruments, piping, valves, fittings and their arrangements. It may also include identification numbers for the equipment, pipelines, pumps, and other auxiliary equipment. The most important feature of P&ID is that it provides a graphical representation of the control structure of the process [68-70]. In industry, P&ID is always made before actually implementing process automation and control for any process. More importantly, P&ID is also used for doing and evaluating HAZOP options which are critical to the implementation of a process.

Case studies

Till date, there are more than 80 excellent publications that use continuous-flow synthesis of high-value molecules where the synthesis involves two and more stages. While choosing the representative case studies we have applied certain classification criteria such that it would cover the broader area in a multistep synthesis. A detailed analysis of more than 80 multistep flow syntheses reported in the literature will be presented separately. The first classification was based on a number of phases involved in the reaction, viz. gas–liquid reaction (viz. amitriptyline synthesis [7]), gas–liquid–solid reactions ((±)-oxomaritidine synthesis [9]) and liquid–solid reactions (viz. (*S*)-rolipram synthesis [4]). The process was also selected on the basis of the heating technique used, viz induction heating (olanzapine synthesis [10]), and conventional heating in a constant temperature bath/circulator. The cinnarizine/buclizine derivative process was selected as it involved in-line quenching [23]. Most of the above processes involve separation units and hence we decided to select telescopic synthesis of tamoxifen and rufinamide as representative case studies [11,14] that do not involve any phase separation. Finally, we selected an ibuprofen synthesis protocol as it had an overall residence time significantly less than the conventional approach [60].

Symbols for block diagram and P&ID

Translating any chemistry to process at industrial scale would require the involvement of engineers from various fields viz. chemical, instrumentation, mechanical and electrical. In such cases, it is desired to describe the process in terms of standard symbols (rather than combined chemical structures and diagrams which are most often used in the literature) which can be understood by process chemists as well as engineers from other disciplines. Figure 2 shows the list of symbols used in the current review. For each case, initially we have described the process chemistry and transformations followed by the approach that needs to be followed to make it a useful method that gives important data that can help it transform into an automated process.

Case study 1: Multistep flow synthesis of olanzapine/zyprexa (induction heating)

Kirsching and co-workers have reported the continuous multistep synthesis of olanzapine (Zyprexa), a drug used for the treatment of bipolar disorder and schizophrenia [10]. The process involves four reaction steps, one inline extraction, and a filtration step. The reaction is shown in Scheme 1. Initially, a Buchwald–Hartwig reaction is carried out between aryl iodide and aminothiazole. Pd_2dba_3 was used as a catalyst and Xantphos as a ligand in an ethyl acetate medium. These reagents are passed through a PEEK reactor filled with 0.8 mm steel beads
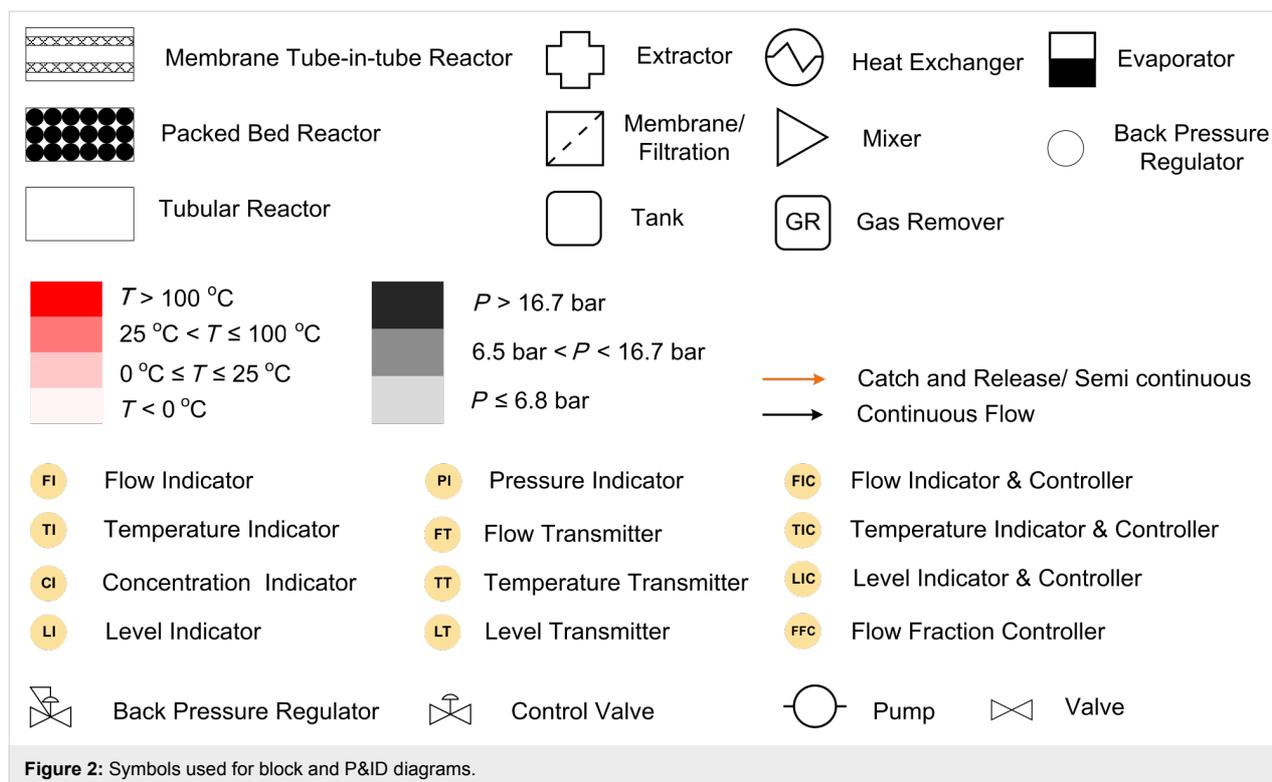
Figure 2: Symbols used for block and P&ID diagrams.
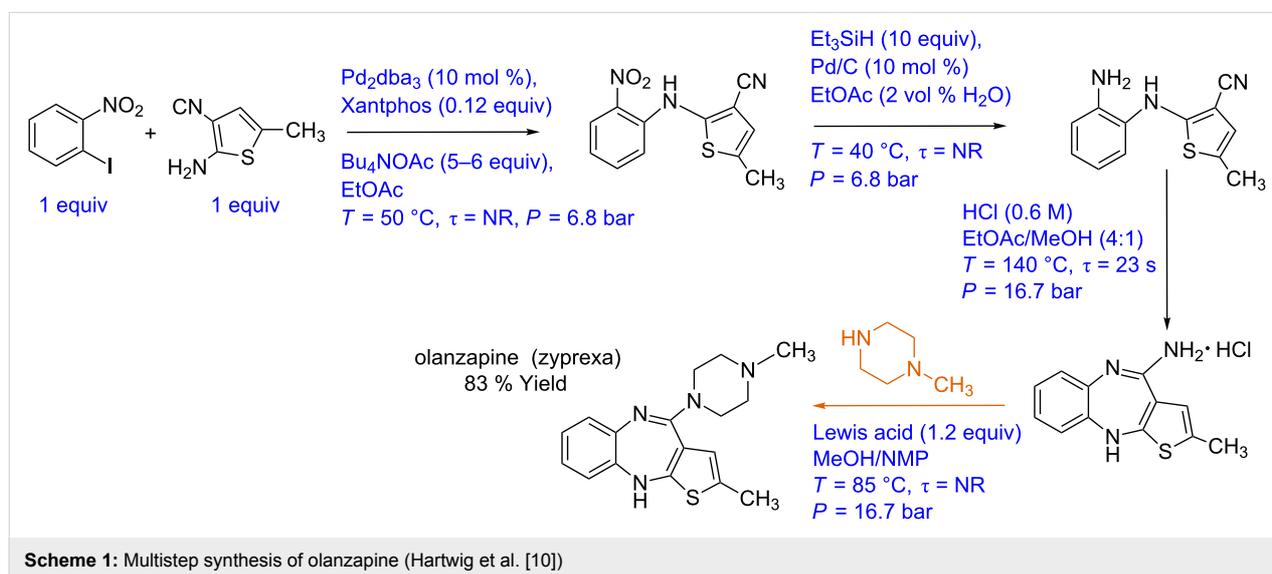
Scheme 1: Multistep synthesis of olanzapine (Hartwig et al. [10])

and were heated at 50 °C by inductive heating (15 kHz). The reaction is subsequently quenched using distilled water and extracted in-line and passed through a silica cartridge to remove the Pd catalyst. The nitroaromatic derivative is mixed with triethylsilane and the mixture is passed through a fixed bed reactor with Pd/C catalyst at 40 °C to reduce the nitro group to an amino group. The yield is reported to be quantitative, and the catalyst activity is reported to be lasted for over 250 h. The reaction mixture is further mixed with HCl in MeOH/AcOEt

and subjected to acid-catalyzed cyclization in a 0.3 mL coiled reactor at 140 °C (inductive heating, 800 kHz). This resulted in 88% overall yield. The isolated product is then mixed with piperazine and passed through the PEEK reactor (3 mL) containing MAGSILICA (inducting material) and silica-supported Ti(OiPr)$_4$ (Lewis acid). The final substitution is reported at 85 °C (25 kHz) that gives olanzapine in 83% yield. These individual synthesis steps can be depicted in the form of a block diagram (Figure 3A). Since each synthesis step is carried out at
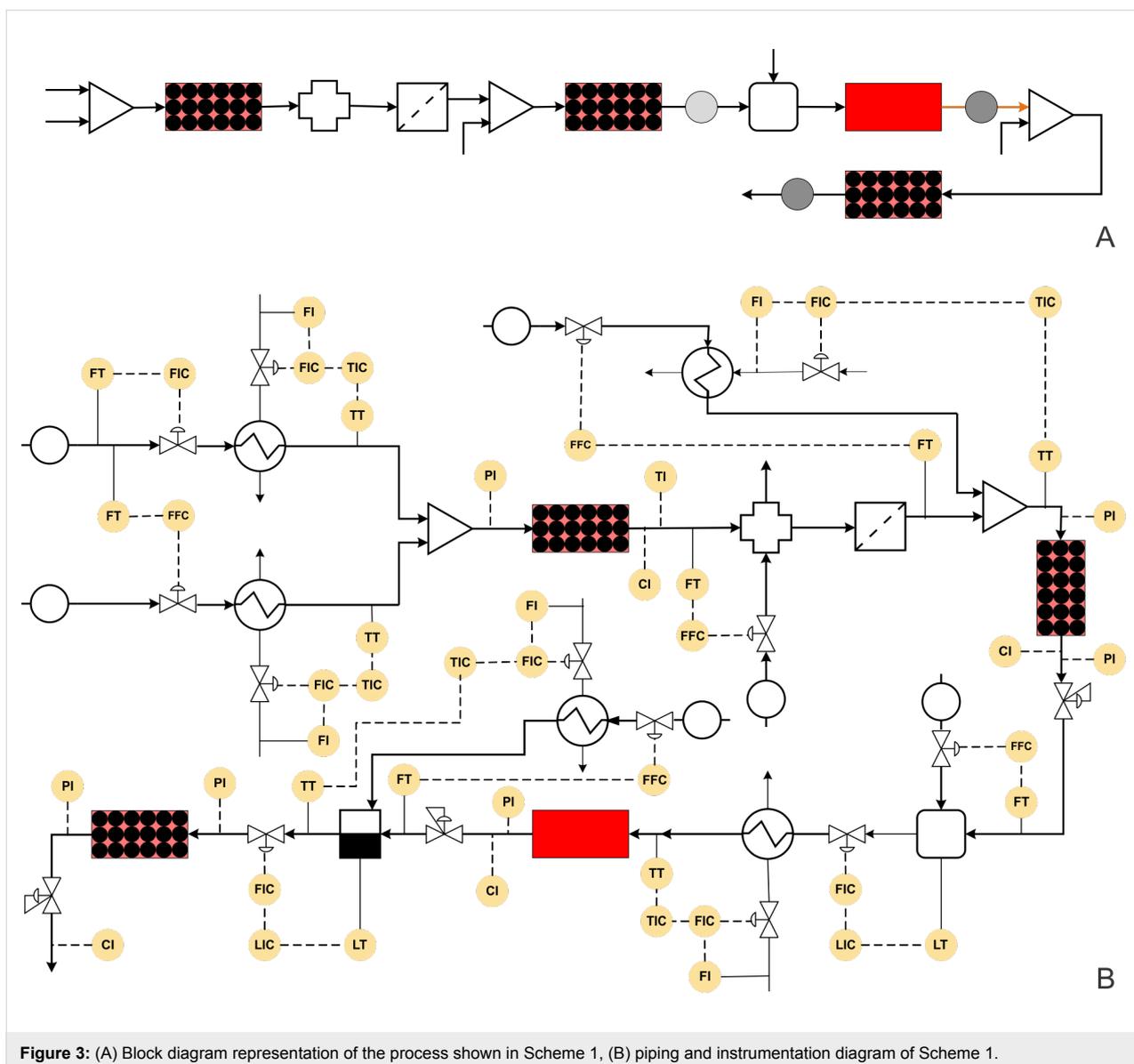
Figure 3: (A) Block diagram representation of the process shown in Scheme 1, (B) piping and instrumentation diagram of Scheme 1.

a very different set of conditions, automation of such a synthesis scheme would need a lot of data from each step including the effects of minor variations in individual parameters at each step. Such an objective would need the intervention of several engineering inputs, which will help to transform this synthesis to a process.

Figure 3B shows the P&ID for the olanzapine manufacturing process. The flow rate of aryl iodide is fixed at a desired set point value using a control valve, which also helps to stop the pump in the case that the reaction temperature or pressure increase beyond a certain set-point over the subsequent reaction steps. The aminothiazole flow rate needs to be controlled using a ratio controller to maintain the molar ratio between aryl iodide and aminothiazole.

Both of these streams can be preheated using a heat exchanger with a feedback controller. The mixed stream can then be passed through the packed reactor with the inductive heating system. The induction heating system should actually be coupled with a suitable cooling system to avoid possible uneven spatial heating effects. Alternatively, unless otherwise needed, the conventional heating system can also be used as it will be more flexible in terms of operation and control. The outlet concentration of the intermediate can be monitored inline using a suitable analytical technique and the reactor conditions should be controlled by manipulating the reactor temperature. The reaction mixture can be quenched by distilled water and extracted in a column, where again the distilled water flow rate can be controlled using a ratio controller. Filtration can remove the Pd catalyst in a continuous manner. This process stream can

be further mixed with preheated triethylsilane at appropriate molar ratio using a ratio controller.

This mixed stream can be passed through a packed bed reactor containing a Pd/C catalyst and maintained at 40 °C using a heating jacket. The reactor outlet concentration can be monitored inline and controlled by manipulating the jacket fluid flow rate of the reactor. The back pressure regulator can be used to maintain the desired pressure. Further, the HCl stream can be mixed with the process stream in a tank at appropriate molar ratio using a ratio controller. The outlet flow rate of the tank can be controlled by maintaining the liquid level inside the tank. The camera based level control systems demonstrated by Ley and co-workers can be a quick option [71]. The solution can be preheated to 140 °C using a heat exchanger and passed through a jacketed reactor. The outlet concentration of the reactor can be measured inline and controlled by manipulating the jacket fluid flow rate. This will help to measure the heat duty for the specific reaction, which can be used for estimating the enthalpy change in the specific reaction. This data is immensely useful for scale-up of this approach. A back pressure regulator (BPR) can be used to maintain the desired set pressure on the entire system. The process stream can be mixed with piperazine (in MeOH/NMP) and subjected to evaporation to remove ethyl acetate solvent. The outlet flow rate of the evaporator can be controlled by maintaining the liquid level inside the evaporator. The process stream can further be passed through a packed bed reactor containing silica-supported Ti(OiPr)$_4$ maintained at 85 °C using a reactor jacket to obtain the olanzapine drug.

While the above mentioned automated protocol can be implemented for the synthesis in Scheme 1, it is not easy to implement a few aspects that are routinely used in the reported multistep synthesis. Here we bring out such challenges and suggest a few alternatives that will help an engineer to transform the protocol to synthesis. To begin with, the merit of this scheme comes from an efficient way of implementing inductive heating. Though inductive heating offers rapid heating, its applicability for large-scale synthesis is yet unreported and may not be economical. For exothermic reactions, the heating unit should also be capable of cooling in case of some undesired events like a runaway reaction or an emergency shutdown. Most of the induction heating systems cool at a slower rate due to natural convection and to some extent radiation. However, an additional set-up (for cooling the induction coil) is required for this which will add cost. Moreover, air needs to be very clean and possibly moisture free as it can corrode the induction coil. With this complex setup, it will be difficult to control the actual set point temperature inside the reactor. If there is a significant temperature difference between two consecutive reactors, then one can preheat (or cool) the process fluid to the desired tem-

perature using conventional heating techniques and then pass it through the reactor for a better performance.

Case study 2: Multistep flow synthesis for tamoxifen (telescope synthesis)

Steven Ley and co-workers have reported a continuous multistep synthesis protocol for tamoxifen, a drug used for treating breast cancer [11]. The synthesis protocol is shown in Scheme 2. A Weinreb amide (1 equiv) and PhMgBr (2 equiv, Grignard's reagent) are reacted in a 10 mL PFA coil at 60 °C for 5 min residence time. The reaction is quenched using aq HCl and the ketone is isolated with 97% yield. The aryl lithium compound is produced simultaneously by reacting aryl bromide (1 equiv) with *n*-BuLi (1.1 equiv) at −50 °C in 10 mL PFA reactor with 7 min residence time. This lithium compound reacts with the ketone intermediate at 30 °C for 2 min in 5 mL PFA reactor coil. The intermediate lithium alkoxide is further reacted with trifluoroacetic anhydride (2 equiv) in a 10 mL PFA reactor at 25 °C for a residence time of 3 min to get the trifluoroacetate, which further reacts with triethylamine in a PFA coil (10 mL) at 100 °C for 5 min to give the final drug molecule. By using Vapourtec V-3 peristaltic pumps, the authors are able to achieve a constant fluid flow rate. Maintaining the mole ratio between ketone (obtained by Grignard's addition) and lithiated compound (obtained by lithiation) is critical. At plant scale, in-line monitoring technique should be used to monitor the outlet concentration of both the reactions. A suitable ratio controller should be employed to control the volumetric ratio (hence the mole ratio) at a larger scale. The entire synthesis can be depicted in the form of a block diagram as shown in Figure 4A. The use of a Vapourtec platform brings a certain level of automation, however, a large variation in the synthesis conditions between two subsequent steps makes it not a fully automated protocol. To make it such a platform, in Figure 4B, we have depicted a process instrumentation diagram for this scheme and subsequently discuss the details.

The P&ID diagram in Figure 4B indicates that the flow rate of the Weinreb amide can be fixed at the desired set point using a control valve as it is the limiting reagent while the flow rate of Grignard's reagent can be controlled using the ratio controller. Both the process streams can be preheated at the reaction temperature (i.e., 60 °C) using a feedback controlled heat-exchanger. The preheated streams have to be mixed in a suitable mixer followed by the reactor. The reactor can be maintained at the desired temperature using a jacket. The flow rate of the jacket fluid can be the manipulating variable to automate the synthesis that can have fixed conversion as a set-point. The outlet concentration or the conversion can be monitored online to check the variation around the set-point value. This process stream containing the ketone intermediate can be precooled to

Scheme 2: Multistep flow synthesis for tamoxifen (Murray et al. [11]).
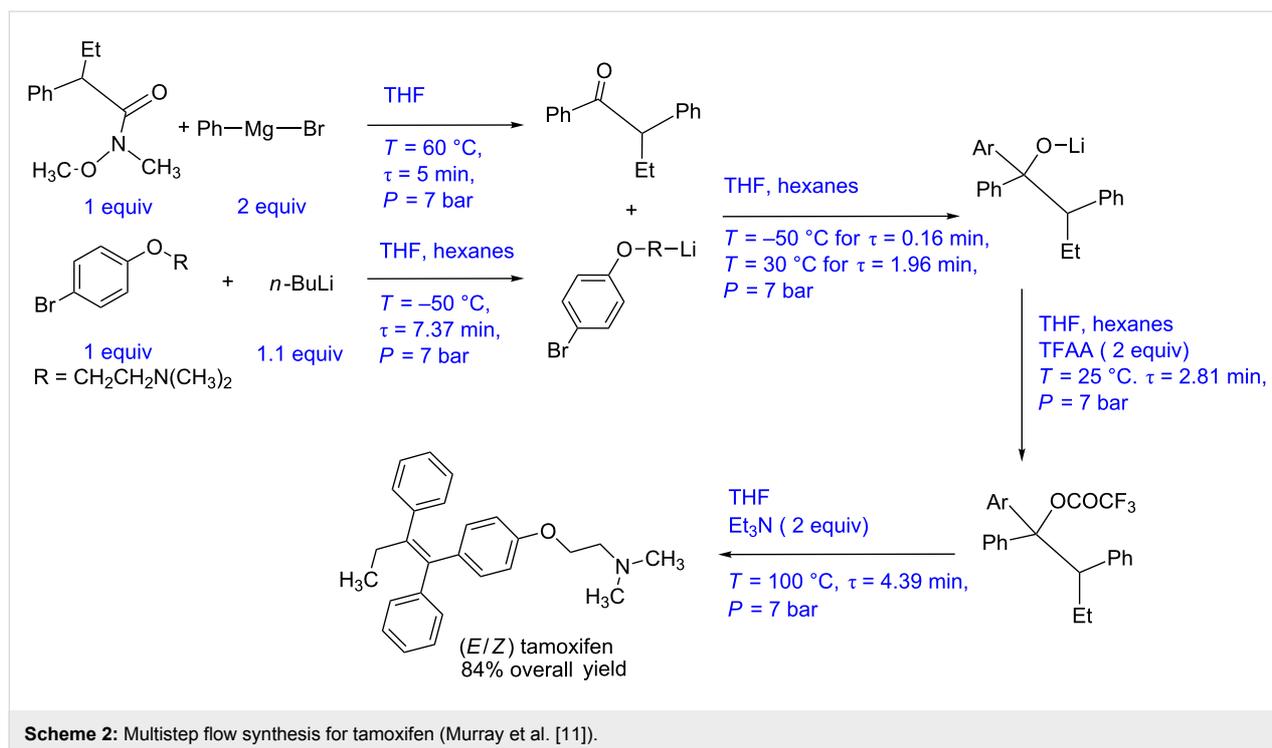
−50 °C. Aryl bromide and *n*-BuLi are precooled at −50 °C and reacted to obtain the lithiated product. The control strategy for lithiation reactor will be similar to the previous reactor. This lithiated intermediate and the ketone intermediate obtained by the simultaneous process can be mixed using a ratio controller at the optimum stoichiometric amount. The obtained lithium alkoxide can be monitored inline using a suitable analytical technique and the reactor control loop will be similar to previously discussed reactors. This process stream can be heated to ambient temperature using a heat exchanger before mixing it with trifluoroacetic anhydride whose flow rate can be controlled using a ratio controller. The intermediate obtained can be mixed with triethylamine using a ratio controller and can be preheated to 100 °C before passing through the reactor. Alternatively, both the process streams can be preheated separately before mixing. The concentration of the tamoxifen thus obtained can be monitored online. The whole system can be pressurized using a back pressure regulator to avoid any intermittent pressure variations due to phase change. It is possible to have a different P&ID structure depending upon the control variable at each stage. However, the merit of any such structure if implemented before optimizing the specific flow synthesis will help to generate very valuable data that can be used for transforming this chemistry into a process.

Lithiation reaction is highly exothermic and a special control strategy should be employed to avoid a runaway situation [44].

However, if a runaway event occurs an appropriate strategy should be developed to stop the reagents flow first and quench the reaction mass. More importantly, moisture sensors need to be installed on the system to avoid the possible contact of water with *n*-BuLi.

Case study 3: Multistep flow synthesis of rufinamide (telescopic synthesis)

Zhang et al. have reported the multistep synthesis of rufinamide, an antiepileptic agent [14] (Scheme 3). The process involves three steps namely azide synthesis, amide synthesis and click reaction or azide–alkyne cycloaddition. For the azide synthesis, the aryl bromide (1 equiv) and sodium azide (1.3 equiv) are reacted in a tubular reactor with 1 min residence time at 25 °C in DMSO medium. This resulted in quantitative yield. The amide synthesis is carried out simultaneously by mixing methyl propiolate (1.5 equiv) and aqueous ammonia (6 equiv) solution in a T-mixer followed by a coiled reactor. The authors report over 95% conversion at 0 °C for a residence time of 5 min. The products obtained by these two reactions are directly mixed and subsequently passed through the copper tube which acted as a catalyst for the cycloaddition reaction. At a temperature of 110 °C and a residence time of 6 min, rufinamide is obtained in 92% overall yield. The whole process is carried out under a pressure of 100 psi. The typical block diagram for this process is shown in Figure 5A, which depicts the simplicity of the experimental set-up for producing an expensive drug.
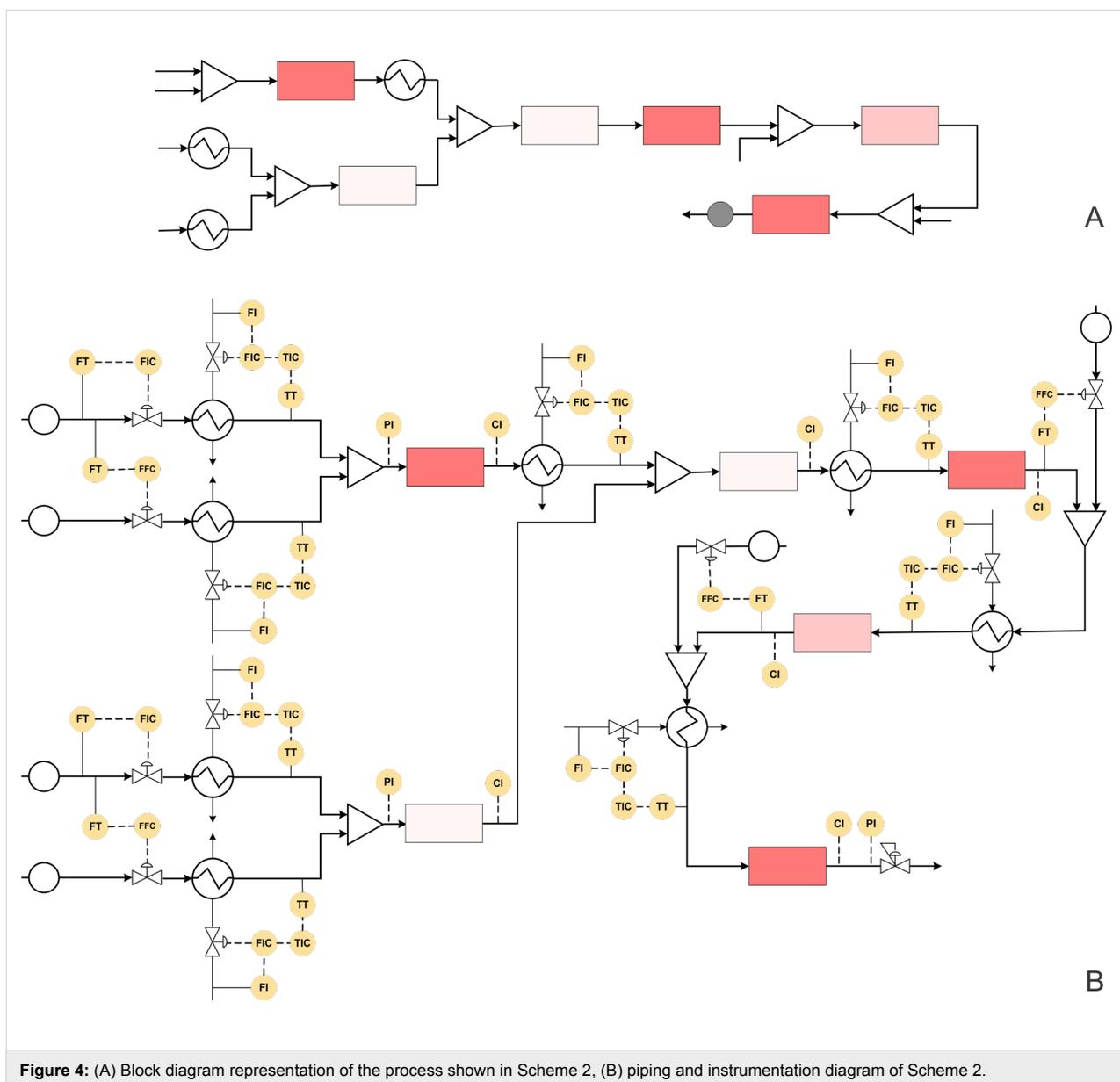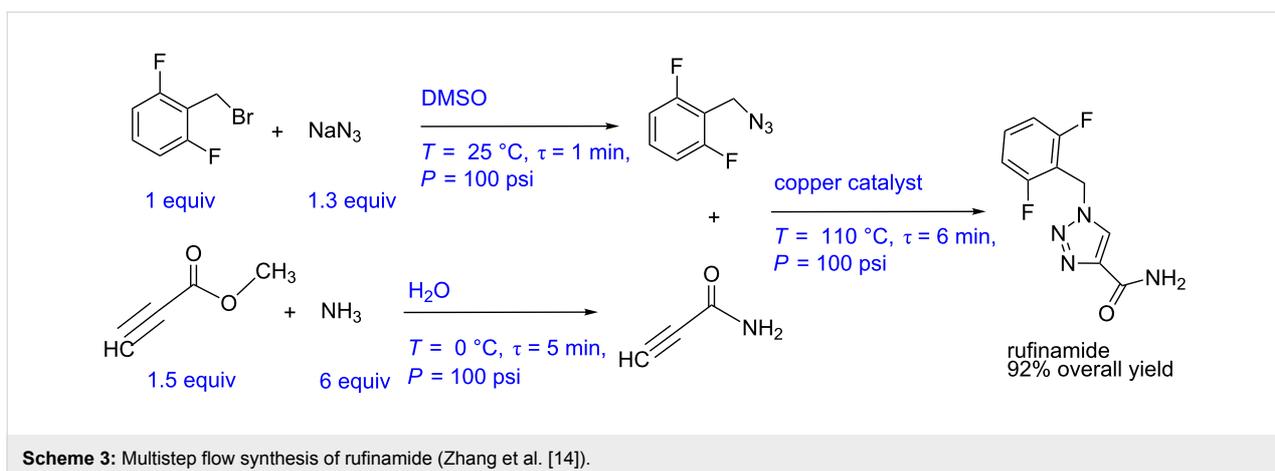
Figure 4: (A) Block diagram representation of the process shown in Scheme 2, (B) piping and instrumentation diagram of Scheme 2.

Scheme 3: Multistep flow synthesis of rufinamide (Zhang et al. [14]).

Figure 5: (A) Block diagram representation of the process shown in Scheme 3, (B) piping and instrumentation diagram of Scheme 3.

The block diagram, when transformed into a piping and instrumentation diagram, helps to know the possible automated flow synthesis platform with better clarity (Figure 5B).

For the said process the automated synthesis can be achieved as follows: The flow rate of aryl bromide can be fixed at a desired set point using a control valve or by setting the pump with feedback in the form of a pressure signal from the system. The flow rate of sodium azide has to be controlled using a ratio controller with respect to the pump for aryl bromide. Both the streams can be heated to the reaction temperature before mixing. This will help to save time in heating the reaction mixture and also to

avoid undesired side reactions possibly due to prolonged contact of the reactants. The mixed stream has to be followed by a flow reactor with a jacket, where the jacket side fluid can be the manipulating variable whereas the outlet concentration of the reactor can be set as a control variable. Simultaneously methyl propiolate and aqueous ammonia can be precooled at 0 °C using a compact heat exchanger (it can even be a coil inside a jacket) before mixing at the desired molar ratio using a ratio control. The amide can be monitored at the reactor outlet using inline monitoring system (like UV, IR or Raman spectroscopy) which may be coupled with the reactor jacket flow rate to maintain the desired conversion. The azide and amide streams can be mixed

and preheated at 110 °C. The preheated stream can then flow through a copper tubing reactor or a packed bed reactor with copper packings, whichever is scalable or easy to replace. The temperature of the reactor can be maintained by manipulating the jacket fluid flow rate. The rufinamide thus obtained can be monitored online. A back pressure regulator can be used to pressurize the entire reactor system.

Case study 4: Multistep synthesis for (±)-oxomaritidine (gas–liquid–solid reaction)

Baxendale et al. have developed a multistep synthesis for (±)-oxomaritidine, a cytotoxic alkaloid of the amaryllidaceae family of natural products [9] (Scheme 4). The process involved seven reaction steps out of which the first two reactions were carried out in parallel. In the first step, 4-(2-bromoethyl)phenol is converted to its azide derivative by passing it through a glass reactor packed with azide exchange resin (20 equiv) at 70 °C to achieve quantitative yield. MeCN and THF were used as solvents. Dimethoxybenzyl alcohol (in THF) is oxidized to the corresponding aldehyde by passing it through a packed column containing tetra-*N*-alkylammonium perruthenate (10 equiv) at room temperature to achieve quantitative yield. Further, these two products are reacted with each other to get the imine intermediate. The catch and flow technique is used with polymer-supported phosphine (20 equiv) as the trapping agent. The imine is further hydrogenated at 25 °C and 20 bar pressure by

using an H-cube reactor with 10% Pd/C as a catalyst [72]. Trifluoroacetylation of the amine intermediate is then carried out in a chip reactor with trifluoroacetic anhydride (in DCM) as a reagent. The reaction temperature and residence time are 80 °C and 3.5 min, respectively. This product further undergoes a coupling reaction in a packed column containing polymer-supported [bis(trifluoroacetoxy)iodo]benzene (PS-PIFA), which yields a seven-membered tricyclic intermediate with 50% yield. The tricyclic intermediate is further mixed with MeOH and water (4:1) and passed through a packed column containing a polymer-supported base at 35 °C. The target compound (±)-oxomaritidine was obtained in 40% yield. The block diagram of different steps performed in this synthesis is shown in Figure 6A. This is a relatively simple approach for a complex transformation. However, there are complexities in terms of the difference in the reaction conditions at each step, where one has to ensure that unreacted reactants do not enter the next step and the heating/cooling rates are managed efficiently to avoid a longer residence time during automation.

The corresponding P&ID diagram and associated complexities that one would need to deal for automating such a synthesis are discussed below. Figure 6B shows the P&ID for the (±)-oxomaritidine manufacturing process. The flow rate of the limiting reagent, 4-(2-bromoethyl)phenol can be fixed at a desired set-point using a control valve. This process stream can

Scheme 4: Multistep synthesis for (±)-Oxomaritidine (Baxendale et al. [9]).

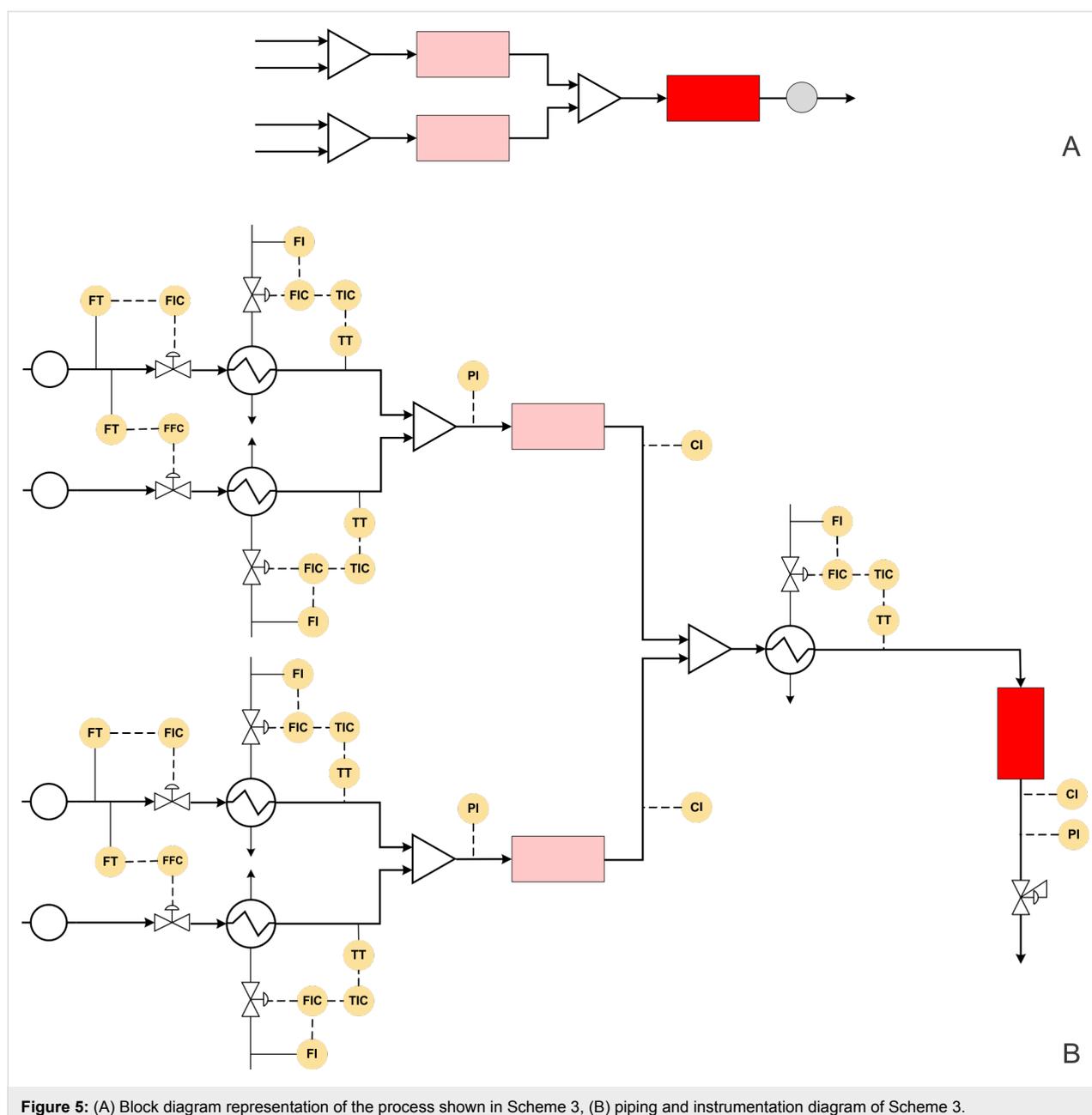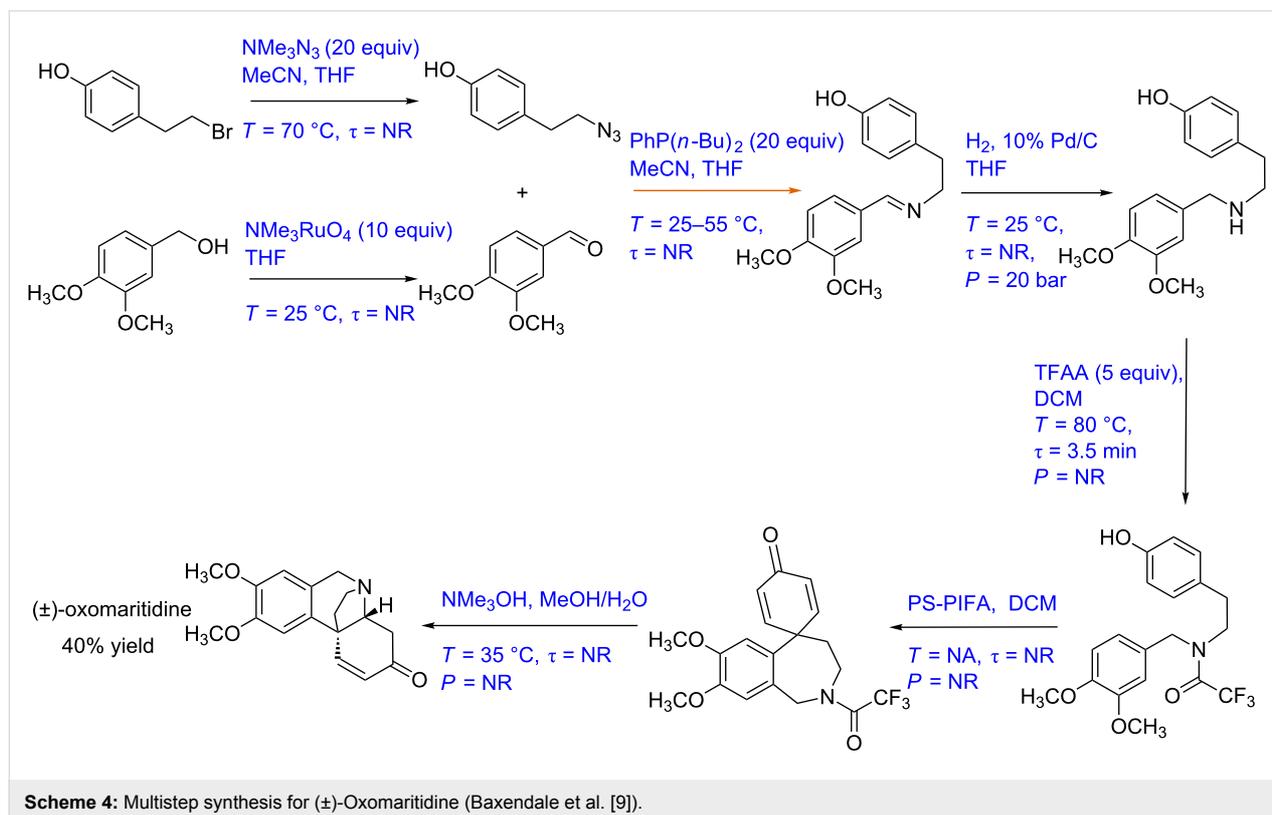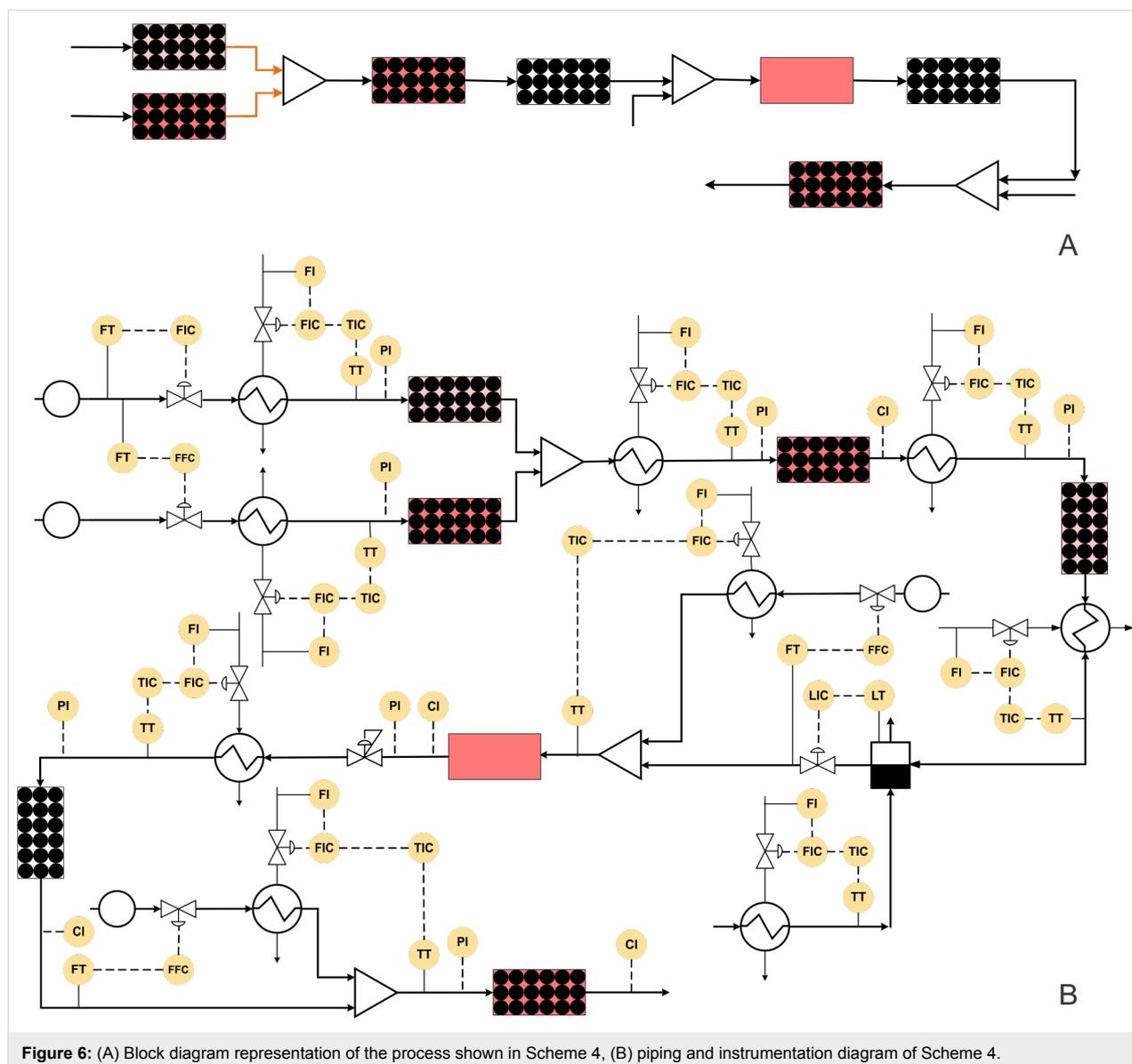**Figure 6:** (A) Block diagram representation of the process shown in Scheme 4, (B) piping and instrumentation diagram of Scheme 4.

be preheated at the reaction temperature (70 °C). It can then be passed through the reactor packed with azide exchange resin maintained at the desired temperature using a jacket. The azide exchange resin will get consumed after some time and the corresponding section needs to be activated or recycled in order to maintain continuous production. In such cases, it is possible to have two parallel reactors containing a packing of azide exchange resin, which can be operated in a cyclic manner to maintain continuous flow or an efficient arrangement of continuous activation of the bed like a simulated moving bed chromatographic reactor (SMB). Alternatively, one can also charge the azide resin as a suspended mass in the flow to avoid this complexity to some extent and to have a filter to keep the resin retained in the reactor. Considering the existing configuration of the packed bed reactor with the cyclic operation, dimethoxy-

benzyl alcohol can be preheated and passed through the packed bed reactor containing the oxidizing reagent as packing material to obtain the corresponding aldehyde. The packed bed reactor control strategy will remain identical for all reagent packed reactors. The azide and the aldehyde intermediate can be mixed and preheated at the reaction temperature and passed through a phosphine-functionalized polymer packed bed reactor to obtain the imine intermediate. This imine intermediate can be reacted with H_2 in a commercial reactor with an integrated control system. After hydrogenation, the solvent switch can be carried out in an evaporator by removing the THF solvent and then re-dissolving the intermediate in DCM as solvent. The outlet flow rate of the evaporator can be controlled by maintaining a fixed liquid level inside the evaporator. Trifluoroacetic anhydride can be preheated and mixed with the amine intermedi-

ate stream and passed through the reactor. The reactor is maintained at the desired temperature using a jacket. The outlet concentration of the reactor can be measured inline and the reactor jacket fluid flow rate should be manipulated to maintain a steady state at the reactor outlet. The process stream can be passed through the heat exchanger to reach the reaction temperature before passing through the packed bed reactor containing polymer-supported [bis(trifluoroacetoxy)iodo]benzene as packing material. The control strategy for the packed bed reactor will be similar as discussed earlier. The process stream containing the tricyclic intermediate can be cooled to 35 °C by mixing a cold stream of MeOH/water at the desired mole ratio using a ratio controller. The mixed stream can be passed through a packed bed reactor containing base to obtain (±)-oxomaritidine. The outlet concentration of (±)-oxomaritidine can be monitored online. Along with the concentration, it is also necessary to monitor the mass flow rate at the outlet to ensure that the reactions and conversions in the entire system are as per the design. The flow regimes in the packed bed reactor described here for liquid–solid reactions will be different based on wettability and such considerations need to be evolved separately as they become rate controlling when one goes for scale-up.

Case study 5: Multistep synthesis for ibuprofen (low overall residence time)

In a fascinating approach, recently Sneed and Jamison have reported a multistep synthesis for ibuprofen with a total residence time of the entire process approximately equal to 3 minutes [60] (Scheme 5). The process involves three reaction steps and one separation step. In the first step, a Friedel–Crafts acylation of

isobutylbenzene (1 equiv) and propionyl chloride (1.17 equiv) in the presence of AlCl$_3$ as Lewis acid was carried out in a tubular reactor. The residence time is one minute, and the temperature is maintained at 87 °C. The outlet of the reactor is mixed with aqueous HCl, and the organic and aqueous streams were separated by using an inline membrane separator. The ketone derivative was obtained in 95% yield (measured at the outlet of the membrane separator). This aryl ketone intermediate is mixed with trimethylorthoformate (8 equiv) in DMF solution and ICI as the promoter (3 equiv) in *n*-PrOH and was subjected to an oxidative 1,2-aryl migration. The reaction is carried out in a coiled reactor at 90 °C and 1 min residence time. The outlet stream is subjected to an alkaline solution of 2-mercaptoethanol, which quenched the ICI and carried further saponification of the ester intermediate in another tubular reactor at 90 °C and 1 min residence time. The entire process is carried out at 200 psi pressure and the yield of the target product ibuprofen is reported to be 83%. This report has been among the most eye-popping works in the recent time. This is largely because of the common usage of this medicine in huge volumes across the globe. As compared to the existing conventional process for ibuprofen, if this approach is to be followed right up to production scale, it needs a very different approach (while keeping the synthesis pathway unchanged). In order to have a first cut analysis of what that approach would involve if the process is to be optimized, in the below we give the synthesis pathway in terms of a block diagram (Figure 7A) that is easy to interpret and then evolve a piping and instrumentation diagram that will allow generating necessary data leading to scale-up. Figure 7B shows the P&ID for the ibuprofen manufacturing process. The flow rate of the limiting reagent, isobutylbenzene can be fixed at the
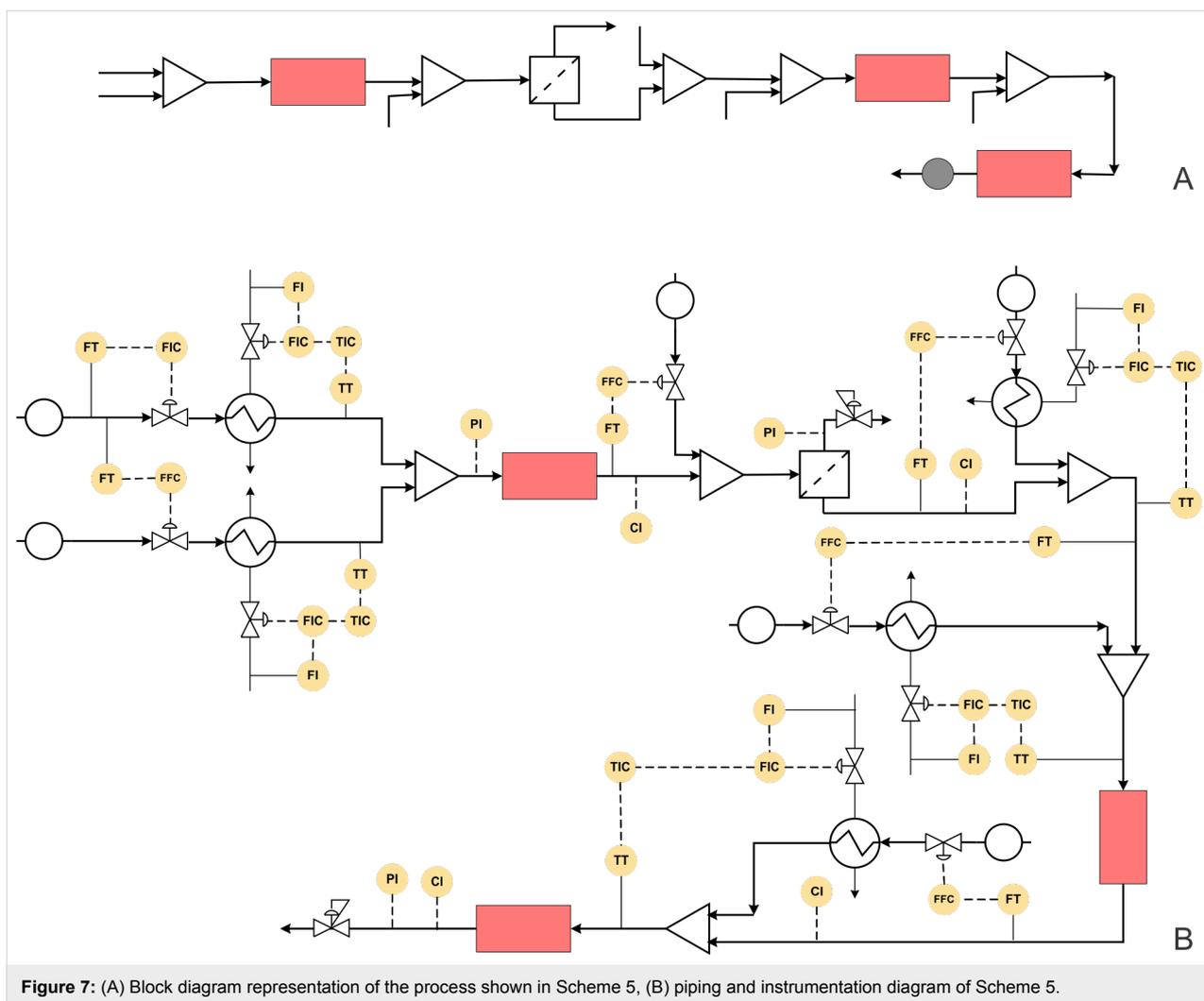

Scheme 5: Multistep synthesis for ibuprofen (Snead and Jamison [60]).
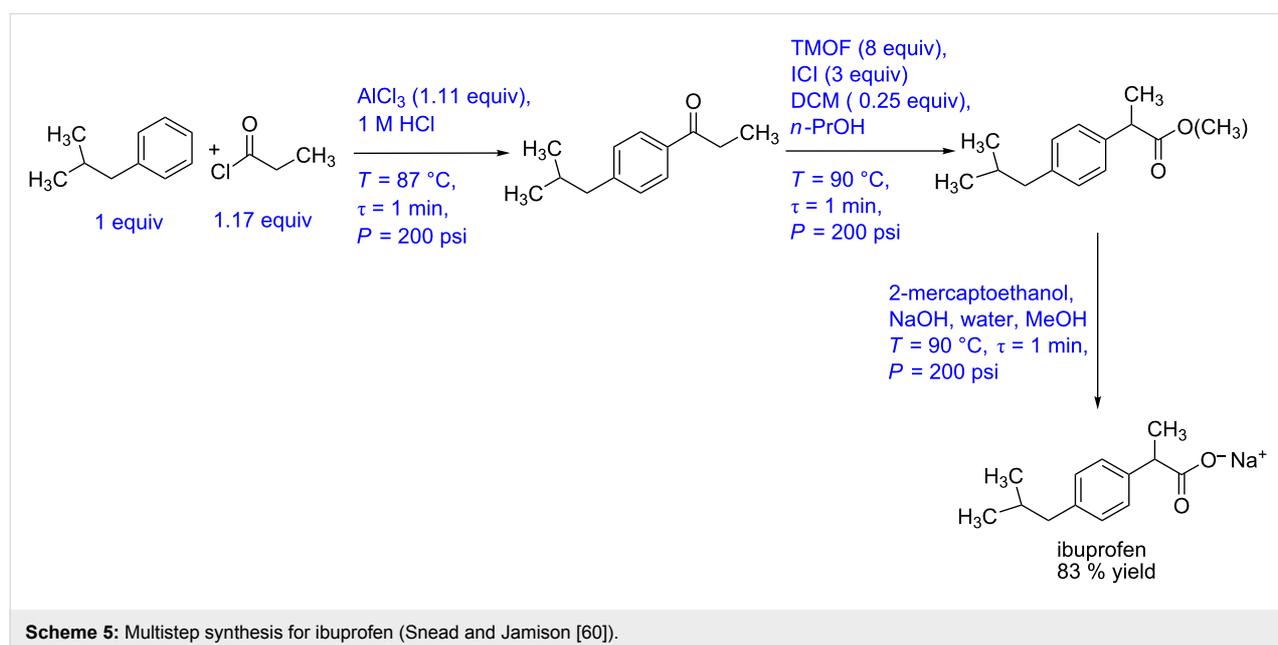
Figure 7: (A) Block diagram representation of the process shown in Scheme 5, (B) piping and instrumentation diagram of Scheme 5.

desired set point using a control valve. The flow rate of the pro-pionyl chloride stream can be controlled by using a ratio controller.

Both these streams should be preheated at 87 °C using a heat exchanger with feedback control. The preheated streams can be mixed in a reactor whose temperature can be controlled by a jacket. The outlet concentration of the intermediate can be monitored online and accordingly the jacket fluid flow rate should be varied for maintaining a steady state. A stream of aqueous HCl is mixed with this process stream using a ratio controller. The aqueous and organic phases will separate in the membrane separator. The back pressure regulator can be installed on the aqueous stream to create the desired pressure and facilitate complete separation. Trimethylorthoformate and ICI promoter also need to be preheated to 90 °C and mixed with the process stream containing the aryl ketone intermediate. The reactor can be maintained at the desired temperature using a jacket or tube-in-tube approach. The concentration of the ester

intermediate can be monitored using the suitable inline analyti-cal technique. The reactor jacket flow rate can be varied to control the intermediate ester concentration thereby ensuring that the reactor temperature is within the set-point and does not lead to side products. This stream can be mixed with a preheated alkaline 2-mercaptoethanol stream using another ratio controller to meet the stoichiometry. The combined stream can pass through a jacketed reactor, and the outlet concentration of ibuprofen can be monitored inline. Once again, as mentioned previously, the jacket fluid flow rate can be used as a manipu-lating variable for controlling the reactor conversion and selec-tivity.
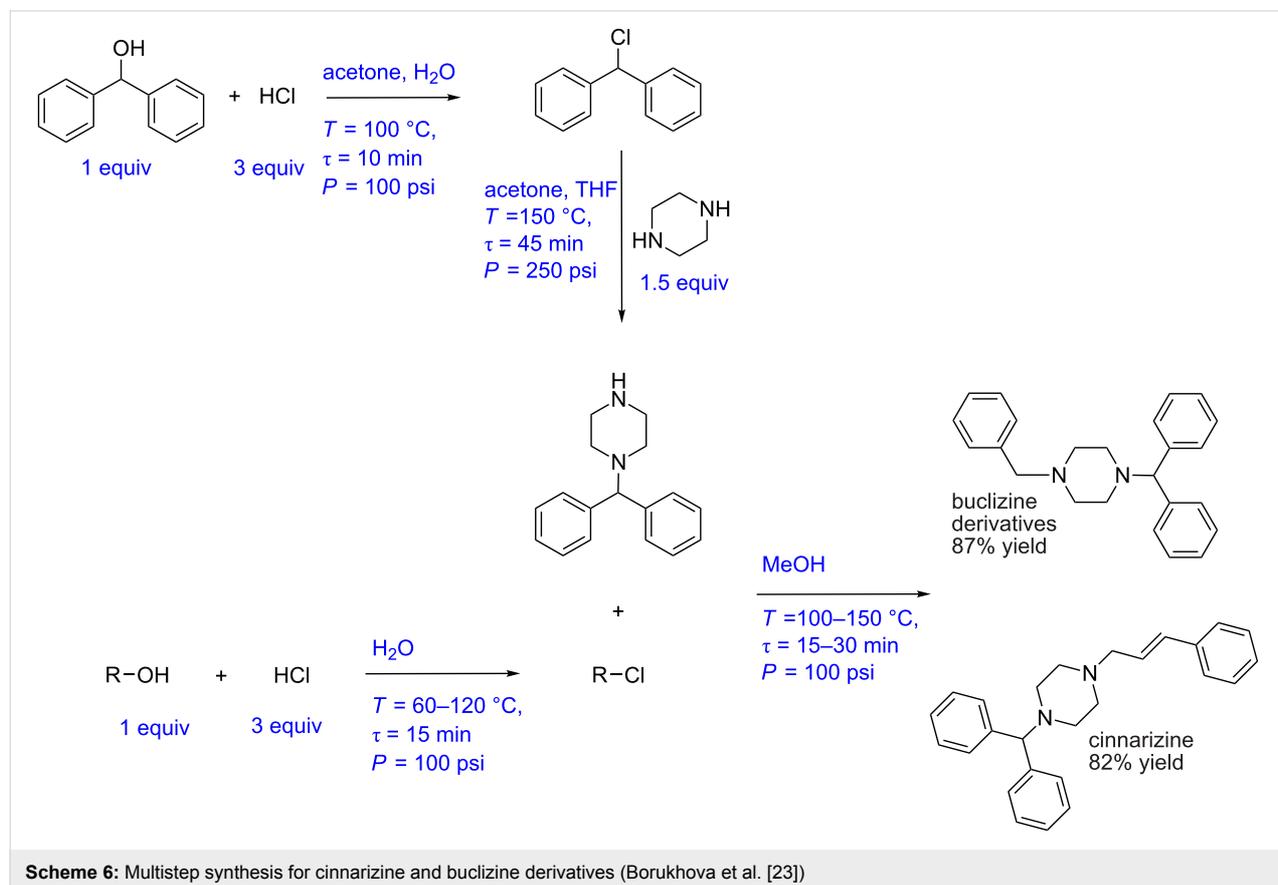
Case study 6: Multistep synthesis of cinnarizine, cyclizine, and buclizine derivatives (inline quenching)

Borukhova et al. have reported a multistep synthesis for cinnar-izine, cyclizine, and buclizine derivatives [23]. These drugs belong to the antihistamine family. The process involves 4 reac-

974

tion steps and two liquid–liquid extraction steps (for cinnarizine and buclizine derivatives). In the first step diphenylmethanol (1 equiv) is mixed with HCl (3 equiv) and passed through a tubular reactor at 100 °C and 10 min residence time. An acetone and water mixture is used as solvent and the reactor is pressurized at 100 psi using a back pressure regulator. The resulting aryl chloride is obtained in 97% yield. The excess HCl is then quenched with NaOH and the process stream is passed through the membrane separator. The outlet pressure of the aqueous stream was maintained at 2 psi pressure resulting in a perfect separation. The aryl chloride is further reacted with piperazine (1.5 equiv) to obtain 1-(diphenylmethyl)piperazine in 92% yield. The optimum conditions were 150 °C, 45 min, and 250 psi. The alcohol substrate is then reacted with HCl in a tubular reactor in parallel to get the corresponding aryl chloride. The temperature range was 60–120 °C for different substrates whereas the residence time and pressure were maintained at 15 min and 100 psi, respectively. The excess HCl was quenched with NaOH, and the organic phase was separated using a membrane separator. Aryl chloride is then mixed with 1-(diphenylmethyl)piperazine (obtained from the previous step) and methanol and passed through a tubular reactor maintained at 100–150 °C, over 15 to 30 min and at 100 psi pressure. The target drugs cinnarizine and buclizine derivatives are obtained

in 82% and 87% yield, respectively (Scheme 6). This process is relatively simple yet involving the use of in-line extraction and separation, which would have very different separation time scales when compared to the reaction time scale. Developing an automated platform for such a synthesis is indeed a challenge. In the below, we describe this approach in a way that can help to build an automated synthesis platform.

Figure 8A and 8B show the block diagram and possible P&ID for the cinnarizine/buclizine derivative manufacturing process. Initially, the flow rate of diphenylmethanol and the alcohol derivative should be fixed at the desired set point using a control valve. These streams can be preheated using a heat exchanger with feedback control. Aqueous HCl can also be preheated to the reaction temperature by applying suitable back pressure, and the stream can be split into two streams with a ratio controller for both the streams. Both the alcohol substrates can be mixed to react with HCl in the separate jacketed reactor to produce the corresponding aryl chlorides. The aqueous NaOH stream can be split into two streams (similar to the HCl stream discussed previously) and mixed with the reaction stream to quench the reaction. Alternatively, an inline pH flow cell can be used to measure the pH of the quenched solution and to send a feedback signal to control the flow rate of the NaOH solution [24].
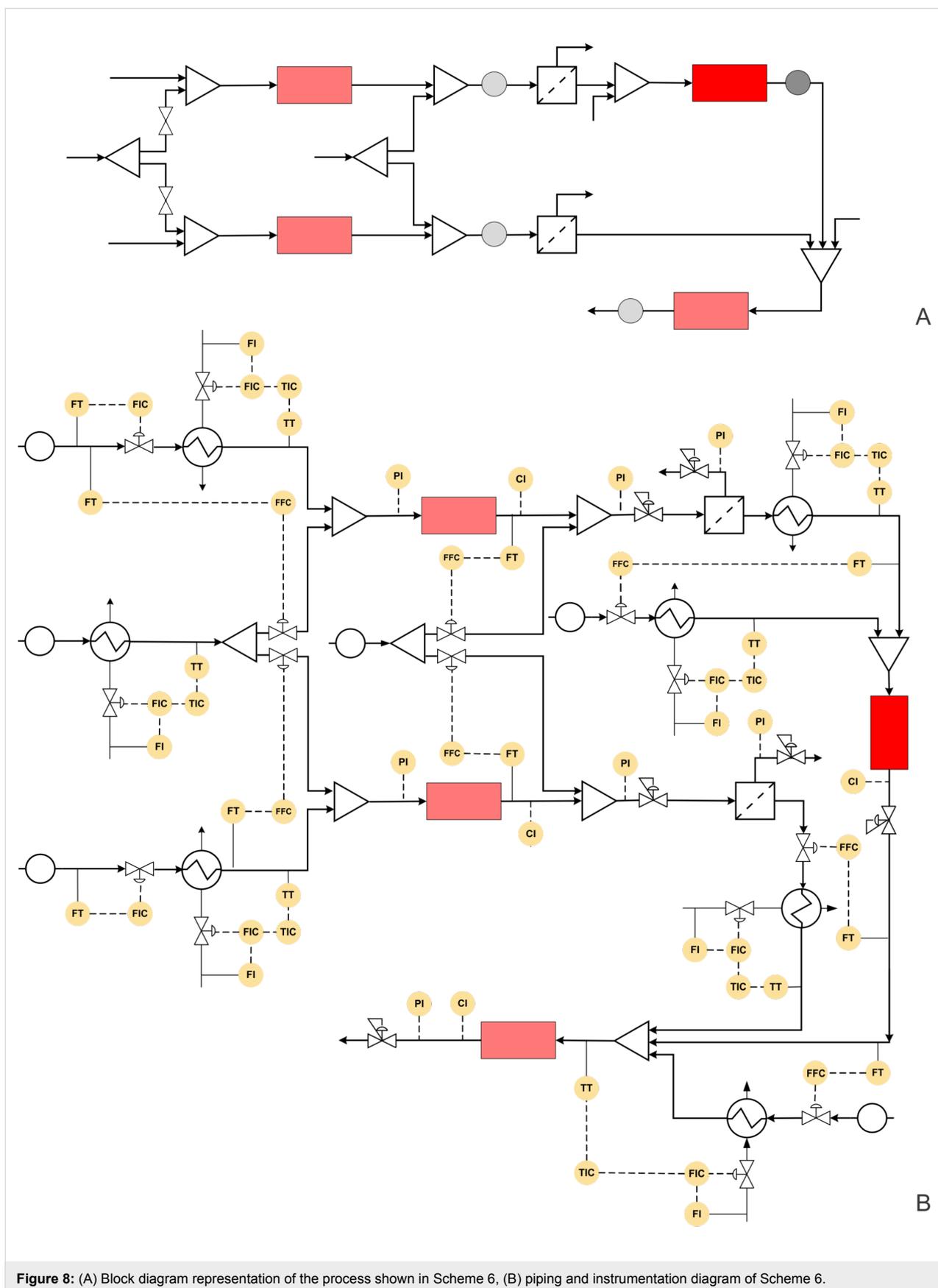

Scheme 6: Multistep synthesis for cinnarizine and buclizine derivatives (Borukhova et al. [23])

Figure 8: (A) Block diagram representation of the process shown in Scheme 6, (B) piping and instrumentation diagram of Scheme 6.

After quenching the reaction, the aqueous and organic phases can be separated using membrane separators. The pressure at the aqueous outlet can be controlled using a back pressure regulator to achieve the desired degree of separation. However, the separator needs to be designed to match the production capacity as it comes from the outlet of the reactor. Moreover, the separator needs to have a pressure transmitter to measure the pressure drop across the membrane to ensure that for higher or lower pressure drop values than the set-point values, an early indication of blocking or wearing of the membrane is given. Piperazine can be preheated and mixed with aryl chloride (obtained from diphenylmethanol) using a ratio controller to maintain the desired mole ratio. The mixed streams should be passed through the jacketed reactor with a jacket flow rate as the manipulating variable and the reactor outlet concentration as a controlled variable. The obtained 1-(diphenylmethyl)piperazine can be mixed with aryl chloride (obtained earlier) and with preheated MeOH at the desired mole ratio using a ratio controller. The mixed stream can then be passed through a jacketed reactor. The control strategy for the reactor can be similar to the above discussed reactor. The concentration of the API, cinnarizine/buclizine can be monitored in real time using an appropriate inline analytical technique. A back pressure regulator can be used to pressurize the entire system. However, if the membranes in the separators do not withstand these oper-

ating pressure for the reaction, one must isolate the zones of different pressure. Also, for the corrosive segments while PTFE or other commonly used flexible tubes would work at laboratory scale, these may not withstand pressure and hence it is advisable to use non-corrosive hastelloy or tantalum lined tubes or glass reactors that can withstand the process pressure.

Case study 7: Multistep synthesis of (*S*)-rolipram (gas–liquid–solid reaction)

Tsubogo et al. developed a multistep synthesis of (*S*)-rolipram, a drug belonging to the GABA family (Scheme 7) [4]. This is an excellent example for the use of several adsorption columns to isolate impurities. This work is a lucrative approach for the end-to-end synthesis of high value drugs. However, using so many packed beds is a challenging task when it comes to scale-up where the feed-back and feed-forward effects of individual packed beds. Before raising more operational complexities in scaling-up this approach, here we briefly describe the synthesis method. In a first step, a solution of aldehyde and nitromethane in toluene is passed through a packed column containing SiO_2-NH_2 and $CaCl_2$ as a catalyst and was maintained at 50 °C. The intermediate nitroalkene is obtained in 90% yield. A solution of malonate and triethylamine in toluene is mixed with the nitroalkene stream and passed through a packed column containing MS 4 Å to obtain stability in the system. This process

Scheme 7: Multistep synthesis for (S)-rolipram (Tsubogo et al. [4])
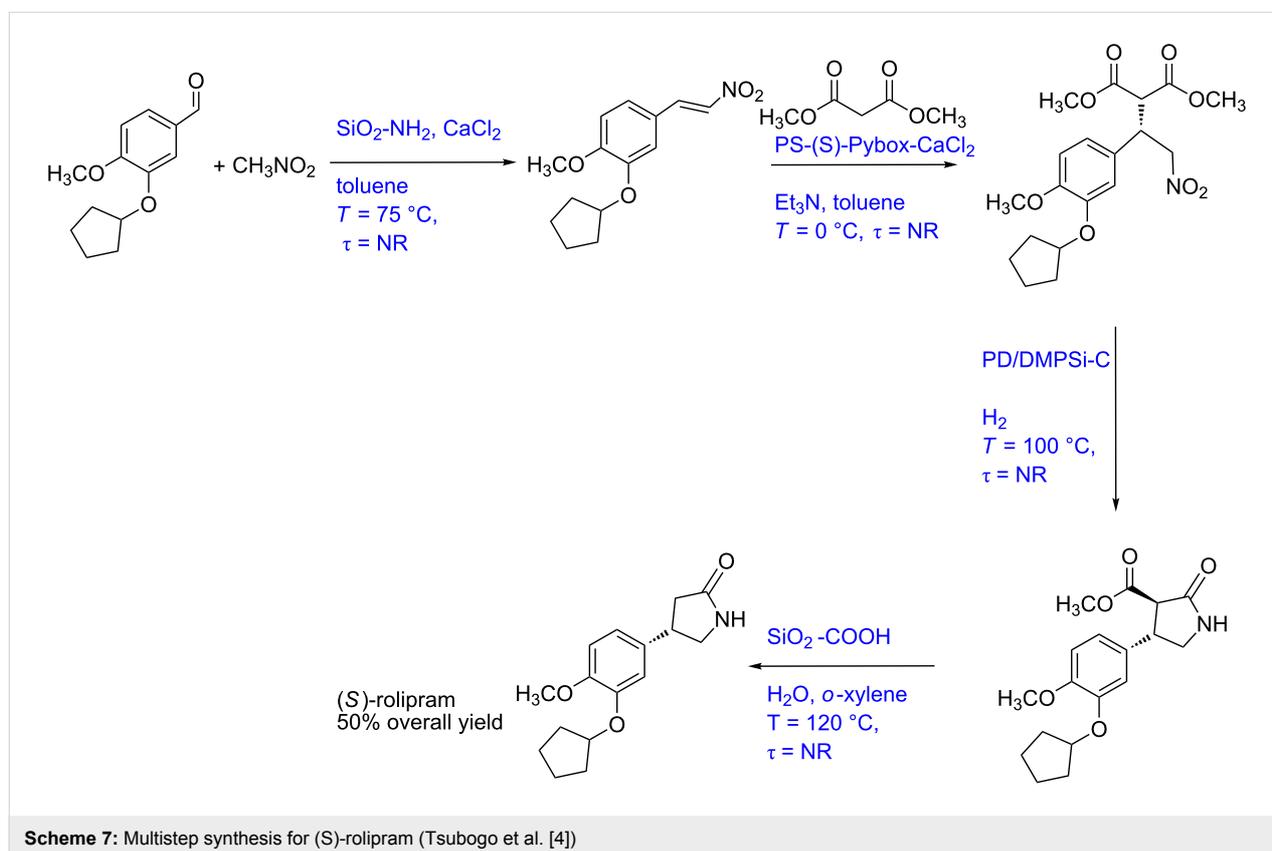
stream is then passed through a catalytic reactor packed with polymer-supported (S)-pybox–calcium chloride maintained at 0 °C. The Michael addition product is obtained in 84% yield which was subsequently reacted with hydrogen in a catalytic reactor containing Pd/DMPSi-C as the catalyst. The optimal operational conditions for the hydrogenation were 100 °C at atmospheric pressure. The γ-lactam was obtained in 74% yield. In the final stage, this product is hydrolysed and decarboxylated by passing it through a reactor containing silica-supported carboxylic acid at 120 °C. The final overall yield of the product (S)-rolipram is reported to be 50%. This synthesis method looks to be the cleanest approach so far as it uses multiple reactors for

individual transformations. Figure 9A shows the block diagram of this synthesis protocol, which actually brings out many challenges for scale-up for this process. In Figure 9B we have shown the P&ID of a possibly automated process for the synthesis of rolipram.

Initially, the flow rate of the aldehyde substrate should be fixed at the desired set point using a control valve while the nitromethane flow rate should be controlled using a ratio controller. Both these process streams should be preheated in a heat exchanger with a feedback controller. The mixed streams can then pass through a catalytic packed bed reactor with a jacket to

Figure 9: (A) Block diagram representation of the process shown in Scheme 7 (colours for each reactor shows different reactor temperatures), (B) piping and instrumentation diagram of Scheme 7.
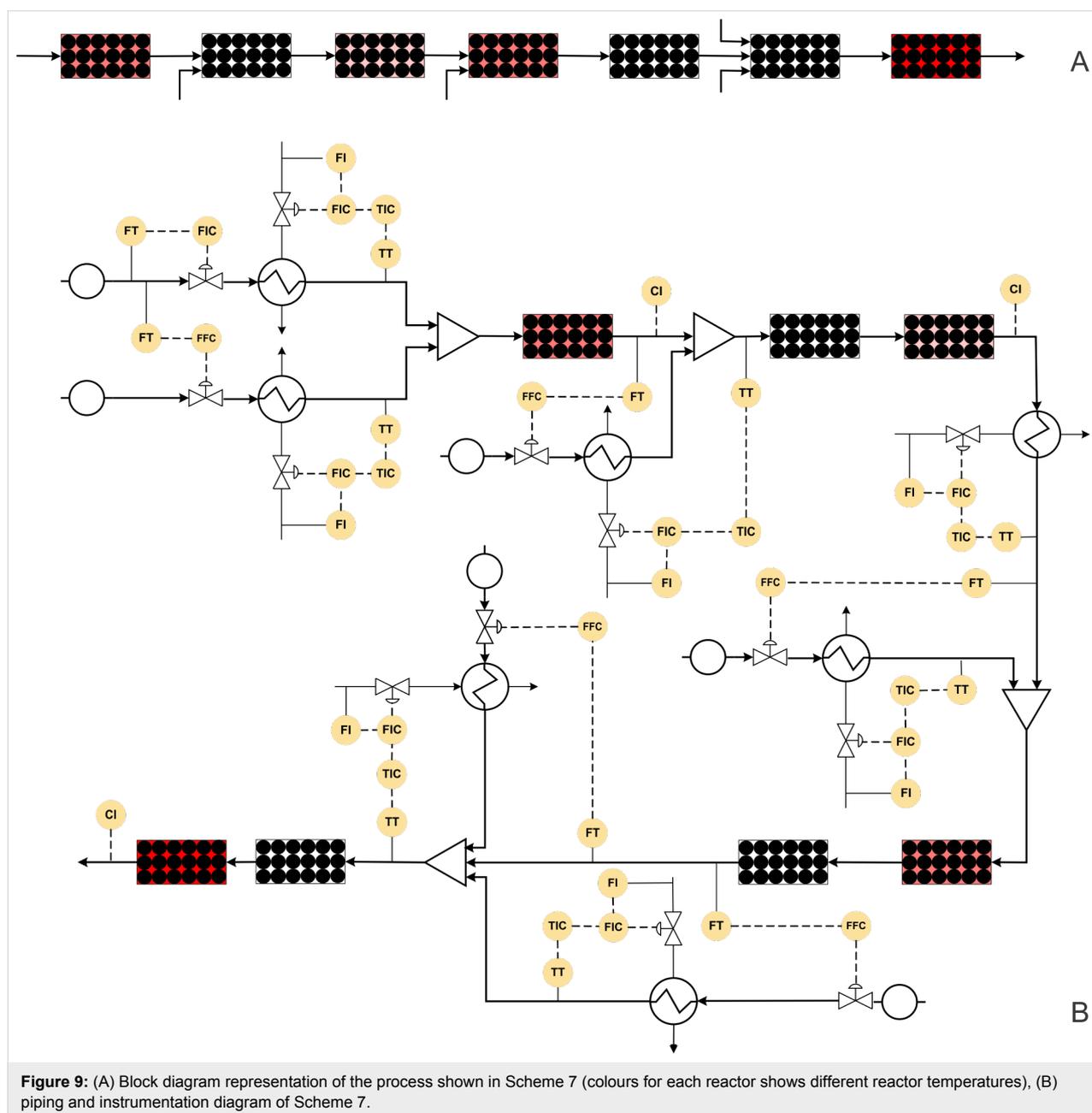
maintain the reaction temperature. The intermediate nitroalkene can be monitored at the reactor outlet, and the jacket fluid flow rate can be manipulated accordingly to maintain a steady state. Typically, for a catalytic reaction in a fixed bed reactor, the temperature profile is not uniform over the cross-section and thus can result in variation of the selectivity. The effect can be minimized by using a multi-tubular fixed bed reactor of smaller tube diameter, provided the flow is uniformly distributed in each tube. The malonate and triethylamine stream can be pre-cooled and mixed with the nitroalkene stream. The mixed stream can be passed through a packed bed reactor containing the catalyst maintained at 0 °C using a cooling jacket. The Michel addition product obtained can be monitored inline and the concentration can be controlled by varying the jacket flow rate. This process stream can be mixed with preheated hydrogen gas using an appropriate ratio controller. This mixed stream can then be passed in a packed bed reactor containing the Pd catalyst and maintained at 100 °C using a heating jacket. Since the temperatures are different for subsequent reactions, the issues related to conjugate heat transfer and reaction progress in the connection section needs to be carefully analyzed. In the case of deviations from the exact or desirable residence time and for the cases where the residence time distribution is non-Gaussian or Gaussian RTD with wider time scale, the formation of impurities and their carry-forward to the next reactor can be detrimental to the process. A systematic model needs to be developed to quantitatively obtain the yields of the products and impurities at different locations spatially and at different scales. The concentration of the hydrogenated product can be monitored and controlled by manipulating the jacket fluid flow rate. This process stream can be mixed with a preheated *o*-xylene and water stream and passed through a

packed bed reactor containing celite which can act as a filter medium. The mixed stream can then be passed to a packed bed reactor containing silica-supported carboxylic acid and was maintained at 120 °C using a heated jacket. A similar control strategy as for the packed bed reactor can be employed. It needs to be realized that since the reaction temperature in each fixed bed is different, an in-line heater is needed wherever necessary so that either quenching of reactions or sudden changes in the conditions can be avoided.

Case study 8: Multistep synthesis for amitriptyline (gas–liquid reaction)

Kupracz and Kirsching have reported a continuous multistep synthesis approach for amitriptyline, an antidepressant drug (Scheme 8) [7]. The process involves six reaction steps. Initially, a lithiation/Wurtz coupling reaction was carried out between benzyl bromide (in THF) and *n*-BuLi (in *n*-hexane) in a coiled steel reactor (1 mm ID and 0.5 mL) at −50 °C and 5 s residence time. This crude mixture of aryl bromide was reacted with CO_2 in a tube-in-tube reactor at −50 °C followed by a PFA reactor coil (0.8 mm ID and 0.5 mL) where the carboxylation took place at 25 °C. After removing the unreacted gas the reaction mixture was mixed with *n*-BuLi (in *n*-hexane). A Parham cyclization is carried out in 0.5 mL PFA reactor coil (0.8 mm ID) at 25 °C to yield 76% of ketone intermediate. This product is dissolved in MeOH and was isolated. This product is dissolved in THF and reacted with the Grignard reagent in a 0.5 mL PFA coil reactor (0.8 mm ID) at 25 °C and 30 s residence time. The crude product is protonated with EtOH and subjected to water elimination. The water elimination took place at 200 °C (using inductive heating) and 30 s residence time in a packed reactor column. The process fluid is cooled to room
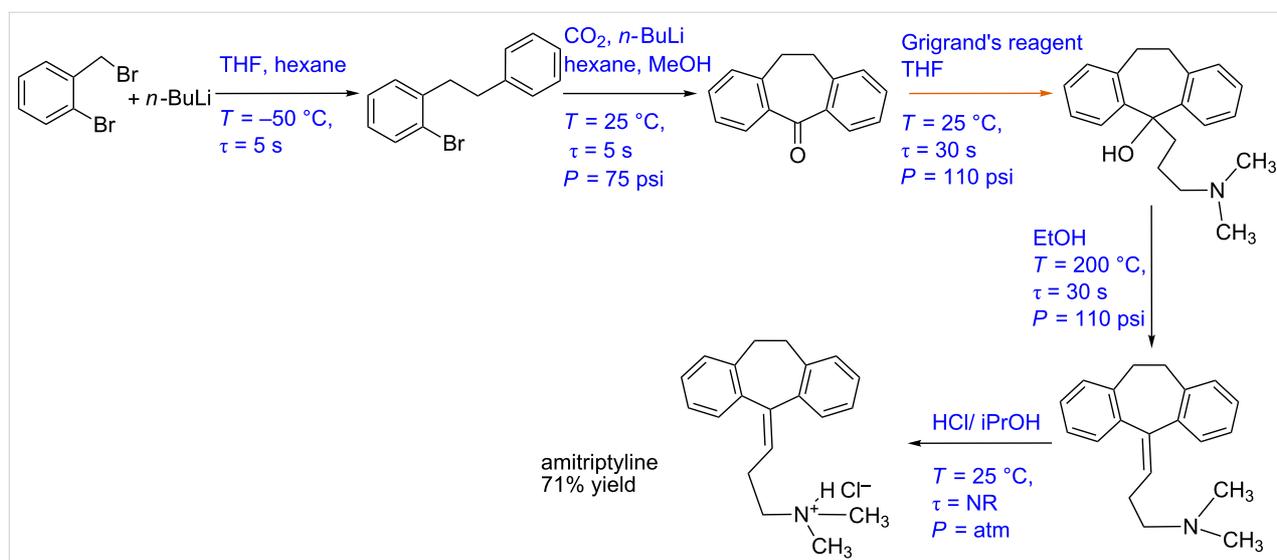
Scheme 8: Multistep synthesis for amitriptyline (Kupracz and Kirsching [7]).

temperature using a heat exchanger and was reacted with HCl (in isopropanol) which gives the corresponding salt. This was further recrystallized from EtOH/Et$_2$O to yield the amitriptyline hydrochloride salt (71%).

Interestingly, the authors have used the tube-in-tube system in series with a coiled reactor for the carboxylation step. While such systems do work for very small scale, the tube-in-tube approach is not easily scalable as the reaction rates enhanced due to higher mass transfer rates at the beginning of the tube would decrease subsequently making it complex to design a reactor for large-scale production. A simple gas–liquid slug flow in the coiled reactor should work. Moreover, it is easy to maintain the mole ratio of CO$_2$ and reactant in the coiled reactor. By selecting an appropriate flow regime, one can maximize the mass transfer rate and hence optimize the reaction. Using very

different solvents throughout the process viz. THF, *n*-hexane, methanol, ethanol, isopropyl alcohol and Et$_2$O will increase the downstream separation cost. We selected this process as it uses a tube-in-tube reactor for gas–liquid reaction along with a complex combination of solvents. Such an approach is going to be challenging for scale-up and specific variations in the process are definitely needed to make it automated. The automation proposed in the rest of this case study is only one such alternative and it will depend upon the choice of flow reactor.

Figure 10A and 10B shows the block diagram and P&ID for the amitriptyline manufacturing process. The mole ratio of benzyl bromide and *n*-BuLi can be controlled using a suitable ratio controller. The flow rate of benzyl bromide can be fixed at a suitable set point value depending on the scale of operation as it is the limiting reagent. Both these process streams can be pre-
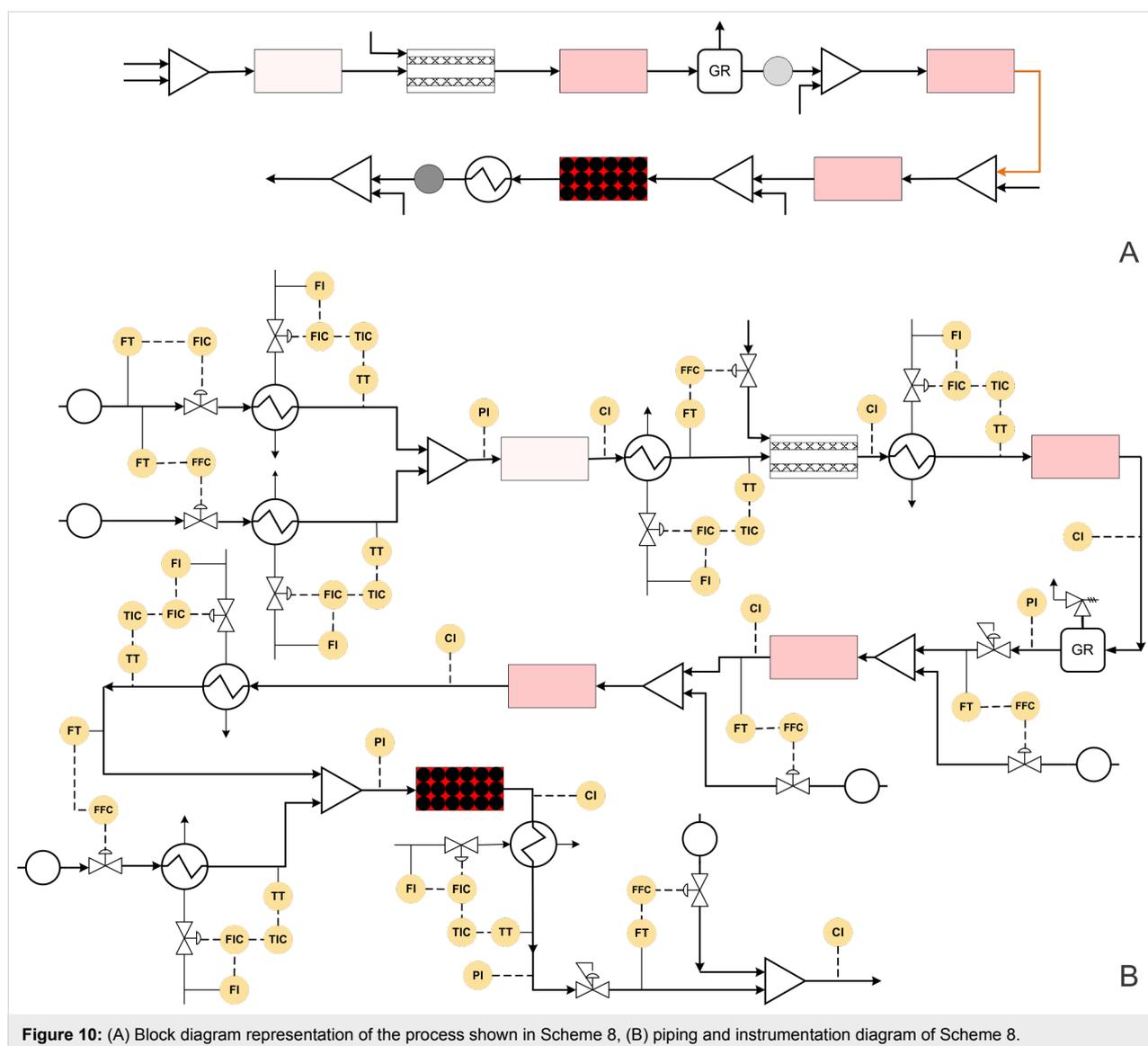

Figure 10: (A) Block diagram representation of the process shown in Scheme 8, (B) piping and instrumentation diagram of Scheme 8.

cooled separately using heat exchangers. For the heat exchanger, the outlet temperature of the process stream will be the controlled variable while the flow rate of the coolant will be the manipulating variable. After precooling, the reactants can be mixed in a suitable mixer and allowed to react in the reactor. The temperature of the reactor can be controlled by the jacket containing coolant (not shown in the Figure). The outlet concentration of the products can be monitored using a suitable inline analytical technique. In this case, the concentration of the reactor outlet can be the controlled variable and the coolant flow rate of the reactor jacket should be the manipulating variable. Alternatively, it is also possible to control the reactor outlet temperature by manipulating the jacket coolant flow rate. The crude mixture can be precooled again as it will be at relatively higher temperature due to absorption of the exothermic heat. This crude mixture can be passed through a heat exchanger to cool it and then passed through a membrane reactor. Using an appropriate ratio controller the flow rate of the CO_2 has to be controlled while measuring the flow rate of the crude mixture. The reaction mixture at the outlet can be heated to ambient temperature using a heat exchanger followed by a reactor. The outlet conversion of the reactor has to be monitored using a suitable inline analytical technique and the reactor temperature should be manipulated to control the outlet conversion. The excess CO_2 can be removed via a gas–liquid separator followed by a gas release valve attached to a pressure regulator. The ratio controller should control the molar ratio of the carboxylated intermediate and the *n*-BuLi. The concentration of the Parham cyclization product can be monitored and controlled at the reactor outlet by manipulating the coolant flow rate of the reactor jacket (not shown in the Figure). The process stream can be further mixed with the Grignard reagent in the desired stoichiometric ratio and passed through the reactor. The reactor temperature is maintained at ambient conditions using a cooling jacket. The concentration of the intermediate is monitored at the reactor outlet and the control action (flow rate of jacket coolant) can be taken accordingly. The process stream can be preheated using a heat exchanger and by mixing with preheated EtOH. Heating oil or high-pressure steam should be employed as a heat exchanger utility as higher temperatures (200 °C) are required. The process stream after passing through the reactor should be cooled at ambient temperature using a heat exchanger. The cooled process stream then can be mixed with HCl at suitable stoichiometry using a ratio controller to get the hydrochloride salt of amitriptyline. The back pressure regulator can be used to pressurize the system at the desired set point.

Examples of laboratory scale automated syntheses

Recently few excellent reports have appeared in the literature where control strategies are implemented at laboratory or bench scales. Saleemi et al. have investigated the effect of different control strategies on crystallization processes [73,74]. Process analytical technologies can be used to monitor concentrations, particle shape and size, and to control the temperature in crystallization processes [73-76]. More details about in-line monitoring techniques and control strategies in the industrial crystallization process can be found in the recent reviews [77-79]. Johnson and co-workers have demonstrated a controlled large-scale continuous-flow synthesis for various processes viz. asymmetric hydrogenation [80], direct asymmetric reductive amination [81] and asymmetric hydroformylation [82] and continuous Ir-catalyzed homogeneous reductive amination reaction [83]. Poh et al. demonstrated a multistep flow synthesis of pyrazole derivatives [84]. The process involved three reactions namely diazotization, reduction, and a hydrolysis/cyclocondensation. In-line flow IR spectroscopy was employed to monitor the concentration of the diazonium salts and the desired carbonyl intermediate. Computer integration with in-line IR and pumps also facilitated the control of the flow rate of the pentane-2,4-dione and HCl for the final hydrolysis/cyclocondensation step. In one of the most sophisticated systems, Adamo et al. have reported a compact (1.0 m (w) × 0.7 m (l) × 1.8 m (h)) and reconfigurable system capable of synthesizing and formulating various active pharmaceutical ingredients [3]. The system had a reconfigurable upstream unit which included a feed reservoir, reactors, pumps, separators and back pressure regulators. The upstream unit was followed by a downstream unit capable of further purification like tanks for precipitation of APIs, crystallizers, filters, etc. Strategic locations in the process were employed with suitable sensors for measuring the temperature, pressure, level and flow and were coupled with data acquisition systems for real-time monitoring. An inline attenuated total reflection (ATR) Fourier transform infrared (FTIR) system (FlowIR) was also employed for online monitoring of the formed APIs namely diphenhydramine hydrochloride, lidocaine hydrochloride, diazepam, and fluoxetine hydrochloride.

Hartman et al. have designed a microfluidic distillation operation and integrated it with a multistep reaction and liquid–liquid extraction [30]. The authors have used a compression chuck that controlled the inlet and outlet temperature of the microreactor and other components using a Thermo Scientific NESLAB RTE-7 refrigerating bath. For controlling the device temperature the authors employed an Omega 120V cartridge heater controlled by an Omega CN9000 series PID controller.

While these case studies are an encouraging sign of taking flow synthesis one step ahead, automation also faces challenges, often from the complexity of integrating various synthesis steps and variability in chemistry including phases of reactants, prod-

ucts, byproducts and catalysts. In the next section of this review, we have highlighted a few of such challenges that one might have to critically review before moving for automation.

Challenges in automation

Challenges to be addressed before automating any process: The discussion so far brings out the approaches for transforming specific continuous synthesis methods to a possible automated platform. There are a few common techniques and tools used in flow synthesis, which can face challenges when automating as well as during the scale-up. Table 1 shows the challenges that need to be addressed before automating any process at pilot scale so that the necessary care can be taken at the laboratory scale to avoid such issues, which can make a route completely unviable. Secondly, safety becomes a major concern during scale-up and the information desired to check the issues relevant to hazard and safety of a synthesis route and conditions has to be monitored right from the laboratory scale synthesis. Thus, creating an automation platform for the specific synthesis is not sufficient but it is absolutely necessary to check the safety of the entire process based on the conditions, reactants, products and their stability.

Table 2 shows the different variables or parameters involved in any reaction or separation processes. Knowing the exact value of these variables like temperature, residence time and pressure is essential for obtaining reproducible experimental results. The reagents are often required to be preheated or precooled if there is a significant difference in the reactor temperature and the ambient temperature. Preheating can be done by simply using a tubular reactor or using a suitable heat exchanger. Preheating or precooling should always be done before mixing reagents. If the reagents are subjected to any reactor maintained at a certain constant temperature (like a thermostat or temperature bath) without preheating or precooling, there can be a noticeable temperature profile in the reactor. This temperature profile can largely contribute to the conversion and selectivity of the reaction under consideration. In such cases the experimental yield is highly sensitive to the temperature profile and thus preheating or precooling should be opted to minimize this sensitivity and make the process more robust. It should be clearly mentioned whether the reported temperature is of the reactor/temperature bath or the process stream. The temperature of the reactor surface and the process fluid can be significantly different in some cases [10]. Residence time is an important time scale for designing any reactor. Residence time along with different time scales like mass transfer, mixing, heat transfer and dispersion are useful in finding the controlling step [86]. This helps in selection of the appropriate reactor device for pilot or commercial scale operations. Surprisingly very few researchers have reported the residence time for a packed bed type reactor [28]. For calculating the residence time in a packed bed reactor, it is essential first to calculate the active volume inside the reactor. The active volume is the volume available in the reactor for reaction (difference of the volume of the unpacked reactor and the packing material). The concentration or the yield of the desired process are always reported, however, the yield of the side product is generally never reported. It is also desired to measure the concentration of the process stream after the separation stage to check its efficiency [3,21,30,60]. If the desired separation is not achieved then temperature, pressure or scavenger loading should be adjusted to optimize the separation process.

Table 1: Common challenges that need to be addressed before automating any process.

Challenges	Comments
Induction heating [10]	• Additional cooling system may be required for cooling the reactor or distillation units. • Will increase the overall cost. • The control system can be complex due to different response times of heating and cooling cycles.
Increasing flow rate from inlet to the final outlet	• The flow rate at subsequent reactors will increase and hence a larger volume reactor will be required to maintain the required residence time. • Set-points for each reaction step will be different and need a different control structure.
Axial dispersion [85]	• Increasing flow rate along the synthesis path will increase the axial dispersion resulting in relatively lower conversions. • Additional volume should be provided for the reactor to overcome the effect of dispersion.
Number of mixers/ joints	• In multistep synthesis, there are relatively more T-joints/mixer which will cause pressure drop. • The control valves will contribute to significant pressure drop.
Material of construction	• At pilot scale, the process will run for a relatively larger time and hence reagents can corrode the reactors/pipelines. • Selecting appropriate material of construction becomes critical before automating any process at pilot scale.

Table 2: Basic variables involved for designing multistep flow synthesis and the status of literature on multistep flow synthesis on adapting suitable automation around these variables.

Author/Reference	Reactor					Separator		
	Preheating or precooling	T	τ	C^a	P	T	P	C
Hartwig et al. [10]	✗	Y	✗^b	✓	✓	✗	✓	✗
Kupracz and Kirschning [7]	✗	Y	✓^c	✓	✓	NA	NA	NA
Murray et al. [11]	✓	✓	✓	✓	✓	NA	NA	NA
Zhang et al. [14]	✗	✓	✓	✓	✓	NA	NA	NA
Snead & Jamison [60]	✗	✓	✓	✓	✓	✗	✓	✓
Borukhova et al. [23]	✗	✓	✓	✓	✓	✗	✓	✓
Baxendale et al. [26]	✗	✓	✗^b	✓	✓	✗	✓	✗
Tsubogo et al. [4]	✗	✓	✗	✓	✓	NA	NA	NA
Adamo et al. [3]	✓	Y	✓	Y	Y	Y	Y	Y
Poh et al. [84]	✗	✓	✓	Y	✓	NA	NA	NA
Hartman et al. [30]	Y	Y	✓	✓	Y	Y	Y	✓
Mascia et al. [24]	✗	Y	✓	Y	Y	✗	Y	Y

Symbols used and their meaning: (✓ - Parameters are either reported or measured offline, ✗ - Parameters are either not reported or not measured and Y - Parameters are measured online or controlled, Superscripts used and their meaning: ^aConcentration at the reactor outlet or yield of reaction at reactor outlet, ^bresidence time was not reported for the majority of the reactors which belonged to packed bed reactor category and ^cresidence time was reported for the majority of the reactors).

Challenges in automating special cases: Each process will have different challenges and it should be addressed separately. Some of the possible challenges are discussed below:

Handling of solids in flow reactors: Clogging of solids is a critical problem in a flow reactor. Recently many researchers have investigated clogging phenomena in micro-reactors and capillaries [87-90]. The event of clogging can be monitored by measuring the pressure [15,87]. The pressure will increase as the solids clog the reactor. Ideally one should identify the operating conditions that result in clogging and optimize the reaction such that clogging in the reactor is avoided. However, this may not be always possible and hence it is desired to develop a control strategy that will take appropriate action to address the clogging and to bring the process back to the steady state. For achieving this it is desired to monitor the pressure of the system and to develop a control strategy that will take appropriate action in the event of clogging. Some of the possible strategies can be (1) switch off the valves of the reactants and flush the reactor with an appropriate solvent to remove the clogging or (2) turn on the sonication while the reactants are flowing through the reactor. This will also minimize the power consumption of the sonication system as it will not be switched on continuously. However, before implementing such control

strategy, one should have experimental data of pressure vs time to understand the time scales of clogging and the unclogging process. The pressure set point/cut-off value can also be obtained from such data. Alternatively, one has to design the flow reactor taking into account the complex solid–liquid flow for the flow synthesis of Grignard reagent as reported by Wong et al. [91].

Maintaining temperature below the maximum allowable temperature: Some reactions like diazotization [92-94], lithiation [7,20], etc. have a maximum allowable temperature as a safety or design criteria. Such a reaction temperature should be monitored along the reactor at strategic locations. The control strategy should take appropriate action if the temperature reaches the maximum allowable temperature to avoid any runaway, decomposition and related hazards.

Maintaining constant conversion: It is desired to achieve a fixed conversion at the reactor outlet to maintain a steady state and constant product quality. This is very challenging when the entire system involves a complex network of dependent variables and parameters. This is usually done by controlling the reactor outlet temperature and manipulating the reactor jacket flow rate. The use of inline measuring techniques can help to

directly monitor the concentration at the reactor outlet [33]. For some reactions like fast or multiphase reactions, the conversion and selectivity will be more sensitive towards the flow regime, velocity, dispersion, etc. In such cases, the flow rate of reactants should be the manipulating variable and the outlet concentration should be the controlled variable. For the systems where there are restrictions on the reaction temperature, due to safety reasons, the temperature is not the recommended manipulating variable.

Conclusion

Automation will have a major role to play for converting the laboratory-scale multistep flow synthesis into industrial processes. In fact, when compared to conventional batch processes, these flow processes will be more logical cases for automation. Till date, except a few exceptions, automation in synthesis has always been interpreted as auto-sampling, in-line monitoring, and self-optimization systems. Auto-sampling and in-line monitoring of process variables like temperature, concentration, pressure, pH, etc. will not only improve the productivity of researchers but also improve the reproducibility of the experiments. The possible variation in the results due to minor changes in the set parameters can also be understood more accurately and used for developing a control structure. Reporting these process parameters can increase the quality of the work as well as the reproducibility.

Self-optimizing systems based on machine learning are the new hot topic in flow chemistry literature. While such systems may give the optimum operating conditions, it may not give insights into the progress of the reaction (like concentration and temperature profiles inside the reactor). If these self-optimization systems are also used for generating kinetic data, the kinetic parameters will add more valve to the research and also take the process one step closer to scale-up. Moreover, selecting right optimization algorithm remains critical for minimizing the time and resources used.

In this review, we have critically reviewed some of the important multistep syntheses in the recent past. The results from multistep flow synthesis indicated are promising and automation can bridge the gap between synthetic chemistry and industrial process. It is shown that automation at laboratory scale is very critical from the operational point of view as it will help to reduce the compounding errors in a big way. Automated control systems are not only responsible for executing normal operations like maintaining a process at steady state but also special purpose operations like a start-up, shut-down, change-over, override and emergency situations. Each operation will have a different protocol, and thorough process understanding is essential for developing an appropriate control logic. Dynamic simu-

lations will be useful for studying special purpose operations. We have also proposed the possible automation cum control logic for a few multistep syntheses and critically investigated the individual process.

The analysis of these representative multistep flow syntheses of a few important molecules indicates that the laboratory scale systems and approaches may not be relevant when one would want to extrapolate them for manufacturing. This means that certain critical sections need to be relooked and a process needs to be re-developed so that necessary time scales at each step are optimized. While these steps are always unavoidable, having an automated synthesis platform at laboratory scale will definitely help to know the issues that one would encounter during scale-up or numbering-up. It is certain that, if such excellent case studies use automated platforms, it will definitely help a true 'lab to market' translation as reported by Mascia et al. [24] and also appeal the chemical engineers and process engineers to work closely with chemists to make sure that the wonderful creations at laboratory scale are translated into practice.

March of machines in organic synthesis has begun long ago and is becoming more prominent as the curiosity of a creative chemist is trying to explore the molecular signatures across a wide range of time durations right from short-lived femtosecond species to living organisms that have a life cycle of few years to space chemistry that would hide mysteries spanning several light years. To be precise deeper understanding of complex syntheses will demand more creative time [95]. However, the true potential of involving machines on a routine basis for chemical synthesis coupled with in-line automation followed by analysis, decision making for the next experiment and identifying the optimal conditions is very close. This will help to take away routine jobs from the life of creative chemists and make them find time for thinking on complex chemistries. Implementation of automation in laboratory scale synthesis will also generate a huge amount of useful data for the process engineers who will find it relatively easy to transform a new chemistry into a process. The evolution of automation, instrumentation, sensing, machines, wireless control and faster logical platforms that allow hardware to interface with software has reached a stage where chemists can rely on the machine-based synthesis and process engineers can rely on the data that does not include a '*possibly ambiguous*' contribution of human errors. In all, it will save a lot of time to move ahead in further exploration in organic synthesis.

Acknowledgements

References

1. Movsisyan, M.; Delbeke, E. I. P.; Berton, J. K. E. T.; Battilocchio, C.; Ley, S. V.; Stevens, C. V. *Chem. Soc. Rev.* **2016,** *45,* 4892–4928. doi:10.1039/C5CS00902B

2. Kim, H.; Min, K.-I.; Inoue, K.; Im, D. J.; Kim, D.-P.; Yoshida, J.-i. *Science* **2016,** *352,* 691–694. doi:10.1126/science.aaf1389

3. Adamo, A.; Beingessner, R. L.; Behnam, M.; Chen, J.; Jamison, T. F.; Jensen, K. F.; Monbaliu, J.-C. M.; Myerson, A. S.; Revalor, E. M.; Snead, D. R.; Stelzer, T.; Weeranoppanant, N.; Wong, S. Y.; Zhang, P. *Science* **2016,** *352,* 61–67. doi:10.1126/science.aaf1337

4. Tsubogo, T.; Oyamada, H.; Kobayashi, S. *Nature* **2015,** *520,* 329–332. doi:10.1038/nature14343

5. Wegner, J.; Ceylan, S.; Kirschning, A. *Adv. Synth. Catal.* **2012,** *354,* 17–57. doi:10.1002/adsc.201100584

6. Lovei, K.; Bana, P.; Orkenyi, R.; Turos, G. I.; Eles, J.; Novak, Z.; Faigl, F. *Chim. Oggi* **2016,** *34,* 18–21.

7. Kupracz, L.; Kirschning, A. *Adv. Synth. Catal.* **2013,** *355,* 3375–3380. doi:10.1002/adsc.201300614

8. Heider, P. L.; Born, S. C.; Basak, S.; Benyahia, B.; Lakerveld, R.; Zhang, H.; Hogan, R.; Buchbinder, L.; Wolfe, A.; Mascia, S.; Evans, J. M. B.; Jamison, T. F.; Jensen, K. F. *Org. Process Res. Dev.* **2014,** *18,* 402–409. doi:10.1021/op400294z

9. Baxendale, I. R.; Deeley, J.; Griffiths-Jones, C. M.; Ley, S. V.; Saaby, S.; Tranmer, G. K. *Chem. Commun.* **2006,** 2566–2568. doi:10.1039/b600382f

10. Hartwig, J.; Ceylan, S.; Kupracz, L.; Coutable, L.; Kirschning, A. *Angew. Chem., Int. Ed.* **2013,** *52,* 9813–9817. doi:10.1002/anie.201302239

11. Murray, P. R. D.; Browne, D. L.; Pastre, J. C.; Butters, C.; Guthrie, D.; Ley, S. V. *Org. Process Res. Dev.* **2013,** *17,* 1192–1208. doi:10.1021/op4001548

12. Guetzoyan, L.; Nikbin, N.; Baxendale, I. R.; Ley, S. V. *Chem. Sci.* **2013,** *4,* 764–769. doi:10.1039/C2SC21850J

13. Battilocchio, C.; Deadman, B. J.; Nikbin, N.; Kitching, M. O.; Baxendale, I. R.; Ley, S. V. *Chem. – Eur. J.* **2013,** *19,* 7917–7930. doi:10.1002/chem.201300696

14. Zhang, P.; Russell, M. G.; Jamison, T. F. *Org. Process Res. Dev.* **2014,** *18,* 1567–1570. doi:10.1021/op500166n

15. Gilmore, K.; Kopetzki, D.; Lee, J. W.; Horváth, Z.; McQuade, D. T.; Seidel-Morgenstern, A.; Seeberger, P. H. *Chem. Commun.* **2014,** *50,* 12652–12655. doi:10.1039/C4CC05098C

16. Martin, A. D.; Siamaki, A. R.; Belecki, K.; Gupton, B. F. *J. Flow Chem.* **2015,** *5,* 145–147. doi:10.1556/JFC-D-15-00002

17. Pellegatti, L.; Sedelmeier, J. *Org. Process Res. Dev.* **2015,** *19,* 551–554. doi:10.1021/acs.oprd.5b00058

18. Lau, S.-H.; Galván, A.; Merchant, R. R.; Battilocchio, C.; Souto, J. A.; Berry, M. B.; Ley, S. V. *Org. Lett.* **2015,** *17,* 3218–3221. doi:10.1021/acs.orglett.5b01307

19. Snead, D. R.; Jamison, T. F. *Chem. Sci.* **2013,** *4,* 2822–2827. doi:10.1039/c3sc50859e

20. Correia, C. A.; Gilmore, K.; McQuade, D. T.; Seeberger, P. H. *Angew. Chem., Int. Ed.* **2015,** *54,* 4945–4948. doi:10.1002/anie.201411728

21. Ghislieri, D.; Gilmore, K.; Seeberger, P. H. *Angew. Chem., Int. Ed.* **2015,** *54,* 678–682. doi:10.1002/anie.201409765

22. Hopkin, M. D.; Baxendale, I. R.; Ley, S. V. *Chem. Commun.* **2010,** *46,* 2450–2452. doi:10.1039/c001550d

23. Borukhova, S.; Noël, T.; Hessel, V. *ChemSusChem* **2016,** *9,* 67–74. doi:10.1002/cssc.201501367

24. Mascia, S.; Heider, P. L.; Zhang, H.; Lakerveld, R.; Benyahia, B.; Barton, P. I.; Braatz, R. D.; Cooney, C. L.; Evans, J. M. B.; Jamison, T. F.; Jensen, K. F.; Myerson, A. S.; Trout, B. L. *Angew. Chem., Int. Ed.* **2013,** *52,* 12359–12363. doi:10.1002/anie.201305429

25. Baumann, M.; Baxendale, I. R.; Kirschning, A.; Ley, S. V.; Wegner, J. *Heterocycles* **2011,** *82,* 1297–1316. doi:10.3987/COM-10-S(E)77

26. Baxendale, I. R.; Ley, S. V.; Mansfield, A. C.; Smith, C. D. *Angew. Chem., Int. Ed.* **2009,** *48,* 4017–4021. doi:10.1002/anie.200900970

27. Baxendale, I. R.; Schou, S. C.; Sedelmeier, J.; Ley, S. V. *Chem. – Eur. J.* **2010,** *16,* 89–94. doi:10.1002/chem.200902906

28. Petersen, T. P.; Ritzén, A.; Ulven, T. *Org. Lett.* **2009,** *11,* 5134–5137. doi:10.1021/ol902101c

29. Adamo, A.; Heider, P. L.; Weeranoppanant, N.; Jensen, K. F. *Ind. Eng. Chem. Res.* **2013,** *52,* 10802–10808. doi:10.1021/ie401180t

30. Hartman, R. L.; Naber, J. R.; Buchwald, S. L.; Jensen, K. F. *Angew. Chem., Int. Ed.* **2010,** *49,* 899–903. doi:10.1002/anie.200904634

31. Webb, D.; Jamison, T. F. *Chem. Sci.* **2010,** *1,* 675–680. doi:10.1039/c0sc00381f

32. Porta, R.; Benaglia, M.; Puglisi, A. *Org. Process Res. Dev.* **2016,** *20,* 2–25. doi:10.1021/acs.oprd.5b00325

33. McMullen, J. P.; Jensen, K. F. *Annu. Rev. Anal. Chem.* **2010,** *3,* 19–42. doi:10.1146/annurev.anchem.111808.073718

34. Matlin, S. A.; Mehta, G.; Hopf, H.; Krief, A. *Nat. Chem.* **2016,** *8,* 393–398. doi:10.1038/nchem.2498

35. Hayden, E. C. *Nature* **2014,** *516,* 131–132. doi:10.1038/516131a

36. Peplow, M. *Nature* **2014,** *512,* 20–22. doi:10.1038/512020a

37. Moore, J. S.; Jensen, K. F. *Angew. Chem., Int. Ed.* **2014,** *53,* 470–473. doi:10.1002/anie.201306468

38. Reizman, B. J.; Jensen, K. F. *Org. Process Res. Dev.* **2012,** *16,* 1770–1782. doi:10.1021/op3001838

39. McMullen, J. P.; Jensen, K. F. *Org. Process Res. Dev.* **2010,** *14,* 1169–1176. doi:10.1021/op100123e

40. McMullen, J. P.; Stone, M. T.; Buchwald, S. L.; Jensen, K. F. *Angew. Chem., Int. Ed.* **2010,** *49,* 7076–7080. doi:10.1002/anie.201002590

41. Fabry, D. C.; Sugiono, E.; Rueping, M. *React. Chem. Eng.* **2016,** *1,* 129–133. doi:10.1039/C5RE00038F

42. Moore, J. S.; Jensen, K. F. *Org. Process Res. Dev.* **2012,** *16,* 1409–1415. doi:10.1021/op300099x

43. Zaborenko, N.; Murphy, E. R.; Kralj, J. G.; Jensen, K. F. *Ind. Eng. Chem. Res.* **2010,** *49,* 4132–4139. doi:10.1021/ie100263p

44. Westermann, T.; Mleczko, L. *Org. Process Res. Dev.* **2015,** *20,* 487–494. doi:10.1021/acs.oprd.5b00205

45. Reizman, B. J.; Wang, Y.-M.; Buchwald, S. L.; Jensen, K. F. *React. Chem. Eng.* **2016,** *1,* 658–666. doi:10.1039/C6RE00153J

46. Fitzpatrick, D. E.; Ley, S. V. *React. Chem. Eng.* **2016,** *1,* 629–635. doi:10.1039/C6RE00160B

47. Harrison, W. *Drug Discovery Today* **1998,** *3,* 343–349. doi:10.1016/S1359-6446(98)01201-X

48. Hann, M. M.; Oprea, T. I. *Curr. Opin. Chem. Biol.* **2004,** *8,* 255–263. doi:10.1016/j.cbpa.2004.04.003

49. Stodden, V.; Leisch, F.; Peng, R. D. *Implementing reproducible research;* CRC Press, 2014.

50. Baker, M. *Nature* **2016,** *533,* 452–454. doi:10.1038/533452a
51. Jämsä-Jounela, S.-L. *Annu. Rev. Control* **2007,** *31,* 211–220. doi:10.1016/j.arcontrol.2007.08.003
52. Stephanopoulos, G. *Comput. Chem. Eng.* **1983,** *7,* 331–365. doi:10.1016/0098-1354(83)80018-0
53. Anderson, N. A. *Instrumentation for Process Measurement and Control,* 3rd ed.; Crc Press, 1997.
54. Baker, R. C. *Flow measurement handbook: industrial designs, operating principles, performance, and applications;* Cambridge University Press, 2005.
55. Dunn, W. *Fundamentals of industrial instrumentation and process control;* McGraw-Hill, 2005.
56. Boyes, W. *Instrumentation reference book;* Butterworth-Heinemann, 2009.
57. Luyben, W. L. *Process modeling, simulation and control for chemical engineers;* McGraw-Hill Higher Education, 1989.
58. Dunjó, J.; Fthenakis, V.; Vílchez, J. A.; Arnaldos, J. *J. Hazard. Mater.* **2010,** *173,* 19–32. doi:10.1016/j.jhazmat.2009.08.076
59. Venkatasubramanian, V.; Vaidhyanathan, R. *AIChE J.* **1994,** *40,* 496–505. doi:10.1002/aic.690400311
60. Snead, D. R.; Jamison, T. F. *Angew. Chem.* **2015,** *127,* 997–1001. doi:10.1002/ange.201409093
61. F³ Factory website. http://www.f3factory.com/scripts/pages/en/home.php (accessed March 6, 2017).
62. Texol website. http://texol.in/ (accessed March 6, 2017).
63. Future Chemistry website. http://futurechemistry.com/ (accessed March 6, 2017).
64. Xytel website. http://www.xytelindia.com/ (accessed March 6, 2017).
65. Britest website. https://www.britest.co.uk/ (accessed March 6, 2017).
66. BIAZZI website. http://www.biazzi.ch/ (accessed March 6, 2017).
67. Snapdragon Chemistry website. http://www.snapdragonchemistry.com/snapdragon-difference/ (accessed March 6, 2017).
68. Couper, J. R.; Penney, W. R.; Fair, J. R. *Chemical process equipment revised 2E: selection and design;* Gulf Professional Publishing, 2009.
69. Towler, G.; Sinnott, R. K. *Chemical engineering design: principles, practice and economics of plant and process design;* Elsevier, 2012.
70. Perry, R. H.; Green, D. W. *Perry's chemical engineers' handbook;* McGraw-Hill Professional, 1999.
71. Ley, S. V.; Ingham, R. J.; O'Brien, M.; Browne, D. L. *Beilstein J. Org. Chem.* **2013,** *9,* 1051–1072. doi:10.3762/bjoc.9.118
72. Saaby, S.; Knudsen, K. R.; Ladlow, M.; Ley, S. V. *Chem. Commun.* **2005,** 2909–2911. doi:10.1039/b504854k
73. Saleemi, A.; Rielly, C.; Nagy, Z. K. *CrystEngComm* **2012,** *14,* 2196–2203. doi:10.1039/c2ce06288g
74. Saleemi, A. N.; Rielly, C. D.; Nagy, Z. K. *Cryst. Growth Des.* **2012,** *12,* 1792–1807. doi:10.1021/cg201269c
75. Powell, K. A.; Bartolini, G.; Wittering, K. E.; Saleemi, A. N.; Wilson, C. C.; Rielly, C. D.; Nagy, Z. K. *Cryst. Growth Des.* **2015,** *15,* 4821–4836. doi:10.1021/acs.cgd.5b00599
76. Powell, K. A.; Saleemi, A. N.; Rielly, C. D.; Nagy, Z. K. *Org. Process Res. Dev.* **2016,** *20,* 626–636. doi:10.1021/acs.oprd.5b00373
77. Nagy, Z. K.; Braatz, R. D. *Annu. Rev. Chem. Biomol. Eng.* **2012,** *3,* 55–75. doi:10.1146/annurev-chembioeng-062011-081043
78. Braatz, R. D. *Annu. Rev. Control* **2002,** *26,* 87–99. doi:10.1016/S1367-5788(02)80016-5
79. Larsen, P. A.; Patience, D. B.; Rawlings, J. B. *Industrial crystallization process control;* IEEE Control Syst. Mag., 2006; pp 70–80.
80. Johnson, M. D.; May, S. A.; Calvin, J. R.; Remacle, J.; Stout, J. R.; Diseroad, W. D.; Zaborenko, N.; Haeberle, B. D.; Sun, W.-M.; Miller, M. T. *Org. Process Res. Dev.* **2012,** *16,* 1017–1038. doi:10.1021/op200362h
81. Johnson, M. D.; May, S. A.; Haeberle, B.; Lambertus, G. R.; Pulley, S. R.; Stout, J. R. *Org. Process Res. Dev.* **2016,** *20,* 1305–1320. doi:10.1021/acs.oprd.6b00137
82. Johnson, M. D.; May, S. A.; Calvin, J. R.; Lambertus, G. R.; Kokitkar, P. B.; Landis, C. R.; Jones, B. R.; Abrams, M. L.; Stout, J. R. *Org. Process Res. Dev.* **2016,** *20,* 888–900. doi:10.1021/acs.oprd.5b00407
83. May, S. A.; Johnson, M. D.; Buser, J. Y.; Campbell, A. N.; Frank, S. A.; Haeberle, B. D.; Hoffman, P. C.; Lambertus, G. R.; McFarland, A. D.; Moher, E. D. *Org. Process Res. Dev.* **2016,** *20,* 1870–1898.
84. Poh, J.-S.; Browne, D. L.; Ley, S. V. *React. Chem. Eng.* **2016,** *1,* 101–105. doi:10.1039/C5RE00082C
85. Nagy, K. D.; Shen, B.; Jamison, T. F.; Jensen, K. F. *Org. Process Res. Dev.* **2012,** *16,* 976–981. doi:10.1021/op200349f
86. Ranade, V. V.; Sharma, M. K.; Kulkarni, A. A. *Chem. Eng. J.* **2015,** *278,* 454–468. doi:10.1016/j.cej.2014.12.050
87. Pal, S.; Kulkarni, A. A. *Chem. Eng. Sci.* **2016,** *153,* 344–353. doi:10.1016/j.ces.2016.07.012
88. Kuhn, S.; Noël, T.; Gu, L.; Heider, P. L.; Jensen, K. F. *Lab Chip* **2011,** *11,* 2488–2492. doi:10.1039/c1lc20337a
89. Hartman, R. L. *Org. Process Res. Dev.* **2012,** *16,* 870–887. doi:10.1021/op200348t
90. Hartman, R. L.; Naber, J. R.; Zaborenko, N.; Buchwald, S. L.; Jensen, K. F. *Org. Process Res. Dev.* **2010,** *14,* 1347–1357. doi:10.1021/op100154d
91. Wong, S.-W.; Changi, S. M.; Shields, R.; Bell, W.; McGarvey, B.; Johnson, M. D.; Sun, W.-M.; Braden, T. M.; Kopach, M. E.; Spencer, R. D.; Flanagan, G.; Murray, M. *Org. Process Res. Dev.* **2016,** *20,* 540–550. doi:10.1021/acs.oprd.5b00268
92. Chernyak, N.; Buchwald, S. L. *J. Am. Chem. Soc.* **2012,** *134,* 12466–12469. doi:10.1021/ja305660a
93. Wedlich, R. C. *Chem. Eng. Prog.* **2001,** *97,* 60–61.
94. Shukla, C. A.; Kulkarni, A. A.; Ranade, V. V. *React. Chem. Eng.* **2016,** *1,* 387–396. doi:10.1039/C5RE00056D
95. Ley, S. V.; Fitzpatrick, D. E.; Ingham, R. J.; Myers, R. M. *Angew. Chem., Int. Ed.* **2015,** *54,* 3449–3464. doi:10.1002/anie.201410744